Multifrequency acoustic target strength of Northern krill

Lucio Calise

Department of Physics and Technology
Faculty of Mathematics and Natural Sciences
University of Bergen

January 2009

Acknowledgements

First, I would like to express my gratitude to my supervisor Professor Halvor Hobæk for his invaluable guidance and support throughout all these years. I sincerely thank him for following up my research work with such interest, encouraging me and believing in my abilities even when things have been difficult.

A special thank goes to my colleague and friend Tor Knutsen, Research Group Plankton at the Institute of Marine Research (IMR) in Bergen, who contributed with fruitful discussions and ideas. Without his encouragement and experience this thesis would not have been possible.

Dr. Webjørn Melle, research manager of the Research Group Plankton of IMR, is also thanked for promoting and supporting my research through the IMR internal program "New feed resources for the Aquaculture industry".

The group leader Dr. Olav Rune Godø and all the colleagues and technicians of the Observation Metodikk Gruppen (OM) of IMR are sincerely thanked for the way they welcomed me as an "associated part" of the group. A particular acknowledgement goes to my co-supervisor John Dalen for his critical comments and helpful advice during the writing part of this thesis. I am deeply indebted to Professor Egil Ona for sharing with me his great knowledge in underwater acoustics and for always inspiring me. As for other young colleagues, I felt "victim" of his contagious enthusiasm. The group consultant Mrs Reidun Heggø Sørensen is also thanked for her great help in solving practical problems during my stay at OM.

Furthermore, I would like to thank Eng. Arve Kristiansen at Aquaculture Research Station of IMR, for his invaluable help during the experimental period at station, and express my gratitude to Dr. Helge Balk, Department of Physics at University of Oslo, for his generosity in providing an enhanced version of the Sonar5 post-processing software and for helping me to explore its many useful features.

I have also particularly appreciated the help of Dr. Lars Nonboe Andersen, Simrad AS, for providing technical information on Simrad echosounders and for giving me free access to the acoustic measurements facilities at Simrad AS in Horten (Norway).

This thesis is in memory of my father.

Contents

List of Papers

Paper I Lucio Calise, Tohru Mukai and Tor Knutsen

Density and speed of sound in winter specimens of Northern krill (Meganyctiphanes norvegica) from a west Norwegian fjord

to be submitted to: ICES Journal of Marine Science

Paper II Lucio Calise, Tor Knutsen and Webjørn Melle

Multifrequency Acoustic Measurements of free swimming northern krill (Meganyctiphanes norvegica) in a mesocosm venue: methodological challenges. Proceedings of the International Conference "Underwater Acoustic Measurements: Technologies & Results", Vol. II, pages 865-871, Heraklion, Crete, Greece, 28th June – 1st July 2005.

Paper III Lucio Calise

Short range performances of a scientific echosounder with emphasis on accurate calibration

to be submitted to: Journal of the Acoustical Society of America

Paper IV Lucio Calise, Tor Knutsen and Webjørn Melle

Multifrequency target strength of horizontally free-swimming Northern krill (Meganyctiphanes norvegica) in a mesocosm venue

to be submitted to: ICES Journal of Marine Science

Paper V Lucio Calise and Tor Knutsen

Multifrequency target strength of Northern krill (Meganyctiphanes norvegica): measurements on tethered specimens and SDWBA theoretical predictions.

to be submitted to: ICES Journal of Marine Science

Paper VI Lucio Calise, Tor Knutsen and Rolf Korneliussen

The impact of echo sounder settings for the discrimination of acoustic scatterers in a multi-frequency survey context. Proceedings of the 2nd International Conference "Underwater Acoustic Measurements: Technologies & Results", Vol. III, pages 1201-1208, Heraklion, Crete, Greece, 25th -29th June 2007.

Sono nato in terra di camorra, nel luogo con più morti ammazzati d'Europa, nel territorio dove la ferocia è annodata agli affari, dove niente ha valore se non genera potere. Dove tutto ha il sapore di una battaglia finale. Sembrava impossibile avere un momento di pace, non vivere sempre all'interno di una guerra dove ogni gesto puo' divenire un cedimento, dove ogni necessità si trasformava in debolezza, dove tutto devi conquistarlo strappando la carne all'osso.
In terra di camorra combattere i clan non è lotta di classe, affermazione del diritto, riappropiazione della cittadinanza. Non è la presa di coscienza del proprio onore, la tutela del proprio orgoglio. E' qualcosa di più essenziale, di ferocemente carnale. In terra di camorra conoscere i meccanismi d'affermazione dei clan, le loro cineteche d'estrazione, i loro investimenti significa capire come funziona il proprio tempo in ogni misura e non soltanto nel perimetro geografico della propria terra. Porsi contro i clan diviene una guerra per la sopravvivenza, come se l'esistenza stessa, il cibo che mangi, le labbra che baci, la musica che ascolti, le pagine che leggi non riuscissero a concederti il senso della vita, ma solo quello della sopravvivenza. E così conoscere non è più traccia di impegno morale. Sapere, capire, diviene una necessità. L'unica possibile per considerarsi ancora uomini degni di respirare.

Roberto Saviano
Gomorra, 2006

Motivation

The central role of the zooplankton within the marine food chain is well known. The secondary production in the marine areas of the world is mostly due to *Calanoid Copepods* and *Euphausiids*, which provide the basis of the energy channelled onwards through the foodweb to the major stocks of directly zooplanktivorous fish, both at larval and adult life stages. In particular, the Euphausiacea order or “krill” is considered a keystone organism that form the basis of the foodweb in the Polar oceans and adjacent regions, being the principal food for whales, fish, squid, pinnipeds and birds.

Therefore, within the framework of an ecosystem approach to manage these important ocean areas, the development of tools and techniques for krill abundance and size distribution estimations are indispensable for understanding the biological processes and the renewable resources.

Scientific echosounders are considered a primary tool for these purposes, and the acoustic properties of krill at different frequencies are key issues in the adopted methodology. Krill produce weak but discernible echoes for a good range of frequencies, and the existing acoustic techniques are in general able to evaluate the distribution of the resources to be managed and to achieve a comprehensive knowledge of them.

However, for purposes that are more specific, such as identification and absolute abundance, the methods are not completely established and there is a strong need for their refinement. This is a focal point in terms of forecasting recruitment abundance fluctuations and the knowledge on the coupling between physical and biological processes. Because of the lack of information on the acoustic backscattering properties from different species, problems arise in the analysis of acoustic data from echosurveys. The acoustically detected swarms of zooplankton are often a mix of species and sizes, with addition of fish larvae, and the species classification is extremely complicated, if not sometimes impossible. In the case of mono-species environment also, the analysis of acoustic data suffers from the lack of accurate

knowledge of target strength and the well-known limitation derived from the associated zooplankton net sampling techniques.

Multifrequency acoustic systems represent a promising tool to overcome the mentioned problems. While general zooplankton acoustics is still in its infancy, following the progress of the acoustic technology and data analysis techniques, dual frequency echosounders and later multifrequency echosounders have been used to assess distribution and abundance of krill, especially for the Antarctic krill (*Euphausia superba*) in South Polar marine areas.

The classification is based on the variation in scattering strength levels between frequencies for various types of scatterers, hence, more accurate discriminations between krill and other species can be obtained. Then, with the help of associated net samples analysis, representative scattering models are applied to derive size distribution and abundance of krill solving the critical conversion of acoustical intensities to biologically relevant quantities.

However, target identification is still indicated as the principal component of uncertainty in acoustical surveys of krill. A rigorous procedure may be performed only if the scattering behaviour, as a function of size and frequency for individual krill species, is well known. Thus, the accurate prediction of krill target strength (TS) becomes the key point of the acoustic method. In few words: “the accuracy of the krill biomass estimation depends directly on the accuracy of the target-strength prediction”.

There are three main approaches to the target-strength estimation: 1) theoretical, by using numerical or empirical models; 2) *in situ*, by measuring acoustic detections of organisms in their natural habitat; 3) *ex situ*, by performing direct measurements on organisms in cages, tanks or enclosures. Due to the complexity of the problem, there is no doubt that the most reliable technique for acoustical assessing of euphasiids lies in combining the best aspects of both the theoretical and empirical approaches.

During the last two decades, large efforts have been undertaken to improve theoretical scattering models, but due the complexity of the scattering processes, exact scattering

models are extremely difficult to establish. Exact solutions can be achieved with analytical restrictions, but with a limited range of applicability, therefore approximate models, either numerical or empirical, are often preferred.

Despite the achieved level, the results still do not satisfy the required accuracy imposed by the capability to explain the ecological processes; investigators have shown that for a specific species the models accuracy depends on the precise knowledge of all the key input parameters. Thus, the verification by comparison with direct multifrequency measurements on target strength of individual or ensemble of krill is still imperative.

To measure directly the target strength of krill both *in situ* and ex *situ* is also problematic. The measurements might be of variable quality because of the difficulties to discriminate multispecies and multitarget scattering *in situ*, and due to significant constraints in animal behaviour when small tanks or enclosures are used in *ex situ* measurements. Very often, the quality of the results cannot always be compared to the engaged effort.

In the present thesis, the outlined problems of both theoretical and empirical approaches are investigated. The *Meganyctiphanes norvegica* (Sars, 1857), also called Northern krill, is used as target species, and the last generation EK60 of Simrad echosounders, already widely used by the scientific community, operating at the common frequencies utilized in fisheries acoustic applications were used.

There is an increasing interest for studying the *M. norvegica* species, both in terms of ecology of Northern marine areas and exploitation in aquaculture as new feed resource. This species is also acoustically relevant as it is assumed to be similar in shape and maturity stages to Antarctic krill.

These features suggest that the *M. norvegica* can be used as an acoustic species model for the krill in general. It is ideal in acoustic studies since generally more accessible to researchers, it has an overlapping length distribution, and its biological aspects related to the acoustical problems, such as diet, growth, biochemical composition and general behaviour, are fairly studied.

Summary

Although this thesis is a dissertation based on articles, an exhaustive overview on the main issues involved is also presented*. This is due to the necessity to summarize the numerous aspects of the problem, as well as the recent works on specific topics and the innovative elements presented in this work of thesis. In some of its parts, it may appear repetitive due to the treatment of the specific topic. The contents of the papers included in the thesis are referred when the related issue is treated.

With the intent to provide a useful guide to the reader, a large effort has also been undertaken to select and indicate specific bibliographic references.

The first chapter describes the background on the acoustic estimation method by using scientific echosounders for zooplankton in general. Then, the specific techniques adopted for identification of krill by using both theoretical and empirical approaches are introduced. The chapter starts with the description of the order Euphausiacea, focusing on its main biological characteristics related to the analysis of the acoustic data. An introduction on the Antarctic krill fishery in Southern Pole areas is also given

In Chapter 2, the theoretical approach on target strength of krill and the key parameters for the modelling are resumed. The krill orientation problem is discussed with reference to the main studies in estimating mean angle and standard deviation of a normal distribution of euphausiids orientation. Paragraph 2.3 explores the methods for the evaluation of the key model parameters being the background for the Papers I. The last Section 2.4 describes in details the distorted wave Born approximation model in its various forms. This is recognized as the state-of-the-art in the physics-based

* Apart from the language and the page margins, there are no restricted guidelines to submit the summary in a PhD dissertation at University of Bergen. The writer may choose the figures, tables, and mathematics formats. For the common fishery acoustics words, it has been chosen to follow the ICES Journal of Marine Science word list guidelines. For references format, it has been chosen not use the typical series/Oxford comma.

models predicting target strength of fluid-like crustacean zooplankton, and deserved a detailed desciption, being also an object of Paper V.

Chapter 3 represents a central point of the entire thesis. *Ex situ* direct acoustic measurements on Northern krill *Meganyctiphanes norvegica* in a novel set-up consisting in a wide mesocosm venue are described. The practical problems and their consequences from this experience are described as a complement to Paper II. The potential of the mesocosm set-up in identifying the targets is discussed, and some specific experiments are described in detail. Papers IV and V represent part of the conclusions obtained from this experience.

As a consequence of the mesocosm practice, the need to evaluate the correctness of the short-range performances of the Simrad EK60 scientific echosounder was addressed. This was done in a controlled way in a tank at Simrad AS in Horten (Norway) and is the subject of Paper III. Chapter 4 justifies the need and presents complementary results to the Paper III.

In Chapter 5, a brief overview describing the general issues for a multifrequency echosurvey for krill estimation is presented. Complexity in suggesting a proper procedure for multifrequency echosurvey in the case of *Meganyctiphanes norvegica* aggregations is emphasized, reflecting Paper VI.

Finally, the historical evolution of the scattering models for fluid-like organisms such as euphausiids is presented in Appendix. This is not directly related to the included papers, and some of its sections may appear too detailed. However, the topic is fundamental for the acoustic method for krill biomass estimation, and the presentation in an appendix was somewhat obligatory. The description is organized as a guide for the interested reader with formulations presented in an easy form for numerical implementation. Some of the models are described in more details; this is based on the opinion of the writer on their importance in general applications.

1. Biomass estimation of krill by scientific echosounders

1.1 Order Euphausiacea or krill: general information

Krill is a general term used to describe about 85 species of open-ocean crustaceans belonging to the order Euphausiacea and known as euphausiids (Mauchline and Fisher, 1969):

Kingdom:	Animalia
Phylum:	Arthropoda
Subphylum:	Crustacea
Class:	Malacostraca
Superorder:	Eucarida
Order:	Euphausiacea

The name “krill” is derived from an ancient Norwegian word that once was applied to larval fish and other tiny marine creatures. It means “young fry of fish” and comes from the Dutch word *kriel* meaning “small fry” (Lloyd and Mitchinson, 2006), now also used to mean both pygmies and small potatoes.

Anatomy

All species of euphausiids have a recognizably crustacean shape (Fig. 1.1). They have a hard chitinous exoskeleton, many legs (used for swimming and gathering food), and a segmented body. This consists of an elongated head-trunk region (cephalothorax) and a muscular segmented tail (abdomen) to which are attached five pairs of paddle-like swimming legs. The head region houses up to thirteen pairs of modified limbs that gather food, manipulate, grind and ingest it. Six of the pairs of thoracic limbs form a specialized “food basket”, with the fine bristles that project from them forming a net-like structure. The adult krill range in size from under 1 cm up to 14 cm long and are considered macro-zooplankton, i.e. the component of the zooplankton that consists of large organisms from 2 to 20 cm in size.

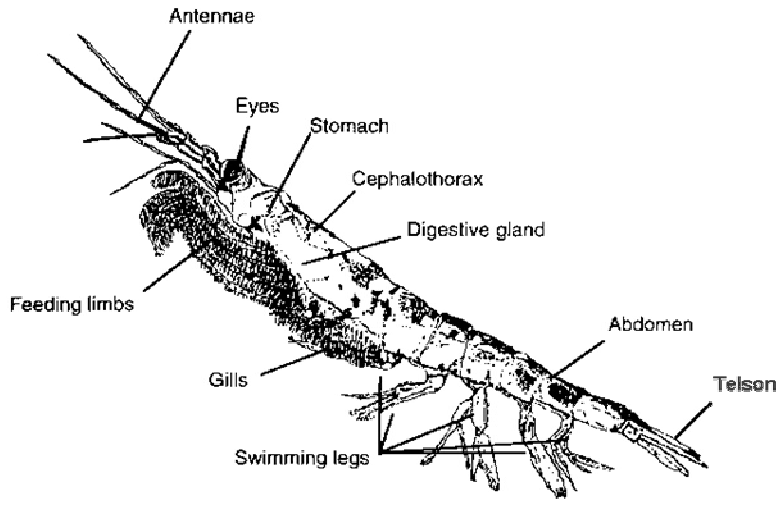

Figure 1.1: *Main anatomical parts of krill.*

Geographic distribution

Krill occur worldwide in all oceans. Most species have transoceanic distribution and several species have endemic or neritic restricted distribution.

Species of the genus *Thysanoessa* occur in both the Atlantic and the Pacific Ocean, which is also home to *Euphausia pacifica* (Hansen, 1911). The *Meganyctiphanes norvegica* (Sars, 1857), also known as "Northern krill", occurs across the Atlantic, from the north to the Mediterranean Sea. The four species of the genus *Nyctiphanes* are highly abundant along the upwelling regions of the California, Humbolt, Benguela, and Canarias Current Systems, where occur most of the largest fisheries activities of fish, molluscs and crustaceans.

In Southern Ocean, euphausiids have a circumpolar distribution and are broadly separated by their latitudinal ranges (Everson, 2000). Seven species are known, one of the genus *Thysanoessa*, the *T. macrura* (Sars, 1885), and six of the genus *Euphausia*: the *E. superba* (Dana, 1852) commonly called "Antarctic krill"; the *E. crystallorophia* (Holt and Tattersall, 1906), also called "ice krill" and dominating south of 74° S and in regions of pack ice (Hosie *et al.*, 2003); *E. frigida* (Hansen, 1911); *E. longirostris* (Hansen, 1908); *E. triacantha* (Holt and Tattersall, 1906); and *E. vallentini* (Stebbing, 1900).

The *Euphausia superba* deserves a particular mention. It is the dominant krill species in the southern polar oceans and has been the subject of many experimental and theoretical acoustic studies. It forms mostly mono-specific aggregations (Miller and Hampton, 1989a), sometime with substantial variability in the length of member animals between closely spaced aggregations (Watkins, 1986). It can be up to 6 cm long and weighs about 1 g, with the life spanning of about 5 to 10 years. Most of the larger Antarctic animals, such as seals, whales and seabirds as well as fish and squid, depend directly or indirectly on Antarctic krill (Everson, 2000). For this reason, the Convention for the Conservation of Marine Living Resources (CCAMLR) denotes the ecosystem of the Southern Ocean as a *krill-centric ecosystem*. Miller and Hampton (1989a) estimates an annual consume of 250 million tons of Antarctic krill by these organisms.

New developments within the aquaculture industry and its increased need of fish feed, and improvements in the catching and processing techniques are fuelling a renewed interest from the fishing industry in exploiting large quantities of Antarctic krill. Since the 1960s, attention has been turned to Antarctic krill, mainly because of its huge geographic extent (around 35 million square kilometres) and colossal abundance.

For an extensive overview of the history, development, ecosystem implications and management of the Antarctic krill fisheries, the following papers: Nicol and de la Mar (1993), Nicol and Endo (1999), Ichii (2000), Nicol and Foster (2003), are suggested.

Antarctic krill are caught by large freezer trawlers, and processed on board into products for aquaculture and aquarium feeds, as bait in sport fishing, or in the pharmaceutical industry. The total global production amounts annually to 100–200,000 tonnes, with more than 90% from the western Atlantic Ocean sector of the Southern Ocean: the Scotia Sea (Kock, 2000).

The Norwegian fishing industry might become a major player in the new generation of krill fishers, by deploying large, modern, highly efficient factory vessels to the remote waters of the Southern Ocean. The new technology involves pumping the krill

constantly from the trawl avoiding the rapid deterioration of the krill, one of the main factors that have limited the catching capacity of krill trawlers until few years ago. As a result, the catching and processing capacity of krill harvesting fleets might expand dramatically in the short-term view. This could stimulate a rapid growth of Antarctic krill fishery with irreversible impacts on krill-dependent species in the Southern Ocean, unless appropriate precautionary management procedures are developed early enough.

The first steps towards management of the krill fishery came in 1991 at the tenth meeting of the Commission for the Conservation of Antarctic Marine Living Resources (CCAMLR), i.e. the body sets up to oversee the implementation of the Convention. The CCAMLR came into force on the 7th of April 1982 as part of the Antarctic Treaty System and was the first international fisheries arrangement to incorporate the ecosystem and precautionary approaches as basic principles. The Commission set the limits on the krill fishery in most of the areas where the Antarctic krill is caught (Figure 1.2). It takes management advices from the Scientific Committee, which in turn is assisted by several working groups. The Working Group on Ecosystem Monitoring and Management (WG-EMM) takes on all relevant technical work in relation to the krill fishery, and is in charge of assessing relevant data in relation to the *krill-centric ecosystem*.

In support of CCAMLR, several national programs have employed the use of acoustic methods to assess the distribution and abundance of Antarctic krill. Since 1981, acoustic surveys are performing almost regularly in important South Pole regions, e.g. Elephant Island area (Hewitt and Demer, 2000), and numerous scientific papers can be found in literature on this topic. They will be referred when relevant for the specific issue.

Growth and reproduction

Krill may live for six to seven years attaining the sexual maturity at two for the female and three for the males (Siegel, 2000). Like all crustaceans, they grow by *moulting*; that is, they cast off the old exoskeleton and expand in size while the new

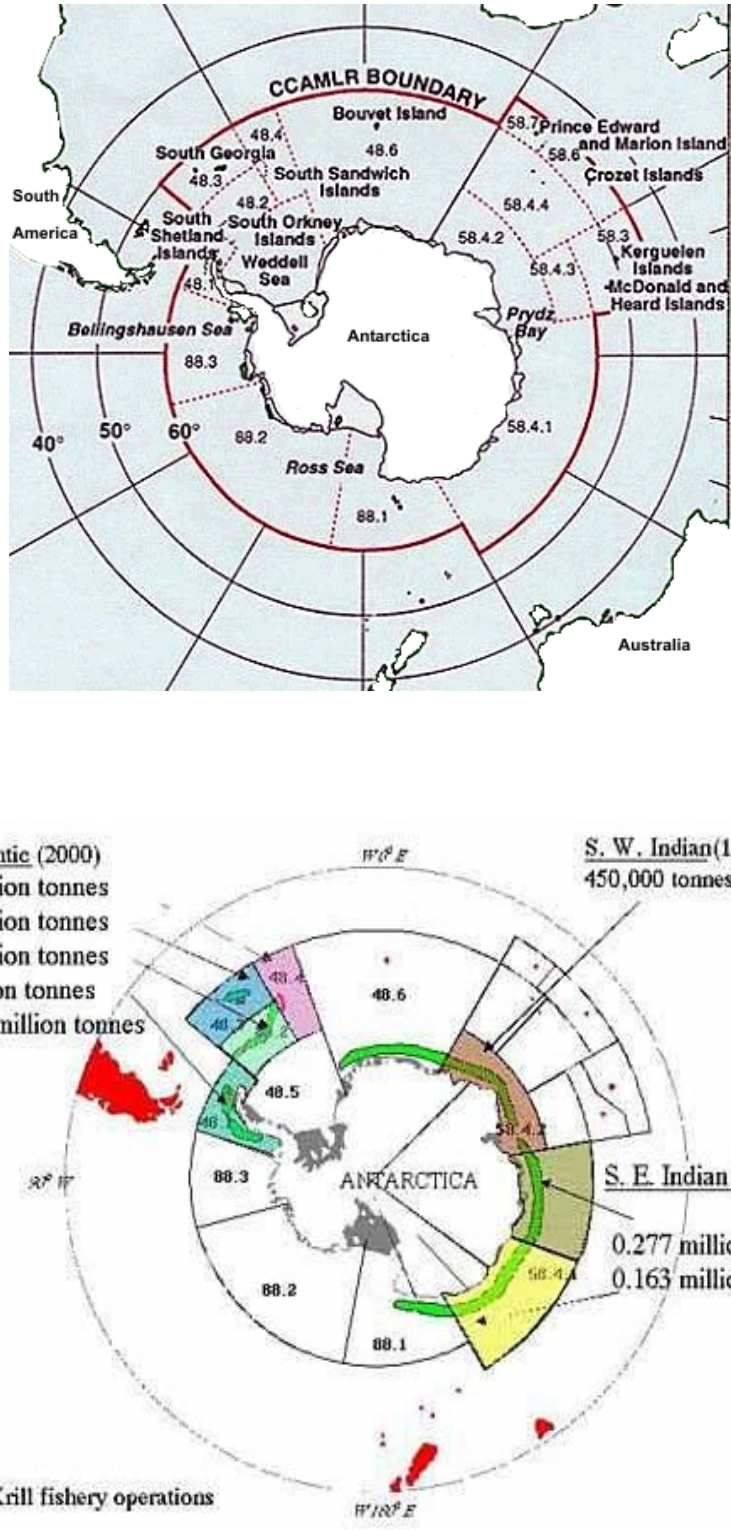

Figure 1.2: *Krill management in Southern Pole area*. *Map of the CCAMLR statistical areas, sub-areas and divisions used for the reporting of krill catch data* (*upper panel*), *and precautionary catch limits in the year 2000 for some of them* (*lower panel*). (CCAMLR 2005: Statistical Bulletin, Vol. 17, electronic version).

one is still soft. This process can be divided in several stages and substages. The duration of the molt cycle is temperature-dependent (Nicol and Stolp, 1990; Cuzin-Roudy and Buchholz, 1999), and they continue to moult regularly even if starved. The cycle highly influences the krill behaviour. Tarling *et al*. (1999) found that the post-moulted *Meganyctiphanes norvegica* specimens do not undertake the diel migration; Thomasson *et al*. (2003) claimed that they have a reduction in swimming capacity. When disturbed, some individuals have been observed to molt instantaneously, leaving the exuvia behind as a decoy. What seems to be unique in krill is the ability to use this process in reverse (in other words, to shrink) when food is absent.

Crustacean age is usually measured by size, but if krill are growing and shrinking in response to a fluctuating food supply, it is unlikely there will be any simple relationship between size and age (Nicol, 1991). This is a problem for fisheries management since the estimates of production are based on assumption of animal lifetime and the natural levels of mortality. Shin and Nicol (2002) suggested the measure of the relationship between eye diameter, which does not seem to change significantly during the two processes, and the body length as indicator of the effect of the long-term starvation.

In summer, krill females may lay up to 10000 eggs at a time, sometimes several times a season, into the surface waters. The eggs are thought to sink to very deep water before hatching (George and Strömberg, 1985). They then begin their long (up to ten days) `developmental ascent', during which the newly hatched larvae journey up towards the sunlit waters to feed. Once krill have surmounted their first hurdle and have reached the surface waters, they begin to grow and change, becoming more likes the adults as time progresses.

Diet

Krill are mainly herbivorous feeding on phytoplankton, which they capture using a dense comb of hair along their legs. Planktonic organisms may also form a part of their diet, especially for the northern oceans species (Saether *et al.*, 1986). It is

believed that krill can survive without eating up to 200 days, shrinking during this time. During feeding, the limbs on the head region are thrown down and outwards enclosing a parcel of water. The water is squeezed out through small flap valves in the `basket' leaving particles trapped on the inside from where they are passed to the mouth. As for all the organisms, substantial composition of the diet components can be different in season and place, depending on the food supply related to the local physical and biological factors. This may give different and significant contribution to the acoustic scattering, hence *in situ* acoustical results. Moreover, the stomach content may vary during the day. Baliño and Aknes (1993) found that the percentage of full stomachs of the *Meganyctiphanes norvegica* in the fjords along the western coast of Norway in January increased from sunset to midnight while it was almost null late in the night.

Behaviour

Although the term “plankton” (from old Greek "planktos") means “wanderer” or “drifter”, and is related to any organism moving under external influence rather than self-generated actions, krill are exceptionally strong and capable to swim. Most of the species have to be consider as nektonic rather than planktonic (Hamner and Hamner, 2000), and their behavioural ecology must be investigated with same methodologies used for study the behaviour of fish schooling.

Their swimming activity is on local scale in both vertical migration and horizontal dimension. Thus, krill are spatially and temporally dynamic species, often behaving as swarming animals[*]. Zhou and Dorland (2004) found that euphausiids aggregate

[*] Hamner and Hamner (2000) have strongly emphasized the incorrect use of the terms “swarmers” and “swarms” attributed to euphausiids aggregations in literature. The term swarm is formally assigned to a congregation of animals that generally do not exhibit polarization of individuals, travelling in different direction and showing not uniform distances with the nearest neighbour. On the contrary, numerous studies (c.f. Hamner and Hamner 2000) state that all the individuals within a krill aggregation are usually polarized, regularly spaced and swimming in the same direction, i.e. school. However, the term swarm is correct when speaking on general aggregations of krill since not always they exhibit the schooling behaviour features. With these meanings, the terms “swarm” and “school” will be kept in this thesis.

more densely in presence of predators, so that swarming, which is formed mainly to reduce energy expense in locomotion, it is also a defensive mechanism intended to confuse predators targeting for single individuals within of a multitude of prey.

Krill may form extremely patchy spatial distributions with a large fraction of their total population biomass aggregated in small fractions of the available habitat (e.g. Watkins and Murray, 1998; Kaartvedt *et al*., 2005). Kils and Marshal (1995) have reported schools of up to 10000-30000 individuals per cubic meter of *Euphausia superba*. Hamner and Hamner (2000) have listed density values for six species of euphausiids found in literature and reported even higher numbers (up to 64000 individuals m^{-3} for *Euphausia superba*), with some case up to 480000 individuals in one cubic metre.

Recent ecological studies have shifted the prevailing viewpoint on the patches. It was assumed as the product of large-scale physical processes only, and the zooplankton as passive members of them. The patchiness is currently considered as originated by a complex iteration between physical processes, population dynamics, food availability, predation, and general behaviour (Folt and Burns, 1999).

Krill have also been observed in various types of aggregations (Greene *et al*., 1988; Watkins and Murray, 1998), and as dispersed scatterers in mixed acoustic recordings (Miller and Hampton, 1989; Madureira *et al*., 1993; Kaartvedt *et al*., 1996; Brierley *et al*., 1998b).

The shape and density of a euphausiid aggregation and activities of individuals may be specific under a given physical and biological environment; thus, depending on the species and the region, there is great variability. In addition, the spatial distributions are influenced by several factor, such as tidal motions, currents, light levels, interspecific competition with other zooplankton (primarily amphipods), and predators.

It is still uncertain to what degree krill populations drift with the currents or whether they are able to maintain self-sustaining populations in particular areas. However, it seems that their larger movements are subject to the currents of the ocean. In addition,

one of the major question marks hanging over their life history is what they do over winter.

Another common and important feature of the euphausiids is the diurnal vertical migration. This topic has been the subject of numerous observations and experiments. Russell (1927) and Cushing (1951) have summarized the earliest and most valuable in their extensive reviews, and more confident results using hydroacoustical observations have been presented after that the methodology was refined (e.g. Everson, 1982; Simard *et al*., 1986; Godlewska and Klusek, 1987). The vertical migration causes aggregations of euphausiids to form and dissipate on a daily basis. The krill ascend to feed on phytoplankton and smaller zooplankton near the surface during darkness, and descend to twilight depths during daylight hours to avoid visual detection by predators (Mauchline, 1980a). Miller and Hampton (1989a) estimated that approximately 40 % of the krill biomass could be present in the upper 5 m during nighttime under certain circumstances. Some species also form surface swarms during the day (Mauchline, 1980a; Nicol and O'Dor, 1985; O'Brien, 1988) for feeding and reproductive purposes, even though such behaviour may be dangerous because the possibilities to escape from predators are limited.

Jaffe *et al*. (1999) and Zhou and Dorlan (2004) found that there is activity reduction with depth, apparently to reduce encounters with predators and to conserve energy by decreasing the metabolic cost and converting food into energy and growth more efficiently. However, krill swim constantly to avoid sinking (Kils, 1981). They normally swim at pace few centimetres per second or 0.2 – 10 body lengths per second (Ignatyev, 1999), using their swimmerets for propulsion. These swimming performances have led many researchers to classify adult krill as micro-nektonic life forms, i.e. small animals capable of individual motion against (weak) currents, while larval forms of krill are generally considered zooplankton.

When in danger, an individual krill shows an escape reaction called *lobstering*: flipping their caudal appendages, i.e. the telson and uropods. They move backwards through the water relatively quickly (Nicol and O'Dor, 1985; O'Brien, 1987),

achieving higher speed in the range of 20 body lengths per second (Ignatyev, 1999). Kils (1981) measure higher tails speed for large *E. superba* means close to 0.6 $m s^{-1}$.

Orientation aspect with respect to the horizontal is a critical parameter for the acoustical backscattering strength predictions of a single organism and it is discussed more in the details in Paragraph 2.1. It is highly variable since it can change when krill hover while feeding, migrate up, down or horizontally, swim against a current, flee from predator, and probably when they avoid the vessel or bodies containing acoustic platform.

1.2 Zooplankton assessments by scientific echosounder

Estimation of zooplankton abundances were routinely obtained by counting sub-samples of specimens caught with towed and vertical nets, bottles and pumps (e.g. Wiebe *et al.*, 1982; Miller and Judkins, 1981; Powlik *et al.*, 1991; Watkins and Macaulay, 2000; Stehle *et al.*, 2007). However, the numerical density of zooplankton is often highly and heterogeneously distributed in space, both in the vertical and horizontal directions (patchiness). Hence, in order to obtain a representative picture of the true distribution of zooplankton, sampling has to be carried out both in time and space in a very intensive basis. This process can be tedious and time consuming. Although it may provide detailed descriptions of species and developmental stages, the sampling methods suffer of many well-known problems. Avoidance and clogging at nets (the net sampling skews biomass estimates in favour of those species that are poor avoiders) (Wiebe *et al.*, 1982; Watkins and Macaulay, 2000), and problems associated with the nature of sequential samples (nets are not able to fully resolve spatial variability), are the most significant. Moreover, the results are not generally available for several months after the original collection.

Therefore, there is a strong need for rapid methods of measuring attributes of the zooplankton community that at the same time provides an acceptably high level of reliability. Since zooplankton produce weak but discernible echoes of transmitted

sound regulated by the same laws as any other object, remote acoustic sampling is a desirable goal for making rapid biomass and size distribution estimates with sufficiently high sampling rate to avoid under-estimation of the zooplankton abundance.

The scattering properties of zooplankton depend on their size, shape, behaviour (i.e. orientation), acoustic material properties and frequency or wavelength. Taking into account these parameters, acoustic tools and appropriate procedures have been used for krill abundance estimation since some decades. In particular, the Acoustic Doppler Current Profilers are promising tools (e.g. Flagg and Smith, 1989; Heywood *et al.*, 1991; Cochrane *et al.*, 1994; Roe *et al.*, 1996; Luo *et al.*, 2000; Zhou and Dorland, 2004; Saunders *et al.*, 2007), but the effort to make the necessary corrections is far from trivial (MacLennan and Holliday, 1996).

Scientific echosounders are the most suitable systems for the purpose. On the base of the specific requirement, these systems may be used in different platform configurations: hull mounted, tow body installations and fixed moored. The acoustic method associated to the echosounder systems has several advantages compared to biological sampling methods but also some limitations; Table 1.I resumes both.

The methodology involved in acoustic zooplankton estimation has its root in fisheries acoustics (McLennan, 1990; Foote and Stanton, 2000), but with some differences. Echo integration and echo counting are the common methods for biomass assessment in oceans, lakes and rivers (Simmonds and MacLennan, 2005). In contrast to fish, zooplankton aggregations are usually consisting of high varieties of species and size, varying in space and time with differentiated acoustic properties. This means that echo counting and target-strength regression methods to identify species are difficult to apply in the same way as for fish (Stanton *et al.*, 1994b; MacLennan and Holliday, 1996). For these reason, although some validating study on echo counting (De Robertis, 2001), the echo integration is the qualified technique for acoustic estimation of the zooplankton biomass.

Table 1.I. Advantages and limitations of the acoustic method for the assessment of zooplankton by using scientific echosounders.

Advantages	Limitations
1. Cost effective (low field man-hours)	1. High initial capital investment
2. Non-invasive, rarely affects organisms behaviour	2. Partial lack of species identification
3. Non-selective, minimizes sampling bias toward size or behaviour	3. Difficulty to obtain information near surface and near bottom boundaries
4. Established theory and methods (at least for fish)	4. Possible impact on some marine mammals and fish
5. High resolutions synoptic observation	5. Relatively complex to use, requiring training and experience
6. Almost real time results	
7. Sampling large volume of water in reduced time	
8. High ability to resolve spatial variability	
9. Collection of large quantity of data for statistical comparison	
10. Minimizing animal avoidance due to visual (?) or vibrational cues	
11. Data can be processed, examined, and stored with replication	
12. Two-dimensional pictures (echograms) and relatively high resolution image is practicable	

It is based on the *linearity principle* (Foote, 1983) applied to quantitative measurements of volume scattering strength. The principle states that the total scattered intensity I_{tot} from a volume containing a random distribution of N scatterers is on average equal to the sum of the scattered intensities from each individual, or more precisely:

$$\lim_{N\to\infty} \frac{I_{tot}}{\sum_{i=1}^{N} I_i} = 1 \qquad (1.1)$$

This means that the phases of the echoes received at the transducer are supposed to be incoherent. The strength of the volume scattering produced by a population of zooplankters is a function of their spatial density and size distribution, as well of the operative frequency. In absolute terms, the acoustical intensity of the received signal is expressed through the *volume scattering coefficient* s_V defined as the sum of the differential acoustical backscattering cross sections (Par. 2.2.1) of all the discrete scatteres within the volume (MacLennan *et al.*, 2002):

$$s_V = \frac{\sum_{i=1}^{n} (\sigma_{bs})_i}{V} \qquad (\mathrm{m}^{-1}) \qquad (1.2)$$

where n is the number of scatterers. The equivalent logarithmic quantity of the Equation (1.2) is the volume backscattering strength $S_V = 10 \log(s_V)$ with units [dB re 1 m^{-1}] *.

If $\langle \sigma_{bs} \rangle$ is the characteristic backscattering cross section of the observed scatterers and ρ_V their numerical density expressed in units of numbers of animals per cubic meter, it is possible to write (Foote and Stanton, 2000):

$$s_V = \rho_V \langle \sigma_{bs} \rangle \qquad (\mathrm{m}^{-1}), \qquad (1.3)$$

which is the equation of the echo integration in terms of volume. The notation $\langle \sigma_{bs} \rangle$ is used in this context to indicate that it is an expected value rather than a mean. It is determined indirectly from the size distribution of net samples and the related length-dependent prediction from a model or an empirical equation.

In practice, scientific echosounders are generally designed to measure s_V. The actual output of a single signal from the principal instruments used in fisheries acoustic is the integral over the range interval $[r_1, r_2]$ of s_V, which is dimensionless and called *area backscattering coefficient* s_a (MacLennan *et al.*, 2002):

* This is also defined as the ratio in decibel between the scattered intensity from a unit volume containing scatterers measured at 1 m from the volume and the intensity incident on the volume.

$$s_a = \int_{r_1}^{r_2} s_V(r)\, \mathrm{d}r \qquad (\mathrm{m}^2\ \mathrm{m}^{-2}). \qquad (1.4)$$

In survey data processing, this relationship is averaged over the specific interval of sailed distance. For large-scale applications, this scaling factor is classically related to 1 nautical mile to define the *nautical area scattering coefficient* (NASC):

$$s_A = 4\pi(1852)^2 s_a \qquad (\mathrm{m}^2\ \mathrm{nmi}^{-2}). \qquad (1.5)$$

Hence, the "working" echo integration equation is expressed in terms of area density ρ_A in units of numbers of animals per square nautical mile:

$$\rho_A = \frac{s_A}{4\pi\ \sigma_{bs}} \qquad (\mathrm{nmi}^{-2}). \qquad (1.6)$$

In some zooplanktonic investigations, it is preferred to use a sailed interval less than 1 nmi; nevertheless, the transformation from density to absolute numbers of zooplanktonic organisms is still unambiguous.

It is evident that the acoustic method provides only measurements of scattered sound, which is a complex function of several parameters (size, shape, physical properties, and behaviour of the scatterers, as well as operative frequency). Therefore, the identification of the particular animals that are the principal source of scattering, and the conversion from acoustic measurements to biologically relevant quantities, such as biomass or animal length, are challenging tasks. Equation (1.3) or the related (1.6) can be used in different ways to convert the acoustic data in absolute biological results (Greenlaw, 1979). Two distinct approaches for the acoustical-biological data conversion are commonly used: the most applied *forward problem*, and the *inverse problem* (Greenlaw and Johnson, 1983).

The solution of the forward problem involves predicting the properties of the acoustic return from a scatterer being known its physical and geometric properties, and the operating system parameters. Due to the variability of the scatterers in ocean, it is reasonable to expect that the calculation is not completely accurate, but through the

procedure, it is possible to have a diagnostic process able to explain the reasons and the causes of the errors.

The inverse problem is concerned with predicting the properties of the scatterer based upon the knowledge of the acoustic return from that object. The processing could be complex, often resulting in non-realistic but mathematically valid solutions. However, in order to attempt to solve the inversion problem, the forward problem must be well posed.

In any case, it is clear that the primary requirements for acoustic estimation methods are a reliable identification of the species of interest and the separation of their backscattering from other sources. Accurate acoustic scattering models may be employed for this purpose. By the relationship of target strength (TS) with the organism size, the acoustic data from an operative frequency can be transformed into biologically relevant data converting the integrated echo energy to absolute numbers of zooplanktonic organisms (Eq. 1.3). This fundamental step relies on the importance of the accurate knowledge of the TS from the target species, as well as the work of this thesis for the euphausiid *Meganyctiphanes norvegica* or for krill in general.

1.2.1 Methods of krill assessment

Since zooplankton is observed in various types of aggregations, verification of scatterers by acoustics only is extremely difficult, and the interpretation of the acoustic data is never straightforward. Therefore, a zooplankton acoustic survey is typically accomplished with target identification net hauls to provide information on sizes and species composition of the schools. However, as mentioned before, net hauls are time consuming and have spatial problem connected, which involves the resolution of questions on zooplankton ecology; thus, improvement of acoustic methods to prevent potential biases from these uncertainties is strongly warranted. In particular, uncertainty in the identification is actually recognized as the largest bias in using acoustic techniques to estimate krill density (Miller and Hampton, 1989a; Foote *et al*., 1990; Everson *et al*., 1990; Demer, 2000).

An individual krill is a weak but discernible scatterer, especially at higher frequencies commonly used in acoustic fishery researches, with stronger scattering levels related to larger sizes. In the last decades, significant progresses in estimation and classification methodology by using scientific echosounders have been achieved. Initially, the investigators have used the *single frequency method* (Pieper, 1979; Cram *et al*., 1979; Sameoto, 1980; Mathisen and Macaulay, 1983; Macaulay *et al*., 1984; Shirakihara *et al*., 1986; Greene *et al*., 1989; Wiebe *et al*., 1996; Greene *et al*., 1998a; Brierley *et al*., 1999)**,** and still using also in recent papers (e.g. Hewitt and Demer, 2000; Kirsch *et al*., 2000; Swierzowski *et al*., 2000; Romaine *et al*., 2002), to describe patterns as swarms or layers of krill in some specific region, or employing volume backscattering technique to study the distribution patterns of Antarctic krill (Everson, 1982; Guzman and Marin, 1983; Richter, 1985b; Everson and Murphy, 1987; Daly and Macaulay, 1988; Miller and Hampton, 1989b; Lawson *et al*., 2004).

The hypothesis on the base of the method is that a single size class of zooplankton is dominant, and the main size is known (Greenlaw, 1979). Nevertheless, single-frequency echosounders cannot generally distinguish between mixtures of different zooplankton sizes or species (Greene *et al*., 1989; Wiebe *et al*., 1990; Holliday and Pieper, 1995) or between zooplankton and collocated turbulent microstructures scattering (Stanton *et al*., 1994a; Trevorrow, 1998). Since the relationship between target strength, size and frequency has a non-monotonic form and varies with shape and aspect angle, Holliday and Pieper (1995) wrote: "*there is no way to distinguish uniquely a change in size or a change in abundance when using a single acoustic frequency*".

Multifrequency acoustic methods have been proposed to overcome this ambiguity. Since the acoustic properties of individual species are known to vary with the operating frequencies (Chu *et al*., 1992), the variation in scattering strength levels between frequencies can be used for identification purposes and discriminate between species. This frequency-dependent identification technique entails to calculate the difference between mean volume-backscattering strength (ΔMVBS or ΔS_V) retrieved at the operating frequencies to identify portions of the echograms representing krill

(Madueira *et al*., 1993; Everson *et al*., 1993; Watkins and Brierley, 2002; Hewitt *et al*., 2003). As Holliday and Pieper (1995) pointed out, in order to render the ΔMVBS technique optimally effective, the frequencies should span the transition from Rayleigh to geometric scattering for all the organisms present in the survey area rather than just those of interest.

Researchers have mostly used the ΔMVBS technique involving the two common frequencies 38 and 120 kHz, the so-called *dual-frequency method*, to improve the accuracy in discriminating and delineating the results between zooplankton species (e.g. Greenlaw, 1979; Madureira *et al*., 1993; Everson *et al*., 1993; Brierley and Watkins, 1996; Mitson *et al*., 1996; Brierley *et al*., 1997, 1998b; Miyashita and Aoki, 1999; Demer, 2000; Everson *et al*., 2007), or distinguish fish from zooplankton (e.g. Cochrane *et al*., 1991; Madureira *et al*., 1993; Demer, 1994; Brierley and Watkins, 1996; Miyashita *et al*., 1997; Simard and Lavoie, 1999; Cochrane *et al*., 2000; Kang *et al*., 2002; Miyashita *et al*., 2004; Onsrud *et al*., 2004; McKelvey and Wilson, 2006; Lawson *et al*., 2008a).

However, the dual method cannot distinguish between animals of very similar sizes and scattering type, and so cannot discriminate among the different species of euphausiid that may be present. Following the progress on the acoustic technology developments, such as systems with more than two frequencies or broadband systems, and using different approaches in the analyses, researchers have delineate more powerful techniques for species identification and abundance estimation. Particular analysis procedures were developed to solve the forward problem (e.g. Cochrane *et al*., 1991; Brierley *et al*., 1998b; Swartzman *et al*., 1999; Cochrane *et al*., 2000; Korneliussen and Ona, 2002, 2003; Hewitt *et al*., 2003; Mair *et al*., 2005; Lawson *et al*., 2006), to improve inversion techniques (Greenlaw and Johnson, 1983; Holliday *et al*., 1989; Napp *et al*., 1993; Martin *et al*., 1996; Mair *et al*., 2005; Lawson *et al*., 2008a), to discriminate between biological and physical sources of scattering under some conditions (Warren *et al*., 2003; Lawson *et al*., 2008b), also applying the neural network technique (Woodd-Walker *et al*., 2003), and deriving more precise long-term

seasonal and inter-annual krill fluctuations by the accumulation of data in a wide area (Cochrane *et al*., 2000, Lawson *et al*., 2008b).

Moreover, multifrequency acoustic systems have been used to describe euphausiids features and aspects that would be difficult or impossible to investigate with direct sampling techniques. Significant examples are the studies on: krill predator performances (Hewitt and Demer, 1993; Veit *et al*., 1993), krill behaviour as prey (Greene *et al*., 1988; Cochrane *et al*., 1991; Simard and Lavoie, 1999; Cochrane *et al*., 2000; Simard *et al*., 2003; Onsrud *et al*., 2004; Nicol *et al*., 2008), general krill behaviour and the study of time-space offsets comparing net sample, pumps and acoustics results (e.g. Costello *et al*, 1989; Daly and Macaulay, 1988; Iida *et al*., 1996; Wiebe *et al*., 1996; Greene *et al*., 1998b; Iida *et al*., 1999; Duportets *et al*., 1998; Cochrane *et al*., 2000; Watkins and Brierley, 2002; Kasatkina *et al*., 2004; Trevorrow *et al*., 2005; Everson *et al*., 2007; Lawson *et al*., 2004; 2008a).

Although krill are usually the dominating scatterers in the areas of investigation, and their aggregations have distinctive features, analysis and quantification of the error associated with various approaches are still difficult. The echo integration method assumes that the total backscattered energy is the sum of echoes from individual scatterers, but krill is often present in high-density schools with related complications due to multiple reflections of the returning echoes, absorption of sound within the aggregation, and shadowing of one portion of the aggregation by another. Authors have also shown how the diel variation in scattering is related to the krill vertical migration (e.g. Everson, 1982; Greene *et al*., 1988; Shirakihara *et al*., 1986; Demer and Hewitt, 1995; Onsrud *et al*., 2004; Lawson *et al*., 2004; Everson *et al*., 2007), and how the season variations in volume scattering strength from krill is associated with the physical features (McGehee *et al*., 2000; Pieper *et al*., 2001; Lawson *et al*., 2004, 2008b). Improvements of the technique have been achieved with the increase of experience, leading to recognize the sources of the variation in scattering levels. Results comparison with other devices could be useful in this context (Sameoto *et al*., 1993; Herman *et al*., 1993; Benfield *et al*., 1998; De Robertis, 2001; Lawson *et al*., 2006, 2008a), as well the study of the theoretical aspects on interference and sound

extinction in densely aggregated zooplankton (Gorska and Klusek, 1998; Chu and Ye, 1999; Gorska, 2000; Gorska and Chu, 2001, 2005).

The dual-frequency method at 38 and 120 kHz, adopted as standard method by CCAMLR in Southern Pole, is substantially effective (Demer, 2000, 2004), but still under improvement. Conti and Demer (2006) have revisited the current practice of using the fixed $\Delta S_V = S_{V,\,120\,\mathrm{kHz}} - S_{V,\,38\,\mathrm{kHz}}$ in the range from 2-4 to 12-16 dB (Hewitt *et al*., 2002; Watkins and Brierly, 2002; Demer, 2004) by proposing a size-adaptive algorithm upon on a *variable*-ΔS_V technique. This takes in account the local seasonal variations in volume backscattering, which are very important especially in periods of lower reproductive success when the acoustic estimates by using the fixed ΔS_V algorithm show increased biomass compared the net-derived biomass (Hewitt *et al*., 2003). The survey area is subdivided in geographic regions (multiple post-stratified areas) according to the length distribution of krill, and the ΔS_V numbers tuned on the base of the theoretical model prediction related to the length distribution of each region. To designate the expected minimum and maximum ΔS_V for *Euphausia superba* estimations in Scotia Sea and South Shetland Islands, Conti and Demer (2006) and Reiss *et al*. (2008) used the parameterized stochastic distorted wave Born approximation model (Par. 2.4) and found significant correlation with both proportional recruitment and krill abundance estimated from zooplankton samples.

Recently, Lawson *et al*. (2008a) have also used a different approach evaluating the threshold level of volume backscattering strength to distinguish euphausiid aggregation from other zooplankton in a multifrequency context. The level was derived on the bases of measurements of euphausiid visual acuity and estimates of the minimum density of the animals over which an individual can maintain visual contact with its nearest neighbour, and thereby with the aggregation as whole. By the results of mean volume back scattering strength on identified aggregation at four frequencies, an inversion method was then developed to estimate simultaneously the mean length and density of euphausiids.

2. Acoustic target strength of krill

Acoustical estimates of zooplankton abundance can be made rigorously if the scattering behaviour as a function of size and frequency for the individual zooplankter is known. Although the individual zooplankton organisms are small and their echoes weak, they are discernible scatterers of sound. The zooplankton gross anatomical features can vary widely across species, and sometimes even within species, resulting in great variation in scattering properties. This means that different types of zooplankton do not contribute equally to the backscattered signal measured during acoustic surveying. Therefore, acoustical characterization of the animals species by species is extremely difficult but in some case possible. Stanton *et al*. (1994a) identified the common types of zooplankton grouped by the gross anatomical similarity and boundary conditions (Fig. 2.1), and modelled them analytically by different theoretical scattering models due to the different boundary conditions:

a) *Fluid-like*, which do no support share wave and generally have material properties close to those of the surrounding water (e.g. decapods shrimp, euphausiid, salp, copepods);

b) *Hard elastic shelled*, with shell thick enough for shear waves of significant energy to travel in it (e.g. pteropods, gastropods);

c) *Gas bearing*, with gas inclusions big enough to produce substantial echo (e.g. siphonophore).

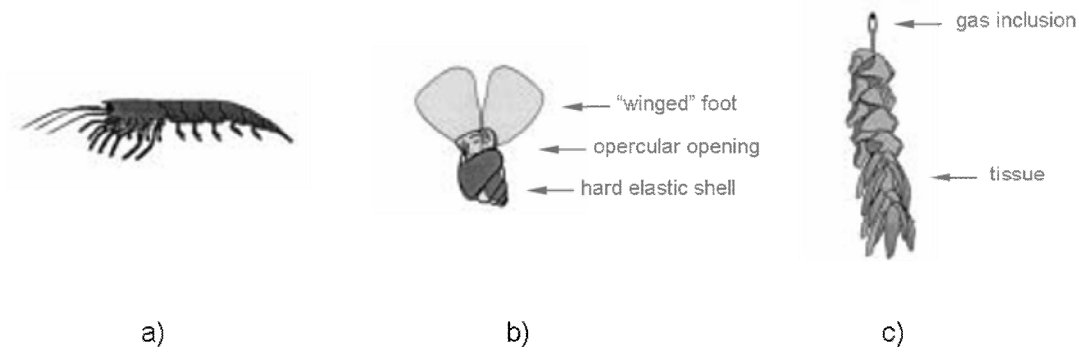

Figure 2.1: *Zooplankton categorized according to their anatomical groups:* (a) *fluid-like,* (b) *elastic shelled, and* (c) *gas-bearing*.

Certainly, these three groups of zooplankton are not the only in the ocean, however they are generally the most important from acoustic point of view and appropriate to identify species groups and estimating plankton size and abundance.

Because of the dissimilarity in morphology, there are consistent differences in the characteristic signatures of each of these classes of zooplankton. The target strengths versus frequency for the same volume or mass of reflecting tissue have a distinct pattern for each animal type and in statistical basis (Stanton *et al.*, 1996, 1998). This is useful to improve solutions for the forward problem, or allowing implementations and improvements of inversion techniques (e.g. Holliday *et al.*, 1989; Pieper *et al.*, 1990; Napp *et al.*, 1993; Martin *et al.*, 1996; Martin Traykovski *et al.*, 1998a; Stepnowski and Moszyński, 2000; Mair *et al.*, 2005; Lawson *et al.* 2008a).

There are three principal approaches to fish and zooplankton target-strength estimation (Foote, 1991): theoretical, *in situ* measurements on free-swimming organisms in their natural habitat, and *ex situ* measurements in cages, tanks or other enclosures. Since the work of this thesis is focused on the acoustic scattering properties of krill, the discussion below will be principally related to the fluid-like organism or group a), and their material properties. The theoretical approach is the object of this chapter and an exhaustive description of the krill target-strength models implemented in the past are presented in Appendix.

It should be emphasized that krill scattering processes are complex and to establish exact model predictions is difficult. Exact solutions can be achieved with analytical restrictions but in limited range of applicability, so that approximate models, either numerical or empirical, are often preferred.

During the last few decades, large effort has been undertaken to improve krill scattering models with different solutions, also because high quality experimental measurements are difficult to obtain. However, with the theoretical approach, problems may arise with the accuracy and the inter-dependence of the many key parameters, for instance: shape, material properties and orientation. Hence, despite the achieved theoretical level, verification of the scattering models is still important

and comparable good quality direct multifrequency measurements on target strength of individual or ensembles of zooplankton are required for the purpose.

In situ and *ex situ* measurements have to be made in the acoustic far field of both the transmitting transducer and the scattering object, assuring that the pressure varies linearly with distance (Medwin and Clay, 1998). In all the cases, since the acoustic scattering has a stochastic nature, it is always difficult to understand how to reduce the related variations in the measurements.

In situ measurements of target strength can be obtained on single animals and aggregation over a range of length and conditions, such as sex, sexual maturity, molt stage, feeding condition and prey and predator activities. As mentioned, due to the multispecies and multitarget problems these measurements might be of variable quality. Moreover, organisms that are acoustically detected cannot be all caught and identified. Submerging acoustic probes with multiple split-beam transducers and single target tracking process may reduce the uncertainties (Demer *et al.*, 1999; Klevjer and Kaartvedt, 2003; Conti *et al.*, 2005b; Klevjer and Kaartvedt, 2006).

In general, the authors reported high variability in TS of a single euphausiid (range often >25 dB) mostly due to change in the orientation. Because of the ambiguities concerning identity of acoustic scatterers related to the species behaviour and the regional biological and physical conditions, the sensitivity of the measurements should be investigated over a range of conditions and densities (ind/m^3). The comparisons of the acoustic returns with results from high-resolution net sampling gears or contemporary photographs, for species and orientation determination, are mostly used (e.g. Greenlaw, 1979; Hewitt and Demer, 1991; Hewitt and Demer, 1996; Lawson *et al.*, 2006; 2008a).

Not mentioning those on *M. norvegica*, which will be discussed in Chapter 3, significant *ex situ* data have been published in the past on free single individual krill (e. g. Richter, 1985a; Pauly and Penrose, 1998), encaged swarm (e.g. Foote *et al.*, 1990) and single tethered animal (e.g. Greenlaw, 1977; Wiebe *et al.*, 1990, Demer

and Martin, 1995; Martin Traykovski *et al.*, 1998; McGehee *et al.*, 1998; De Robertis, 2001; Amakasu and Furusawa, 2006).

Before the introduction and consolidation of the split-beam transducer technology, researchers have adopted an *indirect method* for *ex situ* freely swimming animal measurements (e.g. Foote *et al.*, 1990; Pauly and Penrose, 1998). This was based to yield the TS estimation from a statistical treatment, with a set of assumptions on the scattering regime, of an ensemble of echoes obtained by a single-beam transducer. At present, since the location and the beam compensation of a target with respect of the axis of the beams is assured with high precision by the split-beam technology and calibration, the *direct* methods are more accurate and preferred.

On the other hand, *ex situ* methods are often not reliable and consistent with *in situ* results as many factors are likely to influence organism target strength and may differ with respect to time and volume. Constraints in animal behaviour in small volumes seem to be the main reason. Pressure effects and changes in the physical properties could also produce additional causes, but they are not clarified. Nevertheless, if the set-up assures a good simulation of the natural habitat, and the acoustic calibration assures high accuracy, the results obtained may be remarkable.

The animals under investigation have to be fresh; preservation can reduce the shape (Demer and Conti, 2003b), and produces changes in the material properties (Greenlaw, 1977; Kristensen and Dalen, 1986), usually related with a reduction in target strength (Richter, 1985a; Wiebe *et al.*, 1990).

As straightforward conclusion, due the complexity of the scattering processes and in performing high quality measurements, it is clear that the most reliable technique for acoustical assessing of euphasiids may lie in combining the best aspects of both the theoretical and empirical target strenght approaches.

2.1 Krill orientation problem

Krill have an elongated body shape, hence directional acoustical scattering from these organisms is expected. Greenlaw (1977) and Sameoto (1980) already claimed this important aspect in their earlier valuable studies on krill acoustics.

Several investigators have indicated the orientation as the largest component of the observed variability *in situ* krill target strength (e.g. Klevjer and Kaartvedt, 2006), as well as the cause of the disparities (sometime more than 25 dB) between empirical data and theoretical models (e.g. Greenlaw *et al*., 1980; Everson, 1982; Cochrane *et al*., 1991; Demer and Martin, 1995; McGehee *et al*., 1998; Demer and Conti, 2003a; Amakasu and Furusawa, 2006; Conti and Demer, 2006).

To simplify the description of the the far field scattering phenomenon within the geometric region (Par. 2.2.1) from a fluid-like organism, Stanton *et al*. (1993a; 2004) adopted a ray representation. Each ray is associated with the scattering by a particular physical feature, such as an edge, outer surface, or an organ, and will have an associated amplitude and phase, depending on the size, shape, orientation, position, and material property of the feature, as well as the wavelength of the sound.

Since the euphausiid has a soft body (material properties similar to the surrounding medium), most of the incident acoustic signal passes into body relatively unaffected. The internal acoustic signals reflects off the interface at the far side of the animal, which is facing away from the sound source, propagates back through the animal's body, and finally goes back to the source (assuming a mono-static technology typical of the echosounders). Thus, the scattering may be resumed as occurring primarily from the reflection of the outer boundary of the animal (Figure 2.2).

At broad-side and end-on incidence, there are two main echoes from the animal, coming from the front and back body walls, which interfere according to the acoustic wavelength and the separation between these reflecting faces. At broadside incidence, the interferences correspond to echoes from the front and back portions of the body cross section, while for end-on incidence the echoes from these extended bodies come from the front and backs ends of the bodies (Fig. 2.2a,b). The period of oscillation is

related to the size of the body cross section at broadside incidence, while it is related to the longitudinal length at end-on incidence. In the first case, the echoes interfere mostly constructively, depending of the wavelength with respect to the length of the cross section in the incidence direction, producing a relatively high backscattering level. At other angles, Stanton *et al.* (1998b; 2004) hypothesized that other parts of the body may also contribute significantly to the scattering, giving rise to six or more echoes from the body in mostly destructive interference (Fig. 2.2b).

This is recognized as the major reason of the oscillating pattern of target strength versus frequency in both experimental data and scattering models (Demer and Martin, 1995; Stanton *et al.*, 1998b).

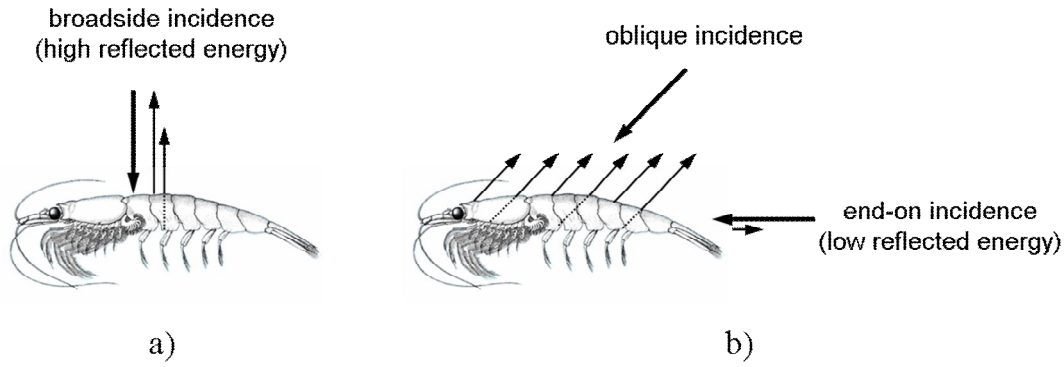

Figure 2.2: *Exemplification of the krill acoustic backscattering phenomena at different angle of wave incidence.*

This general pattern is theoretically confirmed by scattering models involving different techniques. These include the ray representation for the general shape of elongated organisms (Stanton *et al.*, 1993a, 1998c), the pulse compression echoes technique similar to the matched filter process (Stanton *et al.*, 1996; Chu and Stanton, 1998; Stanton *et al.*, 1998b), and the distorted wave Born approximation parameterization (Stanton *et al.*, 1998c).

The deep nulls resulting from constructive and destructive interference complicate the relationship between TS and body size (Stanton *et al.*, 1996), and indicate that the simple TS-length relationships as the Greene model (Par. A3.1) is inappropriate (Demer and Martin, 1995; Demer and Conti, 2005).

The most relevant example is the result obtained by Demer and Conti (2005) re-analysing the data from the CCAMLR 2000 echosurvey in the Scotia Sea (Watkins *et al*., 2000). Hewitt *et al*. (2002) previously estimated a total abundance of 44.3 million metric tonnes [Mt] of krill, on the base of the total energy attributed to these organisms and scaled by the Greene model. By replacing the model with the SDWBA model (Par. 2.4.1b), and incorporating the Demer and Conti, Kills and Endo distributions of orientation (Table 2.I), the krill biomass was re-estimated to be 109.4, 137.4, or 192.4 Mt respectively. As the authors claimed: "*the wide range of the results depends solely on the expected distribution of krill orientation*".

The result indicates that although the effect of the individual orientations is much reduced when the scattering is averaged over a distribution of aspects, the latter still has high space-temporal relevance to the acoustic survey analyses, and the introduction of a proper distribution of orientations in the processing is essential.

There is a range of information available on orientation of free-swimming krill in their natural environment. In general, scuba divers observations indicated that all individuals in a school have the same size, assuming virtually the same orientation, usually swimming horizontally (Hamner *et al*., 1983). However, Demer and Conti (2005) warned that the presence of divers or devices may generally affect the krill natural behaviour, and less invasive investigation is needed. It is reasonable that the orientation will change upon the animal activity and condition as well environmental conditions. Different orientation may be expected when krill hover while feeding, migrate up, down or horizontally, swim against a current, flee from predator, and probably when they avoid the vessel. This last condition is an open matter. While Brierley *et al*. (2002) indicated that krill behaviour is not affected by the survey vessel, Hamner and Hamner (2000) found that the krill response to a towed vehicle depends on its speed; at very low speed (1 kn), a horizontal swim reaction was observed, while when the vehicle was towed at 2-4 kn, tail-flip escape responses occurred. Endo (1993) has also indicated that it can vary even with the maturity stage; mature females would hover at a steeper angle than other krill when migrating. In the

past, Sameoto *et al*. (1985) claimed that anomalous target strength were the results of changes in orientation induced by the ship.

At present, it is clear that the knowledge of the orientation distribution of the krill under investigation is crucial, and methodologies for its determination have to be developed. A valuable approach is to produce simultaneously photographs and acoustic measurements in the volume of water containing krill (e.g. Kristiensen and Dalen, 1986; McGehee *et al*., 1998; Demer and Conti, 2005; Lawson *et al*., 2006; Amakasu and Furusawa, 2006).

Prediction of the orientation distributions based on observations in different conditions may also be a valid support. Predicted distributions can be compared with observed distributions and the models adjusted or redefined as appropriate. Some investigators have claimed the potentials of multifrequency systems with three or more frequencies (e.g. Chu *et al*., 1993) or with broad-bandwidth techniques for determining the orientation as an inverse problem (Martin Traykovsky *et al*., 1998).

Distribution results from observations based on different species, conditions and methods have been reported; Table 2.I resumes the most relevant works. For useful quantitative interpretation, the orientation may be modelled as the angle θ in degrees on respect to the angle between the acoustic wave and the normal to the longitudinal axis of the krill (Figure 2.3), and assuming positive sign for the ‘head-up’ position and negative sign for the head-down

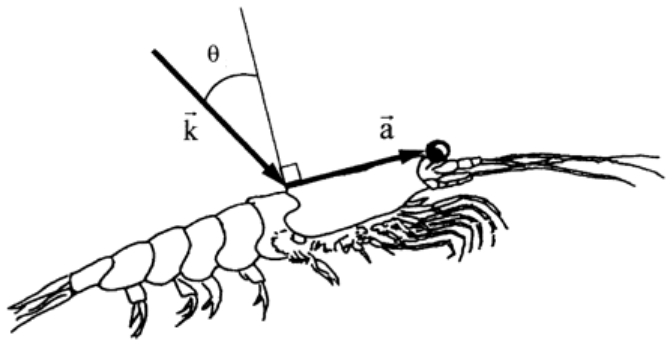

Figure 2.3: *Definition of the angle of orientation* θ: $\vec{a}$ *is the body orientation vector, and* $\vec{k}$ *the incident wave number vector*.
(Amakasu and Furusawa, 2006)

Stanton *et al*. (1993b) demonstrated that the modelling results based on a Gaussian distribution of orientation fit to the measured data when an average of echoes is considered. Thus, the distribution of orientations is typically assumed as a Gaussian distribution defined by its mean and standard deviation values ($\theta = N[\bar{\theta}, std(\theta)]$) in degrees. There is an evident discrepancy among the results of Table 2.I. This is mostly due to the problems related to the conditions of the investigation. Observations in aquarium may be affected by problems related to limited volume, light exposition, and lack of natural habitat conditions such as currents and inhomogeneities. However, high quality observations *in situ* are difficult and the result must be taken with care.

It is interesting to note that in the most recent works (Table 2.I) the mean orientation is supposed closer to the normal incidence ($\bar{\theta} = 0$) with large standard deviation. Hamner and Hamner (2000) also indicated this as resumed result from 20 years of observations by scuba divers, extensive aquarium studies and aboard ship, and asserted that in their life krill are most often oriented horizontally. Falk-Petersen and Kristensen (1985) and Kristensen and Dalen (1986) already suggested such mean orientation with standard deviation of 30° to be applied for survey data on *M. norvegica*. Cochrane *et al*. (1991) and Sameoto *et al*. (1993) found this indication consistent with their *in situ* data and prediction by straight fluid cylinder model (Par. A1.2.1a).

Demer and Conti (2005), Conti and Demer (2006), and Lawson *et al*. (2006, 2008a) have recently applied the close-to-zero mean orientation to the acoustic data on Antarctic krill with success. Their results validate the hypothesis applicable to the survey data analysis that the krill aggregations could be considered composed by individuals horizontally orientated and swimming quickly.

Table 2.I: Summary of the relevant results on distribution of krill orientation $N[\bar{\theta}, \sigma_\theta]$ in degrees as defined in the text.

Author(s), year	**species**	**$N(\bar{\theta}, \sigma_\theta)$**	**Method**
Kils, 1981	*E. superba* *M. norvegica*	N(45.3, 30.4) N(53.8, 64.2)	Observation in aquarium
Kristiensen and Dalen, 1986	*M. norvegica*	N(-9.8, 34.1) N(0, 30)	Observation in situ with underwater photo-camera; Suggestion for no migrating activity
Cochrane *et al.*, 1991, Herman *et al.*, 1993	*M. norvegica*	N(5, 5)	Matching by inversion the High-Pass fluid cylinder model prediction with volume backscattering at 50 and 200 kHz.
Endo, 1993	*E. superba*	N(45.6, 19.6)	Observation in aquarium
Chu *et al.*, 1993	*E. superba*	N(~20, ~20)	Inferred by DWBA model from dual-frequency 38 and 120 kHz target-strength data from encaged animals
Miyashita *et al.*, 1996	*E. pacifica*	N(30.4, 19.9)	Video observation in small aquarium
Demer and Conti, 2005	*E. superba*	N(15, 5)	Matching theoretical prediction by SDWBA model based on biological samples and volume backscattering at 38 and 120 kHz
Conti and Demer, 2006	*E. superba*	N(11, 4) N(4, 2)	As in Demer and Conti 2005, with improved parameterization of the SDWBA model
Lawson *et al.*, 2006	*E. superba*	N(0, 27)	Direct observations from video plankton recorder

2.2 Theoretical prediction

Driven by the need for more accurate scattering prediction, models of increasing sophistication, which take into account the full complexity of the animals' shape and the material properties, have been proposed by the researchers during the years. This leads to increase the accuracy but requires much more effort in the implementation.

With the assumption that the material properties are uniform inside the body, the animal may be represented by digitalization of the outer boundary from low to high resolution as shown in Figure 2.4.

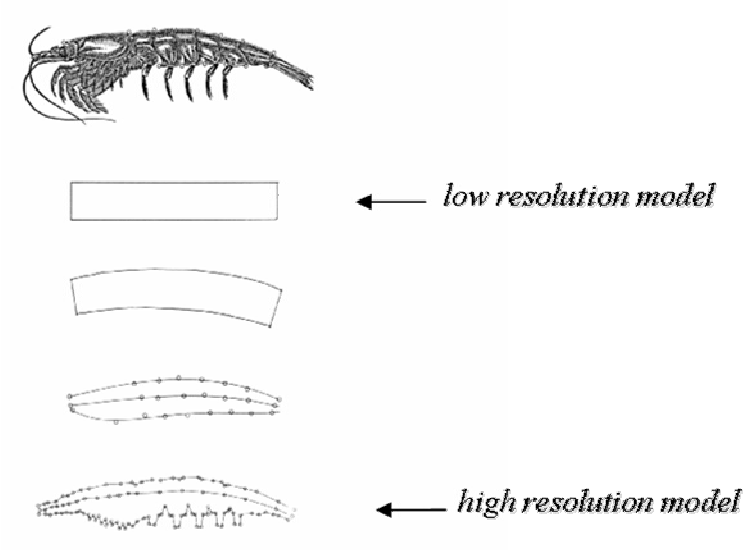

Figure 2.4: *Krill representation for use in physics-based acoustic scattering models*. (Stanton and Chu, 2000)

The scattering predictions show a strong dependence upon shape, orientation and frequency (Stanton and Chu, 2000). Some complex models may be based upon a more rigorous representation of the body shapes, where other animal features are also taking into account. This is the case of the numerical approach based on coupling finite- and boundary-element methods (FEBE) presented by Francis *et al*. (1999) and applied to the multipart body of *Meganyctiphanes norvegica*. The model appears arbitrary in its capacity to be applied to bodies with internal structure for a wider

range of material properties. A more comprensive model should also introduce other elastic properties, such as the transverse-wave sound speed, modulus of rigidity of the organism, or stiffness of carapace (Machlup, 1952).

However, for these complex models, a digitalization in spatial resolution with fraction of the acoustic wavelength (λ) of the order larger than $\lambda/20$ is required (Stanton and Chu, 2000). This induces to conclude that complex approaches have higher range of validity, but simpler approaches have the merit to be reduced to simple analytical forms, which are easier to apply although sometime under limited conditions.

Various examples of such models for fluid-like elongated organisms have been presented in literature (Par. 2.4 and Appendix). As first classification, they were subdivided on the base of their dependence from animal's volume or cross-sectional area (Demer and Martin, 1995). A scattering model is considered dependent on the animal's volume or cross-sectional area if plots of TS as function of log of *ka* and TS versus the log of the animal length have slope of 30 or 20 in the geometric scattering region ($ka>1$) respectively.

2.2.1 Basic scattering formulations

Considering the general case of scattering of sound by any finite-sized object, the pressure field *p* must satisfy both the wave equation and the boundary conditions. The homogeneous wave equation is:

$$\nabla^2 p = \frac{1}{c^2}\frac{\partial^2 p}{\partial t^2} \tag{2.1}$$

where *c* is the compressional speed of sound. As in most physical problems, the solutions of this differential equation are those where the time dependence is sinusoidal in the form $\exp(-i\omega t)$. The boundary conditions require that the pressure and the radial component of the particle velocity must be continuous at the boundary of the object:

$$p_{inc} + p_{scat} = p_{int} \quad ; \quad u_{r_{inc}} + u_{r_{scat}} = u_{r_{int}} \tag{2.2}$$

where p_{inc}, p_{scat} and p_{int} are the respective incident, scattered, and internal pressures evaluated at the boundary of the object, and the letter *u* indicates the related particle velocities. The pressure and the radial component of the particle velocity are related by the expression (Stanton, 1988a):

$$u_r = \frac{-i}{\rho c}\frac{\partial p}{\partial (kr)} \tag{2.3}$$

where ρ is the density of the medium, *c* the sound speed and *k* the wave number (=2π/λ, where λ is the acoustic wavelength) and *r* the position along the wave path.

Moreover, the far field scattered pressure p_{scat} due to any finite-sized object can be written in a compact and commonly used form (Medwin and Clay, 1998):

$$p_{scat} = p_{inc}\frac{10^{-\alpha r/20}}{r} L(\theta, \phi, f) \tag{2.4}$$

where *r* is the distance from the object to the field measurement, α is the absorption coefficient, and $L(\theta, \phi, f)$ is the *complex acoustical scattering length* dependent on the spherical angles and frequency and expresses phase as well as amplitude information.

At backscattering geometry ($\theta = \phi = 0$) the differential backscattering cross section is defined as (Medwin and Clay, 1998)*:

$$\sigma_{bs}(f) = \left| L(0, 0, f) \right|^2 \tag{2.5}$$

where the qualifier Δ used by Medwin and Clay formulation has been omitted as suggested by MacLennan *et al*. (2002) to indicate more generically that σ_{bs} is a continuous function.

Some authors prefer to use the *backscattering amplitude* f_{bs} rather than the acoustic backscattering length. In the far field, the backscattered pressure is proportional to f_{bs},

* The differential backscattering cross section defined in Eq. (2.5) differs by a factor 4π from the often-used scattering cross section σ defined by Urick (1983) ($\sigma = 4\pi\sigma_{bs}$). Korneliussen (2002) showed that if the reference area is 1 m^2, the Urick's definition of TS in terms of sound intensity incident and scattered ratio and the Eq. (2.5) gives the same value for TS.

which indicates the efficiency to which an object scatters sound and is a function of acoustic wavelength, object size, shape and material properties. Since the models are generally based on the backscattering geometry where the phase information is already implicit in the definition, the substitution is made without incongruence. Therefore, efforts to model the scattering from objects like zooplankton will attempt to define f_{bs} or σ_{bs}. Finally, the far field backscattered energy or target strength, in units of decibels relative to 1 m^2, pertaining to a single echo is defined as:

$$\mathrm{TS}(f) = 20\log\left[\left|f_{bs}(f)\right|/1m\right] = 10\log\left[\sigma_{bs}(f)/1m^2\right] \tag{2.6}$$

Hereafter, the target strength units will be reported just in dB, omitting the notation "re 1 m^2" that will be assumed as intrinsic when referring to the far field backscattered energy.

The frequency dependence of the backscattering cross section (as well the target strength) of an object can be divided into two broad regions. 1) A *low-frequency* or *Rayleigh scattering region* (below $ka \cong 1$, with k the acoustic wave number and a the characteristic dimension of the object), where the function monotonally increases proportionally to the fourth power of the frequency (rigid sphere target). 2) A *high-frequency* or *geometric scattering region* (after $ka \cong 1$), where the function has an oscillating trend due to the modal backscattering interference.

Some authors prefer to show their results using the useful *reduced target strength* (RTS) which normalizes the target strength by the square of the characteristic outer dimension of the body; in this way the TS is examined on a dimensionless scale.

2.3 Evaluation of the key models parameters

The theoretical modelling of acoustic scattering from a fluid-like object requires the knowledge of certain organism characteristics based on morphology (size and shape), and physical properties contrasts with the surrounding medium, i.e. the specific mass density and the longitudinal-wave sound speed. The latter are commonly denoted

with *g* and *h* respectively (Greenlaw and Johnson, 1982) and are essential for the accuracy of the models (e.g. Stanton *et al.*, 1994b).

It is obvious that the accuracy of acoustic assessment of zooplankton depends on the ability to measure these model input parameters. In addition to the orientation, the uncertainties in estimations of the materials contrasts are indicated as the principal cause of the discrepancies between the empirical observations of zooplankton target-strength and the theoretical predictions (e.g. Wiebe *et al.*, 1997; Stanton and Chu, 2000). Since *g* and *h* are close to unit (within several percent), small changes in their values will produce dramatic changes of the acoustic scattering level.

In some cases, the investigators have adjusted within reasonable limits the values of *g* and *h* to fit the acoustic data (e.g. Holliday and Pieper, 1980; Wiebe *et al.*, 1997; Lawson *et al.*, 2006).

Direct measurement of the longitudinal-wave sound speed and specific density of zooplankton is extremely difficult because of the general complex shapes and small sizes. There are apparently significant differences in physical properties between orders and species from different environments. Moreover, Greenlaw (1977) reported a substantial difference in *g* and *h* values between alive and dead euphasiids.

For zooplankton in general, the reported contrasts vary from 0.9402 to 1.0622 for *g*, and from 0.949 to 1.096 for *h*. These values have been mostly measured in laboratory (*ex situ*), and for the particular case of krill only for some species were reported, such as *E. superba* and *E. pacifica* and very few measurements on *M. norvegica* and *Thysanoessa* genus.

Inevitably, the results are slightly different. The contrasts are naturally species dependent, and it is generally recognized that for the same species could vary with life stage, season and location (especially due to the diet and food supply that influence the differences in lipid and protein contents) and for some species with the depth (Kils, 1979a; Kristiensen and Dalen, 1986; Køgeler *et al.*, 1987; Mukai *et al.*, 2004; Chu and Wiebe, 2005). They could be also interrelated in some species; Mukai

at al. (2004) studied the annual cycle of the contrasts in the *Euphausia pacifica* and observed that the density increased with a decrease in the sound speed contrast.

It has been also pointed out the dependence of the contrasts from the body length. Chu and Wiebe (2005) claimed that the difference in TS prediction with the DWBA (Par. 2.4) between a juvenile and an adult individual of *E. superba* of length 27 and 53 mm respectively would be about 6 dB more than resulting purely from size difference (Greene model, Par. A3.1 in Appendix).

In conclusion, whatever model is used for the estimation of krill, it should be parameterized according to the length-based and potential seasonal variability in material properties of the organisms present in the area of investigation.

2.3.1 Length

Since the krill species are slightly different in morphometry, the measure of the krill length is not standardized. Investigators have used different limit-body points to measure the length of the individuals under investigation.

In many works, the length measurements are even not described and the limit-body points not defined. This is a source of confusion when the results are compared. Thus, the length definition has always to be declared. Morris *et al*. (1988) summarized and codified various definitions of standard length (SL); their work could be used as precious reference.

In the past, the standard lengths indicated by Mauchline (1980b) have been mostly used. Lawson *et al*. (2006) presented useful interrelationship between the three main Mauchline SL definitions for *Euphausia superba*.

In this thesis, the SL used for *Meganyctiphanes norvegica* is defined from the tip of rostrum to the posterior end of the terminal spine at the end of telson, which is codified as “TT” in the Morris *et al*. (1988) paper. This definition have been preferred for the *M. norvegica* in previous ecological and acoustical studies (e.g. Sameoto *et al.*, 1993; Klevjer and Kaartvedt, 2006; Dalpadado, 2006) because the two body-limit

points are easily recognizable in this species and lead lower uncertainty when measured. In Paper I, conversion relationships between useful lengths definitions for the *M. norvegica* species are presented. However, it should be kept in mind that the length measurement is operator- and tool-dependent.

Another issue to be mentioned is the fact that quite often the animals are preserved (usually frozen or in 4 % formalin solution) prior to the length measurements. This induces to a potential reduction of the actual dimensions (*shrinking*). In this context, it is worth to mention that the measure of the carapax length is known to be much less affected by shrinkage due to various preservatives (Kulka and Corey, 1982). Therefore, proper conversion relationship carapax-SL lengths for fresh specimens of the specific target species is consequently required.

When using the length as key parameter for some theoretical models, the question regarding what is the real “acoustic length”, especially on respect to the orientation, has to be questioned (e.g. Stanton, 1989a). This could have a significant influence when working on field acoustic data. Since the scattering is a non-linear function of krill length, larger individuals in the insonified volume will contribute to the total volume backscattering disproportionately relative to their numerical abundance. Lawson *et al*. (2006, 2008a) suggested that for the *E. superba* the acoustic length has to be measured from the anterior of the eye to the end of the sixth abdominal segment. Morris *et al*. (1988) did not codify this measure.

2.3.2 Sound speed and compressibility

Zooplankton are denser and less compressible than water (Greenlaw and Johnson, 1982), thus their longitudinal-wave sound speed, hereafter just called sound speed, is slightly higher than the surrounding medium.

Foote (1990) found a marked decline in sound speed results with increasing of the sample age, probably due to the deteriorating of the tissue elasticity. This means that the measurements have to be performed as soon as possible after the removal of the krill from the sea.

Estimation of the key model parameter *h* implies measurements of the sound speed or the compressibility of the organism. This was commonly obtained with laboratory measurement involving the time of flight method applied to an inverted *T-shaped velocimeter* with transducers at opposite ends of the horizontal section (Greenlaw, 1977) as in Figure 2.5a. A critical focus on other potential techniques used in the past, such as piezometer operations, resonance and levitation techniques, can be found in Greenlaw and Johnson (1982).

The velocimeter measures the time of flight of an acoustic pulse through a finite volume of a mixture consisting of a reference solution (usually distilled water or seawater) and a number of living organisms uniformly distributed and having similar material properties, i.e. the multiple scattering is negligible. In the common case of acoustic wavelength much shorter than the projected size of the animals, and assuming that the rigidity, the viscous and thermal processes are neglected, the time-average model (Wyllie *et al*., 1958) may be employed and the measured time equated to the sum of the respective travel times due to the solution and the organisms separately. In terms of corresponding sound speeds, it may be written as:

$$\frac{1}{c_m} = \frac{1-V_o}{c_s} + \frac{V_o}{c_o} \tag{2.7}$$

where c_m is the sound speed in the mixture as determined from the measured time of flight, c_s and c_o are the sound speeds in the reference solution and organisms respectively, and V_o is the volume fraction of the organisms in the mixture.

The model of Equation (2.7) is based on a phenomenogical approach described by the application of the geometrical ray theory to a multilayer medium, so that the mixture may be interpreted as a two-phase layered medium where the plane wave with normal incidence on the interface between the layers propagates in one phase at the time.

Foote *et al*. (1996) claimed that the comparison between the acoustic wavelength and the projected dimension of the target organisms is imperative for a full understanding of the measurements. If the operative wavelength is shorter or much longer, the result has to be distinguished as indirect measure of sound speed or compressibility

($=1/\rho c^2$) respectively. In the latter case, all the occurrences of the sound speed in Equation (2.7) should be replaced by the corresponding ρc^2.

Ye and McClatchie (1998) compared the results of Equation (2.7) with those obtained from a wave scattering theory and showed that the empirical equation may be accurate in the Rayleigh scattering regime, i.e. where the acoustic wavelength is much larger than the size of scatteres. More important, they found that Equation (2.7) always underestimates *h* with increasing underestimation as the relative contrasts increases, as well as the ratio between the size of scatterers and the acoustic wavelength. A more comprensive comparative analysis between the Willy *et al.* model and the theoretical scattering theory can be found in Nesse (1998).

The model (2.7) has been used as basis to determine the sound speed in fluid-like organisms with different approaches. The earlier procedure presented by Greenlaw (1977) on *E. pacifica*, and applied on *E. pacifica* and *T. raschii* by Greenlaw and Johnson (1982) and on *M. norvegica*, *T. raschii* and *T. inermis* by Kristiensen (1983) and Køgeler *et al*. (1987), consisted in the following steps:

1. to perform the measurements at various organism concentrations, with the scatterers uniformly distributed along the acoustic path;
2. to measure the volume of the organisms introduced and obtain the volume fraction in the mixture;
3. to determine a linear regression of the measured sound speed versus the organisms volume fraction;
4. to estimate the sound speed from the regression, supposing that the volume is totally filled by the organisms (volume fraction$=1$).

Thereafter, the contrast *h* can be obtained dividing the sound speed of zooplankton by that of seawater determined in the same experiment.

The procedure is suitable for organisms having sound speed close to but greater than the reference solution. However, there are critical points in this procedure. Firstly, the sound speed in a mixture is not generally a linear function of the relative concentration of the constituents and any nonlinear behaviour in the measurements must be discerned. Greenlaw and Johnson (1982) claimed that the regressions tend to

be highly significant and the predicted confidence interval for the sound speed of the zooplankters is generally less than 1 %. The same authors also claimed that the procedure is proper for moderate concentrations of organisms. Hence, uncertainties may arise when determining the exact value at the limit of the regression due to the missing or biased values for higher volume fractions. From a practical point of view, it is difficult to make precise measurements directly from an oscilloscope as well as to assure constant measurement conditions. Since the measure is very sensitive to the temperature, which may vary in the course of the measurement series, the operator has to know accurately its changes and to take into account in the analysis of the data. For example, Greenlaw (1977) has shown that for a variation of temperature from 10.5° to 19° C, the sound speed contrast of preserved euphausiids changes from about 1.0094 to about 1.028.

Foote (1990) overcame the temperature problem by measuring the electrical resistance of a precise potentiometer, whose fine setting accomplished the equalization process, for a high number of measurement series and referring the value to a constant temperature. Then, the resulting referred measurements were averaged. The regression uncertainties were avoided determining the relative increment of the krill sound speed over that of the reference solution at same temperature. By determining the mean and the standard deviation of the increment, the contrast *h* was finally obtained.

The accurate estimation of the total volume of the organisms is the most critical step in practical application of Eq. (2.7). The investigators have used both direct and indirect methods for the volume fraction determination. The Greenlaw (1977) direct method, consisting in recording the changes of level of water in the vertical part of the tube during the addition of the organisms, was adopted in the earlier studies of Kristensen and Dalen (1986) and Køgeler *et al*. (1987) on *Meganyctiphanes norvegica* and *Thysanoessa* species. Measurements of the individual specimen volumes by the direct method of displacement (Wiebe *et al*., 1975) have been used as convenient by Mukay *et al*. (2004). In both the methods, an overestimation of the volume due to the water unavoidably adhered to the animals may be expected.

Therefore, indirect methods by measurements of some properties related to the volume have been preferred. Foote (1990) used specific mass density and morphometric values accomplished with wet weight data. Chu *et al*. (2000a) suggested an empirical approach applied to the resistivity (conductivity) method, which is widely used in geophysical application to estimate the porosity of the sediment (e.g. Evans, 1994). Since the resistivity of the sediment and water are different, different volume fraction of water-animal mixture should result in different resistivity readings.

Measurements of sound speed in winter specimens of *Meganyctiphanes norvegica* at Espegrend Marine Biological Station of the University of Bergen (Norway) in 1998 (Fig. 2.5b) are presented in Paper I. The velocimeter apparatus used in that study was re-fabricated by Trygve Gytre of Institute of the Marine Research in Bergen (Norway), with increased stability and sensitivity, hence precision, compared to the apparatus used by Foote (1990). The paper also describes the inconveniences due to the apparatus and affecting the accuracy of the measurements, and the related adopted solutions. For the volume fraction determination, the Kils (1979a) allometric relationship was used.

The most recent apparatus for sound speed-contrast measurements was presented for the first time by Chu *et al*. (2000a) and named “Acoustic Properties of Zooplankton” (APOP). This apparatus still use the measurable arrival time and the corresponding volume fraction. The first laboratory version consisted of an acoustic chamber with two broadband transducers (350-650 kHz) accomplished with resistivity measurements for the evaluation of the organisms’ volume fraction. Three theoretical models (the DWBA model, the compressibility model and the two-phase ray model) were then used to infer the sound speed contrast. Only results on decapods shrimps (Chu *et al*., 2000a), and eggs and early-stage larvae of cod (Chu *et al*., 2003) are presented with this apparatus.

However, the potential applicability to *in situ* determination of acoustic properties of zooplankton was clear, and few years later Chu and Wiebe (2005) used a modified

APOP version to report the first *in situ h* contrast measurements on *E. superba* and *E. cristallorophias*.

a)

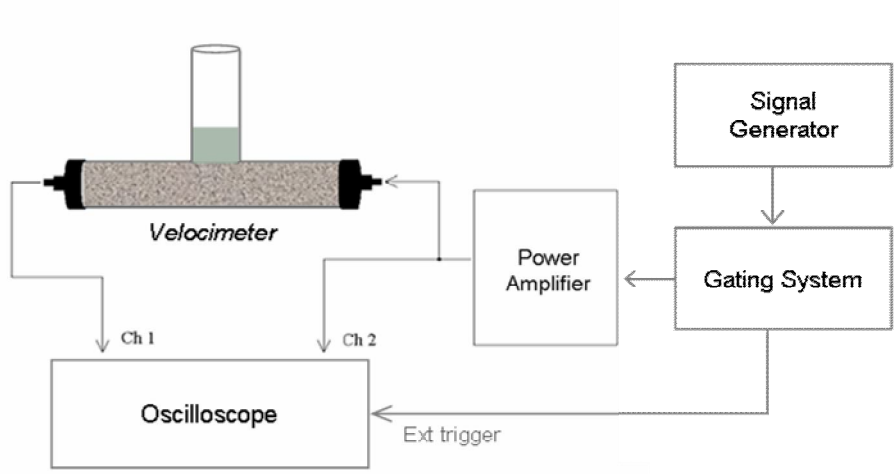

b)

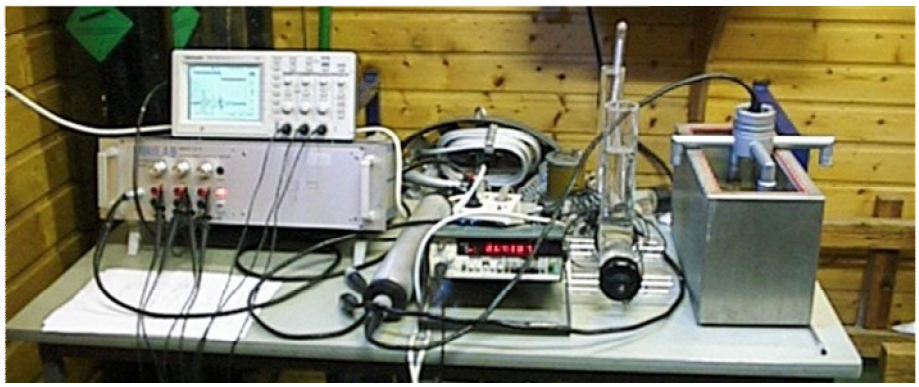

Figure 2.5: a) *Velocimeter schematic set-up* (*redrawn from Kristensen, 1983, and Køgeler et al., 1987*). b) *The Espegrend 1998 sound speed measurement bench-work.*

The new version consists in a dual-chambers acoustic apparatus with identical broadband transducers with increased bandwidth to about 300 kHz and central frequency at 500 kHz, and can be operative from the sea surface to a depth of 220 m. Temperature and pressure measuring systems are also accomplished to the acoustic system. At the reference depth, the received waveforms from the two chambers, one containing animals and seawater and the other containing only seawater, are recorded. The sound speed contrast is then determined by measuring the travel time difference

between the two received waveforms, with estimated uncertainty less then 10 % of the difference contrast from the unity.

The comparison of the results showed insignificant statistical difference in sound speed contrast along the depth for *E. superba*, but not for *E. cristallorophias*. This indicates that krill species could have different depth responses, resulting from either temperature or pressure changes or both. However, the results indicated that there is a dependence on the size of krill, which can be expressed by a linear regression versus the length L in mm by (Lawson *et al.*, 2006):

$$h = 4.981 \times 10^{-4} L + 1.009 \qquad (2.8)$$

2.3.3 Specific density

For small animals with irregular shape, like euphausiids, the measure of the specific density is not simple. Different methods have been used in laboratory measurements in the past. The earliest *method of displacement volume and weight* (Lowndes, 1942; Mauchline, 1967; Wiebe *et al.*, 1975) was the most straightforward. This is an indirect method where the density is determined by the ratio between the weight and the net volume of the animal(s) alone. The measure of these two parameters must be very accurate, but they are difficult to obtain and always affected with errors of a few percent (Chu *et al.*, 2000b).

Another indirect approach for zooplankton is to measure the sinking rate of the organisms (e.g. Knutsen *et al.*, 2001), but it is not suitable for organism with irregular shape as euphausiids.

Direct methods, such as the *density bottles method* and the *gradient density method*, are more accurate and have been mostly used by the investigators. In the first method, the anesthetized animal is immerged in turn in a series of bottles containing homogeneous solution (usually distilled water mixed with colloidal silica) of known and increasing specific gravity. The density of the solution that makes the animal neutrally buoyant (or the mean density between the most dense solution in which the animal sinks and the least density in which it floats) is then assigned to the specimen.

Using this procedure, results on fresh and preserved *E. pacifica* were firstly presented by Greenlaw (1977) and successively by Greenlaw and Johnson (1982), on fresh samples of *E. superba* by Foote *et al*. (1990) and on *E. pacifica* by Mukai *et al*. (2004).

Results of measurements with density bottles method on 0-generation specimens of *Meganyctiphanes norvegica* carried out in 1998 at Espegrend Marine Biological Station of the University of Bergen (Figure 2.6) are presented in Paper I. The measured specimens spanned the range from 10.9 to 26.4 mm. Part of them were collected at the same sea trial as the animals used for the sound speed measurement at Espegrend Station (Fig. 2.5b).

Figure 2.6: *Density bottles method*: *bench-work at Espegrend Marine Biological Station.*

For the second method, a hydrophobic solution is specially treated (usually with salt or sugar) to produce a density gradient in a single container with higher density at the bottom and lower than the animal density at surface. The levels of density are calibrated by using a series of floats with known density immerged in the container. The anesthetized animal is introduced in the gradient column from the surface and

sinks until it reaches the neutral buoyant level corresponding to its specific density. Kristiensen and Dalen (1986) and Køgeler *et al*. (1987) presented specific density and density contrasts for fresh specimens of *M. norvegica, T. raschii* and *T. inermis* using this method.

Due to the set-up, the quality of the measurements with the two methods is variable and the results have generally to be considered with care (c.f. Knutsen *et al*., 2001). Both the methods have similar sources of error, not mentioning the problems that may arise in handling the animals. They require that the animal has to be motionless but alive by anesthetization. When an animal dies, the membrane properties change rapidly as well as the density. Anesthetization is therefore needed, but it will affect the result as influencing the specific density of the organism. Some solutions may also be hypotonic but without apparent deleterious effects on the buoyancy, or give problems associated with osmotic process overall if the observation is elongated in time and solutions have high salinity. Moreover, for an anesthetized animal the legs, antennas and any elongated part of the body may influence the sinking, depending from the aspect position.

To overcome the problems, Chu *et al*. (2000a) presented a new apparatus to infer the density contrast *in situ* using an indirect approach based on the change (reduction) of the acoustic intensity due to the animal in the acoustic path. The intensity reduction results from the scattering-induced attenuation, which is function of the contrasts g and h and the volume fraction. If the contrasts are supposed, it is possible to infer the density contrast from intensity measurements in the forward direction.

The method does not require the animals to be motionless avoiding the anesthetization problems mentioned above and contemporarily overcomes the uncertainty introduced by water unavoidably adhering to the animals as in displacement volume and weight measurements.

Same advantages are obtained by the dual-density method introduced by Chu and Wiebe (2005) but with even higher degree of accuracy. The densities and the associated weights of two fluids, with and without animals, are measured thought a

procedure leading a set of linear equations to be solved. Accurate specific density measurements of living *E. superba* were carried out on board. The result indicated that there is a dependence of the *g* contrast on the size of *E. superba*, which can be synthesized by a linear regression versus the length *L* in mm (Lawson *et al*., 2006):

$$g = 5.439 \times 10^{-4} L + 1.002 \tag{2.9}$$

Since the authors claim a high degree of accuracy, the method may easily become as standard for future measurements.

It is important to note that Kristensen and Dalen (1986) found the specific density of *M. norvegica* linearly decreasing as the size increases[*]. This is also in opposition with the relation (2.9) and the length-based regressions obtained by Kils (1979b) from a set of measurements on *E. superba* and *M. norvegica* specimens lumped together but with most of the animals (112 over 190 specimens) of the latter species. As discussed in Paper I, this disagreement may be attributed to the very different environmental regimes where the two species live and especially significant differences in diet, *Euphausia superba* being herbivorous while the *M. norvegica* are omnivorous or primarily carnivorous during some period of the year (Saether *et al*., 1986).

2.4 The distorted wave Born approximation model

The distorted wave Born approximation (DWBA) is recognized as the state-of-the-art in the physics-based models predicting target strength from fluid-like crustacean zooplankton (Stanton and Chu, 2000; Demer and Conti, 2005). In few words, the prediction of the DWBA model is based upon the coherent summation of scattering from discredited cylinders of varying radius that reproduce the organism body shape when juxtaposed.

* Note the misprinting in sign for the relationships 4a and 4b in Kristensen and Dalen (1986) paper.

In 1968, Morse and Ingard introduced the general DWBA formulation that describes accurately the acoustic scattering by weakly scattering bodies with arbitrary size, shape, orientation, and material properties close to those of the surrounding medium (Morse and Ingard, 1968; Eq. 8.1.20, pag. 413). The formulation is complicated to determine because it involves an evaluation, either analytically or numerically, of the backscattering amplitude expressed by a three-dimensional integral within the volume of the body, in which the immersion-medium wave vector of the ordinary Born approximation is replaced by the internal wave vector in the integration volume.

An alternative approach to the DWBA, easier to calculate but still accurate, was introduced almost contemporary by Stanton *et al*. (1993) and Chu *et al*. (1993), and successively explicitly developed for deformed cylinder in Stanton *et al*. (1998c). The triple integral is numerically replaced by a line integral along the cylinder axis. This is possible with the following assumptions:

1. the animal is elongated and circular in cross-section at every point along a central curve running through its body;
2. the material properties only vary axially;
3. the scatterer has material properties that are close to the water and negligible elastic properties, i.e. weakly fluid-like scatterer.

Despite these restrictions, the DWBA model appears to be well-suited for a wide range of marine animals such as euphausiids and copepods (Stanton and Chu, 2000), shrimps and salps (Stanton *et al.*, 1996, 1998c), post-larval stage without swim bladder of some pelagic species (Miyashita, 2003) and squid (Jones *et al*., 2006; Lavery *et al*., 2007).

For an object that satisfies the assumptions above, two dimensions of the integration can be performed analytically within a cross section at any arbitrary point along the cylinder. Thus, the triple integral is reduced and the scattering amplitude f_{bs} can be predicted as by (Stanton *et al*., 1998c):

$$f_{bs} = \frac{k_1}{4} \int_{\vec{r}_{pos}} a\ (\gamma_k - \gamma_\rho)\ \mathrm{e}^{i2(\vec{\mathrm{k}}_i)_2 \cdot \vec{r}_{pos}}\ \frac{\mathrm{J}_1(2k_2 a \cos\beta_{tilt})}{\cos\beta_{tilt}}\ \left|\mathrm{d}\vec{r}_{pos}\right| \qquad (2.10)$$

where the *k*-subscripts 1 and 2 refer to the surrounding medium and to the fluid-like medium of the zooplankton body respectively, $\vec{r}_{pos}$ is the position vector along the lengthwise axis defining the cylindrical cross section, k_1 and k_2 are the wave numbers, $(\vec{k}_i)_2$ the incidence plane wave vector in the medium 2 ($=\vec{k}_2 = \vec{k}_1 / h$), a is the cross-sectional radius of the cylinder, J_1 is the Bessel function of the first kind of order 1, $\gamma_\rho = (\rho_2 - \rho_1)/\rho_2$ and $\gamma_\kappa = (\kappa_2 - \kappa_1)/\kappa_1$ where ρ is the density and κ the compressibility given by $\kappa_i = 1/(\rho_i c_i^2)$, β_{tilt} is the local angle between the incident wave and the cross section of the body at the point $\vec{r}_{pos}$. The material properties γ_k and γ_ρ are allowed to vary inside the fluid-like volume.

Equation (2.10) is the DWBA-based deformed cylinder formulation and it is similar in form to the modal-series-based deformed cylinder formulation presented by Stanton (1989a) and described in Appendix (Par. A1.2.1c). The differences lie in the fact that the DWBA is only accurate for weakly scattering bodies while the modal-series-based solution can describe a wide range of (axisymmetric) material profiles (elastic shelled body, etc.). However, the advantages of the DWBA formulation derive from the fact that, by the nature of its volume integration, it is accurate for all angles of orientation, in contrast with the modal-series-based solution, which uses modal series coefficients from an infinitely long cylinder and it is accurate only near broadside incidence.

In practice, Equation (2.10) involves the integration of a scattering function along the length of the axis of the body, while at the same time it takes into account the phase shift arising from the deformation of the axis (the exponential term) due to the curvature and the variations in cross-sectional radius.

As a good approximation, the density and sound speed contrasts can be held constant over the krill body, so that the processing is simplified. Certainly, the interior of a krill body is anatomically structured, but there is a general lack of published data available involving heterogeneities of the material properties, and the problem is open to further investigation.

2.4.1 Model parameterizations

In order to solve the Equation 2.10 numerical parameters describing the actual shape of the organism have to be introduced. Since it is still extremely difficult to generate an analytical formulation that fully describes the krill body shape as input for the DWBA model, the researchers have used two geometrical approaches both based on a discredited-bent tapered cylinder shape. These will be introduced in the next two sections.

2.4.1a Uniformly bent cylinder idealization

The krill shape may be idealized as a smoothly tapered uniformly bent cylinder with radius of curvature ρ_c. Thus, the exponent term of Equation (2.10) may be replaced by the relationship $(\vec{k}_i)_2 \cdot \vec{r}_{pos} = k_2\rho_c(1-\cos\beta_{tilt})$ (Stanton *et al.*, 1998c), and using the position $\left|d\vec{r}_{pos}\right| = \rho_c d\beta_{tilt}$, the integral can be performed numerically as the coherent summation of scattering from cylindrical elements of a discrete bent cylinder according to:

$$f_{bs} = \frac{k_1\rho_c}{4}\, e^{i2k_2\rho_c} \int a\,(\gamma_k - \gamma_\rho)\, e^{i2k_2\rho_c\cos\beta_{tilt}}\, \frac{J_1(2k_2 a\cos\beta_{tilt})}{\cos\beta_{tilt}}\, d\beta_{tilt} \qquad (2.11)$$

This represents the DWBA prediction of the scattering amplitude for an individual euphausiid at a given length and single angle of orientation θ, defined as the angle between the line joining the bent cylinder's ends and the horizontal plane. For an animal horizontally oriented in the water and the echosounder vertically aimed, θ is equal to 0°. At broadside incidence, the integral in Equation (2.11) can be performed using the method of stationary phase (Stanton *et al.*, 1998c). At angles away from normal incidence, the phases of the backscattering signals from each element become more important to the summation.

Actually, the body of a euphausiid is not uniformly bented. The dorsal line of the cephalothorax may be considered as a straight line while the abdomen is the primary bented part. Amakasu and Furusawa (2006) investigated the TS-pattern versus angle

of incidence with increased abdominal bending. The results showed that the main-lobe became broader, with maximum TS shifted to negative tilt, and the side-lobe levels increased. However, the idealization to a uniformly bent tapered cylinder replicates in first approximation the actual shape of a krill, and Stanton *et al*. (1993b) asserted that the backscattering cross section averaged over a range of angles of orientation is mostly independent from the cylinder's bend when a value of $\rho_c \geq 2L$ is estimated.

The cross-sectional radius can be incorporated in the model as function of position *z* along the axis. Defining z=0 the animal's midpoint and z=$\pm L/2$ at the animal's ends, the cross-sectional radius *a* can be calculated according to (Chu *et al*., 1993; Stanton *et al*., 1998a):

$$a(z) = a_0 \sqrt{1 - \left(\frac{z}{L/2} \right)^T} \tag{2.12}$$

where a_0 is the radius at the midsection, L is the cylinder length and T is the taper parameter controlling how quickly the cylinder tapers. Chu *et al*. (1993) set this parameter equal to 10 for euphausiids. The other morphometric scatterer properties may depend from the target species conditions. Chu *et al*. chose as radius of the deformed cylinder the value a_0=L/16, with L the total length of the animal measured from the anterior end of the eye to the tip of the telson, and the degree of bend of the animal's central axis characterized by the radius of curvature $\rho_c = 3L$.

Lawson *et al*. (2006) proposed a reasonable approach by using *in situ* observations during the survey to infer properly these key parameters in the uniformly bent cylinder idealization. The cylinder governing the generic krill shape can be simply described by the ratio between length and the cross-sectional radius a_0 and the radius of curvature ρ_c. The first could be determined from samples captured by nets, the second on the base of krill observations by video tools, for example a plankton recorder (VPR). In their analysis for *Euphausia superba* estimation in the Western Antarctic Peninsula, the authors used the values $a_0 = L/18.4$, $\rho_c = 3L$ and the tapered parameter T=10 in Equation 2.12. Still images also helped to derived the krill

orientation, while the physical contrasts *h* and *g* were calculated from the length relationships (2.8) and (2.9) respectively, as derived by Chu and Wiebe (2005) from *in situ* measurements. Lawson *et al*. (2008a) verified with success this parameterization in a multifrequency context.

2.4.1b Body reconstruction by digitalization

As practical alternative to the description of the body shape by the only length and radius of curvature, the animal's body may be discredited by digitalization of the main morphological structures in two-dimension (2D). The 2D approach is validated by the model assumption that the animal is circular in cross-section at every point along a central curve and extremely simplifies the digitalization operation and the model implementation.

The digitizing process implies to outline the dorsal and ventral animal surfaces from an image of a specimen in lateral aspect. A central line can be generated on the base of the digitized points so that the radius *a* and the position vector $\vec{r}_{pos}$ of a discrete body segment can be computed from each dorsal-ventral pair points. The number of digitized points required to characterize the body may vary from size and properties variability of the animal, as well from the spatial resolution of the acoustic wavelength of the frequencies (Stanton and Chu, 2000). In section 2.4.1c, a procedure for krill body reconstruction is suggested.

Other techniques to retrieve animal's shape information can be also used. Lavery *et al*. (2002) employed the DWBA to estimate the scattering as the volume integral over a fully 3-D representation of the decapod shrimps derived from computerized tomography.

Amakasu and Furusawa (2006) examined the opportunity to consider in the model the scattering from pleopods also by adding in the digitalized shape the points corresponding to these important swimming parts of the body. The results showed that the peak level of the side-lobe was increased, while the main-lobe part of the TS-pattern was decreased.

By using Equation (2.10) and digitalized shapes, McGehee *et al.* (1998) found a good fit between DWBA predictions and target strength measured at 120 kHz in a chilled tank on living individual krill in dorsal, ventral or lateral aspect with respect to the transducer. When the animal orientation was away from these aspect angles, the predicted scattering was much less than the measured scattering (5-20 dB). The deviations were explained theoretically by Demer and Conti (2003a, 2004a) using a modified probabilistic DWBA model, the so called *Stochastic DWBA* or SDWBA, which accounts for the stochastic nature of sound scattering and provides probabilities of TS versus all angles of orientation.

The SDWBA assumes that there is variability in the phases of scatter from the krill-scattering elements due to:

1. the stochastic scattering process in a field with noise;
2. the more complex krill shape than juxtaposed cylinders of varying radius;
3. the krill body that flexes as it swims.

Mantaining the same notation of Demer and Conti (2003), the SDWBA form function for θ angle of incidence is obtained by summing the components f_{bs} calculated for each of the N cylinders with a different random phase φ_j:

$$f_{bs}(\theta) = \sum_{j=1}^{N} \left(f_{bs}(\theta) \right)_j \exp(i\varphi_j) . \tag{2.13}$$

For each cylinder j along the body, the phase variability φ_j obtained from a number of realizations of a Gaussian distribution, centred in 0 and standard deviation sd_φ, is applied. When the frequency, the length L and number of cylinders N are given, the sd_φ of the j Gaussians can be estimated empirically by comparison of the SDWBA predictions to the experimental measurements. The backscattering cross section is then obtained from the average of multiple realizations of the ensemble of phase φ_j:

$$\sigma_{bs}(\theta) = \left\langle \left| f_{bs}(\theta) \right|^2 \right\rangle_\varphi . \tag{2.14}$$

On the base of relevant indications (Demer and Conti, 2005; Amakasu and Furusawa, 2006) the SDWBA model have been suggested to be endorsed by the CCAMLR as the Antarctic krill TS model (SC-CAMLR, 2005), as well for the Northern krill *Meganyctiphanes norvegica* (Conti *et al*., 2005a).

McGehee *et al*. (1998) proposed a generic krill shape by digitalizing an *E. superba* specimen of 38.35 mm length from a still image of a video (Table 3 and Figure 7 in the paper), which can be scaled by length to simulate other krill sizes. Investigators have used this last procedure to validate their data (e.g. Conti and Demer, 2006). However, the krill have broadly varying shapes, depending upon their feeding conditions gender and maturity shape, as well as the slightly allometric growth of volume with size (Kils, 1979a). Moreover, the way in which the animals are treated must also be considered. Demer and Conti (2003a) found that freshly caught animals were 40% fatter than the six months starved animals measured by McGehee *et al*. (1998), and suggested to take into account this increment in the computations. In Figure 2.9, the scattering patterns versus angle of incidence for 70, 120 and 200 kHz are shown. It is evident that for same organism length and shape the higher frequencies are more influenced by the orientation.

Demer and Conti (2003a, 2004a) found that the best fit with the empirical data was inferring on the cylinders a phase variability φ_j from 100 random realizations of a Gaussian distribution, centred in 0 and standard deviation $\mathrm{sd}_{\varphi 0} = \sqrt{2}/2 = 0.7071$. The results reduced substantially the dramatic increasing of the krill directivity with animal length and high changes in TS of 10-40 dB versus animal orientation angles previously predicted by the DWBA model and evident in Fig. 2.10. The SDWBA prediction shows a flattening of TS in the side-lobe region, while the DWBA main lobe values are almost not affected[*]. The latter is independent from the applied sd_{φ} (Conti and Demer, 2006).

* The backscattering patterns in Figure 2.10 are different from those showed by Demer and Conti (2003a). For the integral evaluation of Eq. (2.10), the authors used a Matlab function named “quadl” that was inaccurate in software version 6.5 since not intended for the use on complex integrands at that

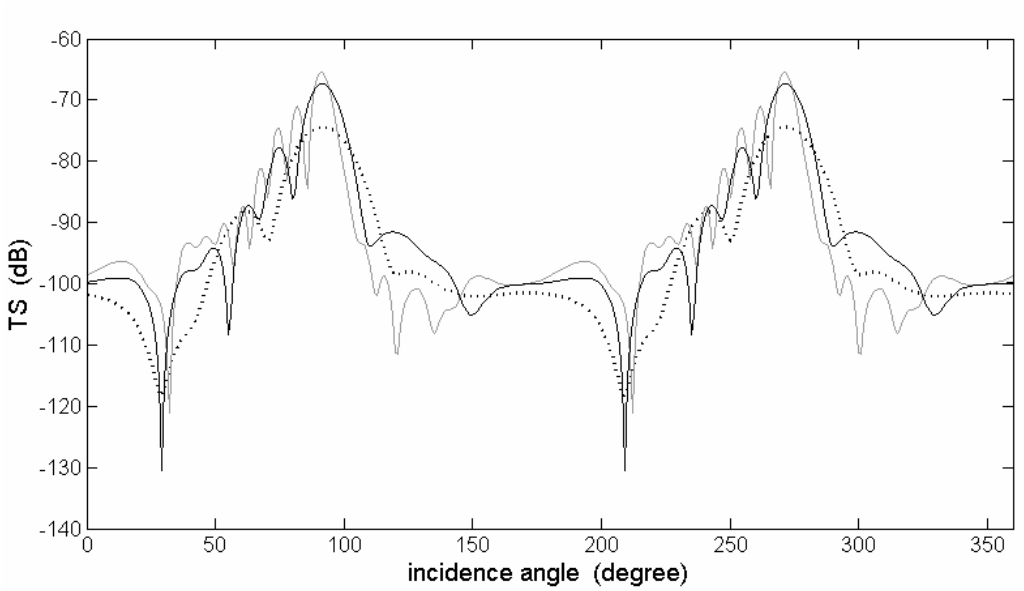

Figure 2.9: *DWBA scattering pattern versus angle of incidence at 70 kHz* (*dashed black line*), *120 kHz* (*black solid line*), *and 200 kHz* (*grey line*) *for the krill standard shape of length L=38.35 mm proposed by McGehee et al. (1998). The key parameters are*: $c=1500\ ms^{-1}$, *digitalized points in Table 3 of referred article, h=1.0279 and g=1.0357.*

Conti and Demer (2006) have also shown that the SDWBA predictions are stable if the number of cylinders *N* is large relative to the ratio of organism length to the acoustic wavelength. Employing the same sd_{φ} for different frequencies, unrealistic off-axis lobes in the TS predictions may be obtained. Hence, in order to ensure general utility of the SWDBA model, the authors proposed an improved parameterization that takes explicitly into account the effects of the interdependence of the four model factors: operative acoustic frequency, length of krill, number of discretized-bent cylinders and amplitudes of inter-element phase variability, and expressing the latter as function of the others.

time (Matlab supporting team, personal comm.). The patterns in Figure 2.10 are evaluated running Matlab version 7 with new function "quadl" corrected for complex integrands and for this reason the same figure is shown here. Dr. David Demer has been informed of that inaccuracy.

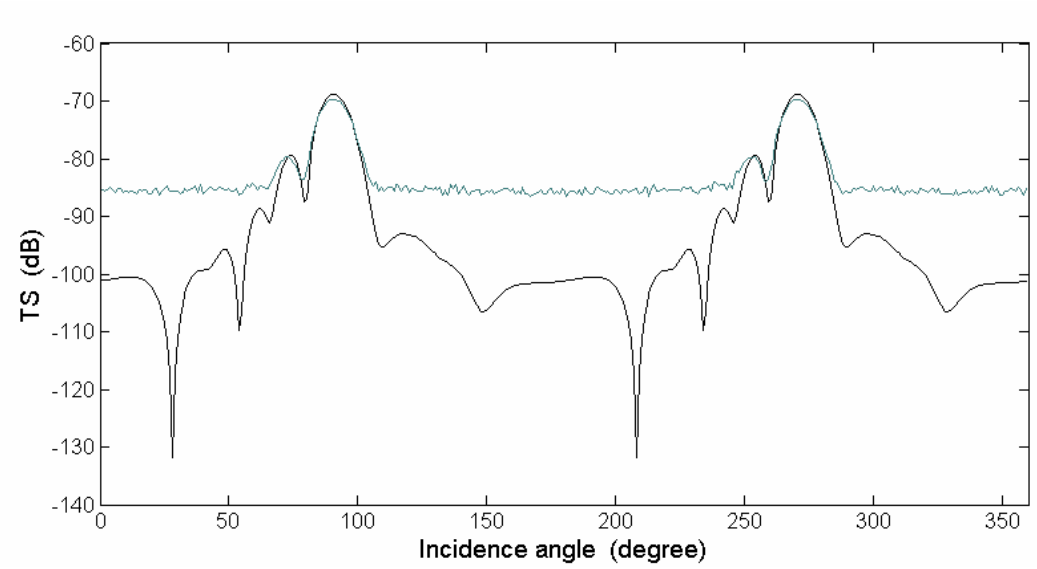

Figure 2.10: *the DWBA (black line) and the stochastic-DWBA (grey line) scattering patterns versus angle of incidence. The key parameters are standard McGehee et al. (1998)*: $L=38.35$ *mm,* $c=1500$ *m*s^{-1}, $f=120$ *kHz, shape in Table 3 of that article,* $h=1.0279$ *and* $g=1.0357$. *The SWDBA is solved with the standard deviation phase variability* $\mathrm{sd}_{\varphi}=0.7071$ *with TS values computed from* σ_{bs} *averaged over 100 realizations of the random phase.*

Again, this general parameterization is based on the parameters used by McGehee *et al.* (1998) to delineate the generic krill body shape and related empirical results. The SWDBA representation for general applications can be obtained from the following basic parameters:

1. the dimensional values governing the generic krill shape defined by McGehee *et al.* (1998): $L_0 = 38.35$ mm, $N_0 = 14$ cylinders, with width increased of 40 % (Demer and Conti, 2003a);
2. the McGehee *et al.* (1998) reference frequency: $f_0 = 120$ kHz;
3. the standard deviation of phase variability φ estimated from comparison of the SDWBA prediction to the experimental measurements by Demer and Conti (2003a): $\mathrm{sd}_{\varphi 0} = \sqrt{2}/2$.

Since the complexity of the body is frequency-dependent, the results in frequency domain over a range of possible orientations are comparable if the product $f_0\,\mathrm{sd}_{\varphi}(f)$ is kept constant, hence with reference to the basic parameters equal to $f_0\,\mathrm{sd}_{\varphi 0}$. In

addition, the spatial resolution of the digitalized body shape must remain constant relatively to the acoustic wavelength. This means that the dimensional ratio involving the length of the animal *L*, the number of cylinders *N* and the wavelength λ ($L/N\lambda$) should be kept equal to $L_0/N_0\lambda_0$. Combining the two positions, the standard deviation of φ and *N* can be adjusted on the base of *f* and *L* according to (Conti and Demer, 2006):

$$N(f,L) = N_0 \frac{f\ L}{f_0\ L_0} \quad ; \qquad sd_\varphi(f,N) = \mathrm{sd}_{\varphi 0} \frac{N_0 L}{N(f,L)L_0}. \tag{2.15}$$

However, the accurate application of the generalized SDWBA model still requires precise information on the orientation distribution and the specific density and sound speed contrasts.

In Figure 2.11, a comparative example of the DWBA and SDWBA TS predictions evaluated for different Gaussian distributions of orientation ($\theta = \mathrm{N}[\bar{\theta}, \sigma_\theta]$ in degrees) reported in recent works (Table 2.I) are shown. The plots can be compared with results from other models shown in Appendix (Figures A.5, A.6 and A.7).

Recognizing uncertainty in the orientation distribution, Demer and Conti (2005) provided a simplified SDWBA version. The expressions (2.10), (2.13) and (2.14) suggest that the TS prediction of SDWBA could be concisely expressed as a function of the product of the acoustic wave number *k* and the mean length *L* of the animals under investigation. The function TS(*kL*) could be expressed by a sixth order polynomial representation and estimated over determined krill orientation distributions. Inverting the SDWBA model in a least-squares sense over volume back-scattering strength measurements at 120 and 38 kHz and net samples from survey data in the Scotian Sea (Hewitt *et al.*, 2002), Conti and Demer (2006) found that the $\mathrm{N}[11°, 4°]$ distribution of orientation gave the better fit to the *in situ* acoustic data. Consequently, averaging the TS(*kL*) function over such distribution they obtained the standard coefficients for convenient estimation of Antarctic krill TS. Presently, this specific polynomial representation is proposed as the model to be endorsed by the CCAMLR for the Antarctic krill predictions (SC-CAMLR, 2005). Regarding this,

Lawson *et al*. (2008a) claimed that, although attractive, the distribution of orientation and the "fatness" polynomial coefficients used to parameterize the SDWBA by Conti and Demer were obtained by fitting the model with empirical results rather than by direct measurements of all necessary parameters obtained during the actual survey.

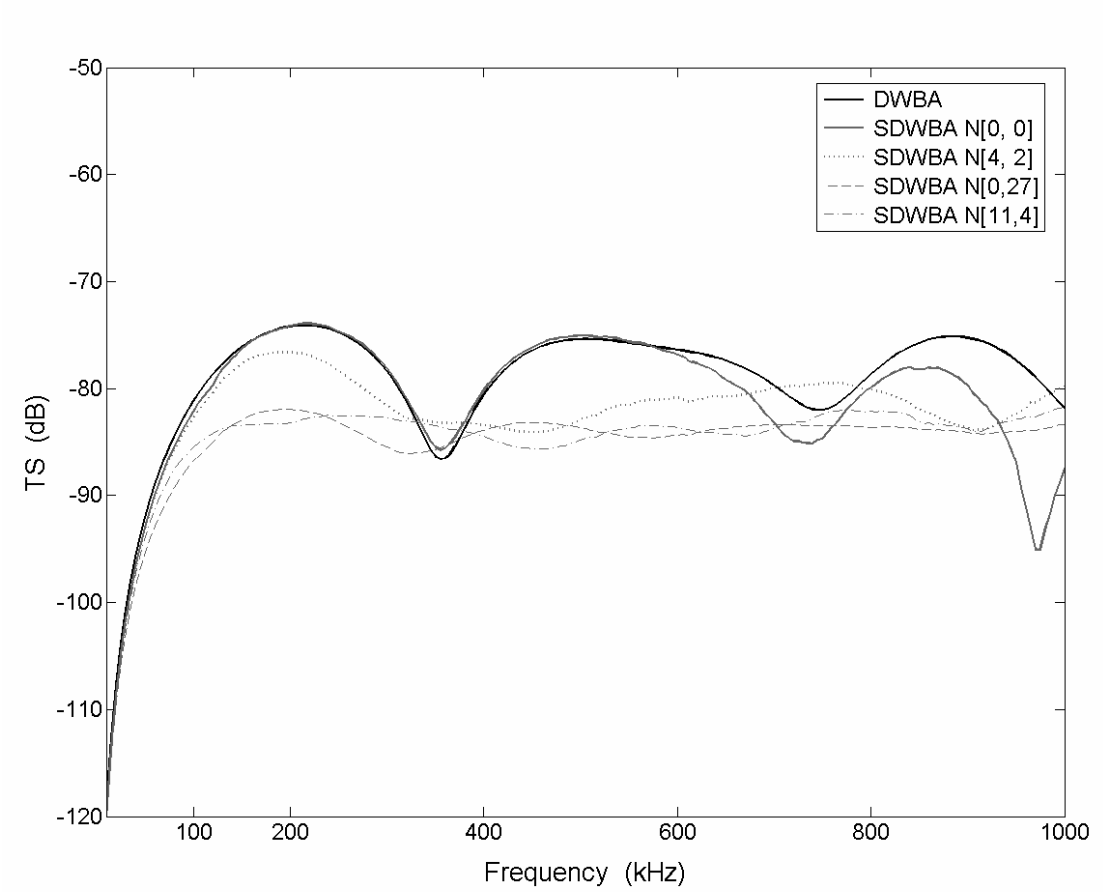

Figure 2.11: *Broadside backscattering DWBA* (*black line*) *and SDWBA* (*grey solid line*) *TS-predictions versus frequency for an individual krill of 23 mm length. The other SDWBA predictions are evaluated for different Gaussian distributions of orientation* $\theta = N[\bar{\theta}, \sigma_\theta]$ *in degrees. The animal shape was scaled from the proposed McGehee et al*. (*1998*) *standard shape and increased by 40 % in width* (*Demer and Conti 2003b*). *The sound speed was* $c = 1500\ m s^{-1}$, *and the contrasts h=1.0205 and g=1.0145 as calculated from of the length relationships 2.8 and 2.9. The SDWBA predictions were solved applying Equations* (*2*.15) *with standard reference parameters indicated in the text. The TS values were computed from* σ_{bs} *averaged over 100 realizations of the random phase*.

2.4.1c A krill body digital reconstruction

In this paragraph, a reconstruction procedure based on the digitalization approach is suggested and described in details. It was used to produce digitalized body shapes of *Meganyctiphanes norvegica* specimens for the model computation presented in Paper V, where it is also described in detail.

To the writer knowledge, examples of krill body digitalization for the DWBA model have been presented in only two published works: 1) McGehee *et al*. (1998) briefly described the digitalization procedure employed on Antarctic krill; the result has been used as standard generic krill shape from other authors to simulate different size krill; 2) Amakasu and Furusawa (2006) presented 12 digitalizations for the same species in a length range of 40.5-51.35 mm, and one animal of 30.3 mm length. The authors did not describe the extrapolation procedure adopted, but, from their Figure 6, it can be supposed that they used a different approach from McGehee *et al*. (1998). It must be emphasised that the digitalization is an operator dependent procedure, at least in the first step. The procedure described below has been arranged in order to reduce as much as possible this dependence.

The first step is to produce a picture showing the animal in lateral view including a metric rule that will be useful for the pixel-to-metric conversion; Figure 2.7 shows an example. On the picture, two body limit-points, one corresponding to the tip of telson and the second to the joint where the peduncle of the first antenna ends, are chosen; they will act as tapered points of the bent cylinder adopted by the model. A vertical grid is then superimposed to the image, and the digit points of the dorsal and ventral body borders intersecting the vertical lines are retrieved.

By retrieving two digit points at 1 cm distance on the rule (Fig. 2.7) and calculating the difference between the horizontal pixel numbers, the conversion factor from pixels to actual centimetre values is determined. Correction for the rule's inclination on the picture can be easily evaluated if needed. With all the points converted in length units, an X-Y Cartesian coordinate system, with zero abscissa and ordinate in

the x-coordinate and y-coordinate of the front and tail tapered points respectively, is established.

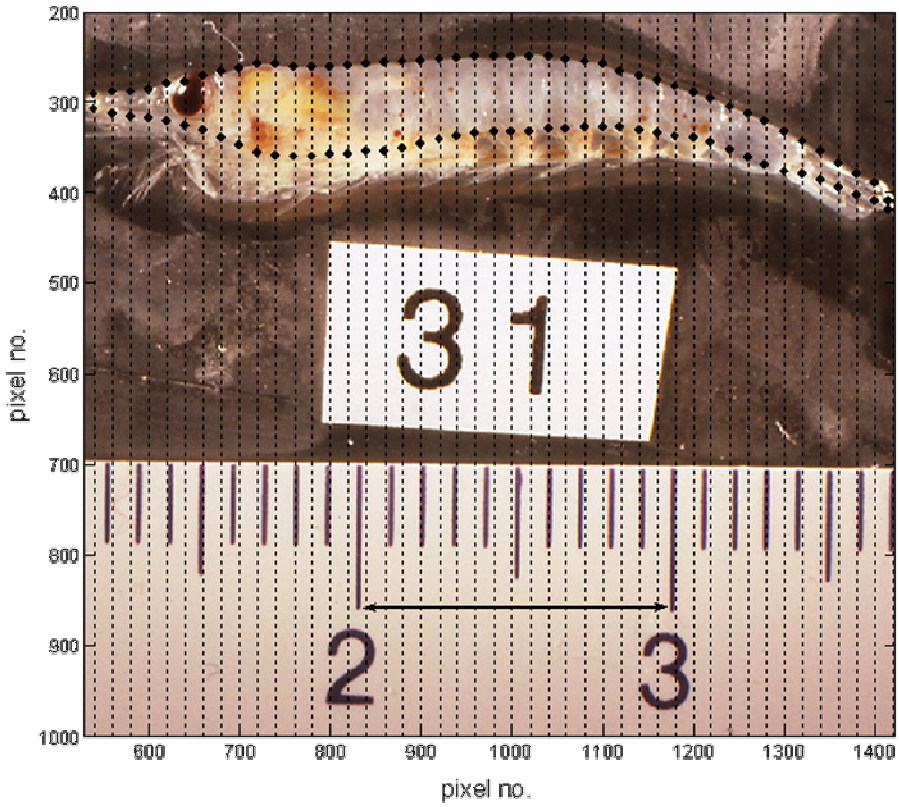

Figure 2.7: *Example of a picture with superimposition of the vertical grid for the extrapolation procedure.*

All the points are then shifted algebraically on respect to those origin coordinates (Figure 2.8a). For each couple of borders points with equal x-coordinate the middle point is calculated. By using the set of middle points, a segmented central line can be generated (Fig. 2.8a). Starting from the tapered-tail point, the line normally intersecting the central segment from each dorsal point is calculated and the intersection point determined. The limits of a single segment are two middle points: the first corresponding the related dorsal point, the second is the next or the previous, depending if the next dorsal point is higher or lower in y-coordinate. The distances between the dorsal points and the intersection points (× markers in Figure 2.8a) will compose the radii array related to the discretized-bent cylinders representing the entire body. In Figure 2.8a, the new ventral points are also plotted with × markers; they are determined along the intersection lines at two times the radius from the

related dorsal points. However, these points are not used in the DWBA processing. Figure 2.8b shows the reconstruction of the body based upon the extrapolated points superimposed to the original image. It can be noted a slight correction on the front part of the body due to the unnatural position when the animal was photographed. The purpose of the digitalization in the DWBA context is to provide the dorsal positions and the related radii vectors arrays utilized as input to the model. In Figure 2.8c, the result of the reconstructed body shape in Figure 2.8b is shown. They are superimposed to the discretized cylinders cross sections in X-Y plane to verify qualitatively how they approximate the acoustically significant animal's body parts.

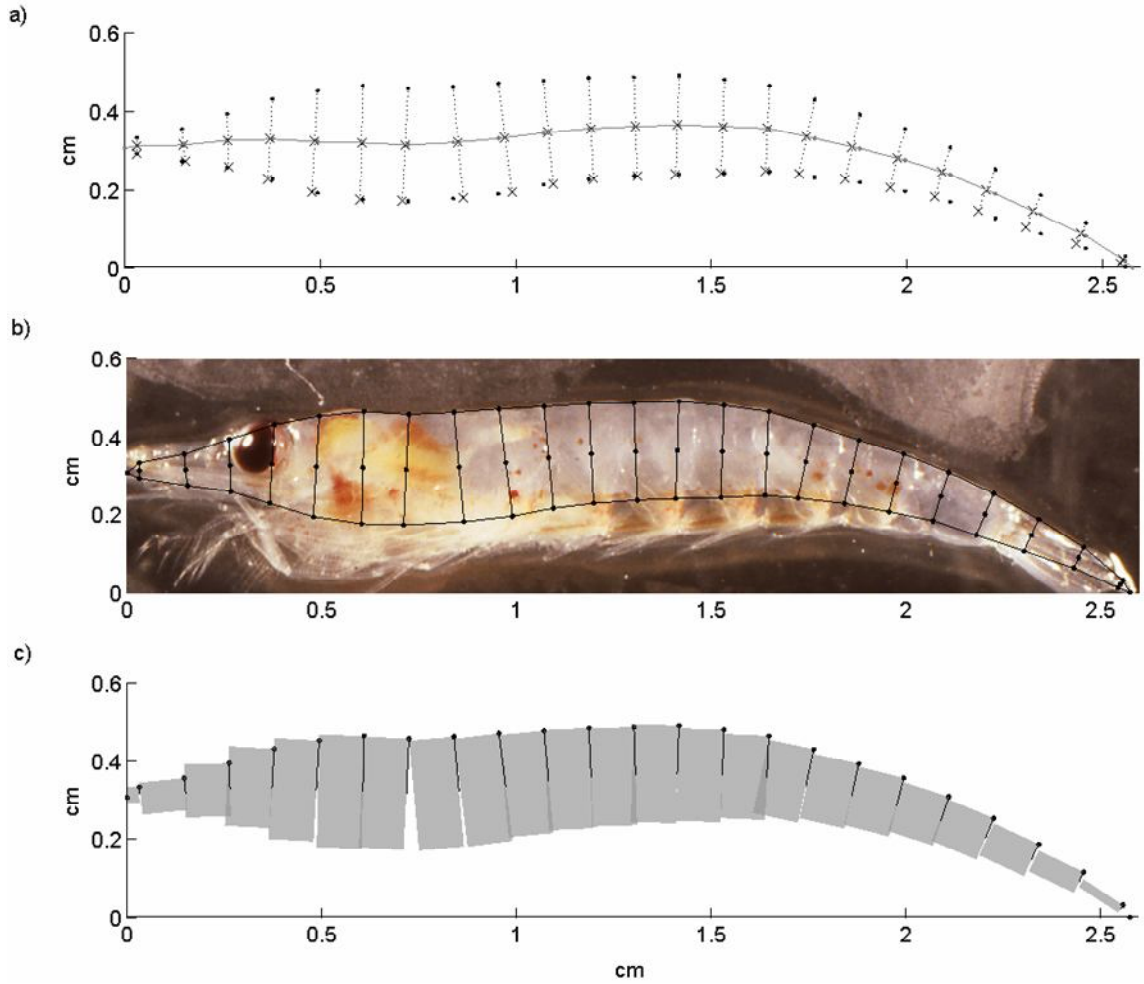

Figure 2.8: *Digitalization procedure in the X-Y plane.* a) *Description of the extrapolation procedure. The dorsal and ventral points are plotted as black dots, the grey dots are the middle points, the solid grey line is the generated segmented central line, the intersection lines are represented by the dashed lines, and the new central and ventral points by the black* × *markers*. b) *Reconstruction of the body based on the extrapolation superimposed to the original image*. c) *Graphical verification* (*grey patch*) *and final position points* (*black dots*) *and related radii* (*black solid lines*) *as will be used in the DWBA model calculation.*

3. Direct measurements on Northern krill in a mesocosm

The Northern krill *Meganyctiphanes norvegica* (Sars, 1857) in Figure 3.1 plays an important role in the ecosystems of the North Atlantic and adjacent seas (Mauchline and Fisher, 1968; Boysen and Buchholz, 1984), as well as in Mediterranean Sea (Labat and Cuzin-Roudy, 1996). This indicates that the *M. norvegica* populations are adapted to very different environments and trophic conditions. There are also indications that occasionally it has been found in the south western part of the North Sea and southwards to North Africa (Mauchline and Fisher, 1969), when the water temperature in February-March is lower.

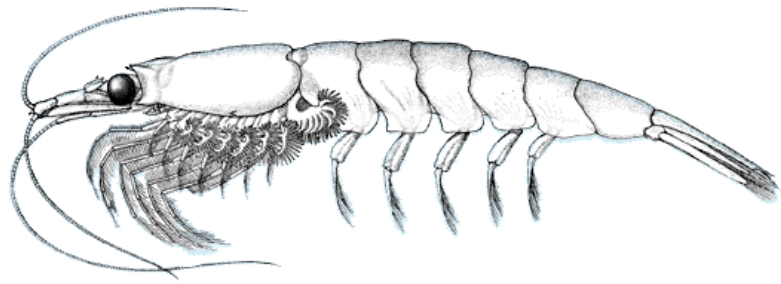

Figure 3.1: The "Northern krill" *Meganyctiphanes norvegica.* (Einarsson, 1942)

M. norvegica stays commonly between 100-400 m during the day and migrates to the surface at night in most regions (e.g. Tarling *et al*., 1999), especially in the coastal waters (Kaartvedt *et al*., 2005; Dalpadado, 2006). It is a large aggregating species and is the food of whales, seals, fish, squid, decapods and birds, particularly in coastal regions. It can reach 45 mm in length and the organism is classified as adult when becomes longer than 22 mm (Dalpadado, 2006), which is related to about one year of age, and becomes sexually mature to breed for the first time. *M. norvegica* may survive close to 3 years, breeding each successive year (Mauchline, 1980) with predicted egg-batch size ranging from 200 to 4000 eggs (Cuzin-Roudy, 2000).

There is an increasing interest on studying the *M. norvegica* in terms of ecological problems (e.g. Dalpadado, 2006), and its exploitation in aquaculture (e.g. Suontama, 2004), due to the growing demand for raw materials for marine feedstuffs and the search for new feed resources. The zooplankton contains lower amounts of environmental toxins than organisms from higher up in the food chain; therefore, it is a preferable feed with respect to the traditional fish raw material used in aquaculture feedstuffs.

M. norvegica is present in huge quantities in North Atlantic. As for its homologous in the Southern Pole the *Euphausia superba*, it is in general thought that moderate levels of harvesting would not significantly affect the amount of food available to fish and marine mammals. However, in order to study the ecological consequences of harvesting in lower trophic levels and prior to recommending the quantity that can be harvested, it is essential to map its distribution and production accurately.

Conti *et al*. (2005a) emphasized similarities in shapes and maturity stages between Northern and Antarctic krill. They found similar values in total target strength, i.e. acoustic energy scattered by an object in all directions, and suggested the *Meganyctiphanes norvegica* as an acoustic organism model for the Antarctic krill. In particular, it is generally more accessible to researchers increasing the possibilities for studying changes in TS due to variation in size, shape and orientation.

Few results of direct acoustic target strength *in situ* on *Meganyctiphanes norvegica* have been presented in literature (Kristensen, 1983; Klevjer and Kaartvedt, 2003; 2006; Everson *et al*., 2007), and with the *ex situ* approach (Kristensen, 1983; Kristensen and Dalen, 1986; Stanton *et al*., 1998c; Conti *et al*., 2005a). Some indication can be also found in Richter (1985a), Greene *et al*. (1989), and Stanton *et al*. (1994b, 1998b)

With the present new acoustic technologies, such as the Simrad EK60 multifrequency scientific echosounder, and applying established procedures and techniques from aquaculture (van der Meer *et al*., 1994), it was possible to get accurate direct

measurements over a wide acoustic frequency range from free-swimming organisms in a wide but limited volume under highly monitored conditions (mesocosm).

A novel experimental set-up for direct multifrequency acoustic measurements of free-swimming krill was established at the Austevoll Aquaculture Research Station of the Institute of Marine Research (Norway) in the period from 20th of January to 2nd of April 2004. A large cylindrical enclosure, vertically suspended in the sea from a raft, was established. After the introduction of a near mono-specific ensemble of living *Meganyctiphanes norvegica*, a set of experimental exercises, including the response of krill to a manipulated artificial light regime as well as measurements on individual tethered animals were performed. Further, results from the EK60 system performances tests, data acquisition procedures and individual measurements were examined.

3.1 The experimental site

The Austevoll Aquaculture Research Station of IMR was established in 1978. It is located on the east coast of Huftarøy, the main island of Austevoll municipality in the Hordland region, Norway.

The station consists of a total indoor area of 4500 m^2 with offices, analytical and experimental laboratories and several outdoor tank facilities. The main research facilities are located in *Sauaneset*, where there are different fish tanks and other facilities such as algae and artemia production, hatchery room, larval silos, start feeding and weaning systems, ongrowing- and broodstock tanks and sea cages.

The staffs consist of circa 45 persons, including scientists, research technicians, administrative staff, students and trainees. The main working tasks is to deal with IMR's goals related to aquaculture of marine species like Atlantic Halibut, Atlantic Cod, Great Scallop, Atlantic Salmon, Wrasses, Hake and Haddock. The research areas deal with fry production, reproductive biology, growth and maturing and include some works related to health and diseases in intensive aquaculture. Moreover,

IMR projects involving acoustic measurements on living encaged fish have been carried out at the station for several years. For this reason, the location is a well-tested area from an acoustic point of view.

An open raft, located in a small bay well protected from severe waves, currents and wind, was chosen as an appropriate site to establish the mesocosm. It is commonly called *GIGA raft,* with dimensions of approximately 16×16 m, and it is connected to the shore by a bridge of about 20 m length (Fig. 3.2). The Giga raft is built to support 4 cages of 6 m diameter, a small wooden cabin as workshop and a zooplankton collector with seawater pumped by an electric pump. The depth around the raft is 11 metres during high tide period, with a change of approximately 0.5 m at low tide.

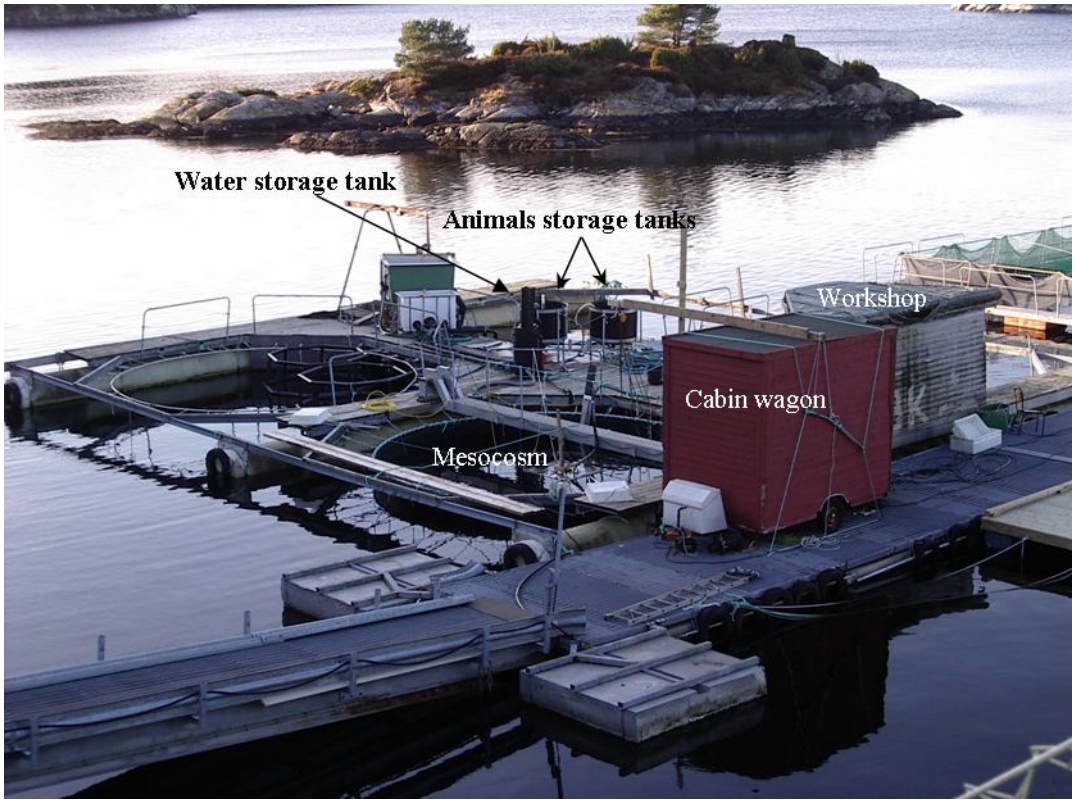

Figure 3.2: *The GIGA raft during the measurements*.

The complete preparation of the mesocosm took two and half weeks. With the invaluable help of Eng. Arve Kristiansen the hydraulic system connection from the central pipe to the raft and the mesocosm in all its parts were established and got ready for the use.

A cabin wagon was placed on the bridge close to the raft, and used as monitoring central board for the experiments. All the electronic devices (PC and transceivers) were there installed and kept safe from adverse weather conditions.

3.2 Mesocosm set-up and monitoring

The mesocosm consisted of a cylindrical-conical enclosure or "bag" of black coloured polyethylene sheeting (three-layer woven PEL with total thickness of 0.15 mm), tapered in the bottom region and suspended in the sea. The overall dimensions of the bag were 6 m of diameter and 8 m deep, with a cylindrical upper part and conical lower part of 5 m and 3 m length respectively, giving a nominal volume of 170 m^3. The complete mesocosm set-up is schematised in Figure 3.3.

The material composing the bag was flexible and impermeable, and the black colour was chosen in order to give the organisms the illusion of being at open deep sea. The bag was suspended vertically oriented in the sea, fastened from its upper edge with a rope to a circular stainless steel ring of 6 m diameter connected to the raft by steel cable and ropes. This means that the raft and bag constituted a single system floating on the sea surface. An aluminium footbridge, placed across the bag slightly off centre, allowed easy access to the measurement venue. Since the distance between the ring and the sea surface was 0.32 m, the exact water volume inside the bag was 160.6 m^3.

In order to insure oxygenation and water circulation in the bag, a hydraulic system was established, being operative during the entire experimental period (Fig. 3.3). More details on the hydraulic system parts and inflow rate can be found in Paper II, Paper IV.

For temporary storage of a small fraction of captured animals, two separate 500-litre seawater tanks placed on the raft to the side of the mesocosm were installed (Fig. 3.2). The two tanks were connected to the same seawater system supply of the mesocosm. A slow ingoing flow was kept by means of a hydraulic valve, and the

extra water in the tanks was simply overflowed via a meshed outlet close to the top of the tanks.

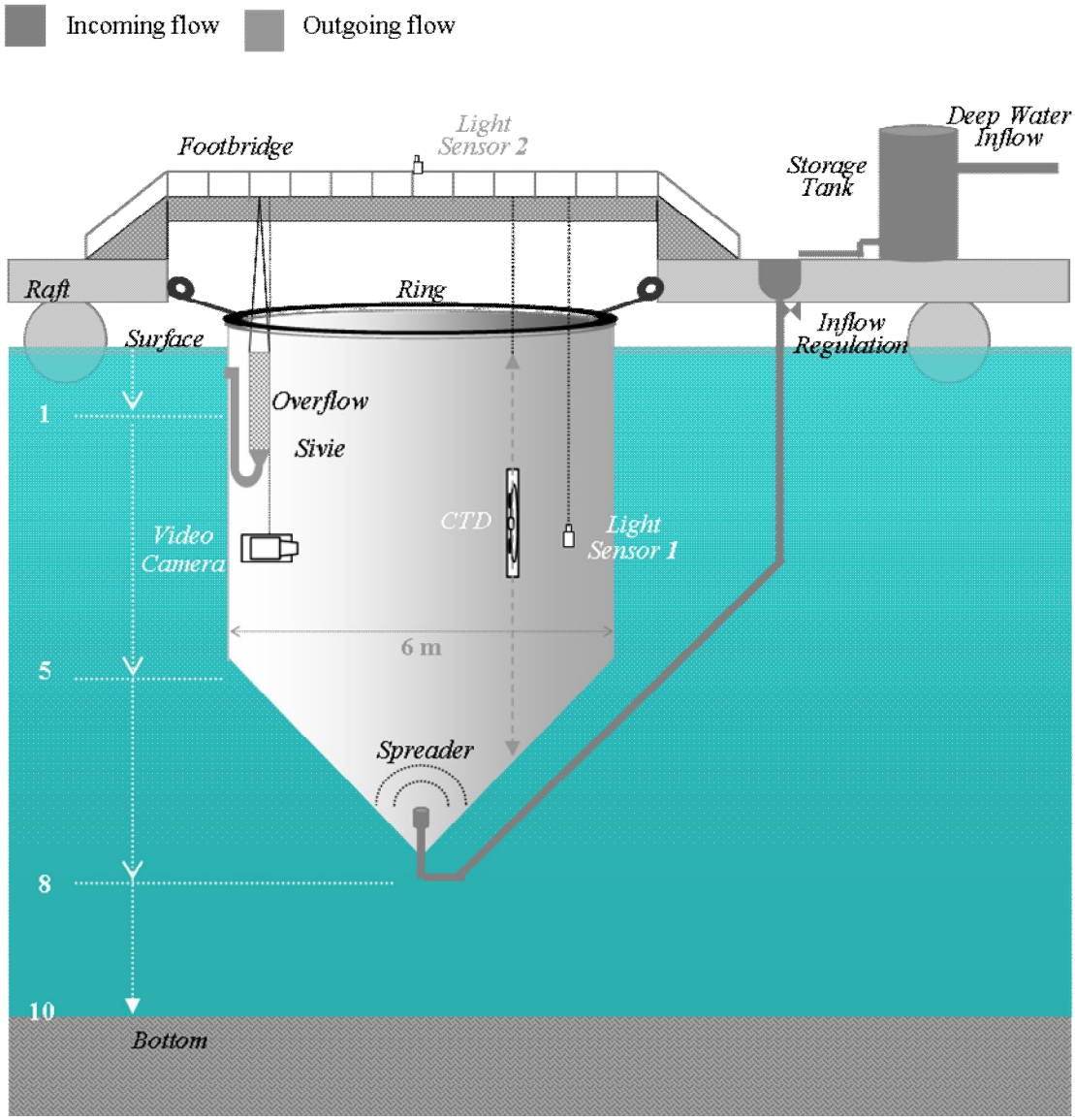

Figure 3.3: *Mesocosm set-up and monitoring schematization.*

To monitor the physical condition of the mesocosm environment different sensors were used. The LICOR light meter system LI-1000 was used to monitor the light intensity during the measurements. Two light sensors were connected to the system: an underwater sensor placed at 4 m depth inside the bag and an air light sensor placed on the footbridge (light sensor 1 and 2 in Fig. 3.3) corresponding to the centre of the bag.

A Simrad Video Camera (SitCam) was also deployed when needed and videos recorded on VHS tapes. Video record was supposed to provide useful information for the estimation of the krill density in the mesocosm volume. Unfortunately, video-recordings were not useful as expected since the sensitivity of the camera and the quality of the images were too low. The camera-rig was acoustically detected if positioned too close to the beams; when outside the acoustic beams, the camera did not supply sufficient information. However, the video filming provided valuable information on the general animal behaviour and the monitoring of the submersed devices when needed.

The temperature and salinity of the internal and the surrounding water to the bag were monitored generally every second day using a calibrated Gytre Mini CTD SD202. Then, the mean values were calculated and inserted in the editable EK60 environmental parameter menu that automatically updated the sound speed to be used in the acquisition processing. From the 2nd of February to the 4th of April 2004, 22 CTD casts were performed; the raw data are shown in Figure 3.4.

Within the entire experimental period, it was found a slight increase in temperature and salinity, from 5.8 to 7.2 °C and from 34.8 to 35.2 psu respectively. This corresponds to a change in sound speed from approximately 1470 to 1480 $m s^{-1}$. The results in Figure 3.4 clearly indicate that, apart from the first meter influenced by the air-water interface exchanges, the mesocosm consisted always of homogeneous water mass in the depth layer from 0.5 to 6 meters, with almost constant temperature and salinity.

3.3 Acoustic system and data processing

The scientific echosounder used for the measurements was a multifrequency system Simrad EK60 (Andersen, 2001). The basic part of the system is the General Purpose Transceiver (GPT), where the signal processing is performed independently at each frequency.

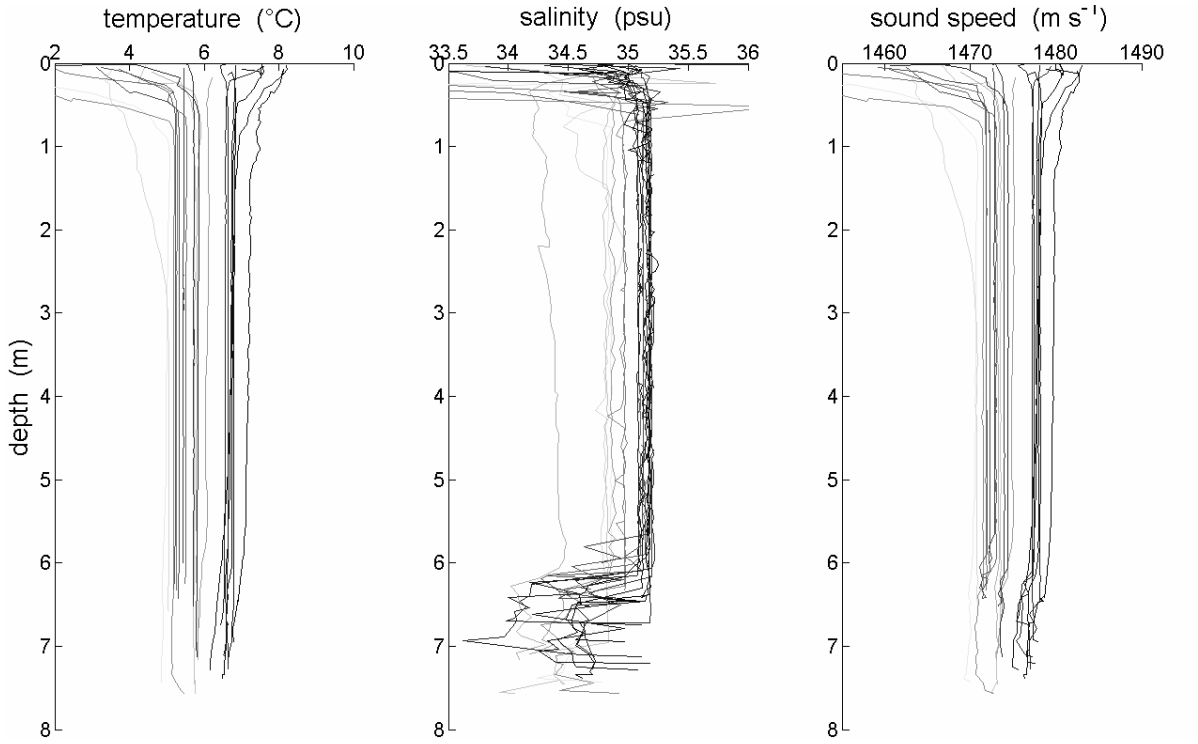

Figure 3.4: *CTD results and indirect sound speed determinations along the mesocosm column water from the 2nd of February (light grey) to the 4th of April (dark grey) 2004.*

The set-up, the acquisition and the storage of data are PC controlled via Ethernet connection by means of the ER60 software, which is part of the entire EK60 system. Seven transmitting frequencies can be run simultaneously with the choice of 5 different pulse durations for each frequency, and without instability in power transmission due to the high duty cycle (Medwin and Clay, 1997), also called "ping interval effect". The angular target resolution (Demer *et al.*, 1999; Reynisson, 1999) is 180/128 electrical phase step degrees per unit (Simrad, 2003).

In receiving mode, the EK60 works by a ping-to-ping process. The basic input parameters are the sound speed c in $\mathrm{m s^{-1}}$ and pulse duration τ in seconds, which define the received resolution length ($=c\tau/2$) in meters (Simmonds and MacLennan, 2005). The entire EK60 Signal Flowchart is shown in Figure 3.5 and systematically described in the Material and Methods of Paper III.

An array of i samples representing the echo signal is realized, and collected and stored in the EK60 raw data file readable by the post-processing software.

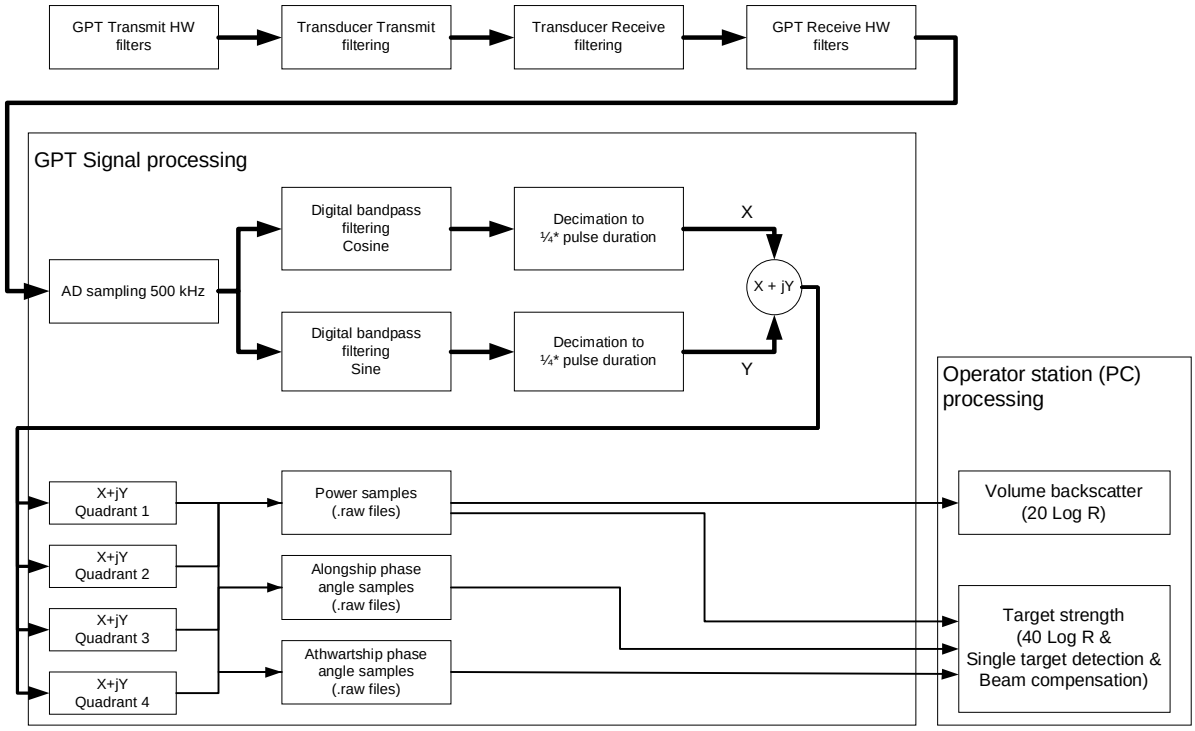

Figure 3.5: *Simrad EK60 receiving signal-processing steps*. (Illustration kindly consented by Lars Nonboe Andersen on behalf of Simrad AS).

Denoting with R_{max} the operator-defined maximum detection range, a number of $i = R_{max}/\Delta r$ samples per ping will be recorded in the raw file. The post-processing software is then demanded to analyse the raw file applying the TVG functions, run the Single Echo Detector (SED) algorithm as well as operate the Beam Compensation. The raw data can be replayed by means of the ER60 and a new raw file can be also generated with new setting of some parameters.

Six EK60 GPTs operating at 38, 70, 120, 200, 364, 710 kHz, and corresponding transducers were used. All transducers were of the new composite type, except the 38 and 710 kHz, and all were with nominal 7° beamwidth split-beam transducers, except the 5° single beam at 710 kHz. The nominal efficiency and angular sensitivity (Reynisson, 1999) in both alongship and athwartship planes of the split-beam transducers were 70 % and 21.9 for the 38 kHz transducer, and 75 % and 23.0 for the others. The ratio between the electrical phase step and the transducer angle sensitivity defines the angular resolution (Demer *et al.*, 1999), being equal to 0.064° for 38 kHz

system and 0.061° for the others. Table 3.I summarizes the acoustic systems and some significant setting parameters.

Table 3.I: EK60 Systems: types and parameters set-up. The nearfield was indicated from Are Johansen on behalf of Simrad AS. The wavelength and bandwidth are for 1480 ms^{-1} sound speed and 0.256 ms pulse duration.

system (kHz)	transducer type	central frequency (kHz)	wavelength (cm)	nearfield (m)	transmitted power (W)	receiving bandwidth (kHz)
38	ES38-B	38.095	3.95	2.7	600	3.68
70	ES70-7C	70.175	2.14	1.5	300	6.16
120	ES120-7C	121.212	1.25	0.9	250	8.71
200	ES200-7C	200.000	0.75	0.5	120	10.64
364	ES400-7C	363.636	0.41	0.3	40	11.84
710	710-30-EP	714.286	0.02	< 0.2	100	12.32

The 70 kHz transducer was the second realized by Simrad AS with this technology. The 364 kHz GPT was usually operating on the research vessel “G.O. Sars” of IMR. It is a modified version of the 400 kHz GPT arranged by Simrad AS under the IMR request to operate with frequencies which are not multiple harmonics of another placed on the same platform (Korneliussen *et al.*, 2008).

Simrad AS arranged the 710 kHz GPT for these specific experiments. Normally, the commercial versions of the EK60 systems are not able to operate with single beam transducers. This special version of GPT permitted to use the 710 kHz single beam transducer, but without the opportunity to select other transmission powers than 100 W. This might affect the 710 kHz data by no linear effects (Pedersen, 2007).

Low transmit power values were set to avoid potential non-linear effects (Tichy *et al.*, 2003; Pedersen, 2007; Korneliussen *et al.*, 2008). Ping rates and pulse duration were set depending of the type of measurement. Generally, the maximum ping rate (Simrad, 2003) and pulse duration of 0.256 ms were used.

3.3.1 The transducers rig

The transducers were mounted on a carefully fabricated aluminium plate (90 x 110 cm and 5 mm thick) as close to each other as space permitted in a minimum packing distance (Fig. 3.6). In collaboration with Tor Knutsen of IMR, the guidelines of the rig design were indicated to Harald Fitje and his assistants at the IMR's mechanical workshop, who contributed with some mechanical solutions and made the complete installation.

The acoustically active transducer surfaces were aligned at the same distance of 9.3 cm from the base of the aluminium plate, sitting on the same horizontal plane. The split-beam transducers were also aligned with identical orientation.

In order to make the transducers rig floating, a 5 cm thick divinycell plate was mounted between the aluminium plate and the transducers, and form-cut of the same material were also inserted to fill up empty space between the transducers. The divinycell is an overall suitable material to reduce back radiation from the transducers. Moreover, an air filled polyethylene tube was mounted underneath the rig to the side of the bigger and heavier 38 kHz transducer to give the correct balance and extra float.

Initially, the 120 kHz transducer was the Simrad ES120-7G type, but after a first period in the mesocosm problems in its functionality had arisen. Hence, it was substituted with the new composite ES120-7C type on the 26th of February. This installation was made on the raft and, as described in the Paragraph 3.5.1, the transducer was discovered to be slightly inclined. Of course, this did not affect the results but only the new geometry of the common insonified volume.

The relative distances between the beam axes were obtained from a digital photo of the rig (Fig. 3.6) setting the centre of the biggest 38 kHz transducer as the origin of a Cartesian coordinate system. The results of the determination are shown in Table 3.II.

Since the accuracy in determining the distances was high, errors related to the inclination of the rig on the picture and the focus could be neglected.

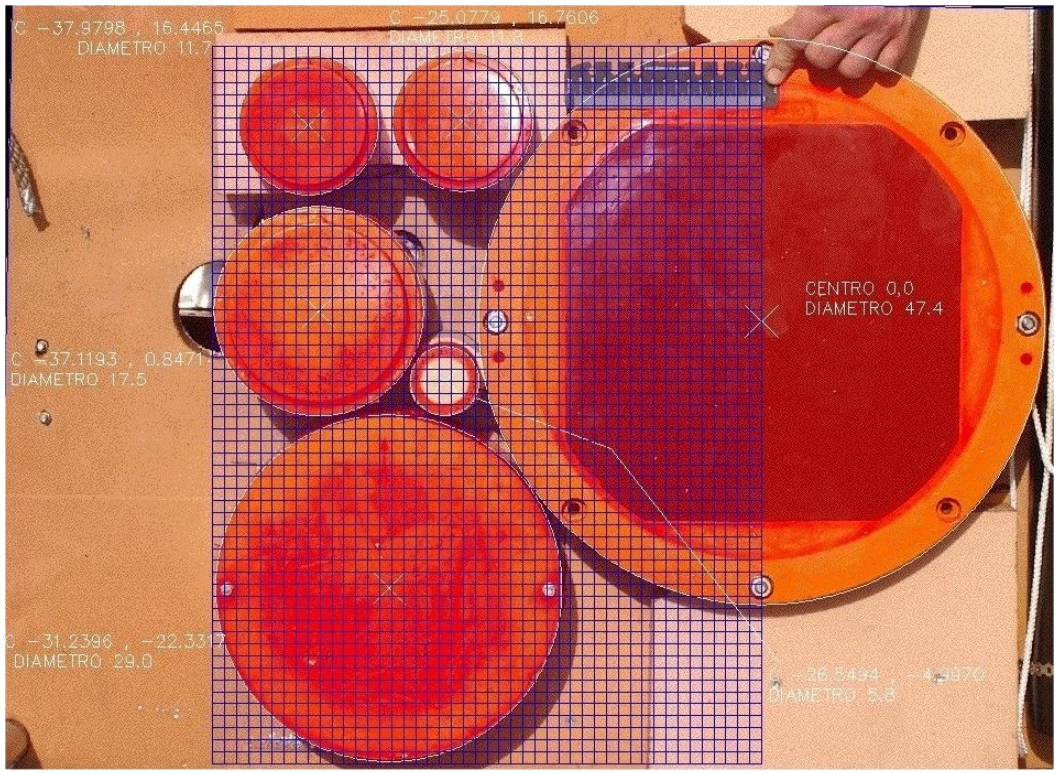

Figure 3.6: *Front view of the transducers mounted on the rig and beam axes distances determination.*

Table 3.II: Beam axes distances in Cartesian coordinate system with origin at the centre of the 38 kHz transducer.

	System (kHz)					
	38	**70**	**120**	**200**	**364**	**710**
x (m)	0	0.312	0.371	0.251	0.380	0.265
y (m)	0	-0.223	0.008	0.168	0.164	-0.050

The knowledge of the relative axis distances permitted a theoretical approach on the interrelationship among the echotrace angle position at different acoustic beams. This evaluation was very useful in several analyses of data and for the calibration of the 710 kHz single beam system.

3.3.2 Calibration

For an EK60 system, the standard target calibration method (Foote *et al.*, 1987) is executed by running the built-in ER60 software "calibration.exe". The normally two separate operations for split-beam calibration, i.e. on-axis sensitivity and acoustic beam pattern (Foote *et al.*, 1987; Reynisson, 1999), are accomplished in one single beam mapping operation to determine the gain *G* and the correction *SaCorr* in dB.

The *SaCorr* is a new parameter introduced by Simrad for the EK60 technology. It is the correction in dB required to harmonize the TS and nautical area scattering coefficient (NASC) (McLennan *et al.*, 2002) measurements for echo-integration estimations*. *SaCorr* is obtained by direct estimation from calibration points near the acoustic axis, and measured as an integrated part of the beam mapping (for more details and formulation see Appendix in Paper III).

Beam models (polynomial and EK-Simrad) are then compared to the acquired data to estimate the beam parameters used for the evaluation of the point-beam compensation by the post-processing software.

The calibration program adjusts the parameters in the beam model to minimise the root mean square error (rms-error) calculated on the recorded data points. The rms-deviations indicate how the beam models fit the recorded data. Hence, they are utilized to evaluate the validity of the calibration, which can be declared satisfactory if the rms-value is less than 0.2 (Simrad, 2003).

The calibration.exe concludes with confirming and updating the transducer parameters inside the GPT of echosounder (Simrad, 2003). A file in ASCII format containing information in a standard form on: calibration parameters, gain and *SaCorr*, beam parameters results, statistical comparison with beam models and echotraces list of the detections involved in the analysis can be also stored.

---

* Following the definitions and symbols in fisheries acoustics after MacLennan *et al*. (2002), the proper notation for this correction term should be $S_A corr$. However, both in the synthesis of thesis and in Paper III the original Simrad notation with lower case *a* is kept.

The mesocosm acoustic systems were calibrated prior to and following the termination of the experiments for different pulse durations and transmit powers. The standard sphere was attached to three 0.4 mm diameter monofilament lines (Fig. 3.7a).

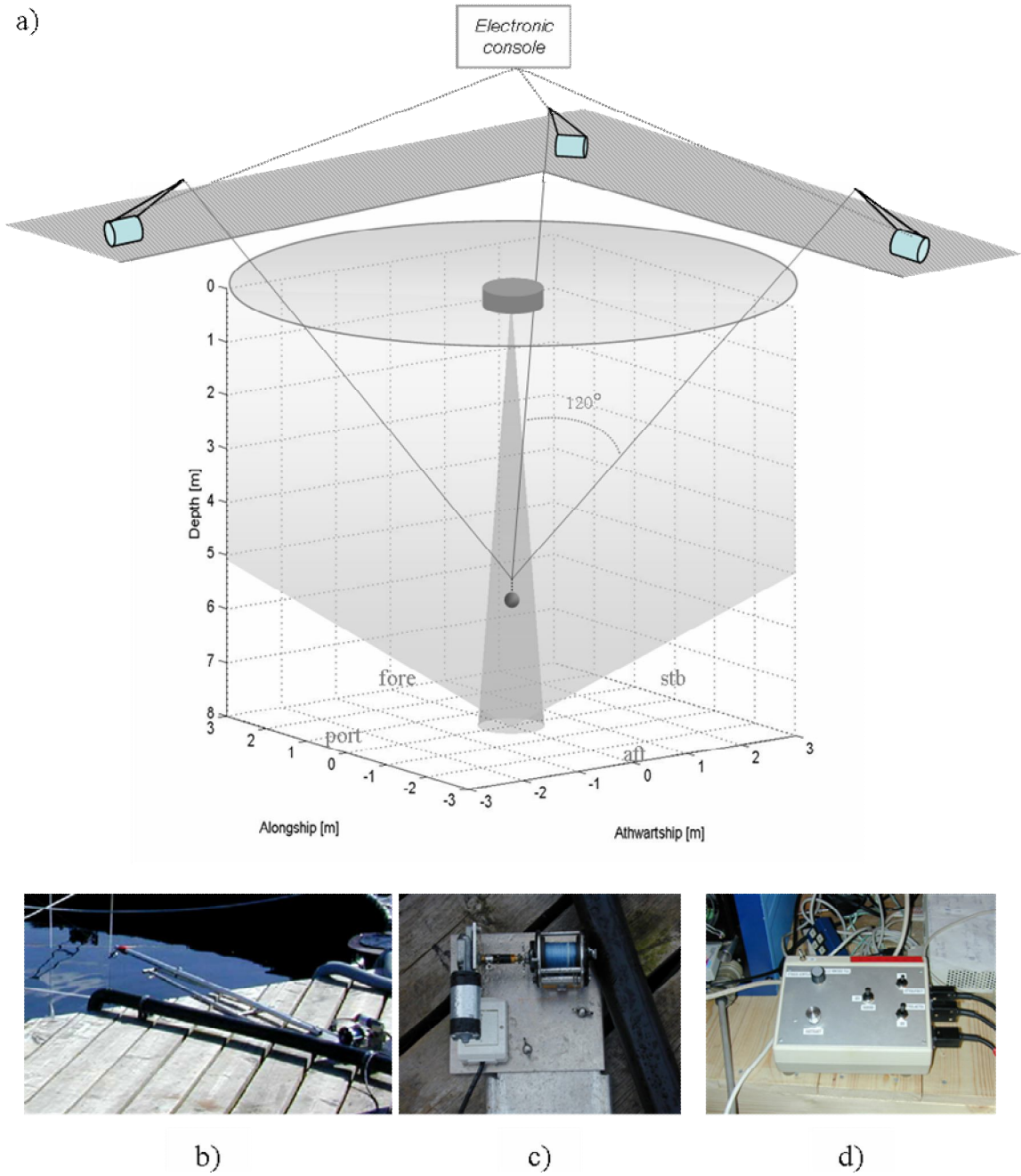

Figure 3.7: *Calibration in mesocosm*. a) *set-up*; b) *one of the 3 winches frames installed on the raft; c) the motor-driven winch system*; d) *the electronic console for remote control of the winches*.

Each line was controlled by a separate motor-driven winch (Fig. 3.7b and c) positioned on the raft along the circular edge of the mesocosm at an angle of 120º each other. The winches were electrically connected to a motherboard electronic console (Fig. 3.7d) which allowed the operator to regulate speed and up-down direction by using joy sticks. In such a way, the sphere was easily moved inside all the detection cells of the acoustic beam. Taking this advantage, the calibration system was also very useful in investigating the geometry of the acoustic beams in mesocosm (Par. 3.5.1) and in a specific experiment on tethered animals (Par. 3.5.3b).

The prior- and after-calibration results for the primary split-beam systems for the most used setting are summarized in Table 3.III together with the standard-sphere type utilized. The two digit values were read directly from the ASCII format calibration files. The results obtained in the post experiments calibration are similar to the previous, indicating consistent performance of the systems and reproducibility of the data. Only the gain at 120 kHz shows a difference between the two calibrations (0.28 dB). This system is known to be slightly unstable (Egil Ona, IMR, pers. comm.) and a minimum variability in results of calibrations performed in different dates might be expected. The variation of the transducer performance with the temperature could be one of the reasons (Demer and Renfree, 2008). Both the 120 kHz calibrations were performed with success, i.e. the rms-errors with respect to the beam model were less than 0.2 (Table 3.III), indicating that the system has slightly changed its stability during the period they were performed.

Since the target strength of an EK60 echotrace is calculated with a term equivalent to two times the gain (Appendix in Paper III) and the post calibration results showed a lower rms-error compared the previous, it has been judged reasonable to apply a date-adaptive compensation to the TS data before the analyses. The amount in dB to compensate this time-dependent deviation was determined in linear domain by interpolating the gains of the two calibrations versus the respective dates. Before any analysis, the calculated compensation, with reference to the day when the measurement was carried out, was multiply by the factor two and added to the output TS.

Table 3.III: Mesocosm calibration results for the 38, 70, 120 and 200 kHz EK60 systems prior and after the measurements. Sphere type (Cu=copper, WC=tungsten carbide with 6% cobalt binder) and diameter in mm, transmitted power to the transducer and pulse duration are in grey colour. Default and calibration Simrad values are also given in grey colour. The dates are referred to the year 2004.

System	rms err. model		detections	GAIN	Sa *corr*	equiv. beam	s. speed	sphere	3 dB beam angle		off-set angle	
and Date	EK	Polyn.				angle [dB]	[m/s]	depth [m]	Along	Athw	Along	Athw
38 kHz	CU 60	600 W	256 ms									
Default				24.00		-20.6			7.1	7.1		
Simrad cal.						-20.9			6.9	6.8		
29-Jan	0.17	0.07	448	24.67	-0.56		1470	5.5	6.98	6.98	0.01	0.01
23-Mar	0.17	0.07	459	24.59	-0.56		1480	5	6.96	6.97	0.00	0.00
difference	0.00	0.00	-11	0.08	0.00				0.02	0.01	0.01	0.01
70 kHz	WC 38.1	300 W	256 ms									
Default				26.80		-21.0			7	7		
Simrad cal.						-20.5			7.2	7.1		
31-Jan	0.17	0.11	459	26.01	-0.70		1473	5.5	6.39	6.40	0.01	0.05
19-Mar	0.14	0.10	478	26.08	-0.71		1480	5	6.50	6.43	0.04	0.03
difference	0.03	0.01	-19	-0.07	0.01				-0.11	-0.03	-0.03	0.02
120 kHz	WC 38.1	250 W	256 ms									
Default				26.58		-21.0			7	7		
Simrad cal.						-20.8			6.95	6.98		
26-Feb	0.15	0.08	482	26.89	-0.62		1475	5.2	6.42	6.41	-0.07	0.07
19-Mar	0.13	0.08	476	26.61	-0.60		1480	4.8	6.66	6.60	0.03	-0.01
difference	0.02	0.00	6	0.28	-0.02				-0.24	-0.19	-0.10	0.08
200 kHz	WC 38.1	120 W	256 ms									
Default				27.00		-20.7			7	7		
Simrad cal.						-20.3			7.5	7.2		
04-Feb	0.21	0.11	482	27.96	-0.45		1474	5.5	6.43	6.50	-0.06	0.07
18-Mar	0.16	0.12	470	27.88	-0.39		1480	5.2	6.61	6.61	-0.02	-0.06
difference	0.05	-0.01	12	0.08	-0.06				-0.18	-0.11	-0.04	0.13

Figure 3.8 shows the result of the interpolation with the dB values multiply by the factor two as in the Simrad TS-echotrace formulation (Appendix Paper III) for the direct compensation of the data.

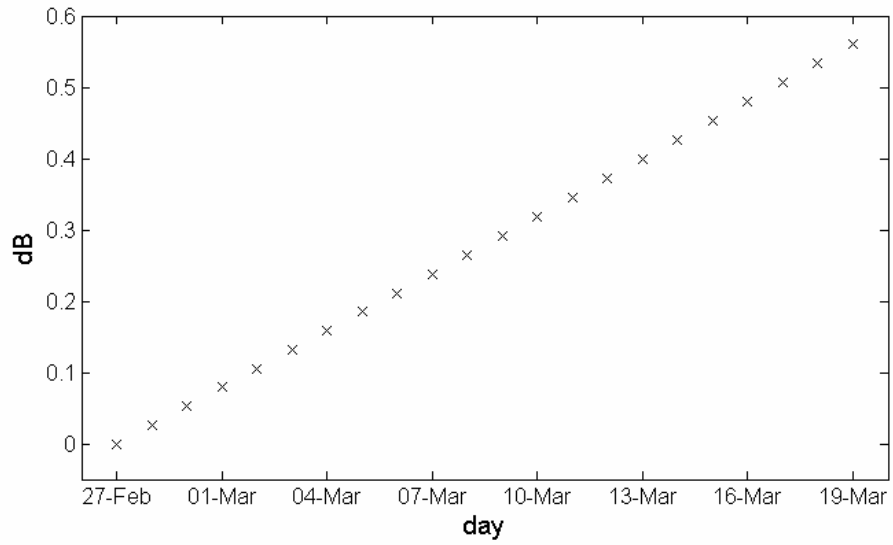

Figure 3.8: *Date-adaptive compensation in dB for the 120 kHz TS data derived from the prior- and post- calibration gain results.*

The 364 kHz system calibration results are not shown in Table 3.III because no calibration has been performed with success for that system. Under the suggestion of the Institute of Marine Research in Bergen the standard sphere WC 38.1 was utilized, and the transducer equivalent two way beam angle was set equal to -20.43 dB instead of the Simrad calibrated -21 dB to take into account the beam deformation due to the change in the GPT central frequency from 400 to 363.6 kHz. Eight calibrations were performed for that system during the experimental period; they all exhibit results with high rms-error deviation value (from 0.42 to 0.65) from the beam models. In only one case, the result was lower than the Simrad defined “not perfect but acceptable” value (Simrad, 2003) of 0.4 dB. Poor acoustic conditions or back scattering objects other than the reference target may cause high rms-error; definitely, these were not the calibration conditions in mesocosm. Figure 3.9 shows an example of the calibration results from the ER60 calibration.exe software. The elliptical beam pattern in the plot view could be referred to the electronic noise in a quadrant during the receiver

process due to the modification of the GPT. However, the real reason was not fully clarified by Simrad. Moreover, the 364 kHz echograms showed always an unexpected noisy picture with a very thin free-noise depth layer. Because of the outlined problems, the recorded data at 364 kHz system were judged too biased and not included in the further analyses.

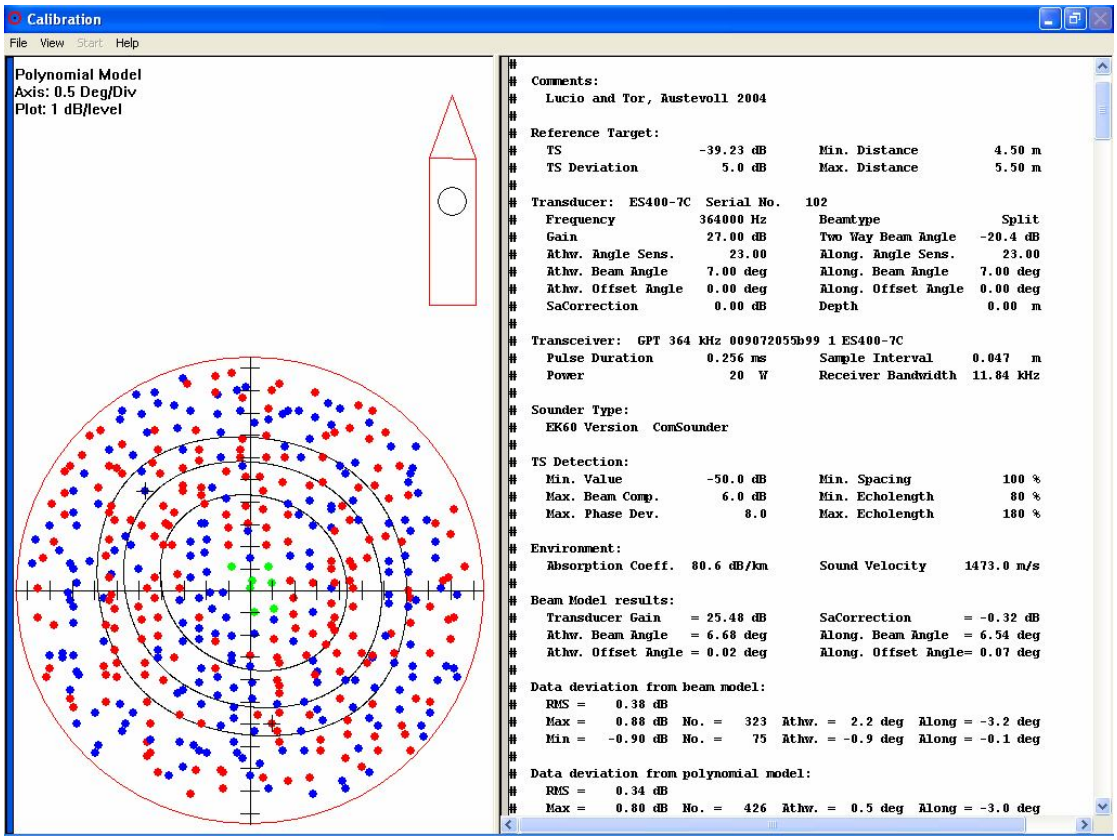

Figure 3.9: *Example of calibration results for the 364 kHz system. The rms-deviation from the EK Simrad beam model was the lowest obtained among eight calibration exercises. Recorded data plotted as blue and red dots indicate the TS values below and above the beam model respectively. The green dots close to the centre axis indicate the points that are utilized for the SaCorr estimation* (*see Paper III, Appendix A*).

3.3.2a Calibration of an EK60 single beam system

The commercial versions of EK60 GPTs are not able to work with single-beam transducers. As a consequence, the ER60 built-in tool calibration software has not this option in its operations. Therefore, a specific procedure was used to calibrate the 710 kHz system that was operating with a single beam transducer. In order to determine the EK60 Gain, the TS-Gain calibration procedure suggested for the previous Simrad EK500 (Simrad, 1996) system was adopted. The sphere WC10 was attached to a 0.12 mm nylon line to the three lines-winches calibration tether system and suspended on the acoustic beam axis. This was assured by using the theoretic geometrical approach based upon the relative distances between the 710 kHz beam and the other split-beams systems, and checking by the oscilloscope window the maximum value determined by the ER60. The observed sphere target strength (TS_{obs}) was then read out from the ER60 numerical view and compared with the theoretical value (TS_{th}) for the operative pulse duration, power and sound speed. The gain G was calculated using the already set gain (G_{old}) by the relationship $G = G_{old} + (TS_{obs} - TS_{th})/2$, and inserted manually in the transducer parameter section of the ER60 software.

The *SaCorr* in dB was determined by comparing the measured and the theoretical NASC values:

$$SaCorr = \frac{10\log_{10}\left[(s_A)_{obs}/(s_A)_{th}\right]}{2}. \qquad (3.1)$$

The measured value was read out from the ER60 numerical view, and the theoretical value calculated according to (Simrad, 1996):

$$s_A = \frac{4\pi r_0^2\ \sigma_{bs}\ (1852)^2}{\psi\ r^2} \qquad [\mathrm{m^2\ nmi^{-2}}] \qquad (3.2)$$

with r_0 the reference distance (1 m), $\sigma_{bs} = 10^{TS_{th}/10}$, ψ the equivalent beam angle expressed in steradiants, and r the range to the sphere in meters (MacLennan, 1990). As for the gain, the determined *SaCorr* was then inserted manually in the transducer parameter section of the ER60 software.

3.3.3 Treatment and analysis of the acoustic data

When ER60 is running, it is possible to store raw files and/or broadcast via Ethernet processed data with high precision in an output binary file called *EK datagram file* with extension .dg. The datagram may contain a number of different parameters selectable from the so-called *output Datagram dialogue box*. The ER60 allows these operations in replay mode also. This is a useful testing feature in the case that the user cannot use appropriate post-processing software. Although time consuming, replaying the same file with different Single-Echo Detection (SED) criteria (Ona and Barange, 1999; Simrad, 2003) it gives the opportunity to lead further analyses, such as to perform investigation of the thresholding effect.

The recorded EK60 raw files from the mesocosm were replayed, and datagram consisting of raw samples and echotrace parameters (Simrad, 2003; Appendix in Paper III) were stored for the analysis. This extraction procedure will be later referred to as the *ER60 extraction*, to distinguish from the *Sonar5 extraction*. The latter consisted in processing the EK60 raw data by an enhanced version of the Sonar5 post-processing software version 5.9.7 (Balk and Lindem, 2005). Due to the flexible and useful built-in tools for the analysis, the Sonar5 was preferred when tracking and more complex multifrequency operations were required.

Following the extraction, the data were analyzed using Matlab (Mathworks, Inc.). A number of Matlab scripts were implemented to read the ER60 raw and datagram binary files, as well as to organize and process the data extracted by both software.

Differences in results between the two extraction methods were also investigated. With same setting of SED criteria, the Sonar5 retrieved higher number of echotraces compared to the ER60. This was due to the thresholding effect in the Simrad ER60 wherein the SED rejects targets with much higher TS of the minTS value.

A slight deviation was also found in target ranges and TS values for the same echo. This is due to the difference in the SED algorithm implemented in ER60 and Sonar5. The SED algorithm has to ensure that only echo samples originating from it are

accepted for the analysis so that the TS of a target is correctly represented. In the case of the ER60 software, the SED algorithm is described in appendix of Paper III.

The Sonar5 SED algorithm determines the range and the TS of a target using the same formulations as the ER60 (Eq. (A2) and (A3) in Paper III, Appendix), but with a different approach after the determination of the peak along the uncompensated array. When a peak is found, Sonar5 trails down on each side and interpolates between samples under and above the -6 dB of the peak value (Helge Balk, pers. comm.). If the result is inside the ranges of the SED criteria, it is accepted as target and an echotrace is generated. In practice, the samples involved in the principle of gravity of Equation (A2) of Paper III have to satisfy the -6dB threshold criteria rather than the range limits [r_p-PL/2; r_p+PL/2] as in ER60 (see Appendix in Paper III). While the analysis produces slightly different results in target range and TS, no difference in beam angles position has been found between the results obtained by the two extraction methods.

3.4 **Biology**

Krill sampling and maintenance

In order to provide live animals for the measurements, three different catching events were carried out during the experimental period. They were conducted in the central part of Raunefjorden (60°16′N 5°09′E), a land-locked fjord on the west coast of Norway near Bergen. In this area the topography consist of a small basin (approx. 0.8 nmi^2), falling down from 120 m depth to a variable bottom depth of 220–240 m, where a Sound Scattering Layer (SSL) is commonly observed (see Figure 1a in Paper VI). This SSL is composed generally of larger crustacean zooplankton, copepods, amphipods, various mesopelagic shrimps and fish.

The samplings were conducted during late evening and night i.e. between 2100 and 0300 hrs, when the *Meganyctiphanes norvegica* were easily available in the surface

layers due to the habit of migrating to these depths in the west Norwegian fjords (e.g. Kaartvedt *et al*., 1988; Baliño and Aksnes, 1993).

The two first catching were performed using the RV “Hans Brattstrøm” on 4-5 February and 6-7 February 2004. The last catch was carried out on 27-28 February 2004 with the smaller vessel MS “Aurelia”. The University of Bergen runs both the vessels. The 3 ft Isaac-Kidd Midwater Trawl (IKMT) with mesh size of 500 μm was used for the sampling. 18 trawl hauls were performed usually at 20-40 m depth with average of 6 hauls per night. More details on sampling procedure can be found in Paper IV and Paper V.

Transport to Austevoll Aquaculture Station took approximately 1 hour following the last catch. The samples were carefully transferred into the mesocosm, with exception of a small part of it that was transferred into the two separate 500-litre seawater tanks situated on the raft to the side of the mesocosm for later use (Par. 3.5.3b).

Along with the krill, a substantial amount of copepods of the genus *Calanus* and *Metridia* were caught with the IKMT net. These are excellent food for the krill *Meganyctiphanes norvegica* and acted as food supply for krill during the experiments. No other food was supplied during the course of the experiments until the mesocosm bag was emptied and all remaining krill were collected from the bag.

During the course of the experimental period, dead animals were regularly removed from the bottom region of the bag by a seawater pump. Other unwanted animals were also immediately removed when observed close to the surface of the bag. All animals removed where identified as species and their size measured.

A critical point in maintenance the animals in good condition over the entire experimental period was the fact that there was no cover on the mesocosm to protect them from intense natural light. This means that during the daytime, although short in winter at such latitude, the animals were under the stress of limited unnatural habitat. It is difficult to estimate how this influenced the mortality of the mesocosm population.

Morphometric measurements

The far most abundant animal caught during sampling was the target krill species *Meganyctiphanes norvegica*. Both during transfer of the animals to the mesocosm and later, all animals that appeared not to be *Meganyctiphanes norvegica* were removed immediately. However, some other krill species were classified from the mesocosm samples obtained after the acoustic data acquisition period.

A number of 2821 specimens were classified and their total length (TL) measured by a Leica MS5 stereozoom microscope at appropriate magnification. The TL was measured from the tip of rostrum to the posterior end of the terminal spine at the end of telson. Morris *et al*. (1988) summarized the definitions for various length measurements on krill and codified the TL as "TT".

The 94.7 % of the sample (2663 individuals) were identified to be *M. norvegica*, the rest belonging to the *Thysanoessa* genus and *Nyctiphanes couchii*. Figure 3.10 shows the length distribution of the sample.

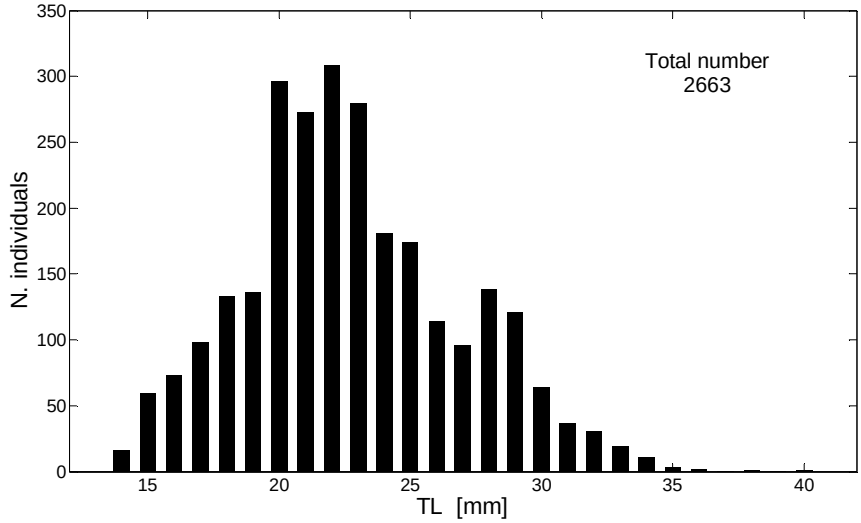

Figure 3.10: *Length distribution of Meganyctiphanes norvegica mesocosm data set.*

The distribution in Figure 3.10 definitely represents winter animals of different generations (0-group: <1 year old, I-group: ~1 ½ year old) at the time of the experiments. The generation 0-group was the dominant size group, probably due to the fact that sampling where conducted in the uppermost part of the water column at

night wherein the youngest generation usually dominate (e.g. Klevjer and Kaartvedt, 2006). Older animals of generation I-group were present but in low numbers. Using the 'mixdist' package as part of the R-environment software, the average length of the dominating cohort of *Meganyctiphanes norvegica* was estimated to 21.8 ± 2.98 mm and for the larger size but significantly less abundant cohort to 27.8 ± 2.68 mm total length (residual results: $Df = 26$, $\chi^2 = 138.34$, $P < 2.2 \cdot 10^{-16}$). Thus, the animals constituting these two cohorts represent 79 % and 21 % of the population of *M. norvegica* in the mesocosm respectively.

Additional morphometric measurements were also performed on a random sub-set consisting of 216 specimens. Those measures were nominally:

- the carapace length (CL), from the base of the carapace eye notch to the posterior lateral edge of the carapace, codified by Morris *et al.* as "S6";
- the body length (BL), from the inner curved part of carapace ("eye notch") to the end of telson, codified by Morris *et al.* as "BT";
- and three measures of body width of animal as seen from dorsal side:
    1. width 1 (B1) across the anterior part of the rostrum;
    2. width 2 (B2) at the end of carapace/joint where the first abdominal segments starts;
    3. width 3 (B3) at the last abdominal segment joints the telson.

Figure 3.11 resumes graphically the three morphometric lengths defined above. It must be noted that prior to the morphometric measurements krill were frozen and a potential small reduction in the actual dimensions could affect the measures (*shrinking*). This seems not the case for the CL that is known to be not or less affected by any preservation (Kulka and Corey, 1982).

Dry weight measurements were also performed on the sub-set by using a Mettler Toledo UMX2 having a working range 2.1 g - 0.1 µg. Details on this procedure can be found in the Paper IV. Figure 3.12 shows the dry weight results plotted versus the carapax length and the total length and the respective regression curves. In Paper I, morphometric relationships for winter *M. norvegica* specimens between commonly used length

measures and dry weight results are also given. Figure 3.13 shows the morphometric relationships of the measured lengths and widths versus the total length and the respective linear regression.

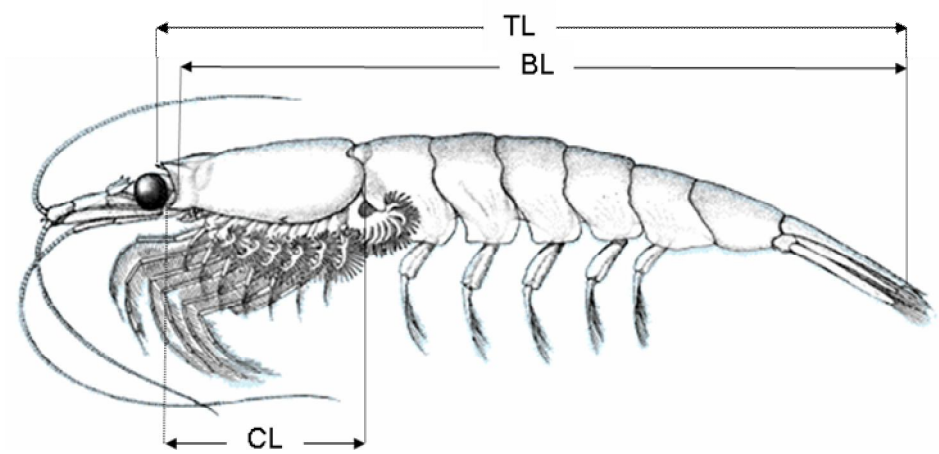

Figure 3.11: *Graphical resume of the length definitions TL, CL and BL measured on the M. norvegica sample and sub-sample, and codified by Morris et al.* (*1988*) *by TT, S6 and BT respectively.*

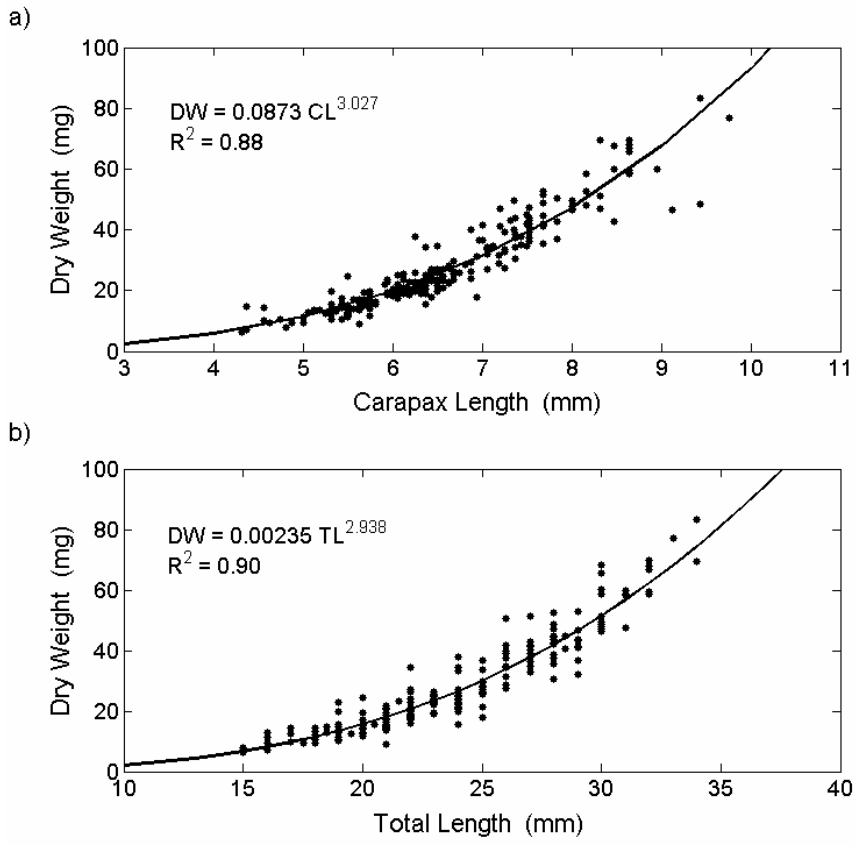

Figure 3.12: *Carapax length* (a) *and total length* (b) *versus dry weight of Meganyctiphanes norvegica mesocosm data sub-set (216 specimens).*

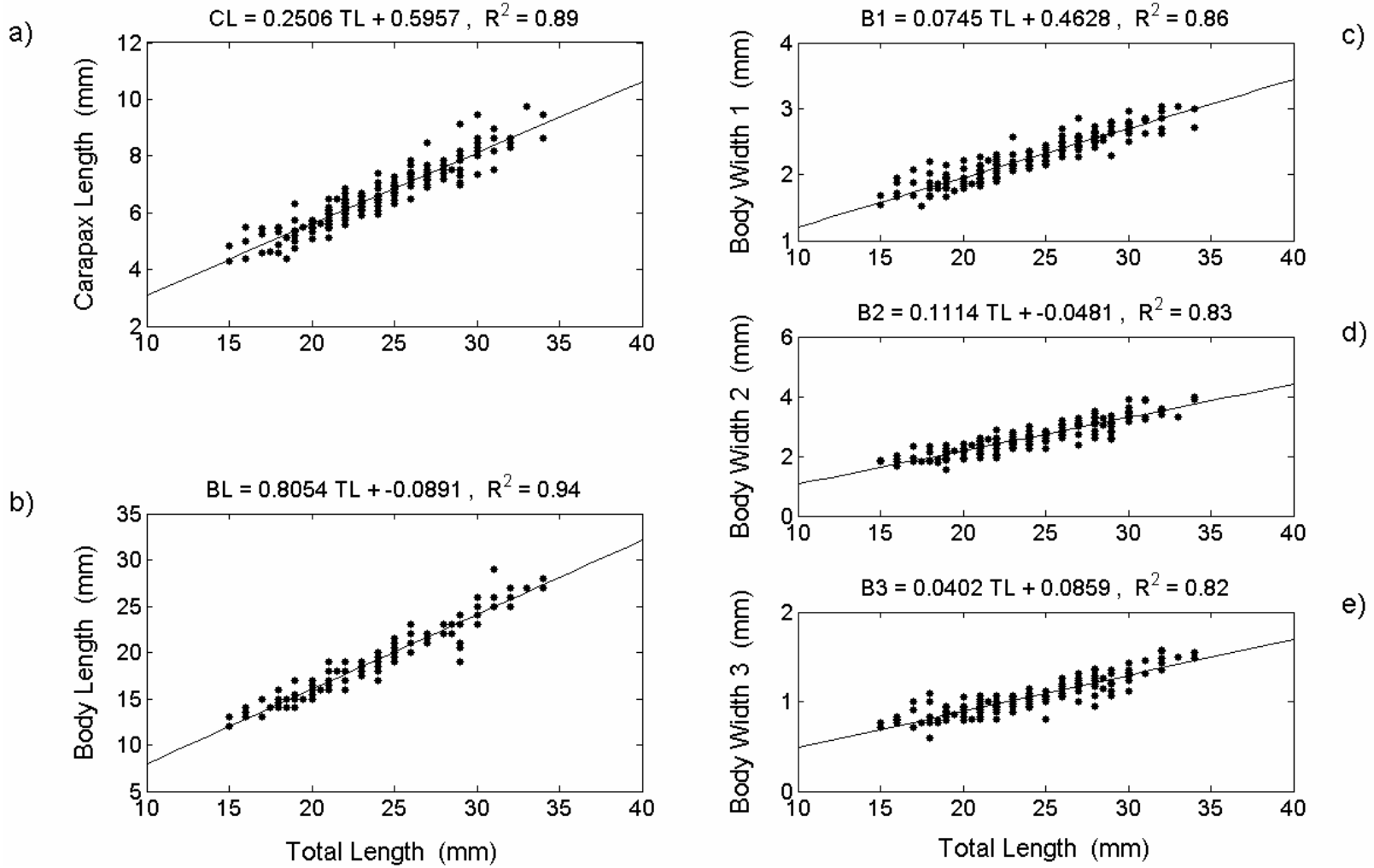

Figure 3.13: M*orphometric measures versus total length of Meganyctiphanes norvegica data sub-set (216 specimens):* a) *carapax length*; b) *body length*; c) *body width 1*; d) *body width 2*; d) *body width 3 as defined in the text.*

3.5 **Acoustic data collection**

The rig was placed neatly floating on the surface at the centre of the mesocosm, with small weights on top to balance it properly and allow a tiny layer of seawater to cover the top surface. By using a simple T-shaped wooden stick turned upside down, it was also possible to attach the rig to the footbridge and to keep it fixed when needed.

Following the recommendation for multifrequency acoustic data collection (Korneliussen *et al*., 2008), the measurements were generally performed setting an identical pulse duration for all the frequencies and with significantly reduced output power to the transducer (Table 3.I) in order to avoid non-linear effects (Tichy *et al*., 2003; Pedersen, 2007; Korneliussen *et al*., 2008).

The common pulse duration at 0.256 ms was found to be the most appropriate to detect targets having distribution and size as recognized in the mesocosm. This corresponds to a sampling distance in EK60 raw data of 4.7 cm.

3.5.1 Systems performance

Empty mesocosm measurements: qualitative results

Before the introduction of krill, measurements on volume reverberation in mesocosm and others tests with the only deep water were performed. Background noise estimates by the Simrad ER60 software and range of the reflection from the bag walls on the echograms were recognized.

With the setting listed in Table 3.I, the estimated background noise was at adequate degree of magnitude (less than -100 dB) for all the frequencies except for the system operating at 38 kHz, which revealed a background noise of -97 dB. Further inspection on that system was carried out at the different settable pulse durations varying the transmitted power from 200 to 2000 watt. The ER60 noise background estimates were observed varying as expected, increasing with pulse duration and power. This indicated a normal functionality of the system althought with low signal-to-noise

ratio. After the introduction of the animal, the background noise was generally estimated at -94 dB during the entire experimental period.

Interference between frequencies on backscattering from standard target spheres

Backscattering data from two standard tungsten carbide spheres, the 38.1 mm (WC38) and the 10 mm (WC10) diameter, were acquired to verify potential interferences between the frequencies.

The spheres were suspended together by a monofilament nylon line of 0.3 mm diameter at a relative distance of approximately 1.2 m. The upper end of the line was connected to the junction of the three 0.4 mm diameter monofilament lines, which formed the suspending part of the system used for the calibration procedure (Fig. 3.7). This leads to locate the spheres everywhere inside the mesocosm volume. With spheres placed on a beam axis, backscattering data were acquired with the relative system set in active mode, while all the others in passive mode. When a satisfactory number of echoes were obtained, the spheres were moved to the next beam set in active and the procedure repeated.

In general, the observation of the echograms with minimum-TS threshold -100 dB showed suitable results. The systems in passive mode slightly detected only the strong backscatteed signal from the bottom and in few cases the reflected signal from the sphere WC 38.1. Particularly, these were the cases for the 364 hHz system when either the 120 or the 200 kHz were set in active; the 710 kHz system when either the 200 or the 364 set in active, and reciprocally for the 38 and 70 kHz system when one was set in active, the other in passive and vice versa.

Beam patterns mapping

With the knowledge of the transducer technical specifications and the transceiver processing parameters, the beam pattern can be theorized. Table 3.IV illustrates the basic beam geometrical features along the depth of the primary system used. The nominal -3 dB circular beamwidth of the split-beams transducer was 7º; however, the

systems will generally accept echoes from larger solid angles (Ona and Barange, 1999). From the cell resolution parameters in Table 3.IV it is evident the potential effect of the finite target size connected to the short-range detection. For example, since in both the split-beam dimensions the nominal angular step is 0.061°, a single horizontal cell resolution at 4 m depth has the area equal to 18.1 mm^2 and the diagonal 6.1 mm. Thus, a 23 mm target subtends at least 4 angular cells at that range. This unequivocally introduces bias in the beam target-position determination and the related beam-pattern loss compensation, especially if the target is moving fast. As discussed in Paper IV, the effect of the interrelation between finite target and angular resolution sizes at short range was evident on the horizontal trajectory of a tracked target, which appared scattered along the actual trajectory.

Table 3.IV. Theoretical geometry of the nominal 7º acoustic beam versus depth. The cell resolution parameters are calculated for angular resolution equal to 0.061º. The cell areas are also listed for the angular resolution 0.064º of the 38 kHz ES38-B transducer.

depth (m)	diameter (m)	base (m^2)	volume (m^3)	cell resolution			
				side (cm)	diagonal (cm)	area (cm^2)	
						38 kHz	others
1	0.122	0.012	0.004	0.11	0.16	0.012	0.011
2	0.245	0.047	0.031	0.21	0.30	0.050	0.045
3	0.367	0.106	0.106	0.32	0.45	0.112	0.102
4	0.489	0.188	0.251	0.43	0.61	0.200	0.181
5	0.612	0.294	0.490	0.53	0.75	0.312	0.283
6	0.734	0.423	0.846	0.64	0.91	0.449	0.408
7	0.856	0.576	1.344	0.75	1.06	0.611	0.555
8	0.979	0.752	2.006	0.85	1.20	0.799	0.725

In order to verify the angle sensitivity of the systems, as well their beam geometry, and derive tolerances for matching target position at two or more frequencies, detections of the two standard spheres WC38 and WC10 were acquired simultaneously at all the frequencies. Using the acquired echoes it was possible to

map completely all the volume of the transducer beams, and identify imprecise mounting that could not be reflected in the 2D photo of the transducer arrangement.

The interrelationships between beam target positions from two transducers mounted adjacently (beam axes parallel) and with active surfaces aligned on the same plane were theoretically illustrated by Demer *et al*. (1999) through simple geometrical considerations. Denoting with *r,* α and β the target range, alongship and athwartship mechanical angles output respectively, the beam position at the transducer 2 is related with that of the transducer 1 by:

$$\alpha_2 = \sin^{-1}\left(\frac{r_1 \sin\alpha_1 - d_\alpha}{r_2}\right) \quad \text{and} \quad \beta_2 = \sin^{-1}\left(\frac{r_1 \sin\beta_1 - d_\beta}{r_2}\right) \tag{3.3}$$

where d_α and d_β are the separations of the beam axes in the planes alongship and athwartship respectively.

The two spheres were suspended as described in the previous section. They were initially moved randomly within the mesocosm volume with all the systems set in active mode, then focusing on the detection inside each beam. The latter operation was performed in turn for each system. The sphere were moved along the split-beam coordinates and around the edge of the detecting beam as indicated from the real-time results in the *single target position windows* of the ER60 software. Figures 3.14 and 3.15 show the results when the spheres were moved to describe the acoustic beam of the 120 kHz system. Comparing the target positions at all the other frequencies, it is evident that the beam axis of the 120 system lies slightly higher in the alongship direction than the expected position based upon the results in Table 3.II. This was also confirmed when the spheres were moved to describe the beam geometry and volume matching of the other systems. Comparing the interpositions in Figures 3.14 and 3.15, it can be noted that the 120 kHz beam axis is slightly higher in the alongship coordinate at deeper range.

From the two figures, it is also clear that the 364 kHz system had poor precision in the angle determination, probably reflecting the internal electronic noise derived from the modification of the original 400 kHz GPT.

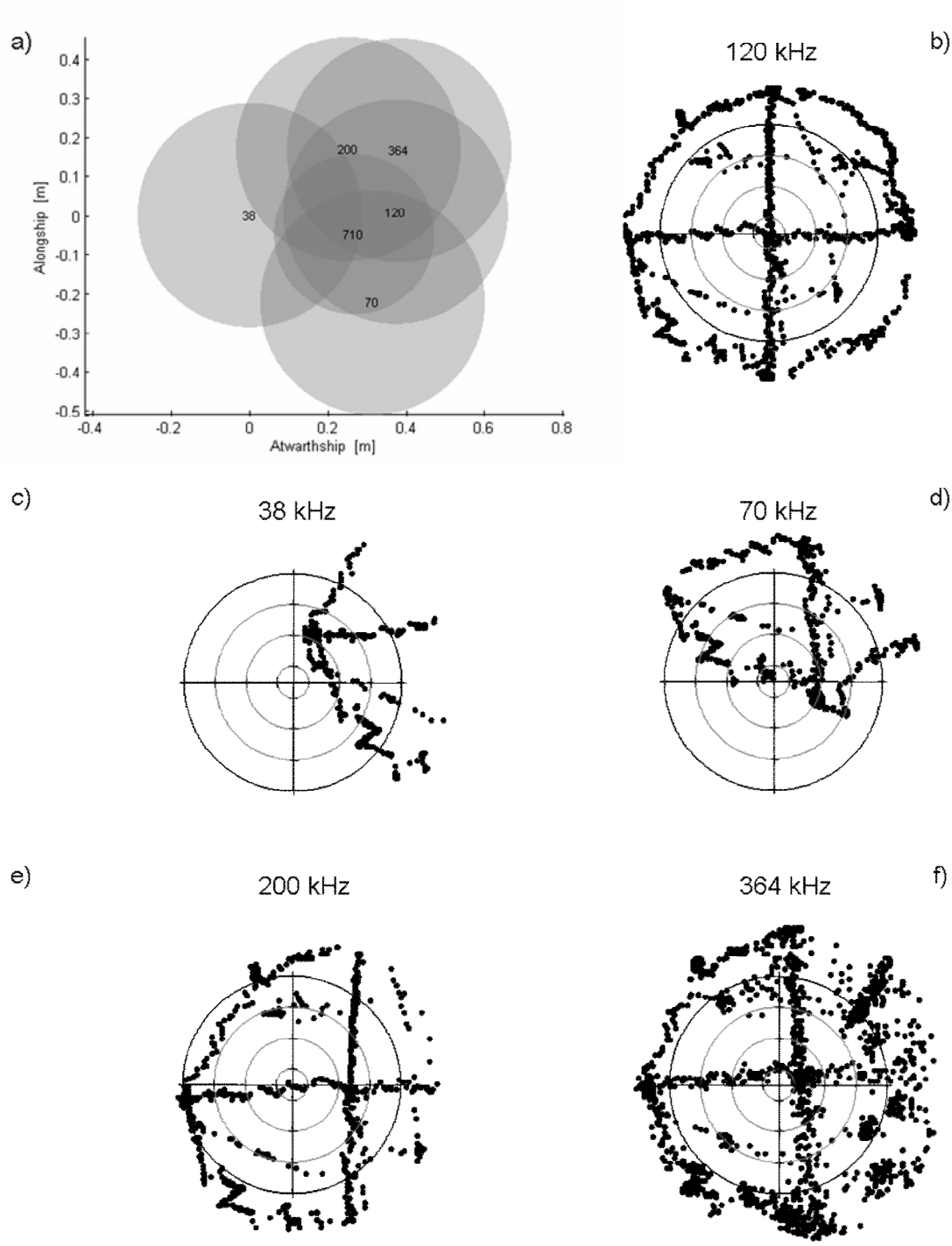

Figure 3.14: *Example of acoustic beam cross sections geometries and matching in the mesocosm*: *trial session with the WC38 standard sphere moved inside the 120 kHz beam at detected mean distance of 4.69 m from the transducer*. a) *Theoretical 7° beam footprints (5° for the 710 kHz system) at the mean depth based upon the measured axes distances described in par 3.2*; b)-f) *ER60 echotraces angular position (atwarthship, alongship) at different frequencies with maximum beam compensation SED criterion set at 6 dB. The grey circles are the beam cross sections at 1, 3 and 5 degree solid angle, the black circles are the nominal 7°.*

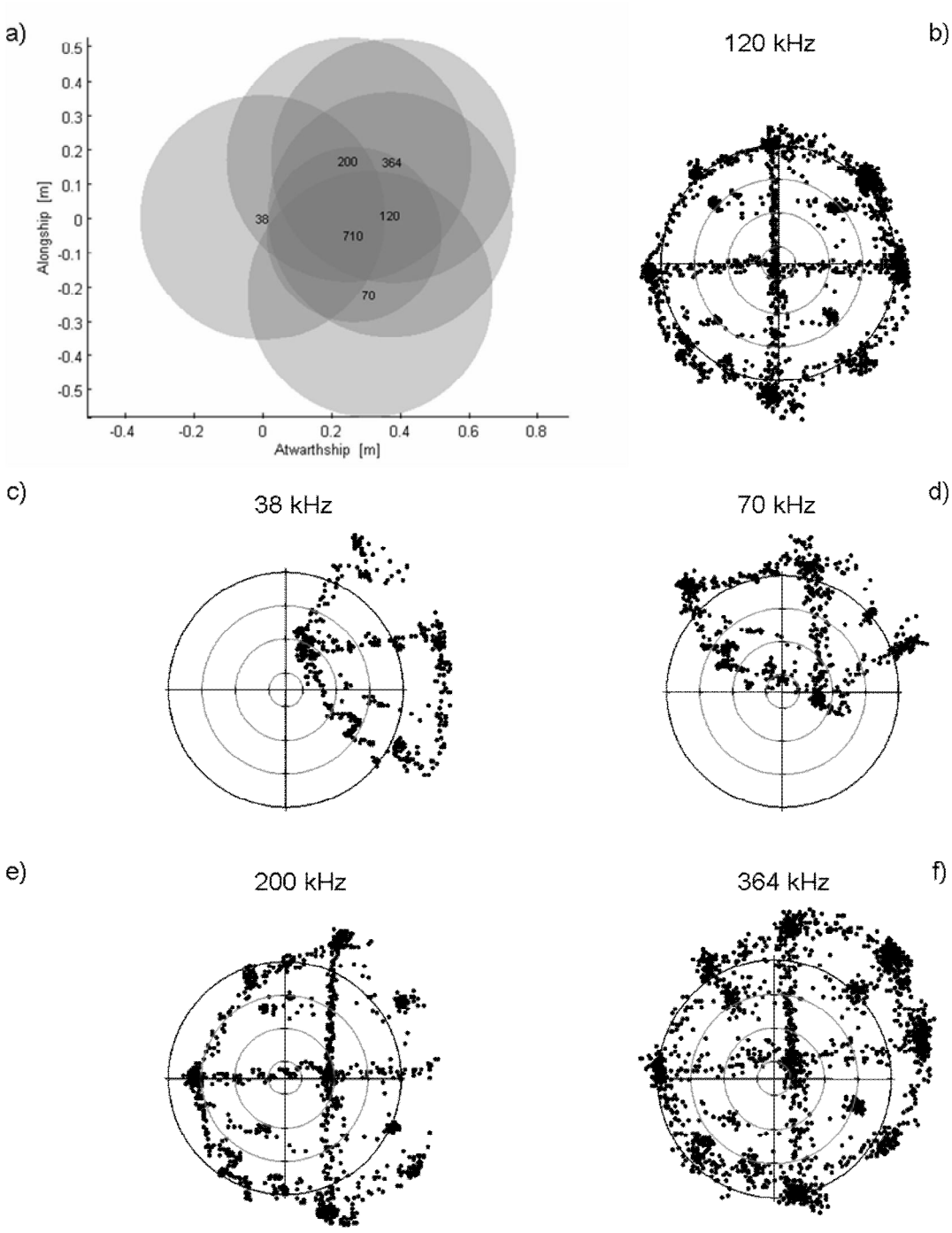

Figure 3.15: *Results from the same trial session of Figure 3.14 for the deeper WC10 standard sphere at detected mean distance of 5.82 m from the 120 kHz transducer*. a) *Theoretical 7° beam footprints (5° for the 710 kHz system) based upon the measured axes distances at the mean depth*; b)-f) *ER60 echotraces angular positions (atwarthship, alongship) at different frequencies with maximum beam compensation SED criterion set at 6 dB. The grey circles are the beam cross sections at 1, 3 and 5 degree solid angle, the black circles are the nominal 7°.*

In order to examine the simultaneously EK60 range detection performances, another test was executed using the same set-up. The two spheres were positioned inside the acoustical common insonified volume in fixed positions and a raw data file composed of 1212 echo pings was recorded. Results from these measurements are shown and discussed in Chapter 4, and the related short-range detection problem of the EK60 systems is the object of Paper III.

3.5.2 Krill behaviour in mesocosm

Since low concentration of scatteres is a primary requirement for TS measurement in a water volume, the number of animals introduced in the mesocosm was kept low but enough for the purposes. Video inspection and acoustic data visualization evidenced no schooling formation during the entire experimental period. The animals were acoustically detected as single target at any time of the day at all the operative frequencies in the depth layer from 0.5 to 6.5 m. They seemed mostly swimming horizontally with almost constant velocity and giving the impression of hovering around searching food.

However, significant differences in target distribution at different natural light conditions were found. The acoustic data acquired during daytime generally showed few animals swimming in the range 2 to 6 meters. Video investigations revealed that the rest of the animals were at the bottom of the bag following their natural behaviour to avoid strong natural light intensity. During nighttime, the krill ascended hovering at any depth within the volume of the mesocosm, and were detected as randomly distributed targets.

The effect of this behaviour on long registration echograms gives the impression of a sort of daily migration. The upper panel in Figure 3.16 shows the volume backscattering strength echogram at 120 kHz of a continuous record of 60 hours duration: from the evening of the 5th to the early morning of the 8th of March 2004. The lower panel shows the range position versus time for the same raw data set of the echo-tracks manually retrieved by using Sonar5. It is evident from both panels the

krill response to the natural light condition in the mesocosm and the similaty with the daily migration.

3.5.3 Specific measurements

During the investigational period, a set of experimental exercises with aim to retrieve significant information on multifrequency TS and acoustic volume backscattering from living krill were conducted. In this section, the motivations of specific experiments that are the issues of Paper IV and Paper V are briefly described and further information are also given.

3.5.3a Experiments with artificial lights

Meganyctiphanes norvegica are known to be attracted to artificial light (Mauchline and Fisher, 1969). Herman *et al*. (1993) reported that this behaviour response is much effective if the submerged source of light is motionless.

This feature was used in the mesocosm to force the krill to swim through the acoustic beams and detect them simultaneously at several frequencies in free-swimming condition. Two different experiments were performed: the first, denominated *internal lamps*, was focused to induce the krill to swim horizontally when crossing the acoustic beams; the second, denominated *internal-external lamps*, was established to verify the potential vertical swimming velocity of the organisms in the mesocosm.

Internal lamps experiment

The internal lamps experiment is the base of Paper IV, where procedure, data analysis and discussion of results are presented in details. It was motivated upon the observations on krill behaviour. Kils (1981) have observed that the tilt angle of krill tends to zero during fast horizontal movement.

Hamner and Hamner (2000) resumed their 20 years observations on *in situ* krill behaviour by scuba diving, and on board and laboratory aquaria asserting that all

a)

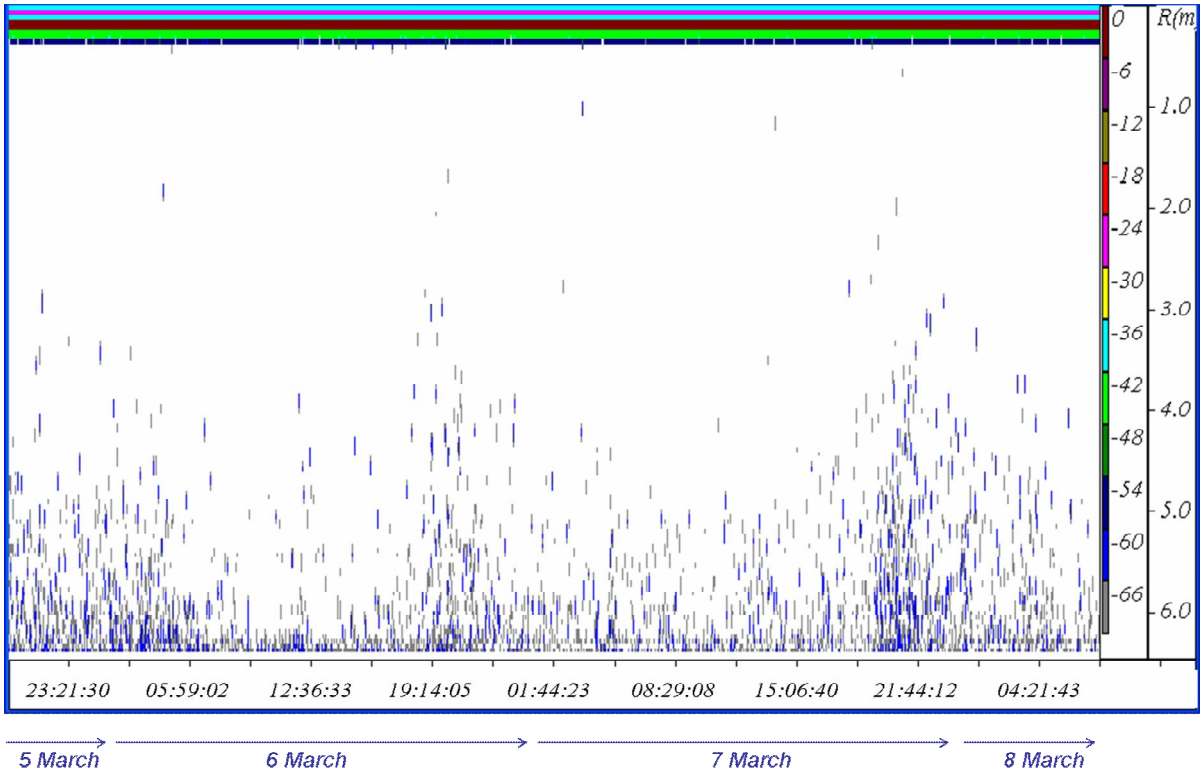

b)

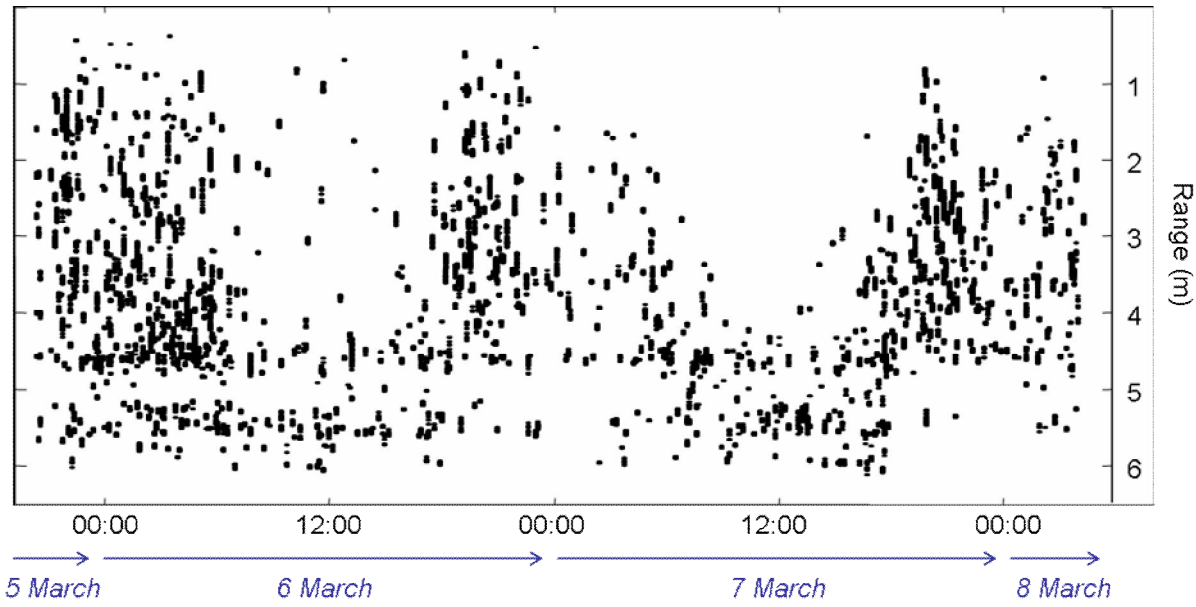

Figure 3.16: *Results of 60 hours record at 120 kHz*: *from 20:06 o'clock on 5th of March to 08:28 on 8th of March 2004* (*60 h 22 min*). *Pulse duration 0.256 ms, ping rate 0.5 (2 pings per second) resulting in 434581 pings.* a) *Compressed volume backscattering strength echogram with -72 dB S_V threshold;* b) *Manually retrieved echo-tracks using Sonar5, TS threshold -100 dB re 1m^2.*

individuals in a school assume virtually the same orientation and spend most of their life swimming horizontally. With the assumption of krill as most often near horizontally oriented and swimming quickly in their natural habitat, Demer and Conti (2005) found the best match of the SDWBA model to their *in situ* acoustic data. Also, by direct observations from video plankton recorder, Lawson *et al*. (2006) found that the mean angle of the krill orientation distribution was close to zero.

Consequently, many authors have inferred data from multifrequency acoustic surveys assuming a mean orientation of the krill population under investigation equal to, or very close to, the horizontal (Cochrane *et al*., 1991; Sameoto *et al*., 1993; Demer and Conti, 2005; Conti and Demer, 2006; Lawson *et al*., 2006; 2008).
However, *in situ* and *ex situ* high quality acoustic measurements on free swimming individuals with contemporary observation of orientation are still strongly required. This is not an easy task since accurate determination of orientation requires high definition images obtainable only with video tools that, due to the rapid attenuation of the light in seawater, have to deploy close to the organisms. This inevitably will influence the natural animal behavior (Hamner and Hamner, 2000), and/or will bring the tools to be detected by the echosounder covering the echoes from the animals.

The mesocosm set-up offered a great opportunity to perform TS measurements with individuals krill swimming horizontally and predict their orientation with good approximation. Hence, it was possible to retrieve TS data with less uncertainty for such situation.

Since *Meganyctiphanes norvegica* is known to be attracted by submersed artificial light (Mauchline and Fisher, 1969; Herman *et al*., 1993) the individual euphausiids were induced to swim horizontally through the active acoustic beams by the attraction of two fixed underwater lamps placed at opposite sides of a split-beam coordinate and alternately switched on-off. Figure 3.17 shows the experimental set-up and the assumed krill path. The two lamps were placed during nighttime at the depth of approximately 4.5 m on the opposite side of the alongship coordinate (fore and aft) close the bag-wall. Five trials were performed with that set-up.

EK60 raw files were acquired during the passages of krill through the beams and the echotrace output parameters analyzed. From the simultaneous TS output at the operative frequencies it was also possible to determine a more confident frequency response in TS domain for a known Northern krill population.

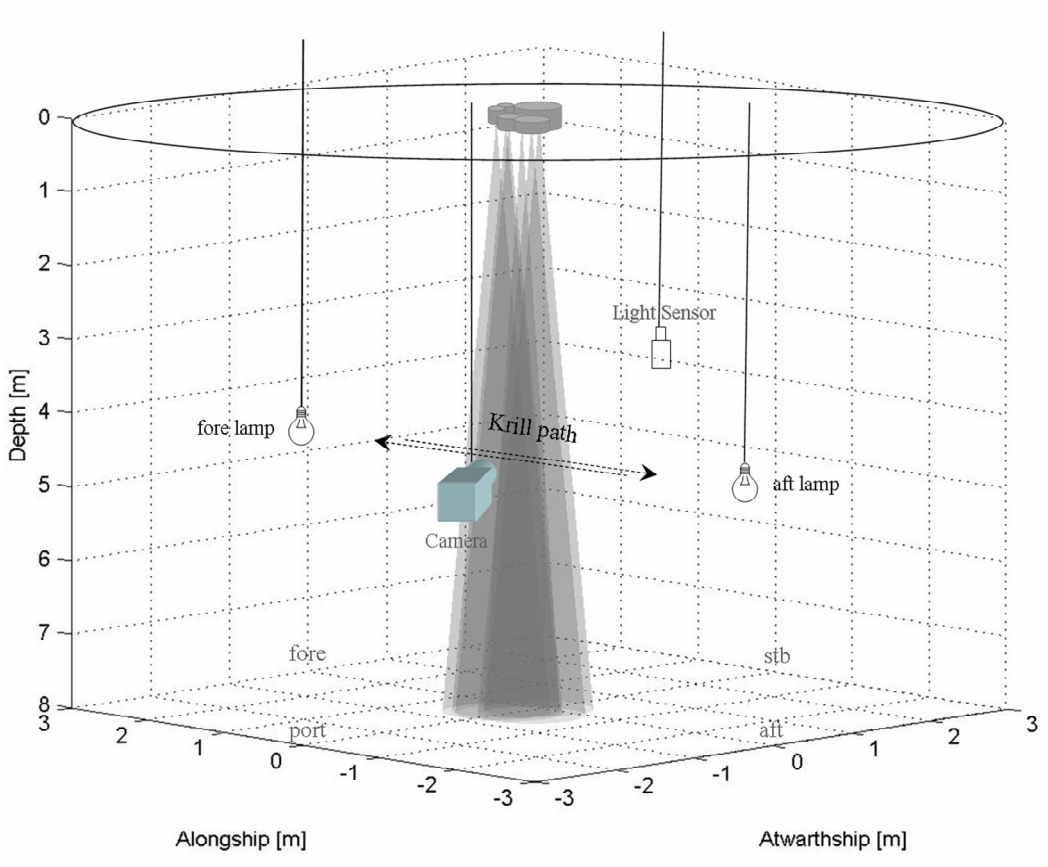

Figure 3.17: *Internal lamps experimental set-up.*

Figure 3.18 is presented in order to illustrate the effectiveness of the experimental set-up. The upper and lower panel in Figure 3.18a show the alongship and the range respectively of the ER60 echotraces at the frequencies 70, 120 and 200 kHz during a time period centred at a specific lamps switching time (dashed vertical line).

The SED criterion maximum beam compensation was set at 6 dB to visualize larger off-axis detections, hence longer tracks. The alongship-echotraces indicate the movement direction of the targets along that coordinate. It is evident that after the switch the targets moved in contrary direction attracted to the aft lamp switched in on.

a)

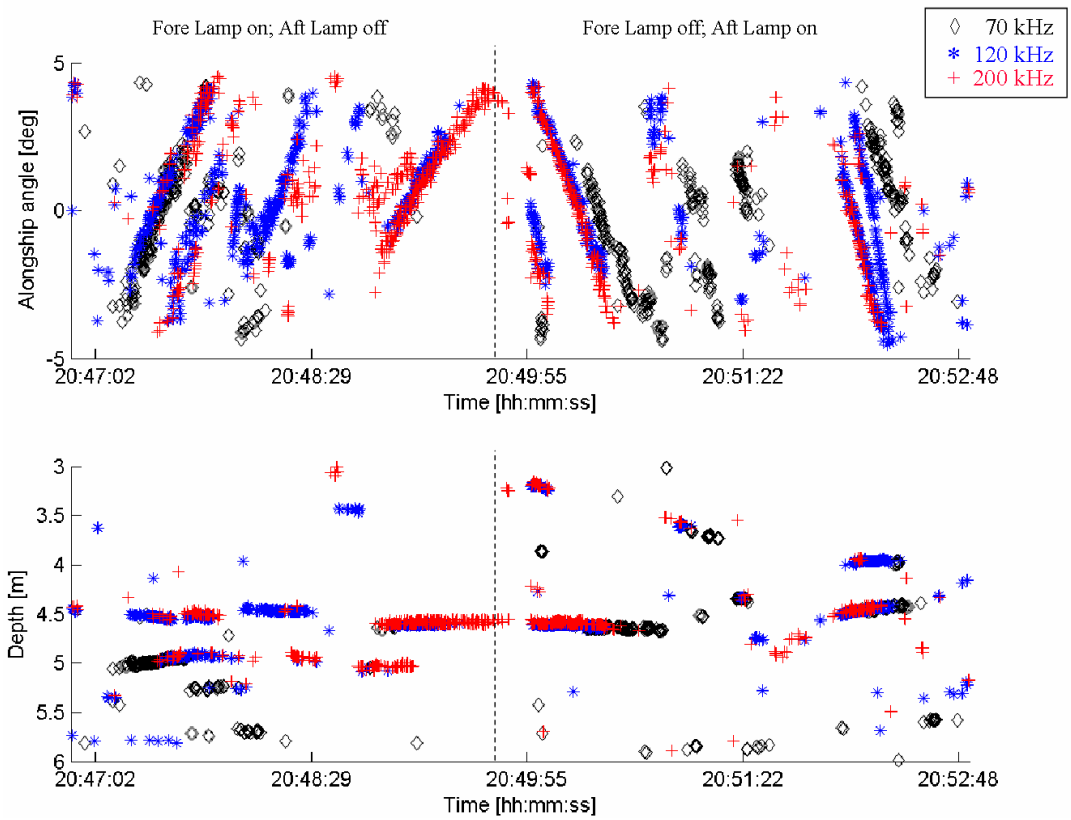

b)

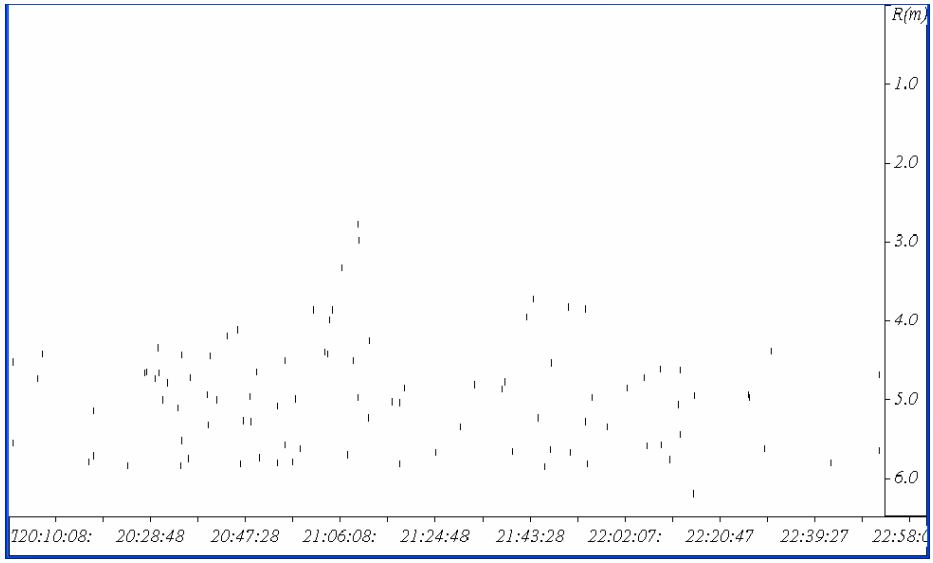

Figure 3.18: I*nternal lamps trial.* a) *Alongship and range ER60 echotraces versus time extrapolated around an on-off switch lamps time* (*dashed line*). b) *Sonar5 single echo detection echogram at 120 kHz. TS threshold -72 dB re 1m*^{2}*, number of pings 184420, pulse duration 0.256 ms, ping rate "maximum"* (*17.5 pings per second*).

Figure 3.18b shows the Sonar5 single echo detection echogram at 120 kHz during an internal lights trial session performed on 2 of March 2004. The TS threshold was set at -72 dB re 1 m^2 to single out detections of animals being mostly horizontally orientated, i.e. stronger TS level at broadside incidence, as theoretically predicted by the DWBA model (Par. 2.4), which is sensitive to the orientation. The scatterers were detected mostly in the layer 4.5–5.5 m in agreement with the assumption of attraction due to the lamps placed at 4.5 m.

Internal-external lamps experiment

Trevorrow *et al*. (2005) reported that krill exhibit a rapid (seconds) response to the vessel lights. This motivated the interest to verify such feature.

Previous tests with a lamp placed outside to the mesocosm water revealed that krill were reacting to the light moving far away from the source, principally descending to the bottom of the bag, similarly as in response to the natural light during daytime.

This reaction suggested performing a measurement exercise using two lamps: an underwater lamp and a second lamp placed outside the water mesocosm close to the surface (Figure 3.19). The submersed lamp was intended to attract the animals in the upper layers of the mesocosm, while the second was intended to induce the escaping response. It must be pointed out that the experiment was performed with the assumption of a pure exercise rather than useful to retrieve valuable data, since the organisms were induced to swim unnaturally fast in vertical direction. Therefore, only few and qualitative results, which are considered of interest to some extent, are shown below.

The halogen lamp JOEL K4-G55TE 55 W model (Denmark) was placed externally at centre of the mesocosm near the water surface, and eye halogen double-lamps 500 W (Iwasaki Electric Co. LTD, Japan), was submerged close the transducers rig at less than 0.3 m depth. Four internal-external lamps trials were performed on different dates. The lamps were alternately switched on-off each 10 or 15 minutes. In some cases, the procedure was completed with periods of darkness between the switching

times. Figure 3.20a shows one of these cases. The output ER60 target ranges versus time as detected at the frequencies of 70, 120, 200 and 710 kHz are superimposed. The krill reaction in moving downward when the external lamp was switched in on is undoubtedly evident.

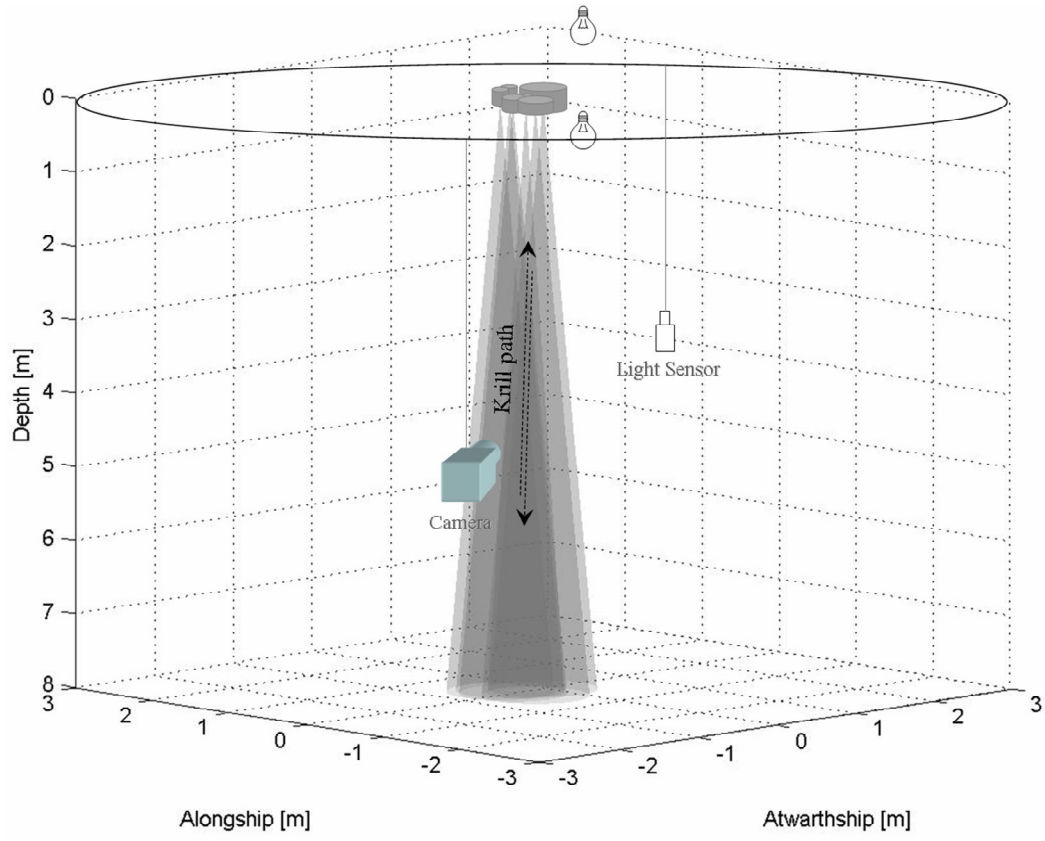

Figure 3.19: *Internal-external lamps experimental set-up.*

Tracking analysis was not fully satisfactory. Within the deeper layers, the patching of the organisms biased the tracking due to the likelihood of multiple targets being interpreted as individuals. In the upper layers, few targets were detected along their actual path due to the conic geometry of the acoustic beams.

Figure 3.20b shows the volume backscattering echogram at 120 kHz of an entire trial. In this case, a timer regulated the switching each 10 minutes without darkness steps. It is easy to observe the fast vertical reaction of the organisms to the different light conditions in mesocosm.

Althought only qualitative, the results shown in Figure (3.20) confirm the chance in using artificial lights in mesocosm for focused study on krill behaviour.

a)

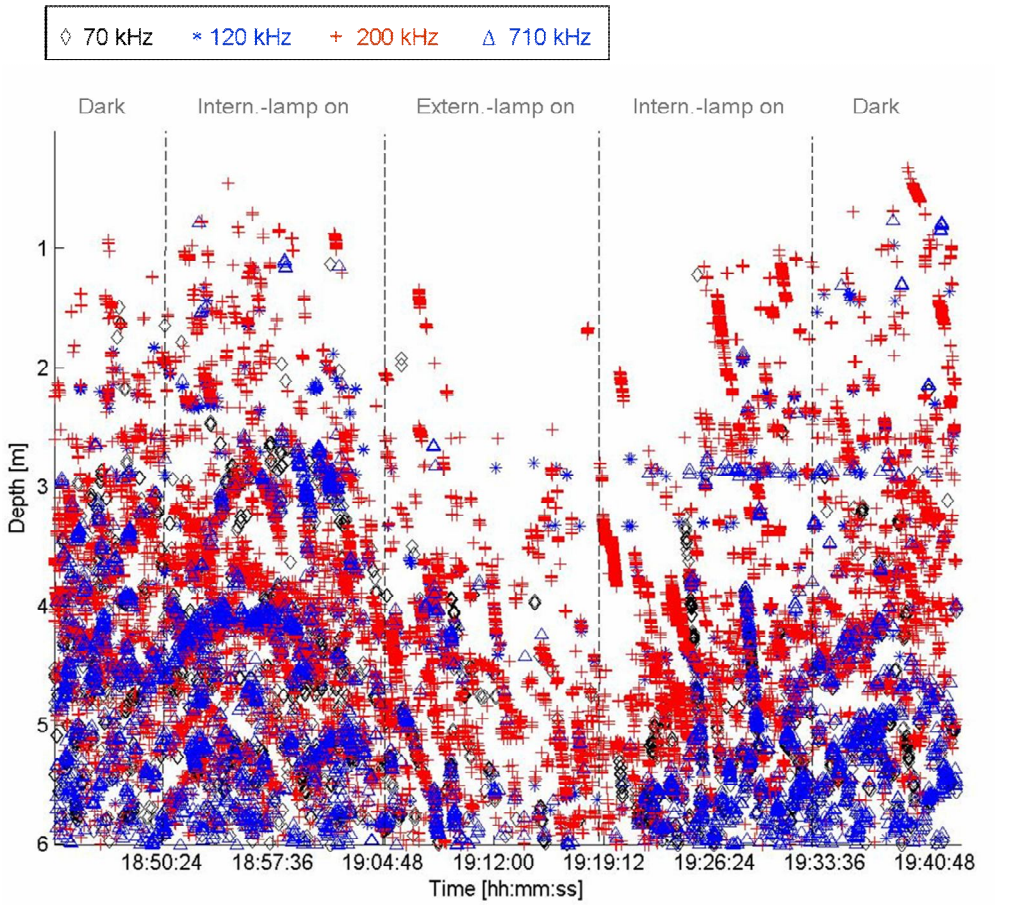

b)

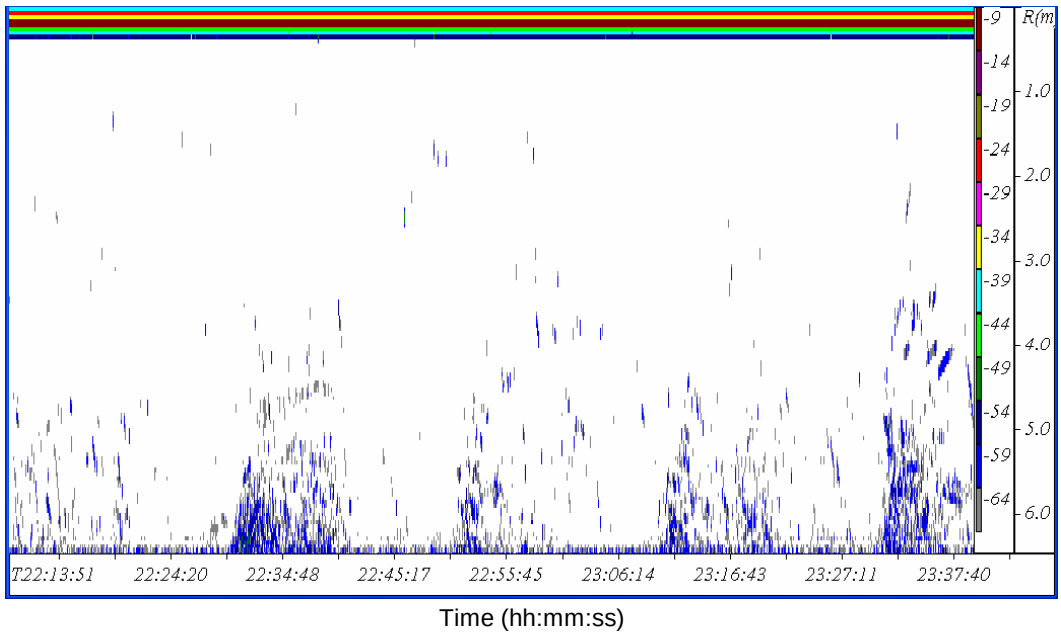

Figure 3.20: I*nternal-external lamps experiment.* a) *ER60 target range output versus time extrapolated during procedural consecutive steps* (*dashed lines*). b) *Mesocosm volume backscattering strength echogram at 120 kHz of an entire trial. S_V threshold -70 dB re 1m^{-1}, pulse duration 0.256 ms, ping rate "maximum"* (*18.4 pings per second*).

3.5.3b Tethered animals

As discussed in the previous section, useful information on natural behaviour and TS patterns of the organisms can be provided combining split-beam information and tracks analysis from data on individual free-swimming measurements. This is valid for both *in situ* (e.g. Klevier and Kaartvedt, 2003; 2006) and *ex situ* measurements. However, the knowledge of the target size is still uncertain.

Models prediction may help to estimate the size with good accuracy only if the backscattering properties of the target are well known and the TS-estimates comparable with available results obtained by measurements made under controlled conditions. These may be achieved through the so-called *suspension method*, where an individual organism is placed under the acoustic beam and forced to move under limited conditions in space and behaviour by an attachment system.

Therefore, a series of measurements on tethered specimens of *Meganyctiphanes norvegica* were performed in mesocosm with the aim to provide valuable multifrequency TS data leading to compare the theoretical predictions with more confidence. Results from such measurements and the comparison with the theoretical predictions derived from the most presently accredited model (the SDWBA, Par. 2.1.1b) are the core of Paper V.

A total of 8 specimens were investigated. This number includes measurements where the procedure was being established and refined. The set-up for tethered krill consisted in a complex system of nylon monofilament fishing lines with a 20 mm diameter tungsten carbide calibration sphere (WC20) mounted at the terminal end.

The set-up is illustrated in Figure 3.17 and described more in detail in Paper V.

The sphere was intended to act as a weight for the line, keeping it steady and vertically aligned, but also to serve as a reference target during the measurements. At a distance of 1.7 meter from the sphere, a very fine line of 15 cm length was attached to the main fishing line by a tiny lasso-like sling. This finer “life-line” held the individual krill specimens during the measurements. At the distal end of it another

sling was prepared and wrapped around the animal between the carapace and the first abdominal segment, as close as possible to the centre of krill body mass (Kils, 1981).

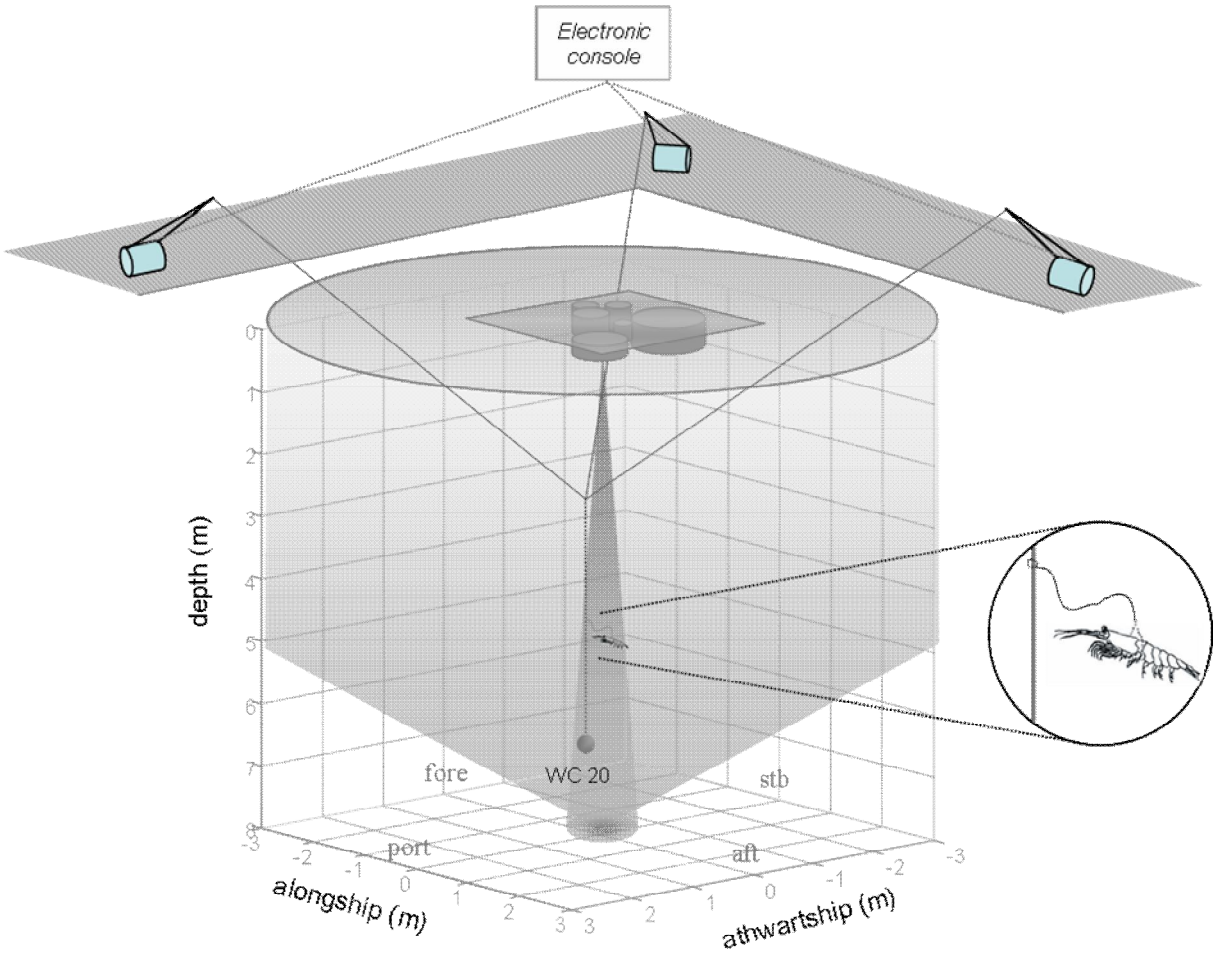

Figure 3.21: *Tethered animal experimental set-up.*

The upper end of the main line was connected at 1.4 m to a junction where three additional 0.4 diameter monofilament lines met. These lines were the suspending part of the system used for the calibration procedure described in Paragraph 3.3.2, which allowed the animal to be positioned wherever inside the mesocosm volume.

With this tethering scheme, the position of the main line could be adjusted and the animal placed close to the beam axis of each individual transducer being operative, as well as moved from one beam to another. In addition, the method of attachment of the lifeline to the animal allowed essentially free swimming, without being severely hampered by the method.

During the acoustic records, the animal was normally kept at 4 to 5 m from the transducer face, slightly depending on the frequency being used and its noise-free part from the side lobe reflection of the enclosure's walls. Placing the animal as close as possible to the beam axis of each system, a high number of detections were acquired

The typical procedure was established with all the systems in active mode. For some animals, a further series of measurements with in active only the system corresponding to the beam axis where the animal was placed and all the other in passive mode was also performed. This procedure permitted to describe the potential of the interferences on the krill TS between the primary frequency and the others.

The entire procedure took from 50 minutes to 2.5 hours, depending on the record sequence adopted. Morphometric measures and the acoustic recording sequence performed for each animal are listed in Table 3.V.

In order to investigate the potential influence on the backscattering, acoustic backscattering data of the life-line without animal were also collected at all the frequencies. This was done using the same set-up and procedure described above. The result showed a partial overlap with some of the acquired backscattering data; hence, a treatment of the linear amplitude of the acquired scattering levels was necessary to remove the line contribution.

Table 3.V: Morphometric measures and acoustic recording sequences for the tethered animals experiment. The day of measurement is referred to March 2004. All the lengths are in mm and the dry weight (DW) in mg.

ID	Day	TL	CL	BL	B1	B2	B3	DW	Record sequence
1	3	33	9.76	27	3.03	3.33	1.50	76.96	Good trial test. All frequencies active for 40 minutes, contemporary record with animal in fixed position
2	5	21	6.12	17	2.02	2.07	0.95	21.05	All frequencies active for 40 minutes, changing position
3	5	32	8.64	25	2.62	2.40	1.57	59.52	10 minutes for each frequency 2 times. All frequencies in active
4	8	26	7.84	21	2.69	2.59	1.17	50.52	5 minutes for each frequency 2 times. All frequencies in active. Bad attachment, animal inclinated.
5	8	22	6.25	18	2.19	2.02	1.00	21.04	5 minutes for each frequency, all frequencies active. Bad attachment, animal inclinated.
6	8	29	8.00	23	2.78	2.56	1.21	46.85	10 minutes for each frequency with all in active. 5 minutes with the other frequencies in passive
7	8	27	7.52	22	2.59	2.71	1.19	43.07	10 minutes for each frequency with all in active. 5 minutes with the other frequencies in passive
8	9	22	6.19	18	2.02	2.31	0.88	26.19	10 minutes for each frequency with all frequencies active.

4. Short range performances of EK60

Although the measurements performed in the mesocosm guaranteed high signal-to-noise ratio, homogenous medium and certainty in resolving the echoes as single targets, potential errors on both the measured target strength and echo energy could arise due to the target detections at short distance from the transducers.

When a target is at short distance from the transducer, the range and the echo strength determinations are biased by wrong estimation of the echo time t_E, i.e. time lag between the transmission and reception of the echo, and the error due to the time varied gain (TVG) functions implemented for the digital echosounder processing. These are denominated by Simmonds and MacLennan (2005) *system* or *electronic delay* and *TVG start error* respectively.

The first is due to the hardware component of the system that necessarily has a finite bandwidth. In the transmitting and receiving processes, the transceiver and the transducer act as band pass filters on the signal, reducing in sharpness the pulse leading edge and biasing the determination of t_E through an apparent delay. Moreover, the determination of t_E could be subject to another uncertainty deriving from the digitalization of the received analogue signal and processing treatment of the samples that may lose information of the actual echo pulse (Ona *et al.*, 1996).

In conjunction, in the modern scientific echosounders the transmission loss compensation, performed by applying the TVG functions (MacLennan, 1990), is not accurate at short range, i.e. t_E close to the pulse duration. The correct application can be obtained by the exact TVG functions, which should take in account the transmitter pulse duration τ, the bandwidth B of the system, and the scattering process of the target (MacLennan, 1986). Since different targets have different scattering properties, it is not possible to realize general formulations that provide the exact compensation of transmission loss.

In software realizations for scientific echosounders this inconvenience is overcome by adopting asymptotic forms of the exact formulations. This is justified with the

consideration that long ranges are generally involved in echosurveys procedures and the deviations are minimized in signal processing.

However, when working with targets at short ranges, users have to be aware that correction in the determinations of the ranges to the targets and their backscattering data can be required to assure sufficient accuracy of the measurements.

In the case of the EK60 systems operating in the mesocosm, the potential bias in range determination was confirmed when results between the frequencies from contemporary detections of two standard spheres (Par. 3.5.1) were observed.

Both the WC38 and WC10 standard spheres were contemporary suspended by a monofilament nylon line, at distance of approx 1.2 m from each other, inside the common insonified volume of the acoustic beams, and kept at fixed depth. Echotraces from an EK60 raw file composed of 1212 echo pings, at 0.256 ms pulse duration were extrapolated by ER60 and Sonar5 software. The mean range results are shown in Table 4.I.

Table 4.I: Mean target range output (m) extracted by the ER60 and the Sonar5 from 1212 simultaneous detections of the WC38.1 and WC10 (deeper) spheres at different systems in mesocosm.

		System (kHz)					
Software	**Sphere**	**38**	**70**	**120**	**200**	**364**	**710**
ER60	**WC38.1**	4.858	4.777	4.772	4.759	4.738	4.721
	WC10	6.019	5.927	5.919	5.903	5.894	5.866
Sonar5	**WC38.1**	4.870	4.777	4.772	4.430	4.750	4.743
	WC10	6.036	5.937	5.933	5.906	5.900	5.882

The maximum standard deviation of the range was found to be 1 cm for the WC38.1 at 38 kHz, while all the other systems revealed insignificant standard deviation less than 2 mm.

In Table 4.I, the differences in range between the frequencies are evident. Differences in echotrace range output at same frequency between the two softwares were also found. This is due to the different SED algorithm implemented in the softwares.

In order to estimate the errors, the short range performances of the EK60 systems operating at 38, 120 and 200 kHz with identical transducers to those used in the mesocosm were examined in a controlled freshwater tank with size 6×6×15 m^3 (width by depth by length) at Simrad AS in Horten, Norway, during the period 1-3 April 2005.

The experimental set-up is schematized in Figure 4.1. By means of a highly accurate mechanical positioning system, standard target spheres were placed along the beam axis at selected distances from the transducers. The range and target strength at the final output of the sounder processing were determined as means based on repeated echo realizations and compared with the actual range and theoretical TS value.

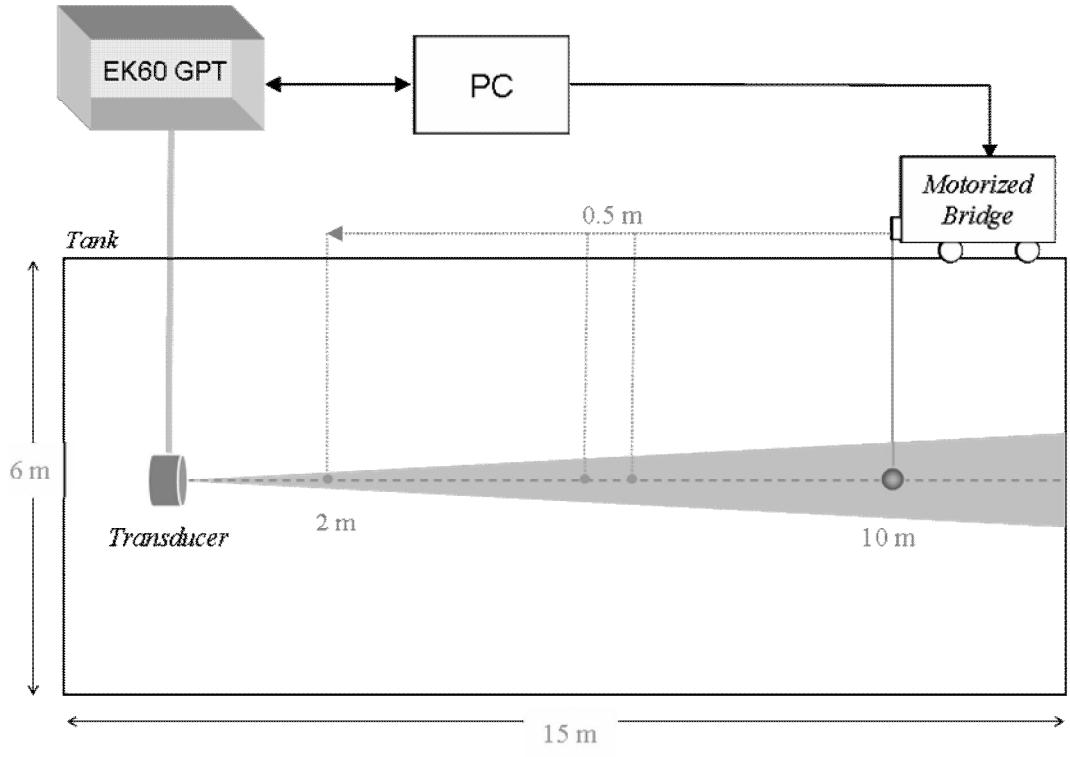

Figure 4.1: *Freshwater tank experimental set-up for the EK60 systems short-range performances tests at Simrad AS, Horten, Norway.*

The investigation is the subject of the Paper III. The reader can refer to the paper for the results on the raw data processed by the ER60, while complementary analyses and results from the same set of raw files but processed by the Sonar5 software are reported in Paragraph 4.3.

4.1 Sources of electronic delay

In order to investigate the electronic effects of the transceiver and transducer on the analogue signal separately, pulse oscilloscope records were retrieved during the ping transmission process, and the influence of the system components on the sharpness of pulse leading edge investigated. The pulse envelopes were determined from the digital records and the rise time at different steps of the process estimated.

The set-up for the transmission-delay investigation is synthesized in Figure 4.2. The signals were recorded by means of a Lecroy 9361 oscilloscope (300 MHz bandwidth and typical error 5 % or 0.17 dB). With the echosounder set in active mode, the oscilloscope was connect first at the two GPT boards before the last amplification, then to the four cables of the split-beam transducer, and finally to a hydrophone placed in the tank at distances of 10 and 5 meters from the transducer and detecting the propagating ping.

The hydrophones Brüel & Kjell 8104 and 8013 were used to detect the ping at 38 kHz and at the two other systems respectively. The hydrophones were mounted at the end of a metal arm fixed to the tank bridge and centred on transducer beam axis by oscilloscope maximum-echo level detection. Scope sampling frequency was typically 10 MHz for the 1.024 ms pulse duration, 25 MHz for the 0.512 ms and 50 MHz for the 0.256 ms.

The pulse envelope is generally defined as the outline of the signal showing the maximum amplitude of the oscillation. Different methods have been developed to determine numerically the envelope of a signal. The most popular are the squaring and the Hilbert transformation approaches. By observing the raw data, the second

approach was chosen for the purpose. The implemented envelope detector run the scope digital records generating an analytic signal with real part the original signal and the imaginary part its Hilbert transform. The envelope (E) was then determined by taking the absolute value (magnitude) of the analytic signal. A digital low-pass filter based on a Hamming window was then applied to smooth and eliminate ringing of the enveloper output. From the envelope, it was possible to evaluate the rise time (RT) of the pulse, defined as the time lag between the estimated starting time of the pulse and the time when the peak value is reached.

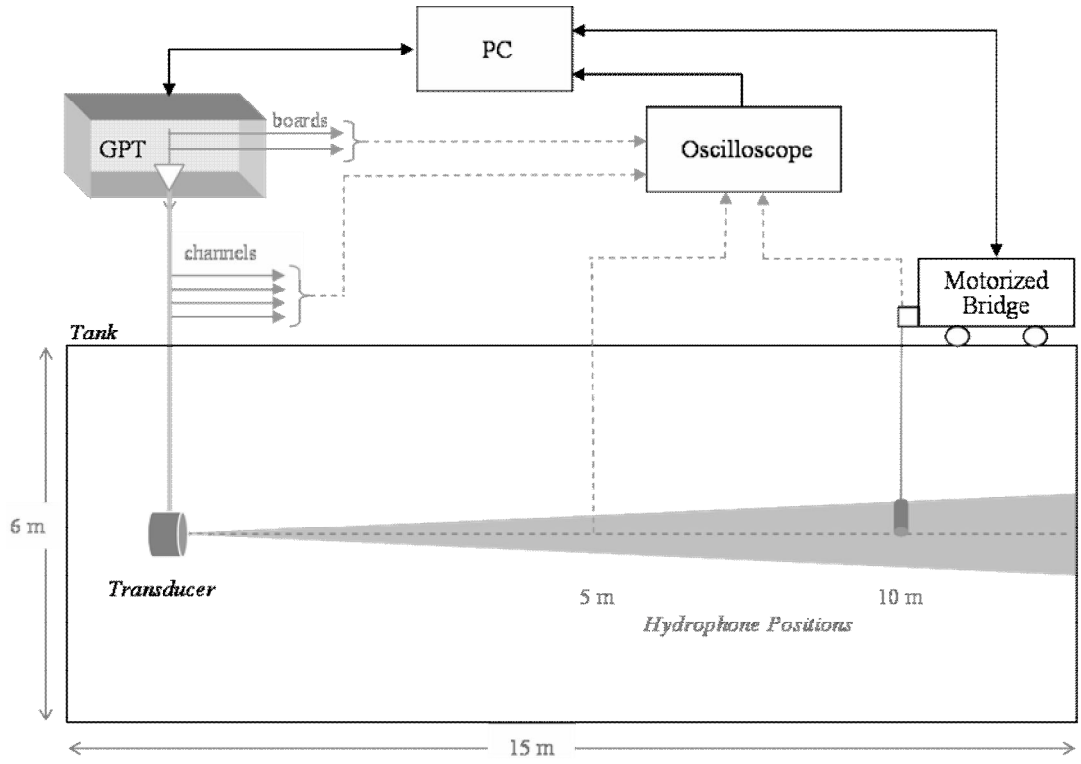

Figure 4.2: Set-up *for the pulse transmission-delay investigation.*

Since the envelope E is a positive and limited function, the peak and the start times were found analyzing the variation ΔE, i.e. the discrete derivate of the samples at the enveloper output. A zero crossing algorithm was run on ΔE, and the times relative to the zero close to the maximum of ΔE were assigned as peak time. The starting time of the pulse was assigned evaluating when the envelope achieved the 2 % of the peak voltage. The latter choice was established in order to avoid eventual signal and

hydrophone bias, which might influence the enveloper output at starting region of the pulse.

It should be noted that the results of the rise time vary upon the size of the Hamming window used to smooth the envelope; thus, it has to be taken as not absolute values. However, when the same Hamming window size is used on records from the same setting, the comparable results are useful for a purely qualitative evaluation of the pulse distortion main sources.

Since the 38 kHz system was found significantly affected from the short-range delay (see Paper III) the analysis was focus on that system. Using the same Hamming window size, the RT of the envelopes at pulse duration 1.024 ms were taken as a typical example. First, the envelope of the signal at the GPT output before the last amplification was produced and the estimated rise time was determined to be 0.12 ms (12 % of τ). For the envelope determined from the signal in the transducer cable, the estimated RT was 0.49 ms (48 % of τ); while in the medium it was found equal to 0.54 ms (53 % of τ).

The results clearly indicate that the transceiver is the main source of the pulse deformation and the major contributor to the electronic delay effect.

4.2 EK60 raw samples variability in tank

The sensitivity of the ER60 range determination is discussed in Paper III. Figure 4.3 shows an example of the recorded data during the tank measurements. The power and the uncompensated TVG40 sample arrays of 100 pings recorded with the 38 kHz system and pulse duration set at 1.024 ms are superimposed. The centre of the CU60 standard sphere was located at the actual distance of 10 m from the transducer face. The sampling distance interval of raw data was 18.9 cm. The power samples involved by the gravity principle method in the target range determination, the peak of the uncompensated array and the echotrace output results are also plotted.

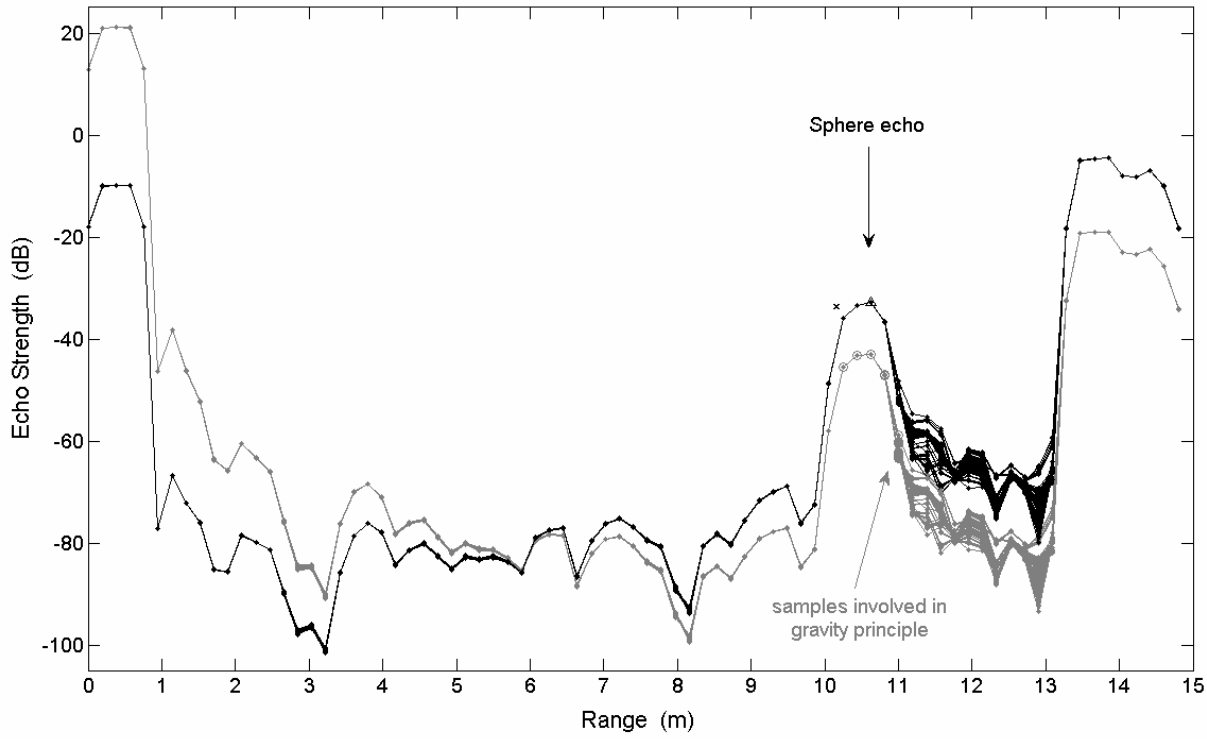

Figure 4.3: *38 kHz tank measurements at 1.024 ms pulse duration. Superposition of 100 pings raw data power (grey) and TVG40 (black) sample arrays. The power samples involved in the gravity principle method* (○), *the peak of the uncompensated array* (∆) *and the echotrace output results* (×) *are also plotted.*

It is clear that the ER60 SED processing on the raw samples in the range 3-10 m may be biased. High amplitude variability of the samples on the right side of the sphere echo is evident. This is probably due to the reverberation between the sphere and the tank wall. In particular, the last sample involved in the principle of gravity shows a high variability that may significantly affect the result. The TS echotrace data set had a variability of 0.3 dB over the 100 realizations. As described in Paper III, this confirms that due to the gravity principle adopted by the ER60 SED algorithm, tank measurements results have to be taken with care. Pre-analysis of the echograms in Simrad “Sp mode” (point backscattering strength data) with ER60 software may help to recognize depth channel free from bias on the EK60 raw samples.

4.3 Short-range errors estimated by *Sonar5* software

The potential errors at short-range detections for raw data processed by the ER60 software are presented in Paper III. Similar analysis has been performed using the Sonar5 software also, and the main results are reported here. The Sonar5 Single Echo Detector has been described in Paragraph 3.3.3.

In Figure 4.4, the range errors versus the actual target range R being determined by Equation (6) in Paper III are plotted. The range to the target was calculated by the mean over the last 100 repeated detections. Since the nearfield for the 38 kHz transducer is 2.7 m (Are Johansen, Simrad, pers. comm.), only data from longer distances are considered for that system.

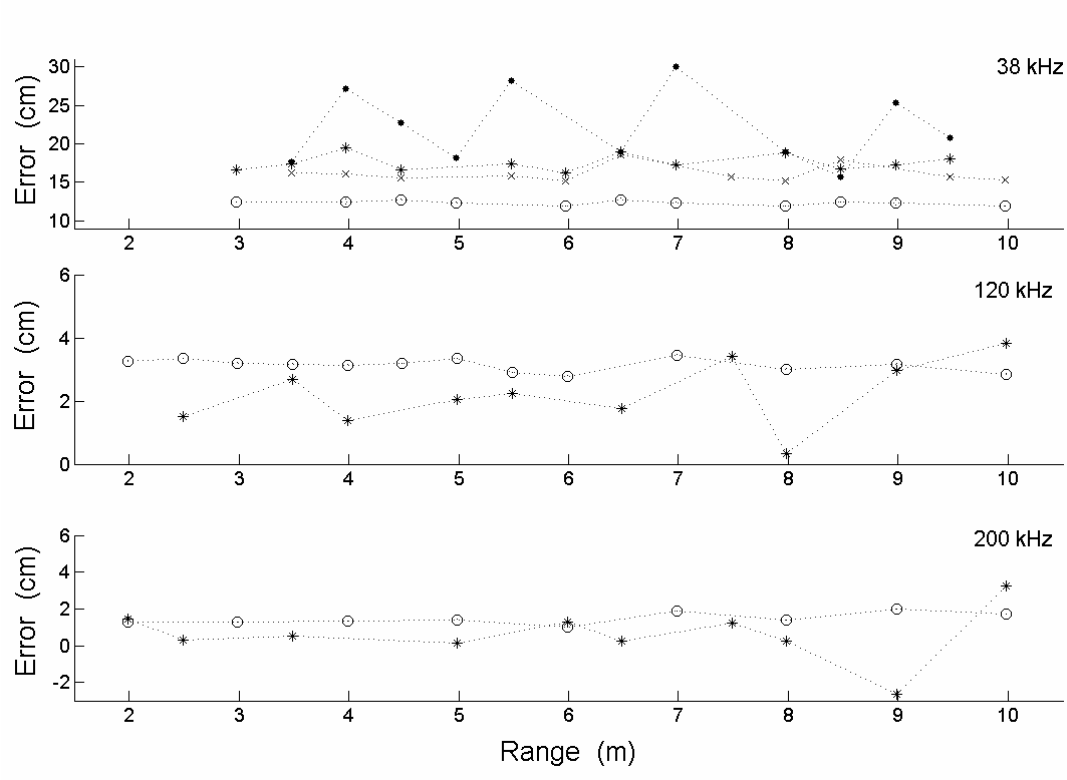

Figure 4.4: *Sonar5 echotrace range errors for three EK60 systems at pulse duration*: *2.048 ms* (•), *1.024 ms* (∗), *0.512 ms* (×) *and 0.256 ms* (o). *The grey dashed lines connecting the consecutive measures are shown for better readability.*

The coefficients of the linear regressions $Err=aR+b$ are listed in Table 4.I. The last column is the calculated intersection with the range axes, i.e. null error. For software

results comparison, Figure 4.4 and Table 4.I can be compared with Figure (8) and Table 2 in Paper III.

Table 4.I. Coefficients of the linear regressions ($Err = a\mathrm{R} + b$) from the Sonar5 echotrace analysis, with R and *Err* in meters defined by Equation (6) in Paper III.

System (kHz)	τ (ms)	$a \cdot 10^3$	b	R^2	$-b/a$
38	2.048	-2.3398	0.2368	0.01	101.21
	1.024	0.0489	0.1724	0.01	-352.52
	0.512	-0.0033	0.1614	0.19	4922.56
	0.256	-0.5685	0.1269	0.00	223.18
120	1.024	0.1748	0.0114	0.17	-6.53
	0.256	-0.0359	0.0333	0.20	92.84
200	1.024	-0.1345	0.0069	0.00	51.34
	0.256	0.0711	0.0105	0.40	-14.81

In general, the errors determined in using the two softwares show similar trends at same frequencies and pulse durations, and the related discussion on the results for the ER60 found in Paper III can be done for the Sonar5 too. However, it is evident the bigger error at 38 kHz and pulse duration 2.048 ms in the Sonar5 output, wich can be attributed to the fact that the interpolation between samples under and above the -6 dB of the peak value operated by the SED algorithm in the Sonar5 is not suitable for that pulse duration.

Figure 4.5 shows the differences between theoretical and measured TS ($\Delta\mathrm{TS} = TS_{th} - TS_{et}$) versus actual range R. The echotrace output TS_{et} is calculated as mean in linear domain over 100 realizations and the theoretical sphere TS_{th} related to the pulse length is given in the last column of Table 1 in Paper III.

The results are similar to those discussed in Paper III for the ER60 software. The general trend is not as expected and only in few cases negative ΔTS values are found as effect of the range error. Since such results were found processing the raw data using the same calibration gains by two different software but with slightly different

SED algorithm, it is possible to conclude that, despite the observed error in range detection, the internal echosounder TS processing is generally not in error for the specific settings used. Hence, no strength correction was applied in the post-processing when data were analized with Sonar5 software.

However, the investigation suggests that this problem needs to be explored by a different approach than the one used here.

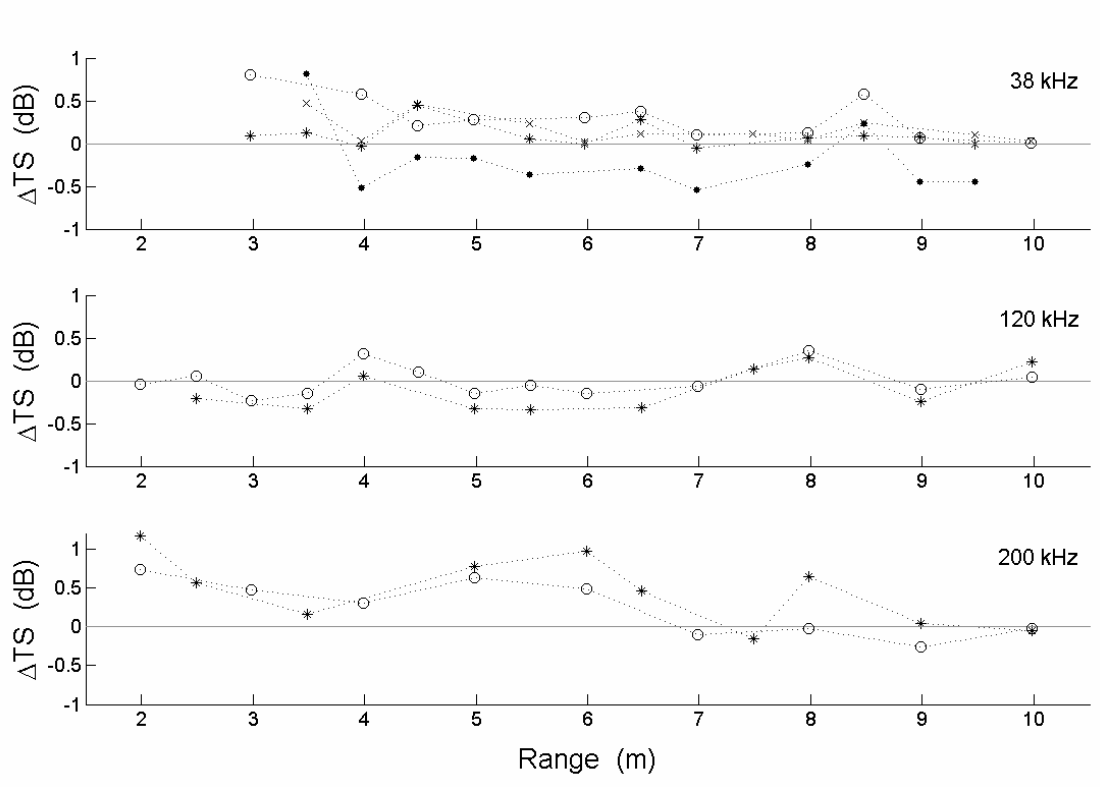

Figure 4.5: *Difference between theoretical TS and mean Sonar5 TS output of standard spheres versus actual range at pulse duration: 2.048 ms* (•), *1.024 ms* (∗), *0.512 ms* (×) *and 0.256 ms* (o). *The zero error line and the grey dashed lines connecting consecutive measures are shown for better readability*.

5. Remarks on Northern krill multifrequency echosurvey

The aim of this paragraph is to describe briefly the general issues concerning a krill multifrequency echosurvey and some of the metodologies presently adopted. Next section introduces the last paper presented in this work of thesis concerning the complexity in discriminating zooplankton species from multifrequency acoustic data acquired in a Norvegian western fjord where the Northern krill *Meganyctiphanes norvegica* species was expected to be the dominating scatterers.

Since Pieper (1971) presented for the first time the scattering cross section of marine euphausiids versus frequency, significant progress has been achieved to obtain adequate results by multifrequency krill echosurvey, in particular for the Antarctic krill species. Detailed studies on the systematic and random components of uncertainty for a generic echosurvey can be found in Tesler (1989), Aglen (1994) and Simmonds and MacLennan (2005), while numerous papers in relation to Antarctic krill echosurvey experiences can be found in literature (e.g. Hewitt *et al*., 2003; Reiss *et al*., 2008). Exploration on the uncertainties related to the current technique adopted in Southern Pole areas can be found in Demer (2004). The topic is still discussed within the CCAMLR Subgroup on Acoustic Survey and Analysis Methods.

Presently, the acoustic method by using multifrequency scientific echosounder can resolve a fine spatial variability, sampling with high resolution in the frequency domain and produce useful data over a satisfactory bandwidth. However, Demer (2004) indicated that target identification and target-strength estimation are two principal components of uncertainty in acoustical surveys of krill. More specifically, he asserted that the accuracy of the krill biomass estimate is directly proportional to the accuracy of the applied target-strength function.

5.1 General issues

Planning

To plan adequately an echosurvey is a fundamental step for the estimation process. Experience and knowledge of the local physical and biological process, especially in relation with the target species, are crucial (e.g. Trathan *et al*., 2001). These are particularly important in making decision on: 1) whether pre-planned or adaptive transects have been carried out; 2) if random or regular and systematic transect separation has to be adopted; 3) to define the survey limits; 4) to determine positions of the net hauls and the CTD casts to be undertaken.

Calibration

The potential in estimating aquatic biomass using quantitative echosounders relies on high accuracy and precision of their calibration, as well as their stability between regular calibrations. Whatever system and number of frequencies are used in the echosurvey, the calibration is obligatory.

The calibration procedure is standardized by the “target calibration sphere method” described in Foote *et al*. (1987) and became an ICES-recommended procedure. It has to be performed in waters having similar physical properties as the survey area, possibly in a geographically close location. The sphere is suspended in a known part of the beam of the immersed transducer as mounted for normal use. The received echo energy from a standard target sphere is compared with the theoretical value to determine the gains of sounder. Hence, with the introduction of power and loss compensation gains to account for both directional properties and losses, the sonar equation applied to the scientific echosounders becomes independent of the input power level and observation point (MacLennan, 1990). Measurement of other object can then be expressed in absolute physical units.

The total error in calibration should be no more than 4 % (Korneliussen *et al*., 2008). In order to reduce the error, Foote *et al*. (1987) suggested to take precisely into account the physical parameters of the seawater at the time of calibration.

It is very important that the echosounders are calibrated at temperature as close as possible to those prevailing within the area in which the survey is conducted. Brierley *et al*. (1998a) estimated an underestimation of Antarctic krill biomass of 52.5 % if the analysis of South Georgia survey data at 120 kHz is executed employing calibration parameters derived from a calibration performed in Norwegian fjord rather than in the survey area waters. Errors in system calibration have also to be considered in relation to the effects of variations in water temperature and salinity on sound speed, absorption, as well as the beam pattern within the survey area (MacLennan, 1990; Demer, 2000; Demer and Renfree, 2008). In practice, it is strongly suggested to execute measurements of salinity and temperature throughout the entire survey and update the echosounder with the actual sound speed value during the acoustic data acquisition.

Multifrequency and identification algorithms

Amakasu and Furosawa (2004) investigated the effective frequency for the acoustic survey of Antarctic krill from the viewpoints of the variation of target strength, detection range, and absorption coefficient. They concluded that the 120 or 70 kHz are the most suitable frequencies. At the present, since there has been no available 70 kHz system of required quantity in the market, the *de facto* international standard frequency for surveying krill is 120 kHz (Demer and Conti, 2005).

However, as previously mentioned, there are several advantages to recommend using dual or multifrequency systems. For the single frequency method, the accuracy of the biomass estimate is directly proportional to the accuracy of the TS estimate. Increasing the number of operative frequencies leads to reduce the general uncertainty of the results if the scattering from dissimilar targets in a volume at different frequencies is predictable. Moreover, the target position information from more transducers improve the accuracy and precision of the results by greatly reducing the occurrence of multiple targets in the analysis (Demer *et al.*, 1999; Conti *et al.*, 2005b) and produce a more realistic results between the frequencies (Kornielussen *et al.*, 2008).

With the adoption of three frequencies, the ΔS_V method could be less biased leading to a better rejection of non-krill species and elucidating the krill patchiness. Moreover, with the improvement of numerical techniques and the validation of the theoretical scattering models, the indirect determination of the orientation could be estimated with better accuracy (Chu *et al*., 1993; Demer and Conti, 2005; Conti and Demer, 2006), also with broad-bandwidth techniques (Martin Traykovsky *et al*., 1998).

For effective multiple-frequency data analysis, the insonified volumes of each frequency have to be spatially similar as far as possible (Demer *et al*., 1999; Kornielussen *at al*., 2008). This may be obtained by using transducers with similar characteristics (i.e. beamwidths) installed with the minimum-space distance criterion, and acquire data with identical pulse duration for each system (Korneliussen *et al*., 2004; 2008).

Theoretical prediction

Both the forward and the inverse approach require prediction of the target strength of krill versus size. Theoretical models will supply this information when direct measurements of target strength in the survey area are not certain.

Although the equation of Greene *et al*. (1991) (Par. A3.1) was accepted as estimator of krill target strength by CCAMLR for several years and had been corroborated with empirical data (Foote *et al*., 1990; Hewitt and Demer, 1991; Pauly and Penrose, 1998), many authors have recognized that the variety of parameters influencing the target strength were not all encompassed in the Greene model. More details on the application of the Greene model can be found in Par. A3.1 in Appendix.

On the base of that remark, the CMLAR subgroup on acoustic survey and analysis method endorsed the change in philosophy from the use of an empirical-only TS model (i.e. Greene *et al.*, 1991) towards the use of theoretically based, empirically-validated models (SC-CAMLR, 2005). Based on the information available at the time, the subgroup agreed that the most appropriate theoretical model for krill target strength was currently the Stochastic DWBA in its parameterized form (Par. 2.4.1b).

The DWBA model has been recognized as the state-of-the-art among the physics-based models (Stanton and Chu, 2000; Demer and Conti, 2005). Nevertheless, it should be emphasized that the distribution of orientation and the "fatness" coefficients used to parameterize the Stochastic DWBA by Demer and Conti (2005) are based on the fitting procedure of empirical data rather than direct measurements of all necessary parameters acquired during the survey. When possible, the latter parameterization is certainly preferable (Lawson *et al*., 2006, 2008a). In Paragraph 2.4.1a, recent parameterizations based on direct observations presented in literature are reported.

However, the potential for reasonable accuracy in practical applications of the ray-solutions, and in some restricted case the volume dependent High-Pass models (Par. A2.2) might be considered as alternative. These simpler models are based on approximations but, since the last observations of the animal orientation in their natural habitat indicate that the mean value could be approximate close to the broadside (Hamner and Hamner, 2000; Conti and Demer, 2006; Lawson *et al*., 2006), their use on measurements of volume backscattering and scattering geometries can be justified (Stanton and Chu, 2000). When the condition of broadside aspect are certain and higher accuracy wanted, the exact bent cylindrical modal solution model (Par. A1.2.1c) could be considered as an extreme alternative.

Krill orientation distribution

The observed variability in krill target strength and the discrepancy between empirical data and theoretical models are mostly due to the uncertainty of the knowledge in animals orientation with respect to the incident acoustic wave (Sameoto, 1980; Everson, 1982; McGehee *et al*., 1998; Martin Traykovski *et al*., 1998; Demer and Conti, 2003a; Conti and Demer, 2006). In a multifrequency context, the observed spatial and seasonal impact on backscattering from krill schools can be explained simply by the variability in orientation of animals (Demer and Martin, 1995; Demer and Conti, 2005; Lawson *et al*., 2004, 2006).

Thus, the knowledge of the orientation distribution is fundamental for acoustic-survey data analysis. Few works have been published on *in situ* krill orientation (Par. 2.1), indicating the strong need of techniques to assure realistic knowledge of the orientation during the data acquisition. To provide certain information on orientation, as well as on density within the schools, information acquired with video or other proper devices should be a standard procedure during the survey, similarly to the net sampling.

Net sampling and length determination

The number of krill per kg decreases exponentially as the length increases (Hewitt and Demer, 2000). This rate is approximately the same since the predicted backscattering cross-sectional area of a single krill increases with increasing length, and implies that the mean length may be used to calculate acoustically biomass densities without introducing substantial errors. In the case of mono-length distribution, the estimates of krill biomass density are relatively insensitive to minor the variations in the frequency distribution of length (Greenlaw *et al.*, 1980; Hewitt and Demer, 1993). Nevertheless, the uncertainty in total net volume of zooplankton is recognized as one of the main source of error in the complete analysis of echosurvey.

Strong strobe lights mounted on the nets and flashing at few seconds interval have been used to shock or blind the animals temporarily minimizing the perception and the avoidance of the net with the effect of increasing (10-20 times) the total catch (Sameoto *et al.*, 1993; Wiebe *et al.*, 2004; Lawson *et al.*, 2004).

There are various definitions of krill length reported in literature. A standard definition is not adopted. It depends on the principal body limit-points recognizable in the target species. The various length definitions were summarized and codified by Morris *et al.* (1988).

Nevertheless, the researchers have used different definitions of total length for the same species, and althought a standard measure has been not established quite often there is a miss of description in the publications. In order to produce comparable results, the definition of krill length used in the analyses must be always declared.

5.2 A case study on Northern krill acoustic estimation

It is recognized that the Antarctic krill is the krill species of main interest, hence the most studied from acoustic point of view also. Antarctic krill forms mostly mono-specific aggregations in the main areas of investigation (Miller and Hampton, 1989a), and this feature, even if sometime substantial variability in the length of member animals between closely spaced aggregations were found (Watkins, 1986), may in some way facilitate in suggesting an appropriate survey procedure designated to be standard and systematic. On the contrary, to suggest an adequate procedure for the Northern krill case is not an easy task. This species is typically found in aggregations that are mix of species and sizes of other zooplankton and fish larvae, especially close the coast, varying with the physical and the biological processes seasonally activated in the area.

This natural feature reflects in different scattering structures and leads to questioning about the use of the methodologies established from the experiences on Antarctic krill for the Northern krill echosurvey case. An example of different conclusions can be found in literature regarding the time of the day for the acoustic data acquisition and net sampling. Demer and Hewitt (1993) and Demer (2000) indicated the daylight as the most favourable time for the acoustic acquisition on Antartic krill because the potential bias attributable to diel vertical migration is minimized. On the contrary, Everson *et al.* (2007) claimed that for a *M. norvegica* echosurvey there are advantages to perform the acoustic acquisition during the night. The TS data have a reduced variance due to the natural dispersion of the organisms comprising the mixed aggregations at that time, and the net sampling are performed during the daylight time.

In Paper VI, multifrequency acoustic results were compared with those obtained from krill-trawl samplings performed in two depth layers where different types of scattering structures were detected: the first with weak and dispersed scatterers, the second a Sound Scattering Layer (SSL) due to a dense aggregation of zooplankton commonly found in the Norwegian western fjords. In both the layers, the Northern

krill *Meganyctiphanes norvegica* species was found to be the dominating scatterers (Table 2 of Paper VI). As supplementary results, in Figures 5.1 and 5.2 the frequency distributions at the different acoustic frequencies of the resolved echoes in the sampling layers from acoustic data acquired during the samplings are shown.

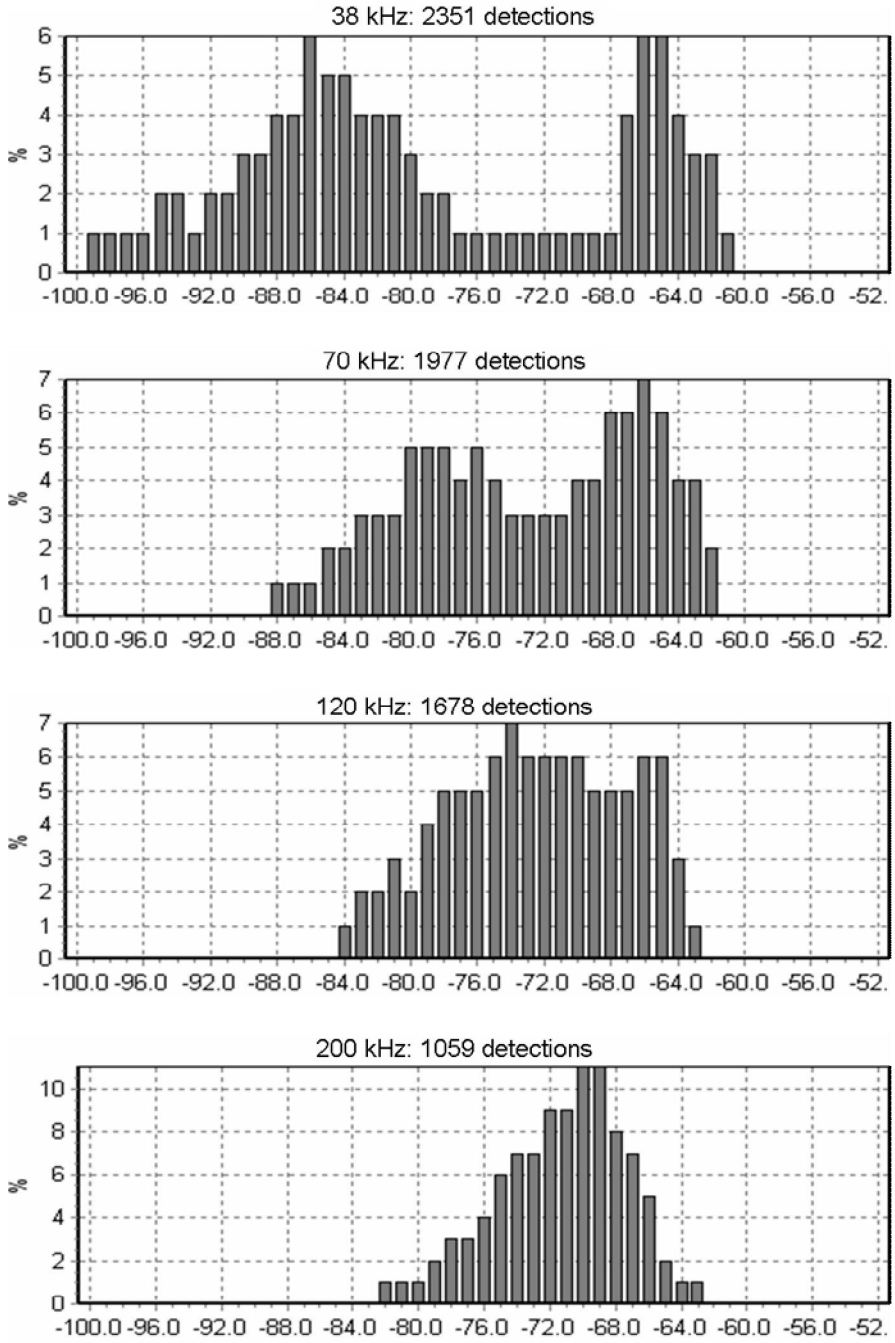

Figure 5.1: *Frequency distributions at the operative acoustic frequencies of the resolved echoes with Sonar5 software within the sampling layer 25-30 m from EK60 raw data contemporary recorded during the catching event krill-Trawl 1. The speed boat was 3 kn, the ping rate and the pulse duration were set for all the sistems at "maximum" and 1.024 ms respectively.*

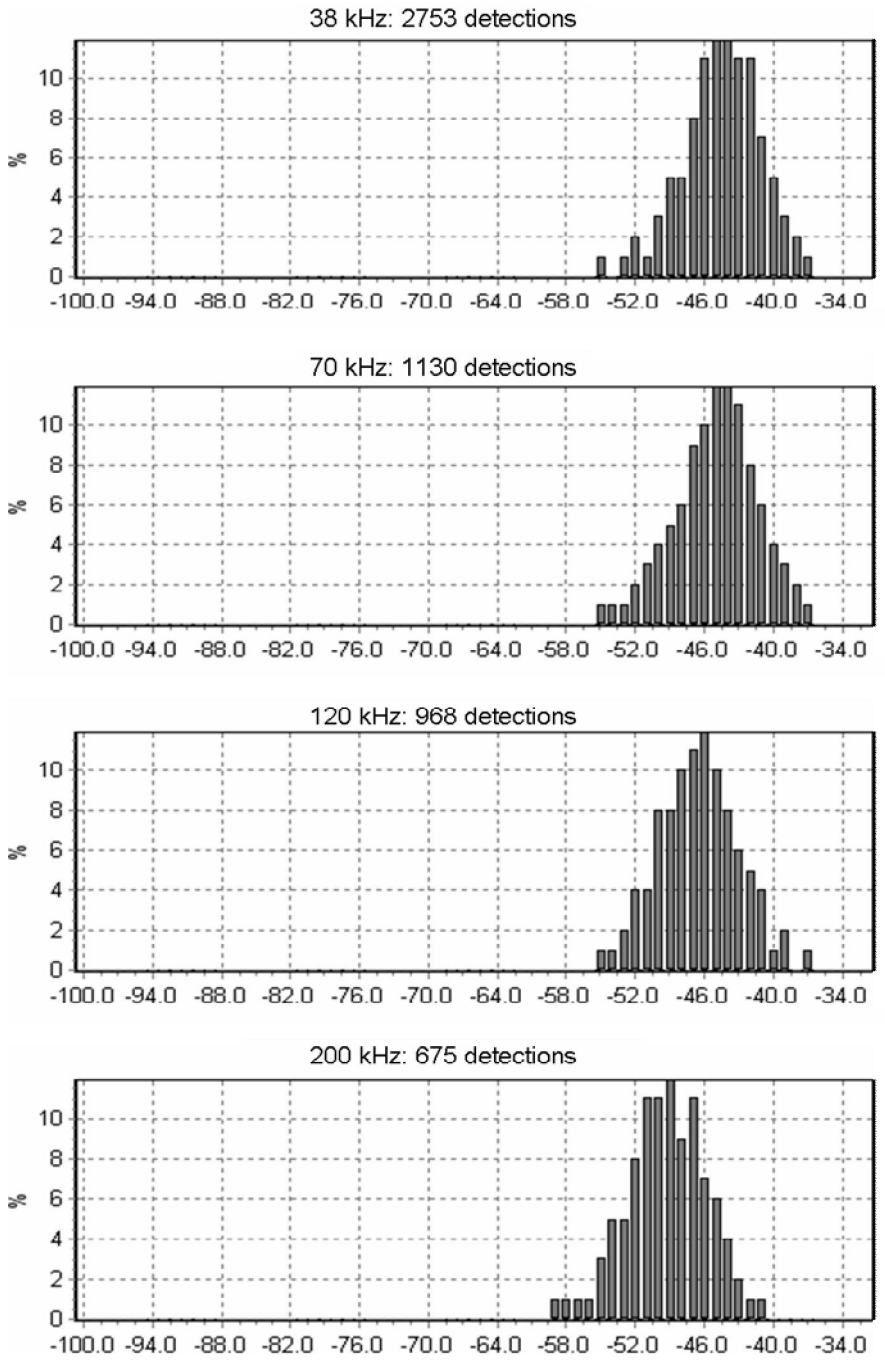

Figure 5.2: *Frequency distributions at the operative acoustic frequencies of the resolved echoes with Sonar5 software within the sampling layer 120-130 m from EK60 raw data contemporary recorded during the catching event krill-Trawl 2. The speed boat was 3 kn, the ping rate and the pulse duration were set for all the sistems at "maximum" and 1.024 ms respectively.*

For both the figures, the echoes were retrieved by Sonar5 with same SED acceptance criteria: TS threshold -100 dB, echo length 40-180 % of the pulse duration, target samples standard deviation in phase measurements less than 8, beam pattern

compensation 3 dB. It is evident the complexity in resolving echo detections of weaker scatterers in the second case, despite the identification analysis of the sample indicated a high number of Euphausiids. Attempts to retrieve weak echoes by “opening” the SED filters (echo length 20-200 % and samples standard deviation 15) were performed without successful.

The results clearly show that for a more complex mixture of scatterers, like typical SSL observed in Norwegian fjords, stronger scatterers (*Müller's pearlside* for the specific case) will prevail and completely mask weaker scatterers like krill to the SED algorithm processing steps.

Before the biological sampling, the same trawl transect was replicated to acquire acoustic data with different echosounder settings, and explore the influence of the key echosurvey parameters like ping rate, pulse duration and vessel speed, on the echo-integration. This is the core of Paper VI; the spatial resolution of acquisition and process parameters of the EK60 systems at the different settings are described and discussed. The relationship of the increasing beam volume along the depth with different pulse durations is also pointed out.

APPENDIX

Survey of acoustic scattering models for fluid-like organisms

A1 Geometrical approximation models

Since it is difficult to describe scattering from the exact shape of most zooplankters, earlier investigators have used simple geometrical forms such as spheres, spheroids, or finite cylinders to approximate the anatomical shape of the organisms. The volume of the geometrical shape is assumed equivalent to that of the animal, and an *equivalent radius* a_{eq} may be determined for every shape. In such way, the scattering become defined in the last approximation as a function of a single linear parameter such as spherical radius or cylinder length.

From the theory, the scattering from an object is given by its size, form and acoustical impedance, which depends on the difference in density and sound speed between the object and the surrounding medium. Thus, an acoustic model can predict the scattering from individual organism (target strength) where the acoustic frequency, size of the organism, density and sound speed contrasts between the animal with its environment are the basic input to the model.

In the rest of the text, the variables without indexed or with subscripts 1 refers to the surrounding medium and index 2 refers to the fluid-like medium of the zooplankton body. The symbols g and h are the standard notification for the contrasts of density ($g=\rho_2/\rho_1$) and sound speed ($h=c_2/c_1$) respectively.

A1.1 The sphere model

In 1950, Anderson developed one of the first models of sound scattering applicable to estimating target strength of zooplankton. He solved the problem of sound scattering from a homogeneous fluid sphere with acoustic properties similar to those of the

medium and with diameter less than several wavelengths. The Anderson model considers an irregular shaped fluid-like target to be acceptably described by a sphere containing an equivalent volume, but does not include other considerations on the target shape. This gives a sense of generality and large approximation to the model, especially for directional scatterers. However, it was the first instructive step in predicting target strength of zooplankton fluid-like species even with complex shapes (e.g. Greenlaw, 1977, 1979; Greenlaw *et al.*, 1980; Holliday and Pieper, 1980; Pieper and Holliday, 1984; Stanton *et al.*, 1987; Foote *et al.*, 1990).

The original fluid-sphere model consists of a summation of an infinite number of vibrational scattering modes. Considering a sphere with centre located at the origin of a polar coordinate system $[r,\theta,\phi]$, for axial symmetry (plane acoustic wave travelling parallel to the polar axis in $-z$ direction) the dependence on ϕ is eliminated, and the general solution of Equation (2.1) is given in terms of spherical harmonics according to (Anderson, 1950):

$$p = \sum_{m=0}^{\infty} A_m P_m(\cos\theta) \begin{bmatrix} j_m(kr) \\ n_m(kr) \end{bmatrix} e^{-i\varpi t} \tag{A.1}$$

where A_m is a constant to be determined by the boundary conditions for p and u by the Equations 2.2, P_m is the Legendre function, j_m is the spherical Bessel function and n_m is the spherical Neumann function, m is the number of modes, ω is the angular frequency, k is the wave number and θ the scattering angle.

For the region $r > a_{eq}$, the scattered wave can be written as:

$$p_{scat} = \sum_{m=0}^{\infty} A_m P_m(\cos\theta)\left[j_m(kr) + i n_m(kr)\right] e^{-i\varpi t} \quad . \tag{A.2}$$

By expanding the incident wave in terms of spherical harmonics and applying the boundary conditions, the scattered wave in the far field of the sphere can be written:

$$p_{scat} = P_0 \frac{i}{kr} e^{-(i\varpi t - ikr)} \sum_{m=0}^{\infty} (-1)^m P_m(\cos\theta) \frac{2m+1}{1+iC_m} \tag{A.3}$$

with P_0 is the amplitude of incident plane wave and

$C_m = \dfrac{(\alpha_m^* / \alpha_m)\ (N_m / J_m^*) - (\beta_m / \alpha_m)\ gh}{(\alpha_m^* / \alpha_m)\ (J_m / J_m^*) - gh}$, where the functions α_m and β_m are defined by:

$$\alpha_m = mJ_{m-1} - (m+1)J_{m+1} \quad ; \quad \beta_m = mN_{m-1} - (m+1)N_{m+1}$$

The unsigned functions have argument k_1a and signed functions with asterisk (*) have argument k_2a, where k is the wave number.

From Equation (A.3), the angle dependence of the scattered wave p_{scat} is given by the Legendre function: $P_m(\cos\phi)$, which for the backscattering process (θ=0) is equal to 1 for all m. Using Equation (A.3), the backscattering cross section of a fluid sphere in the far field can be written according to (Dalen and Kristensen, 1990):

$$\sigma_{bs} = \frac{1}{k_1^2}\left[\sum_{m=0}^{\infty}(-1)^m \frac{2m+1}{1+iC_m}\right]^2 \qquad \text{(A.4)}$$

The sphere model represents an exact solution of the acoustic wave equation for object of spherical shape and all kind of material that support only compressional waves (gas or liquid). It can be considered a first-order approximation under some condition for very complicated scattering process of animals with more complex shape (Stanton *et al*., 1998a).

A1.2 The cylindrical models

The sphere model approximates the body of zooplankters in a truly general way. The shape of many species deviates significantly from that of a sphere and strong differences in scattering values are expected. In particular, euphausiids and decapod shrimps are elongated animal with length-to-width ratios in the order of 5 or higher (Stanton *et al*., 1998a); their body shape is more like a deformed cylinder (elongated and circular in cross section) than a sphere. Wiebe *et al*. (1990), derived regressions relationships relating mean-TS to length, wet weight, dry weight and *ka* (wave number × equivalent spherical radius) basing the analysis on empirical data, and

claiming that crustaceans zooplankton are scattering sound much more like cylinders than spheres.

There have been a number of formulations and applications to the zooplankton scattering using cylinder shapes. The earliest models used an approach based upon the exact modal series solution presented by Stanton in the years 1988 and 1989. Before Stanton's articles, the theory for the scattering models by cylinders was referred to *infinitely* long cylinder theory (e.g. Flax *et al*., 1980). The formulations were complicated, with associated problems in numeric implementation. Stanton overcomes the major theoretical problem considering that the *finite* cylinder has boundary conditions with cylindrical symmetry, but the far field scattered wave spreads spherically.

The modal approach provides exact solutions to the scattering problem at near broadside incidence for a wide range of materials. Numerically, high numbers of terms are needed for the convergence, hence it is time consuming. Very often, simple and rapid estimation of backscattering strength is needed. Approximations of modal formulation, such as the truncated versions and the High-Pass solutions (Par. A2.1 and A2.2), satisfied this requirement. In particular the High-Pass solutions are shown to be also important were the sound is scattered by a large collection of objects of varying size, i.e. swarm of mixed compositions (Stanton *et al*., 1994b).

The modal series solution was an important step to the development of scattering models by elongated animals, but the validity of this approach is limited to target orientated near broadside incidence (Partridge and Smith, 1995) and difficult to manipulate algebraically in the geometric region (Stanton *et al*., 1993a).

With the assumption that many zooplankton organisms are “weakly scattering bodies” (i.e. $g,\ h \cong 1$), and by using this for the boundary conditions and certain other assumptions, Stanton *et al*. (1993a, 1993b, 1994a, 1996, 1998c) and Martin *et al*. (1996) have developed and used a deformed cylinder approach based on ray representation. This reduces the numerical complexity of sound scattering models and may well describe averaged echo levels from aggregation of animals of random

orientation and length. Although approximated, the ray-based solutions (Par. A2.3) are of great utility to predict the frequency dependence in the geometric region, as well a mathematically explicit description of the physical process. Moreover, they are also useful for description of the statistics of the ping-to-ping variability (Stanton *et al.*, 1993b).

A1.2.1 Modal solutions

The theory involving a modal series solution is general enough so that the cylinders can be arbitrarily bent (radius of the curvature can vary along the axis) and the cross-section can vary along the axis provided the bends and rate of change of tapering are gradual. It can be used for a broad range of materials, i.e. the composition can be fluid, elastic, or a combination such as an elastic shell filled with fluid. The directions of the incident wave and receiver position vector, as well the orientation of the cylinder can be arbitrary within a limited range of angles so that the normal or near-normal incidence is maintained to all the tangents of the bent axis (i.e. at end-on incidence, the solution breaks down).

By neglecting the end effects, the volume flow per unit length of the scattered field for the *finite* cylinder is approximated equivalent to the *infinite* cylinder. Therefore, the solution is obtained by integrating this volume flow along the length of the entire cylinder. The following assumptions are made in the general solution for the *infinite* cylinder:

1. There is no dispersion or nonlinearities in the cylinder or surrounding medium;
2. End effects of the scattering by the finite cylinder are not important;
3. Deformations of the cylinder axis, cross-sectional radius, and composition profile vary slowly with respect to the position along the lengthwise axis of the cylinder.

Assumption (2) leads to use the volume flow per unit length of an infinitely long cylinder equivalent to a finite length cylinder. On the other hands, it restricts the solution to geometries where: (a) the direction of incidence and scattering is normal

or near normal to the tangent of the axis of the cylinder and (b) the aspect ratio of the cylinder (length to diameter) is much greater than unity.

In cylindrical coordinate system with the z-axis the axis of the cylinder, the general solution of Equation (2.1) for an *infinitely* long cylinder is:

$$p = \sum_{m=0}^{\infty} A_m \cos(m\phi) \begin{bmatrix} J_m(kr) \\ H_m^{(1)}(kr) \end{bmatrix} e^{-i\varpi t} \tag{A.5}$$

where A_m is a constant to be determined by the boundary conditions for p and u (Eq. 2.2), J_m is the Bessel function of the first kind of order m and H_m is the Hankel function of first kind defined in terms of J_m and the Neumann function (N_m), r is the (polar) distance from the axis of the cylinder to the field point, m is the number of modes; ω is the angular frequency; k is the wave number; ϕ the azimuthal angle that sweeps through the plane perpendicular to the axis of the cylinder ($\phi=\pi$ is the backscatter direction).

For a normally incident plane wave of amplitude P_0 travelling in the positive x direction, the scattered pressure can be expanded in terms of Bessel functions according to (Stanton, 1988a):

$$p_{scat} = P_0 \sum_{m=0}^{\infty} B_m \cos(m\phi)\, H_m^{(1)}(kr) \tag{A.6}$$

The coefficients B_m are determined by satisfying the boundary conditions and are dependent upon the material properties. A general method for the determination of B_m is given in Goodman and Stern (1962). For a fluid cylinder, they are obtained by:

$$B_m = \frac{-\varepsilon_m i^m}{1 + iC_m} \tag{A.7}$$

where ε_m is the Neumann factor equal to 1 for m=0, and to 2 for $m>0$, and

$$C_m = \frac{\left[J_m'(k_2a)\cdot N_m(k_1a)\right]/\left[J_m(k_2a)\cdot J_m'(k_1a)\right] - gh\cdot\left[N_m'(k_1a)/J_m'(k_1a)\right]}{\left[J_m'(k_2a)\cdot J_m(k_1a)\right]/\left[J_m(k_2a)\cdot J_m'(k_1a)\right] - gh} \tag{A.8}$$

with a the equivalent cylindrical radius.

The apparent volume flow per unit length q_a of the scattered field due to the *infinite* cylinder (as observed in the ϕ direction) is derived in Stanton (1988a) as:

$$q_a = \frac{4P_0}{k\rho c} \sum_{m=0}^{\infty} B_m \cos(m\phi) \tag{A.9}$$

where the variables without index are referred to the surrounding medium.

With the assumption 2, it is possible to express the exact scattered pressure per unit length of the *infinitely* long cylinder in terms of q_a, and the generalized deformed cylinder geometry as:

$$\mathrm{d}p_{scat} = \frac{-ik\rho c q_a}{4\pi} \frac{e^{ik(r_s+\delta_s)}}{r_s} \left|\mathrm{d}\vec{r}_{pos}\right| \tag{A.10}$$

where $\vec{r}_{pos}$ is the position vector of a point on the axis of the cylinder, the term $\left|\mathrm{d}\vec{r}_{pos}\right|$ is the differential of the arc-length of the axis of the deformed cylinder, r_s is the distance from a point on the axis at $\vec{r}_{pos}$ to the field point, and δ_s is the distance between the point on the axis at $\vec{r}_{pos}$ and the plane that contains it and the origin which is perpendicular to the direction of the incident plane wave.

Stanton used Equation (A.10) to approximate the (differential) scattered pressure due to a differential element of a deformed cylinder. Each differential element can be considered an infinitesimally thin slice of an infinitely long cylinder with a straight axis in the direction of the tangent to the axis of the deformed cylinder at that location and a constant radius equal to the radius at that location.

The total scattered field due to the entire deformed cylinder is then approximately a summation or the integral of the differential scattered pressures due to the slices. This integral is essentially a quasi-stationary solution and its accuracy depends on the rate at which the composition profile, radius, and tangent to the cylinder axis change along the axis. The slower those properties change the more accurate the solution will be.

Using further approximations (Stanton, 1989a), when the receiver is far away from the cylinder, the sum (r_s+δ_s) can be replaced by the sum of r (distance between the field point and the origin) and a simple dot product, so that the scattered pressure can be written according to (Stanton, 1990):

$$p_{scat} = P_0 \frac{e^{ikr}}{r}\left(\frac{-i}{\pi}\right) \int_{\vec{r}_{pos}} \sum_{m=0}^{\infty} B_m \cos(m\phi)\, e^{ik\, r_{pos}(\hat{r}_i - \hat{r}_r)\cdot\hat{r}_{pos}} \left|d\vec{r}_{pos}\right| \qquad \text{(A.11)}$$

where r is the distance between cylinder and receiver, $\vec{r}_{pos}$ is the vector from the origin to the integration point on axis of cylinder, $\hat{r}_{pos}$ is the unit vector in the direction of integration point on axis of cylinder, $\hat{r}_i$ is the unit vector in direction of the incident plane wave, $\hat{r}_r$ is the unit vector in direction of receiver, $\phi = \cos^{-1}(\hat{r}_{i\perp} \cdot \hat{r}_{r\perp})$ is the azimuthal angle of tangent to cylinder axis (Fig. A.1a), with:

$$\hat{r}_{i\perp} = \frac{\hat{r}_i - (\hat{r}_i \cdot \hat{r}_{\tan})\,\hat{r}_{\tan}}{\left|\hat{r}_i - (\hat{r}_i \cdot \hat{r}_{\tan})\,\hat{r}_{\tan}\right|}\;; \qquad \hat{r}_{r\perp} = \frac{\hat{r}_r - (\hat{r}_r \cdot \hat{r}_{\tan})\,\hat{r}_{\tan}}{\left|\hat{r}_r - (\hat{r}_r \cdot \hat{r}_{\tan})\,\hat{r}_{\tan}\right|}\;,$$

where $\hat{r}_{\tan}$ is the unit vector of tangent to cylinder axis (Fig. A.1b).

The coefficients B_m in Equation (A.11) depend on the composition of the cylinder, whether it is entirely fluid (Eq. A.7), elastic, or perhaps a combination, such as having an elastic outer shell with a fluid core. From Equation (A.11), using the Equations (2.4) and (2.5), the backscattering cross section and the target strength can be obtained.

Equation (A.11) is a general equation that describes the scattering by a deformed cylinder with variable properties and scattering geometries. In general, the integral is relatively complicated and must be evaluated numerically. Only for few cases, such as when the cylinder is straight, it can be integrated analytically.

Stanton *et al*. (1998a) showed that for very low frequencies and certain distributions of orientation angles at high frequencies, the averaged scattering by cylinders would be similar to the scattering by spheres of the same volume.

At this stage, the basic definition of the equivalent radius *a* has to be redefined. Since it is the larger middle portion of the animal that scatters the sound over the smaller outer portion, Stanton (1989a) found reasonable to assume that the " acoustic" radius would be larger than the average radius derived by morphometric relationship (e.g. Greenlaw, 1977; Kils, 1979a). On the base of the fitting between model and direct TS data, he suggested to use a radius 60 % larger than the average cylindrical radius determined from averaged measurements on many animals.

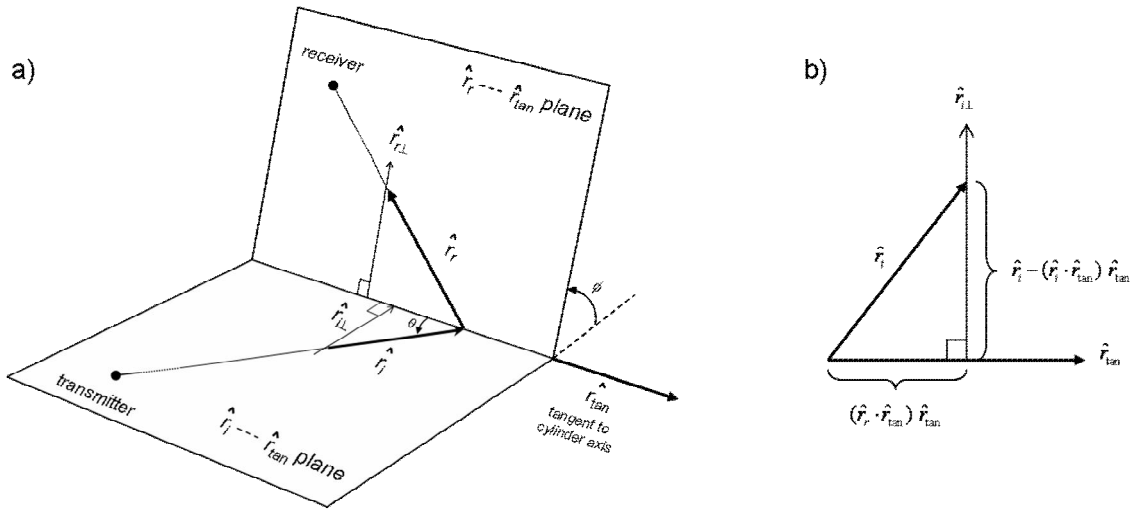

Figure A.1: a) *Scattering geometry of arbitrarily oriented finite cylinder*; b) *Illustration of* $\hat{r}_i$ *and* $\hat{r}_{\tan}$ *components that are used to construct* $\hat{r}_{i\perp}$. (redrawn from Stanton, 1988a).

A1.2.1a Straight fluid cylinder

Assuming the cylinder as straight with length *L* and composed of homogeneous fluid material, the integral of Equation (A.11) can be evaluated analytically (Stanton, 1988a). Because of the simple geometrical shape and uniformity (composition profile is constant along the direction of the axis but may vary along the radial direction), the modal series in Equation (A.11) is constant with respect to the integration and comes out from the integral (as well q_a). For backscattering geometries ($\phi = \pi$), Equation (A.11) can be written (Stanton 1990):

$$\sigma_{bs} = \left(\frac{L}{\pi}\right)^2 \frac{\sin(kL\,\cos\theta)}{kL\,\cos\theta} \sum_{m=0}^{\infty} B_m \cos(m\pi) \qquad \text{(A.12)}$$

where L is the length of cylinder; θ is the angle between the direction of the incident plane wave and the axis of the cylinder, B_m are the coefficients defined in Equation (A.7) with C_m defined by Equation (A.8), and m is the number of modes. At broadside incidence (θ=90°) the directionality function becomes a unity.

The model is valid only when $L > a$ and when the incidence wave is normal or close to normal to the axis of the cylinder (~30°). In addition to the restrictions of being straight and having a constant composition profile, Equation (A.12) has the same assumptions of Equation (2.4): the receiver must be far from the scatterer ($r >> L$) and the length much smaller of the first Fresnel zone of the receiver ($L << 2(r\lambda)^{1/2}$). The latter is an important restriction to take into account as it avoids Fresnel zone interference of the echo and possibly substantial changes in target strength.

It is important to note the difference that occurred using the straight cylinder model from the others. In the geometric scattering region (after the peak or ka>1), the scattering cross-sections of the sphere and bent cylinder (par A1.2.1c) tend to oscillate about a constant value, while the cross-sections from the straight cylinder oscillates about a monotonically increasing value (Figures A.4 and A.5). The trend of the oscillations depends upon whether or not the object is curved in one or two dimensions. At broadside incidence, the surface of the straight cylinder is curved only in one dimension, while the surfaces of the sphere and bent cylinder are both curved in two dimensions. Since in the first case the size of the cylinder remains much smaller than the first Fresnel zone, the trend is constant with respect of frequency.

A1.2.1b Fluid prolate spheroid

The prolate spheroid geometry is a special case of cylinder of finite length with a deformed composition profile and radius that vary along the axis. Despite the krill shape is not close to that of a prolate spheroid, models assuming this regular shape

have been suggested to predict the target strength of krill for species smaller in size like *Euphausia pacifica* (Furusawa *et al*., 1994; Miyashita *et al*., 1996).

For this solution, the spheroid must be oriented at angles where incident and measured scattered waves are normal or nearly normal to the major axis of the spheroid (Fig. A.2). This will correspond to the *z*-axis placing the centre of the spheroid at the origin and the equation for the radius of prolate spheroid is (Stanton, 1989a):

$$a(z) = a_0\sqrt{1-\left[z/(L/2)\right]^2} \tag{A.13}$$

with a_0 length of the semi-minor axis.

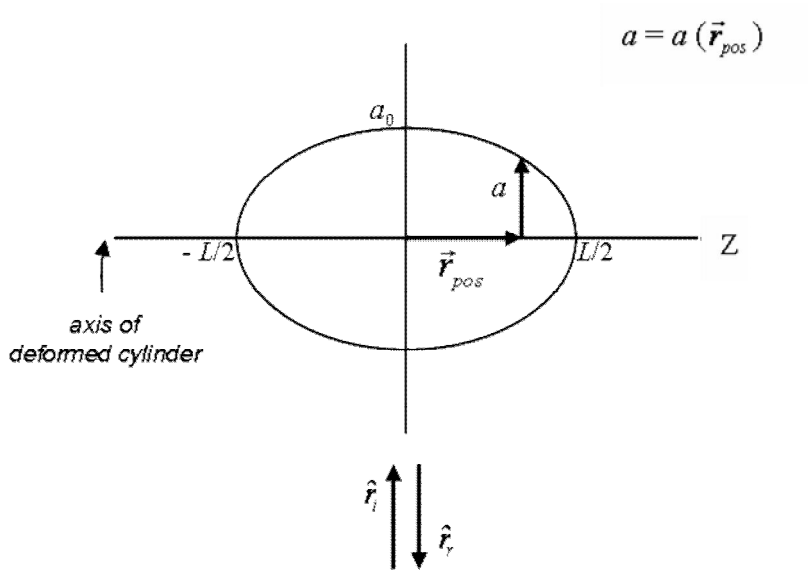

Figure A.2: *Prolate spheroid backscattering geometry of a deformed cylinder*. (redrawn from Stanton 1989a)

With the substitutions $\mu = z/(L/2)$ and $d\mu = dz/(L/2)$ and taking advantage of the fact that the integral is an even function over a symmetrical interval about the origin, and using Equations (2.4) and (A.11), Equation (2.5) is reduced to (Stanton, 1989a):

$$\sigma_{bs} = \frac{L^2}{\pi^2}\left|\int_0^1 \sum_{m=0}^{\infty}(-1)^m B_m \, d\mu\right| \tag{A.14}$$

where now $a(\mu)=a_0(1-\mu^2)^{-1}$, L is the length of the major-axis, B_m are the coefficients defined in Equation (A.7), m is the number of modes, and $\varepsilon=1$ for $m=0$, and $\varepsilon=2$ for $m=1,2,.....$

Equation (A.14) represents a deformed cylinder solution at broadside incidence. The scattering in this model depends on the two parameters a_0 and L separately. Since the cylinder solution is only valid for lengths much greater than the diameter, the model is only valid for axis ratios ($L/2a_0$) greater than 5:1. For lower aspect ratios the end effects are important but they are not included in the model.

A1.2.1c Uniformly bent fluid cylinder

The bent cylinder geometry with constant ray of curvature ρ_c and constant cross-sectional radius is the approximated shape that would resemble an elongated marine organism, such the euphausiid, better than a sphere or a straight cylinder. In this case, the scattering phenomenon becomes more complex. There will be Fresnel zone effects due to both the curvature of the incident and received wave fronts as well as due to the curvature of the object. The radius of the first Fresnel zone due to the bend, which will dictate the scattering levels for the case, is smaller and equal to $(\rho_c \lambda/2)^{1/2}$ (Stanton, 1989a). Thus, for bent cylinder geometry the restriction on the length compared the first Fresnel zone becomes even more significant because it depends on ρ_c also.

For the simpler case of a constant radius of curvature ρ_c at the centre of the x-axis and the cylinder symmetrically bent away from the sonar as in Figure A.3, the angle γ is used to describe $\hat{r}_{\tan}$ and $\vec{r}_{pos}$. Choosing the unit vector $\hat{r}_i = \hat{i}$, which makes $\hat{r}_r = -\hat{i}$, the cross product $\left|\hat{r}_i \times \hat{r}_{\tan}\right|$ is equal to $\left|\cos\gamma\right|$ so that all the wavenumbers in B_m defined by the Equations (A.7) and (A.8) are multipled by this quantity. Thus, the backscattering cross section can be written in terms of arc-length of the bent cylinder L as (Stanton, 1989a):

$$\sigma_{bs} = \frac{L^2}{\pi^2 \gamma_{\max}^2} \left| \int_0^{\gamma_{\max}} \sum_{m=0}^{\infty} (-1)^m B_m \cdot e^{2ik\rho_c(1-\cos\gamma)} \, d\gamma \right|^2 \qquad \text{(A.15)}$$

where the cylindrical radius is supposed to be constant or varying slowly with respect the position along the axis, γ is the angle between the radius vector at the integration point and the radius vector at the centre of the cylinder (Fig. A.3), $2\gamma_{max}$ is the angle subtending the entire cylinder, L is the arc-length ($2\rho_c \gamma_{max}$), and B_m the coefficients defined in Equations (A.7) and (A.8). Due to the symmetry, the integral is calculated from 0. In contrast to the straight cylinder case, here the B_m coefficients are not separable from the integral and at high frequency it has to be performed numerically.

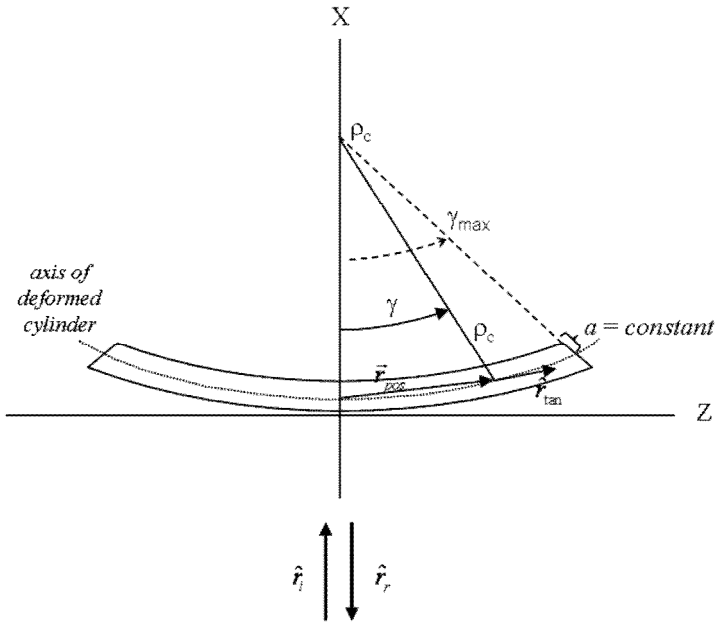

Figure A.3: *Backscattering geometry of a uniformly bent cylinder with constant radius of curvature ρ_c and constant cross-sectional radius*. (redrawn from Stanton, 1989a).

A2 Approximate formulations

A2.1 Truncated versions

Since the zooplankton has a very irregular shape, whatever is the regular geometry of the model neither sphere, straight or bent cylinder, fits exactly the shape of the

animal. Hence, discrepancies between predicted and measured scattering have to be expected.

Pieper and Holliday (1984), Stanton (1988a), and Wiebe *et al*. (1990) showed the highest correlation between backscattering from elongated zooplanktonic organisms and theoretical predictions when the sphere or the straight cylindrical modal series solutions were truncated to the first two modes only. These first two modes represent the monopole ("breathing") and dipole (the oscillatory movement of the surrounding fluid with respect to the entire object) effects, which might be enough to represent the scattering, since the shape of the animals is not regular. It is likely that the higher-order scattering terms are not generated or attenuated in the echo-formation process by irregular object. Another mechanism that can cause deviation from the ideal solution could be the absorption (Stanton, 1989a).

Dalen and Kristensen (1990) found that the first four terms in the summation of the straight fluid cylinder Equation (A.12) were adequate to overlap the first two maxima of that model. Later, Stanton (1989a) showed that in some cases, for animals like Euphausiids, the results from the bent cylinder modal series solution truncated at the first six terms fitted better the backscattering data presented by Greenlaw (1977), depending on how close the geometry of the model fits the actual geometry.

As result, the rapidly varying function in the geometric scattering region is modified, the oscillations are reduced while the amplitude is increased (Figures A.4 and A.5) beginning from a certain “breaking point”. The latter depends on how many modes are supported, so that it has been used to fit empirical data with model truncation by the referred authors.

A2.2 High-Pass versions

Johnson in 1977 proposed the first high-pass model in order to derive simple and rapid calculations for the scattering at all frequencies. He combined heuristically low- and high- frequency limits of the backscattering of the Anderson fluid sphere model.

The high-pass equation was developed in an analogous way to the equations describing the response of a two-pole high-pass electronic filter, where the low frequencies (*Rayleigh scattering region*) are greatly reduced and the high frequencies (*geometric scattering region*) are passed through the circuit.

The model is a smoothed version of the exact modal series solution as the model increases smoothly and monotonically with *ka*, while the modal solution oscillates in the region $ka>1$.

Stanton (1989b) has refined the Johnson's model and extended the approach to the other geometries: the prolate spheroid, straight cylinder and bent cylinder. In addition, he has taken into account the possibility that the object may be either mathematically idealized by simple shape or more realistically approximated (irregular shape).

As a result, Stanton's model passes through intermediate values of the oscillatory high-frequency region, where local reflection coefficients and Fresnel zone interferences become important. It is much like an average, with a constant angle of the curve and it has potential to be applied for a wide range of materials, from gas to rigid and fixed objects. The general high-pass formula can be written as (Stanton, 1989b):

$$\sigma_{bs} = \sigma_{bs}\ (ka << 1,\ fluid)\ G \times \left(1 + \frac{\sigma_{bs}\ (ka << 1,\ fluid)}{\sigma_{bs}\ (ka >> 1,\ rigid/fixed) R^2 F} \right)^{-1} \qquad \text{(A.16)}$$

where R=(gh-1)/(gh+1) is the Rayleigh reflection coefficient to account for the penetrability (at least to a first approximation), F and G are heuristical functions for taking care of lossy materials, irregular shape and resonance-effects.

Both F and G can be empirically derived from calculations of the exact solution or from direct backscattering data. Stanton (1990) presented values for euphausiid determined empirically from the bent cylinder modal series solutions as $F = 3 + 0.005(ka)^4$ and $G = 1\text{-}0.8\exp[\text{-}2.5(ka\text{-}2.05)^2]$. When working on survey data, more complex functional dependencies of G and F may introduce no unique solutions requiring multifrequency observation to resolve the correct prediction (Cochrane *et al.*, 1991). For idealized objects, where the shape is exactly described by a sphere,

prolate spheroid, straight finite cylinder, or uniformly bent finite cylinder and materials lossless with respect to the propagation of acoustic waves, *F* and *G* can be equated to the unity (Stanton, 1990). The equations of the high-pass versions and the associated limits to the modal series solutions for different shapes are given in Table A.I.

It is important to note that when the sound is scattered by a large collection of objects of varying size, the fine structure or modal interferences of the objects occurring at different *ka* values will not be noticeable in the school echo. The scattering strength versus frequency of a collection of un-identical objects will most likely resemble a smoothed version of the exact modal solution such as the high-pass models.

This means that, in addition to its convenience of simple and rapid calculus, the high-pass model has potential for reasonable accuracy in applications in the ocean not only in studies of scattering by marine organism but also for grains of sand (Sheng and Hay, 1988). However, in the case of inversion problem technique on multimodal length distribution of krill, the high-pass versions could produce ambiguities. Kristensen and Dalen (1986) analysed the case and found that the acoustically estimated size distribution by sphere high-pass model contained only one size class. The authors pointed out that the high pass versions do not reflect a decreasing volume-backscattering strength versus frequency and may produce results only for the best-fitted size distribution to the measured values.

Table A.I: High-Pass models and associated limits to the modal series solutions for various approximated shapes and materials (Stanton, 1989b).

shape	***ka*<<1 (fluid)**	***ka*>>1 (rigid/fixed)**	**all *ka* High-Pass model**
Sphere	$a^2(ka)^4\alpha_{\pi s}^2$	$\frac{1}{4}a^2$	$\frac{a^2(ka)^4\alpha_{\pi s}^2 G}{1+\left[4(ka)^4\alpha_{\pi s}^2\right]/(R^2F)}$
Prolate spheroid	$\frac{1}{9}L^2(ka)^4\alpha_{\pi c}^2$	$\frac{1}{16}L^2$	$\frac{\frac{1}{9}L^2(ka)^4\alpha_{\pi c}^2 G}{1+\left[4(ka)^4\alpha_{\pi c}^2\right]/(R^2F)}$
Straight cylinder	$\frac{1}{4}L^2(Ka)^4\alpha_{\pi c}^2 s^2$	$\frac{1}{4\pi}L^2(Ka)s^2$	$\frac{\frac{1}{4}L^2(Ka)^4\pi_{\pi c}^2 s^2 G}{1+\left[\pi(Ka)^3\pi_{\pi c}^2\right]/(R^2F)}$
Bent cylinder	$\frac{1}{4}L^2(ka)^4\alpha_{\pi c}^2 H^2$	$\frac{1}{4}\rho_c a$	$\frac{\frac{1}{4}L^2(ka)^4\pi_{\pi c}^2 H^2 G}{1+\left[L^2(ka)^4\pi_{\pi c}^2 H^2\right]/(\rho_c a R^2 F)}$

Definitions:

$$\alpha_{\pi s}=\frac{1-gh^2}{3gh^2}+\frac{1-g}{1+2g}\quad;\qquad \alpha_{\pi c}=\frac{1-gh^2}{2gh^2}+\frac{1-g}{1+g}\quad;\qquad R=\frac{gh-1}{gh+1}\quad;$$

$g=$ density of body material / density of surrounding fluid;
h = speed of sound in the body / speed of sound in surrounding fluid;
$H=\frac{1}{2}+\frac{1}{2}\frac{\rho_c}{L}\ \sin\left[(\rho_c/L)^{-1}\right]$;
a is the spherical radius (sphere), length of semi-minor axis (prolate spheroid), or cylindrical radius (straight and bent cylinder);
L is the total length of the prolate spheroid and straight cylinder, arc length of the bent cylinder;
ρ_c is the radius of curvature of the axis of the bent cylinder;
k is the acoustic wavenumber (= $2\pi/\lambda$, where λ is the acoustic wavelength);
$K=k\sin\theta$ (straight cylinder);
θ is the angle between the direction of the incident wave and the axis of the cylinder;
$s=\sin(kL\cos\theta)/kL\cos\theta$ (=1 at broadside incidence);
$F=\sum_i F_i(ka)^{\gamma_1}$; $G=\prod_j\left(1+A_j\ \exp\{-B_j[ka-(ka)_{0,j}]^2\}\right)$
where F_i , γ_i , A_j , $\mathrm{B_j}$, $(ka)_{0.j}$ are constants ($-1<A_j<0$ gives null, $A_j>0$ gives peak), and $(ka)_{0,j}$ is the position of the jth peak or null.

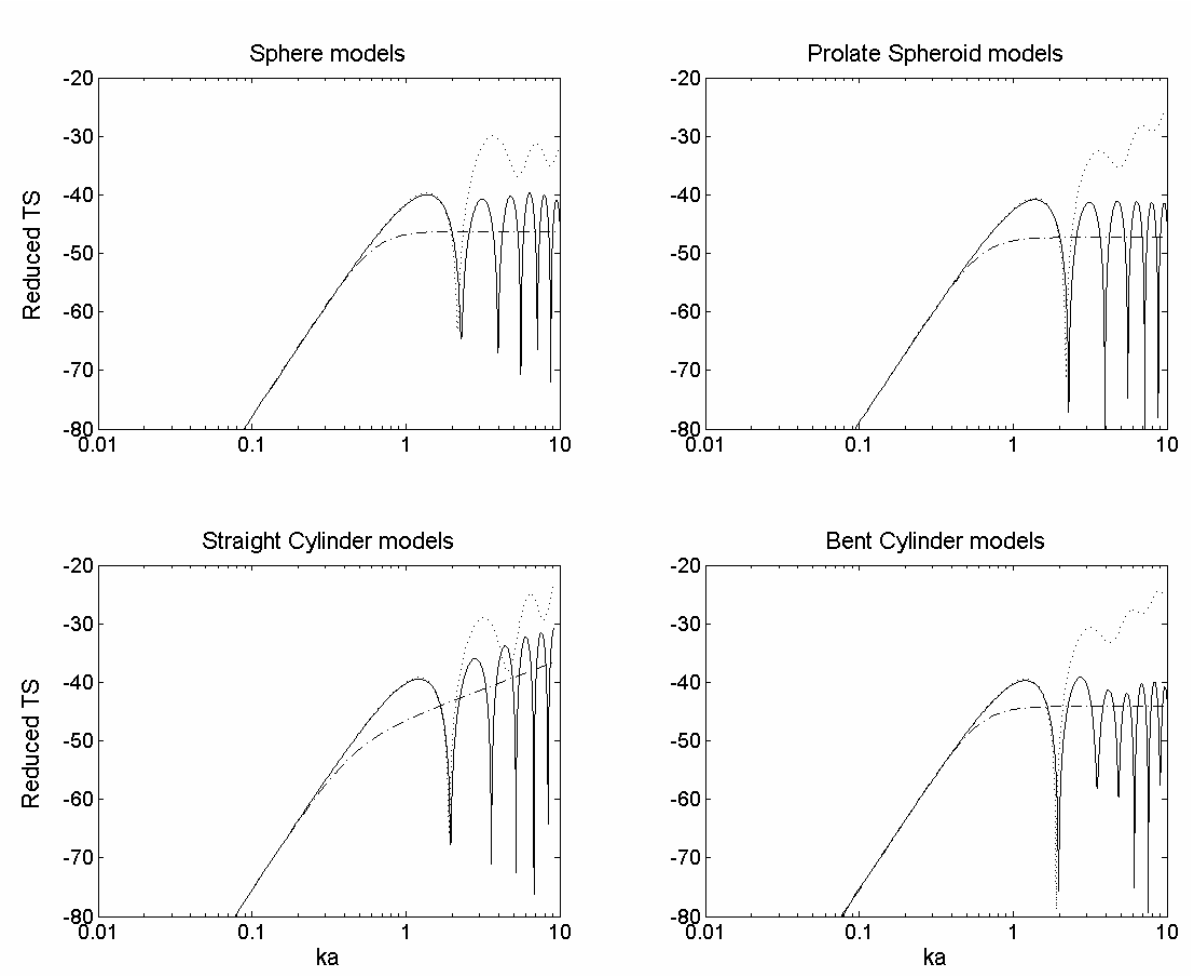

Figure A.4: *Fluid modal series solution* (*solid lines*), *High Pass versions (dash-dotted lines) and truncated versions (dotted lines) predictions for various simple shapes object modelling a krill of length L=23 mm. The reduced target strength is* $10\log_{10}(\sigma_{bs}/\pi a^2)$ *for the sphere and* $10\log_{10}(\sigma_{bs}/L^2)$ *for the other objects. k is the acoustic wave number in the surrounding medium with sound speed c=1500 ms*$^{-1}$*. The modal series solution are calculated using the first 20 modal terms, giving converged solution* (*Stanton, 1989a*), *while the truncated version only the first 2 modal terms. The equivalent radius for the sphere is calculated by the allometric relation* $a_s = 0.095 + 0.134 \cdot L$ (*Greenlaw, 1977*), *while the length related "acoustic cylindrical radius"* $a_c = 2.2$ *mm is used for the cylinders and the calculus of the semi-minor axis of the prolate spheroid* (*Stanton, 1989a*). *The relative dimensions of the bent cylinder are given by* $L = 18.4 a_c$ $\rho_c = 3L$ (*Lawson et al., 2006*). *The input contrasts are h=1.0205 and g=1.0145 as calculated from of the length relationships 2.8 and 2.9.*

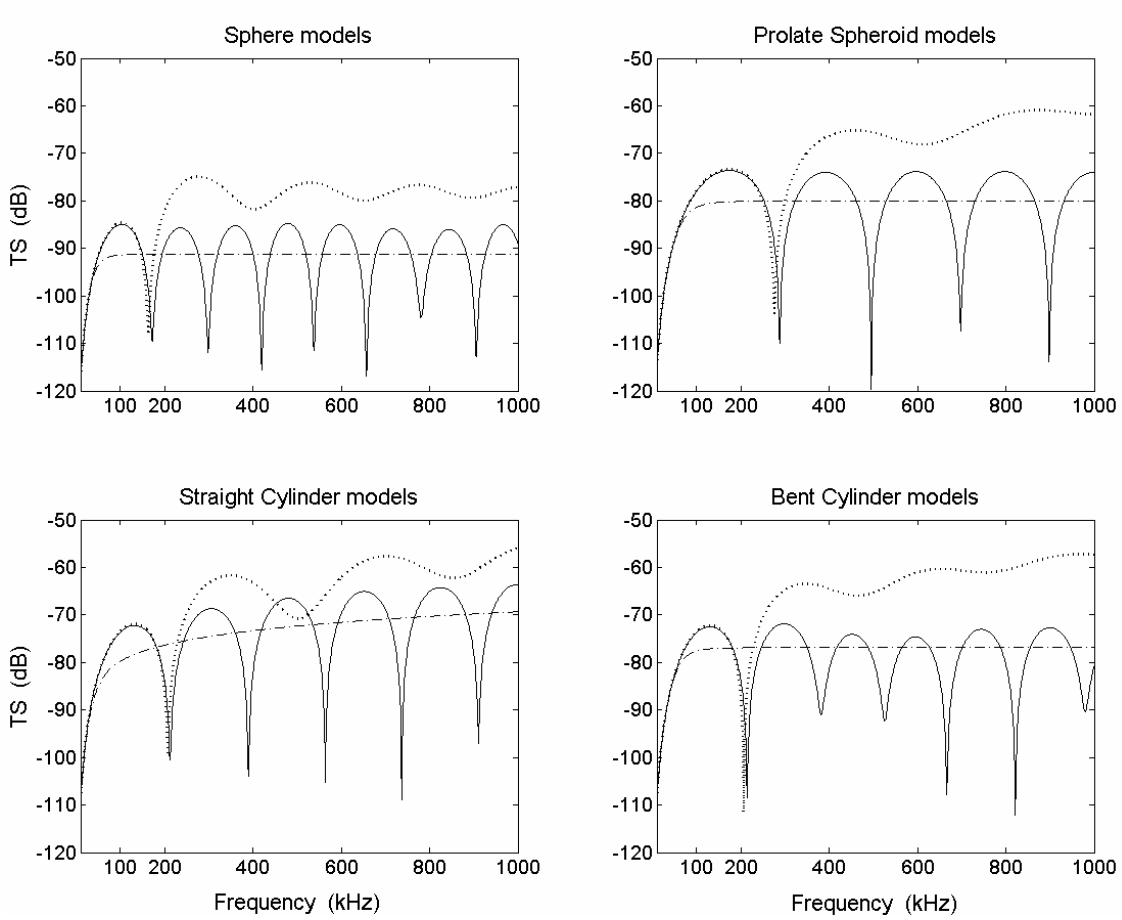

Figure A.5: *Target-strength prediction versus frequency from the various fluid-like models. The solid lines are the modal series solutions, the dash-dotted lines are the High Pass versions and the dotted lines are the truncated versions. All the parameters are the same as in Figure A.4.*

A2.3 Ray-solution representation

The modal series solution requires many terms to converge in the high frequency region and, in general, is very cumbersome if not impossible to manipulate algebraically (Stanton *et al.*, 1993a). Moreover, neglecting the end effects, the approach is only valid for target orientation near broadside incidence and for objects of high aspect ratio. The limited validity of the modal solution for deformed cylinders with different material properties at angular range from broadside is reported in Partridge and Smith (1995).

As discussed in Paragraph 2.3 the acoustical properties of fluid-like organisms are very similar to those of the surrounding seawater, so that the animals tend to behave acoustically as weakly scattering bodies (i.e. $g, h \cong 1$).

Taking in the account this property, Stanton *et al.* (1993a) suggested that a two-ray simplification, which incorporates a close approximation of modal resonances using geometric ray theory, could give a satisfactory description of the scattering. The hypothesis of the ray solution is that in the transitional and geometric region the scattering from weakly infinitely long straight cylinders is the summation of two simple terms: the ones reflected from the front and back interfaces.

This approach facilitates the numerical manipulation in the geometric scattering region ($ka>1$) while at the same time it makes the physics of the process more explicit in the mathematics. Comparing the ray-based solution (approximate) and the modal series solution (exact), Stanton *et al.* (1993a) have shown that the approach is reasonably accurate for scattering by angles of near normal incidence. In contrast, near end-on incidence the solution is inaccurate and predicts levels much lower than at the broadside incidence.

To predict the scattering over all angle of incidence, Stanton *et al.* (1993b) derived ray-based approximate expressions by a heuristic extension of the solution, which describe the echo energy due to sound scattered by finite cylinders averaged over orientation and length. They assumed that the averages over a wide range of angles of orientation are relatively insensitive to the inaccuracies near end-on incidence because the echo near broadside will tend to dominate the average. Stanton *et al.* (1998c) showed that results from the approximated solutions were in agreement with simulations using distorted wave Born approximation (Par. 2.4) on two set of backscattering data; Chu and Stanton (1998) confirmed the effectiveness of the representation comparing the results obtained with the pulse compression technique from three different zooplankton groups.

In Figure A.6, the two-ray target-strength prediction versus frequency for a krill shaped as a uniformly bent fluid cylinder is shown. The length was 23 mm and

$c = 1500$ m s^{-1} for comparison with Figures 2.11 and A.5; the length-width ratio was set equal 8. The simple formulation of the model used in plotting Figure A.6 can be found in Stanton *et al*. (1994b), while the constant values are given explicitly in Stanton *et al*. (1993b).

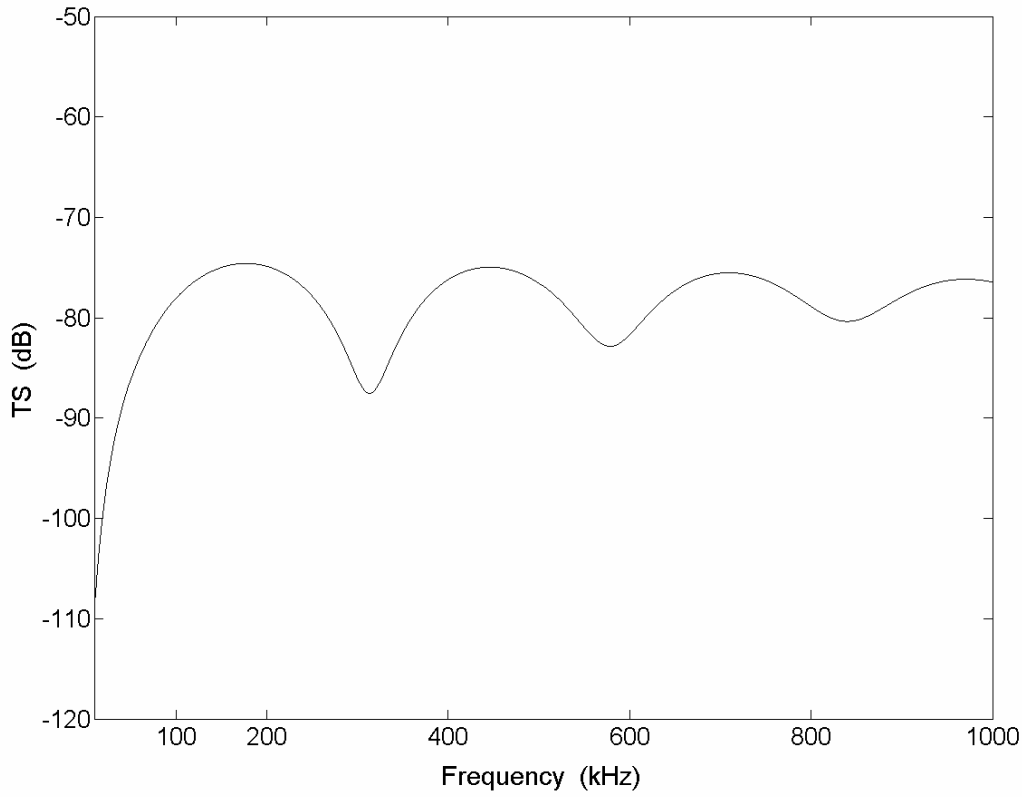

Figure A.6: *Two-rays target-strength prediction versus frequency for a krill of length 23 mm approximated as a fluid uniformly bent cylinder with length-width ratio equal 8.*

As a consequence of the study, Stanton *et al*. (1993b) derived a formula analytically averaged for an ensemble of animals. Through various simplifications, the prediction process can be solved in an easier way without performing an average of the scattering from each individual. For an aggregation of elongated weakly scattering bodies, with narrow distributed length and angle of orientation spanning an arbitrary range with the broadside incidence included, the approximate ray-solution formula gives the average on the differential backscattering cross sections over an ensemble of independent realizations according to (Stanton *et al*., 1993b, 1998c):

$$\left\langle \sigma_{bs} \right\rangle_{L,\,\theta} = 2\mathsf{R}_{1,2}^2\ \bar{a}\ \bar{L}\ \left[1 - e^{-8(k_2 \cdot \bar{a} \cdot s)^2} \cos(4k_2 + \mu_{p=2})\right] \cdot A_{\mathrm{i\,j}} \qquad \text{(A.17)}$$

where $\mathsf{R}_{1,2}$ is the plane-wave-plane reflection coefficient of the body interface, $\bar{a}$ is the mean cylindrical radius, s is the standard deviation of the body length normalized by mean length ($\bar{L}$), and μ is the phase shift term used for values less then k_1a (Stanton *et al.*, 1993b) calculated equal to [-(π/2) k_1a/(k_1a+0.4)]. The term $A_{\mathrm{i\,j}}$ takes on different values for different combinations of shapes and orientation conditions. For the case of uniformly bent cylinders whose orientation angle is Gaussian distributed, Stanton *et al.* (1998c) found that: $A_{\mathrm{i\,j}} = \dfrac{1.44}{16\ s_\theta \sqrt{0.8}}$ were s_θ is the standard deviation of orientation angle in radians and the numbers substituting the parameters are empirically determined from simulation using the distorted wave Born approximation. Equation (A.17) is valid over the frequency range where k_1a>0.1. This is not limiting the application since the animals are generally not detectable at or below the value of $k_1a = 0.1$ (Rayleigh scattering region).

The analysis of the formula showed two important theoretical results. Firstly, under certain condition (for $\rho_c / L \geq 2$), the average cross sections are independent of the bend of the cylinder. The result is essentially the same for both the straight and the bent cylinders of various radii of curvature. Secondly, under all the conditions the averages depend upon the standard deviation of angle of orientation. These results are very important for both forward problem and remote sensing applications that usually involve many realizations. Since the precise bend of free-swimming krill is generally not known, this factor is reduced or eliminated, and the potential to extract other information from data is increased. In particular, the knowledge of the mean angle of orientation and the related standard deviation of the population of euphausiids during the survey becomes primary information to give credit for the transformation of acoustical to biological results.

A3 Empirical models

The large effort undertaken by the researchers to improve theoretical zooplankton scattering models has not been accomplished with the same emphasis on direct acoustic measurements of organisms. Difficulties to retrieve high quality data both *in situ* and *ex situ* have limited the number of studies presented in literature. Since the measurements have been mostly performed on single species, the results have been used to validate specific theoretical models rather to implement models for general groups of zooplankton. Therefore, the empirical models are rarely presented in literature and only two examples have found relevant practical application. They are briefly described below.

A3.1 The Greene model

The Greene model (Greene *et al.*, 1991) was endorsed by CCAMLR starting from 1991 (SC-CAMLR, 1991) until the SDWBA model (Par. 2.4.1b) was proposed in 2005 (SC-CAMLR, 2005). It is a *scaled model* constituted by an empirically derived linear regression relating TS to the log-length of the organism. Greene *et al*. proposed the model on the base of a TS-length relationship obtained from measurement at 420 kHz of 43 individuals of representative zooplanktonic and micronektonic taxa in a 30 m^3 enclosure (Wiebe *et al.*, 1990). As the relationship was based on the single frequency of 420 kHz, with the knowledge of the length L [mm] and sound speed c [m s^{-1}], the ratio of the acoustic wave numbers ($k = 2\pi f / c$), between the frequency of interest and the reference frequency 420 kHz, was used to transform the frequency dependent model.

Since the *de facto* international standard frequency for surveying Antarctic krill is 120 kHz, Demer and Conti (2005) presented a practical formulation of the model based on that frequency:

$$\mathrm{TS}_f = 34.85 \log_{10} L - 127.45 + 10 \log_{10} \frac{k_f}{k_{120\,\mathrm{kHz}}} \qquad \text{(A.18)}$$

where L is measured from the front of the eye to the tip of telson. The relationship A.18 assumes intrinsically that the TS of crustacean zooplankton is dependent on the animal's volume. In practice, it was used in survey analysis transformed in target strength per unit weight (TS_{kg}) by means of weight-length relationships. Figure A.7 shows an example of TS versus frequency for a krill of 23 mm length.

The volume dependence of scattering from krill have been a subject of discussion (e.g. Demer and Martin 1995). McGehee *et al*. (1998) found that using the distorted wave Born approximation model (DWBA, Paragraph 2.4) the krill TS values were 6-8 dB lower than that predicted by the Greene *et al*. model. This reflects differences in biomass estimation; using Kils' krill orientation distribution (Table 2.I), the difference results in a factor roughly increased of 5 in the biomass estimation (Demer and Conti, 2003a). Similarly, Lawson *et al*. (2006) using their DWBA model parameterization (Par. 2.4.1a) found a TS deviation in magnitude of at least 4.4 dB.

The first general objection to the Greene model is that it is a linear relationship not effective to approximate the scattering from zooplankton, which is a highly non-linear phenomenon. Other objections have to be also considered, in part stated in the report of the first meeting of the CCAMLR subgroup on acoustic survey and analysis method (CCAMLR-SG-ASAM, 2005); they can be resumed as follows:

1. It predicts that the TS of crustacean zooplankton is dependent on the animal's volume rather then cross sectional area*.
2. It does not explicitly account for body shape, maturity stage, physical condition, and orientation.
3. It was derived from measurements on "representative zooplankton and micronektonic taxa" at 420 kHz (Wiebe *et al*., 1990) and corroborated at reference frequency of 120 kHz.
4. As the authors themselves claimed, it is only accurate for krill larger than the reference 120 kHz wavelength (e.g. $\lambda_{120\ kHz} \cong 12.5$ mm).

* This conclusion was supported by the results of Richter (1985) and Wiebe *et al*. (1990), but it is in contrast with the current theoretical thought claimed by Demer and Martin (1995) that the TS is dependent on the cross-sectional area.

A3.2 The KRIDA model

On the base of their measurements, Kristensen and Dalen (1986) confirmed the previous observation of Greenlaw (1977) and Holliday and Pieper (1986), that the target-strength data from single krill specimens of a given length group exhibits a resonance-like behaviour in the frequency domain, and also that the krill are highly directive scatterers. The authors proposed an empirical model based on a hybridization of fluid bubble/fluid finite-length cylinder models, successively refined by Dalen and Kristensen (1990). Here, the backscattering cross section area is dependent from the frequency *f*, the equivalent spherical radius *a*, and the tilt angle θ (angle between the incidence wave direction and the longitudinal axis of the animal), and described according to:

$$\sigma_{bs}(f,a,\theta) = \frac{Ca^2\ t(f)\ d(\theta)}{\left[(f_0/f)^2 - 1\right]^2 + \delta^2} \qquad \text{(A.19)}$$

where $t(f)$ is a high-frequency tuning factor chosen to be effective for acoustic radius value *ka* in the range from 8 to 12, f_0 is the organism resonance frequency, and δ and $C = 4\left(\frac{1-gh^2}{3gh^2} + \frac{1-g}{1+2g}\right)^2$ are the model parameters.

In practice, *C* gives a similar backscattering dependence on density and sound speed contrasts as the Johnson high-pass models (Stanton, 1989b; presented in Par. A2.2), determining the scattering strength in the high frequency domain; δ is the damping constant that determines the Q value (ratio peak/bandwidth inside -6 dB limits) at the frequency f_0, corresponding to the resonance frequency of the organism.

To reflect their data on *M. norvegica* and *Thysanoessa* species, as well as on Greenlaw's data from *Euphausia pacifica* (Greenlaw, 1977), Dalen and Kristensen (1990) found that the value $\delta = 0.5$ and the definition $t(f) = (1 + 0.1\ ka)^2$ with the choice $ka = 10$ were appropriate for using the Kils (1979a) equivalent radius-length relationship $a = 0.136\ L^{1.05}$.

The resonance frequency of the organism f_0 is estimated by approximating the animal shape as a fluid sphere. From the relationship $ka = 2\pi fa/c$, the value of f_0 can be determined after that the transition region from Rayleigh to geometrical scattering has been located by comparing the Johnson model prediction and the empirical data. Kristensen and Dalen (1986) found most appropriate to shift downward to about 50 % the resonance frequency ($ka=0.5$ instead of $ka=1$) resulting in $f_0 = c/4\pi a$. When the model was refined also using the high-frequency tuning factor $t(f)$, the value $ka=0.6$ was preferred (Dalen and Kristensen, 1990).

The last function $d(\theta)$ is the scattering directivity factor of the organism; it is derived by similarity from the finite-length object directivity function:

$$d(\theta) = \left[\frac{\sin\left(kL\sin\theta\right)}{kL\sin\theta} \right]^4 .$$

Again, the *ka* value has to be firstly chosen, then the parameter $kL = 2\pi fL/c$ can be calculated by using the Kils equivalent radius-length relationship as $kL=(ka/0.136)^{-1.05}$.

Comparing the size distribution estimations between six scattering models (fluid sphere, high-pass, straight fluid cylinder and truncated versions) on a krill community *in situ* data set, Dalen and Kristensen (1990) found that the KRIDA model produced the best fit between the estimated and the true size distributions.

The main characteristic of the KRIDA empirical model is that the observed resonant peak occurs at $ka\approx0.6$ (Dalen and Kristensen, 1990), giving a transition from Rayleigh to geometric scattering considerably lower in frequency than the generic models ($ka=1$). This is clear comparing Figure A.7 with the predictions of the other models obtained using the same key parameters and shown in Figures 2.11, A.5 and A.6. However, the shift downward of the transition region is consistent with the scattering from bubbles and fish with swimbladders (Medwin and Clay, 1997).

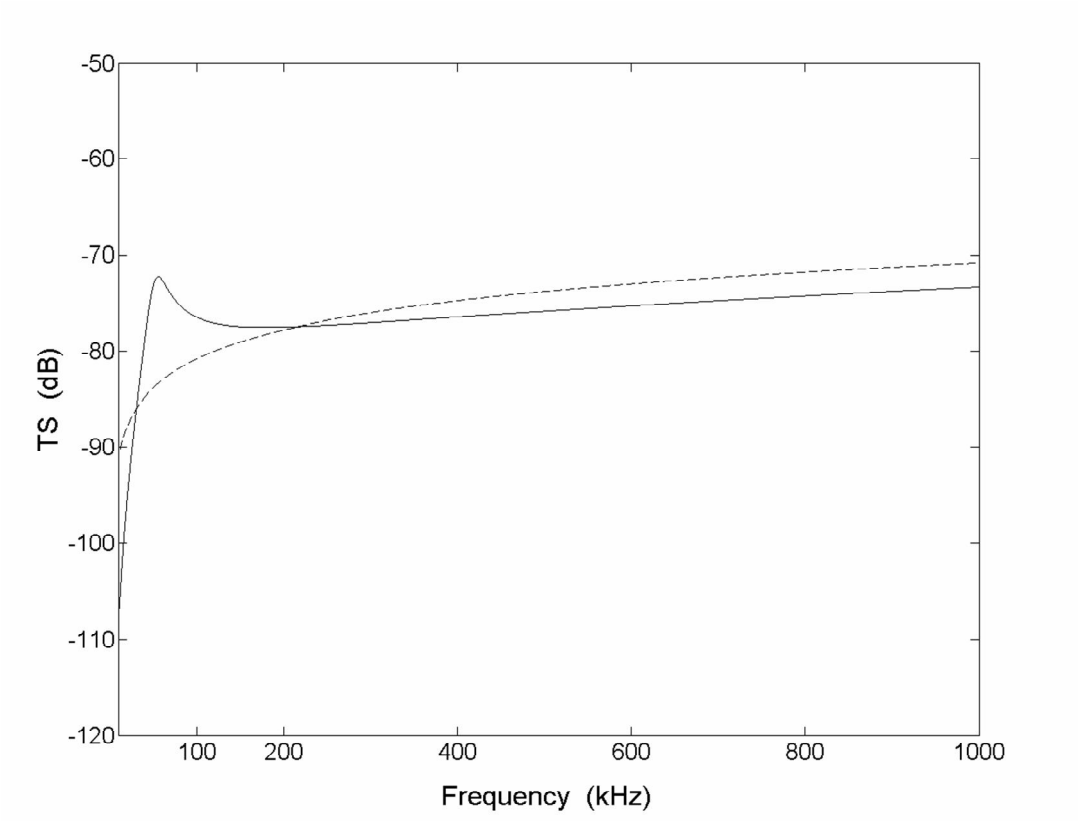

Figure A.7: *Empirical models predictions for a krill of 23 mm length and* $c=1500\ ms^{-1}$. *The dashed line is the Greene model and the solid line the KRIDA model at broadside backscattering* (*angle of incidence* $\phi=90°$). *The input parameters for the KRIDA model are*: *equivalent radius* $a=2.6$ *mm,* $ka=0.6$, $\delta=0.5$, $t(f)=(1+0.1ka)^2$, $h=1.0205$ *and* $g=1.0145$ *as calculated from of the length relationships 2.8 and 2.9.*

Bibliography

Aglen A., 1994. Sources of error in acoustic. estimation of fish abundance. Chapter 7: 107-133 *in* Marine Fish Behaviour in Capture and Abundance Estimation, Edit By A. Fernö and S. Olsen, Fishing news books, Blackwell Science Ltd, Malden, MA, USA, pp. 221.

Amakasu K. and Furusawa M., 2004. Effective frequency for acoustic survey of Antarctic krill. OCEANS 04, MTS/IEEE Techno-Ocean, 1 (9-12): 375-382.

Amakasu K. and Furusawa M., 2006. The target strength of Antarctic krill (*Euphausia superba*) measured by the split-beam method in a small tank at 70 kHz. ICES Journal of Marine Science, 63 (1): 36-45.

Anderson C.V., 1950. Sound scattering from a fluid sphere. Journal of the Acoustical Society of America, 22 (4): 426-431.

Andersen L.N., 2001. The new Simrad EK60 scientific echo sounder system. Journal of the Acoustical Society of America, 109 (5): 2336.

Baliño B.M. and Aksnes D.L., 1993. Winter distribution and migra-. tion of the sound scattering layers, zooplankton and. micronekton in Masfjorden, western Norway. Marine Ecology Progress Series, 102:35-50.

Balk H. and Lindem T., 2005. Sonar4, Sonar5 and Sonar6 post processing systems, Operator manual version 5.9.6. Lindem Data Acquisition Humleveien 4b. 0870 Oslo Norway, 380 pp.

Benfield M.C., Wiebe P.H., Stanton T.K., Davis C.S., Gallager S.M. and Greene C.H., 1998. Estimating the spatial distribution of zooplankton biomass by combining Video Plankton Recorder and single-frequency acoustic data. Deep Sea Research, Part II: Topical Studies in Oceanography, 45 (7): 1175-1199.

Boysen E. and Buchholz F., 1984. *Meganyctiphanes norvegica* in the Kattegat. Marine Biology, 79 (2):195–207.

Brierley A.S. and Watkins J.L., 1996. Acoustic targets at South Georgia and the South Orkney Islands during a season of krill scarcity. Marine Ecology Progress Series, 138: 51-61.

Brierley A.S., Watkins J.L. and Murray A.W.A., 1997. Interannual variability in krill abundance at South Georgia. Marine Ecology Progress Series, 150: 87-98.

Brierley A.S., Goss C., Watkins J.L. and Woodroffe P., 1998a. Variations in echo sounder calibration with temperature, and some possible implications for acoustic surveys of krill biomass. CCAMLR Science, 5: 273-281.

Brierley A.S., Ward P., Watkins J.L. and Goss C., 1998b. Acoustic discrimination of Southern Ocean zooplankton. Deep Sea Research, Part II: Topical Studies in Oceanography, 45 (7): 1155-1173.

Brierley A.S., Demer D.A., Watkins J.L. and Hewitt R. P., 1999. Concordance of interannual fluctuations in acoustically estimated densities of Antarctic krill around South Georgia and Elephant Island: biological evidence of same-year teleconnections across the Scotia Sea. Marine Biology, 134 (4): 675-681.

Brierley A.S., Fernandes P.G., Brandon M.A., Armstrong F., Millard N.W., McPhail S.D., Stevenson P., Pebody M., Perrett J., Squires M.,. Bone D.G and Griffiths G., 2002. An investigation of avoidance by Antarctic krill of RRS James Clark Ross using the Autosub-2 autonomous underwater vehicle. Fisheries Research 60 (2-3): 569-576.

Chu D., Stanton T.K and Wiebe P.H., 1992. Frequency dependence of sound backscattering from live individual zooplankton. ICES Journal of Marine Science, 49 (1): 97-106.

Chu D., Foote K.G. and Stanton T.K., 1993. Further analysis of target strength measurements of Antarctic krill at 38 and 120 kHz: Comparison with deformed cylinder model and inference of orientation distribution. Journal of the Acoustical Society of America, 93 (5): 2985-2988.

Chu D. and Stanton T.K., 1998. Application of pulse compression techniques to broadband acoustic scattering by live individual zooplankton Journal of the Acoustical Society of America, 104 (1): 39-55.

Chu D. and Ye Z., 1999. A phase-compensated distorted wave Born approximation representation of the bistatic scattering by weakly scattering objects: Application to zooplankton. Journal of the Acoustical Society of America, 106 (4): 1732-1743.

Chu D., Wiebe P.H. and Copley N.J., 2000a. Inference of material properties of zooplankton from acoustic and resistivity measurements. ICES Journal of Marine Science, 57 (4): 1128-1142.

Chu D., Wiebe P.H., Stanton T.K., Hammar T.R., Doherty K.W., Copley N.J., Zhang J., Reeder D.B. and Benfield M.C., 2000b. Measurements of the material properties of live marine organisms and their influences on the signatures of the acoustic scattering. Proceedings Oceans 2000 MTS/IEEE, International Symposium, Providence September 11-14, 3: 1963-1967.

Chu D., Wiebe P.H., Copley N.J., Lawson G.L. and Puvanendran V., 2003. Material properties of North Atlantic cod eggs and early-stage larvae and their influence on acoustic scattering. ICES Journal of Marine Science, 60 (3): 508-515.

Chu D. and Wiebe P.H., 2005. Measurements of sound-speed and density contrasts of zooplankton in Antarctic waters. ICES Journal of Marine Science, 62 (4): 818-831.

CCAMLR-SC-CAMLR, 1991. Report of the 10th Meeting of the Scientific Committee, Hobart, Australia (SC-CAMLR-X). Commission for the Conservation of Antarctic Marine Living Resources, Item 3, pp 20.

CCAMLR-SC-CAMLR, 2005. Report of the 24th Meeting of the Scientific Committee, Hobart, Australia (SC-CAMLR-XXIV). Commission for the Conservation of Antarctic Marine Living Resources, pp 564-585.

CCAMLR-SG-ASAM, 2005. Report of the first meeting of the subgroup on acoustic survey and analysis method. La Jolla, USA, 31 May to 2 June 2005.

Cochrane N.A., Sameoto D.D., Herman A.W and Neilson J., 1991. Multiple-frequency acoustic backscattering and zooplankton aggregations in the inner Scotian Shelf Basins. Canadian Journal of Fisheries and Aquatic Sciences, 48 (3): 340-355.

Cochrane N.A., Sameoto D.D. and Belliveau D.J., 1994. Temporal variability of euphausiid concentrations in a Nova Scotia shelf basin using a bottom-mounted acoustic Doppler profiler. Marine Ecology Progress Series, 107: 55-66.

Cochrane N.A., Sameoto D.D. and Herman A.W., 2000. Scotian Shelf euphausiid and silver hake population changes during 1984–1996 measured by multi-frequency acoustics. ICES Journal of Marine Science, 57 (1): 122-132.

Conti S.G., Demer D.A. and Brierley A.S., 2005a. Broad-bandwidth, sound scattering, and absorption from krill (*Meganyctiphanes norvegica*), mysids (*Praunus flexuosus* and *Neomysis integer*), and shrimp (*Crangon crangon*). ICES Journal of Marine Science, 62 (5): 956-965.

Conti S.G., Demer D.A., Soule M.A. and Conti J.H.E., 2005b. An improved multiple frequency method for measuring in situ target strengths. ICES Journal of Marine Science, 62 : 1636-1646.

Conti S.G. and Demer D.A., 2006. Improved parameterization of the SDWBA for estimating krill target strength. ICES Journal of Marine Science, 63 (5): 928-935.

Costello J.H., Pieper R.E. and Holliday D.V., 1989. Comparison of acoustic and pump sampling techniques for the analysis of zooplankton distributions. Journal of Plankton Research, 11 (4): 703-709.

Cram D.J., Agenbag J.J., Hampton I. and Robertson A.A., 1979. SAS Protea cruise, 1978: the general results of the acoustics and remote sensing study, with recommendations for estimating the abundance of krill (*Euphausia superba* Dana). South African Journal of Antarctic Research, 9 (1): 3-14.

Cuzin-Roudy J. and Buchholz, F., 1999. Ovarian development and spawning in relation to the moult cycle in Northern krill, Meganyctiphanes norvegica (Crustacea: Euphausiacea), along a climatic gradient. Marine Biology, 133 (2): 267-281

Cuzin-Roudy J., 2000. Seasonal reproduction, multiple spawning, and fecundity in northern krill, *Meganyctiphanes norvegica*, and Antarctic krill, *Euphausia superba*. Canadian Journal of Fisheries and Aquatic Science, 57 (S3): 6-15.

Cushing D.H., 1951. The vertical migration of planktonic crustacea.Biological Reviews, 26 (2): 158-192.

Dalen J. and Kristensen K-E., 1990. Comparative studies of theoretical and empirical target-strength models of euphausiids (krill) in relation to field-experiment data. Rapports et Proces-Verbaux des Réunions du Conseil International pour l'Exploration de la Mer, 189: 336-344.

Dalpadado P., 2006. Distribution and reproduction strategies of krill (Euphausiacea) on the Norwegian shelf. Polar Biology, 29 (10): 849–859.

Daly K.L. and Macaulay M.C., 1988. Abundance and distribution of krill in the ice edge zone of the Weddell Sea, austral spring 1983. Deep Sea Research, Part A: Oceanographic Research Papers, 35 (1): 21-41.

Demer D.A. and Hewitt R.P., 1995. Bias in acoustic biomass estimates of Euphausia superba due to diel vertical migration. Deep Sea Research, Part I: Oceanographic Research Papers, 42 (4): 455-475.

Demer D.A. and Martin L.V., 1995. Zooplankton target strength: Volumetric or areal dependence?. Journal of the Acoustical Society of America, 98 (2): 1111-1118.

Demer D. A., Soule M. A. and Hewitt, R. P., 1999. A multiple-frequency method for potentially improving the accuracy and precision of in situ target strength measurements. Journal of the Acoustical Society of America, 105 (4): 2359-2376.

Demer D.A. and Conti S.G., 2003a. Reconciling theoretical versus empirical target strengths of krill: effects of phase variability on the distorted-wave Born approximation. ICES Journal of Marine Science, 60 (2): 429-434.

Demer D.A. and Conti S.G., 2003b. Validation of the stochastic distorted-wave Born approximation model with broad bandwidth total target strength measurements of Antarctic krill. ICES Journal of Marine Science, 60 (3): 625-635.

Demer D.A., 2004. An estimate of error for the CCAMLR 2000 survey estimate of krill biomass. Deep Sea Research, Part II: Topical Studies in Oceanography, 51 (12-13): 1237-1251.

Demer D.A. and Conti S.G., 2004a. Erratum - Reconciling theoretical versus empirical target strengths of krill: effects of phase variability on the distorted-wave Born approximation. ICES Journal of Marine Science, 61 (1): 157-158.

Demer D.A. and Conti S.G., 2004b. Erratum - Validation of the stochastic distorted-wave Born approximation model with broad bandwidth total target strength measurements of Antarctic krill. ICES Journal of Marine Science, 61 (1): 155-156.

Demer D.A. and Conti S.G., 2005. New target-strength model indicates more krill in the Southern Ocean. ICES Journal of Marine Science, 62 (1): 25-32.

Demer D.A. and Renfree J.S., 2008. Variations in echosounder–transducer performance with water temperature. ICES Journal of Marine Science, 65 (6): 1021-1035.

De Robertis A., 2001. Validation of acoustic echo counting for studies of zooplankton behaviour. ICES Journal of Marine Science, 58 (3): 543-561.

Duportets L., Gadenne C., Dufour M-C., Couillaud F., Gross M.M., Stevenson P. J., Charette S.L., Pyka G., Marcus R., Greene C. H., Wiebe P.H., Pershing A.J., Gal G., Popp J.M., Copley N. J., Austin T.C., Bradley A.M., Goldsborough R.G., Dawson J., Hendershott R. and Kaartvedt S., 1998. Assessing the distribution and abundance of zooplankton: a comparison of acoustic and net-sampling methods with D-BAD MOCNESS. Deep Sea Research, Part II: Topical Studies in Oceanography, 45 (7): 1219–1237.

Einarsson H., 1942. Notes on Euphausiacea 1–111, Vidensk. Medd. Fra Dansk. Naturk., 106: 263–286.

Endo Y., 1993. Orientation of Antartic krill in an aquarium. Nippon Suisan Gakkaishi, 59 (3): 465-468.

Evans R.L., 1994. Constraints on the large-scale porosity and permeability structure of young oceanic crust from velocity and resistivity data. Geophysical Journal International, 119 (3): 869-879.

Everson I., 1982. Diurnal variations in mean volume backscattering strength of an Antarctic krill (*Euphausia superba*) patch. Journal of Plankton Research, 4 (1): 155-162.

Everson I. and Murphy E., 1987. Mesoscale variability in the distribution of krill Euphausia superba. Marine Ecology Progress Series, 40: 53-60.

Everson I., Watkins J.L., Bone D.G., Foote K.G., 1990. Implications of a new acoustic target strength for abundance estimates of Antarctic krill. Nature, 345: 338-340.

Everson I., Goss C. and Murray W., 1993. Comparison of krill (*Euphausia superba*) density estimates using 38 and 120 kHz echo sounders. Marine Biology, 116 (2): 269–275.

Everson I., 2000. Krill: Biology, Ecology and Fisheries. Oxford: Blackwell Science, 384 pp.

Everson I., Tarling G.A. and Bergström B., 2007. Improving acoustic estimates of krill: experience from repeat sampling of northern krill (*Meganyctiphanes norvegica*) in Gullmarsfjord, Sweden. ICES Journal of Marine Science, 64 (1): 39-48.

Falk-Petersen S. and Kristensen Å., 1985. Acoustic assessment of krill stocks in Ullsfjorden, North-Norway. Sarsia, 70 (1): 83-90.

Fernandes P.G. and Simmonds E.J., 1996. Practical approaches to account for receiver delay and the TVG start time in the calibration of the Simrad EK500. ICES Fish Capture Committee C.M.1996/B:17, 12 pp.

Flagg C. N. and Smith S. L., 1989. On the use of the acoustic Doppler current profiler to measure zooplankton abundance. Deep Sea Research, Part A. Oceanographic Research Papers, 36 (3): 455–474.

Flax L., Varadan V.K. and Varadan V.V., 1980. Scattering by an obliquely incident acoustic wave by an infinite cylinder. Journal of the Acoustical Society of America, 68 (6): 1832-1835.

Folt C.L. and Burns C.W., 1999. Biological drivers of plankton patchiness. Trends in Ecology and Evolution 14 (8): 300-305.

Foote K.G., 1983. Linearity of fisheries acoustics, with addition theorems. Journal of the Acoustical Society of America, 73 (6): 1932-1940.

Foote K.G., Vestnes H.P., McLennan D.N. and Simmonds E.J., 1987. Calibration of acoustic instruments for fish density estimation: a practical guide. ICES Cooperative Research Report, 144, 69 pp.

Foote K.G., 1990. Speed of sound in *Euphausia superba*. Journal of the Acoustical Society of America, 87 (4): 1405-1408.

Foote K.G., Everson I., Watkins J.L. and Bone D.G., 1990. Target strengths of Antarctic krill (*Euphausia superba*) at 38 and 120 kHz. Journal of the Acoustical Society of America, 87 (1): 16-24.

Foote K.G., 1991. Summary of methods for determining fish target strength at ultrasonic frequencies. ICES Journal of Marine Science, 48 (2): 211-217.

Foote K.G., Knutsen T., Baekkevold A.E. Dalpadado P., and Johannessen, S.E., 1996. Initial, collateral measurements of some properties of *Calanus jhmarchicus.* ICES C.M. 1996/L:21, 23 pp.

Foote K.G. and Stanton T.K., 2000. Acoustical methods. In ICES Zooplankton Methodology Manual, Chapter 6: 223-258, Ed. by R. Harris, H.R. Skjoldal, J.Lenz, P. Wiebe and M. Huntley. Academic Press, 684 pp.

Francis D.T.I., Knutsen T., Foote K.G. and Calise L., 1999. Modelling the Target Strength of Meganyctiphanes norvegica. 37th Regular Meeting of the Acustical Society of America and 2nd Convention of the European Acoustics Association, Berlin, 14-19 March 1999;

Acta Acustica, 85 (1): S185; and Journal of the Acoustical Society of America, 105 (2): 1111.

Furusawa M., Miyanohana Y., Ariji M. and Sawada Y., 1994. Prediction of krill target strength by liquid prolate spheroid model. Fisheries Science, 60 (3): 261-265.

Furusawa M., Hamada M. and Aoyama C., 1999. Near range errors in sound scattering measurements of fish. Fisheries Science, 65 (1): 109-116.

George R.Y. and Strömberg J.-O., 1985. Development of eggs of Antarctic krill *Euphausia superba* in relation to pressure. Polar Biology, 4 (3): 125-133.

Godlewska M. and Klusek Z., 1987. Vertical distribution and diurnal migrations of krill - *Euphausia superba* Dana - from hydroacoustical observations, SIBEX, December 1983/January 1984. Polar Biology, 8 (1): 17–22.

Gorska N. and Klusek Z., 1998. Dependence of scattered acoustical-signal intensity on the form of distribution of plankton concentration. Journal of the Acoustical Society of America 104 (1): 141–145.

Gorska N., 2000. Evaluation of sound extinction and echo interference in densely aggregated zooplankton. Oceanologia, 42 (3): 315–334.

Gorska N. and Chu D., 2001. Some aspects of sound extinction by zooplankton. Journal of the Acoustical Society of America, 110 (5): 2315-2325.

Gorska N. and Chu D., 2005. On the echo interference in sound backscattering by densely aggregated targets. ICES Journal of Marine Science, 62 (4):771-778.

Greene C.H., Wiebe P.H. Burczynski, J. and Youngbluth M.J., 1988. Acoustical detection of high-density demersal krill layers in the submarine canyons off Georges Bank. Science, 241: 359-361

Greene C.H., Wiebe P.H. and Burczynski J., 1989. Analyzing zooplankton size distributions using high-frequency sound. Limnology and Oceanography, 34 (1): 129-139.

Greene C.H., Stanton T.K., Wiebe P.H. and McClatchie S., 1991. Acoustic estimates of Antarctic krill. Nature. 349: 110.

Greene C.H., Wiebe P.H., Pelkie C., Benfield M.C. and Popp J.M., 1998a. Three-dimensional acoustic visualization of zooplankton patchiness. Deep Sea Research, Part II: Topical Studies in Oceanography, 45 (7): 1201-1217.

Greene C.H, Wiebe P.H., Pershing A.J., Gal G., Popp J.M, Copley N.J., Austin T.C., Bradley A.M., Goldsborough R.G., Dawson J., Hendershott R. and Kaartvedt S., 1998b. Assessing the distribution and abundance of zooplankton: a comparison of acoustic and net-sampling methods with D-BAD MOCNESS. Deep Sea Research, Part II: Topical Studies in Oceanography, 45 (7): 1219-1237.

Greenlaw C.F., 1977. Backscattering spectra of preserved zooplankton. Journal of the Acoustical Society of America, 62 (1): 44-52.

Greenlaw C.F., 1979. Acoustical estimation of zooplankton populations. Limnology and Oceanography, 24 (2): 226-242.

Greenlaw C.F., Johnson R.K. and Pommeranz T., 1980. Volume scattering strength predictions for Antarctic krill (Euphausia superba Dana). Meeresforschung, 28: 48-55.

Greenlaw C.F. and Johnson R.K., 1982. Physical and acoustic properties of zooplankton. Journal of the Acoustical Society of America, 72 (6): 1706-1710.

Greenlaw C.F. and Johnson R.K., 1983. Multiple-frequency acoustical estimation. Biological Oceanography, 2 (2): 227-252.

Guzman O. and Marin B., 1983. Hydroacoustic and photographic techniques applied to study the behaviour of krill (*Euphausia superba*). Memoirs of National Institute of Polar Research, Special Issue No. 27, 129-152.

Hamner W.M. and Hamner P.P., 2000. Behavior of Antarctic krill (*Euphausia superba*): schooling, foraging, and antipredatory behaviour. Canadian Journal of Fisheries and Aquatic Science, 57 (S3): 192-202.

Herman A.W., Cochrane N.A. and Sameoto D.D., 1993. Detection and Abundance Estimation of Euphausiids Using an Optical Plankton Counter. Marine Ecology Progress Series, 94: 165-173.

Hewitt R.P. and Demer D.A., 1991. Krill abundance. Nature, 353: 310.

Hewitt R.P. and Demer D.A., 1993. Dispersion and abundance of Antarctic krill in the vicinity of Elephant Island in the 1992 austral summer. Marine Ecology Progress Series, 99 (1): 29-39.

Hewitt R.P. and Demer D.A., 1994. Acoustic estimates of krill biomass in the elephant island area 1981-1993. CCAMLR Science, 1: 1-5.

Hewitt R.P. and Demer D.A., 1996. Lateral target strength of Antarctic krill. ICES Journal of Marine Science, 53 (2): 297-302.

Hewitt R.P. and Demer D.A., 2000. The use of acoustic sampling to estimate the dispersion and abundance of euphausiids, with an emphasis on Antarctic krill. Fisheries Research, 47 (3), 215-229.

Hewitt R.P., Watkins J.L., Naganobu M., Tshernyshkov P., Brierley A.S., Demer D.A., Kasatkina S., Takao Y., Goss C., Malyshko A., Brandon M.A., Kawaguchi S., Siegel V., Trathan P.N., Emery J.H., Everson I. and Miller, D.G.M., 2002. Setting a precautionary catch limit for Antarctic krill. Oceanography, 15 (3): 26-33.

Hewitt R.P., Demer D.A. and Emery J.H., 2003. An 8-year cycle in krill biomass density inferred from acoustic surveys conducted in the vicinity of the South Shetland Islands during the austral summers of 1991-1992 through 2001-2002. Aquatic Living Resources, 16 (3): 205-213.

Heywood K.J., Scrope-Howe S. and Barton E.D., 1991. Estimation of zooplankton abundance from shipborne ADCP backscatter. Deep Sea Research, Part A: Oceanographic Research Papers, 38 (6): 677-691.

Hosie G.W., Fukuchi M. and Kawaguchi S., 2003. Development of the Southern Ocean Continuous Plankton Recorder survey. Progress in Oceanography, 58 (2-4): 263–283.

Holliday D.V. and Pieper R.E., 1980. Volume scattering strengths and zooplankton distributions at acoustic frequencies between 0.5 and 3 MHz. Journal of the Acoustical Society of America, 67 (1): 135-146.

Holliday D.V. and Pieper R.E. and Kleppel G.S., 1989. Determination of zooplankton size and distribution with multifrequency acoustic technology. Journal du Conseil International pour l'Exploration de la Mer, 1989; 46 (1): 52-61.

Holliday D.V. and Pieper R.E., 1995. Bioacoustical oceanography at high frequencies. ICES Journal of Marine Science, 52 (3): 279-296.

Ignatyev S.M., 1999. Functional-Morphological Adaptations of the Krill to Active Swimming. Poster on the 2nd International Symposium on Krill, Santa Cruz, California, USA, August 23–27 August.

Ichii T., 2000. Krill harvesting. In: Krill: Biology, Ecology and Fisheries. Fish and Aquatic Resources, Series 6. Blackwell Science, Oxford, 228-262.

Iida K., Mukai T. and Hwang D., 1996. Relationship between acoustic backscattering strength and density of zooplankton in the sound-scattering layer. ICES Journal of Marine Science, 53 (2): 507-512.

Iida K., Mukai T. and Mori H., 1999. Frequency Characteristics of Acoustic Volume Backscattering Strength of Sound Scattering Layer and Estimation of Target Strengths of Constituent Organisms. Nippon Suisan Gakkaishi, 65 (1): 66-72.

Jaffe J.S., Ohmann M.D. and De Robertis A., 1999. Sonar estimates of daytime activity levels of Euphausia pacifica in Saanich Inlet. Canadian Journal of Fisheries and Aquatic Science, 56 (11): 2000–2010.

Johnson R.K. 1977. Sound scattering from a fluid sphere revisited. Journal of the Acoustical Society of America, 61 (2): 375-377.

Jones B.A., Lavery A.C. and Stanton T.K., 2006. An advanced 3-D scattering model for squid. Journal of the Acoustical Society of America, 120 (5): 3106.

Kaartvedt S., Aksnes D.L. and Aadnesen A., 1988. Winter distribution of macroplankton and micronekton in Masfjorden, western Norway. Marine Ecology Progress Series, 45: 45-55.

Kaartvedt S., Melle W., Knutsen T. and Skjoldal H.R., 1996. Vertical distribution of fish and krill beneath water of varying optical properties. Marine Ecology Progress Series, 136: 51-58.

Kaartvedt S., Røstad A., Fiksen Ø., Melle W., Torgersen T., Breien M.T., Klevjer T.A., 2005. Piscivorous fish patrol krill swarms. Marine Ecology Progress Series, 299: 1-5.

Kang M., Furusawa M. and Miyashita K., 2002. Effective and accurate use of difference in mean volume backscattering strength to identify fish and plankton. ICES Journal of Marine Science, 59 (4): 794-804.

Kasatkina S.M., Goss C., Emery J.H., Takao Y., Litvinov F.F., Malyshko A.P., Shnar V.N. and Berezhinsky O.A., 2004. A comparison of net and acoustic estimates of krill density in the Scotia Sea during the CCAMLR 2000 Survey. Ocean. Deep Sea Research, Part II: Topical Studies in Oceanography, 51 (12-13): 1289-1300.

Kils U., 1979a. Preliminary data on volume, density and cross section area of Antarctic Krill, *Euphausia superba* - Results of the the 2. Antarctic Expedition 1977/1978 of the Federal Republic of Germany. Meeresforschung, 27 (3): 207-209.

Kils U., 1979b. Aspect of physiological ecology of *Euphausia superba*. International Council for the Exploration of the Sea ICES, CM 1979/L: 3.

Kils U., 1981. The swimming behaviour, swimming performance and energy balance of Antartic krill, *Euphasia superba*. BIOMASS Scientific Series No.3, 122 pp

Kils U. and Marshall P., 1995. The antarctic krill - feeding and swimming performances - new insights with new methods. In Hempel I. & Hempel G., Biologie der Polarmeere - Erlebnisse und Ergebnisse (Biology of the polar oceans), edit by Gustav Fischer, 201-210.

Kirsch J., Thomas G.L. and Cooney R.T., 2000. Acoustic estimates of zooplankton distributions in Prince William Sound, spring 1996. Fisheries Research, 47 (2-3): 245-260.

Klevjer T.A. and Kaartvedt S., 2003. Split-beam target tracking can be used to study the swimming behaviour of deep-living plankton in situ. Aquatic Living Resources, 16 (3): 293-298.

Klevjer T.A. and Kaartvedt S., 2006. *In situ* target strength and behaviour of northern krill (*Meganyctiphanes norvegica*). ICES Journal of Marine Science, 63 (9):1726-1735.

Kock K.-H., 2000. Understanding CCAMLR's approach to management. Available at: www.ccamlr.org

Knutsen T., Melle W. and Calise L., 2001. Determining the mass density of marine copepods and their eggs with a critical focus on some of the previously used methods. Journal of Plankton Research, 23 (8): 859-873.

Korneliussen 2002. Analysis and presentation of multy-frequency echograms. Dissertation for the degree of philosophiae doctor (PhD), University of Bergen, Norway.

Korneliussen R.J. and Ona E., 2002. An operational system for processing and visualizing multi-frequency acoustic data. ICES Journal of Marine Science, 59 (2): 293-313.

Korneliussen R.J. and Ona E., 2003. Synthetic echograms generated from the relative frequency response. ICES Journal of Marine Science, 60 (3): 636-640.

Korneliussen R.J., Diner N., Ona, E. and Fernandes P.G., 2004. Recommendations for the collection of multi-frequency acoustic data. ICES ASC C.M. 2004/R: 36, 15 pp.

Korneliussen R.J., Diner N., Ona E., Berger L. and Fernandes P.G., 2008. Proposals for the collection of multifrequency acoustic data. ICES Journal of Marine Science, ICES Journal of Marine Science, 65 (6): 982-994.

Kristensen Å. 1983. Acoustic classification of zooplankton. Dr. Ing. Thesis/ELAB Rep STF44 A83 187. University of Trondheim, Norway, pp. 107.

Kristensen Å. and Dalen J., 1986. Acoustic estimation of size distribution and abundance of zooplankton. Journal of the Acoustical Society of America, 80 (2): 601-611.

Kulka D. W. and Corey S., 1982. Length and weight relationships of Euphausiids and caloric values of *Meganyctiphanes norvegica* (M. Sars) in the Bay of Fundy. Journal of Crustacean Biology, 2: 239-247.

Køgeler J.W., Falk-Petersen S., Kristensen Å., Pettersen F. and Dalen, J., 1987. Density and Sound Speed Contrasts in Sub-Arctic Zooplankton. Polar Biology, 7 (4): 231-235.

Labat J.P. and Cuzin-Roudy J., 1996. Population dynamics of the krill *Meganyctiphanes norvegica* (M. Sars, 1857) (Crustacea: Euphausiacea) in the Ligurian Sea (NW Mediterranean Sea). Size structure, growth and mortality modelling. Journal of Plankton Research, 18 (12): 2295-2312.

Lavery A.C., Stanton T.K., McGehee D.E. and Chu D., 2002. Three-dimensional modeling of acoustic backscattering from fluid-like zooplankton. Journal of the Acoustical Society of America, 111 (3), 1197-1210.

Lavery A.C., Wiebe P.H., Stanton T.K., Lawson G.L., Benfield M.C. and Copley N., 2007. Determining dominant scatterers of sound in mixed zooplankton populations. Journal of the Acoustical Society of America, 122 (6): 3304-3326.

Lawson G.L., Wiebe P.H., Ashjian C., Gallager S., Davis C. and Warren J.D, 2004. Acoustically-inferred zooplankton distribution in relation to hydrography west of the Antarctic Peninsula. Deep Sea Research, Part II: Topical Studies in Oceanography, 51 (17-19), 2041-2072.

Lawson G.L., Wiebe P.H., Ashjian C.J., Chu D. and Stanton T.K., 2006. Improved parametrization of Antarctic krill target strength models. Journal of the Acoustical Society of America, 119 (1): 232-242.

Lawson G.L., Wiebe P.H., Stanton T.K. and Ashjian C.J., 2008a. Euphausiid distribution along the Western Antarctic Peninsula – Part A: Development of robust multi-frequency acoustic techniques to identify euphausiid aggregations and quantify euphausiid size, abundance, and biomass. Deep Sea Research Part II: Topical Studies in Oceanography, 55 (3-4): 412-431.

Lawson G.L., Wiebe P.H., Ashjian C.J. and Stanton T.K., 2008b. Euphausiid distribution along the Western Antarctic Peninsula—Part B: Distribution of euphausiid aggregations and biomass, and associations with environmental features. Deep Sea Research, Part II: Topical Studies in Oceanography, 55 (3-4): 432-454.

Lowndes A.G., 1942. The displacement method of weighing living aquatic organisms. Journal of the Marine Biological Association of the United Kingdom, 25 (3): 555-574.

Luo J., Ortner P.B., Forcucci D. and Cummings S.R., 2000 . Diel vertical migration of zooplankton and mesopelagic fish in the Arabian Sea. Deep Sea Research, Part II: Topical Studies in Oceanography, 47 (7-8): 1451-1473.

Lloyd J and Mitchinson J., 2006. The Book of General Ignorance. Ed. Faber & Faber.

Macaulay M.C., English T.S. and Mathisen O.A., 1984. Acoustic characterization of swarms of antarctic krill (Euphausia uperba) from Elephant Island and Bransfield Strait (special issue). Journal of Crustacean, 4 (1): 16-44.

Machlup S., 1952. A theoretical model for sound scattering by marine crustaceans. Journal of the Acoustical Society of America, 24 (3): 290-293.

MacLennan D.N., 1986. Time Varied Gain function for pulsed sonars. Journal of Sound and Vibration, 110 (3): 511-522.

MacLennan D.N., 1990. Acoustical measurement of fish abundance. Journal of the Acoustical Society of America, 87 (1): 1-15.

MacLennan D.N. and Holliday D.V., 1996. Fisheries. andplankton acoustics: past, present and future. ICES Journal of Marine Science, 53 (2): 513-516.

MacLennan D.N., Fernandes P.G. and Dalen J., 2002. A consistent approach to definitions and symbols in fisheries acoustics. ICES Journal of Marine Science, 59 (2): 365-369.

Madureira L.S.P., Everson I. and Murphy E.J., 1993. Interpretation of acoustic data at two frequencies to discriminate between Antarctic krill (*Euphausia superba* Dana) and other scatterers. Journal of Plankton Research, 15 (7): 787-802.

Mair A.M., Fernandes P.G., Lebourges-Dhaussy A. and Brierley A.S., 2005. An investigation into the zooplankton composition of a prominent 38-kHz scattering layer in the North Sea. Journal of Plankton Research, 27 (7): 623-633.

Martin L.V., Stanton T.K., Wiebe P.H. and Lynch J.F., 1996. Acoustic Classification of Zooplankton. ICES Journal of Marine Science, 53 (2), 217-224.

Martin Traykovski L.V., O'Driscoll R.L. and McGehee D.E., 1998. Effects of orientation on broadband acoustic scattering of Antarctic Krill (*Euphausia superba*): Implications for inverting zooplankton spectral acoustic signatures for angle of orientation. Journal of the Acoustical Society of America, 104 (4): 2121-2135.

Martin Traykovski L.V., Stanton T.K., Wiebe P.H. and Lynch J.F., 1998a. Model based Covariance Mean Variance Classification (CMVC) techniques: Algorithm development and application to the acoustic classification of zooplankton. IEEE Journal of Oceanic Engineering, 23 (4): 344-364.

Mathisen O.A. and Macaulay M.C., 1983. The morphological features of a super swarm of krill, Euphausia superba. Memoirs of National Institute of Polar Research, Special Issue No. 27: 153-164.

Mauchline J., 1967. Volume and weight characteristics of Euphausiacea. Crustaceana 13: 241-248.

Mauchline J. and Fisher L.R., 1968. Distribution of the euphausiid crustacean *Meganyctiphanes norvegica* (M Sars). Limnology and Oceanography, 13 (4): 727-728.

Mauchline J. and Fisher L.R., 1969. The biology of Euphausiids. Advances in Marine Biology, 7, 454 pp.

Mauchline J., 1980a. The biology of Mysiids and Euphausiids. Advances in Marine Biology, 18, 681 pp.

Mauchline J., 1980b. Measurements of body length of *Euphausia superba* Dana. BIOMASS Handbook, Ser. 4: 1-9.

McGehee D.E. and Jaffe J.S., 1996. Three-dimensional swimming behavior of individual zooplankters: observations using the acoustical imaging system FishTV. ICES Journal of Marine Science, 53 (2): 363-369.

McGehee D.E., O'Driscoll R.L. and Martin Traykovski L.V., 1998. Effect of Oreintation on Acoustic Scattering from Antarctic Krill at 120 kHz. Deep Sea Research, Part II: Topical Studies in Oceanography, 45 (7): 1273-1294.

McGehee D.E., Greenlaw C.F., Holliday D.V. and. Pieper R.E., 2000. Multifrequency acoustical volume backscattering patterns in the Arabian Sea—265 kHz to 3 MHz. Journal of the Acoustical Society of America, 107 (1): 193-200.

McKelvey D.R. and Wilson C.D., 2006. Discriminant Classification of Fish and Zooplankton Backscattering at 38 and 120 kHz. Transactions of the American Fisheries Society, 135 (2): 488-499.

Medwin H. and Clay C.S., 1997. Fundamentals of Acoustical Oceanography. Academic Press, 712 pp.

Miller C.B. and Judkins D.C., 1981. Design of pumping systems for sampling zooplankton, with descriptions of two high capacity samplers for coastal study. Biological Oceanography, 1: 29-56.

Miller D.G.M. and Hampton I., 1989a. Biology and Ecology of the Antarctic Krill (*Euphausia superba* Dana). BIOMASS Scientific Series 9, Cambridge, SCAR & SCOR, 166 pp.

Miller D.G.M. and Hampton I., 1989b. Krill aggregation characteristics: spatial distribution patterns from hydroacoustic observations. Polar Biology, 10 (2): 25-134.

Mitson R.B., Simard Y. and Goss C., 1996. Use of a two-frequency algorithm to determine size and abundance of plankton in three widely spaced locations. ICES Journal of Marine Science, 53 (2): 209–215.

Miyashita K., Aoki I. and Inagaki T., 1996. Swimming behaviour and target strength of isada krill (*Euphausia pacifica*). ICES Journal of Marine Science, 53 (2): 303-308.

Miyashita K., Aoki I., Seno K., Taki K. and Ogishima T., 1997. Acoustic identification of isada krill, *Euphausia pacifica* Hansen, off the Sanriku coast, north-eastern Japan. Fisheries Oceanography, 6 (4): 266–271.

Miyashita K. and Aoki I., 1999. Acoustic measurements of zooplankton using a dual frequency echo sounder. Marine Ecology Progress Series, 180: 105-109.

Miyashita K., 2003. Diurnal changes in the acoustic-frequency characteristics of Japanese anchovy (*Engraulis japonicus*) post-larvae "shirasu" inferred from theoretical scattering models. ICES Journal of Marine Science, 60 (3): 532-537.

Miyashita K., Tetsumura K., Honda S.,Oshima T., Kawabe R.and Sasaki K., 2004. Diel changes in vertical distribution patterns of zooplankton and walleye pollock (*Theragra chalcogramma*) off the Pacific coast of eastern Hokkaido, Japan, estimated by the volume back scattering strength (Sv) difference method. Fishery Oceanography, 13 (s1): 99-110.

Morris D.J., Watkins J.L., Ricketts C., Buchholz F. and Priddle J., 1988. An assessment of the merits of length and weight measurements of Antarctic krill *Euphausia superba*. British Antarctic Survey Bulletin, 79: 27-50.

Morse P.M. and Ingard K.U., 1968. Theoretical Acoustics. Chapter 8: 400-466, McGraw-Hill, Inc., 67-15428, 911 pp.

Moszynski M. and Stepnowski A., 2002. Time-varied-gain correction for digital echo sounders. Forum Acusticum, Sevilla September 2002, 6 pp.

Mukai T., Iida K., Ando Y., Mikami H., Maki Y. and Matsukura R., 2004. Measurements of swimming angles, density, and sound speed of the krill euphausia pacifica for target strength estimation. Oceans '04, MTS/IEEE Techno-Ocean '04, 1: 383- 388.

Napp J.M., Ortner P.B., Pieper R.E. and Holliday D.V., 1993. Biovolume-size spectra of epipelagic zooplankton using a multi-frequency acoustic profiling system (MAPS). Deep Sea Research, Part I: Oceanographic Research Papers, 40 (3): 445-459.

Nesse Ø, 1998. Sound propagation in emulsions. Dissertation for the degree of Doctor Scientiarum, University of Bergen, Norway, University of Bergen, pp. 159.

Nicol S. and O'Dor R.K., 1985. Predatory behaviour of squid (*Illex illecebrosus*) feeding on surface swarms of euphausiids. Canadian Journal of Zoology, 63 (1): 15-17.

Nicol S. and Stolp M., 1990 A refinement of the moult-staging technique for Antarctic krill (*Euphasia superba*). Marine Biology, 104 (1): 169-173.

Nicol S., 1991. The age-old problem of krill longevity. Bioscience, 40 (11): 833-836.

Nicol S. and de la Mar W., 1993. Ecosystem management and the Antarctic krill. American Scientist, 81 (1): 36–47.

Nicol S. and Endo Y., 1999. Review. Krill fisheries: development, management and ecosystem implications. Aquatic Living Resources, 12 (2): 105-120.

Nicol S. and Foster J., 2003. Recent trends in the fishery for Antarctic krill. Aquatic Living Resources, 16 (1): 42-45.

Nicol S., Clarke J., Romaine S.J., Kawaguchi S., Williams G. and Hosie G.W., 2008. Krill (Euphausia superba) abundance and Adélie penguin (Pygoscelis adeliae) breeding performance in the waters off the Béchervaise Island colony, East Antarctica in 2 years with contrasting ecological conditions. Deep Sea Research, Part II: Topical Studies in Oceanography, 55 (3-4): 540-557.

O'Brien D.P., 1987. Description of Escape Responses of Krill (Crustacea: Euphausiacea), with Particular Reference to Swarming Behavior and the Size and Proximity of the Predator. *Journal of Crustacean Biology*, 7 (3): 449-457.

O'Brien D.P., 1988. Surface schooling behaviour of the coastal krill *Nyctiphanes australis* (Crustacea: Euphausiacea) off Tasmania, Australia. Marine Ecology Progress Series, 42: 219-233.

Ona E., Zhao X., Svelligen I. and Foote K.G., 1996. Some pitfalls of short-range standard target calibration. ICES Fish Capture Committee C.M.1996/B:36, 18 pp.

Ona E., and Barange M., 1999. Single-target recognition. In Methodology for Target Strength Measurements, Ed. by E. Ona, ICES Cooperative Research Report NO. 235: 27-47.

Onsrud M.S.R., Kaartvedt S., Røstad A., and Klevjer T.A., 2004. Vertical distribution and feeding patterns in fish foraging on the krill *Meganyctiphanes* norvegica. ICES Journal of Marine Science, 61 (8): 1278-1290.

Partridge C. and Smith E.R., 1995. Acoustic scattering from bodies: Range of validity of the deformed cylinder method. Journal of the Acoustical Society of America, 97 (2): 784-795.

Pauly T. and Penrose J.D., 1998. Laboratory target strength measurements of free-swimming Antarctic krill (*Euphausia superba*). Journal of the Acoustical Society of America, 103 (6): 3268-3280.

Pedersen A., 2007. Effects of nonlinear sound propagation in fisheries research. Dissertation for the degree of philosophiae doctor (PhD), University of Bergen, Norway, 307 pp. (available on net at: https://bora.uib.no/)

Pieper R.C., 1971. A study of the relationship between zooplankton and high-frequency scattering of underwater sound. Ph.D. thesis, University of British Columbia, 72 pp.

Pieper R.E., 1979. Euphausiid distribution and biomass determined acoustically at 102 kHz. Deep Sea Research, Part A: Oceanographic Research Papers, 26 (6): 687-702.

Pieper R.E. and Holliday D.V., 1984. Acoustic measurements of zooplankton distributions in the sea. Journal du Conseil International pour l'Exploration de la Mer., 41 (3), 226-238.

Pieper R.E., Holliday D.V. and Kleppel G.S., 1990. Quantitative zooplankton distributions from multifrequency acoustics. Journal of Plankton Research 12 (2): 433-441.

Pieper R.E., McGehee D.E., Greenlaw C.F. and Holliday D.V., 2001. Acoustically measured seasonal patterns of Zooplankton in the Arabian Sea. Deep Sea Research, Part II: Topical Studies in Oceanography, 48 (6-7): 1325-1343.

Powlik J.J., St John M.A.and Blake R.W., 1991. A retrospective of plankton pumping systems, with notes on the comparative efficiency of towed nets. Journal of Plankton Research, 13 (5): 901-912.

Reiss C.S., Cossio A. M., Loeb V., and Demer D.A., 2008. Variations in the biomass of Antarctic krill (*Euphausia superba*) around the South Shetland Islands, 1996–2006. ICES Journal of Marine Science, 65 (4): 497-508.

Reynisson P., 1999. Split beam method. In Methodology for Target Strength Measurements, Ed. by E. Ona, ICES Cooperative Research Report NO. 235: 18-26.

Richter K.E., 1985a. Acoustic scattering at 1.2 MHz from individuals zooplankters and copepod populations. Deep Sea Research, Part A: Oceanographic Research Papers, 32 (2): 149-161.

Richter K.E., 1985b. Acoustic determination of small-scale distributions of individual zooplankters and zooplankton aggregations. Deep Sea Research, Part A: Oceanographic Research Papers, 32 (2): 163-l 82.

Roe H.S.J., Griffiths G., Hartman M. and Crisp N., 1996. Variability in biological distributions and hydrography from concurrent Acoustic Doppler Current Profiler and SeaSoar surveys. ICES Journal of Marine Science, 53 (2): 131-138.

Romaine S.J., Cooke K., Keiser R., McFarlane S. and M. Saunders. 2002. Hake and euphausiid acoustic studies in the Strait of Georgia. In Proceeding of the Puget Sound Research 2001, the fifth Puget Sound Research Conference, February 12-14, 2001 Washington.

Russel F.S., 1927. The vertical distribution of plankton in the sea. Biological Reviews, 2 (3): 213 – 262.

Saether O, Ellingsen T. E., and Mohr V., 1986. Lipids of North Atlantic krill. Journal of Lipid Research, 27 (3): 274-285.

Sameoto D.D., 1980. Quantitative measurements of euphausiids using a 120-KHz sounder and their in situ orientation. Canadian Journal of Fisheries and Aquatic Sciences, 37 (4): 693-702.

Sameoto D.D, Cochrane N.A. and Herman A.W., 1985. Response of Biological Acoustic Backscattering to Ships' Lights. Canadian Journal of Fisheries and Aquatic Sciences, 42 (9): 1535-1543.

Sameoto D.D, Cochrane N. and Herman A., 1993. Convergence of acoustic, optical, and net-catch estimates of euphausiid abundance: use of artificial light to reduce net avoidance. Canadian Journal of Fisheries and Aquatic Science, 50 (2): 334-346.

Saunders, R.A., BrierleyA.S., WatkinsJ.L., Reid K., MurphyE.J., Enderlein P. and Bone D.G., 2007. Intra-annual variability in the density of Antarctic krill (*Euphausia superba*) at South Georgia, 2002–2005: within-year variation provides a new framework for interpreting previous ‘annual’ estimates of krill density. CCAMLR Science, 14: 27-41.

Sheng J. and Hay A.E., 1988. An examination of the spherical scatterer approximation in aqueous suspensions of sand. Journal of the Acoustical Society of America, 83 (2): 598-610.

Shirakihara K., Nakayama K. and Komaki Y., 1986. Acoustic estimation of krill biomass in R.V. KAIYO MARU SIBEX I survey area (Indian Sector of the Southern Ocean). Memoirs of National Institute of Polar Research, Special Issue, 40: 140-152

Shin H-C and Nicol S., 2002. Using the relationship between eye diameter and body length to detect the effects of long-term starvation on Antarctic krill Euphausia superba. Marine Ecology Progress Series, 239: 157–167.

Siegel V., 2000. Krill (Euphausiacea) life history and aspects of population dynamics. Canadian Journal of Fisheries and Aquatic Science, 57 (3): 130-150.

Simard Y., Lacroix G. and Legendre L., 1986. Diel vertical migrations and nocturnal feeding of a dense coastal krill scattering layer (*Thysanoessa raschi* and *Meganyctiphanes norvegica*) in stratified surface waters. Marine Biology, 91 (1): 93-105.

Simard Y. and Lavoie D., 1999. The rich krill aggregation of the Saguenay - St. Lawrence Marine Park: hydroacoustic and geostatistical biomass estimates, structure, variability, and significance for whales. Canadian Journal of Fisheries and Aquatic Science, 56 (7): 1182-1197.

Simard Y., Marcotte D. and Naraghi K., 2003. Three-dimensional acoustic mapping and simulation of krill distribution in the Saguenay—St. Lawrence Marine Park whale feeding ground. Aquatic Living Resources, 16 (3): 137-144.

Simmonds J. and MacLennan D., 2005. Fisheries Acoustics: theory and practice, 2nd edn. Fish and aquatic resources series 10, Blakwell Publishing, 419 pp.

Simrad, Norge, 1996. Simrad EK500 Scientific echo sounder. Instruction manual. P2172E, Simrad AS, Horten, Norway.

Simrad, Norge, 2003. Simrad EK60 Scientific echo sounder. Instruction manual. 850-16496/Rev.A. Simrad AS, Horten, Norway.

Stanton T.K., Nash R., Eastwood R. and Nero R.W., 1987. A field examination of acoustical scattering from marine organisms at 70 kHz. IEEE Journal of Oceanic Engineering, 12 (2): 339-348.

Stanton T.K., 1988a. Sound scattering by cylinders of finite length. I. Fluid cylinders. Journal of the Acoustical Society of America, 83 (1): 55-63.

Stanton T.K., 1988b. Sound scattering by cylinders of finite length. II. Elastic cylinders. Journal of the Acoustical Society of America, 83 (1): 64-67.

Stanton T.K., 1989a. Sound scattering by cylinders of finite length. III. Deformed cylinders. Journal of the Acoustical Society of America, 86 (4): 691-705.

Stanton T.K., 1989b. Simple approximate formulas for backscattering of sound by spherical and elongated objects. Journal of the Acoustical Society of America, 86 (4): 1499-1510.

Stanton T.K., 1990. Sound scattering by zooplankton. Rapports et Proces-Verbaux des Réunions du Conseil International pour l'Exploration de la Mer, 189: 353-362.

Stanton T.K., Clay C.S. and Chu D., 1993a. Ray representation of sound scattering by weakly scattering deformed fluid cylinders: Simple physics and application to zooplankton. Journal of the Acoustical Society of America, 94 (6): 3454–3462.

Stanton T.K., Chu D., Wiebe P.H. and Clay C.S., 1993b. Average echoes from randomly oriented random-length finite cylinders: zooplankton models. Journal of the Acoustical Society of America, 94 (6): 3463–3472.

Stanton T.K., Wiebe P.H., Chu D. and. Goodman L, 1994a. Acoustic Characterization and Discrimination of Marine Zooplankton and Turbulence. ICES Journal of Marine Science, 51 (4): 469-479.

Stanton T.K., Wiebe P.H., Chu D., Benfield M.C., Scanlon L., Martin L.V. and Eastwood R.L., 1994b. On acoustic estimates of zooplankton biomass. ICES Journal of Marine Science, 51 (4): 505-512.

Stanton T.K., Chu, D. and Wiebe P.H., 1996. Acoustic Scattering Characteristics of Several Zooplankton Groups. ICES Journal of Marine Science 53 (2): 289-295.

Stanton T.K., Wiebe P.H., and Chu D., 1998a. Differences between sound scattering by weakly scattering spheres and finite-length cylinders withapplications to sound scattering by zooplankton. Journal of the Acoustical Society of America, 103 (1): 254-264.

Stanton T.K., Chu D., Wiebe P.H., Martin L.V. and Eastwood R.L., 1998b. Sound scattering by several zooplankton groups. I. Experimental determination of dominant scattering mechanisms. Journal of the Acoustical Society of America, 103 (1): 225-235.

Stanton T.K., Chu D., and Wiebe P.H., 1998c. Sound Scattering by Several Zooplankton Groups II: Scattering Models. Journal of the Acoustical Society of America, 103 (1): 236-253.

Stanton T.K. and Chu D., 2000. Review and recommendations for the modelling of acoustic scattering by fluid-like elongated zooplankton: euphausiids and copepods. ICES Journal of Marine Science, 57 (4): 793-807.

Stanton T.K., Chu D. and Reeder D.B., 2004. Non-Rayleigh acoustic scattering characteristics of individual fish and zooplankton. IEEE Journal of Oceanic Engineering, 29 (2): 260-268.

Stehle M., dos Santos A. and Queiroga H., 2007 Comparison of zooplankton sampling performance of Longhurst-Hardy Plankton Recorder and Bongo nets. Journal of Plankton Research, 29 (2): 169-177.

Stepnowski A. and Moszyński M., 2000. Inverse problem solution techniques as applied to indirect *in situ* estimation of fish target strength. Journal of the Acoustical Society of America, 107 (5): 2554-2562.

Strand S.W. and Hamner W.M., 1990. Schooling behaviour of Antarctic krill (*Euphausia superba*) in laboratory aquaria: Reactions to chemical and visual stimuli. Marine Biology, 106 (3): 355-359.

Suontama J., 2004. Lack of suitable raw materials for fish feed – could we use plankton?. Marine Research News, 5, edit by Institue of Marine Research, Norway.

Swartzman G., Brodeur R., Napp J., Hunt G., Demer D.A. and Hewitt R.P., 1999. Spatial proximity of age-0 walleye pollock (*Theragra chalcogramma*) to zooplankton near the Pribilof Islands, Bering Sea, Alaska. ICES Journal of Marine Science, 56 (4): 545-560.

Swierzowski A., Godlewska M. and Póltorak T., 2000. The relationship between the spatial distribution of fish, zooplankton and other environmental parameters in the Solina reservoir, Poland. Aquatic Living Resources, 13 (5): 373-377.

Thomasson M.A., Johnson M.L., Stromberg J.O. and Gaten E., 2003. Swimming capacity and pleopod beat rate as a function of sex, size and. moult stage in Northern krill *Meganyctiphanes norvegica*. Marine Ecology Progress Series, 250: 205-213.

Tarling G.A., Cuzin-Roudy J. and Buchholz F., 1999. Vertical migration behaviour in the Northern krill *Meganyctiphanes norvegica* is influenced by moult and reproductive processes. Marine Ecology Progress Series, 190: 253–262.

Tesler W.D., 1989. Bias and precision in acoustic biomass estimation. Proceedings of the Institute of Acoustics, 11 (3):202–211

Tichy F. T., Solli H. and Klaveness H., 2003. Non-linear effects in a 200-kHz sound beam and the conseguences for target-strength measurement. ICES Journal of Marine Science, 62 (3): 571-574.

Trathan P.N., Watkins J.L., Murray A.W.A., Brierley A.S., Everson I., Goss C., Priddle J., Reid K., Ward P., Hewitt R.P., Demer D.A., Naganobu M., Kawaguchi S., Sushin V., Kasatkina S.M., Hedley S., Kim S., Pauly T., 2001. The CCAMLR-2000 krill synoptic survey: a description of the rationale and design. CCAMLR Science, 8: 1–23.

Trevorrow M.V., 1998. Observations of internal solitary waves near the Oregon coast with an inverted echo sounder. Journal of Geophysical Research 103 (C4): 7671-7680.

Trevorrow M.V., Mackas D.L. and Benfield M.C., 2005. Comparison of multifrequency acoustics and *in situ* measurements of zooplankton abundances in Knight Inlet, British Columbia. Journal of the Acoustical Society of America 117 (6): 3574-3588.

Urick R.J., 1983. Principles of Underwater Sound, 3rd edn, McGraw-Hill, New York, 423 pp.

van der Meeren T., Jørstad K.E., Solemdal P. and Kjesbu O.S., 1994. Growth and survival of cod larvae (Gadus morhua L.): comparative enclosure studies of Northeast Arctic cod and coastal cod from western Norway. ICES Marine Science Symposium, 198: 633-645.

Veit R.R., Silverman E.D. and Everson I., 1993. Aggregation patterns of pelagic predators and their principal prey, Antarctic krill, near South Georgia. Journal of Animal Ecology, 62 (3): 551-564.

Warren J.D., Stanton T.K., Wiebe P.H and Seim H.E., 2003. Inference of biological and physical parameters in an internal wave using multiple-frequency, acoustic-scattering data. ICES Journal of Marine Science, 60 (5): 1033-1046.

Watkins J.L., 1986. Variations in the size of Antarctic krill, *Euphausia superba* Dana, in small swarms. Marine Ecology Progress Series 31, 67–73.

Watkins J.L. and Murray A.W.A., 1998. Layers of Antarctic krill, *Euphausia superba*: are they just long krill swarms?. Marine Biology, 131 (2): 237-247.

Watkins J.L. and Macaulay M., 2000. Sampling krill: direct sampling. Chapter 2: 8-49, in Everson, I. (ed.) Krill: biology, ecology and fisheries, Oxford, Blackwell Science, pp. 384.

Watkins J.L. and Brierley A.S., 2002. Verification of the acoustic techniques used to identify Antarctic krill. ICES Journal of Marine Science, 59 (6): 1326-1336.

Watkins J.L., Hewitt R., Naganobu M. and Sushin V., 2004. The CCAMLR 2000 Survey: a multinational, multi-ship biological oceanography survey of the Atlantic sector of the Southern Ocean. Deep Sea Research, Part II: Topical Studies in Oceanography, 51 (12-13): 1205-1213.

Wiebe P.H., Boyd S and Cox J.L., 1975. Relationships between zooplankton displacement volume, wet weight, dry weight, and carbon. Fishery Bulletin, 73 (4): 777-786

Wiebe P.H., Boyd S.H., Davis B.M., and Cox J.L., 1982. Avoidance of towed nets by the euphausiid *Nematoscelis megalops*. Fishery Bulletin, 80 (1): 75-91.

Wiebe P.H., Greene C.H., Stanton T.K. and Burczynski J., 1990. Sound scattering by live zooplankton and micronekton: Empirical studies with dual-beam acoustical system. Journal of the Acoustical Society of America, 88 (5): 2346-2360.

Wiebe P.H., Mountain D.G., Stanton T.K., Greene C.H, Lough G., Kaartvedt S., Dawson J. and Copley N., 1996. Acoustical study of the spatial distribution of plankton on Georges Bank and the relationship between volume backscattering strength and the taxonomic composition of the plankton. Deep Sea Research, Part II: Topical Studies in Oceanography, 43 (7-8): 1971-2001.

Wiebe P.H., Stanton T.K., Benfield M., Mountain D. and Greene C., 1997. High Frequency Acoustic Volume Backscattering in the Georges Bank Coastal Region and Its Interpretation Using Scattering Models. IEEE Journal of Ocean Engineering, 22 (3): 445-464.

Wiebe P., Ashjian C., Gallager S., Davis C., Lawson G. and Copley N., 2004. Using a high powered strobe light to increase the catch of Antarctic krill. Marine Biology, 144 (3): 493-502.

Woodd-Walker R.S., Watkins J.L. and Brierley A. S., 2003. Identification of Southern Ocean acoustic targets using aggregation backscatter and shape characteristics. ICES Journal of Marine Science, 60 (3): 641-649.

Wyllie M.R.J., Gregory A.R. and Gardner G.H.F., 1958. An experimental of factors affecting elastic wave velocities in porous media: Geophysics, 23 (3): 459-493.

Ye Z. and McClatchie S., 1998. On inferring speed of sound in aquatic organisms. Journal of the Acoustical Society of America, 103 (3): 1667-1670.

Zhou M., Nordhausen W. and Huntley M., 1994. ADCP measurements of the distribution and abundance of euphausiids near the Antarctic Peninsula in winter. Deep Sea Research, Part I: Oceanographic Research Papers, 41 (9): 1425-1445.

Zhou M. and Dorland R. D., 2004. Aggregation and vertical migration behavior of *Euphausia superba*. Deep Sea Research, Part II: Topical Studies in Oceanography, 51 (17-19): 2119-2137.

Paper I

Lucio Calise, Tohru Mukai and Tor Knutsen

Density and speed of sound in winter specimens of Northern krill (Meganyctiphanes norvegica) from a west Norwegian fjord

Density and speed of sound in winter specimens of Northern krill (*Meganyctiphanes norvegica*) from a west Norwegian fjord

Lucio Calise, Tohru Mukai, and Tor Knutsen

Abstract

Winter specimens of the euphausiid *Meganyctiphanes norvegica* (Sars, 1857), also known as Northern krill, were caught in late November in Raunefjorden, on the west coast of Norway. Their specific mass density and speed of longitudinal sound waves were measured by density bottles and time-of-flight method respectively. The results permitted the evaluation of the respective contrasts with seawater, which are key input parameters for the theoretical predictions of acoustic target strength of such organisms. The size range of the specimens used for the density measurements varies from 10.9 to 26.4 mm in proper length measure with mean 19 mm and standard deviation 3.4 mm. The results indicate a size-dependence with decreasing density as the size increases, and the specific-density contrast varying from 1.0415 to 1.0373 for the two limit lengths. The trend is in agreement with previous published data on the same species but lower in values. Longitudinal sound speed was obtained from two separate measurement series with a velocimeter apparatus resonant at 500 kHz using a distribution of specimens with overall mean length 18.1 mm and standard deviation 3.6 mm. The overall sound-speed contrast was found equal to 1.0383 ± 0.0066, which is slightly higher than previous results for the same species caught at the same time of the year, but from north Norwegian fjords. Methodological differences, latitudinal conditions and differences in diet could be assumed as the main factors responsible for these discrepancies, including the comparisons with similar data from Antarctic krill *Euphausia superba*. Morphometric relationships between commonly used length measures and dry weight are also given to facilitate comparisons with earlier studies.

Keywords: Euphausiid, *Meganyctiphanes norvegica*, specific mass density, sound speed, morphometry, western Norwegian fiords, acoustic scattering, dry weight.

L. Calise: Department of Physics and Technology, University of Bergen, Allégaten 55, N-5007 Bergen, Norway.
T. Mukai: Faculty of Fisheries Sciences, Hokkaido University, Hakodate, Hokkaido 041-8611, Japan.
T. Knutsen: Research Group Plankton, Institute of Marine Research, P.O. BOX 1870 Nordnes, N-5817 Bergen, Norway.

Introduction

The acoustic scattering from a fluid-like marine organism is theoretically modelled by means of specific key parameters related to the morphological characteristics and significant physical properties contrasts with the surrounding medium. These are nominally the contrasts of specific mass density and the longitudinal-wave sound speed, commonly denoted *g* and *h* respectively, and play a crucial role for the accuracy of model predictions of target strength (e.g. Stanton *et al.*, 1994; Stanton and Chu, 2000).

In the case of krill, in addition to the spatial orientation, the uncertainties in estimating the two contrasts are supposed to be the principal cause of the discrepancies between the empirical observations and the theoretical predictions of target strength (e.g. Wiebe *et al.*, 1997; Stanton and Chu, 2000).

Since *g* and *h* are close to unity within a few percent, small changes in their values will induce significant changes of the predicted scattering level. Already in 1982, Greenlaw and Johnson evaluated this to cause 40 % in changes in the scattering intensity for 1 % changes in either *g* or *h*. More recently, the researchers have employed the distorted wave Born approximation model (DWBA) (Chu *et al.*, 1993; Stanton *et al.*, 1998) to investigate this influence. DWBA is recognized as the state-of-the-art in the physics-based models predicting target strength of fluid-like crustacean zooplankton (Stanton and Chu, 2000; SC-CAMLR, 2005). Chu *et al*. (2000a) presented a systematic analysis varying *g* and *h* within a reasonable range and showed that a few percentage change in these parameters could result in as much as 20 dB error in estimating target strength (TS), corresponding to a 100-fold uncertainty in abundance and/or biomass estimates. Stanton and Chu (2000) performed a series of DWBA simulations at 120 kHz applied to a 30 mm long euphausiid over the published range of material properties values and found that by varying the contrasts from 1 to 6 %, the predicted TS as function of angle orientation exhibits a large change in overall levels of scattering in the order of 15 dB.

A strong dependence of the contrasts from the body size has been also claimed by Chu and Wiebe (2005), who asserted that the difference in TS between a juvenile and an adult individual of *E. superba* with length 27 and 53 mm respectively would be about 6 dB more than resulting from theoretical result based purely on the size difference.

It is clear that, since the parameters *g* and *h* can be so significant in theoretical modelling of echo formation, the effectiveness of the theoretical predictions relies on the ability to measure the material properties of krill with high degree of accuracy.

Precise direct measurements of euphasiids specific mass density and longitudinal-wave sound speed are generally difficult because of the complex shapes of the organisms and the similarity in physical values with seawater. Moreover, Greenlaw (1977) found a substantial difference between live and dead animals and Foote (1990) claimed the influence of the "aging effect" related to a significant decline of longitudinal-wave sound speed results when the time lag between the catch and the measurement increases.

Therefore, the measurements have to be performed on fresh organisms, which have to be easily available to the investigators in a few hours after the catch.

The reported values have mostly been measured *ex situ* in laboratory and only for some species of main interest, such as *Euphausia superba* and *Euphausia pacifica* (Greenlaw, 1977; Kils, 1979, 1981; Greenlaw and Johnson, 1982; Foote, 1990; Foote *et al.*, 1990; Mukai *et al.*, 2004; Chu and Wiebe, 2005), and few measurements on *Meganyctiphanes norvegica* and *Thysanoessa* genus (Kristensen and Dalen, 1986; Køgeler *et al.*, 1987)

As general conclusion, since the lipid content, the size and shape related to the diet and the life stage, and the natural habitat pressure influence the values, the essential physical

properties have to be considered species-dependent, varying with size, stage, geographical location, season, and in some case with the depth.

Due to the high range of variability and the lack of proper data for specific species at the location and time of the measurements, the values of *g* and *h* have often been adjusted to fit the acquired acoustic data (e.g. Holliday and Pieper, 1980; Wiebe *et al*., 1997; Lawson *et al*., 2006). This is especially the case when the attenuation due to the multiple scattering is relevant (Chu and Ye, 1999).

However, when theoretical models are employed for the estimation of krill acoustic scattering, and high accuracy is wanted (especially in the case of single ping analysis) parameterization by contrasts strictly related to the species, the season and the geographical location of the target under investigation is imperative.

The aim of this study was to perform accurate measurements on specific density and longitudinal-wave sound speed, hereafter called sound speed, in winter specimens of *Meganyctiphanes norvegica* (Sars, 1857) and to obtain their corresponding contrasts with respect to seawater in order to improve collateral modelling parameterization. Results from measurements performed at Espegrend Marine Biological Station of the University of Bergen (Norway) in late November 1998 are presented. They aid to fill a gap in current knowledge with respect to theoretical acoustic scattering from euphasiids, and increase the capability to employ acoustical methods for estimation of krill biomass.

Materials and methods

The euphausiid *Meganyctiphanes norvegica* were caught during nighttime in the central part of Raunefjorden (60°16′N 5°9′E), a land-locked fjord on the west coast of Norway near Bergen, with the 11 m long vessel MS "Aurelia", run by the University of Bergen. The sampling gear was an Isaac-Kidd Midwater Trawl (IKMT), with 0.9 m^2 opening and 500 μm mesh size deployed at approximately 15-20 m depth for not more then 15 minutes with a towing speed of 2.6 knots. In lieu of a traditional cod-end bucket, a sturdy, transparent, plastic bag of 30 l volume, partially filled with surface water, was attached to the cod-end by means of a clamp. This arrangement permitted to collect animals in very good condition for the experiments. When brought on board, the contents of the bag were emptied gently into a plastic tub of 50 l capacity. Surface water was added when necessary and dead or damaged animals and unwanted organisms of different species (especially gelatinous forms) were immediately removed using a sieve.

During transport to the Espegrend Station, that took approximately half an hour following the last catch, the tub was covered by a lid to avoid light exposure and loss of water.

For temporal storage, the animals were kept in their tub in a dark cold room maintained at nominal temperature of 6.5 °C, i.e. approximately the *in situ* temperature at the depth of the catch, and aerated continuously by means of an air pump and hose close to the tub bottom. Along with the krill, a small amount of copepods of the genus *Calanus* were visible in the tub, and acted as a natural source of food for the krill during the storage period. Most of the animals were observed to be actively swimming in the bucket. Dead animals were removed from the tub by siphoning from the bottom and by sieving on the surface.

Density measurements

The sampling of krill for the density measurements was carried out on 17 and 25 of November 1998. A total of 113 healthy specimens were measured in the period from 23 to 27 of November 1998 in the cold storage room at 6.5 °C.

Prior to the measurements, the animal was classified and three different lengths of the specimen in lateral aspect were measured using a Leica Wild M10 binocular microscope. These were called total length (TL), body length (BL) and carapax length (CL). They are defined and codified by Morris *et al.* (1988) as follows: 1) total length "TT", from tip of the rostrum to end of telson; 2) body length "S3", from the posterior face of the eye notch to the end of the sixth abdominal segment; 3) carapax length "S6", from the posterior face of the eye notch to the posterior dorsal median end of the carapace. Figure 1 summarizes the lengths and their equivalents with the Morris *et al.* (1988) notations. Other lengths mentioned in this paper are also illustrated in the figure.

The "TT" length measure was found most appropriate for *M. norvegica* because it is defined by two body extremes easily recognizable for the species, leading to less uncertainty when measured.

Together with the specimens from the specific density measurements the other 117 individuals from the catches carried out on 17 and 25 of November were measured in their lengths as defined above. The two data sets consist of a total of 230 specimens, and regressions between different length measures were determined and used when needed.

The density of krill was measured using the density-bottle-method (Greenlaw, 1977). A series of solutions were prepared mixing in appropriate amounts filtered sea water, in which the krill were collected, glycerine and Instant Ocean® Sea Salt, to obtain solutions spanning the range from 1.056 to 1.076 g cm^{-3} with proportions adjusted to give difference in step of about 0.002 g cm^{-3}. A laboratory glass hydrometer was used to check the density of each solution.

Before introduction in the bottles, each specimen was anesthetized individually using a 0.07 g 3-amino-benzoic acid ethylesther methane-sulphonate (MS222) per 100 ml sea water. The measurements started immediately after the animal showed no activity. When transferred from one bottle to the next, the animal was carefully picked up by a glass pipette with rubber bulb and then placed in the next solution using similar pipette with surrounding solution in turn. This procedure was carried out with care, paying attention that the animal had no contact with air, and assuring that only minute amounts of the previous solution were mixed with the next one. The mean density between the densest solution in which the animal sank, and the least dense solution in which it floated, was assigned as the specific density of a specimen. The specific densities of the two solutions were measured again prior to calculating their mean.

Following the completion of the individual density measurement, each specimen was rinsed with fresh water, put in a micro-test tube of 1.5 ml capacity, and placed in a freezer at -20 °C for short-term storage before ultimate measurements of dry weight. These were performed by transferring the euphasiids in an ice-filled container to a Christ Alpha 1-4 freeze drier, being immediately placed in the pre-cooled drying chamber and dried for 24 hours. The animals were then stored over silica gel in a desiccator prior to weighing. Single specimens were transferred to small pre-weighed aluminum cups and dry weight measured to within ±0.001 mg on a Cahn 29 Automatic Electro balance weight.

Sound speed measurements

The time-of-flight-method applied to an inverted T-shaped Plexiglas velocimeter (Greenlaw, 1977), with associated acoustic and electronic instrumentation, was used for the measurement of sound speed. Similar apparatus have been used in a number of previous studies. A schematic draft of the entire system can be found in Køgeler *et al*. (1987) and a description of the transmission process for the velocimeter used in this study is given in Foote (1990). The couple of ceramic transducers resonant at 500 kHz were placed at a distance of 19.05 cm on the opposite horizontal ends of the T-tube, which had an inner diameter of 3 cm.

An ultrasonic velocimeter measures the time of flight of an acoustic pulse through a finite volume of a mixture consisting of a reference solution (usually seawater) and a number of living organisms uniformly distributed. If the acoustic wavelength is much smaller than the projected length of the organisms, the phenomenological model for the determination of elastic wave velocities in porous media by ultrasonic velocimeters introduced by Wyllie *et al*. (1956) and more exhaustively explored in Wyllie *et al*. (1958) may be applied as a good approximation. The mixture can be interpreted as a two-phase layered medium without rigidity and activation of viscous, thermal and scattering processes, where the advancing plane wave with normal incidence on the layers interfaces propagates in one phase at the time. Hence, the measured time t of flight is the time average of the travel times through each layer and can be simply equated to the sum of the travel times t_s and t_k due to the solution and the organisms respectively. This equation may be expressed in terms of the corresponding sound speeds and volume fraction of the organisms (Foote, 1990), defined as the ratio of the volume of the organisms to that of the total mixture, and solved to obtain the sound speed in the organisms c_k according to:

$$c_k = \frac{V\ c\ c_s}{c_s - c\ (1-V)} \tag{1}$$

where V is the volume fraction of the organisms, c is the sound speed in the mixture related to the measured time of flight and c_s is the sound speed in the solution theoretically or experimentally determined.

The velocimeter used in the present study was re-fabricated at the Institute of the Marine Research in Bergen (Norway), having increased stability and sensitivity, hence precision, compared to the apparatus used by Foote (1990). This was confirmed by initial measurements performed with only distilled water or seawater with different salinities in a period prior to the measurements with the animals. The distilled water results suggested a gross precision of 6 parts in 10000.

The improvement in sensitivity addressed to solve necessarily unavoidable system defections. Because of the electronic limitations of the transmitting and receiving circuits effects of the system delays were recognizable in both processes. The first of these effects was clearly evident on the generated square wave. It was due to the limitations of the circuits generating the waveform, whose period was mainly regulated by an R-C oscillator. The rise time needed by the transmitted signal to reach the high level was measurably different to that returning back to low level. Hence, the inevitable deviation of the transmitted pulse from an ideally-square signal was significant. The problem was overcome in practice by reading precisely the period of the square wave and to assign half of the value as the measured time of flight. The reading operation was performed using a digital oscilloscope Tektronics TDS220 (100 MHz bandwidth) operating in time-expanded mode accomplished with a Fluke 1911A frequency multi-counter where the time delay was read out.

The asymmetric effect of the generated square wave also contributed to the entire cumulative system delay due to the successive steps in signal generation and transmission processes. The delay was estimated by the mentioned initial measurements on solutions with known sound speed. For the specific apparatus, a nearly constant time delay equal to 46.82 μs (std=0.38) was found. However, the resulting bias with respect to the measurements was overcome during analysis of the data as described below.

Samples from the catch event on 25 November were used for the measurements with animals. These were performed in a wooden boat-house close to the Espegrend field station during two distinct sessions: the first during the night of 25 November, just after arriving to the station from the fjord; the second in the afternoon the next day, approximately 20 hours after sampling.

Healthy specimens were concentrated in a proper amount of seawater by filtering the content of the buckets with a fine meshed sieve. First, the T-tube was flushed several times with the bucket seawater and then the animals introduced from the open end of the tube until its horizontal part appeared to be uniformly filled with krill without any compression. Before the pulse transmission measurements, the tube was gently shaken to assure uniform distribution of krill across the cross section of the sound path, i.e. the cross section of the horizontal part of the T-tube. During the measurements the animals were mostly aligned along the horizontal axis of the tube with typical pleopod beats activity.

Since the ambient temperature could not be regulated, a thermometer accurate to ±0.05 °C was used to continually monitor temperature changes in the T-tube mixture. It was inserted from the open end of the tube and removed just before pulse transmission. The temperature read just before the removal, was associated to the measured time of flight. Despite the low response, control of the temperature just after the measure was also performed to confirm the temperature to be associated to the measure.

When the sound speed measurements were terminated, the seawater and the krill were separated using a fine meshed sieve. The seawater was preserved in appropriate bottles for salinity determination, while the krill was fixated in 4% formalin solution for later morphometric measurements.

In addition, measurements at a range of experimental temperatures with only seawater from the buckets containing the animals were performed after those with animals. These calibration series were used in a further analysis of data to estimate the response of the system to changes in temperature during the measurements.

Four months after the measurements, the two fixated krill samples were split using a Folsom Plankton splitter and two quarters of each sample worked up independently for species composition and size of the animals. The body length “S3” and carapace length “S6” were measured (c.f. Fig. 1). The latter is known to be much less affected by shrinkage due to various preservatives (Kulka and Corey, 1982) and can easily be converted to total body length when needed.

Since the volume of the samples under investigation was not directly measured, the Kils (1979) length-volume relationship was used to determine the volume fraction of krill in the tube during the pulse transmissions. For an individual krill of length L in mm, the volume V in cm^3 is given by:

$$V = 3.67 \cdot 10^{-6} L^{3.16} \qquad (2)$$

This relationship is indicated from the author as applicable to *Euphausia superba*. However, it was determined lumping together *E. superba* and *M. norvegica* specimens, with most of

the animals (112 over 190 specimens) of the latter species caught in the North Atlantic. Hence, its employment is probably equally justified for measurements on *M. norvegica*.

The Kils length-volume relationship (2) requires that the length *L* in equation (2) is measured from the anterior margin of the eyes to the tip of the telson. This is coded by Morris *et al*. (1988) as length "AT" and shown in Fig. 1. To obtain the length "AT" of the sound speed specimens, a least mean square regression on the length "S6" was determined by measuring both lengths from high definition images (10 Mb in tiff format) of 35 fresh *M. norvegica* specimens, resulting in the following relationship:

$$AT = 3.37 \cdot S6 + 3.46 \tag{3}$$

with $R^2 = 0.95$ and both lengths in millimetres. Volume of the specimens other than *M. norvegica* classified in the samples, i.e. *Thysanoessa inermis* and *Nyctiphanes couchii*, were determined by the volume/length relationships presented by Mauchline (1967) and listed in non-logarithmic form by Greenlaw and Johnson (1982). Because of the lack of proper conversion relationships from length "S3" or "S6" to "AT", equation (3) was also used for these species.

In the worked up sample from 26 November, 20 krill specimens were found damaged and impossible to measure and classify. However, their volume was proportionally taken into account in the analysis on the basis of the species percent reported from the sample classification, and their related mean lengths.

The total length "TT" of the sound speed specimens was also determined by a least mean square regression on the "S6" on the base of measurements on 230 individuals of *M. norvegica* deriving from the sampling of 17 and 25 November with both the lengths in mm:

$$TT = 3.35 \cdot S6 + 1.56 \tag{4}$$

The regression coefficient (R^2) of the relation (4) was equal to 0.96.

Constant measurement conditions are primary requirement to satisfy for the applicability of Equation (1). The variability in temperature during the measurement series persuaded to process the data following a similar procedure as applied by Foote (1990). From the measurements series on seawater from the buckets containing the animals alone, least mean square regressions of c_s on the temperature T related to the each solution of the two measurement sessions were established. For each measurement, the sound speed in the solution c_s introduced in Eq. (1) was referred to a constant temperature and the resulting referred measurements of each series averaged. For the *n* measurements of one series, the mean value of c_s was calculated by:

$$\overline{c_s}(T) = \frac{1}{n}\sum_{i=1}^{n}\left[c_s(T_i) + m(T - T_i)\right] \tag{5}$$

where T_i is the temperature read from the thermometer at the time of the measurement, T is the expected temperature relative to the measurement calculated on the base of the related regression with slope *m*. Finally the sound-speed contrast at each measurement *i* was obtained by the elaborated form:

$$h_i = \frac{c_k(T)}{\overline{c_s}(T)} \tag{6}$$

with c_k(T) calculated by Equation (1) wherein c_s is the value obtained through the related regression at the expected temperature T.

Results and discussion

Length distributions

Figure 2 shows the total length distributions of *Meganyctiphanes norvegica* specimens used in deriving the specific density (Fig. 2a) and the sound speed (Fig. 2b) measurements. They represent winter animals that most probably belong to the 0-group, i.e. individuals less than 1 year old, although some of the bigger animals found within the sound speed samples could belong to the I-group being approximately 1 ½ years old at the time of the experiments. The youngest generation is presumably the dominant size group in the uppermost part of the water column at night, wherein the field sampling was performed. For completeness, differentiations inside the samples are also graphically shown. The partial distribution in grey bars of the specific density sample refers to the animals caught on 17 November; while for the sound speed biological samples (Figure 2b) refers to the animals from the session performed on 25 November. The length of the specimens derived from both catches used for the density measurements span a near identical range. More specimens of length 22 mm from the 17 November sampling (grey bars) were measured. The overall mean and standard deviation were 19 and 3.4 mm respectively. For the sound speed samples, the sample from the session performed on 25 November spans a wider range from 8.6 to 31.6 mm total length. However, for both the grey and black distributions the normal distribution is likely the best fitting, with mean and standard deviation 18.0 and 3.5 mm and 18.1 and 3.7 mm respectively. The cumulative distribution has also a Gaussian trend centred at 18.1 mm and standard deviation 3.6 mm.

Density and dry weight

In Figure 3, the results of the specific density versus TL and the related regression for the total number of measured animals are shown. The TL spans the range from 10.9 to 26.4 mm. Differentiation between animals from the catch events on 17 and 25 of November is graphically emphasized, but no significant difference in the regressions parameters from the two data sets separately has been found (highest p-value found less than 0.02). The results in Figure 3 clearly indicate that the specific density is size-dependent, linearly decreasing as the length increases, as well as the expected contrast with the seawater. They were employed together with the reference density of seawater equal to 1.026 g cm^{-3} to express the linear regression for density contrast g versus TL in mm:

$$g = -2.73\ 10^{-4} \cdot \mathrm{TL} + 1.0445 \qquad (7)$$

The procedure adopted to achieve the results may be debatable, especially because of the low correlation coefficients of the regression. Different methods have been used in the past for laboratory specific density measurements on zooplankton. The earliest indirect method of displacement volume and weight (Lowndes, 1942) was the most straightforward, determining the density by the ratio between the weight and the net volume of the animal. Nevertheless, the measure of both parameters was generally affected by of few percent of errors (c.f. Chu *et al*., 2000b). Another indirect approach for zooplankton is to measure the

sinking rate of the organisms (e.g. Knutsen *et al*., 2001), but it is not suitable for organism with irregular or elongated shapes like euphausiids.

Direct methods, such as the density-bottles method and the gradient-density method, seem to be more accurate and have been adopted by the majority of investigators (Greenlaw, 1977; Greenlaw and Johnson, 1982; Kristensen and Dalen, 1986; Køgeler *et al*., 1987; Foote *et al*., 1990; Mukai *et al*., 2004). They overcome the uncertainty introduced by water inevitably adhering to the animals' appendages, which can introduce serious biases in wet weight and displacement volume measurements. However, due to the set-up the quality of the measurements is variable and in some cases the results have to be considered carefully, especially in the case of gradient-density-method (c.f. Knutsen *et al*., 2001).

Both methods have similar sources of error. They require a particular handling of the animals with associated problems, and the animal has to be motionless but alive. Anesthetization is a common procedure to obtain this requirement, but it could affect the specific density of the organism by influencing the position of the legs, antennas and any elongated part of the body during the sinking. Moreover, problems associated with osmotic processes may arise (Køgeler *et al*., 1987), especially if the observation is prolonged in time and the solutions have high salinities and/or the anaesthetic contains excess salt.

All aspects mentioned above were considered during the density measurement presented in this paper, and partially resolved. The handling was performed with extreme care, and only measurements with animals in perfect shape at the end of the treatment were included in the data set. The amount of MS222 used for the anesthetization was as low as possible and any non-natural aspect of the animal in the bottle was recorded. The measurements were conducted as fast and efficient as possible to reduce handling time and the accomplished use of glycerine and Istant Seasalt allowed to prepare a set of solutions with unknown salinity, but for sure balanced in range around that of the seawater from the buckets wherein the animals were stored.

The most significant result from the density measurements is that the contrast g is size-dependent, decreasing as the krill length increases. Kristensen and Dalen (1986) and Køgeler *et al*. (1987) also found this trend for *M. norvegica* captured in Norwegian sub-Arctic area, and in the second study in different seasons of the year. On the contrary, Kils (1979) reported an opposite trend in specific density with respect to length for a data set of specimens comprising both *Euphausia superba* and *Meganyctiphanes norvegica*. While the latter result is supported for *Euphausia superba* (Chu and Wiebe, 2005), it is uncertain and still an open matter if Kils density relationship is generally valid for *M. norvegica*. The exact location and time of capture of the *M. norvegica* samples were not specified in that paper, and the density was estimated by hydrostatic balance measurements on dead animals.

Differences in lipid (mainly wax ester and triglycerides) and ash contents, which might depend on the physical seawater conditions (i.e. temperature), feeding conditions, gonad maturity and sex may be the primary reason for the size dependency and seasonal changes in specific density. These characteristics have a regional and seasonal variability. Moreover, the specific densities of the lipids strongly depend on temperature (Yayanos *et al.*, 1978).

Raymont *et al.* (1969) investigated the biochemical composition of *Meganyctiphanes norvegica* collected over a 6-month period November-May in west Norwegian fjords near Bergen, i.e. the same region as in this study. They found that the lipid content was highly variable during the time of investigation with lower content associated with smaller animal size from the 0-group generation. Contemporarily, the ash and the protein contents exhibited a reciprocal trend with respect to lipid content. Similar results have been obtained by Falk-Petersen (1981) and Saether *et al*. (1986) in their annual investigations on *M. norvegica* and *Thysanoessa* species from north and central Norwegian fjords. Køgeler *et al*. (1987) argued

that this trend could seriously contribute to the observed decrease in density with increasing length.

A slightly regional difference in biochemical composition have been even observed by Raymont *et al.* (1971) comparing *Meganyctiphanes* collected at same time of the year from the west coast of Scotland and south Norwegian coastal waters. Thus, the geographic location and the actual associated physical conditions strongly influence the specific density of the organisms too, which for the same species at same time of the year can vary with locations.

We speculate that in addition to methodological issues the latitudinal difference is the main reason of the discrepancy when comparing our results with those obtained by Kristiansen and Dalen (1986) and Køgeler *et al*. (1987) on *Meganyctiphanes norvegica* captured in north Norwegian fjords for the same period (November-December) by means of a density-gradient column. For a specimen of 20 mm total length the Kristensen and Dalen regression gives a specific density of 1.0761 g cm^{-3}, while the regression in Figure 3 gives a value of 1.0776 g cm^{-3}. The resulting density contrasts are g=1.0488 and g=1.0503 using the two regressions respectively. Note that Kristiansen and Dalen (1986) measured the total length using the *Morrison et al.* (1988) "BT" length definition, i.e. from base of the eyestalk to the posterior end of the telson (Fig. 1), so that for the same animal a slightly lower length was considered. However, in order to have similar density from the regression, a specimen caught in Raunefjord should have a "TT" length of 14.64 mm. In a more recent paper, the Kristensen and Dalen regression was suggested as appropriate for *M. norvegica* specimens longer than 25 mm (Dalen and Kristensen, 1990).

The regression presented by Køgeler *et al*. (1987) for mid November gives similar results to that of Kristensen and Dalen, but using the coefficients related to September and early November listed in Table 4 of that paper, closer results to those presented here are obtained.

For completeness, in Figure 4 the dry weight of the measured animals is plotted versus TL, and the related power regression is also shown. Biochemical analysis of samples was not carried out. Direct comparison with previous published data may be arduous because of differences in methodology used, especially in the way and the time of drying.

Generation, sex and maturity stage are important parameters for the specific density of a krill as demonstrated by Mukai *et al*. (2004). All our animals measured were presumably 0-group individuals. In November, they are immature and will probably not spawn until April –May the following year. Therefore, specific sexual and stage differentiations were not considered in this study, hence should not have an influence on the results presented in this paper. Previous studies on *Meganyctiphanes norvegica* have indicated that in general sex differences are not apparent in volume-weight relationships (Raymont *et al.*, 1971; Thomasson *et al*., 2003), as well as weight-length relationships (c.f. Brattelid and Matthews, 1978; Kulka and Corey, 1982).

Specific density of the Antarctic krill *Euphausia superba* has been object of several studies. The recent study by Chu and Wiebe (2005) suggested the promising dual-density method. Here the densities and the associated weights of two fluids, with and without animals, are determined through a procedure leading to a set of linear equations to be solved. The method does not require the animals to be motionless, avoiding the associated problems with anesthetization. Since the authors claim a high degree of accuracy, the method may easily become a standard method for future measurements. Their results also indicate that specific density is size dependent for *E. superba* with increasing density as size increases. The difference in density trend between *Meganyctiphanes norvegica* and *Euphausia superba* is difficult to explain. If this pattern could be confirmed in future studies, probably a range of factors are involved. The two species live in very different environmental regimes.

Euphausia superba has a prolonged life-span compared to *Meganyctipanes norvegica,* and they have probably very different life-history strategies. An important aspect could be significant differences in diet, *Euphausia superba* being herbivorous while the *M. norvegica* are primarily omnivorous or carnivorous (c.f. McClatchie, 1985), especially during autumn-winter period (Saether *et al*., 1986). This could induce distinctly different patterns of lipid and protein deposition within both Northern and Antarctic krill, inevitably influencing the specific density as well the longitudinal sound speed.

Sound speed

In Table 1 results from samples classification, total length statistics for each species, and sound speed measurements with associated physical parameters are summarized.

The classification reported specimens of other species than *M. norvegica* in very small numbers. They were nominally *Thysanoessa inermis*, composing 0.9 and 4.4 % of the individuals from 25 and 26 November respectively, and *Nyctiphanes* couchii, composing 2.2 and 5.5 % of the individuals for the respective days. As these species are quite similar in shape to *M. norvergica*, their body volumes were necessarily considered in the krill volume fraction calculation, but the small number of specimens encouraged ignoring their bias on the result that was assigned to the target species.

Among the 25 November sample, two *M. norvegica* specimens with TL bigger than 30 mm were estimated through relationship (4). However, only 6 specimens were bigger than 25 mm, and 8 specimens shorter than 13 mm. Hence, the length distribution for the two samples are interpreted as near identical.

The regression used to determine the values T and *m* in Eq. (5) was based on wider ranges of temperature than the respective ranges during the measurements. This assured a confident applicability of them within the experimental ranges. In particular, the regressions described a temperature gradient in sound speed of 3.4 and 3.3 $m\,(s\,^{\circ}C)^{-1}$ for the measurement with only seawater on 25 and 26 November respectively. The values are in full agreement with the theoretical change in sound speed versus temperature for seawater with the same physical characteristics.

The mean sound speed contrast *h*, obtained from the two series in Table 1 between winter specimens of *Meganyctiphanes norvegica* caught in Raunefjord and seawater is 1.0383±0.0066.

The time-of-flight by velocimeters is the most common method used in zooplankton sound speed measurements. Other methods were suggested in the past; a critical focus on these potential techniques, such as piezometer operations, resonance and levitation can be found in Greenlaw and Johnson (1982). A more modern and sophisticated apparatus that permits *in situ* sound speed measurements is the APOP system presented by Chu *et al*. (2000a) and successively improved (Chu and Wiebe, 2005).

Foote (1990) exhaustively illustrated the conditions to be fulfilled for the applicability of the time-of-flight technique with a T-tube ultrasonic velocimeter. The acoustic wavelength must be less than the projected size of the organisms, the animals used must be as fresh or newly caught as possible, they must be uniformly distributed in the velocimeter during measurements and the precise knowledge and constancy of the physical parameters (mainly temperature) during the measurements are necessary.

In our sound speed measurements, the improved apparatus and the procedure of acquisition and processing assured compliance with the above requirements. Since the second series of

measurements were performed within 24 h of the catch, and the animals were kept in a cold room with near identical physical conditions as *in situ*, the aging effect was considered not affecting that session of measurements.

In practice, determining the krill volume fraction is the most critical step of the analysis. An indirect estimation approach by means of published data on wet weight, or directly derived from the presented dry weight and the density results in Fig. 2, has been judged to be too uncertain due to the large range of variation, also in making appropriate allowances for latitudinal differences on published data. The biochemical composition strictly depends on species, location and time of the year and strongly influences the weight values. Indeed the same is true for the methods used with respect to drying and length determination. To our knowledge no relevant data have been published on *M. norvegica* with strictly same characteristic (specific time period and location) of the specimens considered in this study, the use of the general length-volume relationship (2) has been considered more convenient for the purpose. For a krill length-volume determination the biochemical composition is not important, neither is sex composition (Mauchline, 1967). It should be noted that also Mauchline (1967) gave a volume-length relationship for *M. norvegica*, but this was considered to be inferior compared to Kils (1979) as the predictions from Mauchline's regression for some reason seems to be beyond reasonable limits. Moreover, even if most of the animals used by Kils were bigger compared to those used in the present study, Greenlaw and Johnson (1982) claimed that the krill shape does not change appreciably during growth, so that only the slight allometric changes in volume with respect to length regulated by the Eq. (2), has to be taken into account.

Chu *et al*. (2000a) proposed an indirect method for the volume fraction determination by measuring the resistivity of zooplankton though an empirical approach. Despite attractive, the method was impracticable in the present case.

Mauchline (1967) also reported a length-volume relationship for general *Euphausia* species. The relationship requires the "BT" length (Fig. 1) as defined by Morris *et al*. (1988). Apart from the deviation due to the difference in the starting limit-body points, the Mauchline and the Kils (Eq. 2) relationships give similar results. The Kils relationship was also found in agreement to that determined for *M. norvegica* specimens caught in Gullmarsfjord, on the west coast of Sweden, (M. A. Thomasson, unpublished data) and derived from specimens used by Thomasson *et al*. (2003) for their swimming capacity investigation.

To the authors' knowledge, the unique sources of published data of sound speed in *M. norvegica* species are the studies by Kristensen and Dalen (1986) and Køgeler *et al*. (1987). In both these studies the Greenlaw's procedure was adopted (Greenlaw, 1977), including the questionable method to calculate the krill volume fraction by measuring the displacement of the solution in the vertical part of the T-tube after introduction of organisms. Assuming that it is extremely difficult to introduce dry organisms in good condition, the method does not consider the overestimation of the volume due to water unavoidably introduced with the animals. The regressions obtained by the Greenlaw procedure tend to be highly significant since the relation between sound speed in a mixture and the relative concentration of the constituents is not generally linear, hence the method is suitable for moderate sample sizes (Greenlaw and Johnson, 1982). Despite that, Kristensen and Dalen (1986) and Køgeler *et al*. (1987) reported a series of measurement with a krill volume fraction close to 65 %. Moreover, a practical effect for high volume fractions might also arise since high packing of krill would induce higher and faster mortality of individuals that could bias measurement when proteins in their body coagulate. In addition pleopod activity would be terminated and animals sink to the lower part of the tube, violating the assumption of uniformity in krill distribution along the acoustic path.

Raymont *et al*. (1969) found the general contents and trends in lipid and protein changes remarkably similar in *M. norvegica* and *Thysanoessa inermis* species caught at approximately the same localities and over the same period in west Norwegian fjords near Bergen. Køgeler *et al*. (1987) found that the difference in mean sound-speed contrast between the two species over a year of investigations was of the order of 0.004. Due to this very low value and the presumed similarity in biochemical composition, the presence of other species than the target *M. norvegica* in the measured sample may be considered not biasing the results.

The result of sound-speed contrast obtained in this study is slightly higher than those reported in previous investigations on the same target species and time of the year, but at higher latitude. Kristensen and Dalen (1986) found a value of 1.030 for specimens caught in a north Norwegian fjord during the period November-December. Køgeler *et al*. (1987) found the same value as mean from measurements over a year, but somewhat lower for the period November-December. They found a similar value of sound-speed contrast to this study only earlier in November and in late January the following year.

As for the density contrast, the discrepancy may be attributed to latitudinal conditions and the related physical and biological processes. However, opposite differences in the investigated material properties are not a surprise. Mukai *at al*. (2004) found that the contrasts in *Euphausia pacifica* may be reciprocally interrelated in response to the variations in lipid content, with the density contrast increasing as the sound-speed contrast decreases. On the other hand, this interrelation was not clear in the Køgeler *et al*. (1987) investigation for the same target species as in the present study.

Previous studies on Antarctic species also reported lower sound-speed contrasts in general. These measurements have been usually performed on bigger animals. Chu and Wiebe (2005) found a depth-dependence on sound-speed contrast for *Euphausia crystallorophias* species, but not for *E. superba*, which showed a moderate dependence of sound speed on the size. Unfortunately, it was impossible to investigate the length dependence of sound speed on the target species in this study.

The experiments presented here were performed in a laboratory at atmospheric pressure and the results are presented without considering the potential depth influence on the measured physical properties.

As for the specific density results, the sound-speed discrepancies between the geographically different groups of krill could be mostly attributed to the basic diet of the organisms and the related differences in lipid and protein contents.

Conclusion

Mass density and longitudinal-wave sound speed in winter generation specimens of *Meganyctiphanes norvegica* caught in a fjord of western Norway have been determined by specific measurements. The density and sound-speed contrasts of with seawater are key input parameter and play a primary role in theoretical modeling of the acoustic target strength from fluid-like zooplankton. Thus, the correct knowledge of these parameters and their variability are essential for the employment of acoustic methods for accurate abundance estimation of such organisms. Irrespective of model used, it should be parameterized according to the contrasts length-based and potential seasonal variability.

The fulfillment conditions for the correct applicability of the measurement methods used were fully satisfied. Established procedures employed to obtain more accurate results were also described in details.

For a total body length spanning from 10.9 to 26.4 mm, the density contrast have been found to be size-dependent, decreasing as the length increases through the relation $g = -2.73\ 10^{-4} \cdot TL + 1.0445$. This trend is in agreement with previous published data on the same species captured in the same season, for more northern latitude, but predictions from the regression gives comparably lower values.

The overall sound-speed contrast h was found equal to 1.0383±0.0066, which is also different from results of similar species in earlier studies, but if compared to the specific density results, sound speed values are higher. The inversely reciprocal discrepancy could possibly be explained by the large difference in geographical location and associated physical conditions or methodology, while the differences in material properties between krill groups/species from the two different sub-polar areas have to be attributed to basic diet and associated lipid and protein accumulation.

The results presented in this study have been motivated by the fact that a substantially amount of work have been done regarding measurement of target strength at different frequencies on *M. norvegica* in a mesocosm venue (Calise and Knutsen, 2009). In order to compare such measurements with theoretical scattering model output with respect to target strength, data on sound speed and density contrasts for the same species caught in the same fjord system were considered extremely valuable. However, the data presented in this work are by no means complete. The need for systematic measurements over the year to evaluate seasonal and spatial (including depth) variation of the material properties of *Meganyctiphanes norvegica* is strongly needed. Such studies should also aim to reveal how these material properties relate to processes like maturation and spawning and how the biochemical composition of animals changes with time.

Acknowledgements

The following are thanked for their support of this work: the EU through RTD-contract no. MAS3-CT95-0031 (BASS), the Norwegian Research Council through grant no. 113809/122, and Bergen Large-Scale Facility for Marine Pelagic Food Chain Research. The supervision of Dr. Kenneth Foote, Woods Hole Oceanographic Institution, during all phases of the measurements is particularly appreciated. Trygve Gytre, Institute of Marine Research in Bergen, Norway, is thanked for the technical support in setting up the sound speed apparatus and for practical suggestions and solutions in refining the measurement technique. Professor Halvor Hobæk, University of Bergen, and John Dalen, Institute of Marine Research in Bergen, Norway, are thanked for reviewing the paper and for constructive comments and criticism. L. Calise was financially supported by a University of Bergen Ph.D. fellowship.

Reference

Brattelid, T. E., and Matthews, J. B. L. 1978. Studies on the deep-water pelagic community of Korsfjorden, western Norway. The dry weight and calorie content of *Euchaeta norvegica*

(Copepoda), *Boreomysis arctica* (Mysidacea), and *Meganyctiphanes norvegica* (Euphausiacea). Sarsia, 63: 203-211.

Calise, L., and Knutsen, T. 2009. *Multifrequency target strength of Northern krill Meganyctiphanes norvegica*: measurements on tethered specimens and SDWBA theoretical predictions. In preparation. Paper V of this thesis.

Chu, D., Foote, K. G., and Stanton, T. K. 1993. Further analysis of target strength measurements of Antarctic krill at 38 and 120 kHz: Comparison with deformed cylinder model and inference of orientation distribution. Journal of the Acoustical Society of America, 93 (5): 2985-2988.

Chu D. and Ye Z., 1999. A phase-compensated distorted wave Born approximation representation of the bistatic scattering by weakly scattering objects: Application to zooplankton. Journal of the Acoustical Society of America, 106 (4): 1732-1743.

Chu, D., Wiebe, P. H., and Copley, N. J. 2000a. Inference of material properties of zooplankton from acoustic and resistivity measurements. ICES Journal of Marine Science, 57 (4): 1128-1142.

Chu, D., Wiebe, P. H., Stanton, T. K., Hammar, T. R., Doherty, K. W., Copley, N. J., Zhang, J., Reeder, D. B., and Benfield, M. C., 2000b. Measurements of the material properties of live marine organisms and their influences on the signatures of the acoustic scattering. Proceedings Oceans 2000 MTS/IEEE, International Symposium, Providence September 11-14, 3: 1963-1967.

Chu, D., and Wiebe, P. H. 2005. Measurements of sound-speed and density contrasts of zooplankton in Antarctic waters. ICES Journal of Marine Science, 62 (4): 818-831.

Falk-Petersen, S. 1981. Ecological investigations on the zooplankton community of Balsfjorden, Northern-Norway: Seasonal changes in body weight and the main biochemical composition of *Thysanoessa inermis* (Krøyer), *Thysanoessa raschii* (M.Sars) and *Meganyctiphanes norvegica* (M.Sars) in relation to environmental factors. Journal of Experimental Marine Biology and Ecology, 49: 103-120.

Dalen, J., and Kristensen, K-E. 1990. Comparative studies of theoretical and empirical target-strength models of euphausiids (krill) in relation to field-experiment data. Rapports et Proces-Verbaux des Réunions du Conseil International pour l'Exploration de la Mer, 189: 336-344.

Foote, K. G. 1990. Speed of sound in *Euphausia superba*. Journal of the Acoustical Society of America, 87 (4): 1405-1408.

Foote, K. G., Everson, I., Watkins, J. L., and Bone, D. G. 1990. Target strengths of Antarctic krill (*Euphausia superba*) at 38 and 120 kHz. Journal of the Acoustical Society of America, 87 (1): 16-24.

Greenlaw, C. F. 1977. Backscattering spectra of preserved zooplankton. Journal of the Acoustical Society of America, 62 (1): 44-52.

Greenlaw, C. F., and Johnson, R. K. 1982. Physical and acoustic properties of zooplankton. Journal of the Acoustical Society of America, 72 (6): 1706-1710.

Holliday, D. V., and Pieper, R. E. 1980. Volume scattering strengths and zooplankton distributions at acoustic frequencies between 0.5 and 3 MHz. Journal of the Acoustical Society of America, 67 (1): 135-146.

Kils, U. 1979. Preliminary data on volume, density and cross section area of Antarctic Krill, *Euphausia superba* - Results of the 2. Antarctic Expedition 1977/1978 of the Federal Republic of Germany. Meeresforschung, 27 (3): 207-209.

Kils, U. 1981. The swimming behaviour, swimming performance and energy balance of Antartic krill, *Euphasia superba*. BIOMASS Scientific Series, No.3, 122 pp

Knutsen, T., Melle, W., and Calise, L. 2001. Determining the mass density of marine copepods and their eggs with a critical focus on some of the previously used methods. Journal of Plankton Research, 23 (8): 859-873.

Kristensen, Å., and Dalen, J. 1986. Acoustic estimation of size distribution and abundance of zooplankton. Journal of the Acoustical Society of America, 80 (2): 601-611.

Køgeler, J. W., Falk-Petersen, S., Kristensen, Å., Pettersen, F., and Dalen, J. 1987. Density and Sound Speed Contrasts in Sub-Arctic Zooplankton. Polar Biology, 7 (4): 231-235.

Kulka, D. W., and Corey, S. 1982. Length and weight relationships of Euphausiids and caloric values of *Meganyctiphanes norvegica* (M. Sars) in the Bay of Fundy. Journal of Crustacean Biology, 2: 239-247.

Lawson, G. L., Wiebe, P. H., Ashjian, C. J., Chu, D., and Stanton, T.K. 2006. Improved parametrization of Antarctic krill target strength models. Journal of the Acoustical Society of America, 119 (1): 232-242.

Lowndes, A. G. 1942. The displacement method of weighing living aquatic organisms. Journal of the Marine Biological Association of the United Kingdom, 25 (3): 555-574.

Mauchline, J. 1967. Volume and weight characteristics of species of Euphausiacea. Crustaceana, 13: 241-248.

McClatchie, S. 1985. Feeding behaviour in *Meganyctiphanes norvegica* (M. Sars) (Crustacea: Euphausiacea). Journal of Experimental Marine Biology and Ecology, 86 (3): 271-284.

Medwin, H., and Clay, C. S. 1997. Fundamentals of Acoustical Oceanography. Academic Press, 712 pp.

Morris, D. J., Watkins, J. L., Ricketts, C., Buchholz, F., and Priddle, J. 1988. An assessment of the merits of length and weight measurements of Antarctic krill *Euphausia superba*. British Antarctic Survey Bulletin, 79: 27-50.

Mukai, T., Iida, K., Ando, Y., Mikami, H., Maki, Y., and Matsukura, R. 2004. Measurements of swimming angles, density, and sound speed of the krill euphausia pacifica for target strength estimation. Oceans '04, MTS/IEEE Techno-Ocean '04, 1: 383-388.

Raymont, J. E. G., Srinivasagam, R.T., and Raymont, J. K. B. 1969. Biochemical studies on marine zooplankton – IV.Investigations on *Meganyctiphanes norvegica* (M. Sars). Deep Sea Research and Oceanographic Abstracts, 16 (2): 141-156.

Saether, O, Ellingsen, T. E., and Mohr, V. 1986. Lipids of North Atlantic krill. Journal of Lipid Research, 27 (3): 274-285.

SC-CAMLR, 2005. Report of the 24th Meeting of the Scientific Committee, Hobart, Australia (SC-CAMLR-XXIV). Commission for the Conservation of Antarctic Marine Living Resources, pp 564-585.

Stanton, T. K., Wiebe, P. H., Chu, D., Benfield, M. C., Scanlon, L., Martin, L. V., and Eastwood, R. L. 1994. On acoustic estimates of zooplankton biomass. ICES Journal of Marine Science, 51 (4): 505-512.

Stanton, T. K., Chu, D., and Wiebe, P. H. 1998. Sound Scattering by Several Zooplankton Groups II: Scattering Models. Journal of the Acoustical Society of America, 103 (1): 236-253.

Stanton, T. K., and Chu, D. 2000. Review and recommendations for the modelling of acoustic scattering by fluid-like elongated zooplankton: euphausiids and copepods. ICES Journal of Marine Science, 57 (4): 793-807.

Thomasson, M. A., Johnson, M. L., Stromberg, J. O., and Gaten, E. 2003. Swimming capacity and pleopod beat rate as a function of sex, size and. moult stage in Northern krill *Meganyctiphanes norvegica*. Marine Ecology Progress Series, 250: 205-213.

Wiebe, P. H., Stanton, T. K., Benfield, M., Mountain, D., and Greene, C. 1997. High Frequency Acoustic Volume Backscattering in the Georges Bank Coastal Region and Its Interpretation Using Scattering Models. IEEE Journal of Ocean Engineering, 22 (3): 445-464.

Wyllie, M. R. J., Gregory, A. R., and Gardner, L. W. 1956. Elastic wave velocities in heterogeneous and porous media. Geophysics, 21 (1): 41-70.

Wyllie, M. R. J., Gregory, A. R., and Gardner, G. H. F. 1958. An experimental investigation of factors affecting elastic wave velocities in porous media. Geophysics, 23 (3): 459-493.

Yayanos**,** A. A., Benson, A. A., and Nevenzel, J. C. 1978. The pressure-volume-temperature (PVT) properties of a lipid mixture from a marine copepod, *Cananus plumchrus*: implications for buoyancy and sound scattering. Deep-Sea Research, 25 (3): 257–268.

FIGURES

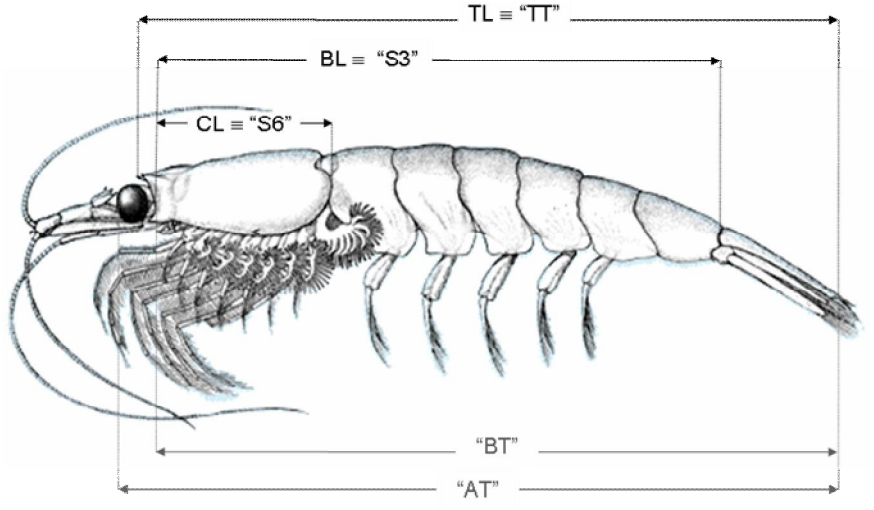

Figure 1. Length definitions and related codes (in quotation marks) after Morrison *et al.* (1988). In black colour the measurements performed on individual krill from the specific density measurements; in grey colour the measure cited in the rest of the text. On the specimens composing the sound speed samples only the measures "S3" and "S6" were performed.

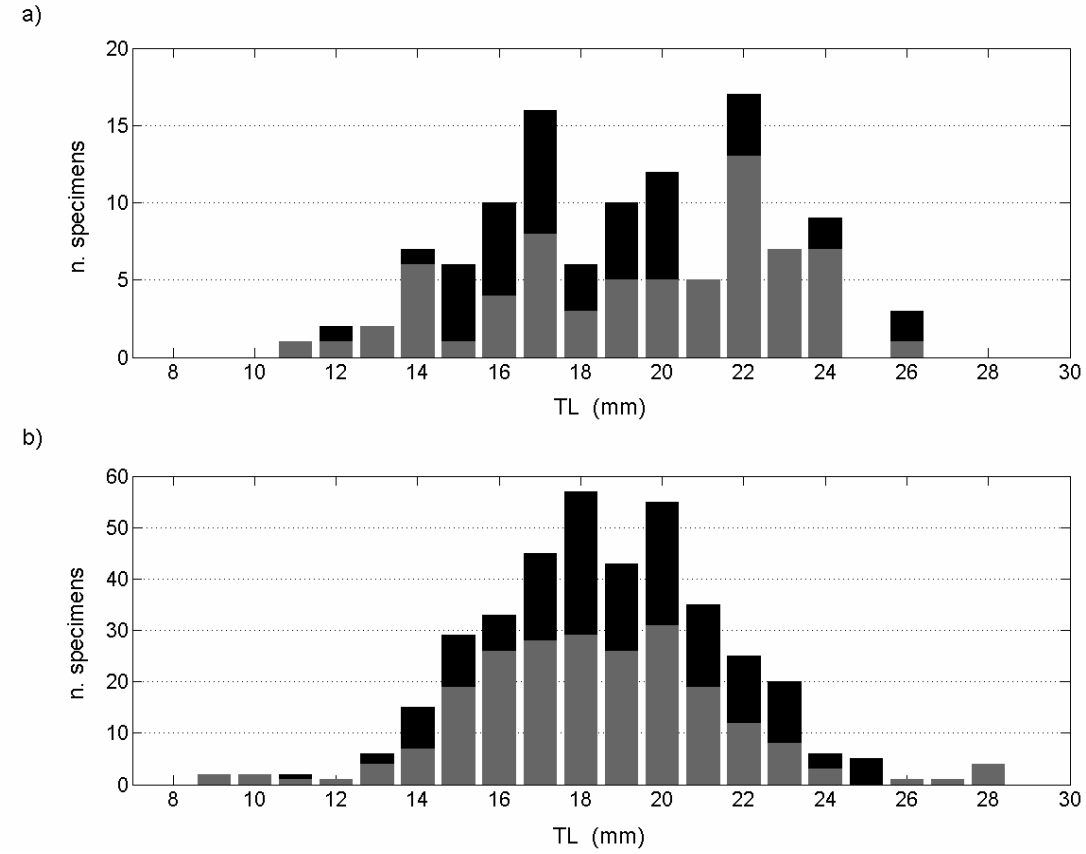

Figure 2. Total Length (TL) distribution of *Meganyctiphanes norvegica* specimens used for the measurements. a) The total sample (n=113) used in the specific density measurements. The partial distributions in grey and black bars refer to the animals caught on 17 (69 specimens) and 25 November (44 specimens) respectively. b) Half of the total sample from the sound speed measurements (n=387); the partial distribution in grey and black bars refers to the animals from the session performed on 25 and 26 November respectively.

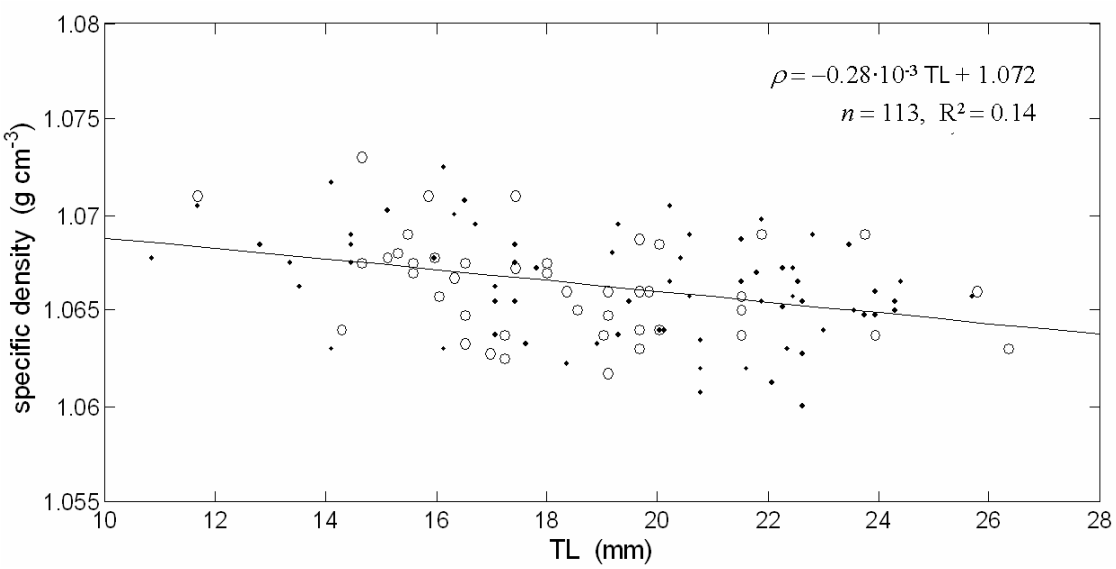

Figure 3. Specific density of *Meganyctiphanes norvegica* versus total length (TL), defined in the text and also shown in Figure 1, at 6.5 °C. The dots represent animals caught on 17 November, while open circles those caught on 25 November.

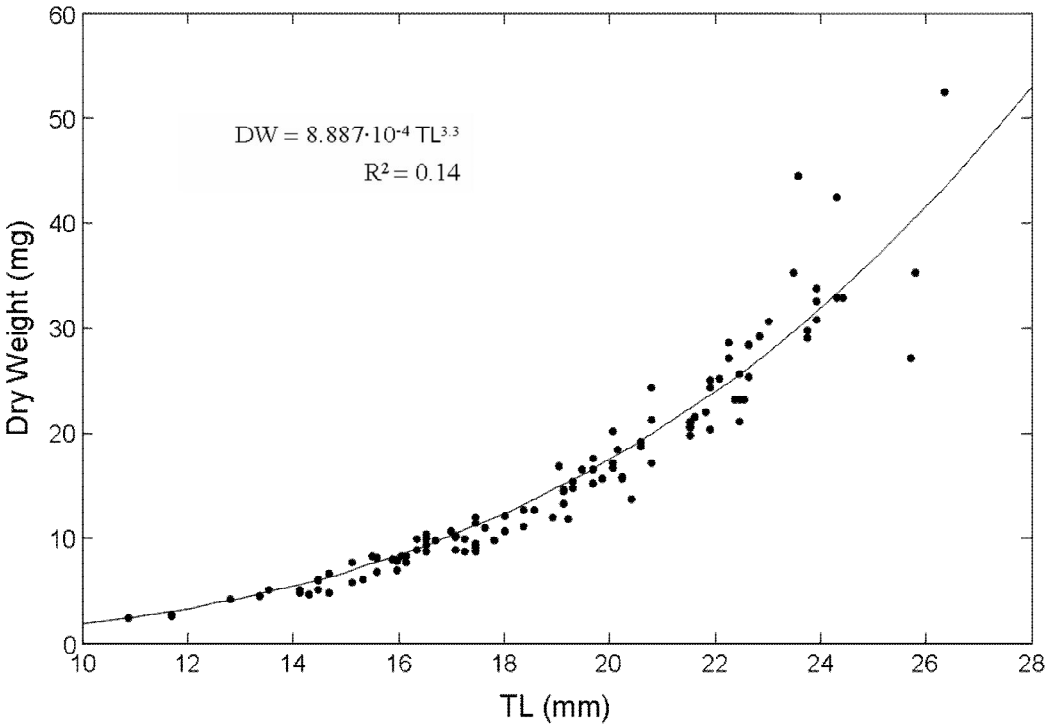

Figure 4. Dry weight versus total length TL (dots) and related power regression (solid line) of the 113 *Meganyctiphanes norvegica* specimens used for the specific density measurements.

TABLES

Table 1. Results from sound speed biological samples and measurements. The date is referred to November 1998. The biological results represent half of the samples. Mn: *Meganyctiphanes norvegica*; Ti: *Thysanoessa inermis*; Nc: *Nyctiphanes couchii*; *n* is the number of specimens identified; TL is the total length defined in Fig.1 and calculated by the Equation (4); n.cl. is the number of non-classified specimens in the sample; V_k is the volume fraction of krill in the horizontal part of the velocimeter; S the salinity; T range is the range of temperature referred to those during calibration series (calibr.) in determining the regression parameters used in Eq. (5) and to the measurements; T is the reference temperature determined by Eq. (5); c_k is the determined sound speed in krill; *h* are the results applying to each transmission Eq. (6).

Date	Species		TL (mm)					V_k	S	T range (°C)		T	c_k (m s^{-1})		*h*	
		n	min	max	mean	std	n.cl.	(%)	(psu)	calibr.	measures	(°C)	mean	std	mean	std
	Mn	224	8.6	31.6	18.2	3.2										
25	**Ti**	2	10.6	12.2	11.4	1.2	-	18.3	31.25	7.4 - 16.6	8.2 - 9.2	12.1	1545	3.7	1.0336	0.0025
	Nc	5	8.2	13.6	10.6	2.0										
	Mn	163	11.5	24.9	19.7	2.8										
26	**Ti**	8	10.5	17.2	12.7	2.1	10	16.6	31.18	7.5 - 17.6	8.4 - 10.1	10.3	1563	3.1	1.0429	0.0021
	Nc	10	7.6	10.9	9.4	1.2										

Paper II

Lucio Calise, Tor Knutsen and Webjørn Melle

Multifrequency Acoustic Measurements of free swimming northern krill (Meganyctiphanes norvegica) in a mesocosm venue: methodological challenges

Proceedings of the International Conference "Underwater Acoustic Measurements: Technologies & Results"
Heraklion, Crete, Greece, 28th June – 1st July 2005

MULTIFREQUENCY ACOUSTIC MEASUREMENTS OF FREE SWIMMING NORTHERN KRILL (*Meganyctiphanes norvegica*) IN A MESOCOSM VENUE: METHODOLOGICAL CHALLENGES

Lucio Calise[a], Tor Knutsen[b], Webjørn Melle[b]

[a] Department of Physics and Technology, University of Bergen, Allégaten 55, N-5007 Bergen, Norway
[b] Department of Marine Environment, Institute of Marine Research, Nordnesgaten 50, P.O. BOX 1870 Nordnes, N-85817 Bergen, Norway

Contact author: Lucio Calise, Department of Physics and Technology, University of Bergen, Allégaten 55, N-5007 Bergen, Norway. Fax number: +47 55589440; email: calise@ift.uib.no

Abstract: *The present work addresses some challenges of direct acoustic measurements of free-swimming krill describing a new set up for acquiring multi-frequency acoustic data in a large but finite volume of water under highly controlled conditions, a so called mesocosm. At Austevoll Aquaculture Research Station of the Institute of Marine Research in Bergen (Norway) a cylindrical enclosure (6 m diameter and 8 m deep) vertically suspended in the sea from a raft was established and a near mono-specific ensemble of living Meganyctiphanes norvegica was introduced. The effectiveness of the Simrad EK60 scientific echosounder pulsating at six frequencies: 38, 70, 120, 200, 364 and 710 kHz, with closely spaced transducers mounted on a floating rig are evaluated and results discussed. Procedures of a set of experimental exercises, including the response of krill to a manipulated artificial light regime and measurements on individual tethered animals are described. The implications for multifrequency acoustic data acquisition and analysis at short ranges are examined.*

Keywords: *Multifrequncy acoustics, Simrad EK60, Short Range, Meganyctiphanes norvegica*

1. INTRODUCTION

Krill comprises an important element of the pelagic food-web in the Polar oceans and adjacent regions. In particular, the northern krill (*Meganyctiphanes norvegica*) plays an important role in the Ecosystems of the Norwegian Sea, adjacent seas, as well as in Mediterranean Sea. Within the framework of an ecosystem approach to management, it is vital to develop techniques to improve the abundance assessment and *in situ* classification of these organisms. In this context the acoustic properties of krill at different frequencies is one key issue.

During the last ten years a large effort has been undertaken to improve zooplankton theoretical scattering models in general, but although many acoustics measurements on living individuals have been performed, both *in situ* and in experimental tanks, high quality experimental measurements on individual organisms and ensemble of animals are still needed. Previous measurements might be of variable quality because of the difficulties to discriminate multi-species and multi-target scattering *in situ* or due to significant constraints in animal behaviour in small experimental tanks or enclosures.

With the present new acoustic technologies, such as the new Simrad EK60 Scientific Echosounder, applying established procedures and techniques from aquaculture it is now possible to get accurate and direct measurements over a wide acoustic frequency range from free-swimming small organisms in a limited volume under highly monitored condition (mesocosms) [1]. In the present work a novel experimental set up for direct multi-frequency acoustic measurements of free-swimming krill is described. A large cylindrical enclosure, vertically suspended in the sea from a raft, was established at the Austevoll Aquaculture Research Station of the Institute of Marine Research in Bergen (Norway) in the period from 20th of January to 2nd of April 2004 and the acoustics performances of the new Simrad EK60 Multifrequency Scientific Echosounder were evaluated. After the introduction of a near mono-specific ensemble of living *Meganyctiphanes norvegica*, a set of experimental exercises, including the response of krill to a manipulated artificial light regime as well as measurements on individual tethered animals were performed. Further, results from EK60 system performances tests, data acquisition procedures and individual measurements are examined.

2. MATERIALS AND METHOD

2.1 Mesocosm set up and monitoring

The mesocosm was establish on an open raft located in a small bay close to the Station, at about 20 m distance from the shore and well protected from severe waves and currents. The depth around the raft was maximum 11 m depth during high tide period.

The mesocosm consisted of a cylindrical enclosure or “bag” of black coloured polyethylene sheeting (three-layer woven PEL with total thickness of 0.15 mm), tapered in the bottom region and suspended in the sea. The dimensions of the bag were: 6 m of diameter and 8 m deep, with a cylindrical upper part and conical lower part of 5 m and 3 m length respectively, giving a nominal volume of 170 m^3.

The material composing the bags was flexible and impermeable, and the black colour was chosen because the black wall gives to the organisms the illusion of being at large depth.

The bag was suspended in the sea vertically oriented, fastened with a rope to a circular stainless steel ring of 6 m diameter connected to the raft by steel cable and ropes. This means that the raft and bag constituted a single system floating on the sea surface. A footbridge was placed across the bag slightly off centre and allowed easy access to the measurement venue.

Because the distance between the ring and the sea surface was 0.2 m, the exact water volume inside the bag was 168 m^3. The complete mesocosm set up is schematised in Fig. 1.

In order to insure oxygenation and water circulation in the bag a hydraulic system was established, being operational during the entire experimental period Fig. 1. That system consisted of two separate parts. First, an incoming water part, supplying sand filtered deep sea water pumped from 165 m depth in the nearby fjord, an intermediary storage tank, a flow regulation system (basket and valve) and finally a tube tapered to the bottom of the bag with at the end a spreader positioned inside the mesocosm. In this way eventual air bubbles were removed. Secondly, an outgoing water part where the extra water was removed by gravity overflow using a vertically adjustable sieve with the terminal part being a tube penetrating the bag wall at approximately 0.3 m depth. It was found appropriate to keep an inflow rate of approximately 18 $l \cdot min^{-1}$ corresponding to a daily recycling of approx 15 % of the water volume.

The temperature and salinity of the mesocosm were monitored almost daily using a Gytre Mini CTD SD202. Then the sound speed in the mesocosm could be calculated and the value inserted in the EK60 environmental parameter menu prior to each recording sequence. During the measurement period it was found a slight increase in temperature and salinity, from 5.8 to 7.2 °C and from 34.8 to 35.2 psu respectively. This corresponds to a sound speed of approximately 1470 to 1480 $m \cdot s^{-1}$. The LICOR light meter system LI-1000 was used to monitor the light intensity during the measurements. Two light sensors were connected to the system: an underwater light sensor placed at 4 m depth inside the bag and an air light sensor on the footbridge (Light Sensor 1 and 2 in Fig.1). A SIMRAD sit Video Camera was also deployed when needed and video recorded on VHS tapes.

2.2 Acoustic System

The new SIMRAD EK60 Multifrequency Scientific Echosounder, using six General Purpose Transceivers: 38, 70, 120, 200, 364 and 710 kHz and corresponding transducers was used to acquire the acoustic data. All transducers were the new composite type, except for the 38 and 710 kHz, and all were nominally 7° split beam transducers, except for the 5° single beam at 710 kHz.

The transducers were mounted on a carefully fabricated aluminium plate (90 x 110 cm and 5 mm thick) as close to each other as space permitted (minimum packing distance) so that the physical transducer faces were aligned at the same distance from the aluminium plate. The split beam transducers were also aligned with identical heading. In order to give the rig float and reduce back radiation from the transducers, between the aluminium plate and the transducers a minimum of 5 cm thick divinycell plates were mounted and form-cut divinycell were also inserted to fill up empty space between the transducers. Moreover, an air filled polyethylene tube was also mounted underneath the rig to the side of the bigger and heavier 38 kHz transducer to give extra float.

The rig was placed neatly floating on the surface to the centre of the mesocosm and with small weights on top to balance the rig properly and allow a tiny layer of seawater to cover the top surface of the rig.

The system was calibrated prior to and following the termination of the experiment using the "standard target calibration sphere method" at different pulse duration and transmitting power [2].

2.3 Collection of data

Following the recommendation for multifrequency acoustic data collection [3], the data were acquired with identical pulse duration for all frequencies and with significantly reduced output power to the transducers in order to avoid non-linear effects (Table 1). Pulse duration of 0.256 ms was found to be appropriate for detecting targets having an abundance and size as found during the present experiment. The geometry of the beam matching volumes and the short-range performance of EK60 were checked, moving a line with two standard tungsten spheres of 38.1 mm (WC38) and 10 mm diameter inside the insonifed volume. The vertical distance between the spheres was 1.2 m. The contemporary detections at different frequencies allowed description of the geometry of the partly overlapping acoustic beams. Thereafter the line with the two spheres was positioned as close to the centre of the common insonified volume as possible, in order to examine the EK60 range detection performance. Data were retrieved from the Echo Trace Telegrams (ETD) involving the Single-Echo Detection (SED) algorithm. The aim of the SED algorithm is to isolate single targets using thresholding with respect to TS, echo length and phase angle deviation (split beam case), and then estimate the position of the accepted targets.

The experiments on single tethered animals were conducted by mounting a single living krill on a vertical 0.12 mm monofilament line with a calibration sphere attached to the end. To the main monofilament line the animal was connected using a 0.07 mm umbilical suture line approximately 15 cm long. Hence, the animal was allowed to swim freely which was also verified through video filming. In this way the animal could easily be put near beam axis and later be moved from one beam to another.

It is a well known fact that krill is attracted to artificial sources of light. This feature was used to force the krill to swim through to the beams placing two underwater lamps at opposite sides of the alongship transducer axis (Fore and Aft directions). The lamps were alternatively switched on and off each 3 minutes during recording. The tilt angle of krill during horizontal swimming has been shown to be close to the horizontal [4], hence TS data for such situations could possibly be retrieved with less uncertainty and with more confidence be compared to model computations.

3. RESULTS AND DISCUSSION

From the present work several challenges arise concerning acoustic measurements at short observation ranges. Table 2 shows the results of range detections for all frequencies when the line holding the two calibration spheres are in fixed position. It is clear that for the different frequencies the computation of distance to the target sphere varies significantly. This is due to the pulse transmission delay (PTD) error, caused by bandwidth limitation of the transmitting and receiving processes, that become serious in the TS measurements at short range, when the range to the scatterer must be determined accurately, and a correct

40Log TVG applied. Measuring several centimetres difference from one transducer to another can also seriously influence the way a defined target can be tracked through different beams in a multi-frequency target tracking analysis. In particular, the data show significant difference between the 38 kHz transducer and the others. This is most probably due to the higher Q value for a discrete piezo-ceramic element transducer compared to the new composite transducer technology. The PTD error is not corrected for in the EK60 at this stage and a thorough investigation of the pulse transmission delay for this system should be conducted.

In Table 3 data on target detection for a tethered krill of 27 mm total length are presented. By varying the TS threshold from –75 to –90 dB and keeping the other SED parameter values constant and identical to what is suggested by the Simrad manufacturer as default, the optimal TS threshold (dB) for different frequencies were derived. The TS threshold values given in Table 3 are the optimal values found in order to obtain the maximum number of detections. Again, the 38 kHz is the most critical system, showing a very low overall percentage detection. This is due to the high signal-to-noise ratio found at such a short range and could most probably be improved by implementing new approaches such as phase stability techniques [5].

Despite some important methodological problems the EK60 multi-frequency set up and mesocosm approach as presented in this work shows the possibility of carrying out direct acoustic measurements of small marine organisms like krill, with high spatial resolution. This is demonstrated through Fig. 2 showing that animals can be controlled and tracked through multiple beams allowing details of behaviour to be revealed and target strength determined for the same animal at different frequencies. This opens new possibilities to explore krill frequency response both in the volume backscattering coefficient (s_v) and TS domains. It is also promising with respect to develop more accurate algorithms for multi-frequency analysis of echosurvey data and classification or categorisation of scatterers in general.

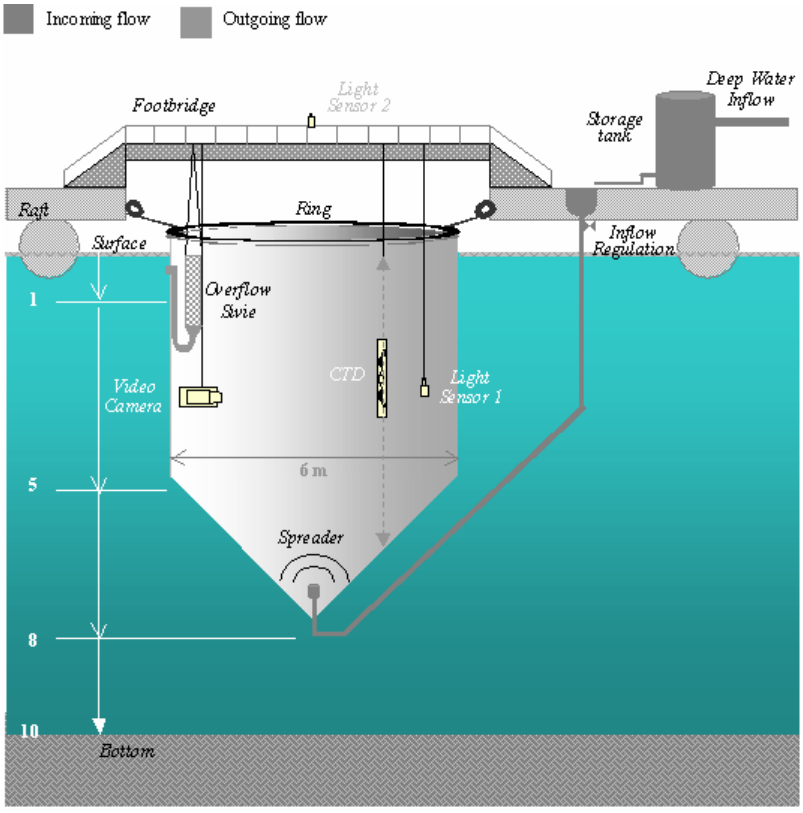

Fig.1: Mesocosm set up

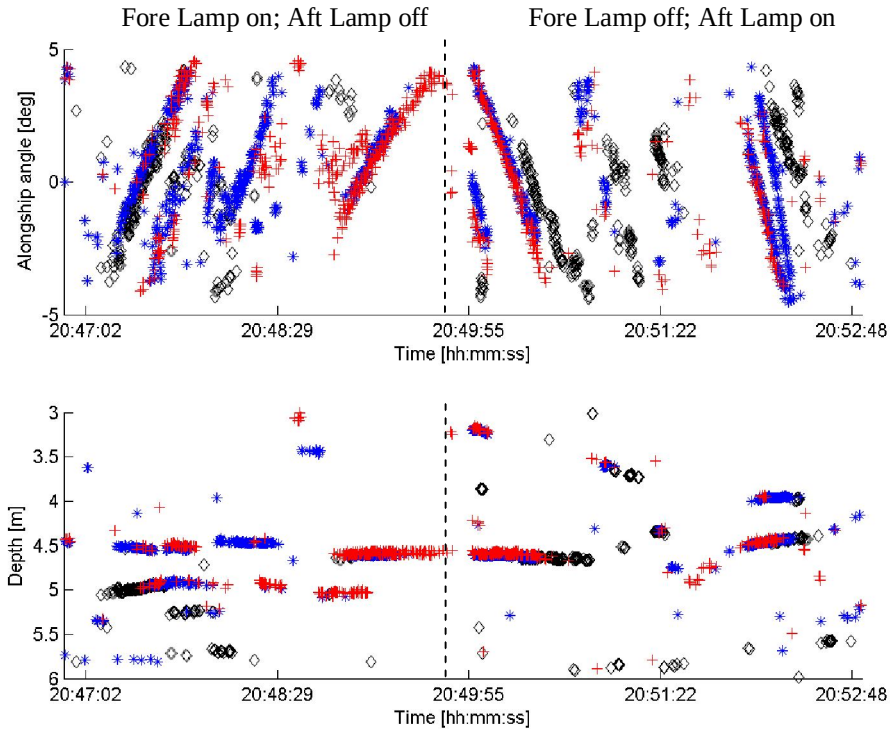

*Figure 2: Target detections during a two lamps exercise session for the frequencies 70 (black◊), 120 (blue *) and 200 (red+) kHz. Upper panel: Alongship angle versus Ping time. Lower panel: corresponding Depth measurement versus Ping time.*

System Frequency [kHz]	Transducer Type	Nominal Frequency [kHz]	Wave Length [m]	Near Field [m]	Transmitted Power [W]	Receiving Band Width [kHz]
38	ES38-B	38.095	0.0395	2.7	600	3.68
70	ES70-7C	70.175	0.0214	1.5	300	6.16
120	ES120-7C	121.212	0.0125	0.9	250	8.71
200	ES200-7CD	200	0.0075	0.5	120	10.64
364	ES400-7CD	363.6363	0.0041	0.3	40	11.84
710	710-30-EP	714.286	0.0002	<0.2	100	12.32

Table 1: Acoustic Systems: types and parameters set up. The Band width values are for the pulse duration of 0.256 msec.

Frequency [kHz]	38	70	120	200	364	710
DD_{WC38} [cm]	4.86	4.78	4.77	4.76	4.74	4.72
DD_{WC10} [cm]	6.02	5.93	5.92	5.90	5.89	5.87

Table 2: Depth Detection (DD) at different frequencies for the two standard calibration spheres used.

Frequency [kHz]	38	70	120	200	364
TS threshold [dB]	-85	-80	-80	-85	-80
No Pings	5531	5486	5501	5490	5498
No Detections	25	3143	2138	2025	1805
%	0.5	57.3	38.9	36.9	32.8

Table 3: Maximum detections found for a tethered krill of total length 27 mm krill and corresponding optimum TS threshold while the other SED parameters are kept constant identical to their default values.

4. ACKNOWLEDGEMENTS

The invaluable assistance of Arve Kristiansen (Aquaculture Research Station of the Institute of Marine Research) is particularly appreciated, helping out with all practical tasks during the experimental period. The Institute of Marine Research (IMR) is thanked for making the project possible through funding via the internal program on "New feed resources for the Aquaculture industry". Harald Fitje at IMR's mechanical workshop is thanked for making the transducer rig on short notice and for elegant mechanical solutions. Mr. Erik Stenersen, Mr. Are Johansen and dr. Frank Reier-Knudsen at Simrad AS (www.simrad.com) are kindly acknowledged for their skilled support through all phases of the experiments and for making available parts of the acoustic system.

REFERENCES

[1] **van der Meeren** T., **Jørstad** K.E., **Solemdal** P., **Kjesbu** O.S., Growth and survival of cod larvae (Gadus morhua L.): comparative enclosure studies of Northeast Arctic cod and coastal cod from western Norway. ICES mar. Sci. Symp., 198, 633-645, 1994.

[2] **Foote K.G., Vestnes H.P , McLennan G., Simmonds,** Calibration of acoustic instruments for fish density estimation: a pratical guide. *Cooperative Research Report, International Council for the Exploration of the Sea***, 144, 69 pp, 1987.**

[3] **Korneliussen** R. J., N. **Diner**, E. **Ona**, P. G. **Fernandes**, Recommendations for the collection of multi-frequency acoustic data. *ICES ASC,* Paper R36, 15 pp, 2004.**Kils** U., Swimming behaviour, Swimming Performance and Energy Balance of Antarctic Krill *Euphausia superba*, BIOMASS Scientific Series 3, 122 p, 1982.

[5] **Aksland** M., An alternative echo-integrating method, *ICES Journal of Marine Science, 62(2), 226-235, 2005.*

Paper III

Lucio Calise

Short range performances of a scientific echosounder with emphasis on accurate calibration

Short-range performances of a scientific echosounder with emphasis on accurate calibration

Lucio Calise

Abstract

Acoustics, signal theory and practical measurements with modern scientific split-beam echosounders indicate that limited hardware bandwidths and approximations in digital processing may bias the measurements, especially if made at short range from the transducer. Both measured target strength and its echo energy may be erroneous at these ranges. This is relevant for field calibrations and numerous applications *in situ* and *ex situ* when performed with targets at short range. If more rigorous solutions are hard or impractical to implement in the echosounder, post-correction of the recorded raw data may be a convenient alternative. The short-range performances of the 38, 120 and 200 kHz Simrad EK60 scientific echosounders are investigated and corrections for post-processing are proposed when necessary. The range and the target strength errors within the range from 2 to 10 meters were estimated for commonly used echosounder pulse durations by using standard calibration targets in a large laboratory tank. The errors were evaluated by comparing the actual range and the theoretical target strength with the respective measured numbers at the final output of the echosounder processing. The processing realization and the single echo detector implemented in the EK60 are described in detail and a method for reviewing and correcting the calibration results is proposed. Due to the procedure and parameters in EK60 calibration, the short-range errors affect only the single scatterer measurements, while the echo integration quantities remain stable. Measurement results indicate that the systems have extremely high range sensitivity. Range correction for the 38 kHz system is theoretically needed to reduce the potential bias in calibration exercises and the related TS measurements. For the 120 and for the 200 kHz systems, the accredited range delay leads to a theoretical TS error smaller than the claimed systematic error in standard calibration exercise starting from 4 m. On the contrary, some observed contradictions between theory and measurements were found: the range errors effects on the TS results were not clearly verified.

Keywords: Echosounder, EK60, calibration, short-range detection.

L. Calise: Department of Physics and Technology, University of Bergen, Allégaten 55, N-5007 Bergen, Norway, tel: +47 55582894; fax: +47 55589440.

Introduction

Acoustical techniques using scientific echosounders are routinely used for investigations of aquatic organisms. Echo integration and echo counting are the common methods for biomass assessment in oceans, lakes and rivers (Simmonds and MacLennan, 2005). The established methods are all based on the echo formation process, theoretically described by the well-known sonar equation (Urick, 1983) involving the transmitted pulse, the transmission loss through the medium, the acoustical scattering by the target and how the echo is sensed and measured by the receiver.

The operational treatment of the sonar equation in scientific echosounders requires that the formulation has to be independent from the input power level and observation point. This is achieved by introducing power gain and loss compensation to account for both directional properties and losses (MacLennan, 1990).

Gain and compensation are determined through standardised calibration and play a key role for the stability and predictability of the equipment performances, but also consequently on the accuracy of the assessment method adopted. Therefore, the prospective of estimating aquatic biomass using quantitative echosounders relies on high accuracy and precision in their calibration, as well as their stability between regular calibrations.

An echosounder system is now typically calibrated by using standard acoustic targets, as described in detail by Foote *et al.* (1987). Here the received echo energy from a standard target sphere is compared with the theoretical value to determine the system gains. The calibration is performed in single-target detection mode, i.e. point-target, where the two-way transmission loss (2TL), due to the attenuation effects: geometric spreading and absorption, is compensated by the range-dependent function $40 \log R + 2\alpha R$, with R being the range in meter to the target and α the absorption coefficient [dB/m] at the particular frequency used, and estimated for the prevailing environmental conditions at the calibration site. The range to the target R is indirectly estimated by $R = c t_e/2$, where c is the sound speed and t_e is the echo time, i.e. time lag between the pulse transmission and reception of the echo. Foote *et al.* (1987) evaluated the error in target range estimation for the calibration method to be 21 %, with a possible relevant reduction if the sound speed is well known.

In the realization of modern scientific echosounders, the echo analogue-digital conversion (A/D) takes place at the first step on the signal processing stage. Digital processing techniques are then utilized to implement the system amplification, compensation for transmission loss, and the echo pulse analysis as well as the target beam compensation in the case of split-beam systems.

The 2TL compensation for single-target detection, as well as for randomly distributed target, i.e. $20 \log R + 2\alpha R$, is digitally realized by its time-equivalent "time varied gain" function (TVG) applied as sample-by-sample basis compensation. This implies no restriction in dynamic range of that function as in analogue echosounders where the compensation was implemented in the hardware. In practice, the TVG functions specify how the receiver gain has to vary with time after the pulse transmission, leading the echo level to be independent from the target range.

When the standard spheres or the targets under investigation are at short distances from the transducer, two sources of uncertainty bias the transmission loss compensation in scientific echosounders (Simmonds and MacLennan, 2005): (1) determination of the echo time t_e, which leads to the so-called *receiver or system delay* t_{del}, due to the echo pulse deformation as consequence of the passages through hardware units of finite bandwidth; (2) the implementation of approximate (asymptotic) rather than exact receiver gain functions, leading to a TVG overcompensation.

Despite being critical for short-range detections, finite bandwidth hardware are obligatory choices for acoustic systems, while the implementation of TVG asymptotic formulations is generally justified with the consideration that usually long ranges are involved in echo-surveys procedures, and the deviations are minimized in the signal processing. In practice, when the pulse duration is much smaller than the detection time $t_e/2$, or equivalently in space when the pulse length is much smaller than R, the asymptotic TVG forms are assumed to provide an adequate compensation for most practical purposes. Nevertheless, this is not always satisfactory. In several acoustic applications, the targets investigated are at rather short ranges from the transducer. Fish pens, rivers, shallow waters, underwater vehicles (ROVs, AUVs, towed bodies), acoustic probes, tanks and enclosure measurements, are example of applications where the errors at short range should not be ignored.

Moreover, it often happens that, due to logistic or physical conditions, the operators are obliged to calibrate their systems in shallow water locations or with the standard sphere suspended not far from the transducer. In these cases, the on axis sensitivity calibration is also not accurate (Foote *et al*., 1987; Sawada and Furusawa, 1993) as well the related values of echo-integration quantities (Fernandes and Simmonds, 1996).

Both the delay t_{del} and the TVG overcompensation effects strictly depend on the echosounder hardware solution and the algorithm realizations. Therefore, general correction methods are not practical as they have to be developed for each specific system. Investigators have suggested different approaches based on processing or empirical equation to quantify and correct the errors for their own system and purposes. Solutions for the earlier popular scientific echosounders are available in some literature (MacLennan, 1986; Sawada and Furusawa, 1993; Ona *et al.*, 1996; Fernandes and Simmons, 1996; Furusawa *et al.*, 1999; Moszynski and Stepnowski, 2002; Korneliussen *et al.*, 2004; 2008).

As a general conclusion, all the authors warn that corrections of the performance of the system being used at short-range calibration and measurements are necessary.

Despite the warning, solutions to the outlined problems have not always been taken into consideration by the echosounder manufacturers, in particular at early stages of commercialization.

The last generation of Simrad echosounders, the EK60, already widely used by the scientific community, does not currently account for the errors at short ranges.

The aim of this work was to investigate the EK60 systems performances at short ranges and derive numerical correction to improve the accuracy in calibration and measurements when performed with targets at short distance.

Theoretical Review

The formulation for the indirect determination of the range to the target ($R = c t_e/2$), obviously indicates that it may be biased from wrong estimations of c and t_e. Wrong values of c are an overall source of error for long-range applications (MacLennan, 1990). At short-range operations, averaging c over the depth channel of interest may be a satisfactory procedure to minimize the error, so that the primary source of error for the precise target range determination is t_e (Simmonds and MacLennan, 2005).

Apart from the intrinsic noise, which may obscure the earliest arrival of the echo pulse, the determination of t_e is compromised by a technological problem due to the impedance in the transducer and the analogue part of the echosounder prior to the A/D conversion. An

echosounder transmits sound bursts of duration τ, called pulses or pings, consisting of several cycles at the operating frequency f_0 and assuring a rather flat top. The generated signal passes through the transmitter electronic filter, then to the transducer, before being transmitted to the medium. Both transmitter and transducer act as a band pass filter so that the effective waveform of the transmitted signal is slightly reduced in sharpness on its leading edge. When the propagating pulse encounters an object, part of its energy is scattered and the transducer receives the backscattered pulse. The latter is stretched out in time, with approximately the same shape as the incident signal, reduced in power by the transmission loss and altered in levels according to the target scattering properties. In the receiving process, the echo signal again passes through the transducer and the receiver, so that the shape is once more altered in sharpness.

Because of the progressive deformation of the pulse shape, the echo pulse start time, which allows in determining t_e and the target range, will be not obviously determined. In some extreme case the pulse does not even reach his maximum value and may have a peaked top (Furusawa, 1991).

The echo waveform being analysed depends on the combined effects of the target scattering properties, the system bandwidth and the transmitter pulse duration. In order to illustrate the relative significance of the last two parameters, the normalized echo pulse envelope (V) can be modelled simulating the response in step time (t) of a resonant receiving system with bandwidth B to a sinusoidal signal with rectangular envelope of duration τ (MacLennan, 1986; Sawada and Furusawa, 1993):

$$V(t) = \frac{1-e^{-\pi \mathrm{B}t}}{1-e^{-\pi \mathrm{B}\tau}} \left[\mathrm{U}(t) - \mathrm{U}(t-\tau)\right] + e^{-\pi \mathrm{B}(t-\tau)}\, \mathrm{U}(t-\tau) \qquad (1)$$

where U(t) is the unit step function, and the first term denominator is introduced for the peak normalization.

Echo pulse waveforms for different $\mathrm{B}\tau$ combinations obtained by Equation (1) are plotted in Figure 1. The input model values are chosen on the base of the actual $\mathrm{B}\tau$ combinations operating in the Simrad EK60 scientific echosounders.

In Figure 1a, the modelled echo envelopes for the 38, 120 and 200 kHz of EK60 at the same pulse duration but different bandwidths are plotted. Clearly, narrower bandwidth system deforms the echo pulse much more than a wider bandwidth, increasing the uncertainty in determining t_e.

On the other hand, the Figure 1b shows three $\mathrm{B}\tau$ combinations of the 38 kHz EK60 system with almost similar bandwidth but different pulse durations. The result is that longer pulse duration implies longer rising time, defined as the time employed to reach the peak. This is the temporal window wherein the echosounder has to assign the echo start time. Longer rising time, i.e. longer pulse duration, increases the uncertainty in the assignation of t_e.

The pulse deformation process may also introduce another bias, involving directly the 2TL compensation implemented in signal processing and the target strength and echo energy estimations.

The two-way transmission loss compensation can be theoretically realized in digital echosounders applying an equivalent time-dependent amplitude gain $a(t)$ to the samples, with t the time after the start of the transmitted pulse. Since the sample levels representing the echo pulse are regulated by the frequency response of the echosounder and target scattering properties, the equivalence between the range- and the time-compensation is not

straightforward. The time varied gain on the sample levels has to take in account of the echo pulse features.

In the case of single target detection, the exact formulation of $a(t)$ is in the form (MacLennan, 1986):

$$a(t) = (ct)^2 \exp\left(\beta \frac{ct}{2}\right) \sqrt{1 + \sum_{i=1}^{4} k_i \left(\frac{\tau}{t}\right)^i} \tag{2}$$

where c is the sound speed in meters per second, β the acoustic absorption coefficient expressed in nepers per meter, τ is the pulse duration in seconds, and k_i are coefficients calculated by moments of the echo waveform normalized to the pulse duration:

$$\begin{aligned} k_1 &= -4I_1 , & k_2 &= -6I_2 + 12{I_1}^2 , \\ k_3 &= -4I_3 + 24I_1I_2 - 24{I_1}^3 , & k_4 &= -I_4 + 8I_1I_3 + 6{I_2}^2 - 36{I_1}^2I_2 + 24{I_1}^4 \end{aligned} \tag{3}$$

where the signal moments I_m are defined as:

$$I_m = \frac{\int_{-\infty}^{\infty} t^m e^{\beta ct} |V(t)|^2 \, dt}{\tau^m \int_{-\infty}^{\infty} e^{\beta ct} |V(t)|^2 \, dt} \qquad m = 1,2,3,4 . \tag{4}$$

wherein the combined effects of B, τ and the target scattering on the echo waveform are taken into account.

Equations (4) reveal that the very knowledge of the system properties is not sufficient to determine the coefficients k_i. They are not unique but vary with the scattering properties of the target and its frequency dependence. Thus, it is not possible to realize a general formulation of Eq. (2) that provides the exact range-compensation in processing operations of echosounders. Moreover, at very short ranges the factor under the square root in Eq. (2) may be negative and $a(t)$ is then undetermined (MacLennan, 1986).

In software realizations for scientific echosounders these inconveniences are overcome by adopting an asymptotic form $a_0(t)$ of Equation (2), commonly called '$40 \log R$' TVG function, which ignores the square root terms, i.e. echo waveform features, and is improperly assumed to be equivalent in time to the 2TL. The equivalence is obtained in practice by substituting $R = ct/2$, as an approximation to the target range, and calculating $20 \log(a_0(t))$ to express the TVG in decibel (MacLennan, 1990; Simmonds and MacLennan, 2005).

In the case of multiple randomly distributed targets, the related '$20 \log R$' TVG function is given by $a_0(t) = ct \exp(\beta\, ct/2)$, ignoring again the square root term in the exact gain function for the case. This is obtained by the sum of the unity plus two time coefficients $k_1 = -2I_1$ and $k_2 = -I_2 + 2{I_1}^2$ with the moments $I_{1,2}$ defined in Equation (4), and can be conveniently rewritten by two time parameters to show more properly the dependence of the exact TVG from the transmitter pulse duration and the echo waveform (MacLennan, 1986):

$$T_1 = \tau I_1 , \qquad T_2 = \tau (I_2 - {I_1}^2) \tag{5}$$

The range-to-time equivalence for the $20 \log R$ function is obtained as for the single target case. It must be emphasized that, since the TVG functions assume a two-way process, the substitution $R = ct/2$ has to be implicitly assumed in the time-to-range conversion.

In theory, the asymptotic formulations compensate the echo level precisely only in the ideal limit of zero pulse duration or at infinite range and infinite bandwidth. Since the square roots of the exact formulations are ignored, the asymptotic TVG functions will produce overcompensation depending on the rate of change in gain, which is range-dependent. For detection at time much smaller than τ, i.e. at short ranges, much higher gain is applied to the digital samples and consequently higher overcompensation with significant bias in target strength estimation.

This is clear in Figure 2, which shows the two-way transmission loss compensation in the range from 0 to 10 m due to the application of exact TVG functions and their asymptotic forms for the 38 kHz Simrad EK60 system at 1.024 ms pulse duration and 2.43 kHz bandwidth. In this example, the exact TVG functions were calculated using Equations (2)-(5) on the envelope of a backscattered analogue signal from a standard 60-mm-diameter copper sphere (Cu60) with centre placed at 3 m from the transducer, see Figure 3. The signal was recorded prior to the amplification stage by a Lecroy 9361 oscilloscope (bandwidth 300 MHz and typical error 5 % or 0.17 dB) with sampling frequency 10 MHz. The moments calculated by Equation (4) result equal to $I_1 = 0.680$, $I_2 = 0.524$, $I_3 = 0.439$, $I_4 = 0.389$. Since the received echo represents a large target located just after the nominal near field of the transducer (Table 1), the set-up represents an extreme case were the deviation from the exact functions are expected to be very large.

It is clear that the TVG overcompensation may be relevant when short-range measurements require high accuracy, as in calibration exercise. On the contrary, it must be noted that at very short range, the application of the asymptotic functions is less conditioned by the system delay error only. Due to the rate of change in gain for an equal t_{del}, i.e. range delay, the error applying the exact compensation will be higher than the one obtained with the asymptotic compensation (Fig. 2).

Echosounders Design and Realizations

In addition to the pulse deformation, the digitalization of the echo signal and the processing of the samples adopted in the receiver software may increase the uncertainty in range determination, as well as target strength and echo energy estimations. These digital solutions are characteristic of the specific echosounder design.

While the theory may help to the general understanding of the problems and suggest better practical realizations, the final errors have to be verified empirically since they are dependent on the specific echosounder. In the past, manufacturers and researchers have implemented and suggested different approaches, based on analytical or empirical equations, to quantify and correct the biases in their operating acoustic system and measurements.

In general, all the results indicated that both the system delay and the TVG overcompensation depend on B and τ in the same way, i.e. increasing with pulse duration and with narrow bandwidth, so that they operate in the same direction.

Foote *et al.* (1987) proposed a procedure for the evaluation of the echo time t_e, which was adopted in the past by Simrad AS in their echosounder processing operations. By determining the point on the leading edge at which the amplitude has risen to half the peak

value, the time from the start of the transmitted pulse to this timed point was considered as the echo time. The procedure is analytically convenient but not always sufficiently accurate to ignore the delay error due to the pulse deformation (Ona *et al.*, 1996; Fernandes and Simmons 1996).

In Figure 3, the recorded 38 kHz Simrad EK60 normalized analogue signal, described before, and its envelope are plotted. The modelled pulse using Equation (1) is also superimposed to illustrate the deviation of the model from the actual echo pulse. Since the model does not consider the hardware filtering of the transmitter the resulting echo shape is less reduced in sharpness and rises fast on its leading edge.

The decaying part of the pulse reflects the interference between different vibration modes in the sphere. These deviate somewhat in frequency, and the interference causes oscillation at a different frequency. By analysing the discrete derivates of the envelope, the peak and the starting time of the actual signal were found, and the point at which the amplitude has risen to half the peak determined (Fig. 3). The rising time was then estimated to be 0.82 ms, which corresponds to a range delay of 121 cm (medium sound speed $c = 1482.3\ \mathrm{m\,s^{-1}}$), while the half amplitude timed point was at 0.18 ms after the pulse start time, corresponding to a range delay of 27 cm. Note that the peak and the starting time values depend on the envelope detector algorithm used. Thus, they should not be taken as absolute values, but rather suitable for relative analysis only. In the present case, the envelope was obtained by a Hilbert transform on the raw data, with subsequent digital low-pass filter based on a Hamming window.

This means that t_e will still appear longer (receiver delay), leading to an overestimation of the target range, hence in a transmission loss overcompensation. For the specific case in Figure 3, the overcompensation is 1.8 dB if the exact TVG function is applied, and 1.5 dB in the asymptotic case.

More precise procedures for target range estimation are still wanted. If the delay t_{del} is well known, it could be taken into account in some manner, for example by subtracting it to the range formulation (MacLennan, 1982; Foote *et al.*, 1987; Fernandes and Simmons, 1996; Simmonds and MacLennan, 2005).

Echo formation theory and knowledge of the system electronics may help to determine the delay t_{del}, but unfortunately the calculations are not simple (Foote *et al.*, 1987). Accurate measurements of the echo energy returned from standard spheres and integrated over the entire echo pulse has been preferred. By using an oscilloscope and a counter timer, Foote *et al.* (1987) reported values of t_e and t_{del} for a specific Simrad echosounder at different $B\tau$ combinations. The results confirmed that the t_{del} tends to increase with increasing pulse duration and is larger at narrow bandwidths. As a general recommendation, the authors suggested to place the spheres at depth not shorter than 15 m to minimize the errors during the standard field calibration procedure.

For the general case of multiple randomly distributed targets, MacLennan (1986) proposed an analytical approximation of the exact TVG function at a given range R_0, obtained by introducing a delay at the start time in the asymptotic form, whose value is calculated by comparison with the exact formulation. This delay, commonly called "TVG start time delay" t_0, is expressed by $t_0 = T_1 + 2R_0/c - [(2R_0/c)^2 - T_2^2]^{1/2}$ with T_1 and T_2 defined by Equation (5). The delay is at least half of the pulse duration and can be applied without a substantial modification of the processing subtracting it to the time term of the first factor in the '$20 \log R$' TVG formulation.

Despite t_0 still depends from the scattering properties of the target, as well as from B and τ, this knowledge can be used for partial corrections of the '$20 \log R$' TVG in software

realizations, for example by introducing the value obtained for the ideal case of rectangular echo pulse long τ and wideband receiver, or during calibration, if the range of the standard target is precisely known (Fernandes and Simmons, 1996). For the specific case in Figures 2 and 3, the t_0 is equal to 0.7 ms (69 % of τ) with excellent agreement between the exact and the approximated TVG starting from 1.5 m.

Sawada and Furusawa (1993) confirmed empirically the theoretical '20 log R' TVG overcompensation. They suggested the use of a more restricted formulation of the integrator output, i.e. the volume backscattering strength S_V, in the calibration procedure, which takes into account the receiving system bandwidth and the TVG overcompensation on the sphere echo shape. Again, the strict formulation is difficult to employ because precise properties of the system and actual echo waveform are required.

Fernandes and Simmons (1996) quantified the underestimation in absolute biomass derived from the '20 log R' TVG overcompensation up to 11 %, if the reference system, the 38 kHz Simrad EK500 (software vers. 5.2) at 1 ms pulse duration and 3.8 kHz bandwidth, was on-axis calibrated (Reynisson, 1999) with the sphere placed at 10 m and the depth sampled channel 100 m. When the error due to the receiver delay was also considered, the total underestimation increased up to 14 %. The authors provided a practical method to correct the delays consistent with the on-axis calibration procedure for the Simrad EK500 system. The receiver delay was first approximated by an oscilloscope through the evaluation of the -6 dB point amplitude and then introduced in calculation to determinate the entire delay. Comparison between asymptotic and corrected TVG functions showed a bias at ranges less then 20 m.

Ona *et al.* (1996) also investigated the origins of short-range dependency effects on calibration of the 18, 38 and 120 kHz Simrad EK500 system version 5.2, and determined the range delay for the different Bτ combinations settable by the systems. In addition, they observed higher variability in the measurements when comparing results from the standard operating software and a special version with an enhanced digitising resolution, indicating further increase of bias due to the loss of pulse information between samples. Finite target size versus angular resolution effect was also recognised as potential bias in target-strength (TS) measurements.

The EK500 system was partly corrected for the electronic delay and the TVG overcompensations starting from software version 5.3 in 1997 (Simrad, 1996). The corrections was made including in the single echo detector algorithm a small peak amplitude gain, and for the volume backscattering algorithm an analysis of effective pulse length rather than the transmitted pulse. The '20 log R' TVG compensation was delayed on a compromise for all the Bτ system combinations by three times the sample interval plus half of pulse duration. However, this choice is not proper at short range for all the settings (Korneliussen *et al.*, 2008).

Moszynski and Stepnowski (2002) proposed a '40 log R' TVG algorithm correction based on the moments (Equations 3 and 4) of the sampled echo wave and applied before the TVG activation. Since this process requires a target detection algorithm before the TVG compensation, it has high computational costs that are not suitable for the echosounder realizations. However, it was used to explore the sources of the echo levels errors due to the delays. Experimental results obtained from a standard sphere and a 200 kHz Biosonics DT echosounder with 5 kHz bandwidth and at different pulse durations showed that the error monotonically decreased with the distance and the TVG time delay was 70 % of the pulse duration instead of the theoretical "MacLennan value" of 50 %. The authors concluded that

the asymptotic time varied functions applied in the referenced echosounder were improper for ranges shorter than 10 m.

Furusawa *et al.* (1999) claimed that it may be a better practice to design echosounders that use intensity based TS measures rather than energy based. In this way, since the measure of the single amplitude at almost flat maximum part of the echo pulse is not needed, the processing becomes independent from the target scattering properties. Although fascinating, the solution restricts the number of suitable $B\tau$ combinations because those that give insufficient amplitude have to be avoided (Furusawa, 1991).

It is clear that the combination of receiver bandwidth and pulse duration is fundamental in designing scientific echosounders with good performances at short range. A large number of selectable pulse durations and bandwidths are desirable to assure a good accuracy for a wide range of purposes. But effective costs of realization and marketing induce the manufactures to limit the option. Moreover, to obtain correct delay for all the settings is not an easy task. Combining short pulse width and narrow bandwidth helps to detect weak echoes but increases the discrepancy of waveform from the rectangular shape and reduces the echo level, hence increase the uncertainty. This is more critical for single target detection operation, especially with low signal-to-noise ratio (SNR). The SNR could be maximized by matching the receiver bandwidth to the transmitter pulse duration but features of the echo pulse shape and/or signal phase, more relevant for single detection applications, are then not preserved (Simmonds and MacLennan, 2005). Echosounder realizations for these specific purposes, has to ensure short pulse duration, i.e. wider spectrum, with related bandwidth not too large but still enough to pass most of the energy in the pulse. With these options, short-range resolution, high cavitation threshold and therefore high SNR will be assured.

Furusawa (1991) suggested a practical method involving graphical consideration on operative frequency, pulse duration and bandwidth to determine the accuracy for different $B\tau$ combinations. The results showed that there is not an optimum combination, but, when the specific purpose is clear the determination of the combined values is more clearly defined. As a general rule, in order to avoid significant loss of echo energy, Simmonds and MacLennan (2005) suggested to design echosounder with $B\tau$ combination equal to 3, or to 1 when the echo detection is limited by broadband noise.

Materials and Methods

The scientific echosounder under investigation was the multifrequency system Simrad EK60 (Andersen, 2001). The basic parts of the system are the General Purpose Transceivers (GPT) where the signal processing is performed independently at each frequency. The set-up, the acquisition and the storing of data are PC controlled via Ethernet connection by means of the ER60 software. Currently, a maximum of seven GPTs can be operating simultaneously with the ER60. The pulse duration is selected for each frequency and combined with fixed receiver bandwidth, which is never more than the 10 % of the central frequency. The EK60 is a split-beam echosounder, where the position of the target in the beam is measured by comparing the received echo on paired quadrants by quadrature sampling. The electrical angular resolution (Reynisson, 1999) is given in electrical phase steps of 180/128 degrees per unit (Simrad, 2003).

In receiving mode the EK60 works by a ping-to-ping process. The sound speed c in meters per seconds and pulse duration τ in seconds are the input parameters of the process. Together

they define the received resolution length ($=c\tau/2$) in meters (Simmonds and MacLennan, 2005). For each of the four split beam transducer quadrants the analogue signal generated on the terminals is digitally converted with sampling frequency of 500 kHz (L. N. Andersen, Simrad AS, pers. comm.). These digital samples are band-pass filtered with both sine and cosine variants in order to construct complex samples from each quadrant. The complex samples are then merged by decimation to ¼ pulse duration. This last operation defines the processing resolution parameters: the sampling time $\Delta t=\tau/4$ and the sampling distance $\Delta r=c\Delta t/2$.

For each sampled time, the power p, in logarithmic based integer, and the split-beam electric phase angles θ and ϕ (Foote *et al.*, 1986) are evaluated on the base of the corresponding decimated quadrant samples. Finally, a set of i samples $S_i(p,\theta,\phi)$ representing the echo ping is realized and can be collected in a storable EK60 raw data file which is readable by the post-processing software. Denoting with R_{max} the operator pre-set maximum detection range, a number of $i=R_{max}/\Delta r$ samples per echo signal will be recorded in the raw data file. The post-processing software is then demanded to analyse the raw data file applying the TVG functions, run the single echo detector (SED) algorithm as well as to apply the beam compensation.

For the present work, the analysis of the raw data was performed using the Simrad ER60 software (vers. 2.1.1), which is part of the entire EK60 system. Since there is a lack of information on the ER60 processing operations, both in the manual and in official literature, helpful details on echotrace extraction and calibration parameters are presented in Appendix. As defined in the Simrad EK60 user manual (Simrad, 2003), the term “echotrace” will be referred to a single echo detection rather than many successive detections of the same target as usually recognized.

The “centre of gravity principle” in ER60 target range determination described in Appendix is a new feature among echotrace extraction methods. The main purpose of the method is to use the most information of the sampled echo pulse. It is an alternative to the previous -6dB peak amplitude echo start method, producing uncertainties at short range as shown by Fernandes and Simmonds (1996) and Ona *et al.* (1996), and discussed in the previous section (Figure 3).

Tank measurements

Performances of the EK60 system in the range of 2-10 metres were examined in a freshwater controlled tank 6×6×15 m^3 (width by depth by length) at Simrad AS in Horten, Norway, during the period 1-3 April 2005.

The water temperature was kept at 20 °C, yielding a sound speed of c=1482.3 $m\,s^{-1}$. The water was stirred and filtered daily to minimize temperature gradients and eventual particle contents, assuring constant sound speed in homogeneous water.

A motorized positioning system, electronically controlled by a PC, assured an independent measure of the target distance from the acoustically active transducer surfaces with an accuracy of 1 mm. The positioning system consisted of an orthogonally crossing bridge, motorized in both the horizontal plane directions and moving with a speed of 3 or 10 cm s^{-1}.

Three echosounder systems operating at the frequency of 38, 120 and 200 kHz with standard Simrad split-beam transducers (Table 1) were examined. These are the systems commonly in use in fisheries acoustic applications.

All the transducers are with nominal 7° half power beam width. They were fixed one at a time on the short side of the tank to a motorized frame and set to a horizontally directed

beam with the axis at the depth of 3 meters. Nominal efficiency and angular sensitivity (Reynisson, 1999) in both alongship and athwartship planes were 70 % and 21.9 for the 38 kHz transducer and 75 % and 23.0 for the 120 and 200 kHz transducers. The ratio between the electrical phase step and the transducer angle sensitivity defines the angular resolution (Demer *et al.*, 1999), being equal to 0.064° for 38 kHz system and 0.061° for the others.

Acoustic backscattering data from the 60-mm-diameter copper sphere (Cu60) at 38 kHz and from the 38.1-mm-diameter tungsten carbide (6 % cobalt binder) sphere (WC38) for the 120 and 200 kHz systems were recorded. Two pulse durations, nominally equivalent to 1.024 and 0.256 ms, were tested for all the frequencies. Additional measurements using pulse durations of 2.048 and 0.512 ms at 38 kHz were also performed. Principal technical specifications of the electronics, transducer types and processing parameters of the systems are listed in Table 1, together with the theoretical TS of the spheres for the actual sound speed (MacLennan, 1981).

The spheres were suspended from the bridge by a 0.4 mm diameter monofilament nylon line and centred on the beam axis by checking the single target detections in the numerical window of the ER60 software. For each system setting, EK60 raw data of more then 100 detections with spheres positioned in step of 0.5 m starting from 10 to 2 m from the transducer were recorded. Only for the pulse duration of 0.256 ms at 200 kHz the distance step was 1 m.

In order to avoid potential non-linear effects (Tichy *et al.*, 2003; Pedersen, 2007; Korneliussen *et al.*, 2008), transmitting powers were set to 600, 100 and 90 W for the 38, 120 and 200 kHz systems respectively. The ping rate of 1 per second was set to minimize interference due to multipath echoes returning from the tank walls, the bottom and the water surface.

Before each session the on-axis gain was evaluated and inserted manually in the transducer parameter section of the ER60 software. The gain G was determined comparing the detected TS_{obs} and the theoretical TS_{th} of the spheres being placed on the beam axis at the maximum measurement distance of 10 m. It was calculated by using the relationship $G = G_{old} + (TS_{obs} - TS_{th})/2$.

After the acquisition, the raw data files were replayed by means of the ER60. The first six echotrace parameters (see Appendix), delivered from the split-beam target detector (SED), were broadcasted directly from the processor of the EK60 and transferred via Ethernet to a binary file, named by Simrad “echo trace datagram” (.dg), for further analysis.

For each distance d, the range error was calculated comparing the mean range to the echotraces ($\overline{r_t}$) and the actually, physically measured, distance R_d:

$$Err_d = \left(\overline{r_t}\right)_d - R_d \tag{6}$$

While the ER60 echotrace range is based on the time difference between the echo start and the ping transmission, the range given by the positioning system used the centre of the sphere as reference. Therefore, in order to compare the two distances, the read-out positioning system distances were corrected before introduced in Equation 6 by subtracting the radius of the sphere in use, and adding the value of 6 mm (Figure 4) to include the thickness of the transducer front layer, i.e. the plastic material covering the acoustically active transducer surface (A. Johansen, Simrad AS, pers. comm.)

Data quality analysis

Even if a controlled tank assures high SNR during the measurements, reverberation, side lobe reflections and possible ringing of the target become crucial for the accuracy. In particular, for the EK60 system the biases on the estimated centre of gravity may highly affect the quality of the data.

Figure 5 shows four examples of digital representation of the echo pulse as recorded in the EK60 raw file. The linear amplitudes [V] of the raw samples from 100 repeated echoes are superimposed. The black dots indicate the samples involved in the gravity principle (Eq. A2). Due to the decimation to ¼ pulse duration, five gravity samples are recognized; among these the central sample is related to the peak of the uncompensated TS array. In panel a) the values of the last two gravity samples are affected by bias probably due to the interference coming from the tank walls and the surface, involving high variability in amplitude of the samples on the right side of the echo pulse. The panels b) and c) show high variability of the gravity samples maybe due in part to the echo signal reflection from the surface which was not perfectly flat as effect of the movement of the bridge. Moreover, in panel b) the secondary side lobe reflection is evident by a right hand shoulder. This was in part expected by the knowledge of the actual transducer beam pattern previously verified. On the contrary, panel d) shows how the echoes on the repeated realization may present stable results and good precision when the sphere was located in a favourable set-up position.

As a consequence, detailed inspection of the variability in the raw samples for some setting distances was necessary for omitting ambiguous results from the analysis. On each repeated run, acceptance criteria based on a minimum standard deviations of range results and cross-correlation on samples' voltage with identical index were stated. Additionally, the direct observation on the graphical behaviour of the power samples was used as a secondary criterion.

As result of the quality analysis, only sampled echo pulse with a trend similar to that of panel d) were considered suitable for further analysis, while measurements having trends similar to that of a), b) and c) were omitted.

It is also clear from these panels that the despite the gravity principle try to use as much information on the echo pulse after the A/D conversion, this was only partially obtained. Panel a) and particularly panel b) are examples where the first sample representing the actual echo is not involved in the calculation, although its contribution could be significant for the range determination. That is a consequence of combination effects due to the pulse deformation, the sampling process and the size and actual range of the target. It is not obvious to foresee when this happens and what the contribution to the error will be.

The effect has to be considered as intrinsic of the signal processing of the echosounder, and the measurements with such behaviour but with stable amplitudes of the gravity samples were included for the error analysis.

Results and Discussion

The present investigation was focused on the EK60 short-range performances and how to produce a post processing-correction on calibration results and on measurements data in the field when these are conducted at similar short ranges. Improvements on hardware design and processing implementation were not considered as aim of the work. However, on the

basis of the results, a discussion on the implemented EK60 signal processing algorithms can certainly be made.

Gravity principle and range resolution

From the Appendix it is clear that by adopting the gravity principle, the ER60 single echo detection algorithm involves several power samples and uncompensated TS peak values. Thus, echo pulse deformation and TVG overcompensation may still prove to be especially troublesome for measurements made at short range.

In order to illustrate in details the sampling process results and the range delay effect, Figure 6 shows the echo pulse uncompensated TS samples versus time and range of the backscattered signal in Figure 3. The values are the averaged in linear domain of samples with same index from 100 repeated detections. The mean echotrace output and the theoretical results are also plotted, to testify the calculated error in range of 17.7 cm.

Throughout the data analysis, the effect of the gravity principle method was particularly evident on the echotrace extraction and data quality investigation. A very high sensitivity in range detection with particular problems was noticed when the sphere were located in positions of unfavourable distances. The range detection sensitivity is generally strictly related to the internal digital processing. Since the ER60 uses the gravity principle when first estimating the range, the target range at the SED output is not associated with the individual sample ranges, as well as the range sensitivity is not equivalent to the sample interval distance Δr.

Equation (A2) indicates that the determined target range can lie arbitrarily in a range-window less than one pulse received resolution length before the recognized uncompensated TS peak.

In Figure 7, range echotraces from datagram (see Appendix) of 106 repeated pings are plotted. The centre of the sphere was at 5 m from the transducer and the 38 kHz system was set with 1 second ping rate and 0.256 ms pulse duration, resulting in sample interval distance Δr of 4.74 cm (Table 1).

The plot shows damped oscillations in range with 21 periods in 100 seconds. This is due to the small angle oscillations of the suspended sphere activated when the bridge was moving from the previous position and then stopped.

Considering a simple pendulum with small angles approximation and neglecting the mass and the influence of the surrounding water, the period of oscillations in air is $T=2\pi(l/g)^{1/2}$, with $g=9.816$ ms^{-2} and l the length of the line in meters. Since the suspending line was approximately 4.67 m long (from the pivot to the centre of the sphere), the calculated period is 4.3 seconds, which is coherent with the approximated period of 4 seconds of the initial oscillation of Figure 7.

The formula is for a simple pendulum, but it is intuitive that for a complex pendulum, consisting in 1.67 m line in air, 3 m in the water and sphere mass, the period should not be so different under the hypothesis of small angle oscillations. The analysis of these unwanted sphere range oscillations permitted to state that the EK60 target range determination has an extremely high sensitivity and the range resolution is independent of and much smaller than the sample interval distance Δr. In other words, the range resolution is not determined by the pulse duration.

The small changes in target range were not clear during the acquisition because the real-time numerical window of ER60 shows the target range in two decimal points digit, i.e.

centimetres. Similar behaviour in target range realizations has been found for other run of measurements (approximately on 35 %), depending on the speed of the bridge and the start of acquisition after it was moved.

For the case in Figure 7, the minimum difference between two successive ranges is 1.2 mm, but shorter values down to 0.5 mm have been found. Inspection of the variation of the linear amplitudes on the same gravity sample indicated that small difference of 10^{-4} V caused a change of 1 mm in range result.

Higher variation in power gravity samples may determine significant differences in results. This indicates that by using the gravity principle, the samples involved in the method play a key role on the single echo detector results.

Errors in range determination

Figure 8 shows the results of the errors in range versus the actual target range R as determined by the Equation (6). The $\overline{r_t}$ were calculated as the mean of the last 100 repeated detections. Since the near field for the 38 kHz transducer is 2.7 m (Table 1), only data for longer distances are considered for that system. The errors seem not to be constant but showing a slight decrease with range.

This may be due to the '$40 \log R$' TVG bias applied to the samples, which decrease with distance and implies a more correct uncompensated peak determination, and also to a better representation of the echo pulse with range.

This range-dependent behaviour may be described by a simple linear regressions in the form $Err = aR + b$. The coefficients and statistical parameters of the linear regressions are listed in Table 2. The last column represents the intersection with the range axes, i.e. null error.

This first order fitting permits to derive practical relationships of the corrected range and the error in range with the detected target range. Combining Equation (6) and the linear regression formulation, the relations are:

$$R = \frac{r_t - b}{1 + a} \qquad \text{and} \qquad Err = \frac{a r_t + b}{1 + a} \tag{7}$$

The results in Figure 8 and the regressions in Table 2 have debatable consequences. In some cases, it is difficult to find the theoretical correlation between the error trends and the system parameters in Table 1.

The digital process parameters play a significant role in this context. The EK60 A/D conversion is pulse duration independent, but the final raw samples, as they result from digital decimation to ¼ of the pulse duration, strongly depend on it.

The raw samples for longer pulse durations are the result of the decimation of a higher number of digital samples and in some case may better represent the echo pulse. The effect of this digitalization process may explain part of the results.

The most evident result is the different in magnitude of the general error between the 38 kHz and the other two frequencies. Apart the difference in wave length, the 38 kHz transducer used was not a composite type. The three longer pulse durations seem to have similar error even if their $B\tau$ values are different (Table 1). This result can be ascribed to the digital process that compensates the difference. The shorter (0.256 ms) pulse duration has a bandwidth similar to the 0.512 ms, but in agreement with the theory it is definitely less affected by the error.

At 120 kHz, the error is bigger for shorter pulse duration, which has also a wider bandwidth. This is in contrast with the theory and only the better representation of the echo pulse in digital process at 1.024 ms could explain the results. For the 200 kHz system, the results show a similar error for both pulse durations. In this case the products $B\tau$ are not so different.

However, the results from systems having the same pulse duration, i.e. same digital process parameters, are in agreement with the theory, showing a larger error at narrow bandwidth.

Measurements at longer ranges may involve regressions with shorter intersection and leading to more sensible results which unfortunately are not obvious here.

Target strength estimation errors

With the knowledge of the range estimating error, the TS data from calibration and measurements may be revisited and corrected. When both calibration and measurements are performed at short range, the correction of the TS data consists of two terms. The first is due to the erratic transmission loss compensation during the measurements, the second one is due to the erratic gain *G* determined during the calibration and included in the formulation of Equation (A3).

Using Equations 6 and A3, the corrected TS (TS_{new}) can be calculated from the echotrace TS (TS_{et}) according to:

$$TS_{new} = TS_{et} - \left(40 \log \frac{r_t}{r_t - Err} + 2\alpha Err \right) + 2(G - G_{new}) \qquad (8)$$

where G_{new} is the correct power gain obtained when the calibration has been revisited with appropriate correction to the observed sphere ranges. For the latter operation and for TS measures obtained by echosounders calibrated with spheres at long range, the last term of Equation (8) is neglected. The Figure 9 shows the correction in dB that should be applied in these two cases. The plots are obtained using general absorption in seawater equal to 10.23, 33.48 and 47.23 dB km^{-1} for the frequencies of 38, 120 and 200 kHz respectively. However the contribution of the absorption term is relatively small (order of 10^{-4}dB).

From Figure 9 is clear that the range error could significantly affect the calibration results for the 38 kHz system. This has implications in using the Equations (A3) and A4 where the range error and the TVG overcompensation are combined. On the contrary, for the 120 and for the 200 kHz systems starting from 4 m the range delay leads to a mean error smaller than the claimed systematic error in standard calibration exercise i.e. $\pm 3.6\,\%$ or 0.15 dB (Foote *et al.*, 1987). It is important to note that the two correction terms in Equation (8) have opposite signs, thus their sum can be null or negligible.

If both calibration and measurements are performed at short range, the last term in Equation (8) has to be introduced. Figure 9 may help to understand the distances where the correction begins to be less important for the accuracy required from the measurements.

The procedure to obtain Equation (8) did not require any analysis on effective TS values with the intention to avoid the random variability in measured target strengths and minimize the contribution of the TVG overcompensation. Nerveless, in most of the cases the investigation on the output TS along the axis has evidenced an intrinsic contradiction. Since r_t has been observed longer than the actual range, an overcompensation in transmission loss is expected (Eq. A3), hence the TS output should be stronger than the theoretical value (TS_{th}) of the sphere, and the difference $\Delta TS = TS_{th} - TS_{et}$ negative.

The plots in Figure 10 show the results of ΔTS versus actual range R, where TS_{et} is calculated as the mean in linear domain over 100 realizations, and TS_{th} the value of the related pulse length listed in the last column of Table 1.

The general trend is not as expected. Negative ΔTS values are found only in part for the 120 kHz and 200 kHz systems, and for the 38 kHz system at 2.048 ms pulse duration. Results for the latter setting have to be taken with care, since the run at 10 m, which were used for the on-axis gain calibration, were omitted after the data quality analysis. This is the same for the 38 kHz system at 1.024 pulse duration, but, as well as for the 120 kHz at 0.256 ms, the TS output trends seem to be almost constant and very close to the theoretical TS of the sphere. These findings indicate that for these specific settings used, despite the error in range detection, the internal echosounder TS processing is not in error, producing more precise results, and no range effects are observed. Hence, no correction has to be applied in the post-processing.

Results for the 38 kHz system at 0.256 ms and for the 200 kHz system at both pulse durations investigated are even more in contradiction with the previous error range results. The ΔTS values are mostly positive, indicating that the theoretical values are stronger than the output TS. This adverse trend, theoretically in opposition with the error range results and the application of Eq. (A3), indicates that for the specific settings the range delay effects are erratic. Similar behaviour has been found by Ona *et al.* (1996) for the Simrad EK500 system transmitting at 120 kHz with $\tau = 0.3$ ms and B=12 kHz. The origins of this effect are somehow obscure even to the system responsible at the manufacturer (L. N. Andersen, Simrad AS, pers. comm.). The present investigation suggests that this problem needs to be explored by a different approach than the one used here.

Results verification

A part of the results has been verified revisiting a set of calibration and measurements performed in a cylindrical-conic enclosure during the period January-April 2004 (Calise *et al.*, 2005). The acoustic systems and the transducer types were identical to those used in the tank measurements. The enclosure was 6 m in diameter and 8 m deep, with a cylindrical upper part of 5 m and conical lower part 3 m long giving a nominal volume of 170 m^3. It was vertically suspended in the sea from a raft and filled with filtered seawater daily recycled in approx 16 % of the volume by a hydraulic system. The transducers were mounted on a fabricated aluminium rig which was placed neatly floating on the water surface at the centre of the enclosure with the transducers vertically oriented downwards. The physical condition of the water was monitored prior the acquisition of acoustic data and found always consisted of homogeneous water. Nine calibrations and specific measurements results were revisited.

The ER60 built-in calibration program can also be run offline without an operational ER60. The final calibration ASCII file (see Appendix) can be loaded and revisited. As first process, the program recalculates the gains on the base of the current echotraces listed in the file. This operation permits to simulate the calibration with new echotrace values and apply the correction to the gain and the *SaCorr* (see Appendix).

The echotraces of the earlier calibration ASCII files were edited with corrected ranges and uncompensated TS by Equations (7) and (8). Then, the calibration program was run with the new files and the new gains obtained. The previous parameters and results of calibration with the new gain and *SaCorr* are listed in Table 3. The last two columns represent the differences between the previous *G* and *SaCorr* and the new values. Again, the 38 system calibration is particularly affected from the range error while for the other two systems the effect could be neglected.

As expected from the harmonization, the differences in *G* and *SaCorr* are similar in absolute value but not in sign. This is an important result because Equation (A5) reveals that even if the *G* and *SaCorr* errors are recognized during short-range calibration of an EK60 system and applied, the related echo integration quantities will be not affect from them since they will compensate each other.

As a secondary verification, the echotraces from contemporary detections at the three frequencies of a WC38 and a WC10 sphere were re-analysed. Both spheres were contemporary suspended by a monofilament nylon line inside the common insonified volume of the acoustic beams, at distance of approx 1.2 m from each other. The pulse duration was set to 0.256 ms for all the frequencies, and the sound speed was c=1481 $m s^{-1}$. The theoretical TS for the WC38 at 38, 120 and 200 kHz were -42.17, -39.57 and -39.32 dB respectively.

The 38, 120 and 200 kHz systems were previously calibrated by the calibration number 4, 6, and 8 in Table 3 respectively. A recorded EK60 raw data file composed of 1212 echo pings was replayed extrapolating the echotrace datagram and the corrections in range and TS using results of Table 2 and 3, and Equation (8), were applied. The previous and new mean values are shown in Table 4. The values in two digit dB are reported as read from the calibration data file results.

The results confirm the validity of the range correction, but not fully the TS correction based on that error. The differences in range among the systems are strongly reduced, overall for the deeper sphere. In particular, between the 38 kHz system and the 120 and 200 kHz the differences in range for the WC38 were reduced from 8.6 and 9.9 cm to 1.1 and 1.6 cm respectively, and for the WC10 from 10 and 11.5 cm, to 0.3 and 0.1 cm. Reduction in range difference less than half centimetre was also obtained between the 120 and 200 kHz systems. When the TS correction was applied, only the new value for the 200 kHz system were slightly closer to the theoretical TS, while for the other two systems no improvement was obtained. This confirms that there is no need to correct the measures in TS domain.

Conclusions

Short-range target detection errors for three of the most commonly used Simrad EK60 echosounders have been investigated within the range 2-10 m.

The errors were accredited to the system delay and in part to the TVG overcompensation that theoretically may affect the accuracy of the measurements both in single and multiple targets measurements

Range sensitivity of the EK60 system was found to be extremely high and not related to the sample interval distance. Potential biases introduced when basing the range measurement to the measured range for energy gravity may compromise the quality of the data. Pre-analysis of the echograms in Simrad “Sp mode” (point backscattering strength data) with ER60 software may help to recognize depth channel free from acoustic noise in calibration procedure and high quality of data.

While error in range determination has been partly recognized, the expected effects on the target strength were not found. This induces to declare that no correction in strength quantities has to be applied in post-processing.

However, due to the procedure and parameters in EK60 system calibration, and the relationship for the multiple targets quantities, the accredited short range errors affect only the single targets measurements, while the echo integration result remains stable.

For measurements at short range using long pulse durations, the range resolution in the present raw data format is too low. It was not possible in the present systems to change the digital sample resolution.

To give the opportunity to the user to set this processing parameter would be an advantage in a scientific echosounder, especially when working at short range.

More accurate algorithms for transmission loss compensation at short range detection are needed. Processing realization based on the echo pulse form and not on the sample basis may be a solution.

Use of others than the ER60 post-processing software commercially available may reduce or even increase the bias, since the single echo detection algorithms are specific and the software manufactures cannot guarantee an exact match.

Acknowledgments

Professor Egil Ona, Institute of Marine Research (IMR), Norway, is thanked for experienced advice on the subject, precious suggestions for the manuscript, and the partial financial supporting of the tank work. Lars Nomboe Andersen on behalf of Simras AS is thanked for permitting access to the tank facility and providing useful information on the EK60/ER60 system. Professor Halvor Hobæk, University of Bergen, Norway, and John Dalen, IMR, are thanked for critical reviewing of the manuscript and helpful comments. Are Johansen (Simrad AS) and Ronald Pedersen (IMR) are thanked for the technical supporting during the tank measurements. The author was financially supported by a University of Bergen Ph.D. fellowship.

Appendix

EK/ER60 Echotrace Extraction and Calibration

The base of the EK60 echotrace extraction is the ER60 single echo detection algorithm (SED) run on the raw data. This is used in real time during calibration exercises by the built-in "calibration.exe" program and during the data acquisition when the operation command is set as "normal".

The ER60 SED algorithm is a one-ping process which searches for pulses along the consecutive ping-samples. Each ping-sample follows the space-time law:

$$r_i = i \cdot \frac{c\,\Delta t}{2} \qquad \text{with} \quad i = 1, \ldots, \frac{\mathrm{R}_{\max}}{\Delta r} \tag{A1}$$

where all the symbols are defined in the text of the paper.

Echo peaks are searched among the uncompensated array, i.e. raw power-samples with '$40\log \mathrm{R}$' TVG, gains and system parameter compensations, calculated for each sample in similar way to Equation A3. When the peak is located the related echo pulse is recognized as single target if it satisfies a set of user-adjustable criteria in terms of: 1) echo strength, 2) echo length with respect to the pulse duration, 3) position in the beam, and 4) angle stability of the representing samples. The acceptance criteria do not differ substantially from those of the SED implemented in the Simrad EK500 system described in (Simrad, 1996), Ona and Barange (1999) and Demer *et al*. (1999). If all the set criteria parameters are satisfied, the SED first determines the target range, and then calculate the target strength.

The target range is calculated by applying the "centre of gravity principle" (H. Solli, Simrad AS, pers. comm.) on the pulse power samples. Let the *p*-th sample to be a peak of the uncompensated array, the "echo centre of gravity" is found scanning the voltage and the range of the samples inside one received resolution length ($=c\tau/2$) spatial window centred at the peak range r_p. The target range r_t in meters is then calculated subtracting half of the received pulse length according to:

$$r_t = \frac{\sum_j \left(\mathrm{V}_j \cdot r_j\right)}{\sum_j \mathrm{V}_j} - \frac{c\tau}{4} \tag{A2}$$

where j are the indexes of the samples in the range limits $[r_p - c\tau/4;\ r_p + c\tau/4]$, V the voltage of the power sample in volt (linear amplitude), r sample range in meters. The echotrace target strength (TS_{et}) is then calculated according to:

$$TS_{et} = P_p + 10\log\left(r_t^4 10^{2\alpha r_t}\right) - 2G + 2G_{BC} - 10\log\left(\frac{P_T r_0^2 \lambda^2}{16\pi^2}\right) \tag{A3}$$

where P_p is the power of peak sample in dB, the second term is the two-way transmission loss compensation evaluated on the base of r_t, G is the one-way power gain estimated during the calibration, G_{BC} is the beam compensation gain (Reynisson, 1999) in dB, calculated by calibration-determined beam pattern parameters and the peak sample-angles. The last term is the system parameter, depending on the electrical power transmitted to the transducer P_T, the wavelength λ related to the operative frequency, and the reference distance for backscattering r_0, with typical value of 1 m (Simrad, 1996).

A Simrad EK60 echotrace datagram is then fully described by seven parameters, nominally: ping time [hh:mm:ss.##], range to the target r_t [m], beam compensated (*TSet*) and uncompensated peak TS [dB re 1 m^2], peak mechanical angles [deg] derived from the split-beam electrical phase differences (Foote *et al.*, 1986) and the *target* s_A [m^2/nmi^2]. The last parameter represents the measure of the target in terms of nautical area scattering coefficient (NASC) (McLennan *et al.*, 2002). It is calculated analysing the *volume backscattering strength-samples* array, i.e. energy samples calculated by Equation (A5). On the base of the peak value, a threshold at -12 dB is performed, and the stronger neighbour power samples are summed in linear domain and multiplied by the sampling distance Δr and the scaling factor $4\pi(1852)^2$.

The aim of the EK60 calibration is to obtain the gain *G*, the Simrad defined correction *SaCorr* [dB] and the beam pattern parameters to evaluate G_{BC} for the echotrace extraction (Eq. A3). They are determined in one single beam mapping operation, moving the standard target across the cells composing the split-beam.

The *SaCorr* number is the correction in dB required to harmonize the target TS and NASC measurements for multiple targets estimations. The harmonization is obtained by calculating *SaCorr* from integrated echoes and uncompensated peak values of *n* detections near the acoustic beam axis, so that it is measured as an integrated part of the beam mapping operation:

$$SaCorr = \frac{10\log_{10}\left(Sa_{\text{int}egration} / s_{A,TS}\right)}{2} \qquad \text{(A4)}$$

$$\text{with} \quad Sa_{\text{int}egration} = \sum_{i=1}^{n}\left(s_A\right)_i \qquad \text{and} \qquad s_{A,TS} = \sum_{i=1}^{n}\frac{4\pi\ 10^{TSu_i/10}\ 1852^2}{r_i^2\ \psi}$$

where TSu_i, r_i and $(s_A)_i$ are the uncompensated TS, the output range and the *target* s_A of the *n* central echotraces and ψ is the equivalent beam angle (MacLennan, 1990) expressed in steradians. The calibration program requires that enough detection (minimum $n = 7$) have to be realized in the central part of the beam, typically within 0.5 degrees of the athwartship and alongship angles.

At the end of a calibration the results are updated in the GPT transducer section and a file in ASCII format can be stored. The file contains information on calibration parameters, gains and beam parameters results, statistical comparison with beam models and list of the detections represented by the seven echo-traces parameters.

With the knowledge of G and *SaCorr*, the accurate volume backscattering strength (S_V) associated to each raw sample *i* with range r_i (Eq. A1) is obtained by:

$$(S_V)_i = P_{r_i} + 10\log\left(r_i^2 10^{2\alpha r_i}\right) - 2G - 2SaCorr - 10\log\left(\frac{P_T r_0^2 \lambda^2 c\tau\psi}{32\pi^2}\right) \qquad \text{(A5)}$$

Where the P_r are the raw power-samples in [dB re 1 W] and the last is the system- dependent term for volume backscattering operations (Simrad, 1996), which takes into account the ping resolution length ($=c\tau/2$).

References

Andersen, L. N. 2001. The new Simrad EK60 scientific echosounder system. Journal of the Acoustical Society of America, 109 (5): 2336.

Calise, L., Knutsen, T., and Melle, W. 2005. Multifrequency Acoustic Measurements of free swimming northern krill (*Meganyctiphanes norvegica*) in a mesocosm venue: methodological challenges. *In* Proceedings of the International Conference "Underwater Acoustic Measurements: Technologies & Results" Crete, Greece, 28th June – 1st July 2005, Ed. by J. S. Papadakis and L. Bjørnø, II: 865-871.

Demer, D. A., Soule, M. A., and Hewitt, R. P. 1999. A multiple-frequency method for potentially improving the accuracy and precision of in situ target strength measurements. Journal of the Acoustical Society of America, 105 (4): 2359-2376.

Fernandes, P. G., and Simmonds, E. J. 1996. Practical approaches to account for receiver delay and the TVG start time in the calibration of the Simrad EK500. ICES Fish Capture Committee C.M.1996/B:17, 12 pp.

Foote, K. G., Aglen, A., and Nakken, O. 1986. Measurement of fish target strength with a split beam echosounder. Journal of the Acoustical Society of America, 80 (2): 612-621.

Foote, K. G., Vestnes, H. P., McLennan, D. N., and Simmonds E. J. 1987. Calibration of acoustic instruments for fish density estimation: a practical guide. Cooperative Research Report ICES, 144, 69 pp.

Furusawa, M., Hamada, M., and Aoyama, C. 1999. Near range errors in sound scattering measurements of fish. Fisheries Science, 65 (1): 109-116.

Furusawa, M. 1991. Designing quantitative echo sounder. Journal of the Acoustical Society of America, 90 (1): 26-36.

Korneliussen, R. J., Diner, N., Ona, E., and Fernandes, P. G. 2004. Recommendations for the collection of multi-frequency acoustic data. ICES ASC C.M. 2004/R:36, 15 pp.

Korneliussen, R. J., Diner, N., Ona, E., Berger, L., and Fernandes P. G., 2008**.** Proposals for the collection of multifrequency acoustic data. ICES Journal of Marine Science, 65 (6): 982-994.

MacLennan, D. N. 1981. The theory of solid spheres as sonar calibration. Scottish Fisheries Research Report, No. 22, 17 pp.

MacLennan, D. N. 1982. Target strength measurements on metal spheres. Scottish Fisheries Research Report, No. 25, 11 pp.

MacLennan, D. N. 1986. Time Varied Gain function for pulsed sonars. Journal of Sound and Vibration, 110 (3): 511-522.

MacLennan, D. N. 1990 Acoustical measurement of fish abundance, Journal of the Acoustical Society of America, 87 (1): 1-15.

MacLennan, D. N., Fernandes, P. G., and Dalen, J. 2002. A consistent approach to definitions and symbols in fisheries acoustics. ICES Journal of Marine Science, 59 (2): 365-369.

Moszynski, M., and Stepnowski, A. 2002. Time-varied-gain correction for digital echo sounders. Forum Acusticum, Sevilla September 2002, 6 pp.

Ona, E., Zhao, X., Svelligen, I., and Foote K. G. 1996. Some pitfalls of short-range standard target calibration. ICES Fish Capture Committee C.M.1996/B:36, 18 pp.

Ona, E., and Barange, M. 1999. Single-target recognition. *In* Methodology for Target Strength Measurements, Ed. by E. Ona, ICES Cooperative Research Report NO. 235: 27-47.

Pedersen, A. 2007. Effects of nonlinear sound propagation in fisheries research. Dissertation for the degree of philosophiae doctor (PhD), University of Bergen, Norway, 307 pp. (available on the net at: https://bora.uib.no/).

Reynisson, P. 1999. Split beam method. *In* Methodology for Target Strength Measurements, Ed. by E. Ona, ICES Cooperative Research Report NO. 235: 18-26.

Simrad Norge 1996. Simrad EK500 Scientific echo sounder. Instruction manual P2172E, Simrad AS, Horten, Norway.

Simrad Norge 2003. Simrad EK60 Scientific echo sounder. Instruction manual 850-16496/Rev.A. Simrad AS, Horten, Norway.

Sawada, K., and Furusawa, M. 1993. Precision calibration of the echo sounder by integration of standard sphere echoes, Journal of Acoustical Society of Japan, (E) 14 (4): 243-249.

Simmonds, J., and MacLennan, D. 2005. Fisheries Acoustics: theory and practice, 2nd edn, Fish and aquatic resources series 10, Blakwell Publishing, 419 pp.

Tichy, F. T., Solli, H., and Klaveness, H. 2003. Non-linear effects in a 200-kHz sound beam and the conseguences for target-strength measurement. ICES Journal of Marine Science, 62 (3): 571-574.

Urick, R. J. 1983. Principles of Underwater Sound, 3rd edn, McGraw-Hill, New York, 423 pp.

FIGURES

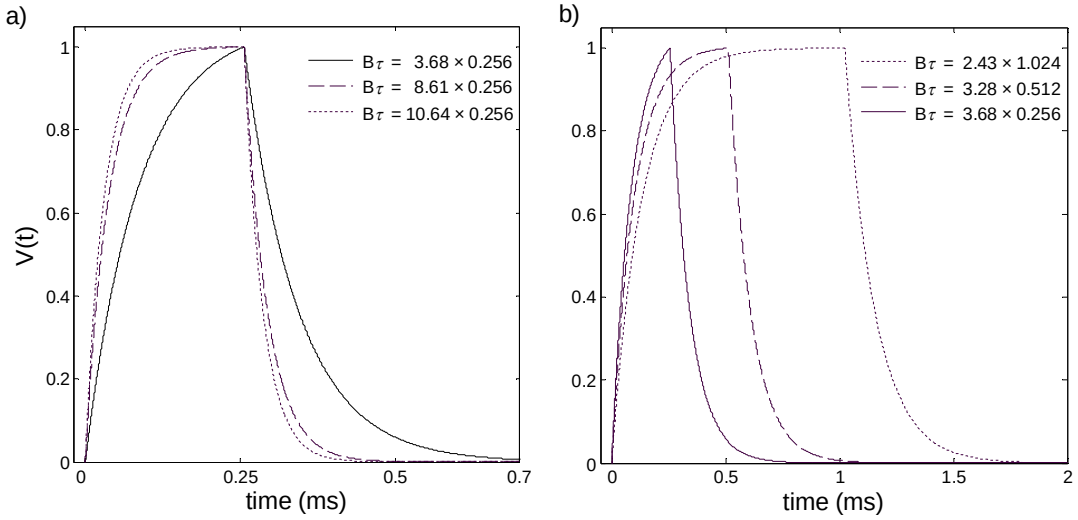

Figure 1. Relative significance of the receiver bandwidth B and the transmitter pulse duration τ on the echo pulse waveform. Simulation of normalized echo pulse waveform for different $B\tau$ combination [kHz×ms]: a) varying B and keeping τ constant, operating in Simrad EK60 38, 120 and 200 kHz ($B\tau = 0.9, 2.2, 2.7$ respectively). b) Varying τ with almost similar B, operating in Simrad EK60 38 kHz ($B\tau = 2.5, 1.7, 0.9$). (Note that the solid line in both the panels refers to the same setting but with different scale of x-axis).

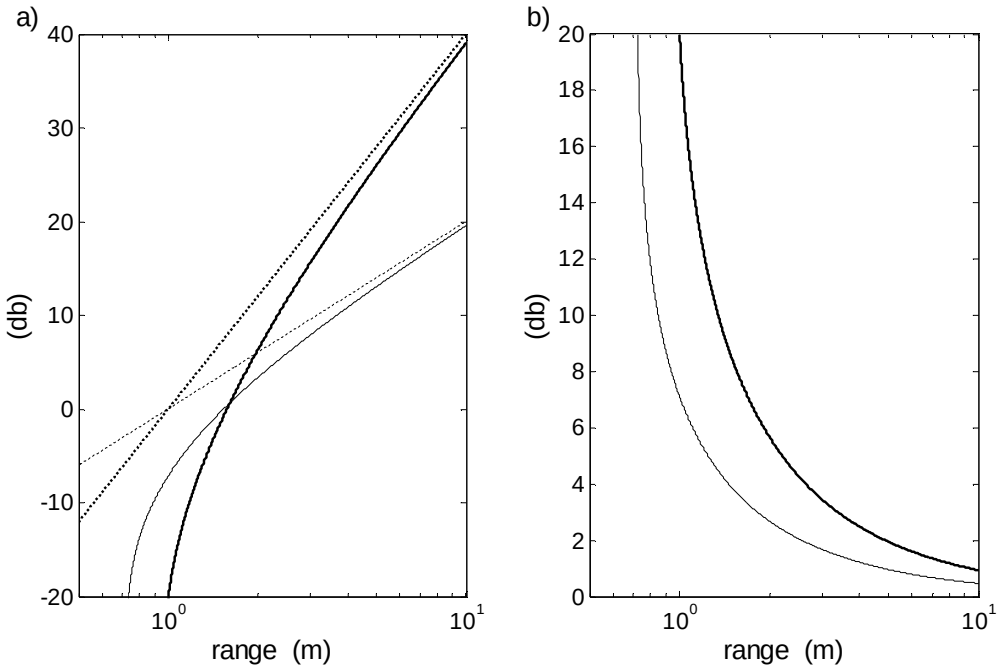

Figure 2. a) Exact (thicker lines) and asymptotic TVG compensations versus range for the 38 kHz Simrad EK60 system with $B\tau = 2.43 \times 1.024$ [kHz×ms]. b) Error in compensation applying the asymptotic forms: '$40 \log R$' and '$20 \log R$' TVG functions. In both panels, the black lines refer to the single target case, the grey lines to the multiple randomly distributed targets.

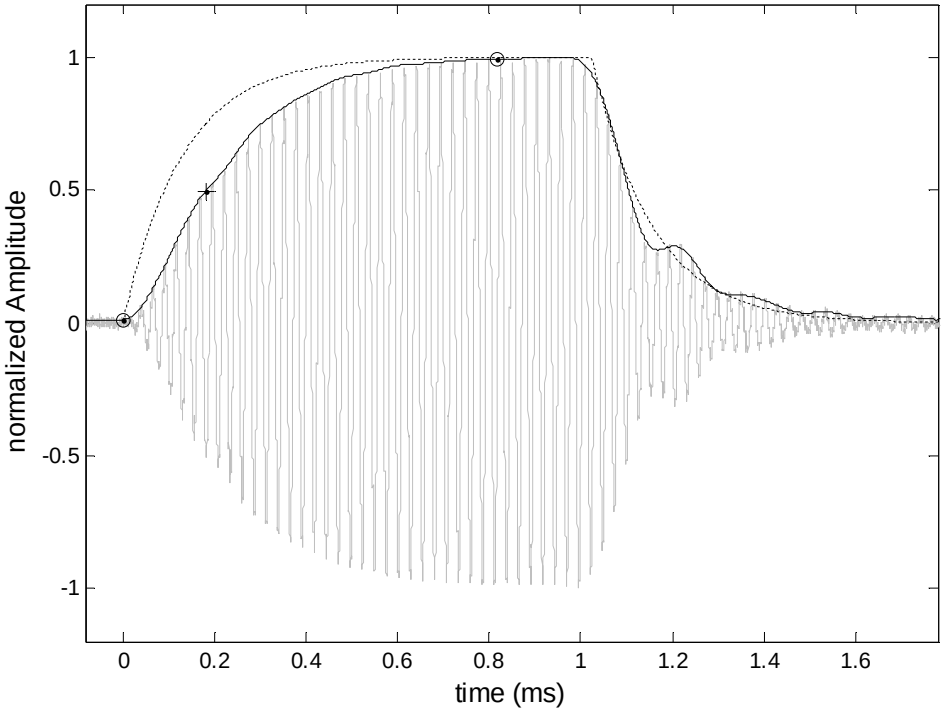

Figure 3. Backscattered analogue signal (grey line) from the CU60 standard sphere placed at 3 m to the transducer as recorded at a receiver board of the 38 kHz Simrad EK60 with 1.024 pulse duration and 2.43 kHz bandwidth. The black solid and dashed lines are the signal envelope and the modelled envelope by Equation 1 (only receiver filtering) respectively. Envelope's start and peak (open circle), and half peak (plus) points are also shown.

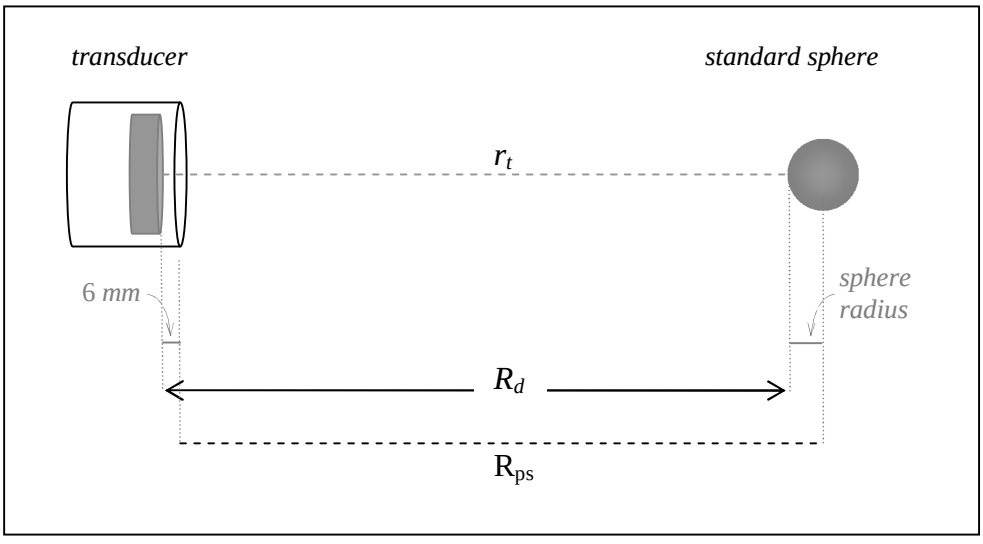

Figure 4. Off-set correction to the positioning system distance (R_{ps}) for comparison with the observed target range (r_t). $R_d = R_{ps}$ - (sphere radius) + 0.006 [m].

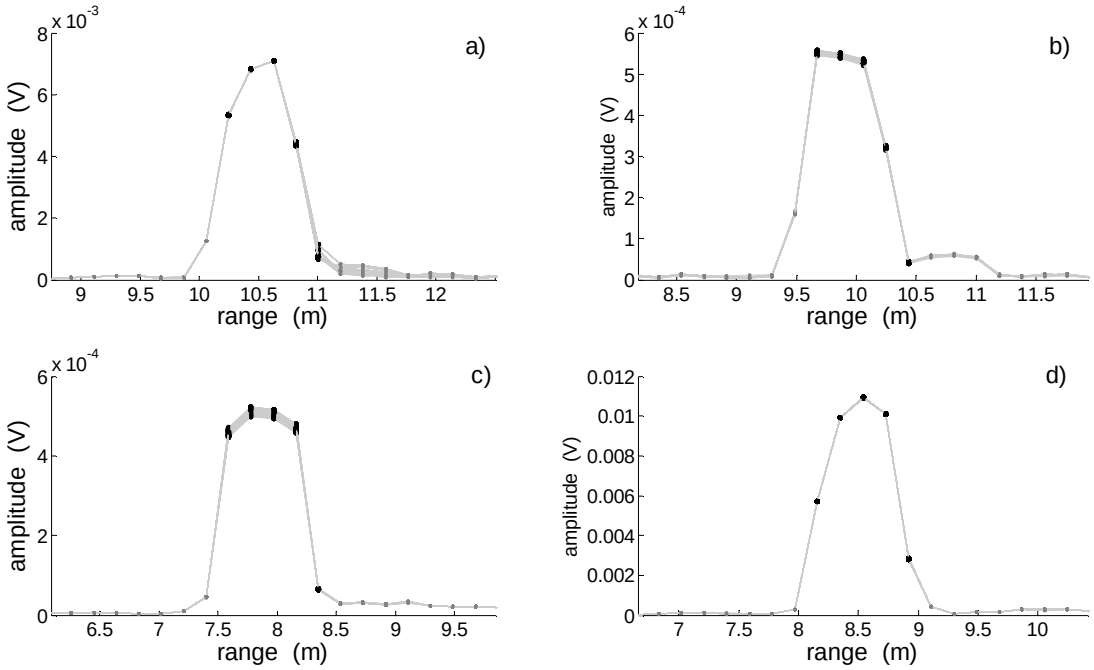

Figure 5. Superimposition of 100 repeated echoes at 1.024 ms pulse duration for different frequencies and distances sphere-transducer [kHz, m]: a) [38, 10]; b) [120, 9.5]; c) [200, 7.5]; d) [38, 8]. All dots are the linear amplitude of EK60 raw power samples ($10\,\hat{}\,(power/20)$); black dots are the values involved in the centre of gravity method.

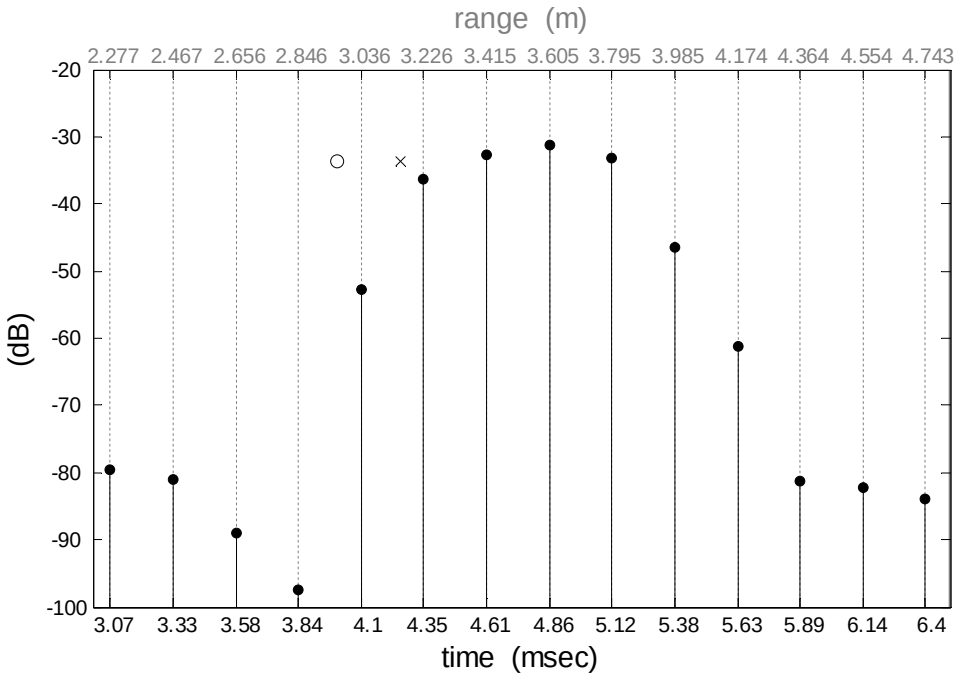

Figure 6. Uncompensated TS samples versus time (lower black abscises) and range (upper grey abscises) of the backscattered signal, the CU60 sphere was at 3 m range for the 38 kHz EK60 system at 1.024 ms pulse duration (see Figure 3). ER60 processing output (cross) and theoretical result (open circle) are plotted to illustrate the range delay.

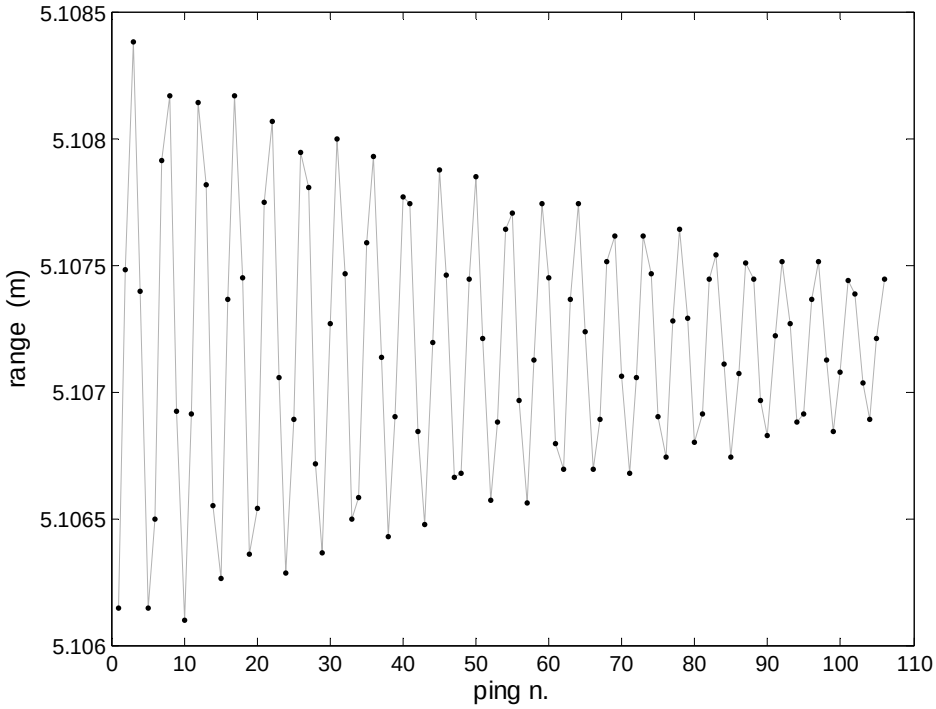

Figure 7. Range sensitivity of EK60. Highest precision echotraces range datagram (dots) of the 38 kHz system with pulse duration of 0.256 ms with the CU60 standard sphere placed at 5 meters from the transducer. Dots are connected by grey lines for better readability.

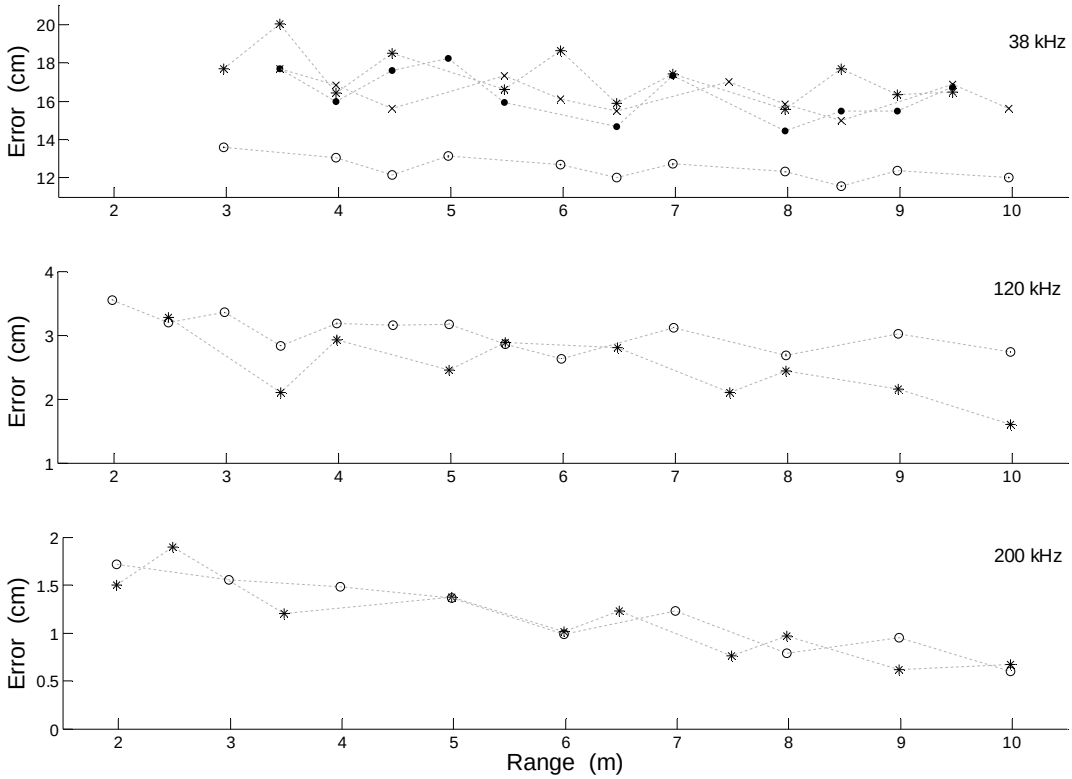

Figure 8. Range errors calculated by Equation 6 for the three EK60 systems at pulse duration: 2.048 ms (black dot), 1.024 ms (asterisk), 0.512 ms (cross) and 0.256 ms (open circle). The grey dashed lines connecting the consecutive measures are shown only for readability.

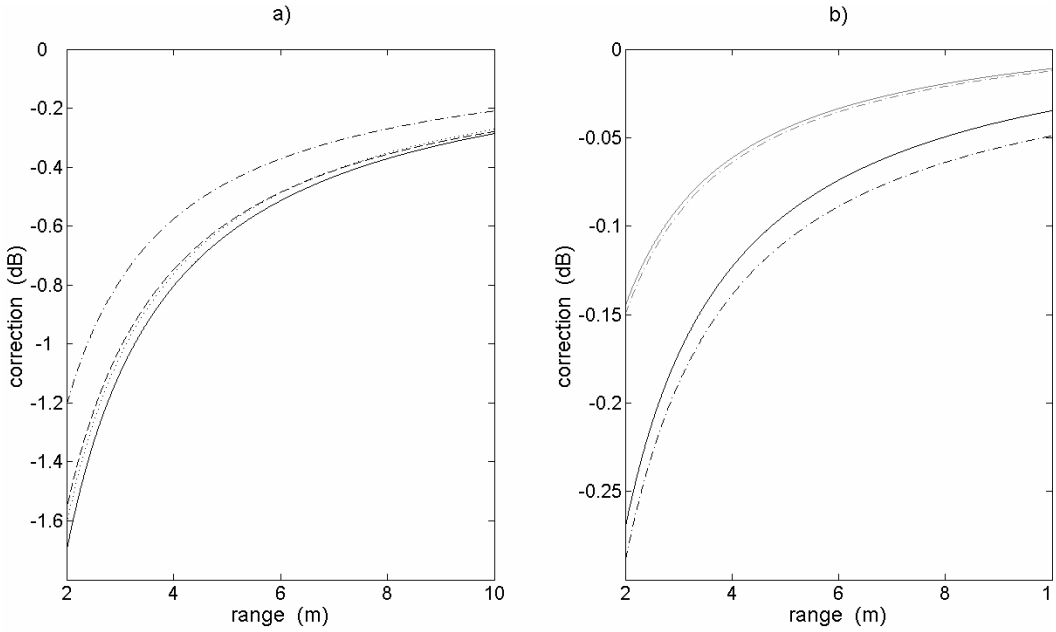

Figure 9. Estimated echo strength correction considering the only error in range detection (second term on right side of Equation 8). Dotted line 2.048 ms; solid line 1.024 ms; dashed line 0.512 ms; dot-dashed line 0.256 ms. Panel a) 38 kHz system; panel b) 120 kHz system (black lines) and 200 kHz system (grey lines).

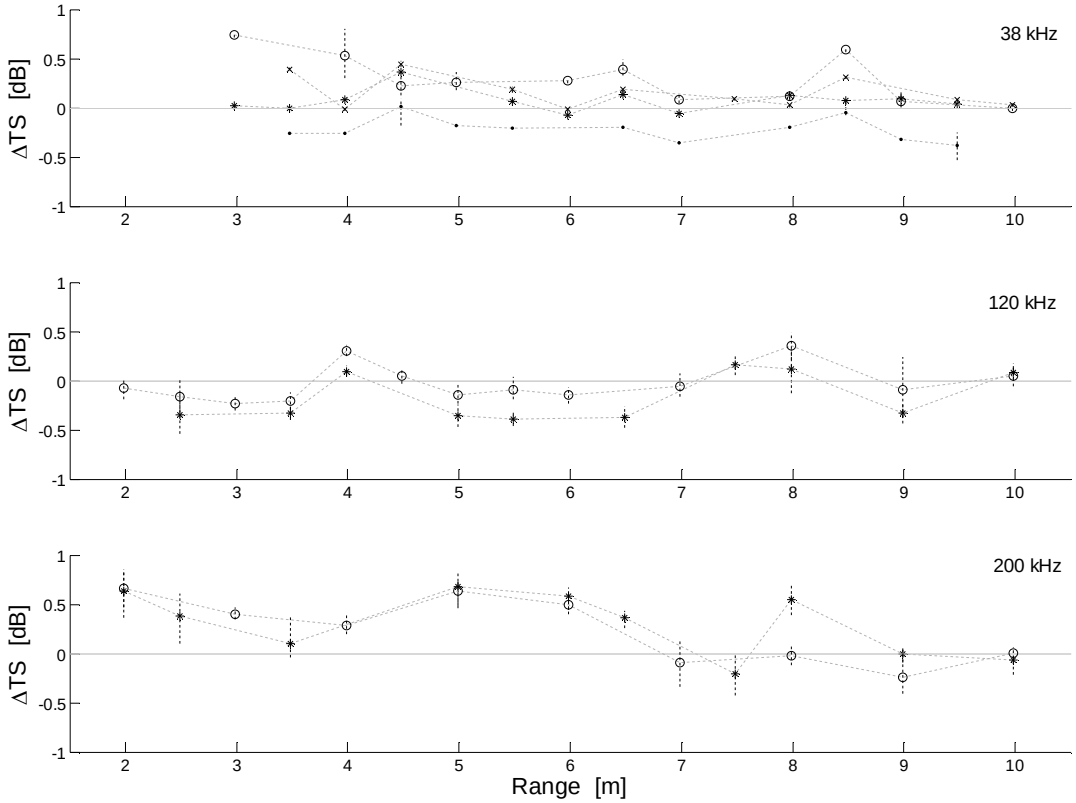

Figure 10. Difference between theoretical and mean output TS of standard spheres versus range. Pulse duration: 2.048 ms (black dot), 1.024 ms (asterisk), 0.512 ms (cross) and 0.256 ms (open circle). The black vertical dashed lines represent the min and max values. The theoretical values are listed in the last column of the Table 1. The output values are calculated as the mean in linear domain over 100 realizations.

TABLES

Table 1. The investigated Simrad EK60 systems, their principal characteristics, and theoretical standard spheres target strength (TS_{th}). The nearfield (n.f.) are theoretical values calculated from d^2/λ (A. Johansen, Simrad AS, pers. comm.), with d the maximum linear dimension of the transducer active face and λ the pulse length related to the GPT central frequency f_0 at $c = 1500$ m s^{-1}. The sample range Δr and the TS_{th} are for sound speed $c = 1482.3$ m s^{-1}. The standard spheres were: the Cu60 for the 38 kHz system and the WC38 for the 120 and 200 kHz systems.

GPT	f_0 (kHz)	Transd. type	n.f. (m)	τ (ms)	B (kHz)	Bτ	Δt (msec)	Δr (cm)	TS_{th} (dB *re* 1 m^2)
38	38.095	ES38-B	2.7	2.048	1.45	3.0	0.512	37.94	-33.56
				1.024	2.43	2.5	0.256	18.97	-33.60
				0.512	3.28	1.7	0.128	9.48	-33.65
				0.256	3.68	0.9	0.064	4.74	-33.68
120	121.212	ES120-7C	0.9	1.024	3.03	3.1	0.256	18.97	-39.50
				0.256	8.71	2.2	0.064	4.74	-39.57
200	200.000	ES200-7C	0.5	1.024	3.09	3.2	0.256	18.97	-39.37
				0.256	10.64	2.7	0.064	4.74	-39.30

Table 2. Coefficients and statistical parameters of the linear regressions determined from Equation (6) with Err and R expressed in meters. R^2 and SE are the R-square and the standard error of the regression.

System	τ (ms)	$a \cdot 10^3$	b	R^2	SE	$-b/a$
38	2.048	-2.982	0.1825	0.24	0.012	61.19
	1.024	-3.082	0.1919	0.27	0.012	62.27
	0.512	-1.718	0.1746	0.19	0.008	101.59
	0.256	-1.924	0.1376	0.54	0.004	71.49
120	1.024	-1.430	0.0335	0.50	0.004	23.43
	0.256	-0.712	0.0342	0.43	0.002	48.07
200	1.024	-1.312	0.0191	0.79	0.002	14.55
	0.256	-1.293	0.0196	0.89	0.001	15.16

Table 3. Enclosure calibration results before and after the correction considering only the range error. c is the sound speed during calibration, P_T the transmitted power to the transducer, $\overline{r_t}$ the detected mean range of the sphere, rms is the root mean square error with respect to the Beam model (BM) and Polynomial Model (PM) defined in the Simrad EK systems.

No.	***Date*** **(2004)**	***c*** **(m/s)**	***f*** **(kHz)**	τ **(ms)**	P_t **(W)**	$\overline{r_t}$ **(m)**	**rms BM**	**rms PM**	***G*** **(dB)**	***SaCorr*** **(dB)**	**New_*G*** **(dB)**	**New_*SaCorr*** **(dB)**	**Δ*G*** **(dB)**	**Δ *SaCorr*** **(dB)**
1	30 Jan	1470	38	1.024	1000	5.34	0.17	0.07	26.74	-0.64	26.45	-0.34	0.29	-0.30
2	30 Jan	1470	38	1.024	600	5.58	0.30	0.09	24.91	-0.57	24.64	-0.29	0.27	-0.28
3	29 Jan	1470	38	0.256	1000	5.32	0.18	0.07	24.63	-0.53	24.41	-0.32	0.22	-0.21
4	30 Jan	1470	38	0.256	600	5.32	0.17	0.07	24.67	-0.55	24.46	-0.34	0.21	-0.22
5	23 Mar	1480	38	0.256	600	5.02	0.17	0.07	24.59	-0.56	24.37	-0.31	0.22	-0.25
6	27 Feb	1475	120	0.256	250	5.30	0.15	0.08	26.89	-0.62	26.83	-0.56	0.06	-0.06
7	19 Mar	1480	120	0.256	250	4.61	0.13	0.08	26.61	-0.60	26.54	-0.53	0.07	-0.07
8	02 Feb	1474	200	0.256	120	5.52	0.21	0.11	27.96	-0.45	27.93	-0.42	0.03	-0.03
9	18 Mar	1480	200	0.256	120	5.24	0.16	0.12	27.88	-0.39	27.85	-0.35	0.03	-0.04

Table 4. Range and TS detection verification of standard spheres enclosure data. The WC38.1 and WC10 sphere range [m] and TS [dB *re* 1 m^2] before and after correction.

	Sphere	38 kHz		120 kHz		200 kHz	
		range	**TS**	**range**	**TS**	**range**	**TS**
before	**WC38.1**	4.858	-42.15	4.772	-39.52	4.759	-39.42
	WC10	6.019	-54.92	5.919	-50.64	5.903	-55.24
after	**WC38.1**	4.729	-42.19	4.741	-39.52	4.745	-39.39
	WC10	5.892	-54.87	5.889	-50.61	5.891	-55.20

Paper IV

Lucio Calise, Tor Knutsen and Webjørn Melle

Multifrequency target strength of horizontally free-swimming Northern krill (Meganyctiphanes norvegica) in a mesocosm venue

Multifrequency target strength of horizontally free swimming Northern krill (*Meganyctiphanes norvegica*) in a mesocosm venue

Lucio Calise, Tor Knutsen, and Webjørn Melle

Abstract

The knowledge of acoustic scattering properties of individual krill at survey operative frequencies is a key issue to improve the acoustic techniques with respect to abundance estimation of these organisms. While substantial improvements have been achieved in general on theoretical scattering models, high quality measurements on free swimming krill with well defined orientation are still wanting. In this work, results from direct multifrequency acoustic measurements on horizontally free swimming krill in a novel experimental setup are presented. A near mono-specific ensemble of living Northern krill (*Meganyctiphanes norvegica*) was introduced into a large seawater mesocosm, vertically suspended in the sea from a raft. Simrad EK60 raw data were collected at frequencies 70, 120, and 200 kHz during a specific experiment. Two submerged lamps placed at opposite sides of the acoustic beam axis and alternately switched on and off, induced individual krill to swim horizontally through the acoustic beams by light attraction. Data analysis on echo tracks also from synchronized detections at the different frequencies allowed to determine krill behaviour parameters like swimming speed, direction and angle, and to derive target strength ranges and frequency response for the Northern krill. The major size group of the mesocosm population had an average total length 21.8 ± 3.0 mm, while the less abundant but larger sized cohort had an average length of 27.8 ± 2.7 mm. On average, the target strength range was found decreasing with the frequency, being inside the range [-88.3, -68.3] dB at 70 kHz, [-83.8, -64] dB at 120 kHz and [-80.8, -63.5] dB at 200 kHz, while the pin-to-ping variability within the tracks increasing with the frequency. The majority of the synchronized detections exhibited stronger TS at 200 kHz compared to 120 kHz, but 19 % showed an opposite trend. It is suggested that this population is composed in such a way that, above a certain size, they are subject to the transition between Rayleigh and Geometric scattering regions. The combined result from these two frequencies might be used in deriving a relative composition of different size groups within an *in situ* aggregation of *M. norvegica*.

Keywords: Multi-frequency acoustics, krill target strength, *Meganyctiphanes norvegica*, frequency response, EK60, mesocosm, krill swimming speed.

L. Calise: Department of Physics and Technology, University of Bergen, Allégaten 55, N-5007 Bergen, Norway.
T. Knutsen and W. Melle: Research Group Plankton, Institute of Marine Research, P.O. BOX 1870 Nordnes, N-85817 Bergen, Norway.

Introduction

Scientific echosounders are considered a primary tool for the evaluation of distribution and abundance of zooplankton and widely used in the last decades (Foote and Stanton, 2000). The present methodology is able to estimate the state of the resources to be managed and get a comprehensive knowledge of them only in part. Especially for specific purposes, such as classification and absolute abundance estimation, it is not fully established. The acoustically detected swarms of zooplankton are often a mix of species and sizes, with addition of fish larvae, and the interpretation of the acoustic data is not straightforward. Also in the case of mono-species environment, the analysis of acoustic data suffer of the lack of accurate knowledge on target strength and the limitation derived from the associated zooplankton net sampling techniques (e.g. Wiebe *et al*. 1982).

Multifrequency systems may potentially overcome part of the problems (Greenlaw, 1979). Since the scattering properties of anatomical group or individual species are known to vary with the operating frequencies (Chu *et al*. 1992; Stanton *et al*., 1998a, 1998b; Martin Traykovski *et al*., 1998), the variation in strength levels can be used for identification and discrimination purposes. In this context, accurate representative scattering models in combination with ground truthed data are essential to derive numerical density, size and taxa of target species. Using this approach, acceptable level of the data analysis techniques have been achieved to assess more accurately the distribution and the abundance of euphausiid organisms, also called krill. Accomplished new acoustic technologies have also helped this progress.

However, researchers still indicate the target identification as the principal component of uncertainty in krill acoustic surveys (e.g. Demer, 2004). This can be made rigorously only if the target strength (TS) of the studied organisms as a function of size, operative frequency and behaviour (i.e. spatial orientation) is well known. The required functions can be obtained by theoretical predictions and *in situ* and *ex situ* direct measurements (Foote, 1991). Due to the complexity of the problem, there are no doubts that the most reliable technique for acoustical assessing of euphasiids lies in combining the best aspects of both theoretical and empirical approaches.

In the case of krill, the results generally show high variability in target strength and substantial differences between measurements and model computations (e.g. Greenlaw *et al*., 1980; Everson, 1982; Cochrane *et al*., 1991; McGehee *et al*., 1998; Demer and Conti, 2003a; Amakasu and Furusawa, 2006; Conti and Demer, 2006; Klevjer and Kaartvedt, 2006). Although the precise knowledge of the material model parameters, i.e. specific mass density and sound speed contrasts, is not fully recognized, the observed deviations are mostly attributed to the changes in krill orientation and the lack of its knowledge during the data acquisition (Greenlaw *et al*., 1980; Everson, 1982; Cochrane *et al*., 1991; Demer and Martin, 1995; McGehee *et al*., 1998; Demer and Conti, 2003; Amakasu and Furusawa, 2006; Conti and Demer, 2006).

Krill orientation depends on their behaviour during own activities, such as feeding, up-down migration, horizontal cruising, and external environmental factors like swim against a current, flee from predators, avoidance from moving acoustic platforms, and in some species with the maturity stage (Endo, 1993). Hamner and Hamner (2000) observing krill behaviour *in situ* by scuba diving and in different aquaria found that all individuals in a school assume virtually the same orientation and spend most of their life swimming horizontally. This has also been observed by *in situ* photographs of *Meganyctiphanes norvegica* (Kristiensen and Dalen, 1986), and from small enclosure and in situ video observations of *Euphausia superba* species (Pauly and Penrose, 1998; Lawson *et al*., 2006).

In analysis of data from multifrequency acoustic survey, mean orientation equal to, or very close to, the horizontal have been often inferred from theoretical predictions matching the acquired acoustic volume backscattering to the biological samples (Cochrane *et al*., 1991, Sameoto *et al*., 1993; Demer and Conti, 2005; Conti and Demer, 2006; Lawson *et al*., 2006, 2008).

However, *in situ* and *ex situ* high quality acoustic measurements on free swimming individuals with contemporary observation of orientation are strongly required. This is not an easy task; accurate determination of orientation requires high definition images obtainable only with video tools close to the organisms that inevitably will influenced their natural behavior (Hamner and Hamner, 2000) and/or detected by the echosounder covering the echoes from the animals.

An alternative is to perform the measurements when the orientation can be predicted with good approximation. In the present work, a specific experiment performed to acquire scattering information at the most commonly survey frequencies on free-swimming krill in expected horizontal aspect is described and the results discussed.

A large enclosure (mesocosm), vertically suspended in the sea from a raft, was established at the Austevoll Aquaculture Research Station of the Institute of Marine Research in Bergen (Norway) during January – April 2004, and a near mono-specific ensemble of living *Meganyctiphanes norvegica* (M. Sars, 1857), also called Northern krill, was introduced.

This species is known to be attracted by submersed artificial light (Mauchline and Fisher, 1969), especially if the light source is motionless (Herman *et al*., 1993). Taking the advantage of this feature, the individual euphausiids were induced to swim through the active acoustic beams by the attraction of two fixed lamps placed at opposite sides of the split-beam coordinate and alternately switched on-off.

Pleopod propulsion is the normal method adopted by krill for forward movement. Kils (1981) described the relationship between forward swimming speed and body angle orientation of *Euphausia superba* by means of a model involving the body centre of mass and the centre of force, which are not located in the same body point. He showed that krill perform forward movement by positioning the body with an angle of orientation θ less than 50°. For faster moving animals there was a clear tendency of orientation angles coming closer to zero ($\theta<10°$). This reduces the drag resistance and allows maximum pleopod stroke amplitude and higher beat rate with minor energy consumption.

Meganyctiphanes norvegica is known to be similar to *Euphausia superba* in the overall body shape but it is smaller at similar stages of maturity. Cochrane *et al*. (1994) argued that for smaller individuals at a given faster swimming speed the square dependence of drag resistance from the length is proportionally more important than the cubic dependence of gravity. Thus, narrower orientation angles are expected when small sized euphausiids are "motivated" to swim in forward direction.

In the experiments presented in this paper *M. norvegica* were induced to swim in "motivated" forward direction by light attraction. Hence, it could be assumed that the individual swimming angles were very close, if not equal to horizontal orientation.

Materials and methods

The mesocosm was established on an open raft, located in a small bay well protected from severe waves, currents and wind, at approximately 25 m from the shore. The depth around

the raft was normally 11 metres during the high tide period, with a decrease of 0.5 m at low tide. The mesocosm consisted of a cylindrical enclosure or "bag" of black colour polyethylene sheeting (three-layer woven PEL with total thickness of 0.15 mm), tapered in the bottom region and suspended vertically orientated in the sea, with geometry illustrated in Figure 1. The material composing the bag was flexible and impermeable, and the black colour was chosen to simulate a deep pelagic habitat giving the organisms the illusion of being at a larger depth. The overall dimensions of the bag were 6 m of diameter and 8 m deep, with a cylindrical upper part and conical lower part of 5 m and 3 m length respectively (Figure 1), resulting in a nominal volume of 170 m^3. The upper edge of the bag was fastened by ropes to a circular stainless steel ring of 6 m diameter connected to the raft and leading the entire structure to be a single system floating on the sea surface. An aluminium footbridge, placed across the bag, allowed easy access to the measurement venue for all the operations needed. The oxygenation in the bag was assured via water circulation of sand filtered deep sea water pumped from 165 m depth in the nearby fjord and pre-monitored in temperature, salinity and oxygen. The inflow rate was kept approximately at 18.2 l min^{-1}, corresponding to a daily recycling of 16 % of the mesocosm water volume. The extra water was removed by gravity overflow using a vertically adjustable sieve suspended by ropes from the bridge and placed inside the bag, with the terminal part being a tube penetrating the bag wall at approximately 0.3 m depth. The sieve was lined by a fine net with mesh size of 250 μm to prevent potential loss of krill from the mesocosm.

Temperature and salinity in the mesocosm and the surrounding seawater were monitored almost every second day using a calibrated Gytre Mini CTD SD202. The mean sound speed of the mesocosm water was then calculated and the value manually entered into the ER60 environmental parameter menu prior to each recording sequence. More details on mesocosm set-up and monitoring can be found in Calise *et al*. (2005).

Three sampling events consisting of 6 hauls each were carried out during night-time on 4, 6 and 27 of February 2004, using a small 3 ft Isaac-Kidd Midwater Trawl (IKMT) with a mesh size of 500 μm. They were conducted at approximately 10-20 m depth in the central part of Raunefjorden (60°16′N, 5°9′E), a land-locked fjord on the west coast of Norway near Bergen. The typical trawling time was 25 minutes with a vessel speed of 2.5 knots and the IKMT was kept at sampling depth not more then 15 minutes. The two first sampling events were performed using the RV Hans Brattstrøm; the last was carried out with a smaller vessel the MS Aurelia, both belonging to the University of Bergen.

A sturdy, transparent, plastic bag with of 30-liters capacity was attached to the cod-end of the IKMT by means of a clamp. It was pre-filled with surface water prior to deployment and allowed to retrieve most of the biological sample in very good condition. When brought on board, the plastic bag was emptied in equal amounts into 3 plastic tubs of 50-liters capacity, partially pre-filled with surface water and with air pumps activated inside. Dead and damaged krill and organisms of unwanted species were immediately removed from the containers. Transport to Austevoll Aquaculture station took approximately 1 hour following the last catch. Here the plastic containers were carefully emptied into the mesocosm after additional inspection and removal of unwanted organisms. Along with the krill, a small amount of copepods of the genus *Calanus* and *Metridia* were caught with the IKMT net. These copepods acted as a natural source of food for the krill in the mesocosm. No other food was supplied during the course of the experiments.

During the course of the experimental period dead animals were regularly removed from the bottom region of the bag by a seawater pump. Other unwanted animals were also immediately removed when observed close to the surface of the bag. All the removed animals where identified to species and their size measured.

At the end the experimental period, 2821 krill specimens were classified and their total length (TL), from the tip of rostrum to the posterior end of the terminal spine at the end of telson was measured. In Morris *et al*. (1988) this total length is denoted "TT".

The acoustic system was the Simrad EK60 (Anderson, 2001) scientific echosounder operating at the frequencies of 70, 120 and 200 kHz. All the transducers were nominally 7° split-beam transducers of the new composite type with angular resolution (Demer *et al*., 1999) equal to 0.061°. The set-up, the acquisition and the storage of data were PC controlled via Ethernet connection by means of the Simrad ER60 software (ver. 2.0.0), which is part of the entire EK60 system. For this study, it is important to note that the EK60 operates without instability in power transmission due to the high duty cycle (Medwin and Clay, 1997), so that the so called ping interval effect is avoided and the pinging is activated simultaneously at all operative frequencies.

The transducers were mounted on a carefully fabricated aluminium plate (90 x 110 cm and 5 mm thick), as close to each other as space permitted, with the acoustically active surfaces aligned in the same horizontal plane and with identical split-beam orientation. A 5 cm thick divinycell plate was mounted between the aluminium plate and the transducers to reduce the back radiation, and form-cut elements of the same material inserted between the transducers to fill up empty space and reduce lateral transducer radiation. The rig was placed neatly floating on the water surface to the centre of the mesocosm, and stabilized by an air filled polyethylene tube and small weights placed on the top.

The acoustic systems were calibrated prior to and following the termination of the experiment period by means of the standard acoustic sphere method (Foote *et al*., 1987). A small deviation in calibration gains was observed for the 120 kHz system. Both the calibrations were performed with success, i.e. the rms-errors with respect to the beam model were less than 0.2 (Simrad, 2003). A date-adaptive compensation was determined by interpolation between calibration gains in the linear domain and used to correct the TS data between calibration dates.

The relative distances between the beam axes were measured from a digital photo of the transducers mounted on the rig setting the centre of the 70 kHz transducer as the origin of a Cartesian coordinate system. Moreover, in order to verify the acoustic angle sensitivity, as well as the beams geometry inside the mesocosm and derive tolerances for matching target positions at two or more frequencies, detections of two standard tungsten carbide spheres with 38.1 (WC38) and 10 (WC10) mm diameter were acquired simultaneously at all the frequencies. The spheres were suspended together, at distance of approx 1.2 m from each other and initially moved randomly by means of the motor-driven system used for the calibration. Then, they were moved inside each acoustic beam along the split-beam coordinates and around the edge as shown in real-time in the *single-target position window* of the ER60 software.

Using the acquired echoes of the standard spheres it was possible to completely map all the volume of the transducer beams, and identify imprecise mounting that could not be reflected in the 2D photo of the transducer arrangement. Figure 2 shows the computed horizontal beam cross-sections and their joint areas at 4.5 m depth. The dotted lines describe the edges of the nominal -3 dB max power beam angle of the transducers equal to 7° solid beam angle, while the grey areas represent the full 6° cross-sections wherein the echoes of the tracks were accepted for the horizontal trajectory determination and the TS analysis.

In order to induce individual krill to swim through the acoustic beams, two underwater lamps, a 500 W Edison model and an eye halogen double-lamp 500 W Iwasaki Electric Co. LTD, Japan, were placed during night-time inside the mesocosm on the opposite sides of the alongship split-beam coordinate (fore-after), at a depth of approximately 4.5 m close to the

bag wall. The lamps were alternatively switched on-and-off using a timer, and EK60 raw files were recorded during the passages of the krill attracted by the light.

All the systems were run with low transmit power to avoid potential non-linear effects (Tichy *et al*., 2003; Pedersen, 2007; Korneliussen *et al*., 2008), with identical pulse duration of 0.256 ms and maximum ping rates i.e. transmitting pings as often as possible. This resulted in a raw sampling distance of 4.7 cm and approximately 18 pings per second.

Table 1 summarizes the acoustic systems, the setting parameters and the performance of the systems in the mesocosm at the time of the experiments.

EK60 raw files from three trials were used for the analysis. Two trials were performed on 2 March, with recording time of 30 and 90 minutes respectively, and one trial of 90 minutes recording on 4 March. In the first trial the lamps were switched on in turn every 5 minutes. Watching the echogram display in real-time apparently the highest activity of animals seemed to be in the first few minutes after the light is turned on, and less activity later. To avoid the animals to habituate to the light source staying close to the light for a longer period, hence being out of the acoustic beam, we chose to run the last two trials with a light switching time of 3 minutes. When a light was turned on, it was easy from the surface to identify and observe single individual krill swimming across the mesocosm most probably attracted by the light.

Acoustic data analysis

The EK60 raw files were processed by an enhanced version of the Sonar5 post processing software (Balk and Lindem, 2005). For each frequency, the single echo detector (SED) criteria (Ona and Barange, 1999) were optimized by means of the Sonar5 built-in-tool "SED pre-analysis". Then, subsequent echoes from the same target, composing the so called echo-track, in the range 1-6.5 m were manually selected and the echotrace variables for each resolved detection extracted. This operation was done by observing the three echograms simultaneously. Echo-tracks recognized at only one frequency were also selected.

In practice, for each echo composing a track, the ping time [hh:mm:ss.##], the range to the target r_t [m], the uncompensated (TSu) and compensated (TS) target strength [dB re 1m] and the mechanical angle positions α and β [degrees] in the beam, were stored for later analysis.

Although varying slightly between frequencies, the typical SED acceptance criteria were set as follows: TS threshold -100 dB, echo length 40-120 % of the pulse duration, target samples standard deviation in phase measurements less than 8, beam pattern compensation 6 dB. The latter parameter was chosen at this stage to visualize larger off-axis detections in the echograms and to obtain longer and easier visualizations of the tracks. In addition, the minimum accepted distance between echoes in the same ping was set to 10 cm to avoid potential detected fluctuations in the echo level.

In all the further analyses on TS and beam angle position data, only echoes detected inside the solid beam angle of 6° (cut-off solid angle) were used. This criterion was chosen to exclude echoes at the outskirts of the nominal beam, where the signal-to-noise-ratio is lower and potential biases might compromise angular position and TS estimation of weak targets (Kieser *et al*., 2000; Fleischman and Burwen, 2000).

The treatment of the extracted tracks and the interpretation of the results had to take into account various biases that could materialize from the instrumentation and processing limitations related to the experimental set-up itself (i.e. short-range detection), as well as animal behaviour and insonified number targets in the mesocosm.

Due to the restriction imposed by the SED criteria parameters, the tracks were not always composed of consecutive pings, but appeared generally segmented in time. Missing echoes were mostly observed when the TS approached lower levels and close to the background noise. In these cases, the raw samples of the echo pulse are strongly biased and the SED standard deviation criterion could cause echo rejection (Soule *et al.*, 1997). Consequently, each track was treated as composed of segments whose limits were defined if four consecutive echoes (i.e. 0.2 second) were missing.

Another and more significant problem appeared as unrealistic changes in range, erroneous split-beam positions and significant jitter in TS levels between consecutive pings in the track. These erroneous measurements and spurious echoes would seriously affect the interpretation of the data and were removed by analysing the tracks with a set of well defined criteria.

To illustrate the full process adopted on a single track, the flow-chart diagram is given in Figure 3. A five-points mean was applied to the absolute values of the ping-to-ping variations versus elapsed-time for each of the four echo variables: range, alongship and athwartship angles, and back scattering cross-section ($\sigma_{bs} = 10^{(TS/10)}$). The means were basically performed on each track segment with the first point considered as start. If the last segment group consisted of less than five echoes, the mean was computed based on the last five points of the segment. For segments with less than five echoes the mean was calculated based on the actual number of points.

For each of the five points the discrete derivate of the variable was calculated and then subtracted from their mean. The resulting deviations were compared to the mean variation of the variable based over the entire track plus two times its standard deviation. For each of the four echo variables data points with deviation exceeding the corresponding track mean value were excluded.

Smoothing the data in vertical plane

Despite the rejection of biased data, unrealistic changes in range between consecutive echoes were still present along the tracks. These were mostly due to the instability in range determination of the EK60 systems with target at short distances from the transducer (Calise, 2009), and required further smoothing of the resolved echoes along the vertical dimension of the entire track.

Different smoothing methods were tested on tracks showing general trends. The weighted cubic smoothing spline (de Boor, 2001) was found the most appropriate for further analysis and applied to the echo ranges of the targets on all the echoes extracted, i.e. with SED beam compensation criteria set to 6 dB. The functions resolved by the smoothing spline technique are determined by minimizing a weighted combination of the average squared approximation error over the observed data and the roughness measure. A smoothing parameter could be imposed to determine how close the smoothing follows the given data, whereas error weight may be introduced to consider some data point more consistent than others and provide additional flexibility during curve fitting. By choosing the smoothing parameter p closer to 1, the smoothed result will lie closer to the actual data point; while letting p closer to 0 a process converging to the least-squares (straight line) fit is operated.

The ping-to-ping changes in range were roughly found in theoretical agreement with changes in TS levels along a track. As a first approximation they could be associated with changes in animal orientation. Therefore, the smoothing was operated on the number of echoes N composing a track by imposing a smoothing array of parameters p_N based on the changes in backscattering cross sectional area and an array of weights w_N relative to the

ping-to-ping changes in range output. In practice, for the single echo *i* the related parameter and weight were determined by:

$$p_i = \frac{(\sigma_{bs})_i}{max(\sigma_{bs})} \; ; \qquad w_i = 1 - \frac{|(\Delta r_t)_i|}{max(|\Delta r_t|)} \tag{1}$$

with $(\Delta r_t)_i = (r_t)_{i+1} - (r_t)_i$. In this way, the parts of the track with stable ranges and stable and strong TS levels were better preserved, while the parts with substantial changes in range and unstable and lower TS were fitted by a least-squares process normalized by TS levels and changes in range. By adopting the relations (1) weak but valid echoes were preserved.

Fitting the data in horizontal plane

The horizontal information from the resolved echoes also needed supplementary treatment. The two mechanical angles β and α describe the direction of the target relative to the acoustic axis and are derived from the split-beam electrical phase differences of the incoming echo between the effective centres of the transducer halves (Foote *et al*., 1987). Therefore, they define the target position uniquely in the athwartship - alongship plane at the detected target range r_t. However, two sources of bias are expected to occur in ping-to-ping track angular positions. These are caused by the magnitudes of the finite target size and the split-beam system angular resolution, and low echo levels closer to the background noise.

With the nominal angular step of 0.061° in both the dimensions, a single horizontal cell resolution at 4.5 m depth is 5×5 mm^2 (with the diagonal of 7 mm). Thus, a 23 mm target subtends at least 4 angular cells (or an angle of 0.3 degree) at that range. This unequivocally introduces bias in the beam target position determination, and even if the target crosses the beam with a straight path, the mechanical angles of the track echoes appear scattered along the actual horizontal trajectory.

In addition, a target with echo level being close to the noise level may be resolved with corrupted phase measurements (Ehrenberg and Torkelson, 1996) resulting in erroneous beam angle position.

Under the hypothesis of straight movements with a constant swimming speed motivated by light attraction, the simple least-squares regression on the angle coordinates versus time was judged to be the correct approach (c.f. Mulligan and Chen, 2000). Since this fitting process assumes that one of the coordinates is known without error, regression versus elapsed time for each angle coordinate was determined, rather than regressing one coordinate on the other. In a further track selection analysis, the two regressions were then combined to obtain the horizontal trajectory across the acoustic beam.

For each echo composing the track, the Cartesian target position was estimated by the spatial coordinates obtained by:

$$z = r_t \cos\phi; \quad x = z \tan\beta; \quad y = z \tan\alpha \tag{2}$$

with $\phi = \tan^{-1}\left(\sqrt{\tan^2\beta + \tan^2\alpha}\right)$, r_t the target range resulting from the smoothing spline process, and α and β the beam angle positions calculated by the respective linear regressions.

By determining the spatial distance and the elapsed time between neighbouring echoes, the vector velocity and the related components (v_x, v_y, v_z) at each point of the track were

obtained. Then, it was also possible to estimate how much of the swimming effort between discrete positions was locally directed as vertical movement by:

$$\theta = \tan^{-1}\left(\frac{v_z}{\sqrt{{v_x}^2 + {v_y}^2}}\right) \quad (3)$$

Finally, the mean velocity of the target along the swimming path was calculated averaging the velocities from each successive echoes *i*:

$$\bar{v} = mean\left(\sqrt{{v_{x,i}}^2 + {v_{y,i}}^2 + {v_{z,i}}^2}\right) \quad (4)$$

The described processing was developed to smooth the data track points based on the assumption that the krill were swimming in the direction of the light more or less horizontally. In order to select a set of tracks that most probably complied with this assumption, a set of criteria was operated on the smoothed tracks: 1) the mean target range of the track should reside within the 2.5 to 6 m depth layer, which also correspond to the noise-free layer with respect to all frequencies compared; 2) at least 4 echoes should be detected inside the 6° beamwidth solid angle, assuring that TS and velocity determination would be based on a sufficient number of high quality data; 3) the slope of the horizontal trajectory should be ≥ |25°| with respect to the athwartship coordinate, to be more confident that an individual crosses the beam due to its attraction to the light; 4) the difference between maximum and minimum target range within the track should be ≤12 cm, i.e. 2.5 times the sample distance interval, to assure that krill were detected by the echosounder in a near horizontal trajectory when crossing the beam. Hereafter, the set of tracks satisfying these criteria is referred as "*horizontal tracks*".

From the synchronized pings, target range, beam position and beams overlapping information, it was possible to compute that 354 individual krill were detected at two or three frequencies along their swimming path. However, the total number of tracks manually retrieved with Sonar5 was 591, distributed by frequency as 203 at 70 kHz, 198 at 120 kHz, and 190 at 200 kHz. Among these, 417 satisfied the horizontal and light attraction movement criteria. The tracks were distributed between frequencies as follows: 138 at 70 kHz, 137 at 120 kHz and 142 at 200 kHz. The average number of echoes and recording time per track were equal to 58 and 6 seconds respectively, representing 174 individual krill.

All the mean-TS presented in this paper are calculated as arithmetic mean in linear domain according to the relationship:

$$\overline{TS} = 10\log\left(\overline{\sigma}_{bs}\right) = 10\log\left(\frac{1}{N}\sum_{i=1}^{N}(\sigma_{bs})_i\right) \quad (5)$$

where σ_{bs} is the backscattering cross section in m^2 and N is the number of TS values.

Results

Mesocosm population

The population of animals in the mesocosm was not solely composed of the Northern krill *Meganyctiphanes norvegica*. By the end of the experiments on 12 March the mesocosm was emptied and all live and dead individuals collected. The result of this sample analysis and the bottom debris containing dead animals collected regularly during the course of the experimental period show that 95 % of the organisms identified were of the target species *Meganyctiphanes norvegica*. The remaining 5 % of the organisms were other euphausiids like *Thysanoessa raschii*, *T. inermis*, *T. longicaudata*, *Nyctiphanes couchii*, while other organisms represented were amphipods (*Gammarus* sp.) and shrimps like *Pasiphea* sp., all in very low numbers.

The size distribution of living *Meganyctiphanes norvegica* by the end of experiments is given in Figure 4. The population represents definitely winter animals of different generations [0-group < 1 year old, I-group: ~1 ½ year old] at the time of the experiments, but the 0-group being the dominant size group, probably due to the fact that sampling where conducted in the uppermost part of the water column at night wherein the youngest generation usually dominate (Klevjer and Kaartvedt, 2006).

Older animals representing the I-group were present but in low numbers. Using the 'mixdist' package as part of the R-environment (Venables *et al.*, 2002) the average length of the dominating cohort of *Meganyctiphanes norvegica* was estimated to 21.8 ± 3.0 mm and for the larger size but significantly less abundant cohort to 27.8 ± 2.7 mm total length ($Df = 26$, $\chi^2 = 138.34$, $P < 2.2 \cdot 10^{-16}$). Thus, the animals constituting these two cohorts represent 79 % and 21 % of the population of *M. norvegica* in the mesocosm respectively.

Hydrography

From 2 February to 4 April 2004, 22 CTD casts were performed both inside and outside the mesocosm. During this period a slight increase in temperature and salinity of mesocosm seawater was observed, from 5.8 to 7.2 °C and from 34.8 to 35.2 psu respectively. This corresponds to a sound speed change of approximately 1470 to 1480 ms^{-1}. Essentially, the measurements showed that the mesocosm volume always consisted of a homogeneous seawater mass from 0.5 to 7 m depth. The variability observed in the upper 0.5 m was most likely caused by the air-water interface processes induced by solar warming, rain and snowfall. For the particular experiments described in this paper, the closest CTD measurements were performed on 1 and 4 March. In both the casts the measured salinity in the mesocosm water column was the same, while the temperature slightly increased by 0.3 °C. The CTD measurements performed on 1 March is taken as representative with a temperature of 5.45 ºC and a salinity of 35.16 psu. After entering these salinity and temperature values to the environmental menu in EK60 the computed seawater sound speed was 1476 ms^{-1}.

Ping-to-ping analysis

In order to illustrate the challenge in obtaining reasonable results from the analysis of the resolved echoes, Figure 5 shows the results before and after the smoothing process on the tracks for an euphausiid attracted by the fore light at the three frequencies. The upper panel a) shows the echoes range as extracted by the Sonar5 software (dots and grey line) with 6 dB max beam compensation. For all three frequencies it is evident the ping-to-ping

variability in target range determination increases when the target tends to change depth. This is particularly evident in the last part of the track at 200 kHz. However, when the target seems to maintain the same depth for a larger number of pings, the computed range to the target is considerably less variable. The coloured solid lines are the result of the smoothing of the range data as illustrated in Figure 3. Also, comparing the synchronized detections at all frequencies it is evident that the target ranges determined by EK60 echosounder are consistently different. The difference between 120 and 200 kHz is generally around to 2.5 cm, but more variable when the 70 kHz is compared with the other systems, from 1 to 4 cm with the 200 kHz data, from 1 to 3 cm comparing the 120 kHz. This is due to the difference in bandwidth of the systems hardware (Table 1) that bias the determination of the echo time, i.e. the time lag between the pulse transmission and reception of the echo, which is used for the indirect determination of the target range (Simmonds and MacLennan, 2005; Calise, 2009).

Figure 5b shows the processing result in the spatial z-coordinate that form the basis for the swimming velocity computations, while in Figure 5c the related TS data are plotted. In both panels, the solid symbols are the echoes estimated inside the 6° solid angle horizontal cross-section and accepted for the further TS analysis. The plots help to understand the effects of the adopted smoothing method and the restriction at 6° beamwidth. The cubic smoothing spline is a process based on the information from the neighbouring points. The lack of information before the start and after the end of a track slightly biases the fitting results. This is evident for the detections of the last part of the 120 kHz track in Figure 5b. Despite the corresponding data in Figure 5a follow the same trend as the 200 kHz, with the slope of both being nearly identical, the final smoothing in z-coordinate deviate substantially from each other. However, the detections in the 120 kHz data are at the periphery of the beam (open diamonds). Hence, by restricting the analysis to the echoes inside the 6° beamwidth the outer boundaries of a track can be ignored. On the other hand, tracks detected entirely outside this border will not be considered, even if they could provide useful information for some steps of the analysis; the 70 kHz track (Figure 5b and c) is such an example.

Observing the 200 kHz data (146 detections in 12.03 seconds) it seems that the target swims almost horizontally and quite fast, with max-min range difference of 8.1 cm along the 48 cm path with a mean velocity of 4 cm s^{-1}. Despite this, the variation in TS is large at all the frequencies (Figure 5c). For the shorter 70 kHz track (53 pings in 4.8 s), the minimum and maximum-TS values are -78.75 and -73.34 dB respectively, which means a difference of 5.4 dB. At 120 kHz the corresponding values are -77.24 and -67.73 dB, while at 200 kHz -79.27 and -67.09 dB, resulting in TS changes of 9.5 dB and 12.2 dB respectively. Comparing the TS-values from simultaneous detections at 120 and 200 kHz suggests that there is not a constant relationship or an explicit rule with respect to which frequency gives stronger backscattering strengths. This varies along the tracks. For some pings, the measured TS at 120 kHz are stronger than at 200 kHz, and vice versa.

It is also realized that changes in TS levels in Figure 5c do not always agree with changes in the vertical position of the animal (Figure 5b). This is particularly evident for the central part of the track at 200 kHz, where the vertical position (z) is very stable, but the corresponding change in TS is in the range of 4 dB, which is significant for an animal at close broadside incidence.

Hence, it is clear that the ping-to-ping data should be handled with care. Straightforward ping-to-ping analysis was performed by evaluating independently the local motion along each spatial coordinate and estimating the local influence of the vertical velocity, which in this set-up can be related to the local animal orientation. For each of the echoes composing the smoothed tracks, the local angle θ was determined by Equation (3) and the associated

TS for echoes with $\theta < 5°$ inside the 6º cut-off solid angle retrieved. Due to the segmentation of the tracks, only successive echoes with elapsed time less than $11/\bar{v}$, i.e. half of the minor krill modal length 22 mm over the mean velocity of track (Eq. (5)) in cm s^{-1}, were selected.

Figure 6 shows the TS distributions of all the selected detections at each frequency. The tails on the left side of the distribution reflect without doubts the inexactness of the smoothing results due to the ambiguities in target range of the echosounder output. If values less than 0.5 % are excluded, the distributions would present a left hand limit equal to -87, -82 and -83 dB for the 70, 120 and 200 kHz respectively. However, the majority of the occurrences are on the right side of the observed distribution range. These clearly show a bi-modal distribution for 70 kHz with modes at -80 and -75 dB, and for 120 kHz, with modes at -73.5 and -70 dB, while for the 200 kHz a left hand mode is much less evident and most of the observations occur around -70 dB. It is worth noting that distances between modes at 70 kHz is larger compared to 120 kHz, 5 and 3.5 dB respectively. Maximum TS values at the different frequencies are -69.73 dB, -63.96 and -65.04 dB for the 70, 120 and 200 kHz respectively.

In first approximation, the results in Figure 6 might be a gross overview of expected TS distributions for a population of euphasiids with lengths described in Figure 4. However, particular animals could be over-represented as the number of detections was not fixed for each tracked animal. In addition, the mentioned ambiguities might favour particular ranges of TS values than others. Despite straightforward, since the results were certainly derived from biased variables, the ping-to-ping analysis was judged to be a sort of instructive step rather than appropriate for ultimate results. Hence, further and more confident analyses were operated comparing the variables determined over the entire horizontal tracks. They are described in the next section.

Track analysis

In Figure 7 the distributions of the mean- and maximum TS determined for each of the horizontal tracks at a given frequency are shown in black bars. The grey bars represent the results of the tracks composed solely of the echoes satisfying the criterion with respect to θ as stated in the previous section. For that case, only tracks composed by at least 4 selected echoes were considered. The number of horizontal tracks was reduced to 286, with average number of echoes and recording time per track equal to 30 and 6.9 seconds respectively, representing 161 individual krill. The results and the simple statistics of the TS sets are listed in Table 2, where the mean and the standard deviation of the ping-to-ping TS variation within the tracks are also listed.

From the scattering theory of a fluid-like elongated organism, the maximum-TS of a krill indicates the scattering level at broadside incidence, i.e. animal in horizontal orientation with its dorsal side facing the transducer. The mean-TS however, indicates the TS value around which the scattering echo levels of a tracked krill are concentrated due also to the contributions of the flexing body, the pleopod beats and small changes in animal orientation during the swimming.

The results in Figure 7 show a bi-modal TS distribution at 70 kHz with modes for the means at -79.5 and -76 dB, and for the maxima at -78 and -75.5 dB. At 120 kHz there are some indications of bi-modality in the data, but less evident compared to 70 kHz. A similar feature can probably be observed for the means at 200 kHz, but not for the maxima. From Figure 7 and Table 2 it is evident the variability of TS at all frequencies is high, ranging from 12.8 to 17.7 dB, but relatively much lower at 200 kHz (12.8-14.3 dB) compared to the two other frequencies studied. Moreover, it can be noted that all the overall mean and

median of the tracks TS sets increase from lower to higher frequencies, as also do the minimum values. This trend is somewhat contradictory for the maximum TS values, where as a general trend the 120 kHz shows the highest TS levels.

Another relevant feature is the increasing ping-to-ping TS variability within the tracks (c.f. Table 2), both in mean value and standard deviation, as the frequency increases.

Comparing the basis of the previous ping-to-ping analysis, these results may better represent the strength levels to be expected from the mesocosm population at the studied frequencies.

However more confident result on the actual TS frequency response, i.e. target TS versus frequency, needed a refined selection among the horizontal tracks. A first attempt was done selecting individual krill tracked at all frequencies while crossing the 6° solid angle beam cross-sections intersection (darkest area in Figure 2) along their swimming path. Tracks related to 53 animals satisfied that condition; they were composed by a mean number of echoes equal to 70 and 7.1 seconds observing average time. Among those, only 27 animals were tracked with at least 3 synchronized pings at all the frequencies. Although of high interest, the number of observed animals was judged too low to represent the mesocosm krill population. Therefore, the horizontal tracks corresponding to individual krill detected by at least two frequencies inside their 6° beams cross-sections intersection (mid dark areas in Figure 2) were selected. Of course, this set of tracks contained the 159 tracks (53×3) recognized in the previous three contemporary frequency sets.

The ping times of these tracks were scrutinized to derive the pair-wise synchronized detections tracks at 70-120 kHz, 70-200 kHz and 120-200 kHz. For each frequency, tracks with at least 3 synchronized pings were grouped and their respective mean and maximum TS values derived. Figure 8 shows a summary of these results. The track means and maxima are plotted in black circles. The grey lines connect the synchronized detections; hence they illustrate the individual TS frequency response. The direct 70–200 kHz connections are not plotted for better readability. However, the single values are visible as isolated circles. The dashed black line is the frequency response relationship with respect to the overall means based on the TS values for each individual frequency and also listed in Table 2. The tracks were composed of an average number of synchronized pings equal to 19 and with a mean observation time of 3.1 seconds, and corresponding to 96 observed animals: 48 at 70 kHz, 91 at 120 kHz and 93 at 200 kHz.

In particular, 2703 synchronized echoes constituted the paired 120-200 kHz tracks. They were related to 88 animals represented by an average number of synchronized pings per tracks equal to 31 with 4.4 seconds mean observing time. The frequency response for that pair-wise data has two distinct patterns. For some tracks, the TS levels are stronger at 120 kHz, this occurs in 19 % and 11 % of the cases for the means and the maxima respectively (Figures 8a and 8b), and mainly for tracks with high 120 kHz TS levels. The differences in TS are 1.5 and 2.6 dB on average, but reaching values up to 3.7 and 5.2 dB for the means and the maxima of the tracks respectively. In 81 % and 89 % of the cases, with respect to the mean and maximum TS, the highest TS levels are observed at 200 kHz. In these cases the steepest slopes between the two frequencies are found for lower TS levels at 120 kHz, and the TS differences are 2 and 2.3 dB in average, with a maximum difference of 6.8 and 6.3 dB for the means and the maxima respectively.

Again, the ping-to-ping TS variation within the tracks increases with the frequency, approximately two times in mean and standard deviation from 70 to 200 kHz, when all the tracks at a single frequency were considered (Table 2). In particular, the mean and standard deviation (dB) of the mean ping-to-ping TS variations within the common 88 synchronized tracks for paired pings at 120 and 200 kHz were (0.8, 0.8) and (1.1, 0.7) respectively; while for the common 32 synchronized tracks at 70 and 120 were (0.7, 0.4) and (0.8, 0.5), and for

the common 36 synchronized tracks at 70 and 200 kHz (0.7, 0.5) and (1.8, 1.5). These results are relevant since the considered tracks are composed by same synchronized pings.

Swimming performance

In Figure 9, results on the computed swimming speeds for all horizontal tracks at the different frequencies are presented. The left panels show the frequency distributions of mean swimming speeds determined by Equation (4). At all three frequencies the majority of swimming speeds are found in the range 2-11 cm s^{-1}, with slightly different modal values from 70 to 200 kHz.

A right hand tail with swimming speeds in the range 11-17 cm s^{-1} is also present at all the frequencies. Referring to the modal krill lengths of the mesocosm population, i.e. 22 and 28 mm, those values correspond to a swimming speed of 4-6 and 5-8 body lengths per second (BL s^{-1}). Fitting each distribution to a theoretical Rician probability distribution function, which seemed to be a likely best fit for all three distributions, the mean values of swimming speed were estimated in the range from 5.7 to 6 cm s^{-1}, which correspond to 2-2.7 BL s^{-1} for the modal krill lengths in the mesocosm.

The right panels in Figure 9 illustrate the relationship of the mean swimming speed versus maximum-TS of the horizontal tracks for the three frequencies separately. The scattered dots are the related values for each of the horizontal tracks, while the solid lines are the least mean squares regressions of the linear amplitude of maximum-TS ($=10^{TSmax/20}$) on the mean swimming speed, retransformed to the logarithmic domain. Maximum TS of tracked targets was selected as the relevant parameter on the assumption that animal swimming capacity increases with size (Kils, 1981; Thomasson et al., 2003) as has often been also found for TS at a specific operative frequency (e.g. De Robertis *et al*., 2003).

The regressions indicate that maximum-TS increases with increasing swimming speed, having a positive slope for all frequencies, but with the steepest slope found at 120 kHz. Moreover, the regressions have also variable significance levels with p-values 0.1, 0.03 and 0.05 for 70, 120 and 200 kHz respectively, indicating that the relationship has the best fit for the 120 kHz data.

Discussion

Measuring target strength of weak scatterers like krill, which are elongate fluid-like zooplankters, is very challenging. Small changes in animal orientation could cause large changes in actually measured backscattering levels. Particularly this is the case at higher frequencies, where the scattering of an animal depend on the combination of the wavelength and its acoustically dimensions on respect to the incident wave. Although in volume backscattering data from a krill echo survey individual backscattering levels are averaged over a distribution of orientations, the effect of individual orientations has high space-temporal relevance (e.g. Demer and Conti, 2005). Thus, rigorous abundance estimation may only be obtained if an appropriate methodology for the determination of *in situ* animal orientation during acoustic acquisition is developed taking also into account all aspects of the animal behaviour in seasonal and daily rhythms. Some practical and numerical approaches using video tools and TS theoretical predictions have been presented recently

(c.f. Demer and Conti, 2005; Conti and Demer, 2006; Lawson *et al.*, 2006), but an appropriate standard and systematic procedure is still not established.

Under the assumption that krill swim mostly horizontally in their natural habitat, the present study represents an attempt to identify the actual differences in scattering intensity between common survey frequencies that can be realistic in future abundance estimation works. Although the established mesocosm simulated quit well a deep pelagic habitat, the results were obtained by forcing the animals to swim directionally by light attraction and assuming a more defined orientation rather than rely on measurements of scattering from the organisms free to swim in the mesocosm volume without any stimulation. Such an approach, assuming a close to zero-mean distribution of orientations *in situ*, mat also lead to a more convincing comparison in a multifrequency context between theoretical predictions and measured scattering intensities. In addition, the analyses executed on the data were refined in successive steps to assure a more controlled process and confidence of the results.

Methodological aspects

The effectiveness of the krill attraction to the lamps in the mesocosm venue established at Austevoll Aquaculture Research Station is discussed in Calise *et al*. (2005). The observed trajectories of the detected krill when crossing the beams were all found to be directional during light periods, either towards the positive or the negative alongship split-beam coordinate, depending on the lamp being activated.

Video inspections executed during the entire experimental period in the mesocosm, as well as acoustic visualizations during the current study revealed no evidence of krill schooling behaviour. The animals were acoustically detected as single targets at any time of the day at all operative frequencies in the depth layer from 0.5 to 6.5 m. Higher concentration in the lower layers during daylight hours were observed, while during night time the animals were mostly uniformly distributed within the entire mesocosm volume.

For the analysis of the specific experiment described here, due to the narrow depth channel being examined, as well as the possibility of magnifying the echograms and the restriction in SED settings, we are confident that no multiple echoes were retrieved during the manual tracking of individual targets. By means of a built-in Sonar5 tool, the maximum Sawada index (Sawada *et al.*, 1993), i.e. the average number of targets within the sampling volume, among the parts of echograms representative of the light switching periods was found equal to 0.02, which is much less than the acceptable limit. It must be also mentioned that within the complete data set, multiple targets were detected only for 8 pings, but at most only two targets in a given ping.

Short range detections might bias the adopted vertical smoothing process as well the observed TS levels. The synchronized detections of an individual krill in Figure 5a showed differences in target range output between the three systems. When a target is at short distances to the transducer error in target range determination has to be expected. This is the effect of the so called “receiver or system delay”, which is due to the echo pulse deformation being a consequence of the passages through hardware units with finite bandwidth (Simmonds and MacLennan, 2005). The delay depends on the pulse duration and system receiver bandwidth. The latter was different for the operating EK60 systems (Table 1) at similar pulse duration, and reflects the differences in simultaneous detected range of the same target. Measurements on standard target spheres in a monitored tank at fixed distances from transducers showed that the range delay for the EK60 systems decreases with increasing distance from the transducer face (Calise, 2009). In the range of 2-10 m this effect could be modelled using a simple linear regression relationship. However, inspection

on the synchronized krill detections showed that the differences in range between the frequencies were neither constant nor significantly dependent on the depth. This indicates that for short range detections of weak mobile targets the ER60 target range algorithm is highly and unsystematically biased. Thus, it has been judged more convenient to not implement a general range delay correction before the smoothing of the current data set. The potential bias in TS output due to the range determination error has also been ignored. Calise (2009) showed that the expected range effects on the target strength from standard targets were not clearly defined, suggesting that no correction in strength quantities has to be applied during post-processing. There is an urgent need to conduct more specific work that addresses these unresolved issues.

The criteria established to select the horizontal tracks were substantially justified by the experimental set-up, acoustic instrumentation and considerations with respect to krill behaviour. The choice to restrict the slope of the horizontal trajectory to $\geq |25°|$ with respect to the athwarthship coordinate derived from the fact that the light field was not directional and the acoustic axes were more than 2.5 m away from the light sources. Additional analysis with wider slope angles up to 40º showed no significant changes in the trends of the TS distributions in Figure 7, but only a minor reduction in number of selected tracks. Similar inspections on the parameters set for the other criteria revealed that the TS results were more sensitive to the "minimum target range variability" within a track. In some way this was not a surprise since this criterion more directly related to the selection of krill tracked during their horizontal swimming, and confirms the general efficacy of the adopted methodology. Setting this parameter equal to 2.5 times the sample distance interval was chosen considering the EK60 system processing, in particular the principle of gravity used by the ER60 for target range determination (Calise, 2009). In that formulation, the quantity $c\tau/4$, with c the medium sound speed in m s^{-1} and τ the pulse duration in seconds, related to half of the sample distance interval is subtracted from a summation of the samples ranges around the pulse peak. Since the target range was recognized very sensitive to biases, this criterion parameter was set assuming a potential error of one sample distance interval plus $c\tau/4$ over the entire track. Thus, the parameter was set equal to 12 cm which was large enough to obtain a good number of tracks and assure range errors within reasonable limits. For larger values of this parameter, the TS distributions were slightly different, with particular increasing Δ in Table 2.

With a relatively restricted insonified volume in the mesocosm, it is clear that the probability to detect a target was quite low, especially simultaneously at the three frequencies. The hypothesis that the entire distribution of mesocosm population has been represented by the results in Table 2 and Figure 7 is the main concern in this study. It might also be possible that particular sizes of individuals have faster responses to a switching light environment; hence such animals might have been overrepresented. However, the wide range of TS levels and swimming speed results strongly support that the initial set of tracks were representative of the krill mesocosm population.

Target strength

Due to the orientation, highly oscillating patterns of krill target strength have been recognized in experimental measurements at a specific frequency (e.g. Demer and Martin, 1995; Stanton, *et al.*, 1998a; McGehee *et al.*, 1998; Martin Traykovsky *et al.*, 1998; Amakasu and Furusawa, 2006; Klevjer and Kaartvedt, 2006). In general, the target strength must always be considered a stochastic parameter characterising the scatterer over a large distribution of values (MacLennan, 1990). In the case of krill, when an individual swims the

body flexes, and the separate contributions to the scattering from the exoskeleton segments, the tail, the antennas and the eyes, as well its pleopod beats certainly increase the stochastic nature of the process. Theoretical predictions also indicate that there is no linear dependence on TS with respect the length for the frequencies that has been applied in the present work and for those commonly used during scientific survey work, underlining the uncertainties in applying identification algorithms to the survey data.

In this study, except the initial step in skipping echoes with unrealistic jitter (Fig. 5), no restrictions on TS have been applied. Although the orientation of the tracked krill could be assumed close to horizontal, large variability in the TS statistics of a selected track has been found for all frequencies (Table 2). Such variability would be much less evident analysing acoustic volume backscattering survey data being determined by integration of a large ensemble of data, thus representing an average quantity. Higher variability may also be explained by the extreme sensitivity of the acoustic instrumentation used. However, it has been documented that the ping-to-ping TS variation between consecutive echoes from an animal swimming with identical 3D spatial direction and speed, was very low (c.f. Figure 5). Klevjer and Kaartvedt (2006) found higher *in situ* ping-to-ping TS variability for later identified *M. norvegica* with almost the same length distribution as in the present work, but over a presumably wider range of orientations.

Few results of direct acoustic target strength *in* or *ex situ* on *Meganyctiphanes norvegica* specimens have been presented in the literature (Kristensen and Dalen, 1986; Greene *et al*., 1988; Stanton *et al*., 1998a; Conti *et al*., 2005; Klevjer and Kaartvedt, 2006). Some related results are also reported in Richter (1985), and Stanton *et al*. (1994; 1998a).

Due to the range of operative frequencies, length of the animals under investigation, location and seasonal aspects with respect to when animals were caught as well as the methods and instrumentation used in acquiring the data, it is difficult to proceed to a proper comparison with other studies. In general, our target strengths measured seem to be slightly higher then the earlier observations. It must be also noted that, to our knowledge, the non-linear effects for high-power transmissions at higher frequencies were not considered in any of the previous studies. The magnitude of the energy transferred from the fundamental frequency into higher harmonics is indeed important (Tichy *et al*., 2003; Pedersen, 2007). In specific cases, the related attenuation at the nominal frequency lead to significant and unpredictable reduction of the acquired target strengths levels, representing an additional reason of the difficulty of appropriate comparison between studies.

This seems to be also the case for the results presented by Klevjer and Kaartvedt (2006) at 120 kHz from a *M. norvegica* population measured *in situ*. In their study, the animals were of similar mean lengths (c.f. TT in Morris *et al*., 1988) to those investigated here, and observed approximately in the same season (November 2003 – February 2004) in Oslofjord, a location probably not very different from Raunefjord, i.e. location where the animals of the present study were caught. This should favour the comparison of the results since the animals investigated in the two studies would be quite similar in terms of biological and physical properties. The reported average TS are in some cases close, but generally lower than in the present study. In Table 2 of Klevjer and Kaartvedt paper, the listed average TS levels vary from -76.6 to -70.1 dB at 120 kHz for animals in the range 19.6 – 32.4 mm mean length; while in the present study the average TS at 120 kHz and similar sized animals have a range from-71.9 to -69.6 dB (Table 2). Klevjer and Kaartvedt (2006) did not mention the EK60 power setting when detected free swimming *M. norvegica* specimens, mostly at a typical range of 10 m from the transducer. In a personal communication, T. A. Klevjer confirms that a power setting of 400 W was used during their investigation.

For an operative EK60 at 120 kHz with close transmit power to the transducer of 500 W, Pedersen (2007) estimated a non linear attenuation to approximately 0.5 dB at 9 m distance from the transducer. However, while in the present study it is assumed that the animal orientation is close to broadside incidence, in the Klevjer and Kaartvedt study the animals were measured *in situ* and their results may reflect a wider range of animal orientations reflecting also lower TS levels. The combination of the above mentioned effects could actually explain the difference between the two studies. In addition, in Klevjer and Kaartvedt work the time lag between the acoustic measurements and the trawl identification of scatterers could have induced a bias in their TS-length relationships. This may to some extent explain their finding of higher levels of TS for smaller sized animals (c.f. Table 2 in their paper), which according to the current knowledge and the present work are somewhat unexpected at 120 kHz.

Both this study and the work of Klevjer and Kaartvedt (2006) on *M. norvegica* show higher target strength at 120 kHz compared to the reported average TS from Antarctic krill of approximately the same length (Foote *et al*., 1990; McGehee *et al.*, 1998; Pauly and Penrose, 1998; Lawson *et al.*, 2006). However, differences in TS levels between the two species have to be expected. *Euphausia superba* has different diet preferences and most likely biochemical composition compared to *M. norvegica*, probably throughout its life cycle. The time of measurement with respect to animal maturation processes might also be a key factor in determining the range as well as peak target strength values. The body material properties involved in the scattering process could therefore be considerably different, considering *Euphausia superba* being a herbivorous species throughout its life span (e.g. McClatchie, 1985) while *Meganyctiphanes norvegica* are normally omnivorous, but often carnivorous during autumn and winter seasons depending slightly on the size of the animals (Saether *et al.*, 1986).

The inspection of the synchronized echoes from the paired 120-200 kHz tracks in Figure 8 reveals that for the majority of tracked animals target strength was found higher at 200 kHz compared to 120 kHz. For the remaining cases, target strengths at 120 kHz were higher than at 200k Hz. This suggests that animal size is a key parameter influencing target strength for identically oriented animals, but from the present study this influence cannot be directly quantified. However, the range of krill lengths represented in the mesocosm population reflects the variability of the transition between Rayleigh and Geometric scattering regions. The combined result from these two frequencies might thus be used in deriving a relative composition of different size groups within an *in situ* aggregation of *M. norvegica*. A separate paper on measurements performed on tethered *M. norvegica* spanning the length range from 22 to 33 mm addresses this aspect, suggesting a possible change in transition region starting from a body length starting of approximately 27 mm (Calise and Knutsen, 2009).

Swimming speed

Since the schooling formation during the acquisition was without doubt excluded, the estimated swimming speeds presented here have to be ascribed to single swimming behaviour rather than as effect of krill schooling formation. In general, the results are favorably in agreement with previous reports on euphausiid species noticeably summarized in De Robertis *et al*. (2003). Similar results have been also recently obtained by Klevjer and Kaartvedt (2003; 2006) tracking targets *in situ* and later identified as *M. norvegica* specimens.

As mentioned, because of the species and the size of the organisms investigated in this study, it could be assumed that the single individuals were horizontally orientated when swimming straightforward, to reduce the energetic costs of locomotion (Cochrane *et al*., 1994). On the contrary, Miyashita *et al.* (1996) have observed smaller euphausiid species *Euphausia pacifica* in aquaria reaching high speeds with swimming angles much different from zero. The tank utilized by Miyashita *et al.* (1996) was very small (60×30×35 cm) and this might induce significant constraints on animal behaviour, especially at high concentrations of animals. The authors have also reported contacts between specimens during the swimming activity, which is particularly atypical since during aggregate swimming, the specimens maintain constant interindividual distance by detecting the propulsion jet of the surrounding individuals with the antennular flow receptors (e.g. Wiese and Ebina, 1995; Patria and Wiese, 2004). However, Miyashita *et al.* (1996) claimed that the difference in mean swimming angles found between *Euphausia pacifica* and published values of the Antarctic krill *Euphausia superba*, which is more similar to *M. norvegica*, could be attributed to differences in body form, although this interpretation might be somewhat speculative given the nature of their experiments.

The mesocosm used in the present study seems to offer a large enough volume to simulate a deep pelagic habitat and let the animals swim without any external or behavioural constraints, allowing perfect conditions for a swimming investigation. The swimming speed distributions at all the frequencies support the notion that the majority of animals are quite similar in terms of their swimming speed capacity. However, a smaller group of individuals seem to have a greater swimming capacity, hence could reflect the presence of the larger size group of krill found in the mesocosm.

At 120 and 200 kHz the swimming speed distributions are very similar, while the somewhat right skewed distribution at 70 kHz (c.f. Figure 9) might reflect that smaller and slower individuals are less well detected at this frequency because they are weak targets having backscattering intensities close to the background noise. It could also be due to data treatment when skipping unrealistic echoes (c.f. Figure 2). Since the range of extracted TS at this frequency compares with the other two frequencies this issue is still not fully explained.

Thomasson *et al*. (2003) in their specific investigation of swimming capacity of *M. norvegica* found that there is no significant difference between males and females. This gives us confidence that sexual difference in swimming performance is a non-issue with respect to the present study. Ovarian development and related lipid contents may certainly influence body shape, hence animal swimming capacity. The animals in the present study were mostly 0-group individuals that at the time of investigations were either immature or maybe only in a very early phase of maturation. Therefore it was not given particular attention to how this could affect animal swimming speeds nor target strengths of the animals.

Conclusion

Studying krill in a large mesocosm, as during the present work, has proved a valuable way of obtaining high quality measurements of *M. norvegica* target strength. It allows various approaches and methods to be applied, and to a certain extent also control krill behavior using underwater lamps. For sure the techniques used in the present work can be further

developed, in particular on the determination of the size of each individual krill or the concentration of individuals being used for the experiments.

For the mesocosm population of *Meganyctiphanes norvegica* having a total length "TT" in the range 14 – 34 mm, the target strength range decreases with the frequency and in some cases quite large (up to 20 dB), despite the orientation was anticipated to be close to horizontal. At 70 kHz the TS range was [-88.3, -68.3] dB with a mean value of -77.2 dB, while at 120 kHz the TS range was [-83.8, -63.9] dB and mean -71.5 dB and at 200 kHz [-80.8, -63.5] dB with a mean of -70.9.4 dB. On the contrary, the ping-to-ping variability inside the tracks was found to increase with the frequency. However, when a horizontally swimming krill maintains its depth with a more or less constant swimming speed and presumably tilt angle, variability in target strength is significantly reduced.

The individual frequency response of the studied krill in the TS domain shows particular differences at 120 and 200 kHz. For the majority of tracked animals the target strength was found higher at 200 kHz compared to 120 kHz for synchronized ping detections, but a good number showed an opposite trend. The intriguing differences found between these two frequencies suggest that the size mixture of krill in the mesocosm is exposed to the physical effects of the transition between Rayleigh and Geometric scattering regions.

The swimming speeds of the animals in the mesocosm when attracted to the submerged lamps seem to support the notion that there were two size groups of animals with significantly different swimming capacity. It is realized however, that it is not the maximum swimming speed that was measured, but rather a swimming speed that can be related to the animals' motivation to direct their attention in a special direction.

It is suggested that future work on krill target strength should proceed through studies conducted in large enclosures such as the mesocosm described in the present work. Understanding and quantifying target strength and its variability should be a key task in all works concerning target organisms for acoustic survey abundance estimation and acoustic modelling.

In order to refine our understanding of acoustic scattering and the potential for acoustic characterization and identification of scatterers, the application of wide-band systems is a natural next step for better understanding of TS patterns and more accurate comparison with theoretical model predictions. Conti *et al.* (2005) suggested that *Meganyctiphanes norvegica* may be used as an acoustic krill model species. However, present results suggest that utmost care is necessary when applying results from Northern krill to that of Antarctic krill. With respect to the adoption of the frequency response and inversion techniques as tools in acoustic classification, the need for improved resolution is warranted. Also in this case broadband instrumentation seems a very promising and necessary pathway to explore.

Acknowledgements

Arve Kristiansen, Aquaculture Research Station of the Institute of Marine Research (IMR), Norway is particularly thanked for the help on all the practical tasks during the experimental period. Harald Fitje and his assistants at IMR's mechanical workshop are thanked for making the transducer rig on short notice and for elegant mechanical solutions. Mr. Are Johansen and Dr. Frank Reier-Knudsen at Simrad AS are acknowledged for their skilled support through all phases of the experiments and for making available parts of the acoustic system. The IMR is thanked for making the project possible through funding via the internal

program on “New feed resources for the Aquaculture industry”. The Research Council of Norway (RCN) is thanked for partial support through the project “Harvesting at lower trophic levels - stock assessment and ecological consequences” project no. 178447. This is also a contribution to The Barents Sea Ecosystem Programme and the Norw**e**gian Sea Ecosystem Programme at IMR. The University of Bergen (UiB), Norway, is thanked for the LC financial supporting under the UiB PhD fellowship program.

References

Amakasu, K., and Furusawa, M. 2006. The target strength of Antarctic krill (*Euphausia superba*) measured by the split-beam method in a small tank at 70 kHz. ICES Journal of Marine Science, 63 (1): 36-45.

Andersen, L. N. 2001. The new Simrad EK60 scientific echo sounder system. Journal of the Acoustical Society of America, 109 (5): 2336.

Balk, H., and Lindem, T. 2005. Sonar4, Sonar5 and Sonar6 post processing systems, Operator manual version 5.9.6. Lindem Data Acquisition, Humleveien 4b, 0870 Oslo, Norway, 380 pp.

Calise, L., Knutsen, T., and Melle, W. 2005. Multifrequency Acoustic Measurements of free swimming northern krill (*Meganyctiphanes norvegica*) in a mesocosm venue: methodological challenges. Proceedings of the International Conference “Underwater Acoustic Measurements: Technologies & Results”, Vol. II, pages 865-871, Heraklion, Crete, Greece, 28th June – 1st July.

Calise, L. 2009. Short-range performances of a scientific echosounder with enphasis on accurate calibration. In preparation. Paper III of this thesis.

Calise, L., and Knutsen, T. 2009. Multifrequency target strength of Northern krill Meganyctiphanes norvegica: measurements on tethered specimens and SDWBA theoretical predictions. In preparation. Paper V of this thesis

Chu, D., Stanton, T. K, and Wiebe, P. H. 1992. Frequency dependence of sound backscattering from live individual zooplankton. ICES Journal of Marine Science, 49 (1): 97-106.

Cochrane, N. A., Sameoto, D. D., Herman, A. W., and Neilson, J. 1991. Multiple-frequency acoustic backscattering and zooplankton aggregations in the inner Scotian Shelf Basins. Canadian Journal of Fisheries and Aquatic Sciences, 48 (3): 340-355.

Cochrane, N. A., Sameoto, D.D., and Belliveau, D. J. 1994. Temporal variability of euphausiid concentrations in a Nova Scotia shelf basin using a bottom- mounted acoustic Doppler current profiler. Marine Ecology Progress Series, 107: 55-66.

Conti, S. G., Demer, D. A., and Brierley, A.S. 2005. Broad-bandwidth, sound scattering, and absorption from krill (*Meganyctiphanes norvegica*), mysids (*Praunus flexuosus* and *Neomysis integer*), and shrimp (*Crangon crangon*). ICES Journal of Marine Science, 62 (5): 956-965.

Conti, S. G., and Demer, D. A. 2006. Improved parameterization of the SDWBA for estimating krill target strength. ICES Journal of Marine Science, 63 (5): 928-935.

de Boor, C. 2001. Calculation of the smoothing spline with weighted roughness measure. Mathematical Models and Methods in Applied Sciences, 11 (1): 33-41.

De Robertis**,** A., Schell**,** C., and Jaffe, J. S. 2003. Acoustic observations of the swimming behavior of the euphausiid Euphausia pacifica Hansen. ICES Journal of Marine Science, 60 (4): 885 – 898.

Demer, D. A., and Martin, L. V. 1995. Zooplankton target strength: Volumetric or areal dependence?. Journal of the Acoustical Society of America, 98 (2): 1111-1118.

Demer, D. A., Soule, M. A., and Hewitt, R. P. 1999. A multiple-frequency method for potentially improving the accuracy and precision of in situ target strength measurements. Journal of the Acoustical Society of America, 105 (4): 2359-2376.

Demer, D. A., and Conti, S. G. 2003. Reconciling theoretical versus empirical target strengths of krill: effects of phase variability on the distorted-wave Born approximation. ICES Journal of Marine Science, 60 (2): 429-434.

Demer, D. A. 2004. An estimate of error for the CCAMLR 2000 survey estimate of krill biomass. Deep Sea Research Part II: Topical Studies in Oceanography, 51 (12-13): 1237-1251.

Demer, D. A., and Conti, S. G. 2005. New target-strength model indicates more krill in the Southern Ocean. ICES Journal of Marine Science, 62 (1): 25-32.

De Robertis, A., Schell, C., and Jaffe, J. S. 2003. Acoustic observations of the swimming behavior of the euphausiid Euphausia pacifica Hansen. ICES Journal of Marine Science, 60 (4): 885–898.

Ehrenberg, J. E., and Torkelson, T. C. 1996. Application of dual-beam and split-beam target tracking in fisheries acoustics, 53 (2): 329-334.

Endo, Y. 1993. Orientation of Antartic krill in an aquarium. Nippon Suisan Gakkaishi, 59 (3): 465-468.

Everson, I. 1982. Diurnal variations in mean volume backscattering strength of an Antarctic krill (*Euphausia superba*) patch. Journal of Plankton Research, 4 (1): 155-162.

Fleischman, S. J., Burwen, D. L., 2000. Correcting for position-related bias in estimates of the acoustic backscattering cross-section. Aquatic Living Resources, 13: 283–290.

Foote, K. G., Vestnes, H. P., McLennan, D. N., and Simmonds E. J. 1987. Calibration of acoustic instruments for fish density estimation: a practical guide. Cooperative Research Report ICES, 144, 69 pp.

Foote, K. G., Everson, I., Watkins, J. L., and Bone, D. G. 1990. Target strengths of Antarctic krill (*Euphausia superba*) at 38 and 120 kHz. Journal of the Acoustical Society of America, 87 (1): 16-24.

Foote, K. G. 1991. Summary of methods for determining fish target strength at ultrasonic frequencies. ICES Journal of Marine Science, 48 (2): 211-217.

Foote, K. G., and Stanton, T. K. 2000. Acoustical methods. In ICES Zooplankton Methodology Manual, Chapter 6: 223-258, Ed. by R. Harris, H.R. Skjoldal, J.Lenz, P. Wiebe and M. Huntley. Academic Press, 684 pp.

Greene, C. H., Wiebe, P. H., Burczynski, J., and Youngbluth, M. J. 1988. Acoustical detection of high-density demersal krill layers in the submarine canyons off Georges Bank. Science, 241: 359-361

Greenlaw C.F., 1979. Acoustical estimation of zooplankton populations. Limnology and Oceanography, 24 (2): 226-242.

Greenlaw, C. F., Johnson, R. K., and Pommeranz, T., 1980. Volume scattering strength predictions for Antarctic krill (Euphausia superba Dana). Meeresforschung, 28: 48-55.

Hamner, W. M. 1984. Aspects of schooling in Euphausia superba. Journal of Crustacean Biology, 4 (1): 67–74

Hamner, W. M., and Hamner, P.P. 2000. Behavior of Antarctic krill (*Euphausia superba*): schooling, foraging, and antipredatory behaviour. Canadian Journal of Fisheries and Aquatic Science, 57 (S3): 192-202.

Herman, A. W., Cochrane, N. A., and Sameoto, D.D. 1993. Detection and Abundance Estimation of Euphausiids Using an Optical Plankton Counter. Marine Ecology Progress Series, 94: 165-173.

Holliday, D. V., and Pieper, R.,E. 1995. Bioacoustical oceanography at high frequencies. ICES Journal of Marine Science, 52 (3): 279-296.

Kieser R., Mulligan T. K., Ehrenberg J. E. 2000. Observation and explanation of systematic split-beam angle measurements. Aquatic Living Resources, 13: 275–281.

Kils, U. 1981. The swimming behaviour, swimming performance and energy balance of Antartic krill, *Euphasia superba*. BIOMASS Scientific Series, No.3, 122 pp.

Klevjer, T. A., and Kaartvedt, S. 2003. Split-beam target tracking can be used to study the swimming behaviour of deep-living plankton in situ. Aquatic Living Resources, 16 (3): 293-298.

Klevjer, T. A., and Kaartvedt, S. 2006. *In situ* target strength and behaviour of northern krill (*Meganyctiphanes norvegica*). ICES Journal of Marine Science, 63 (9):1726-1735.

Korneliussen, R. J., Diner, N., Ona, E., Berger, L., and Fernandes, P. G., 2008. Proposals for the collection of multifrequency acoustic data. ICES Journal of Marine Science, 65 (6): 982-994.

Lawson, G. L., Wiebe, P. H., Ashjian, C. J., Chu, D., and Stanton, T.K. 2006. Improved parametrization of Antarctic krill target strength models. Journal of the Acoustical Society of America, 119 (1): 232-242.

Lawson, G. L., Wiebe, P. H., Stanton, T. K., and Ashjian, C. J. 2008. Euphausiid distribution along the Western Antarctic Peninsula – Part A: Development of robust multi-frequency acoustic techniques to identify euphausiid aggregations and quantify euphausiid size, abundance, and biomass. Deep Sea Research Part II: Topical Studies in Oceanography, 55 (3-4): 412-431.

MacLennan, D. N. 1990. Acoustical measurement of fish abundance. Journal of the Acoustical Society of America, 87 (1): 1-15.

Martin Traykovski, L. V., Stanton, T. K., Wiebe, P. H., and Lynch, J. F., 1998. Model based Covariance Mean Variance Classification (CMVC) techniques: Algorithm development and application to the acoustic classification of zooplankton. IEEE Journal of Oceanic Engineering, 23 (4): 344-364.

Mauchline, J., and Fisher, L. R. 1969. The biology of euphausiids. Advances in Marine Biology, No. 7, 454 pp.

McClatchie, S. 1985. Feeding behaviour in *Meganyctiphanes norvegica* (M. Sars) (Crustacea: Euphausiacea). Journal of Experimental Marine Biology and Ecology, 86 (3): 271-284.

McGehee, D. E., O'Driscoll, R. L., and Martin Traykovski, L. V. 1998. Effect of Oreintation on Acoustic Scattering from Antarctic Krill at 120 kHz. Deep-Sea Research Part II, Topical Studies in Oceanography, 45 (7): 1273-1294.

Medwin, H., and Clay, C. S. 1997. Fundamentals of Acoustical Oceanography. Academic Press, 712 pp.

Miyashita, K., Aoki, I., and Inagaki, T. 1996. Swimming behaviour and target strength of isada krill (*Euphausia pacifica*). ICES Journal of Marine Science, 53 (2): 303-308.

Mulligan, T. J., and Chen, D. G. 2000. Comment on "Can stationary bottom split-beam hydro-acoustics be used to measure fish swimming speed in situ?' by Arrhenius et al. Fisheries Research, 49 (1): 93-96.

Ona, E., and Barange, M. 1999. Single-target recognition. *In* Methodology for Target Strength Measurements, Ed. by E. Ona, ICES Cooperative Research Report NO. 235: 27-47.

Pauly, T., and Penrose, J. D. 1998. Laboratory target strength measurements of free-swimming Antarctic krill (*Euphausia superba*). Journal of the Acoustical Society of America, 103 (6): 3268-3280.

Patria, M. P., and Wiese, K. 2004. Swimming in formation in krill (Euphausiacea), a hypothesis: dynamics of the flow field, properties of antennular sensor systems and a sensory–motor link. Journal of Plankton Research, 26 (11): 1315-1325.

Pedersen, A. 2007. Effects of nonlinear sound propagation in fisheries research. Dissertation for the degree of philosophiae doctor (PhD), University of Bergen, Norway, 307 pp. (available on net at: https://bora.uib.no/).

Richter, K. E. 1985. Acoustic scattering at 1.2 MHz from individuals zooplankters and copepod populations. Deep Sea Research, Part A: Oceanographic Research Papers, 32 (2): 149-161.

Sameoto, D., Cochrane, N., and Herman, A. 1993. Convergence of acoustic, optical, and net-catch estimates of euphausiid abundance: use of artificial light to reduce net avoidance. Canadian Journal of Fisheries and Aquatic Science, 50 (2): 334-346.

Sawada, K., Furusawa, M., and Williamson, N. J. 1993. Conditions for the precise measurement of fish target strength in situ. The Journal of the Marine Acoustic Society of Japan 20:73–79.

Simmonds, J., and MacLennan, D. 2005. Fisheries Acoustics: theory and practice, 2nd edn, Fish and aquatic resources series 10, Blakwell Publishing, 419 pp.

Simrad, Norge 2003. Simrad EK60 Scientific echo sounder. Instruction manual 850-16496/Rev.A. Simrad AS, Horten, Norway.

Soule, M., Barange, M., Solli, H., and Hampton, I. 1997. Performance of a new phase algorithm for discriminating between single and overlapping echoes in a split-beam echosounder. ICES Journal of Marine Science, 54 (5): 934-938.

Stanton, T. K., Wiebe, P. H., Chu, D., Benfield, M. C., Scanlon, L., Martin, L. V., and Eastwood, R. L. 1994. On acoustic estimates of zooplankton biomass. ICES Journal of Marine Science, 51 (4): 505-512.

Stanton, T. K., Chu, D., Wiebe, P. H., Martin, L. V., and Eastwood, R. L. 1998a. Sound scattering by several zooplankton groups. I. Experimental determination of dominant scattering mechanisms. Journal of the Acoustical Society of America, 103 (1): 225-235.

Stanton, T. K., Chu, D., and Wiebe, P. H. 1998b. Sound Scattering by Several Zooplankton Groups II: Scattering Models. Journal of the Acoustical Society of America, 103 (1): 236-253.

Thomasson, M. A., Johnson, M. L., Stromberg, J. O., and Gaten, E. 2003. Swimming capacity and pleopod beat rate as a function of sex, size and. moult stage in Northern krill *Meganyctiphanes norvegica*. Marine Ecology Progress Series, 250: 205-213.

Tichy, F. T., Solli, H., and Klaveness, H. 2003. Non-linear effects in a 200-kHz sound beam and the conseguences for target-strength measurement. ICES Journal of Marine Science, 62 (3): 571-574.

Venables, W. N., and Smith, D. M. 2002. An Introduction to R. Network Theory Limited, Bristol, United Kingdom. pp. 156.

Wiebe, P. H., Boyd, S. H., Davis, B. M., and Cox, J. L. 1982. Avoidance of towed nets by the euphausiid *Nematoscelis megalops*. Fishery Bulletin, 80 (1): 75-91.

Wiese, K., and Ebina, Y. 1995. The propulsion jet of Euphausia superba (Antarctic krill) as potential communication signal among conspecifics. Journal of the Marine Biological Association of the United Kingdom, 75 (1): 43–54.

FIGURES

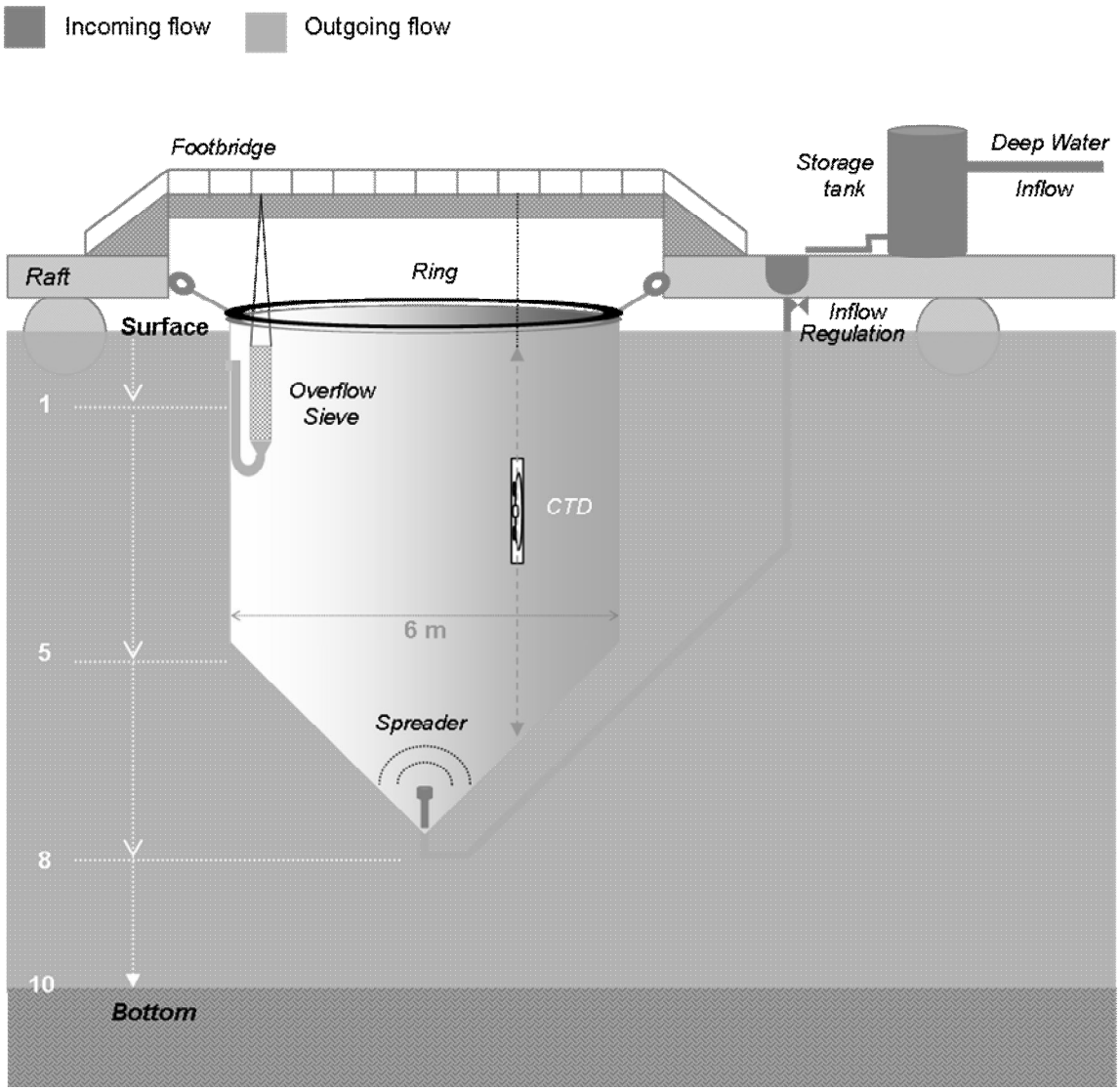

Figure 1. Mesocosm set-up and monitoring at Austevoll Aquaculture Research Station.

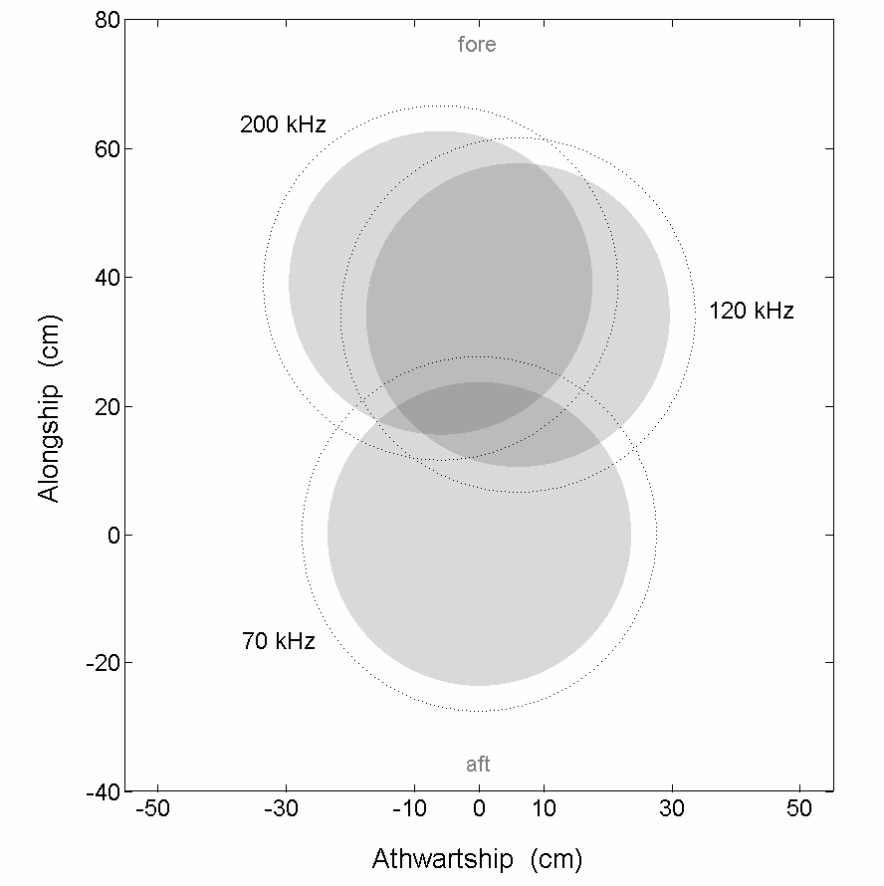

Figure 2. Horizontal beam foot-prints and joint areas in athwartship-alongship coordinates at 4.5 m depth. Dotted lines are the edges of the nominal -3 dB max power beam angle (7°); grey areas represent the full 6° degree sections wherein the echoes were accepted for the TS analysis. The fore and aft directions of the alongship split-beam coordinates are also indicated to illustrate the lamp positions.

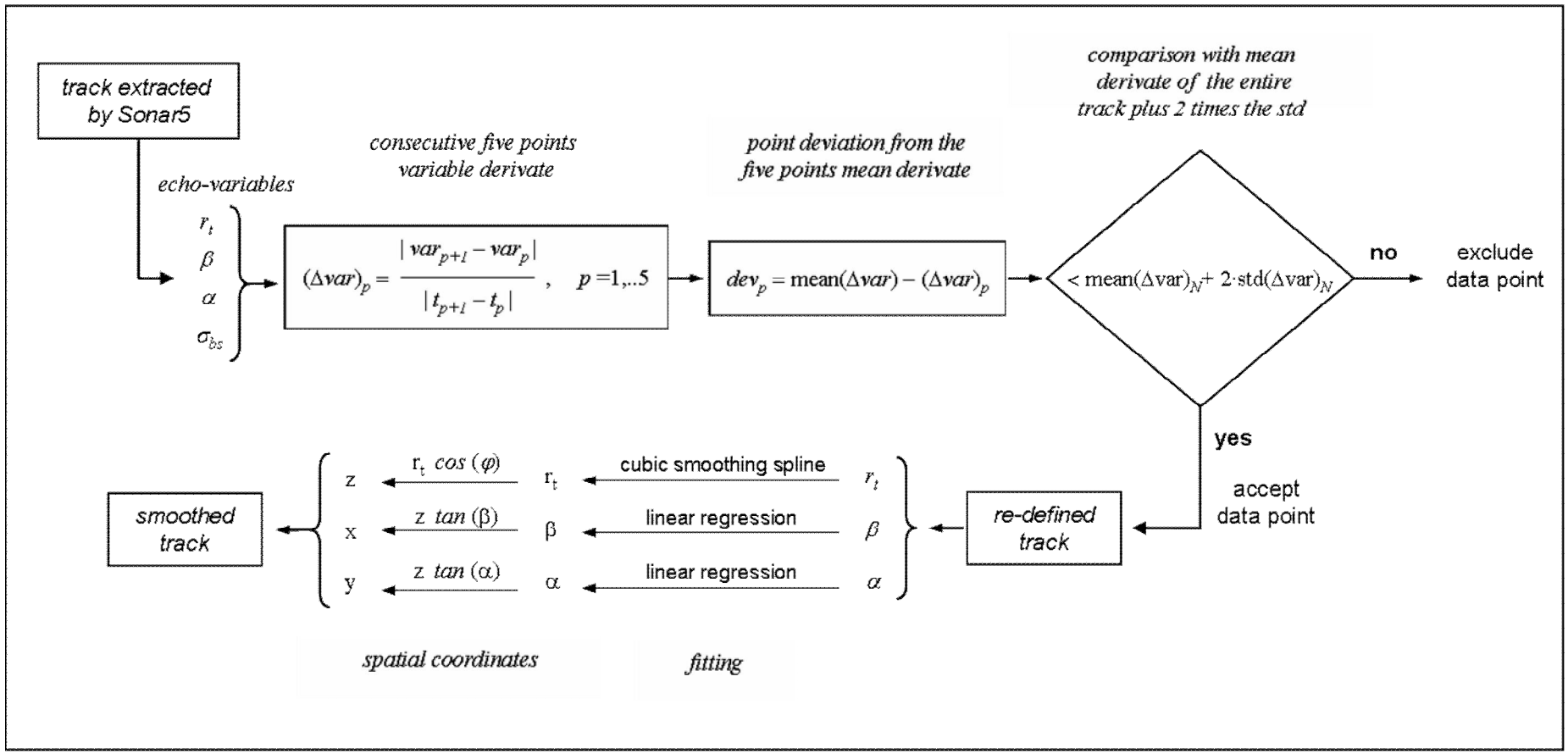

Figure 3. Processing steps on a single track composed by *N* echoes extracted by the Sonar5 post-processing software. The upper part is the skipping process for echoes with improper jitters on each echo-variable (*var*). The lower part is the fitting process associated with final Cartesian coordinate system conversion.

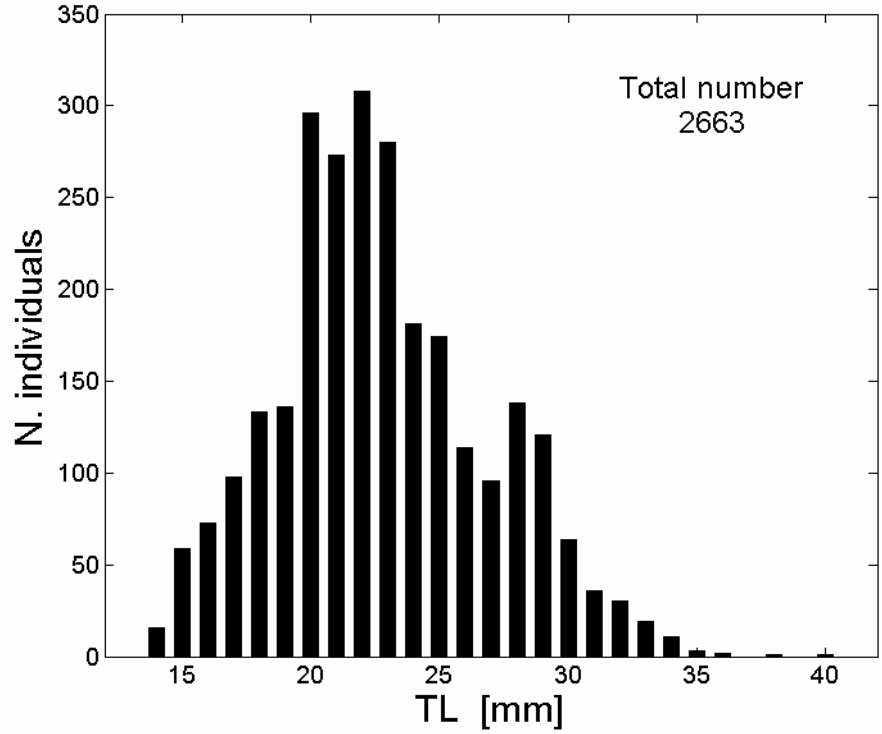

Figure 4. Length distribution of *Meganyctiphanes norvegica* in the mesocosm by the end of the experiments.

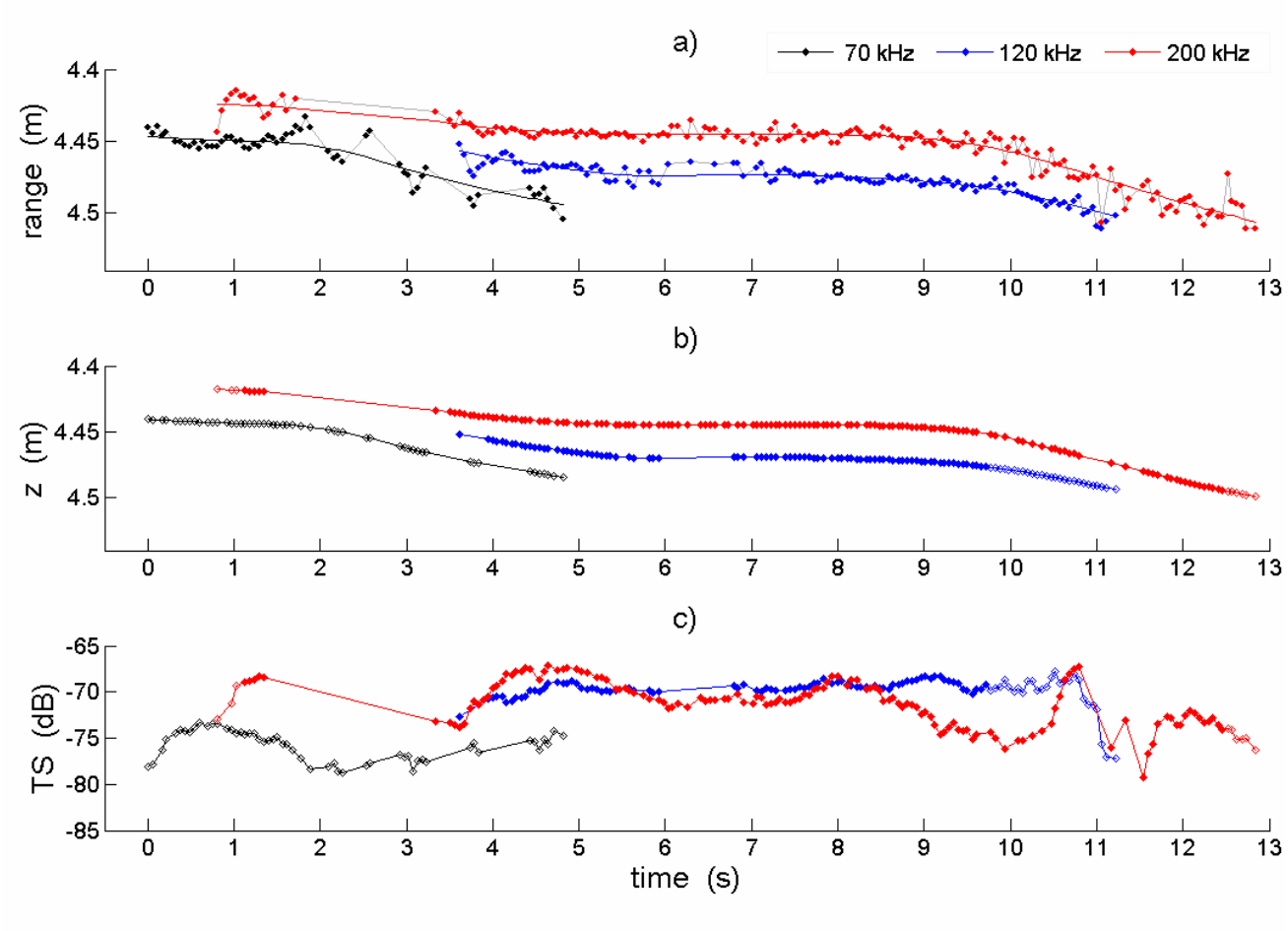

Figure 5. Data processing on the resolved echoes at the three frequencies for an euphausiid tracked as it is attracted by the fore light source. a) Target range (dots and grey line) as extracted by the Sonar5 software, and results of the smoothing (colour solid line). The solid grey lines connecting the data are plotted for readability. b) Cartesian z-coordinate at the end of the smoothing process calculated by the first of equations (2). c) TS of the resolved echoes. In panel b) and c) solid symbols are the echoes detected inside the horizontal 6° beam cross section while open symbols are outside.

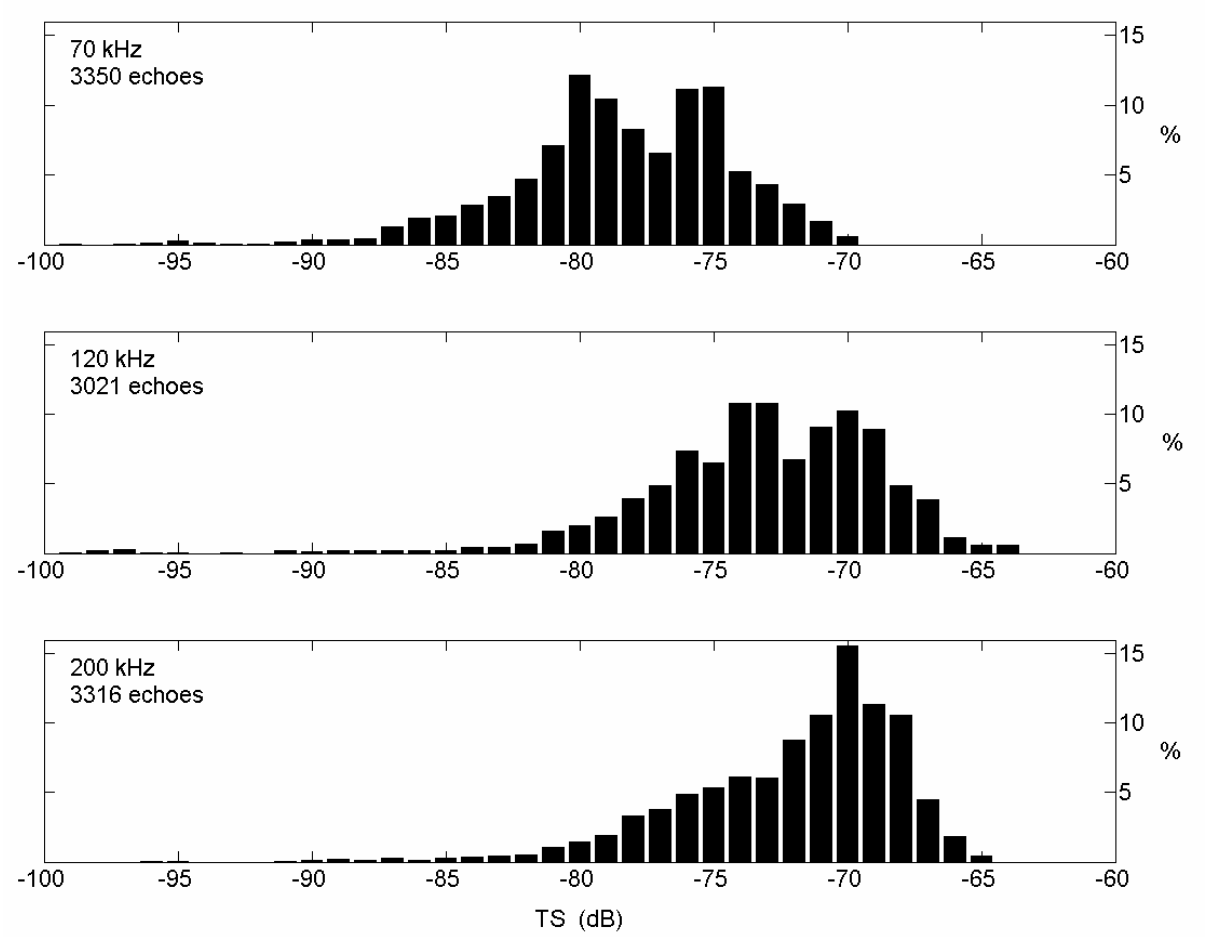

Figure 6 Ping-to-ping analysis. TS Frequency distributions of detections with vertical velocity angle less than 5º for each of the frequencies.

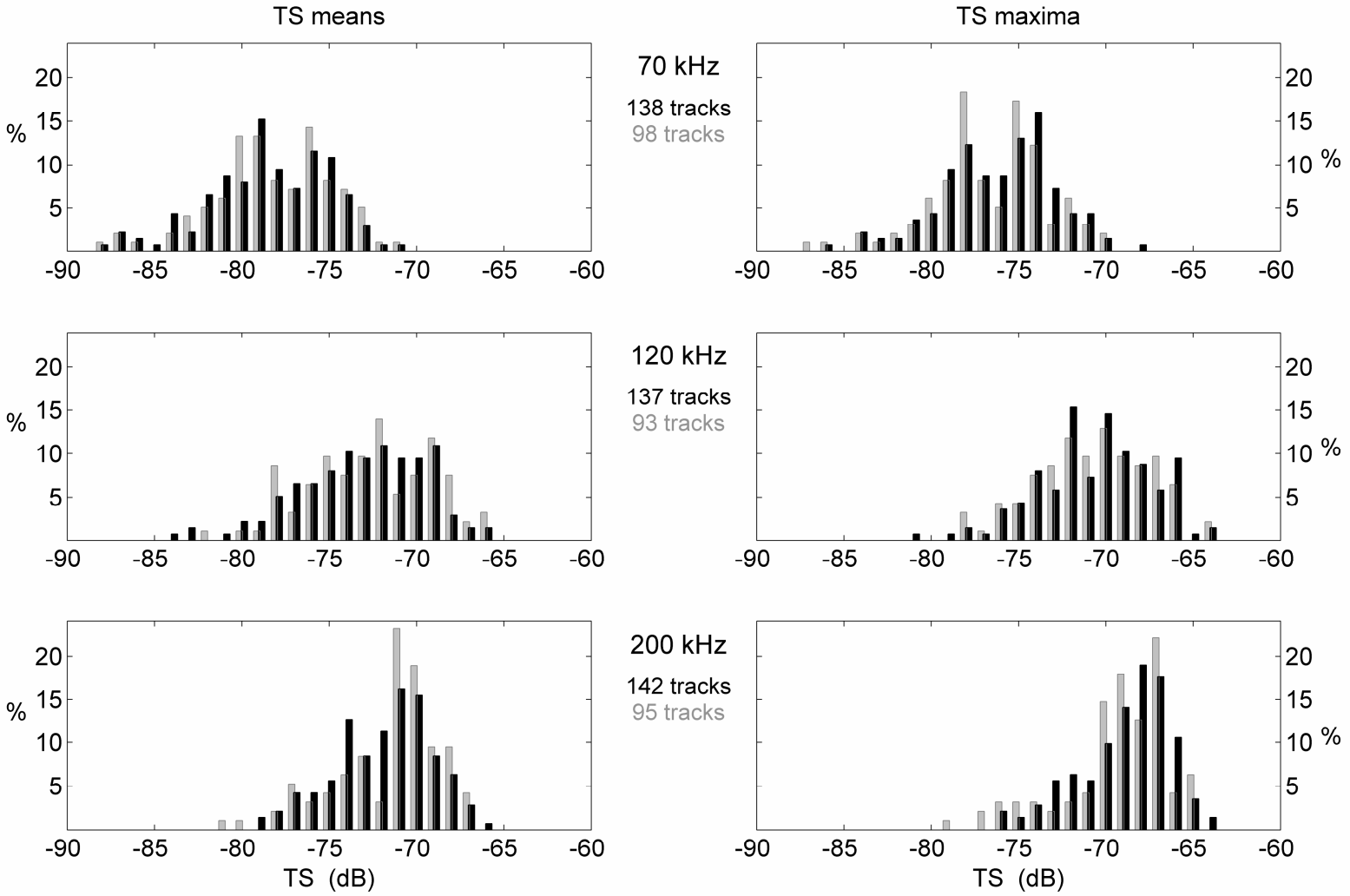

Figure 7. Frequency distributions of the means (left column) and maxima (right column) TS of krill derived from the horizontal tracks for each acoustic frequency. The black bars are the results on the entire tracks, while the grey bars are considering the tracks composed by only echoes (minimum 4) with vertical velocity angle $\theta < 5°$. The number of observed individual krill was 174 and 161 for the two cases respectively.

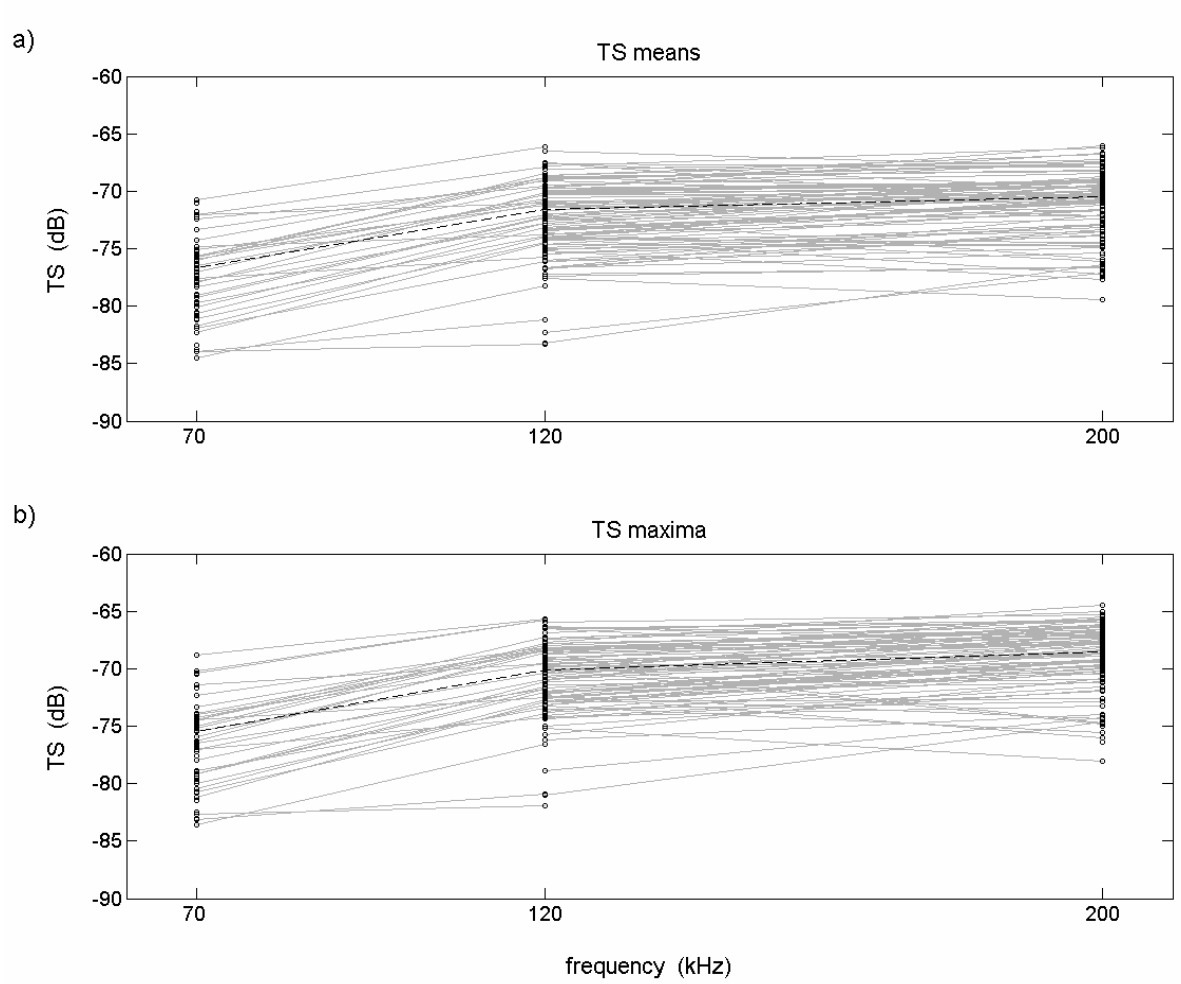

Figure 8. Mean TS (a) and maximum TS (b) derived from horizontal tracks with synchronized detections for at least two frequencies. Values are plotted as black circles while the individual frequency responses (grey lines) are superimposed. The tracks relate to 96 individual krill which have been simultaneously detected by at least two frequencies. The 70-200 kHz connections are not plotted for better readability. The dashed black lines are the relationships between the overall means.

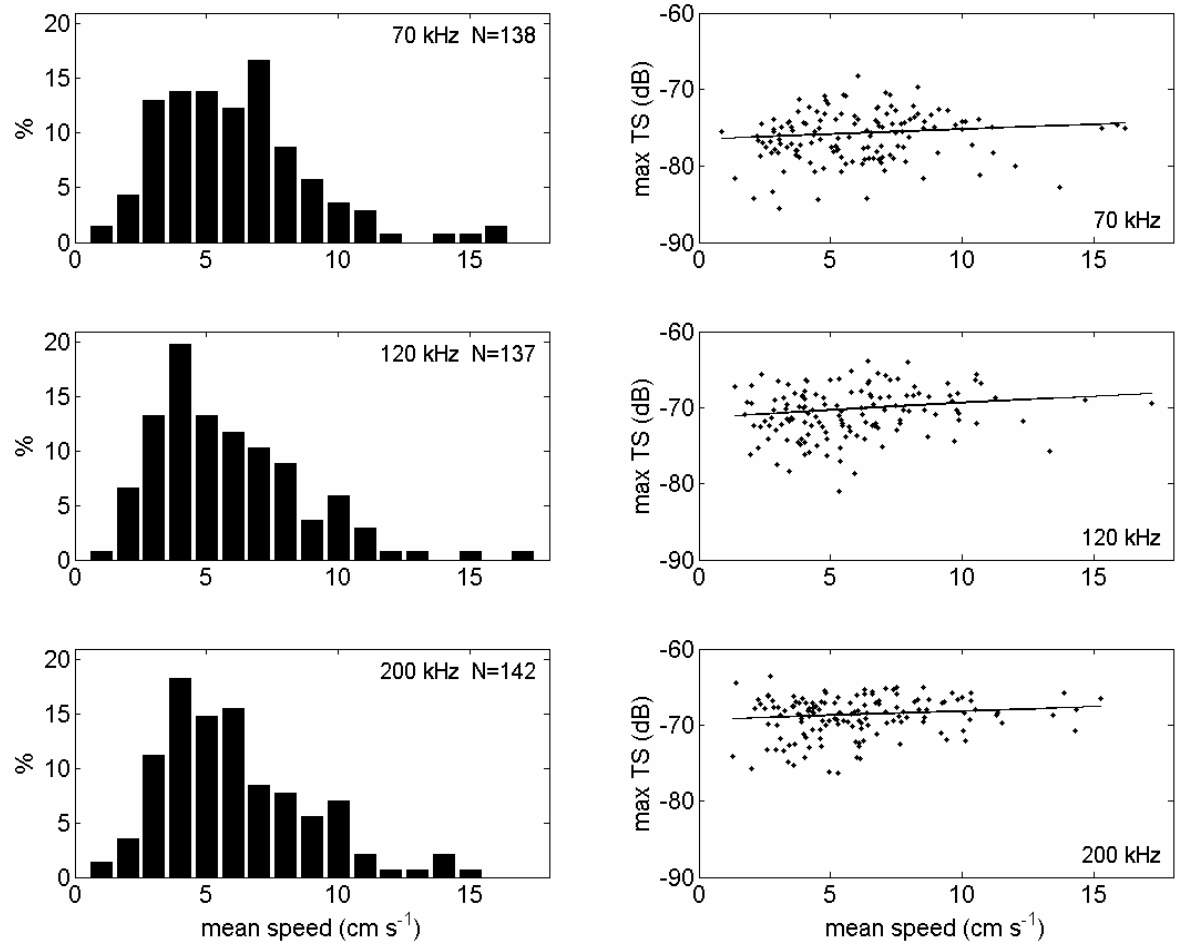

Figure 9. Mean speed frequency distribution (panels on the left column) and relationship with observed maximum-TS (right column) at each of the three frequencies for krill recognized by the horizontal tracks data set.

TABLES

Table 1. Simrad EK60 acoustic systems: General Purpose Transceiver (GPT) and transducer parameters, settings, and performances in Austevoll mesocosm for the pulse duration 0.256 ms. f: nominal frequency; f_0: central frequency; NF: transducer near field; x, y: distances between the centres of the transducers and the centre of the 70 kHz (taken as origin of a Cartesian coordinate system); EP: electric power transmitted to the transducer; RB: receiver bandwidth, fixed by Simrad for the given pulse duration; SL: source level estimated by Sonar5; AP: acoustic power in the medium determined by Sonar5; BN: background noise estimated by the Simrad ER60 software.

GPT		***Transducer***				***Setting***		***Performance in Mesocosm***		
f (kHz)	**f_0 (kHz)**	**Type**	**NF (m)**	**position (cm)**		**EP (W)**	**RB (kHz)**	**AP (W)**	**SL (dB *re* 1 μPa at 1 m)**	**BN (dB)**
				x	**y**					
70	70.175	ES70-7C	1.5	0	0	300	6.16	116.8	221.5	-98
120	121.212	ES120-7C	0.9	5.9	23.1	250	8.71	119.9	221.6	-102
200	200.000	ES200-7C	0.5	-6.1	39.1	120	10.64	74.8	219.5	-110

Table 2. Summary of TS results in dB re 1m from analyses on the horizontal tracks set. *N.* krill is the number of observed krill; f is the frequency in kHz; *N.* tracks is the number of krill tracked at the relative frequency; $\overline{N}$**.**ping is the mean number of pings composing the tracks; $\bar{t}$ is the mean observing time. Mean and standard deviation (*std*) of the mean ping-to-ping (p-to-p) TS variability within the tracks are also listed. For each selected track, the mean- and maximum-TS were determined and grouped at each frequency. The simple statistical parameters of the values in dB re 1m are listed in the last five columns; Δ is the range of values.

horizontal tracks composed by	***N.* krill**	***f***	***N.* tracks**	$\overline{N}$**. pings**	$\bar{t}$ **(sec)**	***p-to-p TS variability*** *mean*	*std*	***tracks TS data***	***f***	**min**	**max**	**Δ**	**mean**	**median**
all echoes	174	**70**	138	55	5.5	0.8	0.5	means	**70**	-88.3	-71.2	17.1	-77.4	-78.5
									120	-83.8	-66.1	17.7	-71.9	-72.8
		120	137	57	5.6	0.9	0.6		**200**	-79.3	-66.4	12.9	-71.1	-71.5
								maxima	**70**	-85.5	-68.3	17.2	-75.1	-75.8
		200	142	31	3.7	1.2	0.8		**120**	-81.0	-63.9	17.0	-69.6	-70.4
									200	-76.3	-63.5	12.8	-68.2	-68.4
only echoes with low vertical movement	161	**70**	98	29	6.9	0.7	0.6	means	**70**	-88.1	-71.0	17.1	-77.0	-78.1
									120	-81.8	-65.8	16.1	-71.2	-72.2
		120	93	28	6.7	0.7	0.5		**200**	-80.8	-66.5	14.3	-70.7	-70.9
								maxima	**70**	-86.7	-69.7	16.9	-75.5	-76.4
		200	95	31	6.9	1.0	0.7		**120**	-78.5	-64.0	14.5	-69.7	-70.7
									200	-78.9	-65.0	13.9	-68.5	-68.7
at least two frequencies synchronized echoes	96	**70**	48	12	2.3	0.7	0.5	means	**70**	-84.5	-70.8	13.8	-76.7	-77.9
									120	-83.3	-66.1	17.1	-71.6	-72.2
		120	91	22	3.6	0.9	0.7		**200**	-79.4	-66.0	13.4	-70.5	-70.8
								maxima	**70**	-83.6	-68.9	14.8	-75.5	-76.4
		200	93	21	3.1	1.4	1.2		**120**	-81.9	-65.7	16.2	-70.1	-71.0
									200	-78.0	-65.0	12.2	-68.5	-68.6

Paper V

Lucio Calise and Tor Knutsen

Multifrequency target strength of Northern krill (Meganyctiphanes norvegica): measurements on tethered specimens and SDWBA theoretical predictions

Multifrequency target strength of the Northern krill *Meganyctiphanes norvegica*: measurements on tethered specimens and SDWBA theoretical predictions

Lucio Calise and Tor Knutsen

Abstract

Direct acoustic target strength measurements on four tethered individuals of the Northern krill *Meganyctiphanes norvegica* species were made in a large enclosure, vertically suspended in the sea from a raft and filled with filtered deep seawater. The specimens spanned a length range from 22 to 33 mm representing the Northern krill generations of the northern Atlantic and adjacent seas during the winter period. A new suspension set-up allowed the individual krill to swim almost freely and gives the opportunity for a more confident comparison between the acquired data and theoretical predictions. The scientific echosounder Simrad EK60 operating at the four frequencies 38, 70,120 and 200 kHz, was used for the acoustic acquisition and the data compared with the Stochastic Distorted Wave Born Approximation model (SDWBA) predictions. A novel digitalization procedure for the reconstruction of the body shape to be used in the model is described and three shapes relative to different Northern krill lengths are proposed. The SDWBA was run over three selected distribution of orientation to simulate the possible behaviour of the animals during the measurements. Acoustic results in TS domain and from echo statistic analysis are shown. They show that the scattering process is highly variable and sensitive to the size and angles of orientation of the organisms. Large range of TS values were observed for all animals at all the frequencies. A particular feature of the mean and maximum TS values when comparing 120 and 200 kHz data for animals with length 27 and 29 mm specifies a presumable frequency transition region that may help to provide direct estimates of the Northern krill size by echosurvey data. Modelling results reflect the scattering complexity but have been found much lower than the empirical strength levels. The cause of deviations is obscure. It can be mainly ascribed to erroneous material properties values, but it seems more likely to be attributed to a combination of numerous factors and their interrelationships in the formulation.

Keywords: Krill target strength, *Meganyctiphanes norvegica*, echo statistics, DWBA, digitalization, SDWBA, Simrad EK60, mesocosm

L. Calise: Department of Physics and Technology, University of Bergen, Allégaten 55, N-5007 Bergen, Norway.

T. Knutsen: Research Group Plankton, Institute of Marine Research, P.O. BOX 1870 Nordnes, N-85817 Bergen, Norway.

Introduction

The order Euphausiacea or krill is considered a key ecosystem component in the majority of the world's oceans (Mauchline, 1980). Especially this is the case in the southern ocean where the species *Euphausia superba* (Dana, 1850), also called Antarctic krill, is the principal food of whales, fish, squid, pinnipeds and birds. For this reason, the Convention for the Conservation of Antarctic Marine Living Resources (CCAMLR) often denotes the ecosystem of the Southern ocean as a "krill-centric" ecosystem.

In the North Atlantic and adjacent seas, including the Mediterranean, the "Northern krill" *Meganyctiphanes norvegica* (Sars, 1857) is by far the most abundant krill species (Mauchline and Fisher, 1968; Boysen and Buchholz, 1984; Labat and Cuzin-Roudy, 1996), being an important prey item for a range of zooplanktivorous fish and whales. Within the framework of an ecosystem approach to management, measuring krill abundance and size distribution in an optimal way is a key issue in order to forecast changes in abundance and recruitment of these biological resources.

Acoustic methods using scientific echosounders are considered a primary tool to conduct rapid biomass estimation with a sufficiently high sampling rate, avoiding in part the underestimation and the unresolved spatial variability of the euphausiid communities typical of traditional biological sampling tools (e.g. Wiebe *et al*., 1982; Watkins and Macaulay, 2000). Nevertheless, to undertake an accurate abundance estimation of euphausiids from acoustic surveys is not straightforward because it implies to distinguish these organisms from other scatterers that have similar acoustic characteristics.

At present, the identification and discrimination between organisms is obtained by adopting multifrequency techniques, formerly indicated as a promising method by Greenlaw (1979). The knowledge of the variation in target strength (TS) versus the operative frequencies is crucial for the effectiveness of the method, both in the scrutinizing process and in converting acoustic data to absolute biological units when estimating population abundance. In general, the acoustic target strength of an organism is a function of its size and shape, and of the density and the sound speed contrasts with the surrounding medium. For a fluid-like elongated object, such as euphausiids, the scattering is a directional process so that organism behaviour (i.e. spatial orientation) constitutes an important aspect significantly influencing the target strength, hence abundance estimation from acoustic surveys (e.g. Stanton *et al*., 1993; Martin Traykovski *et al*.,1998; McGehee *et al.*, 1998; Demer and Conti, 2005).

During the last decades, large efforts have been undertaken to improve theoretical scattering models (e.g. Stanton and Chu, 2000), but some investigations have also performed direct target strength measurements on individual krill or similar organisms *ex situ* in small laboratory tanks (Richter, 1985; Kristensen, 1983; Wiebe *et al*., 1990; Stanton *et al*. 1994; Demer and Martin, 1995; McGehee *et al.*, 1998; Stanton *et al*. 1998a; De Robertis, 2001; Lavery *et al.*, 2002; Conti *et al*. 2005; Amakasu and Furusawa, 2006), on encaged individuals (Pauly and Penrose, 1998; Foote *et al*., 1990) and *in situ* (e.g. Falk-Petersen and Kristensen, 1985; Kristensen and Dalen, 1986; Greene *et al*. 1988; Klevjer and Kaartvedt, 2006).

When there is confidence in what species are located within the acoustic beam, it is suggested that measuring target strength directly *in situ* or in large volume tanks is superior to derive it solely from theoretical scattering models. However, since the scattering process from a fluid-like elongate organism is very complex, both theoretical and empirical approaches should be addressed in combination to obtain the most reliable comparison for acoustic assessment works.

In order to provide primary acoustic information and develop more accurate algorithms for echo survey data and krill classification in a multifrequency context, direct acoustic measurements on *Meganyctiphanes norvegica* were conducted at Austevoll Research Station of the Institute of Marine Research (Norway) during January – April 2004. The euphausiid *M. norvegica* were caught in large numbers in a neighbouring fjord locality at night and transferred to an enclosed bag, "mesocosm", which was fully monitored with respect to its physical and biological characteristics.

A set of experimental exercises were conducted with the aim to retrieve significant information on multifrequency TS and acoustic volume backscattering from live krill. In this paper, results from measurements on tethered individual krill in excellent condition are presented. Data from six commonly used frequencies in fisheries research were acquired (38, 70, 120, 200, 364 and 710 kHz), but only from the four lowest frequencies are analyzed in the present work.

Tethering individual krill could limit the animal behaviour with respect to what can be considered "natural" swimming activity, on the other hand it allows much greater control of the individual, positioning it underneath the acoustic beams and assuring the knowledge of the size and the morphological features. The method of attachment used in this study allows the animal to swim almost freely. For this reasons and because animal size and shape are precisely known, this would favour a more confident comparison with theoretical scattering model predictions.

Driven by the need for more accurate scattering prediction, models of increasing sophistication, which take into account of the full complexity of the animals' shape and the orientation, have been proposed in the last two decades. At present, the distorted wave Born approximation model (DWBA) (Chu *et al.*, 1993; Stanton *et al.*, 1998b) is recognized as the state-of-the-art in the physics-based models predicting target strength of fluid-like crustacean zooplankton such as krill (Stanton and Chu, 2000). In the present work the stochastic version of the DWBA model (SDWBA) (Demer and Conti, 2003, 2005; Conti and Demer, 2006) has been the primary model applied.

Materials and methods

The mesocosm was established in an open raft located in a small bay well protected from severe waves and currents, at about 20 m distance from the shore. It consisted of a cylindrical enclosure or "bag" of 6 m in diameter and 8 m deep of flexible and impermeable black coloured polyethylene sheeting with thickness 0.15 mm (three-layer woven PEL), tapered in the bottom region and vertically suspended in the sea from the raft. The upper cylindrical and lower conical parts were 5 and 3 m long respectively, resulting in a nominal volume of 170 m^3.

The bag was fastened by ropes to a circular stainless steel ring of 6 m diameter that was connected to the raft by steel cables and ropes. This means that the raft and the bag constituted a single system floating on the sea surface. In order to insure recharging of new seawater in the bag a hydraulic system was established and kept operative continually during the experimental period. Seawater from 165 m depth was pumped in from a neighbouring fjord and driven inside the mesocosm through a tube mounted at the bottom of the bag. The introduced water was priory filtered and directed through a temporary storage tank to eliminate eventual air bubbles. Temperature, salinity and oxygen characteristics of the seawater were routinely monitored before the introduction. The inflow to the mesocosm

was kept equal to 18.2 litres per minute, assuring a change rate of approximately 16 % of the total water volume per day. Additional water was removed by gravity overflow by means of a sieve suspended in the bag with the terminal part out from the wall bag at approximately 0.3 m from the sea surface.

A footbridge placed on top of the raft allowed easy access, mounting of gear and instrumentation as well as maintenance work. Before the acoustic measurements, average temperature and salinity along the vertical dimension in the mesocosm were monitored by using a calibrated Gytre Mini CTD SD202. The values were then used to update the sound speed to be set in the echosounders during the acoustic acquisition. More details on mesocosm set-up and monitoring procedures can be found in Calise *et al*. (2005; 2009a).

Krill sampling and measurements

The krill used for the measurements were collected using the MS Aurelia of the University of Bergen, during the night of 28 of February in Raunefjorden (60° 16' N, 5° 9' E) sited near Bergen on the west coast of Norway. The 3 ft Isaac-Kidd Midwater Trawl (IKMT) with an opening of 0.9 m^2 and mesh size of 500 μm was utilized. A total of 7 trawl hauls were performed at approximately 15-25 m depth, where the krill was easily available during the night. More details on the sampling methodology may be found in Calise *et al*. (2009a)

Transport to Austevoll Aquaculture Station took approximately one hour following the last catch. Here, the contents of most of the sample was introduced into the mesocosm, while the contents of two 50 litres buckets (2/3 of one catch) were stored in two separate 500-litres seawater tanks, situated on the raft close to the mesocosm, to kept the animals in optimal conditions until they were used for the experiment described in this paper.

The two tanks were connected to the same seawater supply system of the mesocosm, which provided sand filtered deep seawater pumped from the nearby fjord at 165 metres depth and monitored in temperature, salinity and oxygen. A slow ingoing flow was kept by means of a hydraulic valve and surplus water was removed by gravity overflow.

Along with the krill, a small amount of copepods of the genus *Calanus* and *Metridia* were caught with the IKMT net and acted as food supply for the krill until the experiments terminated. No other food was supplied until the acoustic measurements were performed in the period 5-9 March 2004.

Following the acoustic experiments the animals were frozen at -18 °C in individually marked Eppendorf-tubes for later measurements of lengths, widths and dry weight. Approximately four months later, the individual specimen was partly defrozen and the lengths measured to the nearest millimetre below by means of a Leica MS5 stereomicroscope at appropriate magnification. The total length (TL) was measured from the tip of rostrum to the posterior end of the terminal spine at the end of telson; the carapace length (CL) was measured from the base of the carapace eye notch to the posterior lateral edge of the carapace. These are codified by Morris et al. (1988) as lengths “TT” and “S6” respectively. Another measure denoted body length (BL) was taken from the inner curved part of carapace (“eye notch”) to the end of telson. In addition, three measures of body width of the animal as seen from the dorsal side was also taken: 1) width across the anterior part of the rostrum (B1); 2) width at the end of carapace/joint were first abdominal segments start (B2); 3) width where the last abdominal segment joints the telson (B3).

Subsequently, the animals were stored in pre-weighed aluminium dishes and put for short-term storage in a freezer ready for freeze drying. Dry weight was measured after freeze-drying using a Heto FD8 freeze-drier initially set to pre-freezing. When the krill was entered to the freeze dryer they were still frozen. Then the vacuum pump was turned on and the krill freeze dried

over night at 10°C, after which the temperature were increased to 18°C for 3 hours more. Thereafter the krill was taken out, put in an exicator and weighed later the same day. A Mettler Toledo UMX2 having a working range 2.1 g - 0.1 µg was used for weighing the krill.

Acoustic data collection

The measurements on tethered animals were performed during day time when the free swimming krill inside the mesocosm water volume were observed to reside close to the bottom of the bag.

Data from four SIMRAD EK60 echo sounders, consisting of the General Purpose Transceivers (GPT) and corresponding split-beam transducers operating at 38, 70, 120, 200 kHz were acquired and analyzed. The set-up, the acquisition and the storing of data were PC controlled via Ethernet connection by means of the Simrad ER60 software (ver. 2.0.0). Systems set-up and principal parameters are listed in Table 1.

All transducers were 7º nominal beamwidth and the new composite type, except for the discrete elements 38 kHz transducer. They were mounted on an aluminium plate 90 x 110 cm and 5 mm thick, as close as possible to each other, with the active face lying on the same plane and identical split-beam orientation. Between the aluminium plate and the transducers, a minimum of 5 cm thick form-cut divinycell plates were mounted to minimize the back radiation from the transducers and obtain better floating stability. Extra weights were added on the upper side of the rig to balance the frame influenced by the heavier 38 kHz transducer. The rig was placed, with transducers facing downward, close to the centre of the mesocosm, neatly floating on the surface, with a tiny layer of seawater to overflow the top of the rig. In addition, by using a simple T-shaped wooden stick turned upside down the rig was attached to the footbridge and kept in fixed position for truly stable measurements.

Prior to and after the four months experimental period, the systems were calibrated using the "standard target method" (Foote *et al.*, 1987) and the Simrad ER60 built-in software calibration.exe. A small deviation in the pre- and post-calibration results was observed for the 120 kHz system. Therefore, a date-adaptive correction was determined by interpolation between the two gains in the linear domain and the data were then compensated by estimating the deviation related to the day of the measurements. This was determined to be 0.19 and 0.29 dB for the days 5 and 9 March respectively.

Acoustic data were acquired with identical pulse length of 0.256 ms for all frequencies, resulting in 4.7 cm raw sample distance, and using significantly reduced transmission power to the transducer (Table 1) to avoid potential non-linear effects (Tichy *et al.*, 2003; Korneliussen *et al.*, 2008). In order to retrieve a high number of echoes representing a broad range of krill tilt angles, the ping rate was set to maximum, i.e. transmitting pings as often as possible, generally resulting in 18.2 pings per second.

The experimental set-up is shown in Figure 1. The tether system consisted of a main blue nylon monofilament line of 0.4 mm diameter, with the standard tungsten calibration sphere of 20 mm diameter (WC20) mounted at the terminal end. The sphere was intended to act as a weight for the line, keeping it steady and vertically aligned, and as a reference target when positioning and moving the animal between the transducer beams. At a distance of 1.7 meter from the sphere, a secondary and finer line was attached to the main line by a tiny lasso like sling. This finer line held the individual krill specimens during the measurements. The "life-line" was a thinner 0.12 mm Berkley Fireline (EFLFS12-42) from Pure Fishing, 1900 18th Street, Spirit Lake, IA 51360-1099 (www.berkley-fishing.com) 1-800-237-5539, USA. In one case, for the smaller animal no. 8, another type of line was used, namely an Ethicon

Prolene, EH7242 6/0, 0.07-0.09 mm thick with the additional description "blau monofilament Polypropylen chirurgisches nahtmaterial nicht resorbierbar". The two lines are referred to as L1 and L2 respectively.

At the distal end of the "life-line" a sling was prepared and wrapped around the animal between the carapace and the first abdominal segment, as close as possible to the point of centre of krill body mass (Kils, 1981). This operation was performed in a small seawater-filled dish in order to avoid air bubbles being trapped between the animal's legs or otherwise attached to its body. After cutting surplus line from the sling, the dish with the tied animal was immediately submerged into the mesocosm water and the animal lowered to measurement depth. The length of the "life-line" holding the krill varied from 15 to 17 cm, and allowed the krill to swim almost freely without being severely hampered by the method of attachment.

The upper end of the main line was connected to a junction where three additional 0.4 mm diameter monofilament lines met (Figure 1). Each line was controlled by a separate motorized winch positioned on the raft, and otherwise used for calibration purposes. The three winches were mounted along the circular edge of the mesocosm, at an angle of 120º relative to each other and electrically connected to a motherboard electronic console leading to control the lines, hence the tethered animal, using joy sticks. The distance from the junction to the animal was generally 1.4 m.

With this tethering scheme, the position of the main line could be adjusted and the animal placed close to the beam axis of each individual transducer being operative, as well as moved from one beam to another.

A Simrad Video Camera (SitCam) was also used to perform video recordings of the tethered krill. Video-recording of the animals during the acoustic acquisition was not possible as the camera-rig was acoustically detected if positioned too close to the animal. When outside the acoustic beam, the camera did not supply sufficient information on krill behaviour. However, the video filming provided valuable information on the general animal behaviour when tethered, and qualitative information on its main spatial orientation. A white rope with a weight attached at the lower end was deployed hanging vertically on the other side of the bag with respect to the camera. This rope was intended to indicate the true vertical direction, i.e. parallel to the direction of the acoustic wave, for the video inspection of the animal position by contrasting with the dark background of the video image.

Before and after the acoustic measurements the activity of the animal was checked by the video camera and recordings made on VHS cassette. Animals without any sign of swimming activity, showing an odd body posture or unnatural behaviour were immediately removed and replaced with a fresh animal. Only measurements on animals showing adequate swimming behaviour before and after the acoustic measurements are reported here.

After a first try with one animal, a more appropriate acquisition procedure was established as follows: prior to the start of each measurement session, the tethered animal was gently shaken as an additional precaution to help release potential air bubbles attached to the body or appendages, and its activity checked by the camera. Then the animal was positioned as close as possible to one of the beam axes within the appropriated depth layer for the target frequency by checking the real-time echogram in Simrad "Sp mode" (point backscattering strength data) with ER60 software, and freely allowed to move around that point. The animal was generally kept for all the acquisition time at a range of 4-5 m from the transducer face, slightly depending on the better noise-free part ("acoustic window") of the frequency being used. If it seemed to stop its activity, the line was gently twisted to induce it to move again. When a satisfactory number of echoes were obtained at a given frequency the animal was slowly moved to the next active beam and the procedure repeated. The entire

procedure took not less then 50 minutes. The data were normally acquired with all the four systems pinging synchronously. In some cases the procedure was repeated with the target frequency in active mode and all the others set in passive mode.

A total of eight animals were measured during the cited period. However, a detailed inspection of the video recordings and examination of the acoustic data suggested that four of the investigated animals should be discarded from the later analysis. While for the first animal the hanging procedure was not fully established providing unsatisfactory comparisons of data, in two cases the animal was slightly inclined on one side on respect to the transducers faces; in the last case, the extra line of the sling was not completely cut contributing to an evident bias on the measurements at the higher frequencies.

The recorded EK60 raw data files were processed by an enhanced version of the Sonar5 post processing software (Balk and Lindem, 2005). The optimum Single Echo Detector (SED) criteria (Ona and Barange, 1999) were established for each frequency and case (line-alone and animal with different size) by means of the Sonar5 built-in tool "SED pre-analysis". In some cases, the beam compensation criterion was set to 6 dB for better visualization of the targets in the echograms.

Following the SED optimization procedure, echo-tracks of the target were manually scrutinized from the Sonar5 echograms visualized in single echo detection mode. The krill echotrace was generally easy to recognize in the echograms. For weaker echoes, such as smaller animals at 38 kHz, the calibration sphere and the upper 3-line junction knot were used as additional references. For all the cases, the minimum TS criterion was set to -100 dB re $1\,m^2$.

Single echotrace parameters for the echoes composing the tracks were retrieved for the analysis. These were nominally: ping time [hh:mm:ss.##], range to the target r_t [m], uncompensated and compensated (TS) target strength [dB re $1m^2$] and the mechanical beam angle positions α and β [degrees]. Hereafter, when the target strength units are reported in dB only, it is assumed that the omitted notation "to 1 m^2" is intrinsic to the far field backscattered energy definition.

In the further analysis, in order to exclude echoes at the outskirts of the nominal beam, where the signal-to-noise-ratio is lower and potential biases might compromise angular position and TS estimation of weak targets (e.g. Kieser *et al.*, 2000), only echoes detected inside the solid beam angle of 6° (cut-off solid angle) were used.

Data treatment

In order to investigate the potential influence of the tether, acoustic backscattering data of the "life-line" alone were also collected. This was done by moving the main and life lines in exactly the same manner underneath each transducer as when the animal was attached.

The inspection revealed that the line L1 was detectable at 70, 120 and 200 kHz, whereas the thinner L2 was detected at 120 and 200 kHz only; Table 2 resumes the results. At the other frequencies the scattering was most probably below the background noise threshold (Table 1) and the potential line contributions could be readily ignored. For the thickest line L1 the mean TS at 200 kHz was the largest (-85.5 dB) and lowest at 70 kHz (-94.1 dB); while mean TS for line L2 at 120 and 200 kHz were much below and approximately to -90 dB respectively. The backscattering distributions had a marked Gaussian trends centred at similar levels of the mean observed echo.

Since the backscattering data from the lines alone showed potential contribution to the acquired measurement data-sets and even partial overlap with some of the recorded level

ranges, a filtering treatment on the acquired scattering intensities was necessary to remove these contributions and to express the backscattering due to the animal contribution alone.

The filtering approach was based in terms of probability theory assuming that the received scattered intensity from the animal plus the line is on average equal to the sum of the scattered intensities from each individual contribution. This is the same to say that the contributions to the echo of the line and the animal received at the transducer are supposed to be incoherent. A recorded echo-data set (E) can be interpreted as the result of the sum of two random signals due to noise line (L) and the animal (A) respectively. Hence, given $A=E-L$ the probability distribution of the animal contribution can be determined by:

$$PDF\left[A(n)\right] = E(n) - \sum_{m} PDF\left[L(n)\right] \cdot PDF\left[E(n+m)\right] \quad (1)$$

where $PDF[\ ]$ denotes the probability distribution function, and n and m are the sets of all possible outcomes for E and L respectively. The last term on the right side of equation (1) is conceptually similar but different in the form from the regular discrete cross-correlation used to control the similarity between two random signals (Bracewell, 1999); it evaluates the incoherent effect of the L value in n-th bin on the relative higher signal E bins.

Equation (1) was applied in TS domain to the cases where the lines appeared to be acoustically significant, as given in Table 2, with bin resolution of 0.05 dB. The actual $PDF[L]$ used for the filtering process was the Gaussian distribution fitting the line backscattering data. As an example, the histograms in Figures 2a and 2b show the probability distributions of the recorded echoes at 200 kHz from the L1 alone and of the echo data-set relative to the *Meganyctiphanes norvegica* length 27 mm plus L1 respectively. It can be observed a clear overlap in the TS echo-signal range [-92,-78] dB. In Figure 2a, the Gaussian fitting distribution used in the process is superimposed to the line data as black solid line. Figure 2c shows the result of the treatment after the application of Equation (1) to the recorded data. Negative occurrences due to the process are not showed in figure; they were omitted in the further analysis.

Among all the cases where the Equation (1) was applied, the example shown in Figure 2 represents the extreme one where the filtering had the highest impact on the original data set. The total probability of the resolved *PDF* due to the animal contribution alone was calculated to be 76.8% of the initial $PDF[E]$.

Subsequently, the resolved data array was reconstructed. For each bin resolution interval, the number of detections due to the animal only were calculated on the base of the original target echo-realizations times the ratio between the probabilities of the resolved animal contribution and the original data-set. Figure 2d shows the final probability distributions of the reconstructed krill data set for the specific case.

The reconstruction was necessary in order to perform appropriately the successive step consisting in echo statistic analysis in echo amplitude domain. Direct transformation of the *PDF* from logarithmic to linear domain was judged inconvenient for the numerical and graphical control of the results, since the increments for representing the linear amplitude for the constant resolution of 0.05 dB was logarithmical spaced rather than uniformly incremented. For the same reason the filtering was not performed in linear domain since the TS was the primary acoustic quantity of the raw date output from the Sonar5 software.

Together with the echo data-sets related to the cases where the filtering treatment was not necessary, the reconstructed data-sets constituted the hereafter called “krill data-sets”, which were further analyzed to produce the final results.

The statistic analysis was performed in the linear domain through the conversion of the backscattering data to the target echo-amplitude *e* that is proportional to the square root of the backscattering cross section σ_{bs} in m^2:

$$e \cong \left(\sigma_{bs}\right)^{1/2} = 10^{(TS/20)} \tag{2}$$

Clay and Heist (1984) claimed the theoretical Rice *PDF* to be a likely model for echo-amplitude distribution from an individual live fish. Wiebe *et al*. (1990) found that the Rice *PDF* well describes the fluctuations of the observed echo amplitudes from decapod shrimps also. These organisms seem to be acoustically similar to krill.

The formulation of the Rice *PDF* is based on two parameters representing the concentrated and distributed scattering components derived from the coherently and incoherently scattered powers respectively. These two parameters are easy to estimate from the data and their ratio γ describes the shape of the *PDF*. The parameter γ can be associated to the average of the observed σ_{bs} so that the Rice formulation can be transformed in to a more convenient form to describe the statistics of the echoes from the organism (Clay and Heist, 1984). By varying γ, it is possible to find the best fit to the observed distribution. The Rayleigh and the normal distributions are particular cases of the Rice *PDF* with γ equal to 0 and very large respectively.

A least-squares approach was applied on each krill data-set, searching iteratively the minimum sum of squares of the differences between the *PDF* values of the animal echo amplitudes and a set of theoretical Rice probability functions parameterized by different γ (minimized sum analysis). Hence, the Rice probability function related to the minimized sum (MS) is considered to be the best fitting estimation of echo amplitude and describes the scattering characteristics of the organism.

Modelling *M. norvegica*

The DWBA prediction is based upon the coherent summation of scattering from discretized cylinders of varying radius that reproduce the krill body shape when juxtaposed. To include a more precise description of the krill body through its parameterization, McGehee *et al*. (1998) proposed a generic krill shape obtained digitizing the body of a *Euphausia superba* specimen of 38.35 mm length image in lateral aspect, which can be scaled to simulate other krill sizes. Demer and Conti (2003) found that freshly caught animals were 40 % fatter than the six months starved animal measured by McGehee *et al*., and suggested to take this increment into account for the computations. The stochastic version of the model (SDWBA) introduced by Demer and Conti (2003) uses such a standard shape and takes into account the stochastic nature of the scattering process, such as the along axis deformation and changes in animal body curvature during swimming. This is done incorporating a phase variability term φ for each discrete cylinder along the body obtained from a number of realizations of a Gaussian distribution, centred in 0 and with standard deviation sd_{φ}.. With a specific parameterization for *Euphausia superba* (Demer and Conti, 2005; Conti and Demer, 2006) the proposed SDWBA has been recently endorsed by the CCAMLR as the “Antarctic krill TS model” (SC-CAMLR, 2005).

M. norvegica is known to be similar to *E. superba* in the overall body shape and with respect to maturation; hence the DWBA model could be also appropriate for that species (Conti *et al*., 2005). However, the scaling process from a standard shape is debatable. Krill could have slightly varying shapes, depending upon feeding condition, gender and degree of

maturity. For a specific species and condition, the allometric growth of volume with size (e.g. Kils, 1979) should be considered and the roughness and the degree of bend may vary with the stage, influencing the angular dependence of the scattering (Stanton and Chu, 2000; Amakasu and Furusawa, 2006).

Thus, despite the similarity between the two species, an effort was undertaken to reproduce more precisely the shape of *M. norvegica* individuals at different lengths. In doing this, the digitalization procedure was also revisited. The purpose of the digitalization is to obtain a 2-D composite box model of an individual krill consisting of a number of rectangular elements along the body designed to reflect its original shape. The DWBA model assumes that the organism is circular in cross-section at every point along a central curve running through its body, so that the rectangular elements are later interpreted as discrete cylinders.

The *M. norvegica* composite box model was generated from high definition colour images in lateral view (10 Mb in tiff format) of animals caught during late winter in Raunefjord and photographed the next day after being stored live in a seawater tank overnight. A metric ruler was present in each image to allow the pixel-to-metric conversion. When digitizing the animal, two points were used to close the resulting polygon. These were the tip of telson and the joint where the peduncle of the 1st antenna ends. The perimeter along the ventral side of the body was slightly more difficult to determine compared to the dorsal side. It was chosen to digitize only the solid body structure, and not include the thoracic and abdominal legs as well as those parts of the exoskeleton that cover the abdominal legs. A vertical grid with appropriate longitudinal spatial resolution was superimposed to the image, and for every point where the vertical lines crossed the perimeter of the animals dorsal and ventral sides the x,y-coordinates were retrieved. For each element of the x,y-coordinates sets having identical x-coordinates, the midpoint between them were computed, hence a segmented centreline of the digitized animal was generated from the results. Starting from the tapered-tail point (i.e. tip of telson), for all the dorsal-side points the normal line to the centreline was determined and the coordinates of the points defined by the intersecting lines retrieved. One concern was to determine for a given dorsal point to which side of this point the normal to the centreline should be established. To a certain degree, it depends on the curvature of the animal and the digitized dorsal points, that is, whether the next dorsal point had a y-value greater or lesser then the preceding point. Finally, the tapered and the dorsal points define the position vector $\vec{r}_{pos}$, while their distances to the corresponding intersection points define the related radii. Together, they compose the arrays defining the discrete cylindrical body segments used as input to the DWBA model. So, it is apparent that only the upper part of the digitized body forms the basis of the final krill body reconstruction used for model computations.

In Figure 3 the proposed shapes obtained by the digitalization of three selected images with *M. norvegica* specimens of total length equal to 32.36, 26.8 and 21.87 mm are illustrated. The body shape resulting from the digitalization is shown in grey colour, the final points forming the $\vec{r}_{pos}$ position vector the related radius utilized as input for the DWBA models calculation as black dots and lines respectively. In some cases, it is evident that the distance between the tapered point and the closest dorsal point is different from the adopted spatial resolution. This is because the grid was chosen independently from the tapered points. In Table 3, morphological results for the three digitalized specimens and the main parameters of the digitalization process are listed. The differences between the shapes and their effect on the model results are commented in the Discussion section.

The formulations of the DWBA and its stochastic versions have been described in several articles (Stanton *et al.*, 1998b; McGehee et al., 1998; Demer and Conti, 2003; 2005; Conti and Demer, 2006). In all the versions, the material properties are allowed to vary inside the

fluid-like organism volume. However, as a good approximation they can be held constant over all the discretized-bent cylinders. This approximation is kept also in the present study; the sound speed contrast value was set to $h = 1.0383$ and the density contrast was based on the length relationship $g = -2.73\ 10^{-4} \cdot \mathrm{TL} + 1.0445$, being both determined by Calise *et al.* (2009b) for winter specimens of *Meganyctiphanes norvegica* captured in Raunefjord.

Conti and Demer (2006) showed that the SDWBA predictions are comparable in frequency domain if the number of cylinders N is large relative to the ratio of organism length to the acoustic wavelengths. For N close to the ratio, the use of the same $\mathrm{s.d.}_{\varphi}$ at different frequencies reflects to unrealistic off-axis lobes in the TS-predictions versus incidence angle. Hence, in order to ensure utility of the SWDBA model over a range of frequency, the SWDBA parameterization has to take explicitly into account the effects on the results of the interdependence of the four model factors: operative acoustic frequency, length of krill, number of discretized-bent cylinders and amplitudes of inter-element phase variability, and expressing the latter as function of the others.

A first inspection on the SDWBA run with the suggested Conti and Demer (2006) phase standard deviation $\mathrm{s.d.}_{\varphi_0} = \sqrt{2}/2$ over the proposed *M. norvegica* digitalized shapes revealed that unrealistic off-axis were obtained for frequencies higher than $f_0 = 100$ kHz for the form shapes of *M. norvegica* body length 32.36, and 26.8 mm, and $f_0 = 120$ kHz for the form shape from the 21.87 mm long specimen (c.f. Table 3).

Thus, following Conti and Demer (2006), for each of these shapes, the SDWBA predictions at frequencies f higher than the respective reference frequency f_0 were calculated adjusting the number of cylinders N and the standard deviation of the phase variability term φ by:

$$N(f, L) = N_0 \frac{f}{f_0} \frac{L}{L_0}\ ; \qquad \mathrm{s.d.}_{\varphi}(f, N) = \mathrm{s.d.}_{\varphi_0} \frac{N_0}{N(f)} \frac{L}{L_0} \tag{3}$$

where N_0 is the number of discredited-bent cylinders composing its basic shape, and the dimensional lengths ratio in both the equations is used to scale the digitalized shape of reference length L_0 to a generic L of a krill if needed. In Table 3, f_0 and N_0 for each of the proposed shapes are given.

For frequencies higher than the respective f_0, the original $\vec{r}_{pos}$ vector and radii values were resampled with higher sample rate, using a polyphase implementation and applying an anti-aliasing (low-pass) FIR filter, to reconstruct the shape through $N(f, L)+1$ points.

In all the further analyses, the SDWBA TS-predictions are then computed from the backscattering cross section areas averaged over 100 realizations of the random phase and specific distribution of orientation.

In practical works, the distribution of the angle of orientation θ is typically assumed as a Gaussian-like distribution defined by its mean and standard deviation values ($\theta = \mathrm{N}[\bar{\theta}, \mathrm{std}_{\theta}]$) in degrees. For comparison with the acoustic measurements, three different distributions of orientation were used as reference in the present study: 1) the N[0,0] distribution as expectation of the maximum TS-prediction related to the horizontally orientated position (broadside incidence) of the krill body; 2) the N[0,30] distribution observed *in situ* for no migrating activity of a *M. norvegica* individual by Kristiensen and Dalen (1986) analysing underwater photo-camera images, and very much close to the more recent observed N[0,27] by Lawson *et al.* (2006) on *Euphausia superba* images from video plankton recorder; 3) the N[11,4] distribution suggested for *E. superba* individuals in aggregation by Conti and

Demer (2006) derived matching SDWBA predictions based on average length from biological samples and volume backscattering data at 38 and 120 kHz.

In appendix, the simplified version of the SDWBA model provided by Demer and Conti (2005) is introduced, and the polynomial coefficients for the three proposed shapes determined over the selected distributions of orientation listed.

Results

Mesocosm environment

Two CTD casts were carried out in the mesocosm to determine the seawater physical characteristics at closest dates of measurements on 6 and 8 of March 2004. Temperature and salinity along the water column, as well the sound speed, were nearly constant with mean values of 5.72 and 5.82 °C, and 35.16 and 35.14 psu respectively. By entering manually the values into the environmental parameter menu of the Simrad ER60 software the computed seawater sound speed during the acoustic acquisition on tethered animals was 1476 ms^{-1}.

Biology and behaviour

Results of the morphological measurements for the four investigated animals are shown in Table 4. In Figure 5, plots of the total length versus carapax length and dry weight are shown. The grey dots are the measures on a random subset of animals (216 specimens) performed at the end of the experimental period. The related regressions in solid lines show the general trend of the *M. norvegica* mesocosm population. Black dots and open circles represent the measures of the accepted tethered animals used for the acoustic experiment and those digitized respectively. It can be observed that these specific individuals span a size range from 22 to 33 mm and align quite well with the general trends giving confidence that they may well represent the *M.* norvegica generations available in the northern Atlantic and adjacent seas during the winter period (0-group: < 1 year old, I-group: ~1½ year old). In terms of dry weight the tethered animals spans a range from 25 to 60 mg, with a factor of 2.3 from the smallest to the largest animal measured.

Video observations showed that the animals were generally moving in nearly horizontal direction with head-up orientation, stopping their activity for few seconds (mostly due to the attachment that limited the movements from the main line at longer distance of the life-line length) and start to swim again, usually changing direction. In these stop-and-go steps, the swimming speed appeared noticeable variable.

For each animal, an attempt was made to qualitatively estimate the range of orientation from a number of selected video frames recorded before the acoustic measurements with the body in lateral aspect when the eyes where collimate on respect to the camera. The orientation of the animal was then estimated by determining the angle between the white rope hanging vertically on the other side of the bag on respect to the camera (c.f. Materials and Methods section) and the dorsal border of the animal's carapax. Since the video records and the acoustic detections were not acquired contemporary, and the pour quality of the image limited the accuracy, the results from this analysis were judged to provide only a qualitative interpretation of the general orientation related to the behaviour. Some differences were found among the animals, the biggest ID 3 of 32 mm length and the smaller ID 8 of 22 mm length showed smaller range of orientation. Greater angles of orientation were always found

after that the animal stopped its swimming activity before to restart to swim. The estimated maximum angle was found for ID 6 of length 29 mm in the range 45-50º.

A**coustics**

For animals ID 6 and 7, measurements were additionally conducted for one given active frequency while all others were set in passive mode. This scheme was repeated until data were acquired for all frequencies. The data were then compared with those obtained using the normal procedure with all the systems set in active during the acquisition. The results did not show any particular difference between the two sets, especially in terms of PDF. Thus, the potential interferences on TS between the primary frequency and the others were considered null, or unimportant, on the results obtained.

A summary of the target strength measurements for the four chosen tethered specimens is given in Table 5. For each trial, recording time, number of pings and number of resolved echo realizations within the 6º solid beam angle are also given to illustrate the challenge of detecting the target inside the beam during measurements. For the smaller animal ID 8, it was initially difficult to see the target by the real-time echogram of the ER60 without pre-defining optimum SED parameters. However, by optimizing the SED criteria using the Sonar5 software, a satisfactory number of echotraces were retrieved also for this case.

The next two columns in Table 5 refer to the filtering process of Equation (1); p is the probability of the resolved animal contributions *PDF* related to that of the initial echo data-set and "krill echoes" is the number of the detections determined to be due to the animal after the reconstruction of the backscattering data-set.

The central part of the table is related to the results from the krill data-sets in logarithmic domain; the TS-mean was calculated in linear domain via the mean over of the corresponding backscattering cross sections in m^2. On the right side of the table, results derived from the minimized sum analysis on the echo amplitudes probability distributions are shown. The statistical mean ($\overline{TS}$) is the mean value of the theoretical best fitting curve transformed to logarithmic domain; shape parameter γ and the minimized sum (MS) of the fitting functions are also given.

Figures 5 and 6 show the graphical summaries of the results in logarithmic and linear domain respectively. In Figure 5 the frequency distributions of krill TS data-set are illustrated. The panels are horizontally ordered from bigger to smaller animal size and vertically by increasing frequency. For those cases whose it was needed to remove the line contribution by Equation (1), the frequency distribution of the original echo data is shown by the grey line. For a better readability, the histograms and the grey curves are plotted with 0.5 dB spaced bins while the actual analysis was performed grouping the data in 0.05 dB bin intervals. Figure 6 shows the summary of the echo-amplitude probability distributions of the backscattering krill data (grey bars) with the best fitting theoretical functions (black solid lines) determined from the minimized sum analysis superimposed. The MS listed in the last column of Table 5 were the sum of the square of the difference between the *PDF* values of the animal echo amplitudes and the points on the theoretical Rice *PDF* curve corresponding to the histograms and plotted in the panels of Figure 6 as black dot.

An expected characteristic of the results is that the TS distributions for bigger animals and low frequencies in Figure 5 exhibit a marked main mode. This is not the case for the smaller animal of 22 mm length and almost all the distributions at 200 kHz. These different trends are reflected in the linear echo-amplitude domain (Figure 6) by a Gaussian-like fitting having higher γ values (c.f. Table 5), while where there is a stronger tendency of bimodal

character in TS domain, the echo-amplitude distribution is better represented by a Rayleigh-like fitting curve distribution with γ values close or equal to zero.

In general, the TS-range are quite large and tends to increase with the frequency (Table 5), except for the bigger animal ID 3, which at 200 kHz has smaller range of values compared 70 and 120 kHz, and for the ID 7 that exhibits similar range of values from 70 to 200 kHz. At 120 kHz, all the distributions have the more similar TS-range. As expected, the TS-maximum increases with frequency for all the animals with exception of the biggest ID 3 of 32 mm length that exhibits a lower value at 120 kHz compared to the 200 kHz. The mean- and median-TS seem to have similar relative trends for the bigger and the smaller animals, increasing with the frequency. Interestingly, this does not appear for the middle sized animals in the transition from 120 to 200 kHz. For both the animal of 27 and 29 mm length, stronger mean values at 120 kHz compared 200 kHz were observed, even if the TS-maximum was recorded with different trend, being 2 dB stronger at 200 kHz.

For each animal, the statistical mean $\overline{TS}$ has a similar trend of the observed TS-mean and TS-median. It is always stronger than the TS-mean, while the comparison with the TS-median shows high variability: $\overline{TS}$ is always lower for the biggest ID 3 animal, stronger for the smallest ID 8 animal, and without a definite trend for the middle sized animals.

However, the comparison between animals must be taken with caution since the tether might have influenced differently the orientation of each specimen. A more confident comparison can be done between the frequencies for each of the specimens investigated.

For the bigger animal ID 3 of 32 mm total length the main mode of the distributions is maintained with increasing frequency, as well as the observed averages and the statistic mean increase. This is fully reflected in the linear echo amplitude domain, with the shape parameter γ inversely related to the TS-range. It is interesting to note the tendency for a modest main bimodality of the distribution at 70 and 120 kHz. While the lower part of the distribution at 120 kHz can be suspected to be in part influenced by the coherent scattering from the line, the apparent secondary mode, close to the primary, is certainly due to the animal contribution and its changes of orientation.

The TS distribution at 38 kHz for the smallest specimen ID 8 of 22 mm length is clearly limited in its left part by the bias of the high background noise for that system (Table 1). This influences the statistics results too and most probably the actual Gaussian-like fit of the echo amplitude distribution should be shifted to lower levels as well the value of the statistical mean. Comparing the frequency results for that animal, it is evident that the fitting curve tends to Rayleigh-like distribution with the increasing of the frequency and γ tends to zero, reflecting the largest range of TS values obtained. Similar trends are shown by the ID 7, despite in this case the inverse relationship between γ and the range of TS values is not respected at 70 kHz. This is due to the noticeable Gaussian-like character of the distribution at high values of TS.

The distributions for the ID 6 of 29 mm length relative to the frequency appear different in both the domains. At 70 kHz the echo amplitude has already a Rayleigh-like character, with γ having the same value and almost similar to the fitting curves at 120 and 200 kHz respectively. In TS domain (Figure 5) the value are not as concentrated as for the other animals, but appear more distributed within the observed range. At 120 kHz, a secondary mode related to the lower TS levels becomes more distinct, until to be primary at 200 kHz. This frequency trends can be attributed to the changes of orientation and it is an issue for the Discussion section.

In Figure 7, the major SDWBA modelling results are superimposed to the measurements and statistics of the observed TS frequency distributions. The vertical bars extend over the

range of acquired TS. The TS-median and the third and first quartiles of the distribution are also shown as described in the caption of the figure. The black dotted lines connect the statistical mean $\overline{TS}$ of the data-sets (Table 5). The SDWBA models were run with the same sound speed $c = 1476$ m s^{-1} as during the measurements, an the material properties contrast $h = 1.0383$ and g(TL) given in Table 3 as determined by Calise *et al.* (2009b) for winter specimens of *Meganyctiphanes norvegica* from a Norwegian western fjord. For each shape the number of cylinders and the standard deviation phase variability were varied with the frequency according to Equations (3) and reference parameters are given in Table 3. Results using the three reference distribution of orientations N[0,0] (grey solid lines), N[0,30] (grey dotted lines) and N[11,4] (grey dashed lines) are shown.

It is firstly observed that the model results at 38 kHz for the 22 mm length show a close to -10 dB offset compared to the observed median and statistical mean. As mentioned above, this is quite certainly attributed to the related low signal-to-noise ratio below -90 dB for this system. A similar offset is found for the 27 mm length at 38 kHz, but now being reduced to about -5 dB, and in this case the modelling results are found within in the relative lower range of the actual measurements from around -87 to -92 dB. For the 32 mm animal the model fits better at 38 kHz compared to the two smaller animals. For the different orientation angle realizations the results are quite similar at lower frequencies around 38 kHz. At higher frequencies the model computations slightly deviate from each other, but the realizations with N[11,4] seems in general to fit the measured values better than the other two. This is particularly evident for the 32 and 22 mm lengths. As expected, the model realizations over N[0,0] gives the highest TS values for all animals over the presented frequency range, except for the 32 mm length above 220 kHz. For all the lengths, the predictions for this orientation are also clearly above the median and mean TS values for the two highest frequencies, and for the 32 mm length the value (-69.3 dB) is quite close to the measured maximum TS at 200 kHz (-68.1 dB). For animal with that length, the highest target strength was observed at 120 kHz (-65.7 dB), the model prediction for N[0,0] is not so close (-68.8 dB), but indeed slightly higher than for 200 kHz. For the intermediate sized animal, the others orientation predictions at 70 and 120 kHz are offset approximately -5 dB to -10 dB compared to median and mean target strength values measured.

Discussion

There is an increasing interest on studying the Northern krill *M. norvegica* species in terms of ecology of Northern marine areas and exploitation in aquaculture as new feed resource (e.g. Suontama, 2004; Dalpadado, 2006). For this reason, correct and rapid methods for the abundance estimation of this important pelagic ecosystem component are strongly wanted. Multifrequency acoustic technique is the answer to such requirement, and the knowledge of the *M. norvegica* target strengths and its variability at the common survey frequencies is the key for the correctness of its application.

In addition, *M. norvegica* is also acoustically relevant as it is assumed to be similar in shape and maturity stages with the very important species Antarctic krill (Conti *et al.*, 2005), but it is more accessible to researchers. It has a typical overlapping length distribution and its biological aspects related to the acoustical problems have been the object of several studies. Thus, *M. norvegica* could be used as a suitable acoustic model for krill in general.

Many problems may arise in acoustic studies of *M. norvegica* species *in situ* since it is mostly found in locally and seasonally variable aggregations composed of species and sizes of other zooplankton and fish larvae. Therefore, the identification and discrimination of the scatterers from multifrequency acoustic data becomes definitely a challenge (e.g. Calise *et al*., 2007; Korneliussen *et al*.; 2007; 2009). Model predictions may help in this step only if the backscattering properties of the target are well known and the TS-estimates comparable with available results obtained by direct measurements made under controlled conditions.

The present study represents a step forward in this sense. Accurate multifrequency acoustic backscattering measurements on living individuals of *M. norvegica* achieved through a suspension method are compared to the theoretical predictions derived from the most accredited model at present.

Methodological aspects

As mentioned in the Material and Methods section, a total of eight animals were suspended under the acoustics beams and acoustically measured, but only four specimens were considered correctly attached to the life-line. This may well explain the practical difficulties in measuring small fluid-like organisms with such method. However, the suspending method gives the opportunity for a more confident comparison between the acquired data with theoretical scattering model predictions since the animal size and shape can then be precisely known. Fortunately, the range in length spanned by the selected animals covered the requirement for the purpose of the experiments.

Despite the individual organism was forced to move under limited conditions in space and behaviour by the attachment system, we are confident that the animals exhibited a natural behaviour during the acoustic acquisition. The large volume of the mesocosm and the use of deep seawater assured that no other physical restriction influenced the animal behaviour. Video observations indicated that all the animals were in health condition and swimming almost freely with typical pleopod propulsion before and after the session of measurements.

The main worry during the acquisition was related to the time needed for an entire session of measurements wherein the animal could be held in suspending condition without stress and activation of proteins coagulation that could have changed its acoustic characteristics. This could be a potential effect during the acquisition with the last frequencies used in the session of measurements and compromise the correctness of the comparison between frequencies. For this reason the time of observation at all the frequencies was cut as short as possible, particularly for small animals. Although this limitation, each trial of measurement was performed over a time interval allowing to acquire a good number of detections without perceptible regression of the animal' activity. Since post measurements inspection by video camera confirmed this impression, the effects of the stress were considered not present. With the exception of the smaller ID 8 of length 22 mm at 38 kHz, the number of observations at each frequency was judged large enough to be comparable, and no random selection to obtain equal number for each frequency was applied.

Apart from the observed maximum TS values, the filtering process on some of the recorded backscattering data-set was a concern for the confidence of the results. The consequence of the processing were noticeable only for the data-sets at 200 kHz, while for the other cases it was very weak, if not considered null (Table 5). The filtering was focused on removing only the incoherent contribution from the line. It is very likely that coherent scattering exists; it would be dependent on the random animal-line interrelationship at each of the resolved echoes, and to eliminate correctly such effect is not an easy task. Thus, no such attempt has been made. However, the coherent contribution can be roughly estimated as double in

strength (6 dB) of the line data backscattering alone (assuming equal strength of line and animal contributions). This means that these contributions can be supposed quite low in level with respect to the animal backscattering which is a much stronger scatterer than the line.

Other techniques to remove the incoherent part, such as regular discrete cross correlation and discrimination of the echoes in each bin by scaling the echoes with a factor equal to the ratio between the detections in it, were tested but judged inappropriate.

Since Stanton and Chu (2000) claimed that for single ping investigations the organism shape and material properties must be known with high degree of precision for accurate TS predictions, it was judged worthy to extrapolate new shapes for *Meganyctiphanes norvegica* at different lengths, and compare the results with those obtained using the krill standard shape proposed by MacGehee *et al*. (1998) from an *Euphausia superba* long 38.35 mm. Figure 8 illustrates the importance of the shape in the model prediction. The SDWBA TS-predictions obtained by scaling different krill shapes to the length 21.87 mm are shown for the three reference distributions of animal orientation. Results from backscattering strengths retrieved from the tethered specimen ID 8 of length 22 mm are superimposed for a comparison.

In general, there is a big discrepancy between the results. It seems that for higher than zero mean orientation, closer TS-predictions are obtained. This was to some extent expected since the errors due to imperfect representation of the shape or material profile can become negligible once averaged (Stanton and Chu, 2000). For the orientation N[0,0] (Fig. 8a) the curves substantially deviate from each other and none of them predicts values close to the maxima of the experimental results. The results obtained by scaling the shape derived from the 26.8 mm specimen are the closest. At 200 kHz the TS prediction for this curve is -67.03 dB, which means 1.2 dB lower than the experimental maximum. The curve obtained using the shape derived from the 21.87 mm and the scaled from 32.36 mm length specimens shape are closer to each other, at least until 250 kHz.

With the orientation N[0,30] (Fig. 8b), the deviations between the curves are smaller in the range of the experimental frequencies; while in the range from 240 to 300 kHz all the curves surprisingly predict an equal result with maximum difference at 285 kHz of 0.2 dB. Apart from the experimental 38 kHz result, which must be taken with care, the results obtained scaling the shape derived from the 26.8 mm specimen seem to fit better with the experimental median values. This is the same for the curve obtained from the 21.87 mm specimen shape and that from the scaled McGehee *et al*. shape when the orientation N[11,4] is imposed (Fig. 8c). In this case the two curves are more close. At 70 kHz the first predicts a TS value equal to -84.1 dB while the second -83.2 dB, being closer to the experimental median -83 dB. At 120 kHz they show quite similar results to the experimental median predicting -78.1 and -78.2 dB respectively. At 200 kHz the first predicts -75.9 dB and closer to the experimental median (-75.6 dB), while the second -76.81 dB.

The main difference between the digitalization procedure presented in this study and that proposed by McGehee *et al*. (1998) is the choice of extrapolating the points by superimposing a regular grid to the image rather than follow the changes in shape of the dorsal outer of the animal. This was done in order to assure the constancy of spatial resolution relative to the wavelength and to respect the condition for stability of the SDWBA (Conti and Demer, 2005) by obtaining uniformly spaced cylinders. Moreover, the use of a grid permits to simply choose the increment for the body reconstruction, hence the spatial resolution of the digitalization. Stanton and Chu (2000) claimed that a very rigorous approach in model TS-prediction has to involve a digitalization of the shape (and in the case of the material properties also) in increments much smaller than the acoustic wavelength λ.

In the present study, for the grid increment Δ used to extrapolate the proposed shapes (Table 3), the ratio λ/Δ at the frequencies used for the measurements is less than 10 only at 200 kHz for all the shapes, with a minimum of 5.2 for the shape a) relative to the 32.36 mm long specimen and at 120 kHz (8.9) for the same shape a).

Examples of krill body recontruction via digitalization have been presented in Amakasu and Furusawa (2006) also. In this study 12 digitalizations of specimens of Euphausia superba in a length range of [40.5, 51.35] mm and one animal of 30.3 mm length are presented. The authors did not describe the extrapolation procedure adopted, but from their Figure 6 it can be supposed that they used a grid approach as in the present study.

From figure 3, the bend appears to increase for smaller sized animal. This can be an artefact due to the position of the animal when photographed. On the other hand, the segments of the abdomen are relatively smaller for such animal length, and seem less flexible as than bigger size so that small animals seem to swim with the body positioned more bent than straight.

Acoustic results and theoretical approach

An evident characteristic of the results is the large range of TS values found for all animals at all the frequencies. Following the swimming angle-speed model for Euphausiid proposed by Kils (1982), the behaviour observed by video records could reflect in a wide range of animal orientation. Therefore, since the TS range depends upon general animal orientation, the observation of large range in backscattering levels was fully possible.

A specific inspection on consecutive or neighbouring echoes also revealed a relative high degree of ping-to-ping TS variability, especially at 200 kHz for all the animal lengths. This was also an expected result since the separate contributions to the scattering from the different anatomical parts (such as exoskeleton segments, tail, antennas and the eyes, as well the pleopod beats) certainly change when the animal swims, and increase the stochastic nature of the TS (stochastic roughness).

It is clear from Figures 5 and 6 that the orientation plays a key role in both the overall scattering levels as well as the statistical behaviour of the echoes. Indeed, the statistical properties of the observed echoes are related to the dominant scattering processes associated with shape and orientation of organisms, and operative frequencies (Martin Traykovski *et al.*, 1998; Stanton *et al.*, 2004). With respect to the wavelength, the scattering has to be associated at any particular physical feature, such as an edge, outer surface, or an organ. The total scattered field will be comprised of the sum of the contributions from each of those features. As the orientation of the organism changes so will the interrelation of the contributions, and the statistical fluctuations of the echo amplitude may exhibit a high degree of ping-to-ping variability. At larger wavelength compared to the maximum dimension of the organism, a Gaussian-like echo distribution has to be expected, since there is a stronger contribution, mainly from the entire body, which vary with the orientation.

Thus, from the echo statistic results in Figure 6 and Table 5, it is clear that in the case of krill the shape parameter γ of the fitting curve does not indicate the behaviour of the animal, as claimed for fish by Clay and Heist (1984), rather it is related to the fluctuation due to the interrelationship between orientation and frequency.

To illustrate the predicted backscattering dependence on both frequency and angle of orientation, theoretical TS as a function of angle of incidence (90º-angle of orientation) for the three proposed shapes are plotted in Figure 9. While the absolute TS values have to be considered with caution since substantial discrepancies were found with the empirical

results (Figure 7), the behaviour of theoretical functions versus angle of incidence may partially help to explain the backscattering distributions of Figure 5, with confidence that the filtering process did not neglect some contributions from the animal.

As mentioned, the comparison between animal results can be inappropriate since the tether might have influenced the orientation of each specimen differently.

In general, it can be seen that the orientation dependence of the backscattering increases with increasing frequency, and the level of sophistication of the model is less critical at angles close to broadside. Focusing the attention on the range of incident angle on the left side of the main lobe, corresponding to the qualitative video results for the angle of orientation, it can be noted that for the bigger animal of length 32.36 mm (Fig. 9a) the 200 kHz curve is lower than the 120 kHz in the range [80, 90] degrees, but higher in the range [65, 80]. Within the range [62, 90] degrees it is much more smoothed than the 120 kHz curve without showing deep nulls. On the contrary, the 120 kHz shows relative maxima at 68º and an evident null at 73º. This may clarify the smaller TS-range at 200 kHz and the modest main bimodality at 120 kHz observed in the TS distributions relative to the ID 3 in Figure 5. For the 70 kHz the observed bimodality is not explained by the relative curve in Figure 9a, while the 38 kHz Gaussian-like distribution in Figure 5 is fully justified.

For the middle size animal of length 26.80 mm (Figure 9b) the 200 kHz is clearly stronger compared to the 120 kHz in the range [84, 90] degrees and lower in the range [77, 84]. The relative maximum at 75º and the null at 80º may to some extent explain the marked bimodality observed in the TS distribution, with the majority of echoes in the lower levels. The 120 kHz curve decreases smoothly until 73º and may clarify the related distribution in Figure 5 for the ID 7 that does not show a marked separation from the higher to lower TS values but appear uniformly decreasing. The smoothed curves for the 38 and 70 kHz reflect the Gaussian-like distribution observed for the relative ID 7 distributions in Figure 5. The latter observation can be similarly made for the curves in Figure 9c and the related TS distributions for ID 8 of 22 mm length in Figure 5.

A number of acoustic studies on euphasiids using the suspending method, tethering the animal by a human hair or very thin nylon lines, and involving single ping investigation have been presented in literature (Kristensen, 1983; Wiebe *et al*., 1990; Stanton *et al*. 1994; Demer and Martin, 1995; McGehee *et al.,* 1998; Stanton *et al*. 1998a; De Robertis, 2001; Amakasu and Furusawa, 2006). In some cases, the animals were anesthetized before the acquisition. Due to the range of frequencies used, species (mostly Antarctic krill) and length of the animals, and the type of instrumentation used in acquiring the data, it is difficult to proceed to a direct comparison with this study. In general, our measured target strengths are slightly higher than what has been observed in the cited studies. *In situ* TS results on *Meganyctiphanes norvegica* in a location not very different from that where the animals of the present study were caught, show a good agreement with our TS results. A similar trend has also been found in a specific experiment on free swimming animals in the same mesocosm venue (Calise *et al*., 2009a). In that paper, one of the principal reasons of discrepancy was attributed to the non-linear effects of high-power transmissions at higher frequencies which were not considered in the previous studies. However, since in this case the length and the shape of the animals under investigation are well known, it is possible to hazard the claim that for equal length of specimen the Northern krill seems to be a stronger scatterer compared to the Acoustic krill. Differences in biochemical composition, hence in acoustic impedance contrast, due to the diet (Calise *et al*., 2009b) may be a plausible cause.

Previous studies have indicated the changes in orientation and the relative highly oscillating patterns of krill target strength as the main reason of the discrepancy between measurements and model predictions (e.g. Demer and Martin, 1995; Stanton, *et al*. 1998a; 1998b;

McGehee *et al*., 1998; Martin Traykovsky *et al*., 1998; Demer and Conti, 2003, 2005; Amakasu and Furosawa 2006). The deviation was mostly evident in the side-lobe of the predicted TS versus angle of incidence pattern, while a good agreement near the main-lobe (broadside incidence) was generally found.

The results plotted in Figure 7 revealed a substantial discrepancy between measurements and SDWBA model predictions in this study too. In addition, the comparison with the distribution of orientation N[0,0] (grey solid lines in Figure 7) indicates that the deviation is relevant at broadside incidence also, i.e. main lobe of the predicted TS-pattern orientation.

A similar deviation (in some cases 10 dB lower) for the DWBA model main-lobe was found by De Robertis (2001) for *Euphausia pacifica* specimens from 8 to 22 mm long anesthetized with MS222 and tethered under a 445 kHz acoustic system beam.

Several factors can be the cause of the discrepancy. They can be related to the reconstruction of the body shape (bending of abdomen, pleopods beats and scattering, separate contributions to the scattering from the tail, the antennas and the eyes, circular approximation of the body in 3D) and to the key parameters used as input of the model.

In a first evaluation, it can be presumed that the bending of abdomen and the scattering contribution from pleopods may be the main causes. The krill body is perhaps more straight when the animal swims than when it is observed at a fixed position on a laboratory dish, while the pleopods were ignored in the body digitalization. Amakasu and Furusawa (2006) separately investigated the TS-pattern of the DWBA model versus angle of incidence when the abdominal bending is increased and the pleopods are included to the digitalized shape. In the first case, the results showed a broader main-lobe, with maximum TS shifted to negative tilt, and the side-lobe levels increased. In the second case, the peak level of the side-lobe was increased, while decreased in the main-lobe of the TS-pattern. Therefore, it may be possible that these two reasons do not particularly affect the case in this study.

The use of erroneous material contrast values is also known to be a cause of the discrepancies between the empirical observations and the theoretical predictions of target strength. The contrasts are species-dependent, varying with size, stage, geographical location, season, and in some case with the depth. Stanton and Chu (2000) performed a series of DWBA simulations at 120 kHz over the published range of material properties values and found that by varying the contrasts from 1 to 6 %, the predicted TS as function of angle of orientation exhibits a large change in overall levels of scattering in the order of 15 dB. The use of the same sound speed contrast for different animal lengths can explain some of the deviations found in this study, but to estimate the actual effect it is not an easy task due to the lack of certain data relative to the *Meganyctiphanes norvegica* species and krill in general.

It is possible to ascribe the cause of deviation to the material contrasts values, but to identify a definite cause through a single factor is not reasonable. It is more likely that in single ping investigations the model deviations from the observed scattering levels have to be attributed to a combination of numerous factors and their interrelationships in the formulation. To estimate these highly variable effects seems extremely complicate, if at all possible.

Conclusions

Accurate multifrequency acoustic backscattering measurements on live tethered specimens of the Euphausiid *Meganyctiphanes norvegica* have been performed in a large enclosure and

compared to the model predictions derived from the most accredited model at present: the Stochastic Wave Born Approximation (SDWBA).

The enclosure was vertically suspended in the sea from a raft and filled with filtered deep seawater assuring a homogeneous and optimal medium for the acoustic measurements. The Euphasiids were caught during nighttimes in the upper layer of a Norwegian western fjord and kept in good condition in a large tank filled up with same deep seawater for a few days before being employed for the measurements.

The tethered system allowed the animals to swim almost freely, without being severely hampered by the method of attachment, and permitted an easy control of the animal's position inside the volume of the measurement venue. With such system the animal was placed in turn close to the beam axes of four Simrad EK60 systems, operating at the frequencies of 38, 70, 120 and 200 kHz, and a good number of detections at each frequency was acquired.

Despite difficult to realize, the entire procedure of acquisition was performed with success for four specimens spanning a length range from 22 to 33 mm and well representing the *M. norvegica* generations of the northern Atlantic and adjacent seas during the winter period.

Acoustic results in TS domain and from echo statistic analysis have shown that the scattering process is highly complex and very sensitive to the size and angles of orientation of that organism, particularly for the higher frequencies utilized. Large range of TS values and high ping-to-ping variability increasing with the frequency were observed for all animals at all the frequencies. The maximum recorded TS increases with the frequency also, but in this case with exception of the biggest 32 mm long specimen that seems to be a weaker scatterer at 120 kHz compared 200 kHz. For animals with length in the range from 27 to 29 mm the observed mean values were stronger at 120 kHz than at 200 kHz, despite the maximum TS was 2 dB stronger at 200 kHz. This particular feature indicates a presumable transition frequency that may help to provide directly estimates of the size of Northern krill by acoustic data *in situ*. In this sense, the data comparison between the 120 and the 200 kHz is an attractive way from the viewpoint of length variability.

Previous digitalization for the reconstruction of the body shape has been revisited and three shapes relative to different Northern krill lengths have been proposed. The SWBA was run over three selected distributions of orientation to simulate the possible behaviour of the animals when tethered under the acoustic beams.

Modelling results and predictions reflect the scattering complexity but have been found much lower than the empirical strength levels. No single factor seems to be causing this deviation. Instead it must be due to a combination of numerous factors

The high level of complexity and variability of the observed scattering indicates that sophisticated models are necessary to reproduce the different aspects of the process, but at same time they should be less sensitive to the potential error in the key input parameters.

Appendix

Simplified SDWBA estimations for Northern krill target strength

Demer and Conti (2005) indicated that the SDWBA TS-prediction over a definite distribution of orientation could be simplified as a function of the product of the acoustic wave number k and the mean length L of the animals under investigation. The function

TS(kL) is concisely expressed by a sixth order polynomial representation with coefficients estimated over the specific animal orientation distribution:

$$\mathrm{TS}(kL) = \mathrm{A}\left(\frac{\log_{10}(\mathrm{B}kL)}{\mathrm{B}kL}\right)^{\mathrm{C}} + \mathrm{D}(kL)^6 + \mathrm{E}(kL)^5 + \mathrm{F}(kL)^4 + \\ + \mathrm{G}(kL)^3 + \mathrm{H}(kL)^2 + \mathrm{I}kL + \mathrm{J} \tag{A1}$$

The first term of Equation (4) reflects the non-linear behaviour of the prediction, and it is found by estimating the three coefficients of a non-linear regression using a least-squares estimation approach. The other coefficient can be then found by polynomial fitting to the TS predictions in the least-squares sense.

In Table 6, the resulting coefficients of Equation (A1) for the three proposed shapes in Figure (3) over the selected distributions of orientation N[0,0], N[0,30] and N[11,4], and the related error in decibels between the exact and the simplified SDWBA prediction are listed.

Acknowledgements

Mr. Erik Stenersen, Mr. Are Johansen and dr. Frank Reier-Knudsen at Simrad AS in Horten (Norway) are acknowledged for their skilled support through all phases of the experiments and for making available parts of the acoustic system. Professor Halvor Hobæk, University of Bergen, Norway, is thanked for the constructive review of the manuscript. The IMR is thanked for making the project possible through funding via the internal program on “New feed resources for the Aquaculture industry”. The Research Council of Norway is thanked for partial support through the project “Harvesting at lower trophic levels - stock assessment and ecological consequences” project no. 178447. This is also a contribution to The Barents Sea Ecosystem Programme and the Norw**e**gian Sea Ecosystem Programme at IMR. The University of Bergen is thanked for the LC financial supporting under the UiB PhD fellowship program.

References

Amakasu, K., and Furusawa, M. 2006. The target strength of Antarctic krill (*Euphausia superba*) measured by the split-beam method in a small tank at 70 kHz. ICES Journal of Marine Science, 63 (1): 36-45.

Balk, H., and Lindem, T. 2005. Sonar4, Sonar5 and Sonar6 post processing systems, Operator manual version 5.9.6. Lindem Data Acquisition, Humleveien 4b, 0870 Oslo Norway, 380 pp.

Boysen, E., and Buchholz, F. 1984. *Meganyctiphanes norvegica* in the Kattegat. Marine Biology, 79 (2):195–207.

Bracewell, R. N. 1999. Pentagram Notation for Cross Correlation. In: The Fourier transform and its applications. New York: McGraw-Hill, 3rd ed., 624 pp**.**

Calise, L., Knutsen, T., and Melle, W. 2005. Multifrequency Acoustic Measurements of free swimming northern krill (*Meganyctiphanes norvegica*) in a mesocosm venue: methodological challenges. Proceedings of the International Conference "Underwater Acoustic Measurements: Technologies & Results", Heraklion, Crete, Greece, 28 June – 1 July 2005, Vol. II: 865-871.

Calise, L., Knutsen, T., and Korneliussen, R. J. 2007. The impact of echo sounder settings for the discrimination of acoustic scatterers in a multi-frequency survey context. Proceedings of the 2nd International Conference "Underwater Acoustic Measurements: Technologies & Results", Vol. III, pages 1201-1208, Heraklion, Crete, Greece, 25th -29th June 2007.

Calise, L., Knutsen, T., and Melle, W. 2009a. Multifrequency target strength of horizontally free swimming Northern krill (*Meganyctiphanes norvegica*) in a mesocosm venue. In preparation. Paper V of this thesis.

Calise, L., Mukai, T., and Knutsen, T. 2009b. Density and speed of sound in winter specimens of Northern krill (*Meganyctiphanes norvegica*) from a west Norwegian fjord. In preparation. Paper I of this thesis

Chu, D., Foote, K. G., and Stanton, T. K. 1993. Further analysis of target strength measurements of Antarctic krill at 38 and 120 kHz: Comparison with deformed cylinder model and inference of orientation distribution. Journal of the Acoustical Society of America, 93 (5): 2985-2988.

Clay, C. E., and Heist, B. G. 1984. Acoustic scattering by fish acoustic models and a two-parameters fit. Journal of Acoustics Society America, 75 (4): 1077-1083.

Conti, S. G., Demer, D. A., and Brierley, A. S. 2005. Broad-bandwidth, sound scattering, and absorption from krill (*Meganyctiphanes norvegica*), mysids (*Praunus flexuosus* and *Neomysis integer*), and shrimp (*Crangon crangon*). ICES Journal of Marine Science, 62 (5): 956-965.

Conti, S. G., and Demer, D. A. 2006. Improved parameterization of the SDWBA for

Dalpadado, P. 2006. Distribution and reproduction strategies of krill (Euphausiacea) on the Norwegian shelf. Polar Biology, 29 (10): 849–859.

Demer, D. A., and Martin, L. V. 1995. Zooplankton target strength: Volumetric or areal dependence?. Journal of the Acoustical Society of America, 98 (2): 1111-1118.

Demer, D. A., and Conti, S. G. 2003. Reconciling theoretical versus empirical target strengths of krill: effects of phase variability on the distorted-wave Born approximation. ICES Journal of Marine Science, 60 (2): 429-434.

Demer, D. A., and Conti, S. G. 2004. Erratum - Reconciling theoretical versus empirical target strengths of krill: effects of phase variability on the distorted-wave Born approximation. ICES Journal of Marine Science, 61 (1): 157-158.

Demer, D. A., and Conti, S. G. 2005. New target-strength model indicates more krill in the Southern Ocean. ICES Journal of Marine Science, 62 (1): 25-32.

De Robertis, A. 2001. Validation of acoustic echo counting for studies of zooplankton behaviour. ICES Journal of Marine Science, 58 (3): 543-561.

Everson, I., Tarling, G. A., and Bergström, B. 2007. Improving acoustic estimates of krill: experience from repeat sampling of northern krill (*Meganyctiphanes norvegica*) in Gullmarsfjord, Sweden. ICES Journal of Marine Science, 64 (1): 39-48.

Falk-Petersen, S., and Kristensen, Å. 1985. Acoustic assessment of krill stocks in Ullsfjorden, North-Norway. Sarsia, 70 (1): 83-90.

Foote, K. G., Knudsen, H. P., Vestnes, G., MacLennan, D. N., and Simmonds E. J. 1987. Calibration of acoustic instruments for fish density estimation: A practical guide. ICES ICES Cooperative Research Report, 144, 69 pp.

Foote, K.G, Everson, I., Watkins, J. L., and Bone, D. G. 1990. Target strength of Antartic krill (*Euphausia superba*) at 38 and 120 kHz. Journal of Acoustics Society America. 87 (1): 16-24.

Greene, C. H., Wiebe, P.H., Burczynski, J., and Youngbluth M.J. 1988. Acoustical detection of High-Density Demersal Krill Layers in the Submarine Canyons off Georges Bank. Science, 241: 359-361.

Greenlaw, C. F. 1979. Acoustical estimation of zooplankton populations. Limnology and Oceanography, 24 (2): 226-242.

Kieser, R., Mulligan, T. K., Ehrenberg, J. E. 2000. Observation and explanation of systematic split-beam angle measurements. Aquatic Living Resources, 13: 275–281.

Kils, U. 1979. Preliminary data on volume, density and cross section area of Antarctic Krill, Euphausia superba. Meeresforsch., 27:207-209.

Kils, U. 1982. Swimming behaviour, swimming performance and energy balance of Antarctic krill, *Euphausia superba*. Biomass Scientific Series, 3. pp.121.

Klevjer, T. A., and Kaartvedt, S. 2006. *In situ* target strength and behaviour of northern krill (*Meganyctiphanes norvegica*). ICES Journal of Marine Science, 63 (9): 1726-1735.

Korneliussen, R. J., Lebourges-Dhaussy, A., and Knutsen, T. 2007. Estimation of size and type of zooplankton by the use of operational post-processing systems. *In* Proceeding of the 2nd International Conference ”Underwater Acoustic Measurements: Technologies & Results”, Heraklion, Crete, Greece, 25-29 June, 2007.

Korneliussen, R. J., Diner, N., Ona, E., Berger, L., and Fernandes, P. G. 2008. Proposals for the collection of multifrequency acoustic data. ICES Journal of Marine Science, 65. In press.

Korneliussen, R. J., Heggelund, Y., Eliassen, I. K., Øye, O. K., Knutsen, T., and Dalen, J. 2009. Combining multibeam sonar and multifrequency echo sounder data: example analysis

and imaging of large euphausiid schools. Submitted to ICES Journal of Marine Science, 69: 000–000.

Kristensen, Å. 1983. Acoustic classification of zooplankton. Dr. Ing. Thesis/ELAB Rep STF44 A83 187. University of Trondheim, Norway, pp. 107.

Kristensen, Å., and Dalen, J. 1986. Acoustic estimation of size distribution and abundance of zooplankton. Journal of the Acoustical Society of America, 80 (2): 601-611.

Labat, J. P., and Cuzin-Roudy, J. 1996. Population dynamics of the krill *Meganyctiphanes norvegica* (M. Sars, 1857) (Crustacea: Euphausiacea) in the Ligurian Sea (NW Mediterranean Sea). Size structure, growth and mortality modelling. Journal of Plankton Research, 18 (12): 2295-2312.

Lavery, A. C., Stanton, T. K., McGehee, D. E. and Chu, D. 2002. Three-dimensional modeling of acoustic backscattering from fluid-like zooplankton. Journal of the Acoustical Society of America, 111 (3), 1197-1210.

Lawson, G. L., Wiebe, P. H., Ashjian, C. J., Chu, D., and Stanton, T. K. 2006. Improved parametrization of Antarctic krill target strength models. Journal of the Acoustical Society of America, 119 (1): 232-242.

Martin Traykovski, L. V., O'Driscoll, R. L., and McGehee, D. E. 1998. Effects of orientation on broadband acoustic scattering of Antarctic Krill (*Euphausia superba*): Implications for inverting zooplankton spectral acoustic signatures for angle of orientation. Journal of the Acoustical Society of America, 104 (4): 2121-2135.

Mauchline, J. 1980. The biology of Mysiids and Euphausiids. Advances in Marine Biology, 18, 681 pp.

Mauchline, J., and Fisher, L.R. 1968. Distribution of the euphausiid crustacean *Meganyctiphanes norvegica* (M Sars). Limnology and Oceanography, 13 (4): 727-728.

McGehee, D. E., O'Driscol, R. L., and Martin Traykowski, L.V. 1998. Effects of orientation on acoustic scattering from Antarctic krill at 120 kHz. Deep-Sea Research II, Topical Studies in Oceanography, 45 (7): 1273-1294.

Morris, D. J., Watkins, J. L., Ricketts, C., Buchholz, F., and Priddle, J. 1988. An assessment of the merits of length and weight measurements of Antarctic krill *Euphausia superba*. British Antarctic Survey Bulletin, 79: 27-50.

Ona, E., and Barange, M. 1999. Single-target recognition. *In* Methodology for Target Strength Measurements. ICES Cooperative Research Report, 235: 27-47.

Pauly, T., and Penrose, J. D. 1998. Laboratory target-strength measurements of free-swimming Antarctic krill (*Euphausia superba*). Journal of Acoustical Society of America, 103 (6): 3268-3280.

Richter, K. E. 1985. Acoustic scattering at 1.2 MHz from individuals zooplankters and copepod populations. Deep-Sea Research Part A, 32 (2): 149-161.

SC-CAMLR 2005. Report of the 24th Meeting of the Scientific Committee, Hobart, Australia (SC-CAMLR-XXIV). Commission for the Conservation of Antarctic Marine Living Resources, pp 564-585.

Stanton, T. K., Chu, D., Wiebe, P. H., and Clay, C. S. 1993. Average echoes from randomly oriented random-length finite cylinders: zooplankton models. Journal of the Acoustical Society of America, 94 (6): 3463–3472.

Stanton, T. K., Wiebe, P. H., Chu, D., Benfield, M. C., Scanlon, L., Martin, L. V., and Eastwood, R. L. 1994. On acoustic estimates of zooplankton biomass. ICES Journal of Marine Science, 51 (4): 505-512.

Stanton, T. K., Chu, D., Wiebe, P. H., Martin, L. V., and Eastwood, R. L. 1998a. Sound scattering by several zooplankton groups. I. Experimental determination of dominant scattering mechanisms. Journal of the Acoustical Society of America, 103 (1): 225-235.

Stanton, T. K., Chu, D., and Wiebe, P. H. 1998b. Sound Scattering by Several Zooplankton Groups II: Scattering Models. Journal of the Acoustical Society of America, 103 (1): 236-253.

Stanton, T. K., and Chu, D. 2000. Review and recommendations for the modelling of acoustic scattering by fluid-like elongated zooplankton: euphausiids and copepods. ICES Journal of Marine Science, 57 (4): 793-807.

Stanton, T. K., Chu, D., and Reeder, D. B. 2004. Non-Rayleigh acoustic scattering characteristics of individual fish and zooplankton. IEEE Journal of Oceanic Engineering, 29 (2): 260-268.

Suontama, J. 2004. Lack of suitable raw materials for fish feed – could we use plankton?. Marine Research News, 5, edit by Institue of Marine Research, Norway.

Tichy, F. T., Solli, H., and Klaveness, H. 2003. Non-linear effects in a 200-kHz sound beam and the conseguences for target-strength measurement. ICES Journal of Marine Science, 62 (3): 571-574.

Watkins, J. L., and Macaulay, M. 2000. Sampling krill. Chapter 2: 8-39 in Krill: biology, ecology and fisheries, Edited by Inigo Everson, Blackwell Science, Oxford, pp. 384.

Wiebe, P. H., Boyd, S. H., Davis, B. M., and Cox, J. L. 1982. Avoidance of towed nets by the Euphausiid Nematoscelis megalops. Fishery Bulletin, 80 (1): 75-91.

Wiebe, P. H., Greene, C. H., Stanton, T. K., and Burczynski, J. 1990. Sound scattering by live zooplankton and micronekton: Empirical studies with a dual-beam acoustical system. Journal of the Acoustical Society of America, 88 (5): 2346-2360.

FIGURE

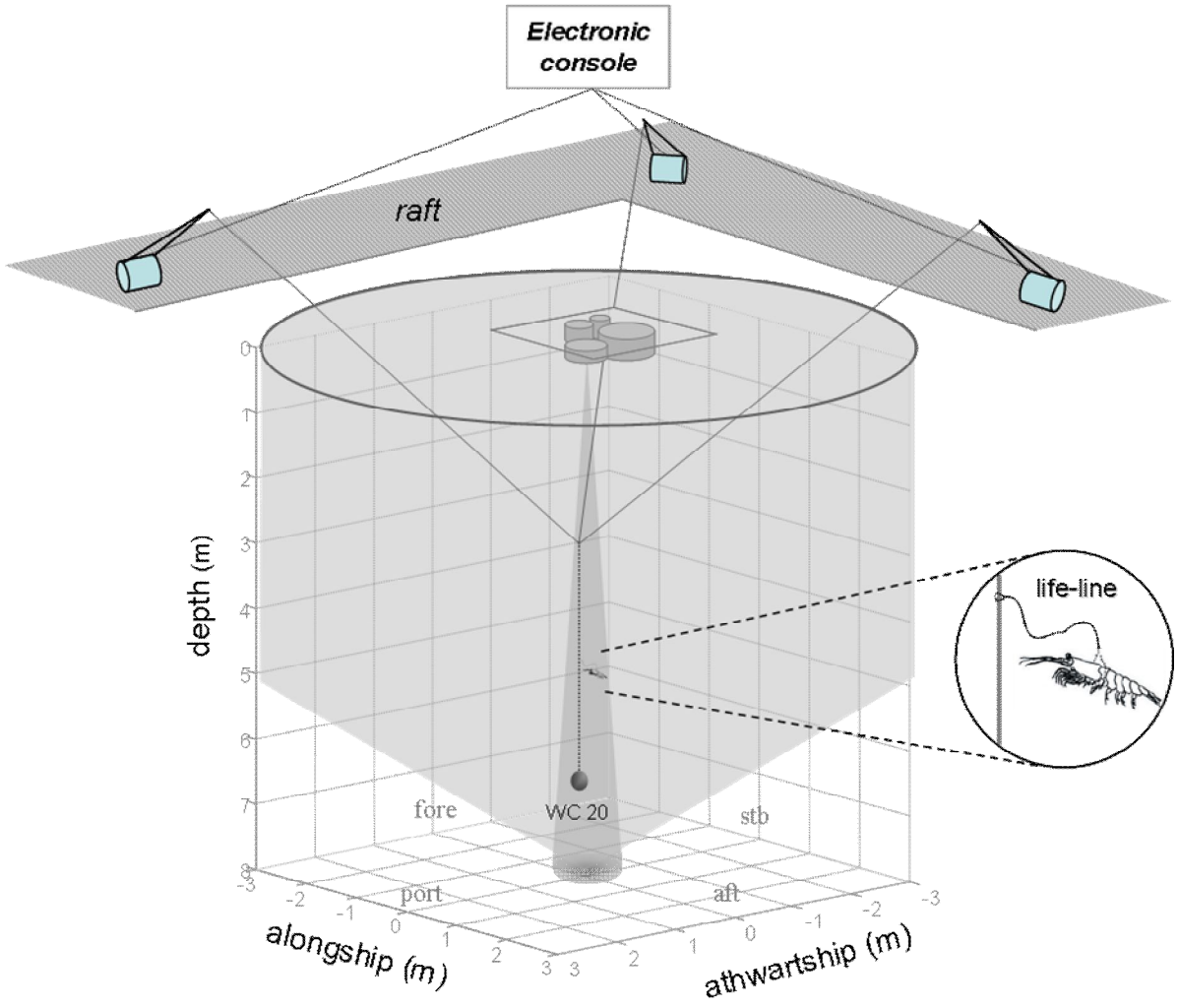

Figure 1: Tethered animal experimental set-up in the mesocosm. (The enlarged picture of the tethered krill is included with the kind permission of Dr. Kazuo Amakasu).

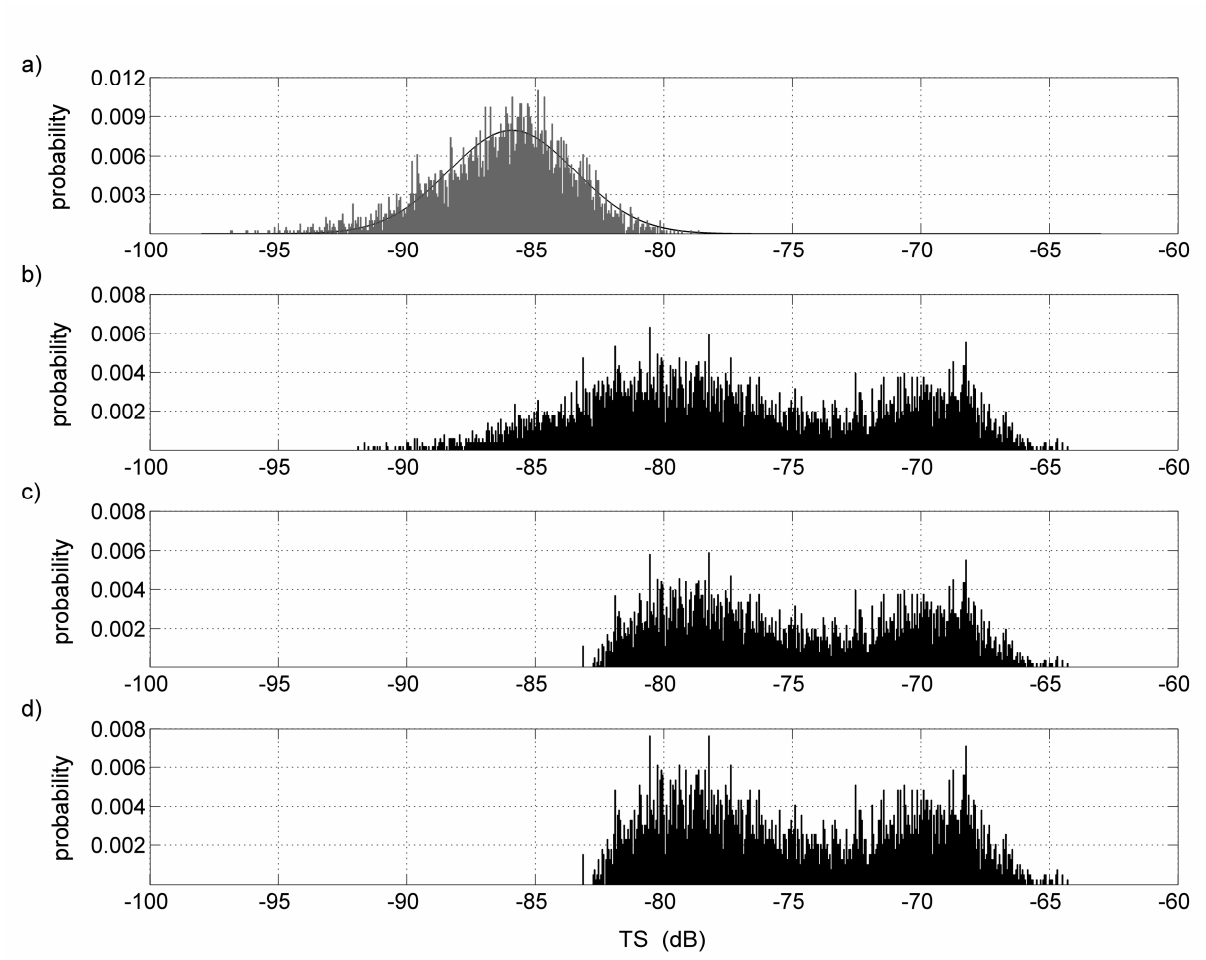

Figure 2. Example of echo data treatment using Equation (1) at 200 kHz. Probability distributions of backscattering echoes (TS) with resolution 0.05 dB from: a) line L1 (3913 detections) and its Gaussian fitting distribution (black lines); b) echo data set: animal ID 7 of length 27 mm plus line L1 (5050 detections); c) resolved *PDF* of the animal contribution (total p=0.77); d) Probability distributions of the reconstructed krill data set (3888 echoes; total p=1).

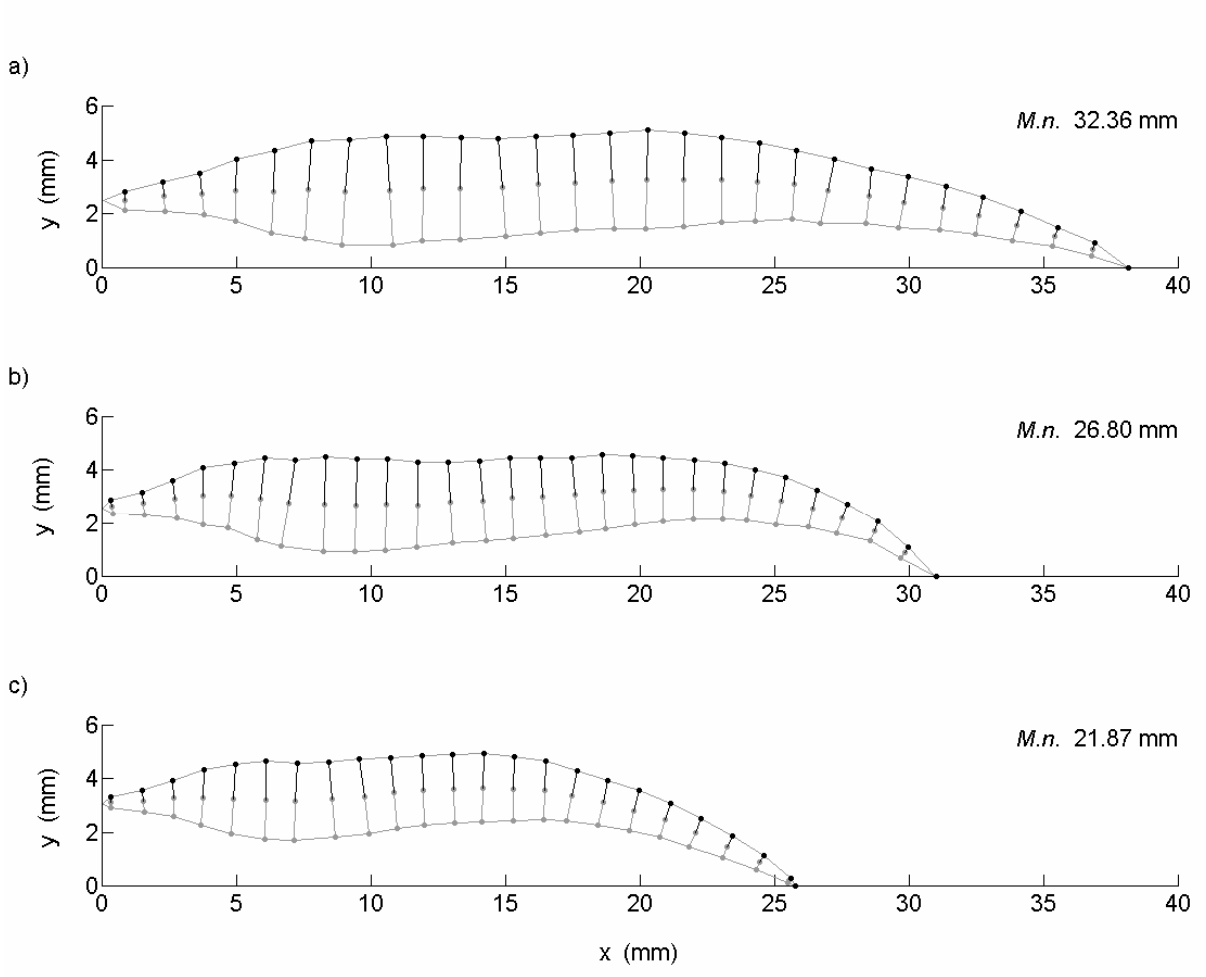

Figure 3. Proposed digitalized body shapes of *Meganyctiphanes norvegica* specimens with total length: a) 32.36 mm; b) 26.80 mm; c) 21.87 mm, measured from the tip of rostrum to the posterior end of the terminal spine at the end of telson. The body shapes resulting from the digitalization is shown in grey colour, black dots and black solid segments are the extrapolated points forming the $\vec{r}_{pos}$ position vector and the related radii as used in the DWBA models calculation.

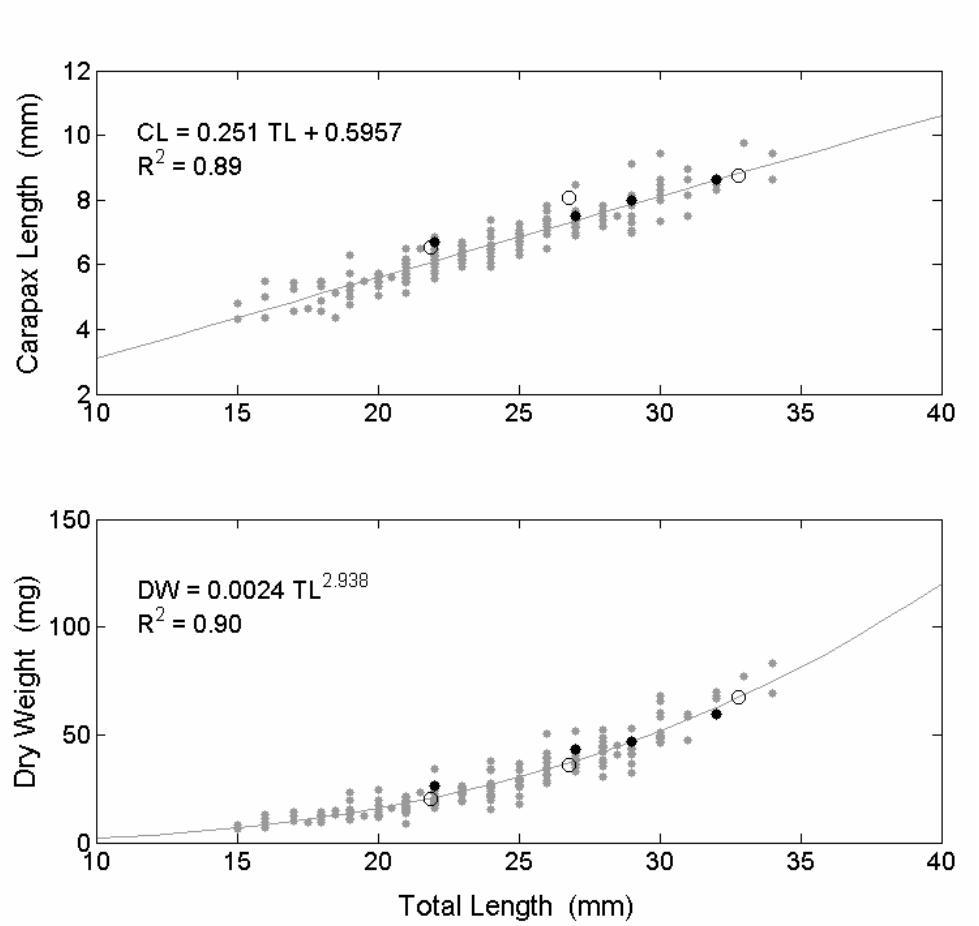

Figure 4. Total length versus carapax length and dry weight of individuals *Meganyctiphanes norvegica* caught in Raunefjord (west coast of Norway) in February 2004. The grey dots are the 216 animal used for the regressions determination; the black dots are the individuals used for the tethered experiment (also included in regressions determination); the open circles are the digitalized specimens.

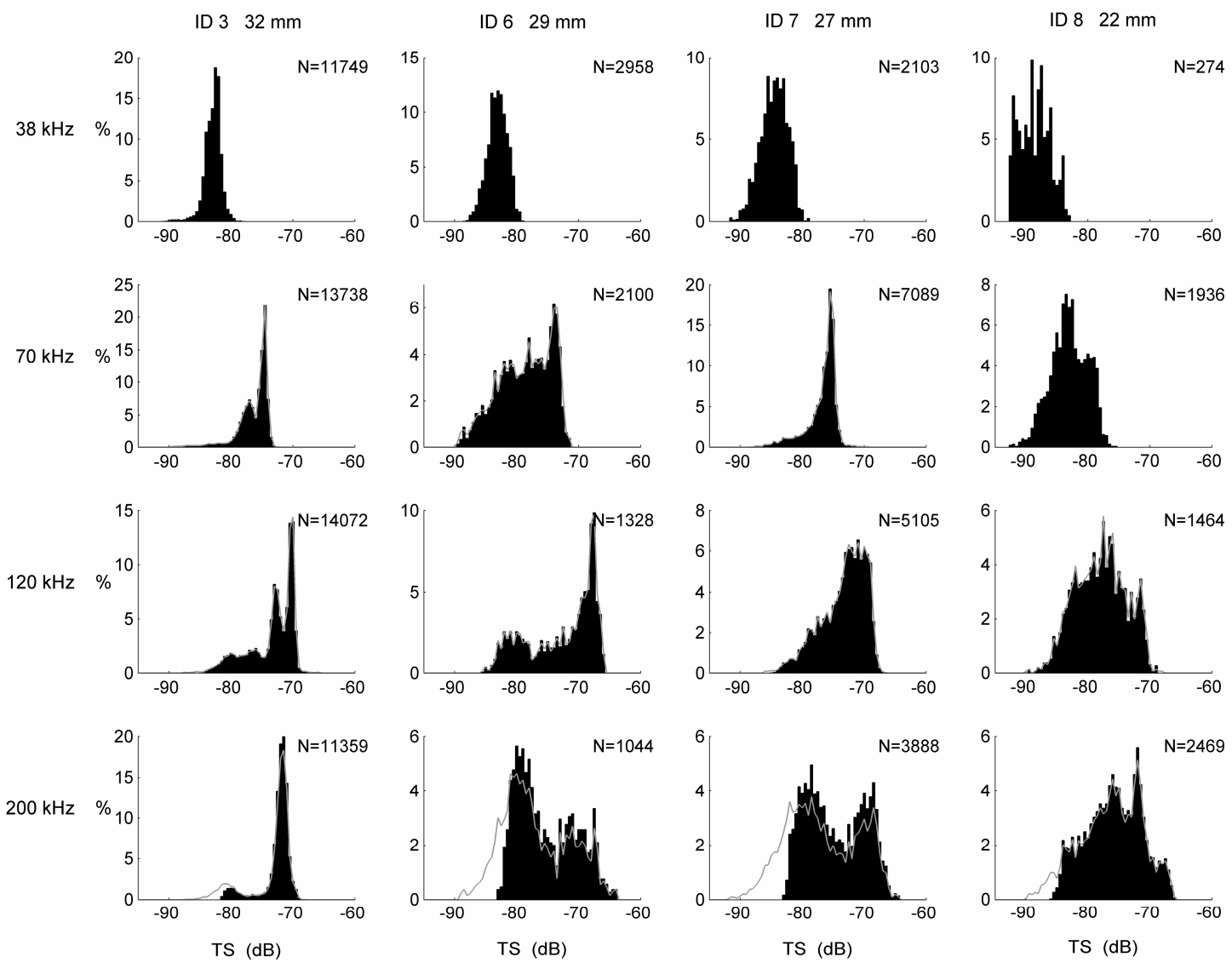

Figure 5. Frequency distributions of krill TS-data for the investigated ID specimens at different frequencies. For those cases whose the Equation (1) has been applied, the grey lines refer to the original echo data-sets before the process and the black histograms are the distributions of the krill detections arrays after the reconstruction. Length refers to total length (TL) defined in the text. N in the upper corner of the panels is the number observations. Details on the data sets are given in Table 5. Note differing scales.

Figure 6. Echo-amplitude probability distributions (grey histograms) and best fitting theoretical functions (solid lines) of the backscattering data from the four ID specimens at different frequencies. Echo- statistics parameters of the fitting curves are given in Table 5. The black dots on the curve are the corresponding points to the histograms used for the curve error estimation. Note differing scales.

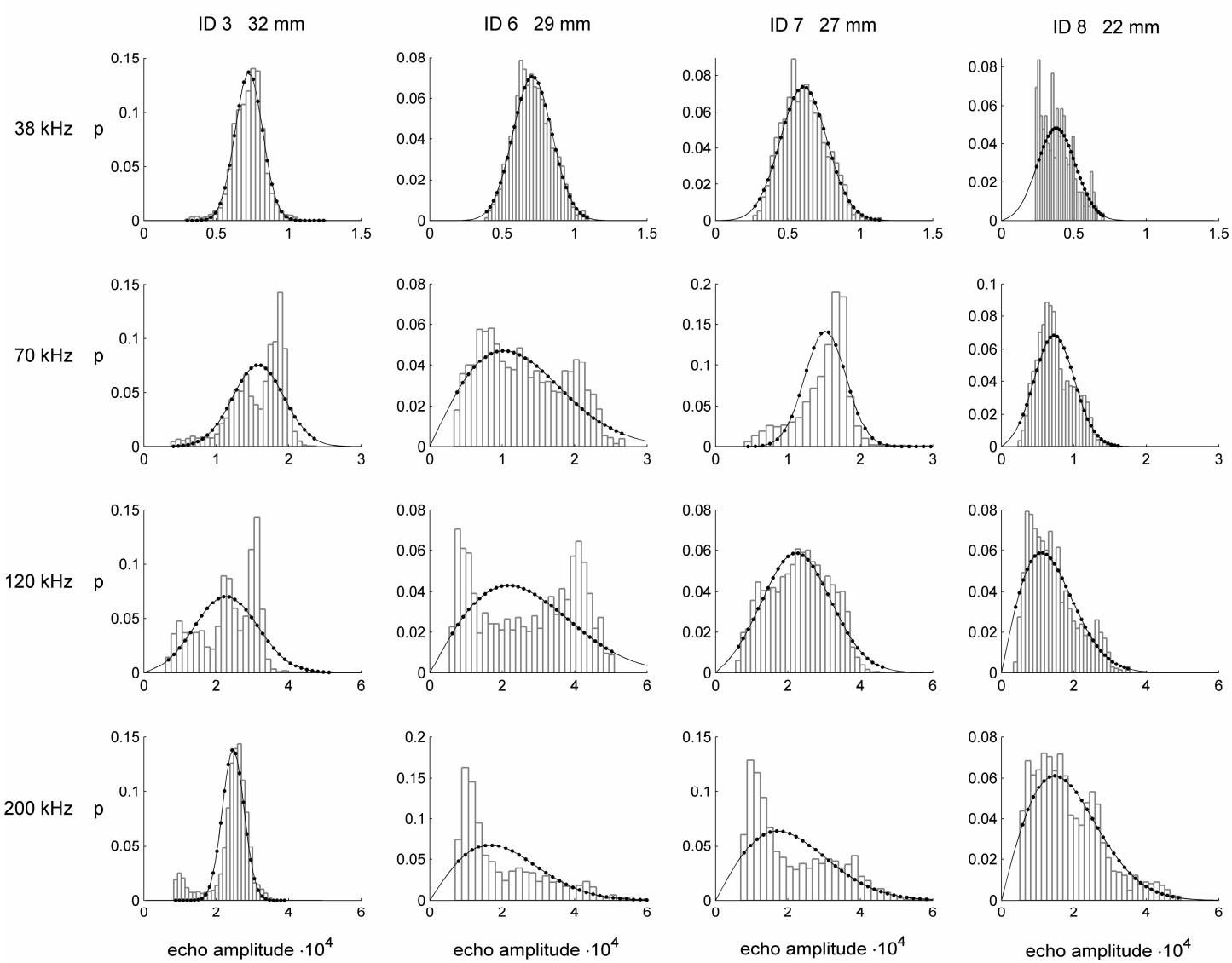

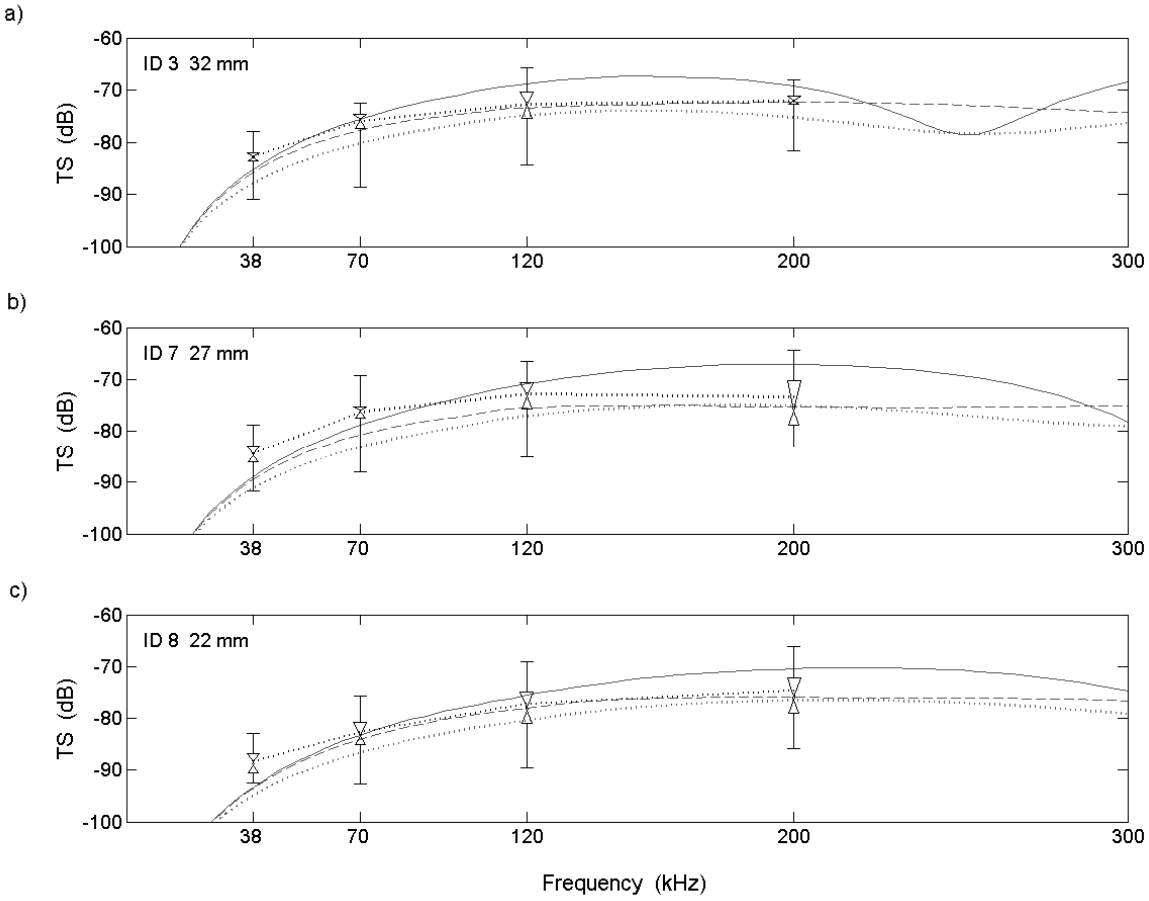

Figure 7. Comparison between direct TS measurements (black bars) for three of the tethered animals: a) ID 3 with length 32 mm; b) ID 7 with length 27 mm; c) ID 8 with length 22 mm, and the SDWBA TS-predictions (grey lines) using the related shape models in Figure 3. The vertical whiskers extend over the range of acquired TS. The common vertex of the triangles is the median, while the upper and lower triangles are the third and first quartiles respectively. The black dotted lines connect the statistical mean TS of the data-sets (Table 5). The SDWBA predictions were run with key parameters: $c = 1476$ m s^{-1}, $h = 1.0383$ and g(TL) given in Table 3. For each shape, the number of cylinders and the standard deviation phase variability were function of the frequency according to Equations (3) with reference parameters given in Table 3. Predicted TS functions were computed from σ_{bs} averaged over 100 realizations of random phase for the following distribution of orientations N[0,0] (grey solid lines), N[0,30] (grey dotted lines) and N[11,4] (grey dashed lines).

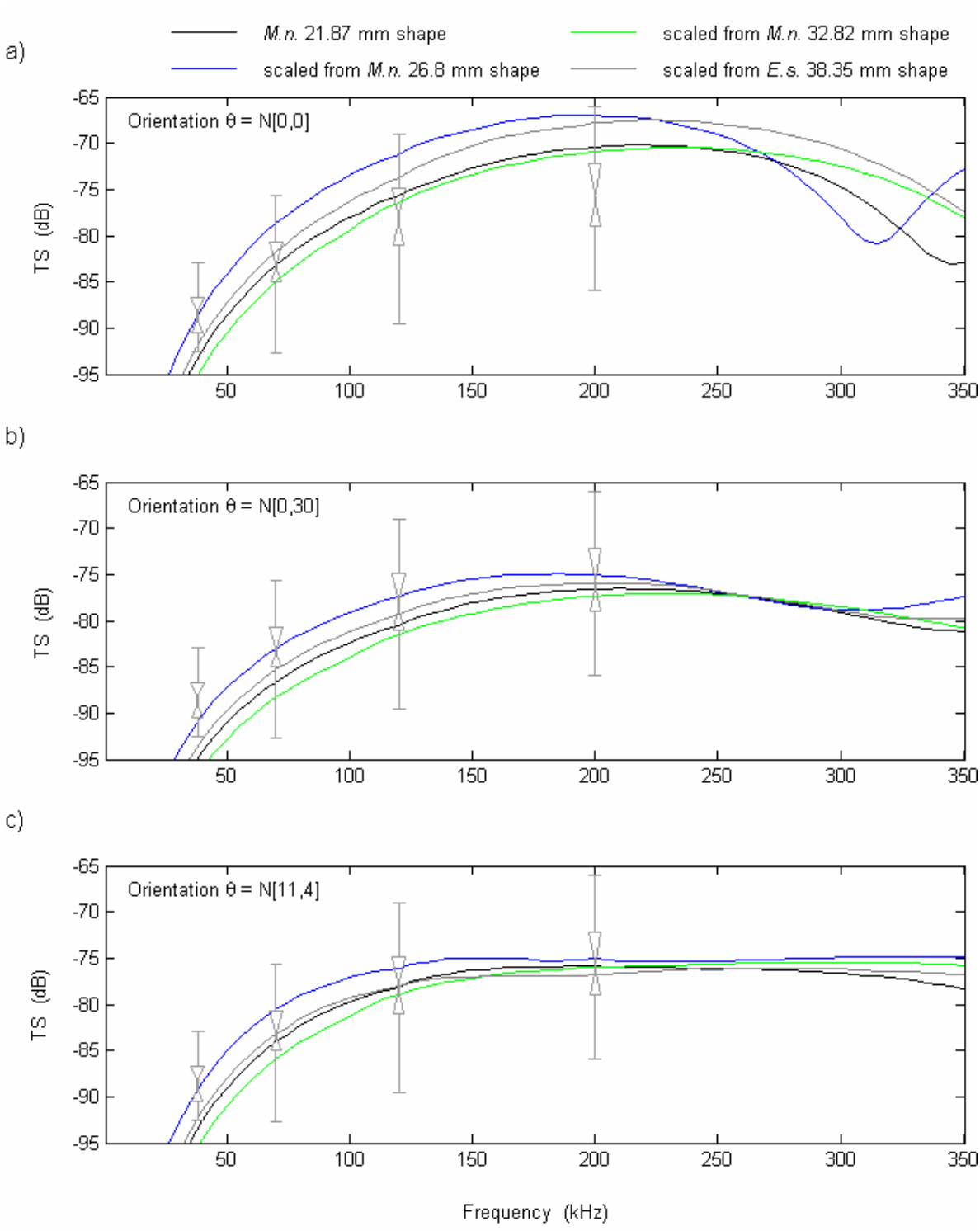

Figure 8. SDWBA TS-predictions (TS) for a 21.87 mm long krill obtained by scaling different krill shapes for three distributions of animal orientation: a) N[0,0], b) N[0,30], c) N[11,4]. Backscattering strengths retrieved from the tethered specimen ID 8 of length 22 mm are also plotted in grey colour bars as described in the caption of Figure 7.

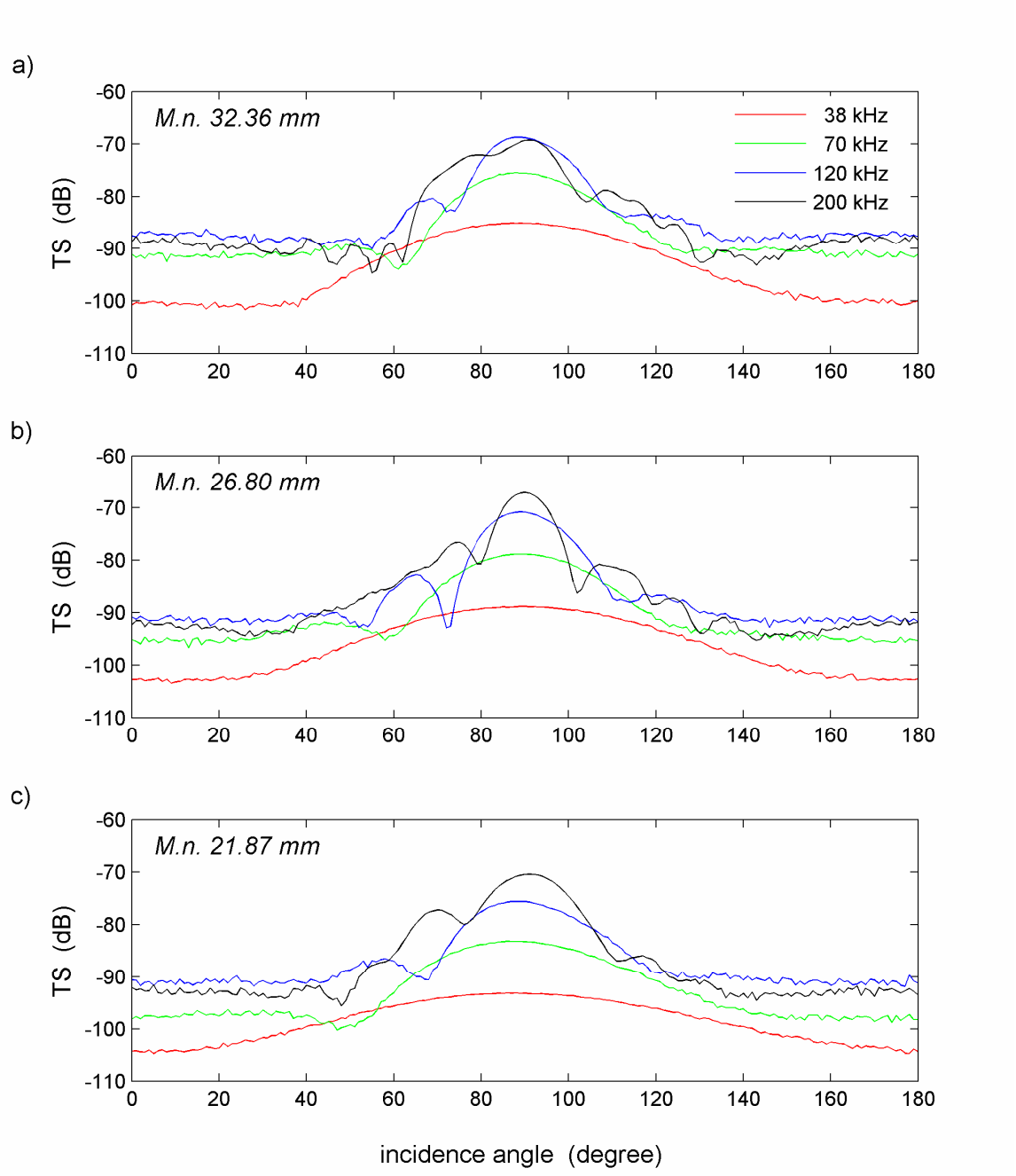

Figure 9. SDWBA target strength predictions versus angle of incidence for the proposed *Meganyctiphanes norvegica* shapes of length: a) 32.36 mm; b) 26.80 mm; c) 21.87 mm. The key parameters were: c = 1476 ms^{-1}, h = 1.0383 and g(L) given in Table 3. The number of cylinders and the standard deviation phase variability were function of the frequency according to Equations (3) with reference parameters also given in Table 3. TS values were computed from σ_{bs} averaged over 100 realizations of random phase. The dorsal aspect corresponds to a 90º incident angle.

TABLES

Table 1. Simrad EK60 acoustic systems: types, settings and performances in mesocosm. All transducers are 7º nominal beamwidth. The receiving bandwidth are for the pulse duration 0.256 ms. The near-fields are theoretically calculated from d^2/λ (A. Johansen, Simrad AS, pers. comm.), where d is the maximum linear dimension of the transducers active face and λ the wavelength related to the GPT central frequency at c=1500 ms^{-1}. The term power refers to the electrical transmit power to the transducer.

EK60 system (kHz)	**central frequency (kHz)**	**transducer type**	**λ (m)**	**near-field (m)**	**power (W)**	**receiving bandwidth (kHz)**	**source level (dB *re* 1 μPa at 1 m)**	**background noise (dB)**
38	38.095	ES38-B	0.039	2.7	600	3.68	223.2	-95
70	70.175	ES70-7C	0.021	1.5	300	6.16	221.5	-98
120	121.212	ES120-7C	0.012	0.9	250	8.71	221.6	-102
200	200.000	ES200-7C	0.007	0.5	120	10.64	219.5	-110

Table 2. Key backscattering data from the tether life-lines alone acquired on 9 March 2004. The diameter of the lines (∅) is in mm; the recording time is in mm:ss; the TS levels are in dB re 1 m^2 from echoes resolved within the solid beam angle of 6°. The TS mean was calculated as the arithmetic mean in linear domain through the mean of the backscattering cross section in m^2.

line	∅	***f***	**rec. time**	**n. pings**	**echoes in 6º**	**TS**			
						min	*max*	*mean*	*med*
L1	0.12	**70**	5:03	5459	2096	-100	-88.86	-94.08	-94.40
		120	5:03	5505	1592	-99.69	-83.76	-90.77	-91.46
		200	9:59	9842	3913	-96.83	-78.64	-85.54	-86.02
L2	0.08	**120**	8:06	8717	5622	-99.70	-87.83	-94.62	-95.02
		200	7:00	6495	5456	-99.84	-82.56	-89.95	-90.36

Table 3. *Meganyctiphanes norvegica* digitalized specimens and related SDWBA model parameters. The shape refers to the Figure 3. The lengths measures TL, BL, and CL are in mm and defined in the text. The dry weight (DW) is in mg; Δ is the spatial resolution in mm of the grid used in the digitalization procedure for the body reconstruction; N_0 is the number of discrete cylinders reproducing the krill shape; f_0 is the reference shape frequency in kHz where Equations (3) start to be applied for the stability of the SDWBA model. The model was run with sound speed contrast h=1.0383 for all the shapes and density contrast determined by the length relationship $g = -2.73\ 10^{-4} \cdot TL + 1.0445$ (Calise *et al*., 2009b) kept both constant over all the discretized-bent cylinders.

shape	TL	BL	CL	B1	B2	B3	DW	Δ	N_0	f_0	g
a)	32.36	26.16	8.76	2.96	3.69	1.32	67.665	1.39	27	100	1.0355
b)	26.80	21.57	8.06	2.60	3.16	1.13	35.856	1.14	27	100	1.0372
c)	21.87	18.48	6.05	2.14	2.55	1.04	20.141	1.16	23	120	1.0385

Table 4. Morphological results for the four tethered animals investigated. All the lengths are in mm and defined in the Material and Methods section. The dry weights (DW) are in mg.

ID	TL	BL	CL	B1	B2	B3	DW
3	32	25	8.64	2.40	2.62	1.57	59.517
6	29	23	8.00	2.56	2.78	1.21	46.846
7	27	22	7.52	2.59	2.71	1.19	43.068
8	22	18	6.19	2.02	2.31	0.88	26.189

Table 5. Resume of results for the four tethered animal backscattering data sets. Asterisk (*****) refers to the data-sets filtered from the life-line according to Equation (1); the recording time is in (mm:ss); p is the probability of the resolved animal contributions *PDF* relative to that of the initial echo data-set (=1). Krill echoes is the number of the detections determined to be due to the animal after the reconstruction of the backscattering data-set All the TS are in dB re 1 m^2. The krill TS-mean was calculated in linear domain through the mean over of the corresponding backscattering cross sections. The Rice *PDF* parameters are derived from the minimized sum analysis; the statistical $\overline{TS}$ is the mean value of the theoretical fitting curve transformed to logarithmic domain; the minimized sum (MS) is the sum of squares of the differences between the *PDF* and the fitting curve values in each bin.

ID	TL	*f*	rec. time	pings	echoes in 6°	p	krill echoes	krill TS					Ricean echo statistics		
								min	*max*	*range*	*mean*	*med*	$\overline{TS}$	γ	MS
3	32	**38**	20:11	21787	11749	1	11749	-90.93	-78.01	12.9	-82.91	-82.72	-82.79	28.6	0.0021
		70 *	25:29	27522	13793	0.99	13738	-88.55	-72.45	16.1	-76.31	-75.40	-76.01	9.1	0.0174
		120 *	20:09	21747	14184	0.99	14072	-84.40	-65.70	18.7	-73.32	-72.35	-72.76	2.7	0.0217
		200 *	20:20	21808	12482	0.91	11359	-81.65	-68.10	13.6	-72.58	-71.90	-72.16	33.6	0.0115
6	29	**38**	10:06	10987	2958	1	2958	-88.41	-79.19	9.2	-83.11	-83.08	-82.98	13	0.0008
		70 *	10:07	11001	2110	0.99	2100	-89.45	-71.40	18	-78.64	-78.10	-77.96	0.2	0.0027
		120 *	10:05	11002	1329	0.99	1328	-85.30	-65.85	19.5	-72.77	-70.80	-71.42	0.2	0.0128
		200 *	10:05	10992	1291	0.81	1044	-83.10	-64.05	19	-75.22	-76.45	-73.62	0	0.0253
7	27	**38**	10:04	11001	2103	1	2103	-91.73	-78.82	12.9	-84.53	-84.42	-84.31	6.5	0.0011
		70 *	10:07	10970	7090	0.99	7089	-88.00	-69.30	18.7	-76.78	-75.95	-76.38	13.6	0.0212
		120 *	10:05	10989	5125	0.99	5105	-85.05	-66.60	18.5	-73.36	-72.65	-72.82	2.1	0.0015
		200 *	10:06	10971	5050	0.77	3888	-83.15	-64.30	18.9	-74.68	-75.25	-73.37	0	0.0160
8	22	**38**	5:02	5468	274	1	274	-92.58	-82.99	9.6	-88.54	-88.45	-88.36	3.4	0.0077
		70	5:04	5542	1936	1	1936	-92.74	-75.74	17	-83.04	-83.04	-82.64	2.8	0.0037
		120 *	5:03	5504	1465	0.99	1464	-89.50	-69.00	20.5	-77.91	-77.75	-77.19	0	0.0035
		200 *	10:06	11023	2606	0.95	2469	-85.85	-66.10	19.8	-75.73	-75.60	-74.7	0	0.0024

Table 6. Coefficients of the simplified SDWBA model for the proposed *Meganyctiphanes norvegica* shapes of Figure (3). The function TS(*k*L) expressed by Equation (A1) was averaged over different distributions of orientation $\theta = N[\bar{\theta}, \text{std}(\theta)]$ in degrees. Exponential notation (·10^#) is denoted by ‘‘e#’’. The coefficients can be used for values of *k*L smaller than 50; δ is the mean error in decibels between the exact and the simplified SDWBA calculated by $\delta = 10 \log_{10}(\sigma_{exact}^2 / \sigma_{simpl}^2)^{½}$.

L	**32.36 mm**			**26.8 mm**			**21.87 mm**		
θ	N[0,0]	N[0,30]	N[11,4]	N[0,0]	N[0,30]	N[11,4]	N[0,0]	N[0,30]	N[11,4]
A	1.23140711e+1	8.74124830e-1	1.40004796	1.49251360e+1	6.92934718	8.81252056e-1	1.78975186	4.48492084	1.50616181
B	1.18407346e-1	-3.47103555e-3	-2.56930386e-3	1.26326690e-1	1.10624062e-1	-2.37526090e-3	-4.95319652e-3	1.10486727e-1	-9.29509769e-3
C	3.71224500e-1	4.12965378e-1	4.14191472e-1	3.87155872e-1	3.76040529e-1	4.27141922e-1	4.59389706e-1	3.24845706e-1	3.45547341e-1
D	-1.51404457e-7	-1.24457751e-8	4.39589100e-8	1.58699294e-7	-6.17821282e-8	1.41589083e-7	8.31660466e-7	-6.21667725e-8	-7.70758954e-7
E	2.36252154e-5	9.72925294e-7	-7.76620994e-6	-1.69922331e-5	9.28651325e-6	-2.18613944e-5	-1.03289554e-4	9.39173404e-6	9.73969329e-5
F	-1.33752171e-3	3.86316046e-5	5.26181472e-4	6.58966042e-4	-4.96235291e-4	1.29504205e-3	4.96930065e-3	-4.98295823e-4	-4.85233253e-3
G	3.32480859e-2	-5.09972874e-3	-1.69295067e-2	-1.26161095e-2	1.11206853e-2	-3.61836017e-2	-1.17149063e-1	1.09498581e-2	1.21491439e-1
H	-3.49607855e-1	1.30870683e-1	2.51003567e-1	1.49063873e-1	-9.36045450e-2	4.60366968e-1	1.36924935	-8.99014277e-2	-1.62507531
I	1.31731988	-8.56233329e-1	-1.29001174	-9.00665911e-1	2.12638489e-1	-1.97256644	-6.47719762	1.98638620e-1	1.12851560e+1
J	-8.60778794e+1	-6.95408043e+1	-6.67796762e+1	-8.51183922e+1	-8.56680499e+1	-6.93913288e+1	-6.51067161e+1	-8.68145468e+1	-1.10023174e+2
δ	0.85	0.24	0.19	0.70	0.20	0.29	0.52	0.17	0.52

Paper VI

Lucio Calise, Tor Knutsen and Rolf Korneliussen

The impact of echo sounder settings for the discrimination of acoustic scatterers in a multi-frequency survey context

THE IMPACT OF ECHO SOUNDER SETTINGS FOR THE DISCRIMINATION OF ACOUSTIC SCATTERERS IN A MULTI-FREQUENCY SURVEY CONTEXT

Lucio Calise[a], Tor Knutsen[b] and Rolf J. Korneliussen[b]

[a] Department of Physics and Technology, University of Bergen, Allégaten 55, N-5007 Bergen, Norway
[b] Institute of Marine Research, Nordnesgaten 50, P.O. BOX 1870 Nordnes, N-85817 Bergen, Norway

Contact author: Lucio Calise, Department of Physics and Technology, University of Bergen, Allégaten 55, N-5007 Bergen, Norway. Fax number: +47 55589440; email: calise@ift.uib.no

Abstract: *In many ocean regions, scattering structures are complex, and a diverse mixture of plankton and fish are often found in a given volume of water. In this paper we aim to understand the importance of key echo-survey parameters like ping rate, pulse duration and vessel speed, as these influence the echo-integration values for specific acoustic structures of the water column. Traditionally the setting for fish echo-surveys is standardized by a typical 1 ms pulse duration, a vessel speed of 10 knots and a 1 second ping rate. The present work explores the echo-integration results from different types of scattering structures using five multi-frequency echo survey settings. We discuss whether the standard procedures used for many fish surveys are appropriate if the abundance and size distribution of krill, other zooplankton and fish should be determined simultaneously. Consequences when frequency response techniques used for classification and zooplankton inversion techniques are also discussed.*

Keywords: *Multi-frequency survey, Simrad EK60, echo-integration, krill acoustics*

1. INTRODUCTION

Zooplankton in general and krill in particular are key ecosystem components of the world's oceans. For nearly a decade multi-frequency acoustic methods have been used to assess the distribution and abundance of Antarctic krill [1], while general zooplankton acoustics is still in its infancy. In the northern Atlantic, *Meganyctiphanes norvegica* is probably the most important krill species along with *Thysanoessa inermis* [2]. Identical challenges with respect to the abundance estimation are evident for these stocks as for the stock of *Euphausia superba* in the southern ocean, Hence, methods to safely delineate krill from other similar type of scatterers needs further attention and elaboration.
The scattering properties of zooplankton strongly depend on their size, behaviour, acoustic frequency and material properties. The variation in scattering strength levels between frequencies for various types of scatterers can be used for classification purposes and to discriminate between species. Scattering models representative for particular groups of zooplankton [3] can also be used to derive both the abundance and size distribution of scatterers applying the use of inversion techniques [4]. Krill is observed in various types of aggregations and as dispersed scatterers in mixed acoustic recordings. In these latter types of acoustic registrations verification of scatterers by acoustics only, is extremely difficult and improvement of acoustic methods is warranted.

In this paper we aim to understand the importance of key echo-survey parameters like ping rate, pulse duration and vessel speed. These significantly influence how integrator values for specific structures of the water column vary. Traditionally the setting for fish echo-surveys is standardized by a typical 1 ms pulse duration, a vessel speed of 10 knots and a 1 second ping rate. The investigation allows us to explore echo-integration for different types of scattering structures in a multi-frequency context. We question whether the standard procedures used for many fish surveys are appropriate if the abundance and size distribution of krill, other zooplankton and fish should be determined simultaneously. This is particularly a concern when frequency response techniques are used for classification and zooplankton inversion techniques applied.

2. MATERIAL AND METHODS

The tests were performed in the central part of Raunefjorden (60°16' N, 5° 9' E), a land-locked fjord on the west coast of Norway near Bergen. In this area the topography consist of a small basin (approx. 0.8 nmi^2), falling down from 120 m depth to a variable bottom depth of 220- 240 m, where a Sound Scattering Layer (SSL) is commonly observed. This SSL is composed generally of larger crustacean zooplankton, copepods, amphipods, various mesopelagic shrimps and fish.

The data were collected on board of the R/V G. O. Sars of the Institute of Marine Research in Bergen, during the night between 20-21 of January 2006 with very calm meteo-marine conditions (light NW 14° wind and dry air with temperature of 2.3 °C). The physical conditions were monitored using a Sea-Bird SBE 9*plus* CTD profiler during the period of measurements. No significant changes in structure were observed.

In order to obtain a quantitative understanding on the composition of the scatterers at different depths, biological samplings were performed using a WP2 vertically operating plankton net and a krill trawl with a mouth opening of 6x6 m = 36 m^2.

Two WP2 net hauls were carried out before the acoustic measurements: the first from 100 to 0 m covering the upper part of the water column where mostly dispersed targets were observed. The second haul was carried out from 230 to 0 m to include the SSL.

Following the acoustic transects, two krill trawl hauls were conducted. The towing speed was 2.8-3 knots and the net depth and the mouth opening were monitored constantly using a Scanmar acoustic trawl control system, allowing information on catch depth and the computation of volume filtered. The first krill haul was performed in the depth channel of 25-30 m, where the previous acoustic observations suggested the presence of very few and weak scatterers. The second haul was performed between 120-130 m depth, to provide the SSL biological information. When on board, catch sub-samples were either fixated (WP2 samples) or immediately frozen (krill trawl catches) for later counting, species and size determination. Krill total length (TL) was measured from the tip of the rostrum to the posterior end of the terminal spine at the end of telson.

The acoustic data were collected with four Simrad EK60 echo sounders connected to hull vertical 7° split beam transducers at frequencies of 38, 70, 120 and 200 kHz. Following the recommendation for multi-frequency acoustic data collection [5], the data were acquired with identical pulse duration for all frequencies and with significantly reduced output power to the transducers in order to avoid non-linear effects. The echo sounders were calibrated two days before the measurement in the same area of investigation.

Four different system settings were consecutively tested along the same 1.5 nmi transect. The time between the first and the last measurement was of 1.5 hour. The ping rate of 1 ping per second was set for all the transects, and pulse duration (PD) of 1.024 and 0.256 ms, and vessel speed of 5 and 10 knots were interchanged to differentiate the four transects (Table 1). Moreover, the acoustic data during the first trawling, acquired with PD=1.024 ms, 3 knots vessel speed and maximum ping rate, resulting in 2.2 pings per second, were also used for comparison (c.f. Transect 5). The procedure assured that the same volume of water with approximately similar biological conditions was acoustically sampled with different degree of horizontal and vertical resolution (Table 1).

Transect	*PD* [msec]	*Speed* [kn]	*Pings* in 0.1 nmi	*Horiz Pings. distance* [m]	*EK60 raw Vert. Interval* [cm]	*EK60 raw Samples* in 10 m depth	*EK60 raw Samples* in 1 cell
1	0.256	5	72	2.57	4.7	211	15162
2	0.256	10	36	5.14	4.7	211	7581
3	1.024	5	72	2.57	19	53	3790
4	1.024	10	36	5.14	19	53	1895
5	1.024	3	120	0.70	19	53	6317

Table 1: Transects settings and averaged spatial resolutions of acquisition and process.

The EK60 raw files were processed using the LSSS software [6] with –82 dB S_V threshold for all the frequencies. The acoustic values were compensated for the alongship transducer offset and corrected for the frequency-dependent delay. Further, the data were slightly smoothed and noise corrected [7]. The echograms were subdivided in defined cells of 10 m thickness and 0.1 nmi (182.5 m) length, and the Nautical Area Scattering Coefficient (NASC), s_A [m^2/nmi^2] [8] were retrieved for each cell. Based on geographical

coordinates, 10 consecutive integration intervals (1 nmi in total) for each transect were considered aligned and the s_A of the related depth cells were used for the comparison.

Since each transect also represents a time series of n=10 observations, each dependent on the previous one, an autoregressive (AR) time series analysis was performed on the s_A values of the single transect using the stationary first order Burg method [9]. The method produces a stable AR model with advantage of high resolution for short data records. The variance (*var*) of the mean s_A for each transect and layer channel is estimated by [10]:

$$\mathrm{var}\left(\overline{s_A}\right) = \frac{\mathrm{var}(s_A)}{n^2} \cdot \left[n + 2 \cdot \sum_{i=1}^{n-1} i\, a^{n-i} \right] \qquad (1)$$

where the AR coefficient a for distribution with mean $\neq 0$ is calculated by:

$$a = \left[\sum_{i=1}^{n-1} \varphi_i \cdot \varphi_{i+1} \right] \Big/ \left[\sum_{i=2}^{n-1} {\varphi_i}^2 + \frac{1}{2}\left[{\varphi_1}^2 + {\varphi_n}^2 \right] \right] \qquad \text{with } \varphi_j = \left(s_A\right)_j - \overline{s_A}$$

Finally, the 95% confidence interval (*c.i.*) of the s_A mean can be estimated by $c.i. = \overline{s_A} \pm \left(1.96 \cdot \sqrt{var\left(\overline{s_A}\right)}\right)$ and the transects results in the same channel can be compared.

3. RESULTS AND DISCUSSION

A Sound Scattering Layer (SSL) was observed at 100-160 m depth (Fig.1a), as is also commonly found during most of the year. In the upper part of the water column mostly weak and dispersed scatterers were found. The krill *Meganyctiphanes norvegica* was by far the most prominent component in terms of number of animals per unit volume (Table 2), having an average size of 21±4 mm. A few stronger scatterers like fish larvae and gobies were found in this layer, but their abundance was very low.

	Krill trawl 1, 25-30 m		**Krill trawl 2, 120-130 m**	
Species/Group	**No. ind.**	**No. ind. per 1000 m^3**	**No. ind.**	**No. ind. per 1000 m^3**
Meganyctiphanes norvegica	26057	507.6	49346	961.2
Thysanoessa inermis	253	4.9	145	2.8
Pasiphea sivado	203	3.9	381	7.4
Shrimp indet.	51	1.0	1633	31.8
Gammaridae (Amphipoda)	152	3.0	----	----
Euchaeta norvegica (Copepoda)	203	3.9	145	2.8
Cephalopoda	51	1.0	----	----
Aphya minuta (transparent goby)	101	2.0	163	3.2
Maurolicus muelleri (Müller's pearlside)	----	----	7057	137.5
Sygnathus acus (greater pipefish)	1	0.02	18	0.4
Fish larvae/juvenile	51	1.0	----	----
Etmopterus spinax (velvet belly lantern shark)	----	----	7	0.1

Table 2: Abundance and species composition from trawl samples.

The SSL was a.o. composed of larger crustacean zooplankton of which euphausiids was a key component. *Meganyctiphanes norvegica* was by far the most dominant krill species, but also *Thysanoessa inermis* was found in very low numbers. Another important

component was the mesopelagic fish Müller's pearlside (*Maurolicus muelleri*). Larger mesopelagic fish was probably also present but their abundance must have been very low as no such fish were caught in the trawl samples. The zooplankton community also included several small copepod species, small gastropods and bivalves, as well as siphonophores, but all in very low numbers. For details see [11]. The mesopelagic shrimps *Pasiphea sivado* was more important in the SSL then at shallow depths (Table 2).

The interpretation of the acoustic results has to take in account three effects that might bias the comparisons. First, the time lag between transects; secondly there might be a slight geographical offset between transects and thirdly, the entire procedure due to both the internal EK60 digital processing and the low number of integration intervals, hence their statistical properties.

Figure 2 shows the average s_A and its variability for a selected set of depth strata and frequencies. For the shallow layer represented by the depth strata 20-30 m (Fig. 2a), average s_A for all frequencies and transects are very low (<1.0 m^2 nmi^{-2}). There seems to be a tendency that average s_A is increasing with increasing frequencies although from a statistical point of view no significant difference between means are evident. This layer corresponds to the first krill trawl haul where krill was the dominant scatterer in terms of number of individuals per unit volume (~0.5 $ind.m^{-3}$). However, a few small fish larvae and transparent gobies were also found. It seems that for such a weak scattering structure, although consisting mostly of one type of scatterer (krill), the integration cell is to small to obtain comparable s_A values at various frequencies as the number of targets per unit volume is so low. Figure 2b shows a trend with respect to average s_A that is similar for all frequencies and higher absolute s_A values compared to Figure 2a. Figure 1b shows the frequency distribution of mean Target Strength (TS) from tracking analysis obtained at 120 kHz from a non-moving vessel for the 20-30m and 50-60m layer respectively. Near identical distributions were obtained from the single target detections at the same frequency during all transects (not shown). This suggests that stronger scatterers are present in the 50-60m channel.

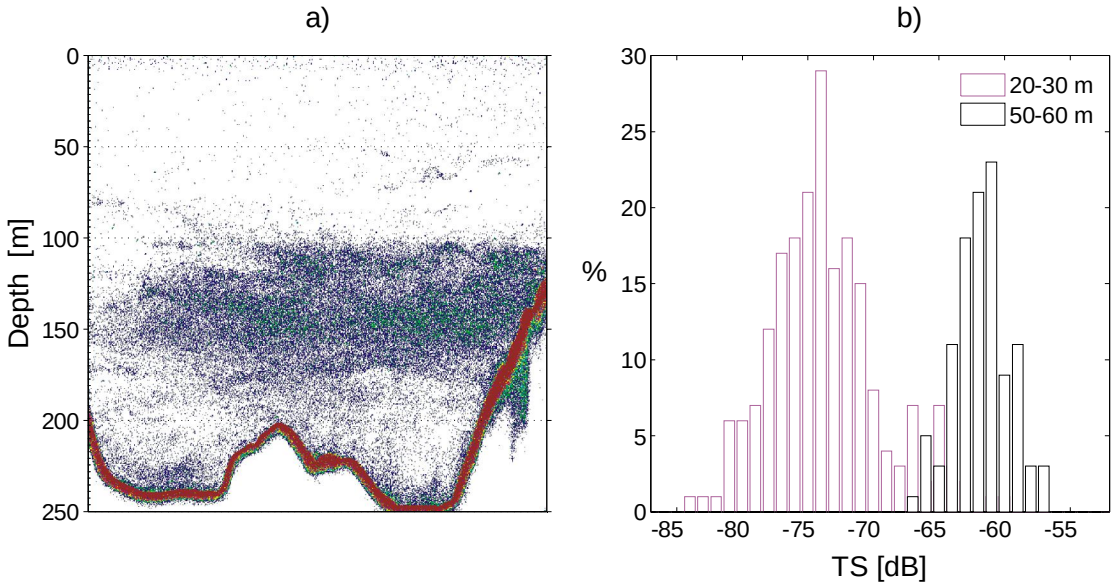

Fig. 1: a) Typical echogram of the basin at 120 kHz (Transect 4); b) Frequency distribution of mean target strength (minTS=-100 dB) based on target tracking using the software SonarX [12] for the layers 20-30 m and 50-60 m at 120 kHz during a 10 minutes record with vessel in no-moving position.

A particular feature seen in this layer was the higher average s_A for transects 1 and 2, both obtained for a PD=0.256 ms. Both at 120 and 200 kHz average s_A values for this pulse duration is significantly higher then for the transects run with 1.024 ms. Single TS detection analysis from consecutive transects revealed that this is a time effect. A significant reduction in number of smaller targets were evident between transect 1 to transect 3, suggesting that a fair amount of scatterers left the measurement volume prior to transect three.

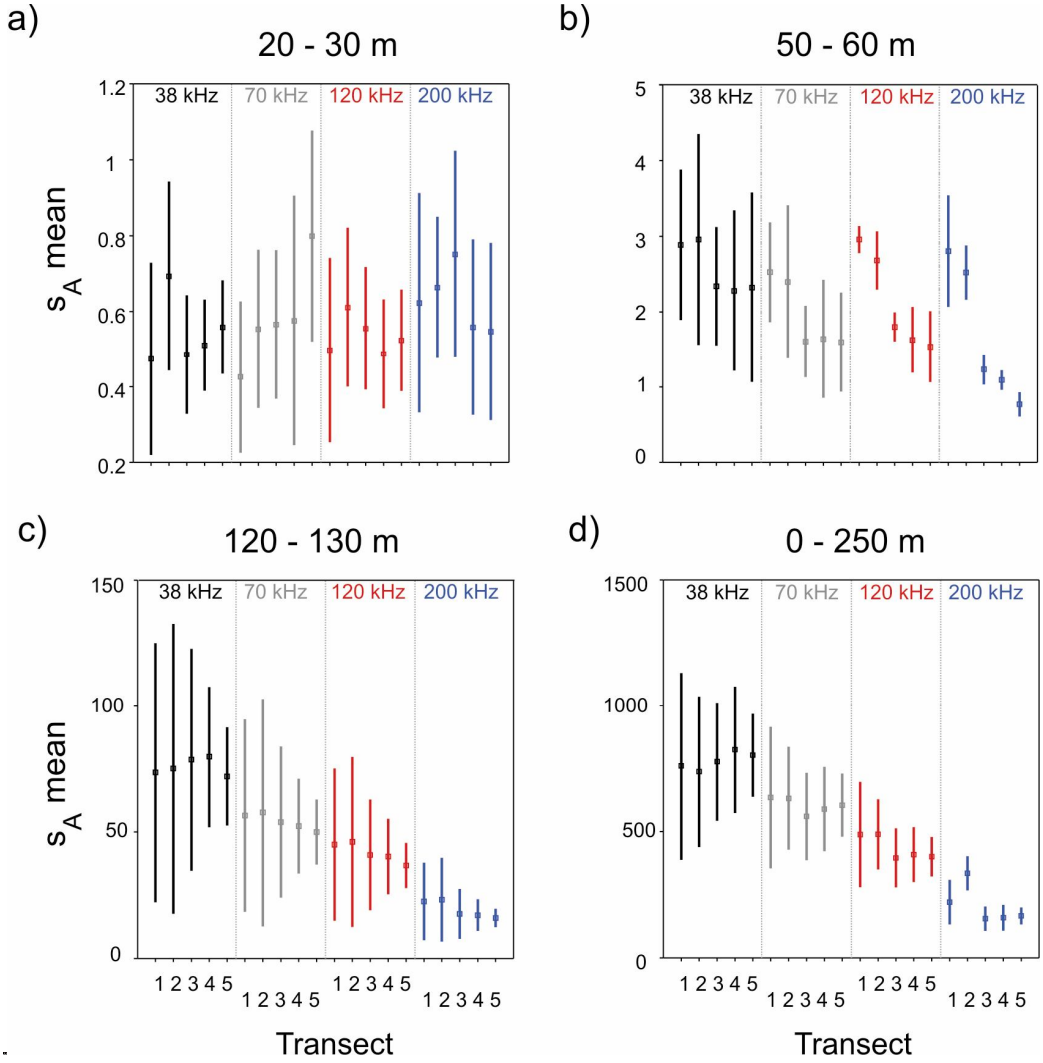

Figure 2: Mean s_A and estimated confidence intervals for a selected set of depth strata.

Figure 1c corresponds to the depth layer for the second trawl haul inside the SSL, where density of scatterers is significantly higher than in the upper layers (Fig. 1a) and also types of organism more diverse (Table 2). It is apparent for a PD=0.256 ms that there is a much higher variability in average s_A than for a PD=1.024 ms, and that mean s_A decrease with increasing frequency. The frequency response suggests that some dominating scatterer other then zooplankton is causing the trend. The only scatterer abundant enough to explain this trend is the small fish, *Müller's pearlside* (cf. Table 2), which next to *Meganyctiphanes norvegica* is the dominant organism present in this layer. The same trend is evident in Figure 2d where the integration over the entire investigated volume is presented. This suggests that this fish is distributed over a greater part of the

SSL, since the trend for the whole water column is near identical. The high s_A mean value at 200 kHz for transect 2 in Figure 2d could be an effect of a small geographical offset, or due to some change in boundary conditions for this particular transect and frequency.

In general, the higher s_A variability at shorter pulse length is initially caused by how EK60 internally process the analogue signal. The EK60 A/D conversion is pulse duration independent but the final output (raw data file), as it resulting from digital decimation to ¼ of the pulse length ($c\tau/2$), strongly depends on it (Table 1). This means that the raw data for the longer PD of 1.024 ms are averaged based on a higher number of digital samples, and will have lower variance compared to data retrieved with a short PD of 0.256 ms. This variance will be reflected in the echo-integration results. Moreover, with respect to echo-integration shorter pulse duration implies higher variability in s_A compared to a longer pulse duration for otherwise identical sampling volumes.

The ping-to-ping variability related to the horizontal resolution is another effect to consider. This variability is less as shorter is the distance between two consecutive transmissions, because the respectively beam volumes are overlapped. This explains the lower variability of the Transect 5 compared the Transect 3 and 4, obtained with the same pulse duration.

In conclusion, in order to determine the number and type of organisms in a structure of dispersed, weak or stronger and near mono-specific scatterers, at least there has to be a sufficient amount of these scatterers within the measurement volume, weather a short or longer pulse duration is being used. The benefit of short pulse duration in this context is the retrieval of target strength measurements of the weak scatterers, contrary to the pitfall of multiple targets if a longer pulse duration is used.

For a more complex mixture of scatterers like the SSL observed in this study, stronger scatterers like the *Müller's pearlside* will completely mask a weaker scatterer like krill, which in fact is twice as abundant in the SSL as in the 25-30m layer described above. This is also exemplified by the use of the inversion technique for the same data as presented in [11]. The results of the inversion gives mostly the "gas filled" model solution for a greater part of the SSL, truly suggesting that fish is the dominant scatterer in the SSL, but the krill component is not resolved. However, an overall aim should be to resolve also the krill and possibly other plankton components, even if they reside within a volume of stronger scatterers. The resolution of the acoustics sampling in time and depth should aim to delineate stronger from weaker scatterers more satisfactorily. With respect to the adoption of the frequency response and inversion techniques as tools in acoustic classification the need for improved resolution is warranted. However, it is currently not realized how this can be achieved with the technology and methods presently available.

4. ACKNOWLEDGEMENTS

Vidar Hjellvik of Institute of Marine in Bergen (Norway) is thanked for the statistical advice.

REFERENCES

[1] **Hewitt** R.P. and **Demer** D.A., The use of acoustic sampling to estimate the dispersion and abundance of euphausiids, with an emphasis on Antarctic krill, *Fisheries Research* 47, 215-229, 2000.

[2] **Mauchline**,J., The biology of mysids and euphausiids, *Adv. mar. Biol.*, 18, 1-681, 1980.

[3] **Stanton** T.K., **Chu** D. and **Wiebe** P.H., Sound Scattering by Several Zooplankton Groups II: Scattering Models, *Journal of the Acoustical Society of America*, 103, 236-253, 1998.

[4] **Holliday** D. V. **and Pieper,** R. E**.** Volume scattering strengths and zooplankton distributions at acoustic frequencies between 0.5 and 3 MHz. *Journal of the Acoustical Society of America,* 67, 135-146. 1980.

[5] **Korneliussen** R. J., **Diner** N., **Ona** E. and **Fernandes** P. G., Recommendations for the collection of multi-frequency acoustic data, *ICES ASC*, Paper R36, 15 pp, 2004.

[6] **Korneliussen** R. J., **Ona**, E., **Eliassen**, I., **Heggelund**, Y., **Patel**, R., **Godø**, O.R., **Giertsen**, C., **Patel**, D., **Nornes**, E., **Bekkvik**, T., **Knudsen**, H. P., **Lien**, G., The Large Scale Survey System – LSSS, *Proceedings of the 29th Scandinavian Symposium on Physical Acoustics*, Ustaoset 29 January – 1 February 2006, 2006.

[7] **Korneliussen**, R. J., Measurement and removal of echo integration noise, ICES *Journal of Marine Science*, 57, 1204-1217, 2000.

[8] **MacLennan** D.N, **Fernandes** P.G. and **Dalen** J., A consistent approach to definitions and symbols in fisheries acoustics, *ICES Journal of Marine Science*, 59, 365-369, 2002.

[9] **Orfanidis**, J. S., Optimum Signal Processing: An Introduction. Second Edition. Macmillan Publishing Co., New York, NY, 1988.

[10] **Brockwell**, P. J., and **Davies**, R. A., Time Series: Theory and Methods. Second Edition Springer, pages 577, 1996.

[11] **Korneliussen** R. J**.**, **Lebourges-Dhaussy** A. and **Knutsen** T., Estimation of size and type of zooplankton by the use of operational post-processing systems, in *Proceeding of the 2nd International Conference "Underwater Acoustic Measurements: Technologies & Results"* Heraklion, Crete, Greece, 25-29 June, 2007.

[12] **Balk** H., and **Lindem** T., Sonar 4 and Sonar 5-Pro post processing systems. Operator Manual. Lindem Data Acquisition, Oslo, Norway, 2002.